

**A REVIEW OF RESEARCH
ON
AERONAUTICAL FATIGUE IN THE UNITED STATES**

2015 - 2017



Compiled by
Dr. Ravinder Chona
Air Force Research Laboratory
Wright-Patterson Air Force Base, Ohio, USA

**FOR PRESENTATION AT THE MEETING
OF THE
INTERNATIONAL COMMITTEE ON AERONAUTICAL FATIGUE**

5 JUNE 2015 – 9 JUNE 2017

NAGOYA, JAPAN

TABLE OF CONTENTS

<u>Section</u>	<u>Page</u>
9.1. INTRODUCTION.....	9/7
9.2. NON-DESTRUCTIVE INSPECTION/EVALUATION	9/11
9.2.1. Improving NDI Confidence	9/11
9.2.2. Single Pass Aircraft Structure Inspection – Challenges and Solutions.....	9/14
9.2.3. Ultra Low Frequency Eddy Current System Using Magnetoresistive Sensor Arrays for Inspection of Multilayer Structures	9/16
9.2.4. Bolt Hole Eddy Current Inspections – From Detection to Characterization.....	9/18
9.2.5. Laser Shearography NDI	9/21
9.2.6. Every Nook and Cranny: An Etchant Qualification Test Program for Pre-Fluorescent Penetrant Inspection on the A-10 Canopy Bow Casting	9/24
9.2.7. Fatigue Damage Characterization Using In-situ Computed Tomography for Validation of No-Growth and Slow-Growth Analysis Methods.....	9/26
9.3. STRUCTURAL HEALTH MONITORING	9/31
9.3.1. Structural Health Monitoring, Risk, and Reliability	9/31
9.3.2. Implementation Challenges for Small Fleet Structural Monitoring.....	9/33
9.3.3. Structural Health Monitoring: Integrity Assessment of Bonded Structures	9/34
9.3.4. Commercial Application of Structural Health Monitoring	9/36
9.4. STRUCTURAL TEARDOWN ASSESSMENTS	9/39
9.4.1. B-52 Inboard Wing Teardown	9/39
9.4.2. T-38 Wing Teardowns – Making a Molehill Out of a Mountain.....	9/42
9.4.3. F-16 Block 50 Full-Scale Durability Test – Test Findings	9/45
9.4.4. Structural Teardown Analysis.....	9/47
9.4.5. T-38 Wing Teardowns	9/49
9.5. LOADS AND ENVIRONMENT CHARACTERIZATION	9/53
9.5.1. Determination of Vibratory Loads for the HH-60G Pave Hawk Helicopter	9/53
9.5.2. Flight Maneuver Recognition for the UH-1N Helicopter	9/55
9.5.3. Comparison of Flight Loads of Single-Engine Air Tankers with Agricultural Operations.....	9/57
9.5.4. Mission Utilization Impact on Individual Aircraft Tracking Data.....	9/59
9.6. CHARACTERIZATION, MODELING & TESTING	9/61
9.6.1. Comparing Starting Crack Size Estimates (EPS and EIFS) Based on the Same Experimental Crack Growth Life Data	9/61
9.6.2. Effective Corrosion Prevention Control Plans.....	9/64
9.6.3. In Situ Thermoelastic Stress Analysis of the F-35 – An Improved Approach to Airframe Structural Model Validation.....	9/66
9.6.4. Impacts on Crack Growth Analysis of Titanium 6Al-4V Small Crack Test Data.....	9/69
9.6.5. Relationship Between Galvanic Corrosion and Local Plastic Deformation – A7050-T7451	9/73
9.6.6. Progress Toward Accelerated Corrosion Testing and Asset Management Tools.....	9/75
9.6.7. Cumulative Corrosion Damage Modeling: A Novel Approach to Evaluating Environmental Attack on Aerospace Alloys.....	9/78
9.6.8. Improved Life Cycle Management Tools for Prediction of Corrosion Damage of Airborne Systems	9/82
9.6.9. Damage-Tolerant Analyses Using Load-Shedding ΔK -Rate Data is Inappropriate for Aircraft Spectrum Loading Life Predictions	9/85

TABLE OF CONTENTS (*Cont'd*)

<u>Section</u>	<u>Page</u>
9.6.10. Modeling Cracks in Obliquely Loaded and Tapered Lugs	9/88
9.6.11. StressCheck + Fracture: Best Practices and Live Demo	9/93
9.6.12. A-10 Failure Analysis Case Study of High Strength Nuts.....	9/94
9.6.13. Continued Development of the NASGRO Software for Fracture Mechanics and Fatigue Crack Growth Analysis	9/97
9.6.14. Advances in Boeing Composite Durability Analysis	9/100
9.6.15. Revised Approach for Efficient Surface Crack Analysis.....	9/101
9.6.16. Fatigue and Damage Tolerance of Tension Fittings	9/103
9.6.17. Cost and Flow Reduction via “Smarter Testing” and Improved Analysis Methods	9/104
9.6.18. Smarter Testing for Metallic Structures.....	9/106
9.6.19. Metallic Materials Properties Development and Standardization (MMPDS).....	9/108
9.6.20. Methodology for Evaluating High-Temperature CMAS (Calcium-Magnesium- Aluminosilicate) Attack of Protective Coating Materials.....	9/109
9.6.21. Investigation of the Correlation Between Surface Topology Changes and Fatigue Crack Propagation.....	9/112
9.6.22. A Combined Dislocation Fan – Finite Element (DF-FE) Method for Stress-Field Simulation of Dislocations Emerging at the Free Surfaces of 3D Elastically Anisotropic Crystals.....	9/114
9.6.23. Open-Hole Tension-Tension Fatigue of Three-Dimensional Woven Composites.....	9/118
9.6.24. Tension-Tension Fatigue Investigation of Three-Dimensional Woven Composites: Effect of Various Epoxy Resin Matrices	9/121
9.6.25. Thermal Cycling Fatigue of Thermal Barrier Coatings	9/124
9.6.26. New Damage Tolerance Methodology to Model High Temperature Dwell Crack Growth in Nickel-Based Superalloys	9/126
9.6.27. Cyclic Fatigue and Dwell Fatigue Crack Growth Response of Ti-6Al-4V	9/128
9.6.28. Role of Deformation Heterogeneities in Life-Limiting Fatigue Failures in a Two-Phase Titanium Alloy.....	9/129
9.7. PROGNOSTICS & RISK ANALYSIS.....	9/133
9.7.1. Risk Assessments per DoD System Safety, USAF Airworthiness and USAF ASIP	9/133
9.7.2. Risk-Shaping the Building Block Development Process for Certification of Composite Structure.....	9/138
9.7.3. Aircraft Structural Reliability Under the Cumulative Effect of Structural Repairs	9/139
9.7.4. Probabilistic Damage Tolerance Using the FAA-Sponsored SMART DT Software.....	9/141
9.7.5. HH-60G Risk-Based Service Life Assessment.....	9/143
9.7.6. Probabilistic Risk Assessment – The SMART Approach to Continued Operational Safety	9/146
9.7.7. Building Robust Initial Flaw Size Distributions for T-38 Risk Analysis	9/149
9.7.8. Fatigue Path Probability Integration (FPPI) for Fatigue Management with Multiple Maintenance Options Using Nondestructive Inspections (NDI) or In-situ NDI.....	9/153

TABLE OF CONTENTS (*Cont'd*)

<u>Section</u>	<u>Page</u>
9.7.9.	A Comparison of Risk Methods in Problems of Varying Complexity 9/155
9.7.10.	Durability Risk Analysis for Random Double Cracks at a Hole 9/157
9.7.11.	Continued Development of the DARWIN Software for Probabilistic Damage Tolerance Analysis and Risk Assessment 9/160
9.7.12.	Risk Assessment and Risk Management Methods for Small Airplane Continued Operational Safety (COS), SMART Software 9/163
9.8.	LIFE ENHANCEMENT CONCEPTS..... 9/167
9.8.1.	Fatigue Enhancement of a Critical A-10 Structural Detail Using Engineered Residual Stress 9/167
9.8.2.	Residual Stress Management Using X-Ray Diffraction and Slitting Methods to Assess Significant Stress Corrosion Cracking in Extruded 7075-T651 Wing Skin Integral Risers on Australian Air Force P-3C Aircraft 9/171
9.8.3.	B-1 Wing Repair – Unique Hole Geometry Cold Expansion Solutions 9/176
9.8.4.	Implementation of Deep Engineered Residual Stresses into the Damage Tolerance Paradigm – Reducing Sustainment Costs and Improving Aircraft Availability 9/180
9.8.5.	Structural Certification of Laser Peening for F-35 Safety Critical Aluminum Forgings 9/182
9.8.6.	Analytical Tools for CX Holes: Where We Are and Where We're Headed 9/187
9.8.7.	SMA Sleeve Method to Coldwork Holes 9/188
9.8.8.	B-1 Wing Lower Skin Repair and Structural Life Enhancement 9/191
9.8.9.	Aleatory Uncertainties in Crack Propagation Life Predictions From Cold-Expanded Holes 9/196
9.8.10.	Low Plasticity Burnishing Mitigates Fretting Fatigue Failures in AV-8B Harrier Engines Restoring Fleet Readiness 9/198
9.8.11.	LPB Treatment of P-3 and C-130 Propellers Reduces Maintenance and Ownership Costs 9/200
9.8.12.	Low Plasticity Burnishing of LPC1 Vanes Mitigates Fatigue Failures of AV-8B Harrier Engines 9/203
9.8.13.	Shot Peen Residual Stress Redistribution During Bending Loading 9/206
9.9.	REPAIR CONCEPTS 9/211
9.9.1.	TRAINING: Design of the Full Strength, Damage Tolerant Repairs for Metallic Aircraft Structure: The Art Behind the Science 9/211
9.9.2.	Finite Element Analysis of Bonded Repairs and Analysis Methods for the ASIP Engineer 9/214
9.9.3.	Lower Forward Corner Fitting Life Extension 9/216
9.9.4.	Bonded Repairs in Metallic Structure..... 9/220
9.9.5.	Effect of Environment on the Mechanical and Fatigue Behavior of Adhesive Bonded Repairs..... 9/220
9.9.6.	Bonded Repairs of Composite Airframe Beam Structure..... 9/223
9.10.	REPLACEMENT CONCEPTS 9/225
9.10.1.	Process-Induced Bulk Residual Stress Finite-Element Model and Validation Measurements of an Aluminum Alloy Forged and Machined Bulkhead 9/225
9.10.2.	Inclusion of Forging Residual Stresses in Large Component Structural Design..... 9/227

TABLE OF CONTENTS (*Cont'd*)

<u>Section</u>	<u>Page</u>
9.10.3. Evaluation and Implementation of Additive Manufacturing Technologies for Structural Applications	9/228
9.10.4. Advanced Aluminum-Lithium (AL-LI) for Primary Structure.....	9/230
9.10.5. Assessment of Emerging Metallic Structures Technologies Through Full-Scale Test and Analysis	9/232
9.11. OVERVIEWS	9/235
9.11.1. Damage Tolerance for Life Management of Composite Structures – Part 1: Modeling	9/235
9.11.2. Damage Tolerance for Life Management of Composite Structure – Part 2: Nondestructive Evaluation	9/239
9.11.3. ADS-89-SP: A Standard Practice for U.S. Army Rotorcraft Structural Integrity Programs	9/240
9.11.4. Digital Thread/Digital Twin Benefits Assessment	9/241
9.11.5. B-1 Wing FSFT Progress and Lower Skin Trailing Edge DaDT Analysis	9/245
9.11.6. C-130 Full-Scale Wing Durability Test with an ESL Wing: Coupon Test Program.....	9/249
9.11.7. Long Term Viper: Flying the F-16 to 8,000 Hours and Beyond!	9/253
9.11.8. F-16 Block 50 Full-Scale-Durability Test – Leveraging the Data.....	9/255
9.11.9. The Evolution of the USAF Aircraft Structural Integrity Program	9/257
9.11.10. A-10 ASIP Adaption to Digital Data; Tactical Advantages, Lessons Learned and Future Plans.....	9/260
9.11.11. F-35 Lightning II Joint Strike Fighter Full-Scale Durability Tests.....	9/264
9.11.12. T-38 Full-Scale Fatigue Test of Two Legacy Wings (Milling Away at Durability Correlations).....	9/267
9.11.13. F-16s Fly with Cracks? Safely Dealing with the Reality of an Aging Airframe.....	9/270
9.11.14. Structural Integrity in Aging USAF Landing Gear.....	9/272
9.11.15. Expanded Dent Limits for C-5 Honeycomb Panels.....	9/274
9.11.16. F-15 Full-Scale and Component Fatigue Tests.....	9/277
9.11.17. F/A-18 Service Life Assessment Program (SLAP) and Service Life Extension Program (SLEP).....	9/279
9.11.18. Structural Life Management of International Space Station (ISS)	9/280
9.11.19. P-8A Poseidon Full-Scale Fatigue Test	9/282
9.11.20. Boeing 787 Full-Scale Fatigue Test Program	9/284
9.11.21. An Assessment of the Potential for Widespread Fatigue and Multi-Site Damage in the 727/737 Forward Pressure Bulkhead.....	9/286
9.11.22. Structural Damage Capability – Reintroducing Fail-Safety into FAA Part 25 Airworthiness Standards	9/287
9.11.23. Active Flutter Suppression (AFS) – The Development of a Research Plan	9/288
9.11.24. U.S. Air Force Academy Center for Aircraft Structural Life Extension (CAStLE) Support to USAF Aircraft Structural Integrity Program (ASIP).....	9/290
9.11.25. U.S. Air Force Academy Center for Aircraft Structural Life Extension (CAStLE) Basic Research.....	9/292
9.11.26. Impact of Material Degradation on Fatigue.....	9/295

9.1. INTRODUCTION

Leading government laboratories, universities and aerospace manufacturers were invited to contribute summaries of their recent aeronautical fatigue research activities. This report contains several of those contributions. Inquiries regarding a particular article should be addressed to the person whose name accompanies that article. The generous contributions of each participating organization is hereby gratefully acknowledged.

Government

- FAA – Aircraft Certification Service
- FAA - Transport Airplane Directorate
- FAA – William J. Hughes Technical Center
- Los Alamos National Laboratory
- NASA Glenn Research Center – Materials and Structures Division
- NASA Johnson Space Center
- Ogden Air Logistics Complex
- Sandia National Laboratories
- USA – Aviation Development Directorate
- USA – Aviation Engineering Directorate
- USA – Vehicle Technology Directorate
- USAF A-10 ASIP
- USAF B-1 ASIP
- USAF C-5 ASIP
- USAF C-130 ASIP
- USAF F-16 ASIP
- USAF F-22 ASIP
- USAF HH-60G ASIP
- USAF Life Cycle Management Center
- USAF Research Laboratory – Aerospace Systems Directorate
- USAF Research Laboratory – Materials and Manufacturing Directorate
- USAF Sustainment Center
- USAF T-38 ASIP
- USAF UH-1N ASIP
- USAF Warner Robins Air Logistics Complex
- USN - NAVAIR

Academia

- Drexel University
- Michigan State University
- Mississippi State University
- Perdue University
- St. Mary's University
- University of Dayton Research Institute
- University of Maine
- University of Texas at Arlington
- University of Texas at El Paso
- University of Texas at San Antonio

- University of Virginia
- University of Washington
- USAF AFIT
- USAFA - CASTLE
- Wichita State University

Industry

- Adirondack Analytics
- Albany Engineering Composites
- Alcoa Technical Center
- Alion Science and Technology
- Arconic Technical Center
- A.S.K. INTERNATIONAL, Inc.
- Battelle Memorial Laboratories
- Bombardier Inc.
- Booz Allen Hamilton
- Constellium
- Curtiss-Wright
- Delta Airlines
- DSTG – Australia
- Elder Research
- Engineering Software Research & Development, Inc.
- Fatigue Technology, Inc.
- Hill Engineering, LLC
- Independent Consultant
- Jacobs Technology, Inc.
- LabSys, LLC
- Lambda Technologies
- Laser Technology Inc.
- Lockheed Martin Aeronautics
- Lockheed Martin F-35 Program
- Mercer Engineering Research Center (MERC)
- Nuss Sustainment Solutions
- PredictionProbe, Inc.
- Sabreliner Aviation
- Southwest Research Institute
- Textron Aviation
- The Boeing Company – B-1 ASIP
- The Boeing Company – B-52 Program Office
- The Boeing Company – Commercial Airplanes
- The Boeing Company – Defense, Space, and Security
- The Boeing Company – Engineering Operations & Technology
- The Boeing Company – F-15 Program
- The Boeing Company – F-35 Program
- The Boeing Company – Military Aircraft
- The Boeing Company – Research & Technology
- The Boeing Company – Small Airplane Directorate
- The Boeing Company – Structures & Mechanical Systems

- The Boeing Company – Test & Evaluation
- The Boeing Company – Transport Aircraft Directorate
- Tom Brussat Engineering, LLC
- TRI/Austin, Inc.
- VEXTEC

References, if any, are listed at the end of each article. Figures and tables are integrated into the text of each article.

The assistance of Jim Rudd and Pam Kearney, Universal Technology Corporation, in the preparation of this report is greatly appreciated.

One of the goals of the United States Air Force is to reduce the maintenance burden of existing and future weapon systems by eliminating programmed repair cycles. In order to achieve this goal, superior technology, infrastructure and tools are required to only bring down systems when they must be repaired or upgraded in order to preserve safety and effectiveness. This requires a condition-based-maintenance capability utilizing structural integrity concepts (CBM+SI). Knowledge is required for four Emphasis Areas: 1) Damage State Awareness, 2) Usage, 3) Structural Analysis and 4) Structural Modifications (Figure 9.1-1). The following nine Technology Focus Areas are identified to provide this knowledge: 1) Non-Destructive Inspection/Evaluation, 2) Structural Health Monitoring, 3) Structural Teardown Assessments, 4) Loads and Environment Characterization, 5) Characterization, Modeling and Testing, 6) Prognostics and Risk Analysis, 7) Life Enhancement Concepts, 8) Repair Concepts, and 9) Replacement Concepts. The aeronautical fatigue research activities of this report have been categorized into these nine Technology Focus Areas, plus a tenth category titled “Overviews” that cuts across two or more of the nine Technology Focus Areas.

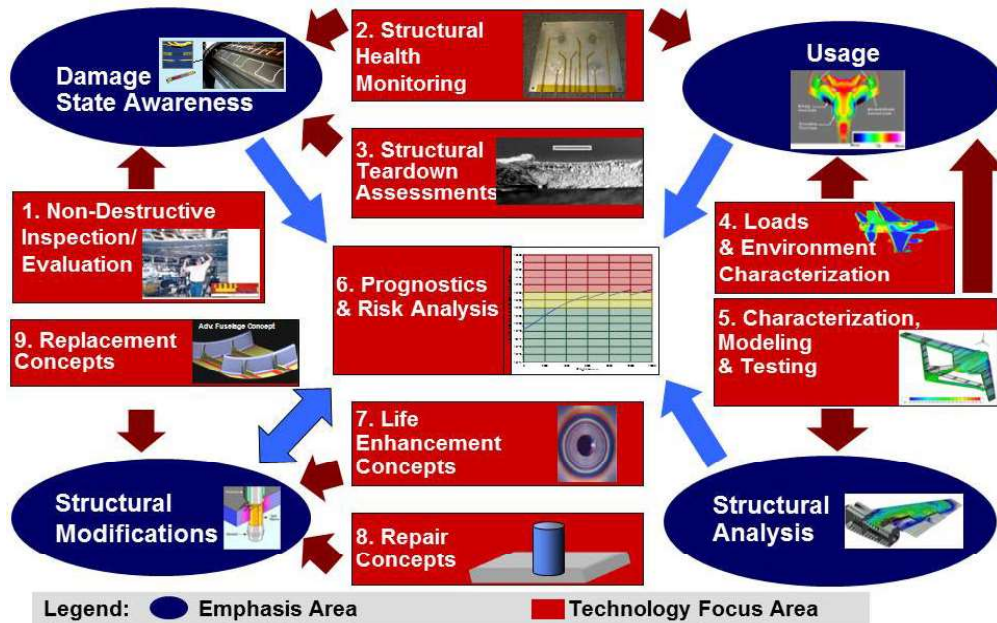


Figure 9.1-1. Condition Based Maintenance + Structural Integrity (CBM+SI)

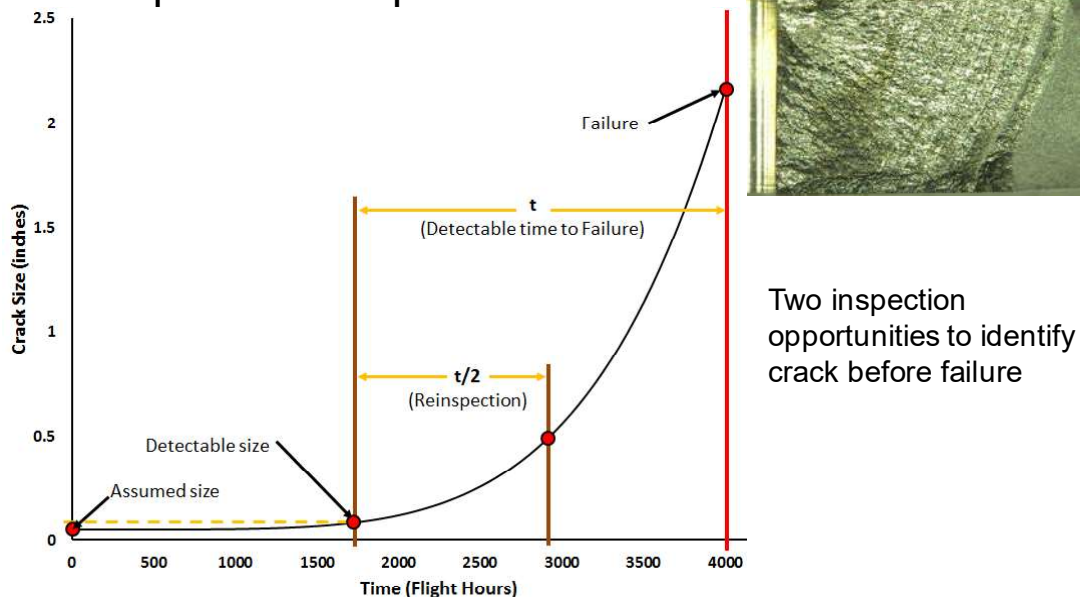
9.2. NON-DESTRUCTIVE INSPECTION/EVALUATION

9.2.1. Improving NDI Confidence

Jacob Warner, USAF F-22 ASIP

The damage tolerance design paradigm relies heavily on accurate Non-Destructive Inspection (NDI) data to project safe flight intervals (Figure 9.2-1). With the increased use of light-weight materials, such as titanium and composites, inspections are becoming more complex and more difficult to interpret. Unfortunately, no additional training opportunities have been provided to inspectors in the United States Air Force (USAF) to account for the increased complexity of inspections. To assist the inspector until further training opportunities can be provided, a bolt-hole-eddy-current study was performed to capture inspection responses of numerous materials, defects and stack ups to create a guide and a tutorial to assist the USAF inspector in interpreting inspection results (Figures 9.2-2 and 9.2-3). The guide includes an isometric view of a hole with the induced flaws and locations identified accompanied with the eddy-current-signal response for that flaw. The goal was to further enable the inspector to correctly call a hole “acceptable”, “uninspectable” or “rejectable” as “uninspectable” hole responses can be very similar to “rejectable” responses (Figure 9.2-4). Correctly identifying hole responses can reduce aircraft maintenance and improve safety of flight. Field studies were completed at two USAF bases to determine the effectiveness of the guide and tutorial. The field studies confirmed the usefulness of the guide/tutorial and identified other inspector needs such as practice specimens (in addition to reference standards) and inspection videos. Three inspection videos were made that show the inspection signal response simultaneously with inspection probe location to clearly demonstrate signal response when transitioning between material layers (Figure 9.2-5). The study concluded that aids such as the videos, guide and tutorial are helpful to the inspector, but that training requirements also need to be reviewed. It is recommended that the guide and tutorial created be made available to the USAF inspector, possibly by incorporation into Technical Orders TO 33B-1-1 or TO 33B-1-2.

- Damage tolerant design relies on successful inspections to prevent failure



Two inspection opportunities to identify crack before failure

Figure 9.2-1. Critical Role of NDI

- Purpose:
 - Identify hole conditions that affect damage indication
 - Create a tutorial and guide to improve inspectors signal interpretation skills
 - Use information to update/supplement TO 33B-1-2
- Created 19 specimens, 232 holes
 - Varying layers (Ti, Al, composite, sealant, shims), thicknesses, and hole diameters
 - Varying damages (gouges, sealant, corrosion, out of round, EDM, etc.)

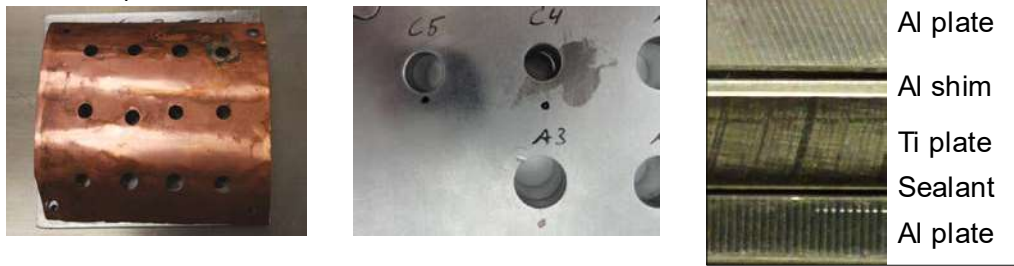


Figure 9.2-2. Eddy Current Capability Study

- EC uses magnetic fields to detect anomalies in conductive materials
- Bolt Hole display:

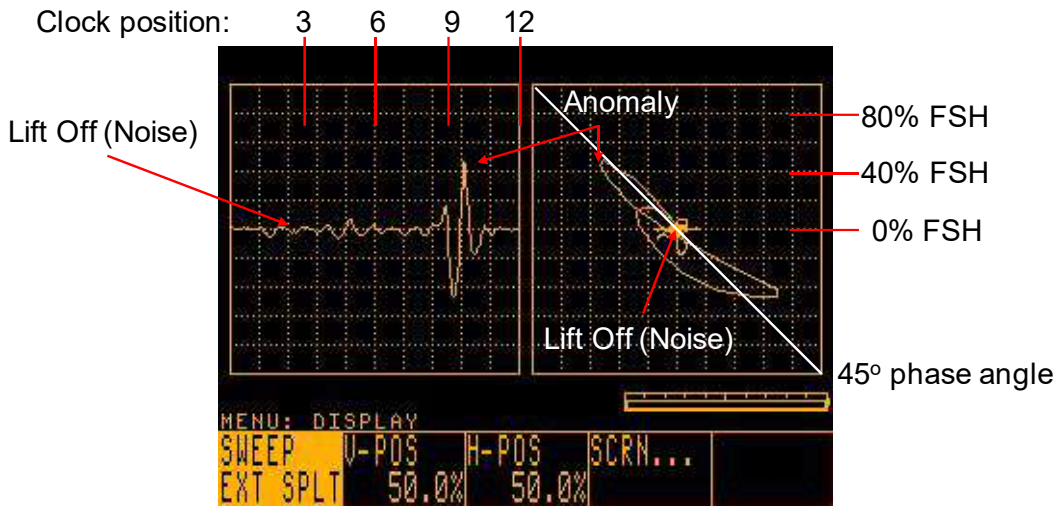
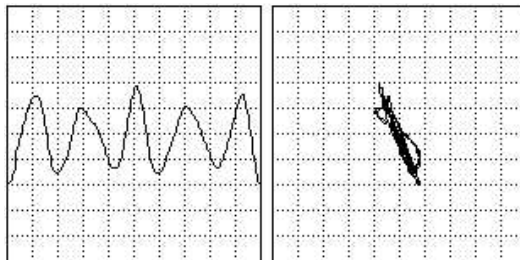


Figure 9.2-3. Eddy Current Background

- Tutorial:
 - An EC reference explaining the physics behind EC
 - Suggests possible causes of signal response
- Interpretation Guide:
 - Document to assist inspector in making more educated conclusions
 - Rejectable vs. Uninspectable



Crack or noise?

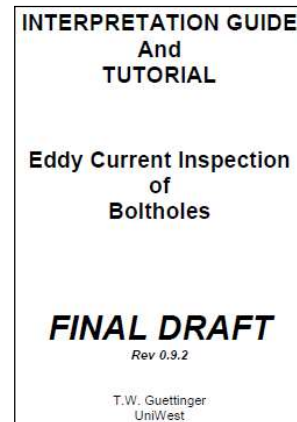


Figure 9.2-4. Tutorial and Interpretation Guide

- Created videos inspecting EC study panels
- Created three on aircraft videos
 - Two for Eddy Current inspection
 - One for Ultrasonic inspection
- Identified method for including video into TOD or USAF NDI web portal

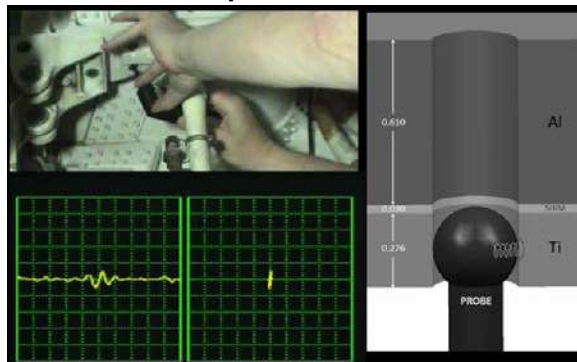


Figure 9.2-5. Videos

9.2.2. Single Pass Aircraft Structure Inspection – Challenges and Solutions

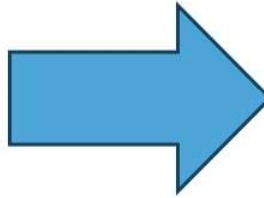
Eric Lindgren, John Brausch, and Charles Buynak, USAF Research Laboratory – Materials and Manufacturing Directorate; David Campbell, USAF Sustainment Center; Ward Fong, USAF Ogden Air Logistics Complex; Tommy Mullis, USAF Warner Robins Air Logistics Complex; Michael Paulk, USAF Life Cycle Management Center

A desired capability expressed by management in the aircraft sustainment community has been and continues to be the single pass inspection of aircraft. In this embodiment, colloquially referred to as the “Nondestructive Inspection (NDI) Car Wash,” an aircraft would be processed through a gantry or other representative envelopment system to enable full inspection of the entire aircraft structure to meet all inspection needs, including those addressing ASIP requirements, without burdensome aircraft preparation/disassembly. This approach is intended to address the perception that there is significant time and cost to perform an assessment of an aircraft using current NDI technology (Figure 9.2-6). Various approaches have been suggested to address this desired capability, including several that cite the neutron radiography system that was located at the Sacramento Air Logistics Center (Figure 9.2-7). This technical activity presents a review of previous efforts to address single pass aircraft inspection, including the expected capabilities, successes/shortfalls of these efforts, and the outcomes from attempts to implement these systems. In addition, the technical activity reviews the physics of each NDI-based sensing method, the challenges that need to be addressed for each method, and the anticipated performance/capability that could be realized based on each technique. Representative simulations for some inspection scenarios are included to illustrate the requirements of the excitation and detection systems needed to obtain typical ASIP-based required sensitivity for fatigue cracks in metallic structures. While comprehensive “return-on-investment” scenarios are not addressed, the economics of possible single pass systems are covered. In addition, the possibility of using embedded sensors to shape the desired outcome is discussed, together with an analysis of multiple requirements that would need to be satisfied before such an approach could be used. The technical activity concludes with several possible scenarios that could begin to address the need for single pass inspection as a function of sensing modality, material type, and detection requirements. Pros and cons for each approach are touched upon together with perspectives on which approach has the highest degree of realism for integrating all parameters that must be addressed to realize this capability.

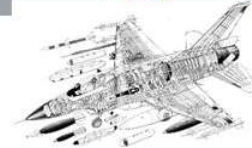
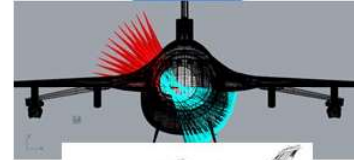
Desire to go from this:



Ref. Jones et.al. ICAF 2015



To this:



- Perception: a major maintenance cost driver is time/cost of Nondestructive Inspection (NDI)
- Perceived solution: single pass inspection process
 - No disassembly (major cost driver)
 - Accelerated inspection rate

Figure 9.2-6. Motivation

X-ray Radiography

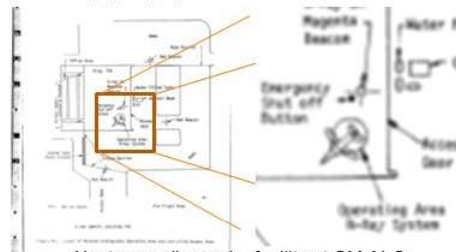
- SM ALC: x-ray source/detector gantry system for water entrapment in honeycomb
- WR ALC: x-ray source/detector gantry system for water/FOD in honeycomb
 - Gridlock in flight controls decreased requirement, low use rate



X-ray gantry system at SM ALC and WR ALC

Neutron Radiography: SM ALC

- Neutron source in cart to circle around aircraft for corrosion detection
 - Only when water present with corrosion
 - Risk of irradiating some materials



Neutron radiography facility at SM ALC

NOTE: most common application is water entrapment/FOD
Current study: cracks smaller than 0.35" cannot be reliably detected
Physics of ionizing radiation limits capability

Figure 9.2-7. Ionizing Radiation: Previous Work

9.2.3. Ultra Low Frequency Eddy Current System Using Magnetoresistive Sensor Arrays for Inspection of Multilayer Structures

Donald Palmer, Jr., The Boeing Company – Research & Technology; Yue Huang, LabSys, LLC; Lalita Udpa, Michigan State University; Charles Buynak, USAF Research Laboratory – Materials and Manufacturing Directorate

Detection of cracks in aging aircraft continues to be a major concern from a structural integrity standpoint. This is especially the case for thicker structure, where manual nondestructive inspection methods are frequently used. Often times, these manual methods require the removal of fasteners and partial disassembly in order to gain access to perform the inspection at an acceptable level of reliability. The United States Air Force Research Laboratory initiated the “Magnetoresistive Sensing Development (MRS-D)” program to build on previous programs that demonstrated some advantages in using giant magnetoresistive (GMR) sensor arrays for inspection of thick and/or multi-layer structure (Figures 9.2-8 through 9.2-10). This program brings together Michigan State University’s modeling and sensor engineering skills in developing optimized array configurations for challenging applications, LabSys LLC’s sensor array manufacturing skills in fabricating high performance GMR arrays, and Boeing’s nondestructive evaluation (NDE) system development skills in producing integrated systems solutions adaptable to the depot maintenance environment (Figure 9.2-11). Specifically, this technical activity will include (1) a discussion on sensor design, with an emphasis on numerical model based design optimization and physics-based signal processing of the measured data, (2) highlights on sensor array performance, including sensor characterization and array integration, and (3) information on systems related topics, including sensor packaging, cabling, hardware integration, and software algorithms for data acquisition, processing and interpretation (Figure 9.2-12). In addition, preliminary validation results obtained using representative multi-layered standards and initial depot inspection experiences are presented.

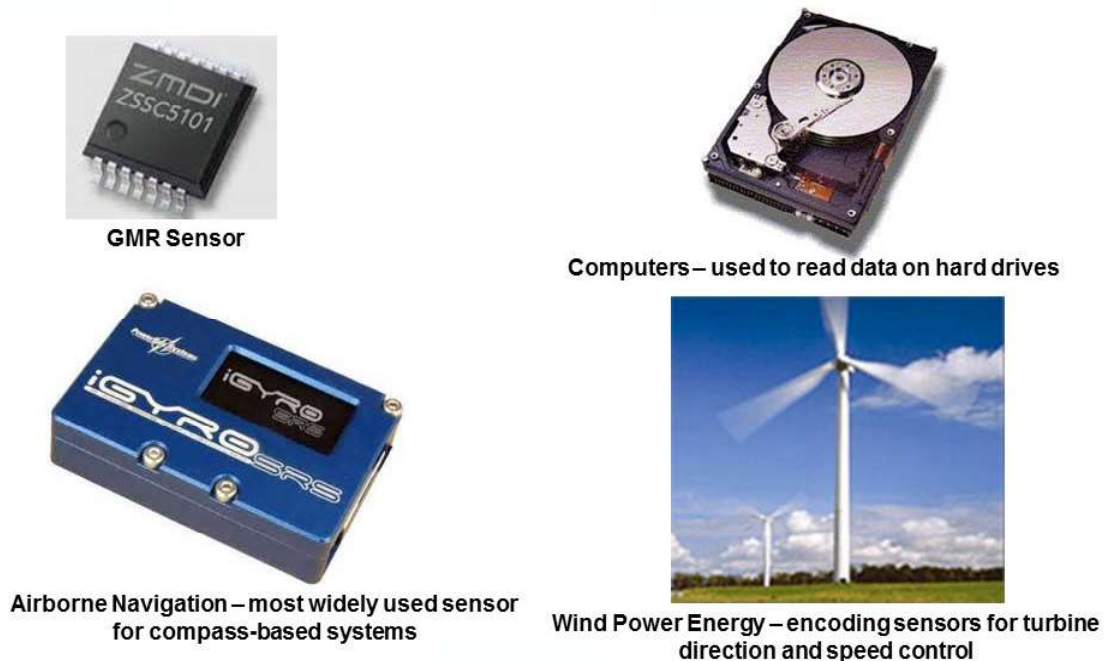


Figure 9.2-8. Traditional GMR Sensor Applications

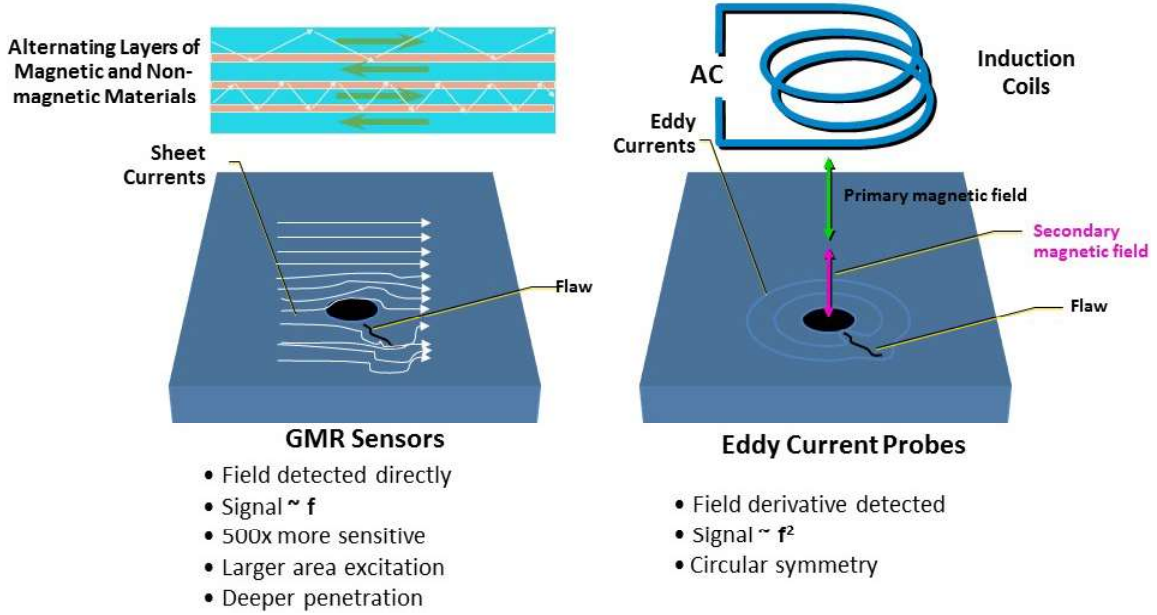
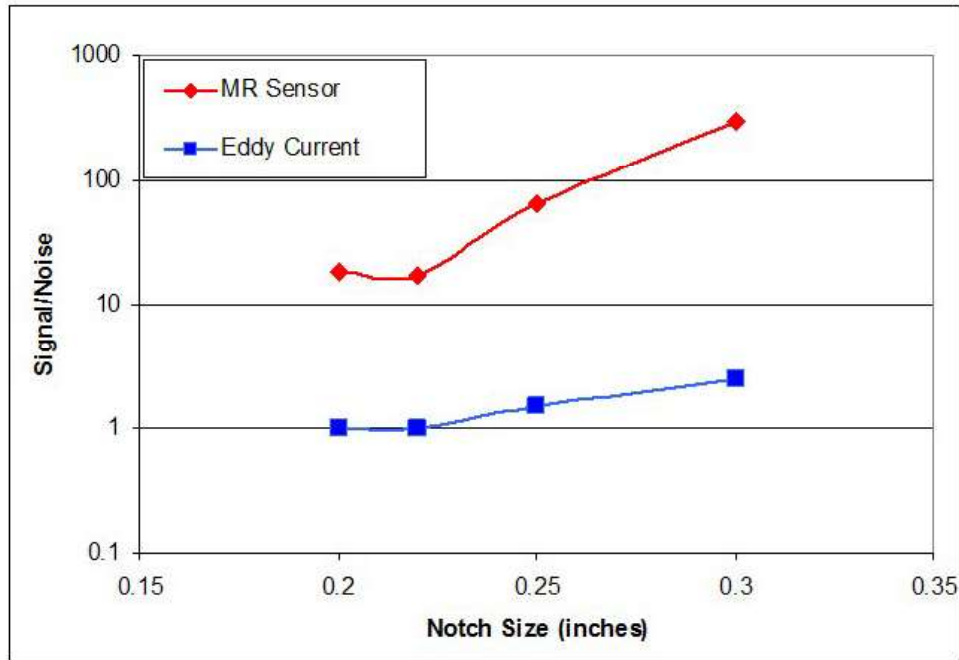


Figure 9.2-9. MR Sensors vs. Eddy Current Probes

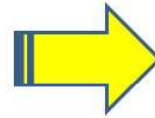


Signal-to-Noise vs. Notch Size through 0.350" Aluminum

Figure 9.2-10. Quantitative Comparison Through Thick Aluminum

Sensor Engineering/Field Modeling

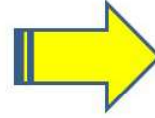
- Detailed Engineering Approach
- Field Modeling
- Parametric Evaluation



Michigan State University
East Lansing, MI

Sensor Manufacturing

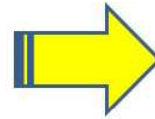
- Develop Robust Sensor Array Designs
- Repeatable Sensor Array Performance
- Simplified Manufacturing/QC Processes



LabSys, LLC
East Lansing, MI

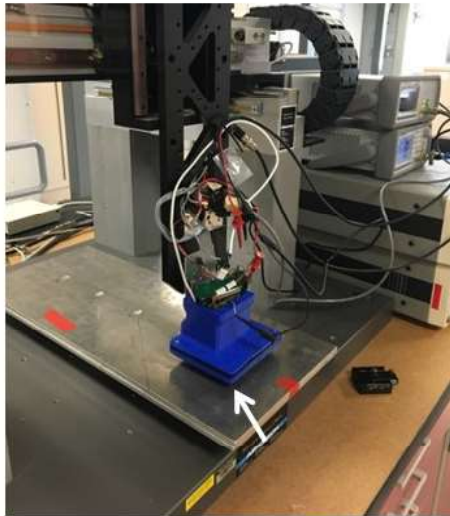
Improved System Hardware/Software

- Chassis Features
- Sensor Packaging
- Cabling
- Software (DAQ and Image Interpretation)

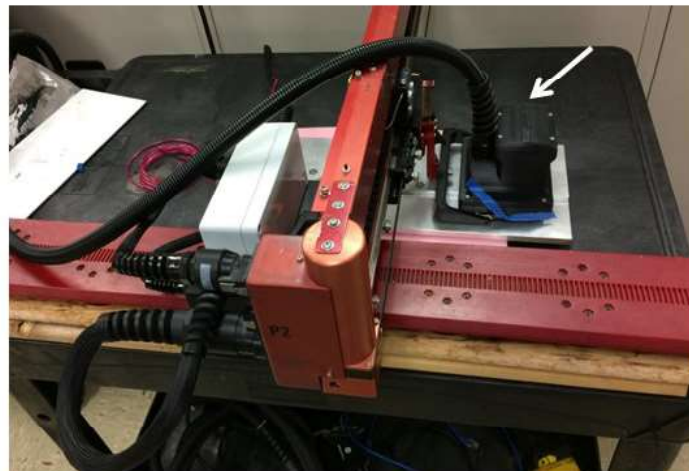


The Boeing Company
St. Louis, MO

Figure 9.2-11. Key Needs Derived From Initial Prototype Program



β-Prototype Array Testing at MSU/LabSys



Scanning Using MAUS Track System at Boeing

Figure 9.2-12. Scanning Using β-Prototype Array

9.2.4. Bolt Hole Eddy Current Inspections – From Detection to Characterization

David Forsyth, TRI/Austin, Inc.

As part of the movement from simple detection to damage characterization, the United States Air Force is sponsoring efforts to verify and validate new inspection hardware and inversion software to support the detection and sizing of cracks in fastener holes. Bolt hole eddy current (ET-BH) inspections are a common technique for inspection of fastener holes in Air Force aircraft structure. In current practice, the inspector holds a small rotary motor with an ET probe attached, and moves the probe up and

down in the hole while viewing the live results on an ET instrument (Figure 9.2-13). These inspections are very sensitive, and a large amount of data exists to support the good probability of detection (POD) of ET-BH in many applications. Shortcomings of the current ET-BH techniques are in the ability to distinguish between fatigue cracks and scratches or other marks on the hole surface, the ability to deal with stackups of different materials, and the ability to size cracks. A new ET-BH system is being validated that automatically indexes the probe through the hole, and records and displays a resulting map of the hole (Figure 9.2-14). It also supports simultaneous recording of multiple ET frequencies and multiple coil arrangements. These hardware developments assist in discrimination of fatigue cracks from non-relevant signals, in the ability to work in multiple material stackups without recalibration, and in the ability to visualize crack lengths on the bore. A new ET inversion software is being validated to support the sizing of fatigue cracks in depth (Table 9.2-1). This is important in the selection of appropriate repairs, and the minimization of material removal. In this technical activity we present the design of the program to verify and validate these complementary, new technologies. Preliminary results on fatigue crack detection and sizing capabilities are also shown.



Figure 9.2-13. Current State of the Art



Figure 9.2-14. Latest and Greatest

Table 9.2-1. Inversion Model Results

• Results: New 15 EDM Notch Aspect Ratio (NIAR) Test Panel:

L notch orientation									
Flaw ID #	Known Depth (mils)	Known Length (mils)	Estimated Depth (mils)	Estimated Length (mils)	Estimated Width (mils)	Estimated Depth (%)	Estimated Length (%)	Known Aspect Ratio ()	Estimated Aspect Ratio ()
1	4.8	37.0	4.97	35.59	0.82	3.6%	3.8%	7.7	7.2
2	5.9	29.9	6.57	28.76	0.88	11.3%	3.8%	5.1	4.4
3	7.5	25.1	8.22	24.11	0.83	9.6%	3.9%	3.3	2.9
4	8.6	22.3	9.18	23.19	0.80	6.8%	4.0%	2.6	2.5
5	10.0	19.9	10.07	21.30	0.56	0.7%	7.0%	2.0	2.1
6	5.0	37.7	5.27	34.46	0.96	5.4%	8.6%	7.5	6.5
7	5.9	29.7	6.75	27.39	0.76	14.4%	7.8%	5.0	4.1
8	7.6	25.0	7.89	24.33	0.72	3.9%	2.7%	3.3	3.1
9	8.8	22.0	8.94	22.63	0.84	1.6%	2.9%	2.5	2.5
10	9.9	19.5	10.06	21.83	0.71	1.6%	11.9%	2.0	2.2
11	5.0	20.0	5.71	21.82	0.76	14.3%	9.1%	4.0	3.8
12	6.4	17.2	6.73	18.31	0.78	5.1%	6.4%	2.7	2.7
13	7.6	15.2	8.07	16.35	0.74	6.2%	7.6%	2.0	2.0
14	8.7	12.3	8.85	14.46	0.92	1.7%	17.6%	1.4	1.6
15	10.0	9.9	11.08	11.79	0.94	10.8%	19.1%	1.0	1.1

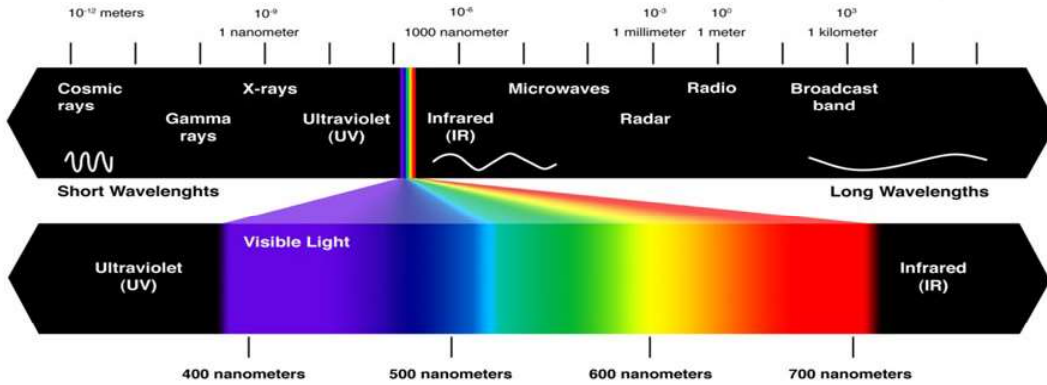
9.2.5. Laser Shearography NDI

Flynn Spears, Laser Technology Inc.

The use of Shearography nondestructive inspection refers to the use of laser-based imaging interferometers to detect, measure and analyze surface and subsurface anomalies in materials and structures by imaging submicroscopic changes to a test part surface when an appropriate stress is applied (Figure 9.2-15). This process can be used to detect defects such as impact damage, disbonds, delamination, near surface porosity, wrinkled fibers, fiber bridging and cracks. Laser Shearography is a mature inspection method that is part of the traditional NDI family of radiography, eddy current, ultrasonics, magnetic particle, liquid penetrant, and visual (Table 9.2-2). All are used on a wide range of aerospace NDI applications including composite aircraft panels, control surfaces, metal honeycomb or foam core panels and solid composite laminates (Figure 9.2-16). As with all the NDI methods, the limitations of Shearography inspection must be understood. Applications must be qualified through test verification, the development of written procedures, and operator training. Once qualified, Shearography methods can be highly cost effective and achieve production throughputs from 25 to 1200 sq. ft/ hour depending on the method and application. Through the increased use of Shearography as an overall screening tool it can quickly and efficiently detect and image flaws as compared to other current techniques. This is achieved by using inspection parameters such as wide FOV (field of view) for large area coverage, real-time image analysis, and automatic image processing and stitching. A typical Shearography NDI system consists of a laser light source, shearing image interferometer, image processing computer, display monitor, and a means to provide a controlled and repeatable stress to the test object. The Shearography optical system is what is referred to as a common path imaging interferometer that offers significant advantages. Shearography cameras are relatively resistant to environmental vibration and motion that can degrade holography images. Shearography cameras create images showing the first derivative of the out-of-plane deformation of the test part surface in response to a change in load. Shearography is relatively insensitive to the global bending or deformation test when it is stressed with heat or vacuum but still highly sensitive to local deformation caused by a defect. Shearography NDI systems can be used in portable on aircraft field inspection (Figure 9.2-17) or fixed production applications. Fixed production systems may also use test chambers to allow vacuum stress and scan gantries to inspect large panels or structures. With the advent of composite structures, materials and advanced weapons systems such as fixed wing, rotor, unmanned, and with low observable coatings this technology is gaining huge importance in the materials manufacturing arena.

• **Wavelength Classification**

- **Ultraviolet** **180 Nm - 400 Nm** **LTI M5100 532Nm**
- **Visible** **400 Nm - 700 Nm** **LTI M7200 660Nm**
- **Infrared** **700 Nm - 1 Nm** **LTI M2100 660Nm**



Visible light is defined as the region between 400 Nm and 700 Nm where the human eye is sensitive.

Figure 9.2-15. Laser Methods

Table 9.2-2. NDT Method Comparisons

Test Method	Sensitivity to Cracks	Sensitivity in Ferromagnetic materials	Accuracy	Contact Requirement	Speed
Eddy Current	Decreases with depth	Surface only	High	> 2 mm liftoff acceptable	Fast
Ultrasonic	Penetrates	Penetrates	High	Couplant	Slow
Liquid Penetrant	Surface only	Surface only	Subjective	Clean Surface	Slow
Magnetic Particle	Decreases with depth	Decreases with depth	Subjective	Contact	Slow
Radiography	Penetrates	Penetrates	Moderate	Through access	Slow

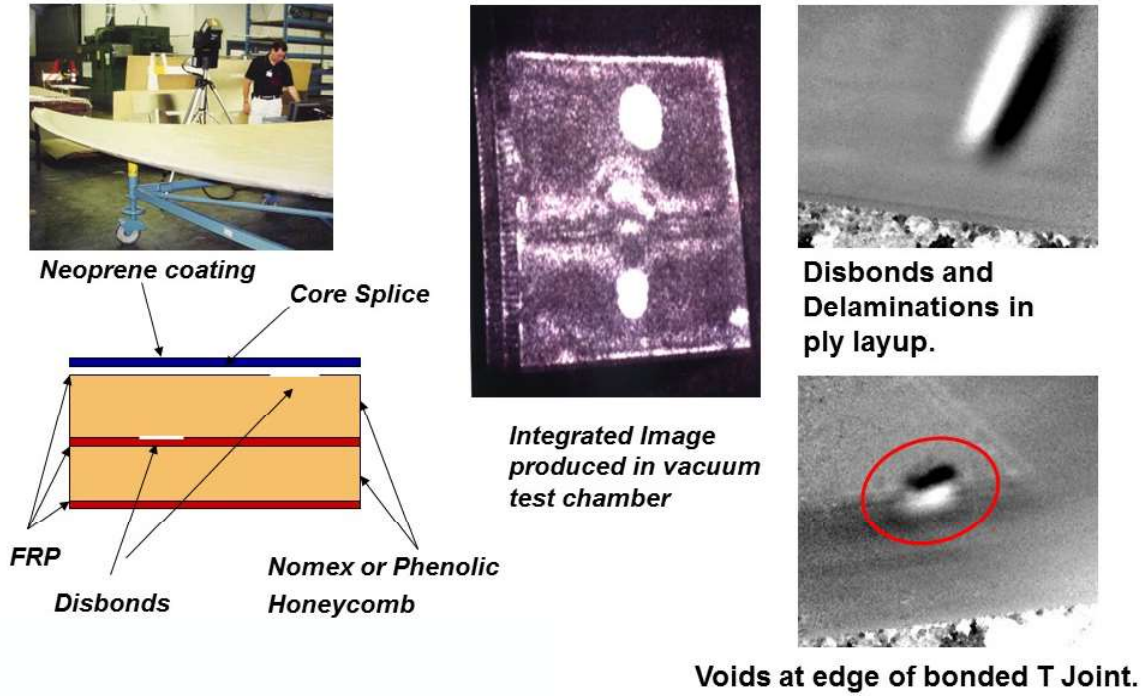


Figure 9.2-16. Shearography Applications



• **Example Activity:**

Shearography Results F-35 Honeycomb Matrix Panel 3-21 Ply, Disbonds 1.0-0.28 in. 36"x26" Panel

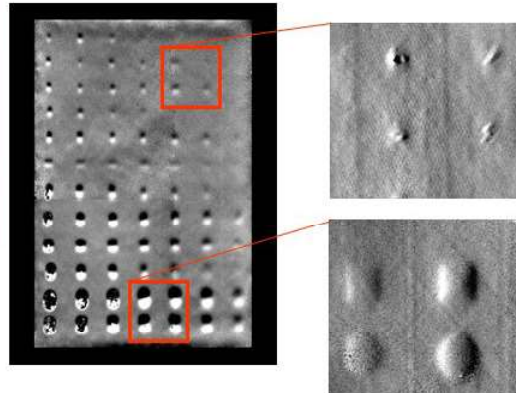


Figure 9.2-17. Portable Shearography Equipment

9.2.6. Every Nook and Cranny: An Etchant Qualification Test Program for Pre-Fluorescent Penetrant Inspection on the A-10 Canopy Bow Casting

Dallen Andrew, Southwest Research Institute; Dennis Vickery, USAF A-10 ASIP; John Brausch, USAF Research Laboratory – Materials and Manufacturing Directorate

An A-10 aircraft (Figure 9.2-18) experienced a fracture of the left side canopy bow clevis lugs resulting in a section of the clevis and pin releasing into the airstream and being ingested in the first-stage fan of the left hand motor. After an initial inspection of the aircraft and the canopy bow was completed, the lower left side of the bow was cut out of the windscreen and shipped to Southwest Research Institute (SwRI) for a thorough metallurgical evaluation to determine the root cause of the failure (Figure 9.2-19). At the time, Technical Orders authorized field units to blend mechanical damage identified during inspections of the lugs. Cursory inspections of aircraft in the field as well as data from the failure investigation made it evident that blending was prolific throughout the fleet. These blends reduced the strength of the lugs in addition to creating impediments for penetrant inspections. Mechanical grinding, blending, and sanding processes result in smearing of the base material (Figure 9.2-20). This smearing has the potential to close or reduce the surface opening of any existing discontinuities or cracks significantly reducing the effectiveness of a fluorescent penetrant inspection (Figure 9.2-20). Fluorescent penetrant was the method of choice for this application, in lieu of eddy current inspection, due to the complex geometry and high eddy current signal noise typical of aluminum castings. To facilitate fluorescent penetrant inspections, a reliable etchant process was critical in order to remove any smeared metal and expose the crack to the surface. This technical effort will discuss the evaluation of multiple etchants and the overall qualification process. Etchant differences to include etchant rates as a function of temperature and post-etch metallurgy to evaluate pitting will be discussed (Figure 9.2-21). The technical effort will also discuss lessons learned for future etchant evaluations.



Figure 9.2-18. Failure Location



Figure 9.2-19. Failure Origin

■ Example of smearing

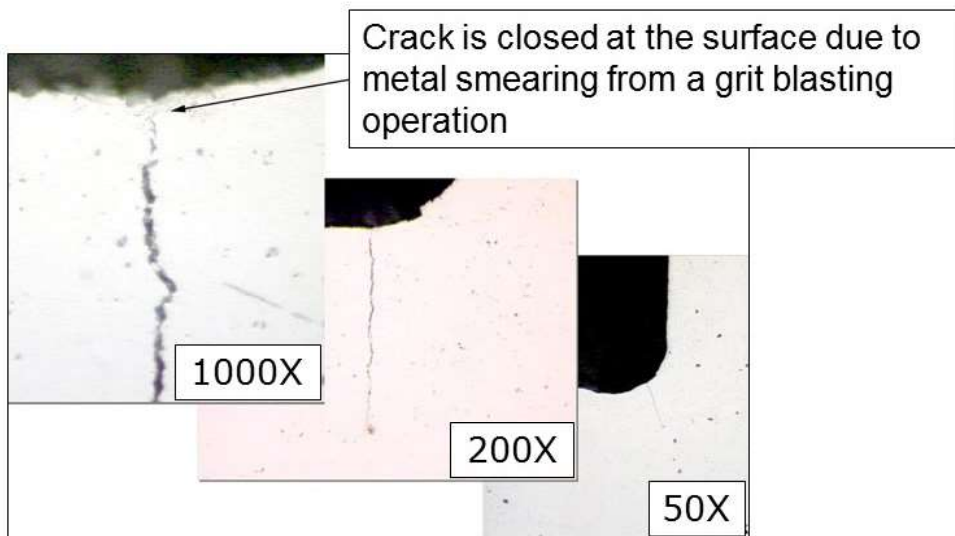


Figure 9.2-20. Inspections: FPI After Blending

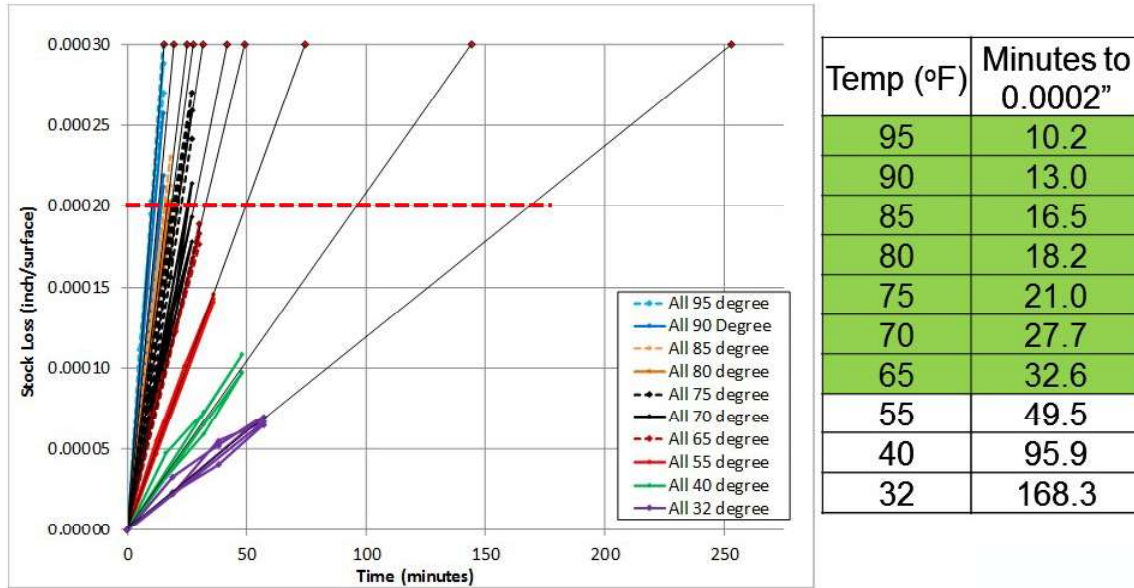


Figure 9.2-21. Etching Results

9.2.7. Fatigue Damage Characterization Using In-situ Computed Tomography for Validation of No-Growth and Slow-Growth Analysis Methods

Joseph D. Schaefer*, Salvatore L. Liguore, Brian P. Justusson, The Boeing Company – Research & Technology (*Corresponding Author: josephschaefer@boeing.com)

High Flight Hour (HFH) aircraft such as the F/A-18 C/D have exceeded their original design life and are experiencing fatigue and environmental damage in primary composite structure. Typical damage identified from teardown structure includes transverse micro-cracking (TMC), adhesive micro-cracking (AMC) (near pylons), and widespread delaminations near free-edges, steps, and highly-loaded fasteners (Figure 9.2-22). These damage types were not identified by standard fleet-level inspection techniques. Critically, AFRL, NASA, and ONR have recently initiated programs to develop progressive damage analysis (PDA) techniques to predict initiation and growth of these damage mechanisms in composite structure. The intent of these techniques is to provide an analysis basis for damage growth predictions, inspection intervals, and design-space expansion. However, implementation of PDA techniques is severely limited by the lack of supporting inspection data to provide metrics for in-situ damage growth.

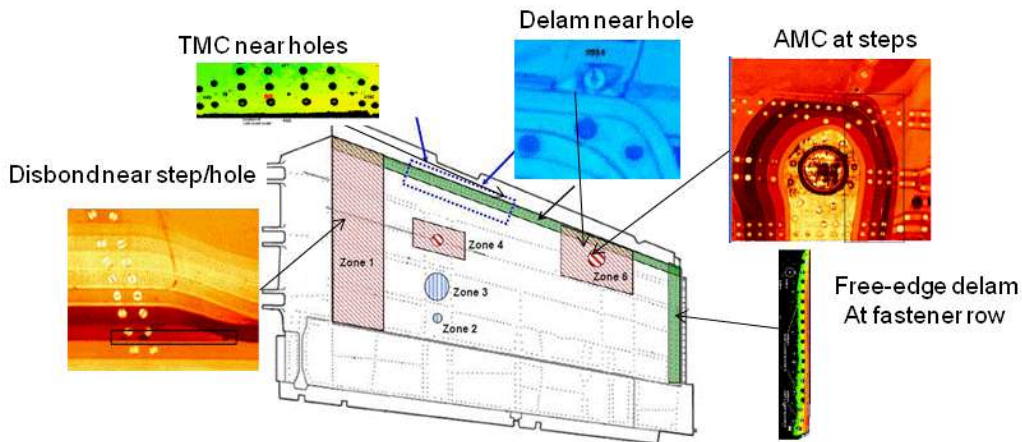


Figure 9.2-22. Damage Mechanisms Around Fastener Holes

An exploratory test program was initiated under the Predictive Composite Failure Methods Program to characterize composite damage using the emerging technique of in-situ computed tomography (in-situ CT) to provide enhanced characterization of damage on a ply-by-ply and damage-mode basis. Quasi-static and fatigue tests were performed on open hole tension (OHT) specimens to identify the initiation and propagation of damage modes noted in Figure 9.2-22. The results provided unprecedented data for comparison to analysis predictions on a layer-by-layer and failure-mode basis. The results for static damage initiation are shown in Table 9.2-3. The results were plotted to develop a novel Damage Map for correlating analysis predictions to the characterized material behavior, as shown in Figure 9.2-23.

Table 9.2-3. Damage Initiation of Embedded Plies Identified Using In-situ CT

Specimen No	% of Ultimate Load by which First Damage Observed		
	90° Plies	45° Plies	0° Plies
1	16	32	32
2	19	32	47
3	22	32	N/A
4	20	32	47
5	25	32	47

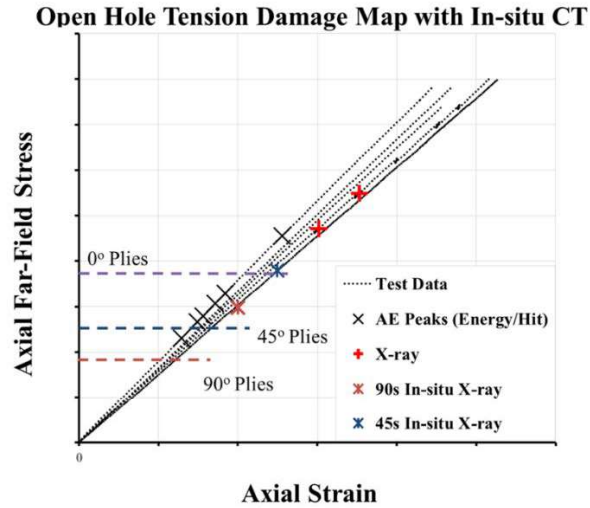


Figure 9.2-23. Lamina Scale Damage Map (Static) for Damage Initiation Indicated by Inspection Technique – Dashed Lines Indicate In-situ CT

Fatigue testing was performed on an additional specimen subset to identify the growth of the damage types noted in the static investigation. Initial CT scanning was performed to identify the undamaged material state in the region of interest. A specimen was quasi-statically loaded to 70% UTS and subsequently scanned. Following the static loading, the specimen underwent a fatigue loading block ($R = 0.1$) consisting of 50,000 cycles at 70% UTS. The specimen was then loaded quasi-statically to 70% of UTS and scanned using in-situ CT. The resulting scans are shown in Figures 9.2-24 through 9.2-26.

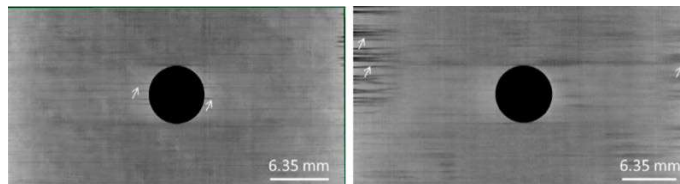


Figure 9.2-24. 90° Embedded Ply Damage for Static Loading (Left, Arrows Indicated Ply Cracking) and After Fatigue Loading (Right, Arrows Indicate Edge Damage); 4th Ply

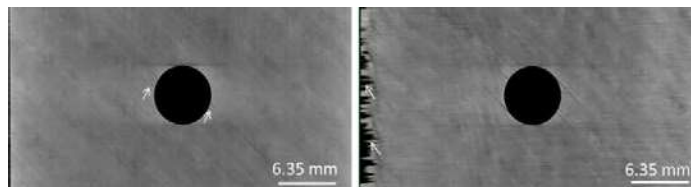


Figure 9.2-25. 45° Embedded Ply Damage for Static Loading (Left, Arrows Indicate Ply Cracking) and After Fatigue Loading (Right, Arrows Indicate Edge Damage); 3rd Ply

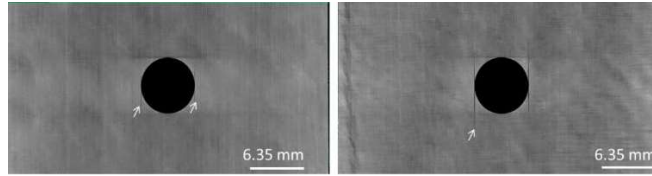


Figure 9.2-26. 0° Embedded Ply Damage for Static Loading (Left, Arrows Indicate Ply Splitting) and After Fatigue Loading (Right, Arrows Indicate Ply Splitting Extension); 2nd Ply

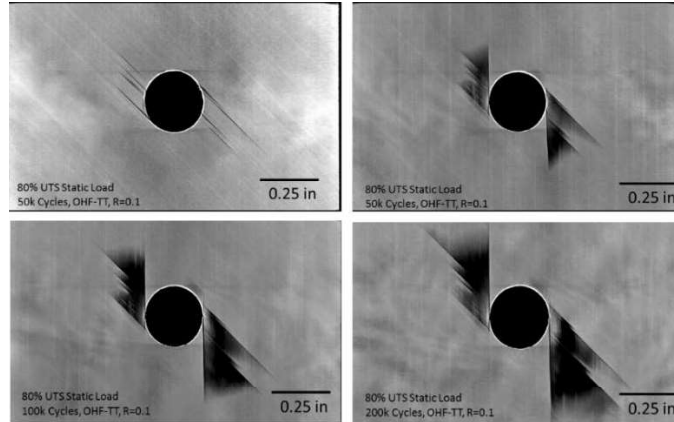


Figure 9.2-27. In-situ Characterization of Damage Progression for OHTT, R=0.1, 80% UTS

Key new insight into the development of edge delamination and stress reduction mechanisms at the hole edge was obtained. It was observed that strain relief at the hole edge in embedded 0° plies occurred due to a splitting damage mode. A requirement for accurate use of PDA techniques may be to predict the presence of splitting. The novel investigation undertaken by the PCDFM team was extended to provide metrics for fatigue damage growth on the ONR High Fidelity Test Program (N00014-14-C-0128). A subcontract with the University of Texas-Arlington Advanced Materials and Structures Lab was completed to evaluate the development of fatigue damage within composite specimens similar to those noted above in OHTT, R=0.1, from loadings of 20% UTS to 90% UTS (5320-1/IM7). An example of delamination growth at 80% UTS from 50-200k cycles is shown in Figure 9.2-27. The interaction of in-plane ply damage and delamination modes was observed to most severely develop for fatigue loadings above 60% UTS at 50,000 cycles. The ongoing investigation is contributing significantly to the BR&T technical strategy of analysis validation, and has already provided value to the NASA Advanced Composites Project. Further, AFRL feedback has indicated that BR&T is the industry leader for effective implementation of these advanced inspection, analysis, and validation techniques. This technical focus is additionally reinforced through four technical publications within the past calendar year at CAMX, SAMPE, and ASC. The partnerships developed on this program additionally support CRAD capture.

9.3. STRUCTURAL HEALTH MONITORING

9.3.1. Structural Health Monitoring, Risk, and Reliability

David Forsyth and Jake Montez, TRI/Austin, Inc.; Juan Ocampo and Harry Millwater, University of Texas at San Antonio

Structural health monitoring (SHM) has long been proposed as an alternative to nondestructive inspection (NDI). If SHM is going to replace NDI for ASIP-managed structure, then the probability of detection (POD) for the SHM must be determined in order to support ASIP Task V. The risk is then managed by scheduling inspections of a known POD at an interval of usage that prevents damage from progressing to a dangerous size (Figure 9.3-1). Many questions still remain about the correct calculation of POD and risk for SHM onboard systems. There are conflicting approaches in the literature regarding the effectiveness of the ability to have very many inspections at a single location using SHM (Figures 9.3-2 through 9.3-4). We propose a method to assess POD for SHM with the consideration of the ability to perform sensor readings at various intervals. We then demonstrate how the SHM-specific POD calculation can be used to support a risk calculation. Both NDI data and SHM data are presented in support of the theory.

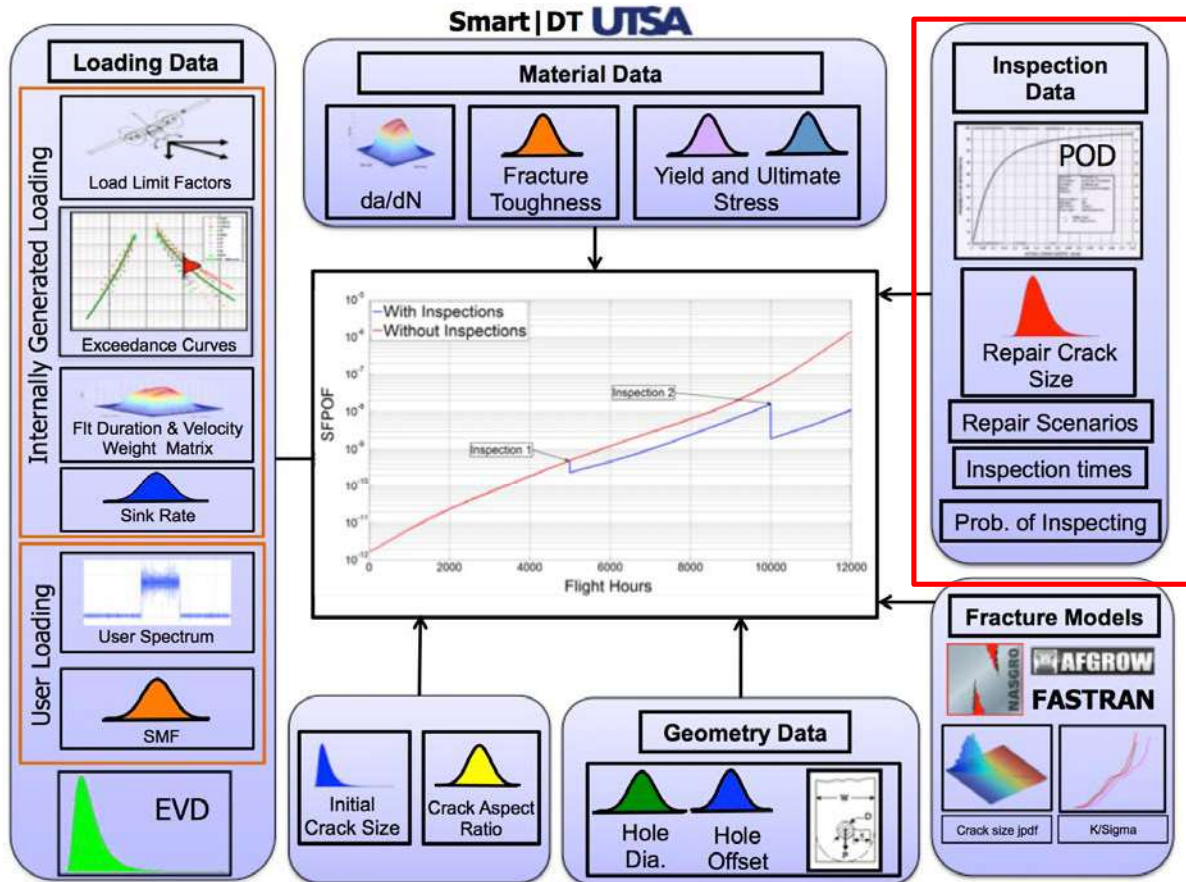


Figure 9.3-1. Replace NDT with SHM in Risk Calculation



Figure 9.3-2. Manual ET Inspection for Fatigue Cracks

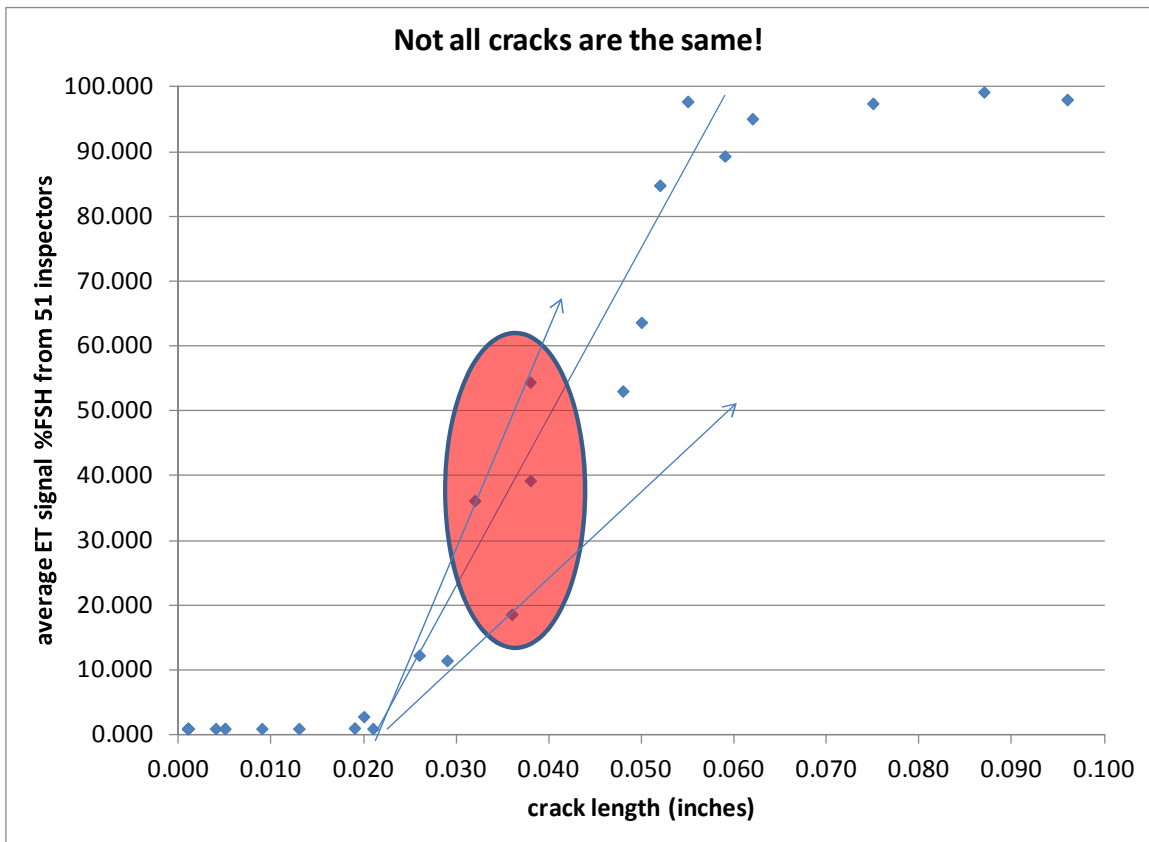
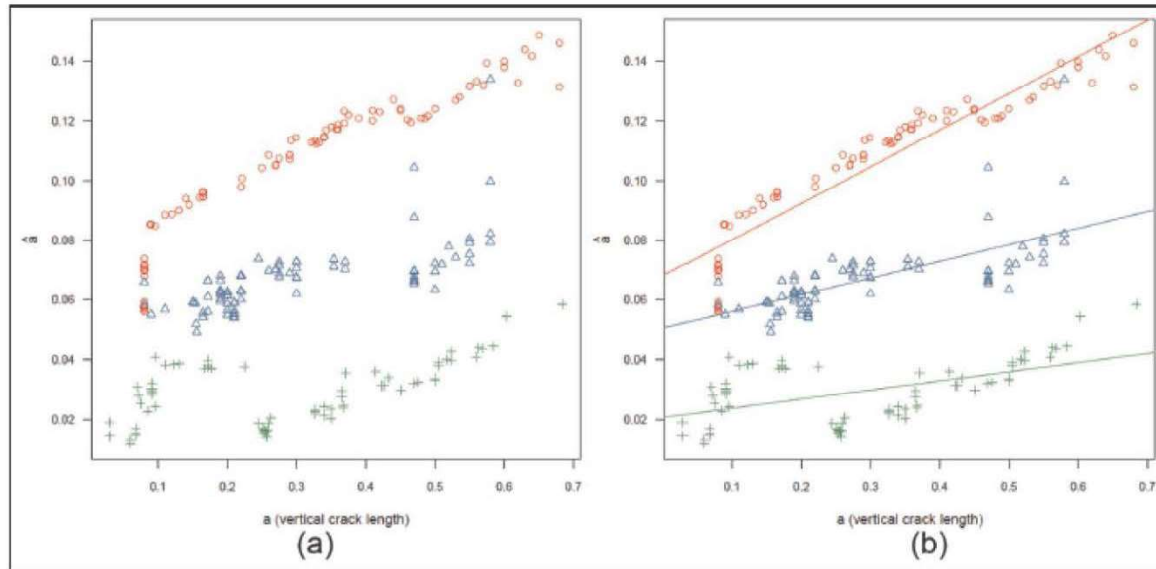


Figure 9.3-3. Average ET Signal vs. Crack Length



Scatterplots of the square root transformed single sensor output versus vertical crack length for each of the three specimens: (a) without and (b) with fitted regression lines.

Figure 9.3-4. Crack Variability

9.3.2. Implementation Challenges for Small Fleet Structural Monitoring

Thomas Melia, Curtiss-Wright

Well established ASIP methods and procedures continue to result in life extension and increased availability for strategic aircraft assets. This situation contrasts sharply with small aircraft fleets globally, who have not benefitted in the same way and have limited resources to implement structural monitoring programs on the same scale. The majority of aging aircraft tails within these small fleets remain unmonitored, where monitored implemented sample sizes are small and vulnerable outliers remain unidentified. This technical activity reviews the technical and economic challenges faced by small fleet managers in the context of a structural monitoring implementation (sensor specification, hardware procurement, certification, analysis, restricted budget) and proposes a complete "sensor-to-screen" solution for small fleets (Figure 9.3-5).

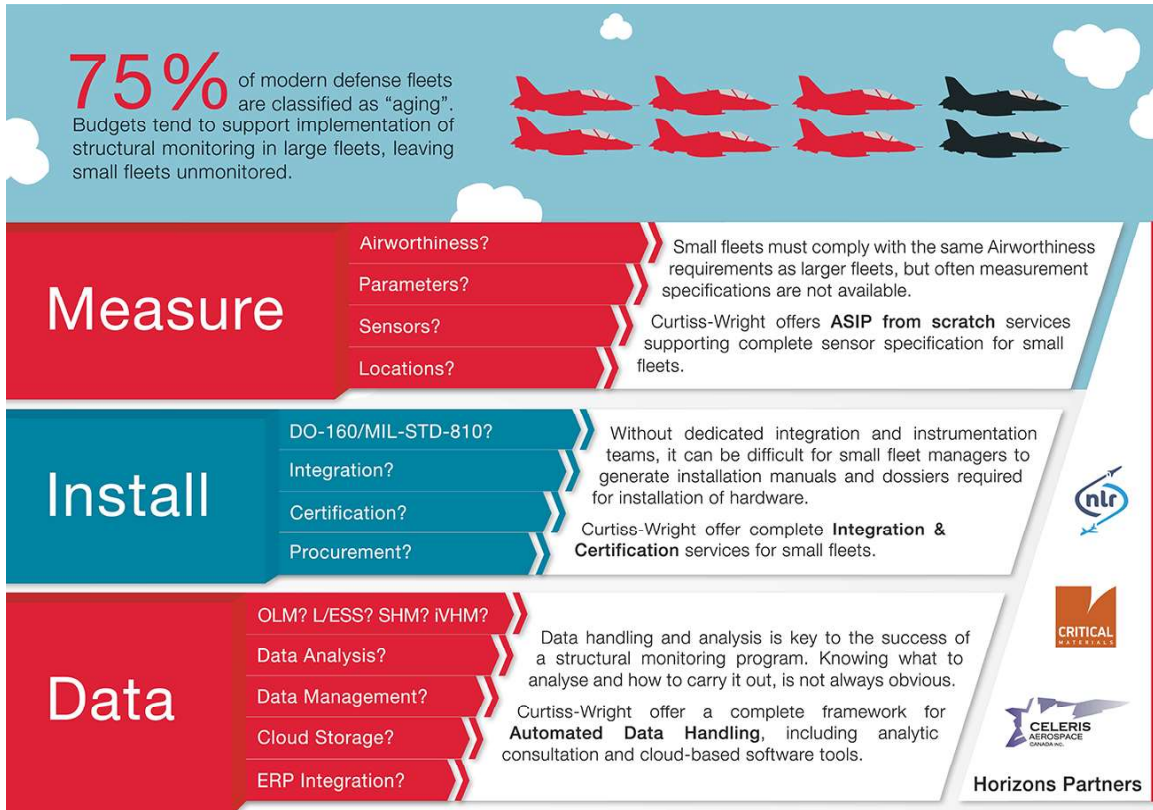


Figure 9.3-5. Challenges for Small Fleets

9.3.3. Structural Health Monitoring: Integrity Assessment of Bonded Structures

Mark Jahanbin, The Boeing Company – Commercial Airplanes; Jeong-Beom Ihn, The Boeing Company – Research & Technology

Damage nucleation and growth behavior can be complex and rich in hybrid structures and multilayered laminated composites that are constructed from two or more materials with different mechanical properties. Presently there is not any reliable damage growth analysis method to evaluate the bonding integrity of such structures. Depending on the geometry and accessibility of hybrid joints and composite plies, some Non Destructive Evaluation (NDE) techniques are being used for inspection of these structures, but they are limited to localized damage detection and not to the extent of verifying the bonding integrity of hybrids and composites.

This study is devoted to the use of a Structural Health Monitoring (SHM) system to assess hybrid structures by examining ultrasonic wave behavior at the interface of such structures. The essence of SHM technology is to develop autonomous built-in systems for the continuous (or on-demand) monitoring, inspection, and damage detection of structures with minimum labor involvement. A reliable SHM system has the potential benefits of cost saving, reduction in human error which is critical to NDE methods and also real-time monitoring and reporting of the structure’s condition in a service environment. Typically, SHM systems are a built-in network of sensors that collect data, and then a software for damage identification by interpreting the collected data from sensors, which is translated from the physical condition of the structure.

The focus of this research lies in the real-time in-situ health monitoring of the interface between two media with different materials (Figure 9.3-6). Ultrasonic Guided waves are a widely used approach

in SHM. In-situ ultrasonic inspection has been demonstrated as a viable technique to investigate the condition of both isotropic metallic and anisotropic composite structures. This work suggests a novel inspection method to evaluate the bond integrity of such structures, by use of interface guided waves.

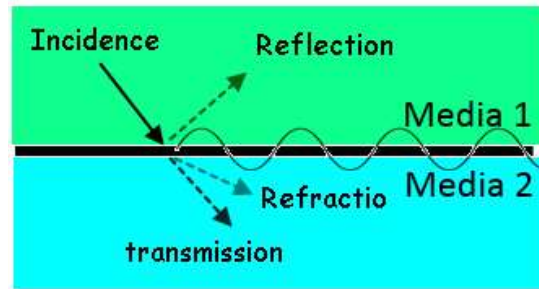


Figure 9.3-6. Schematics of Wave Propagation at Two Media

The preferred inspection method for both constituents of hybrid structures (composite and metallic) is using ultrasound. Ultrasonic waves can propagate in the material and reflect from its boundaries and are scattered by interfacial defects. The velocity of waves depends on material properties (modulus of elasticity and density), and characteristics such as disbonds at interfaces or any other types of damage in both sections of interface (Figure 9.3-7).

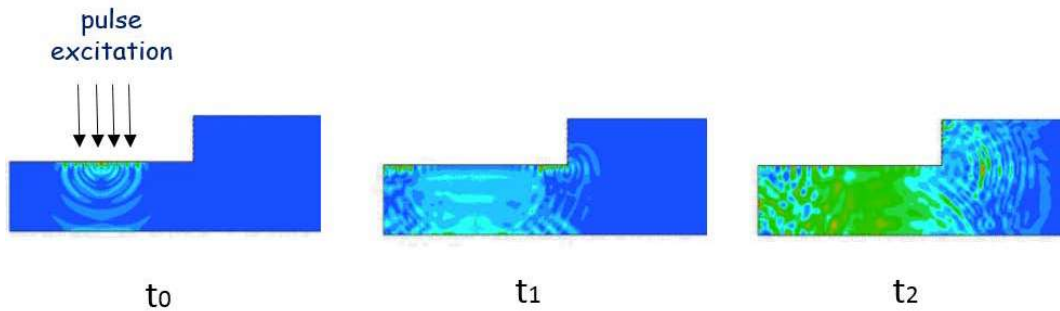


Figure 9.3-7. Wave Propagation at Interface of Two Media with Close Material Properties

Ultrasonic waves can be distinguished by longitudinal waves (compressional waves) and shear waves. A three-dimensional medium bounded by one surface allows for propagation of surface waves (Rayleigh waves and Love waves). A plate of finite thickness and two bounding parallel surfaces allows the propagation of guided waves called Lamb waves, which are broadly used and considered for diagnostics and NDE. There are also waves that propagate on media boundaries (so called interface waves) with their names derived from their discoverers for any combination of media. For example, the wave propagating along the interface between two solids is called a Stoneley wave, and the wave traveling along the interface between solid and a liquid is referred to as a Scholte wave. There are many other forms like Love waves, leaky waves, creep wave, etc. The interface waves between two sections of a hybrid structure which have significant mechanical property differences are the main focus of this study (Figure 9.3-8).

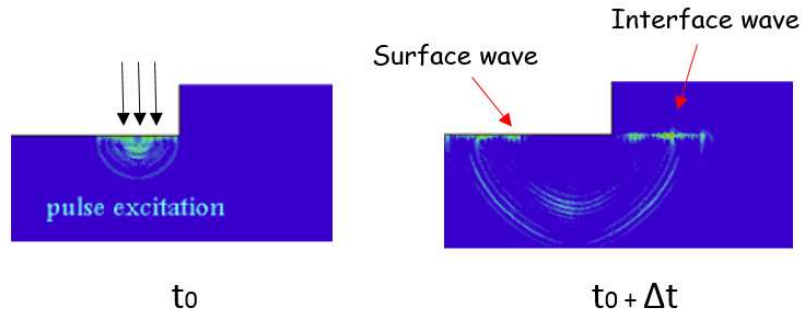


Figure 9.3-8. Wave Propagation at Interface of Two Media with Different Material Properties

A hybrid structure model was constructed to demonstrate the interface wave behavior at the bondline of perfectly bonded isotropic and anisotropic interface. This model was used to study the interface wave behavior at the typical damage mode for a bonded structure. The investigation of bonding integrity in hybrid structures by computational modeling of ultrasound propagation is a novel concept which highly depends on the structure configuration to effectively simulate the interface guided wave.

Boeing is modeling interface waves for different range of material selection and geometrical configuration very similar to the co-cure and co-bonded structures. These models will be utilized in the solution of the ‘inverse’ problem. The inverse problem involves identifying the location, size, and shape of defects by analyzing the scattered signals received at sensor and comparing the distortion with respect to the pristine undamaged state of the structure. This work demonstrates the cases in which interface waves are sensitive to bond defects and consequently wave form distortion can be used for damage detection purposes. The size and location of damage significantly influence the leaky wave behavior and propagation of interface wave. The results of these modeling techniques and damage simulations might be of particular interest in the development of experimental test setups for SHM of laminated and hybrid structures.

9.3.4. Commercial Application of Structural Health Monitoring

Paul Swindell, FAA – William J. Hughes Technical Center; Dennis Roach, Sandia National Laboratories; David Piotrowski, Delta Air Lines; John Linn, The Boeing Company

Industry is promoting new technologies, such as structural health monitoring (SHM), to reduce long-term maintenance costs, improve safety, reduce labor costs, and reduce human error. However, to enable the insertion of SHM in commercial transport airplanes for current and future applications, including fatigue monitoring and condition-based maintenance, data are needed to assist the FAA in developing SHM certification and continued airworthiness requirements.

For this multi-year project, the FAA is partnering with Sandia National Laboratories, Delta Air Lines, and The Boeing Company to conduct a trial SHM certification and integration activity using embedded comparative vacuum-monitoring (CVM) sensors to detect the formation of cracks in a critical load-bearing structure. The goal is to integrate SHM into the regulatory framework and transition the use of the technology from its prototype status into mainstream maintenance.

The application chosen was remote hot-spot sensing of the center wing box front spar shear fittings, at Body Station (STA) 540, on seven of Delta Air Lines’ Boeing 737-700s, shown in Figure 9.3-9a. This area of the aircraft is prone to high stress levels and has known cracking issues, as indicated by a Boeing service bulletin requiring inspections after 21,000 flights. Designed as a passive system, the CVM sensors have an array of embedded galleries to which a vacuum is applied (Figure 9.3-9b). Any leaking path of atmospheric pressure detected produces a measurable change in vacuum level, indicating the presence of a crack. If no crack is present, a vacuum is achieved. Seventy CVM sensors were

installed (Figure 9.3-9c). In June 2016, Boeing issued a revised Service Bulletin with CVM as an alternate means of compliance, which is officially the first approved use of SHM in the U.S. commercial transport fleet.

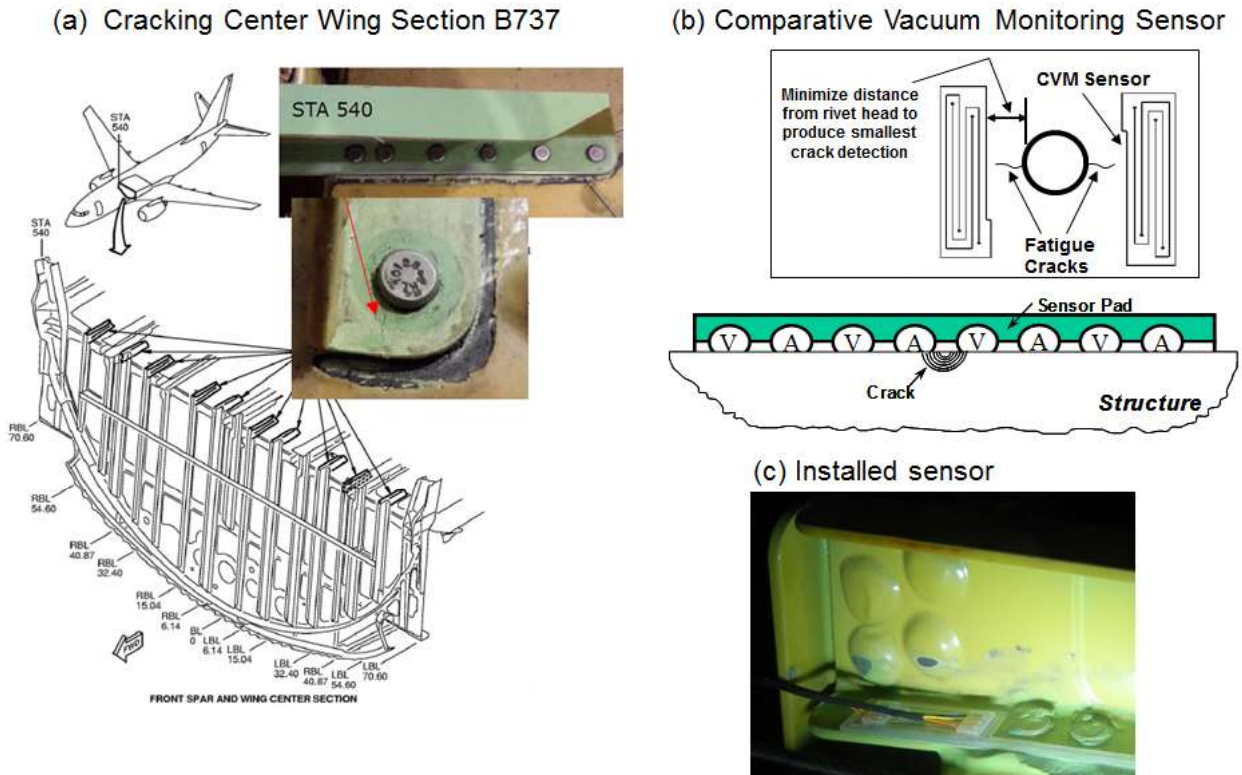


Figure 9.3-9. SHM Certification and Integration Activity

9.4. STRUCTURAL TEARDOWN ASSESSMENTS

9.4.1. B-52 Inboard Wing Teardown

Jennifer Wilson, The Boeing Company – B-52 Program Office

B-52 aircraft (Figure 9.4-1) are projected to be in service beyond the year 2040. At that time, the aircraft will have been flying for over 80 years. During their lifetime they have been exposed to severe operational environments. A disciplined approach to airframe structural integrity has been in place for several decades and is implemented primarily through Programmed Depot Maintenance (PDM). Structural teardown evaluations perform invasive inspections on salvaged B-52 structure to identify damage that cannot be detected during normal PDM inspections with the use of conventional Non-Destructive Inspection (NDI) methods. A thorough visual and metallurgical examination of retired aircraft structure is performed to determine the mid-life health of the B-52H fleet. A teardown of inboard wing structure from three aircraft was completed in 2014 (Figure 9.4-2). The upper wing surface is the life limiting area on the B-52, so there was particular interest in the condition of this structure. The teardown evaluation showed minimal fatigue damage, with an average crack size below 0.05". Stress Corrosion Cracking (SCC) and corrosion damage was also found throughout the inboard wing structure. This technical effort provides an overview of the teardown process and all findings from the evaluation (Figures 9.4-3 through 9.4-6). It also summarizes the measures that will be taken as a result of the findings in order to maintain the structural integrity of the B-52 fleet through the remainder of its service life.

- **76 active aircraft**
 - Boeing built and delivered 744 B-52 aircraft
- **First B-52 delivered February 1955**
 - Active fleet delivered between 1960-1961



Figure 9.4-1. B-52 Aircraft History

■ **Three aircraft selected for teardown**

- Aircraft #1
 - Partial inboard wing sections from two different aircraft
 - 1A: 57-6488: 14,831 FH
 - Corrosion rating = 2.63
 - Highest corrosion rating at AMARG
 - 1B: 58-0222: 16,563 FH
 - Corrosion rating = 0.68
- Aircraft #2
 - 57-6510: 18,199 FH
 - Corrosion rating = 1.85
 - Near high-time B-52G at AMARG
- Aircraft #3
 - 58-0226: 15,533 FH
 - Corrosion rating = 1.28

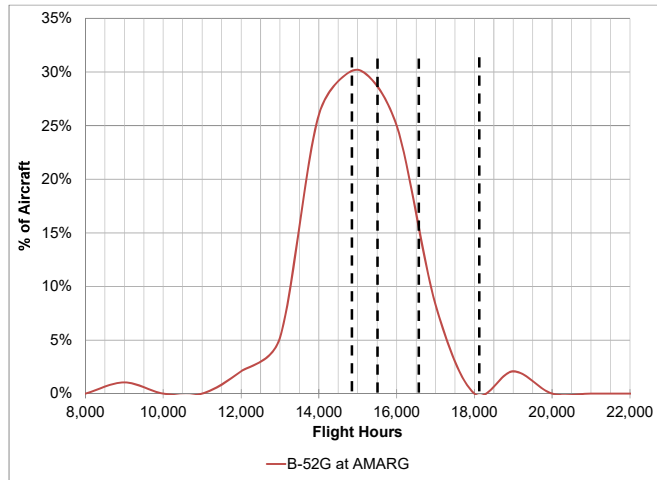


Figure 9.4-2. Teardown Aircraft

■ **Primary damage consists of fatigue, corrosion or stress corrosion cracking**

- This presentation will only cover primary damage
- Mechanical damage and damage due to disassembly was minor and is not addressed
- **Some type of primary damage was found in 124 (22%) of the 550 cubes**

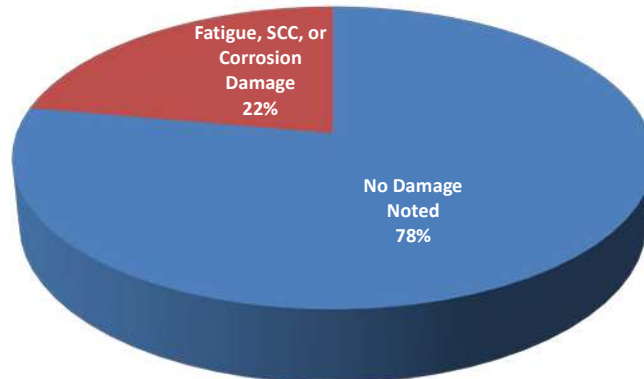


Figure 9.4-3. Summary of Findings

- Chart on right provides a breakdown of the primary damage by type
- Corrosion damage includes the following:
 - Exfoliation
 - Light surface pitting
 - Moderate material loss
- Corrosion damage consistent with that observed during normal maintenance
- Teardown analysis focused on fatigue and SCC damage

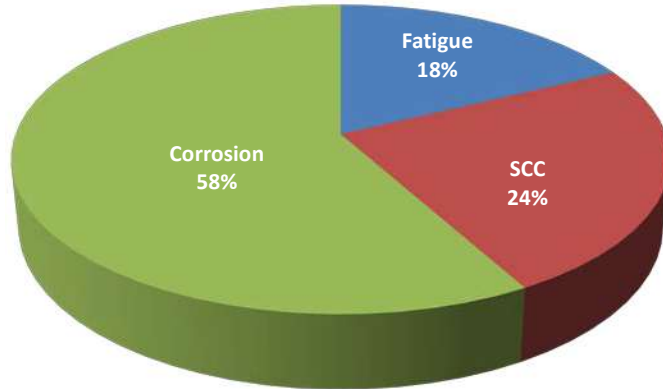


Figure 9.4-4. Breakdown of Primary Damage by Type

- **Twenty-four fatigue cracks found during the teardown**
 - Majority of fatigue damage found in stiffeners or spar chords in the lower half of the wing between WS 520 and WS 1025
 - Crack lengths ranged from less than 0.05” to 0.3”

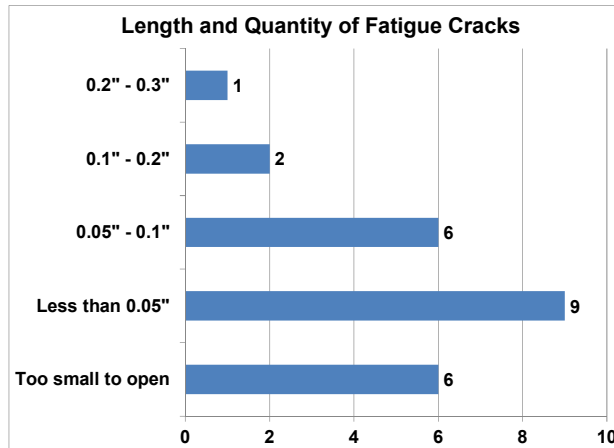


Figure 9.4-5. Summary of Fatigue Cracks

- **Twenty-six SCC cracks found during the teardown**
 - Majority of SCC damage found in chords and stiffeners in the upper half of the wing
 - Upper wing skin material (7075-T6) is more prone to SCC than the lower wing skin material (2024-T351)
 - Crack lengths ranged from 0.01” – 20”
 - Repairs already developed and in use for these types of cracks
 - Majority of SCC’s (57%) were accompanied by an area of general corrosion

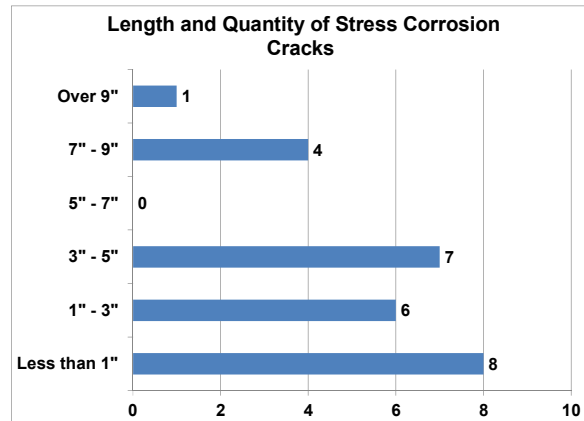


Figure 9.4-6. Summary of Stress Corrosion Cracking

9.4.2. T-38 Wing Teardowns – Making a Molehill Out of a Mountain

Paul Clark and Isaac Grothe, Southwest Research Institute; Jim Greer, USAF Academy-CASTLE; Mike Blinn, USAF T-38 ASIP

The T-38 (Figure 9.4-7) has been the primary fighter trainer for the Air Force since the early 1960s and was in production for over a decade with the last delivery taking place in 1973. Since that time it has had numerous modifications and configuration changes to address problems or improve some aspect of the airframe. Analysis and fatigue testing do not capture the time related component of aging; field data can capture cracks, corrosion and other means of degradation, but only for those areas accessible to the field or where previous modifications were employed. A full teardown shows reality. It captures fatigue cracking, wear, corrosion and all of their synergies that frequently result in some form of mixed mode failures. Teardown work is historically performed on one article, often after a full-scale test, providing relatively small sample sizes. However, the sample has tremendous value and is heavily relied on by engineering; but it still remains a small sample. The T-38 is in the process of tearing down nine wings (known as -29 wings) as part of the T-38 Aircraft Structural Integrity Program (ASIP) sustainment activities. Part of the hope is to provide a robust set of data from which to draw safe and confident conclusions. Like many fleets, the T-38 has been flown by different organizations over the years, each of which has their own requirements. Some of the effects to the airframe are more severe than others; however, only total flight hours have been consistently tracked for the airframe leaving questions about the true condition of the structure. The overarching goals of this destructive teardown of multiple condemned T-38 wings are three-fold: 1) Establish a robust set of teardown data for further management of the existing wings (i.e., the -29 wing) including developing data with sufficient samples to perform risk analyses with confidence. 2) Compare pre-teardown inspections discoveries with teardown inspections evaluations. 3) Provide a more holistic and proactive approach towards improved determination of structural life impact and criticality for existing and new fatigue critical locations (FCLs). A team of engineers from Center for Aircraft Structural Life Extension (CASTLE), Sabreliner, and Southwest

Research Institute (SwRI) collaborated with the T-38 ASIP on this effort. The teardown articles were first sent to Sabreliner Aviation Inc. for pre-teardown inspection. Sabreliner and SwRI technicians and engineers documented the condition of the wings. In addition, the team performed an initial nondestructive inspection (NDI) on the article for later evaluation against teardown indications. Upon completion of the pre-teardown inspection the articles were shipped for destructive teardown investigation. The procedures for aircraft structure teardown analysis, as established by CASTLE, were the foundation for all teardown activities as required by the contract. These efforts are still in process. This technical activity will report on the processes and provide information on the logic used to down select from hundreds of indications to a representative number of locations to be promoted for failure analysis (Figures 9.4-8 and 9.4-9, plus Table 9.4-1).



Figure 9.4-7. T-38 Aircraft

- Results for 4 wings (SP-5XX, SP-6XX, SP-7XX, SP-8XX)
- Focus: Lower Wing Skin
- Upper Wing Skin and Substructure
- Fasteners Removed

Disassembly Observations	TO 0034 Wing Serial Numbers				Totals
	SP-5XX	SP-6XX	SP-7XX	SP-8XX	
Fasteners Removed	2322	2324	2335	2321	9302
Fastener Removal Damage	164	52	18	47	281
Manufacturing or Maintenance Damage	131	105	9	125	370
Fastener Knockout/Punch Damage	28	0	3	2	33
Total Mechanical Damage	323	157	30	174	684

- Damage excluding manufacturing and maintenance
 - Pressure to not induce teardown damage
 - Approximately 3% damage from teardown process
 - If damage exists, not all value is lost ... *potentially*

Figure 9.4-8. Teardown Details

- Non Destructive Inspection
 - Fluorescent Penetrant Inspection (FPI)
 - Close Visual Inspection (CVI)
 - Eddy-Current Inspection
 - Surface (SSEC)
 - Bolt Hole (BHEC)

~200 Failure Analyses

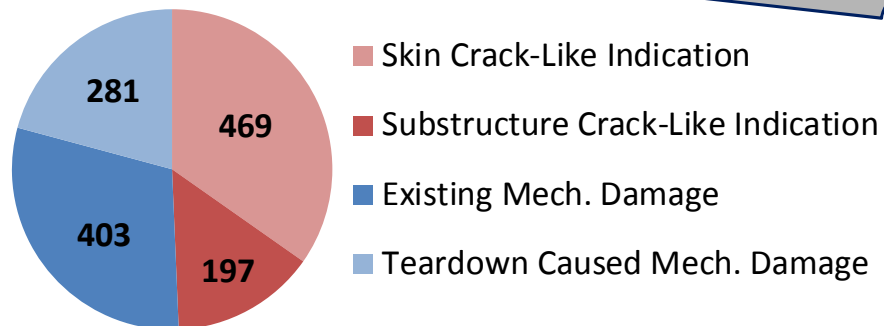


Figure 9.4-9. NDI Indications From 4 Wing Teardowns

Table 9.4-1. Failure Analysis Summary

Failure Analysis Finding	Teardown Article				Totals
	SP-5XX	SP-6XX	SP-7XX	SP-8XX	
Failure Analyses completed	50	50	56	45	201
Fatigue Cracks	66	58	101	50	275
Limited Evaluation Fatigue	1	41	32	3	77
General Corrosion	1	0	0	2	3
Stress Corrosion Cracking	0	0	1	0	1
Intergranular Corrosion	0	0	2	0	2
Pitting Corrosion	0	0	1	0	1
Mechanical Damage	3	2	7	2	14
Inconclusive	1	1	0	1	3

9.4.3. F-16 Block 50 Full-Scale Durability Test – Test Findings

Carlos Cordova, Lockheed Martin Aeronautics

The F-16 Program completed the teardown of its third Full-Scale Durability Test Aircraft (Figure 9.4-10). The durability test was conducted in support of an extension of the Certified Service Life of the Block 40 and Block 50 configurations to 12,000+ hours (Figure 9.4-11). Teardown of the test aircraft is used to identify the extent and severity of cracking on the aircraft structure at the conclusion of the test. The teardown data will be used to identify aircraft structure needing modifications, update the durability and damage tolerance analysis models, validate or update current structural maintenance requirements, and develop maintenance requirements for newly identified control points in the structure. This technical activity will focus on the test and teardown findings (Figure 9.4-12 through 9.4-14) and how these compare to the pre-test predicted damage.



Figure 9.4-10. F-16 Full-Scale Durability Test Aircraft



Figure 9.4-11. Installed SLEP Modification

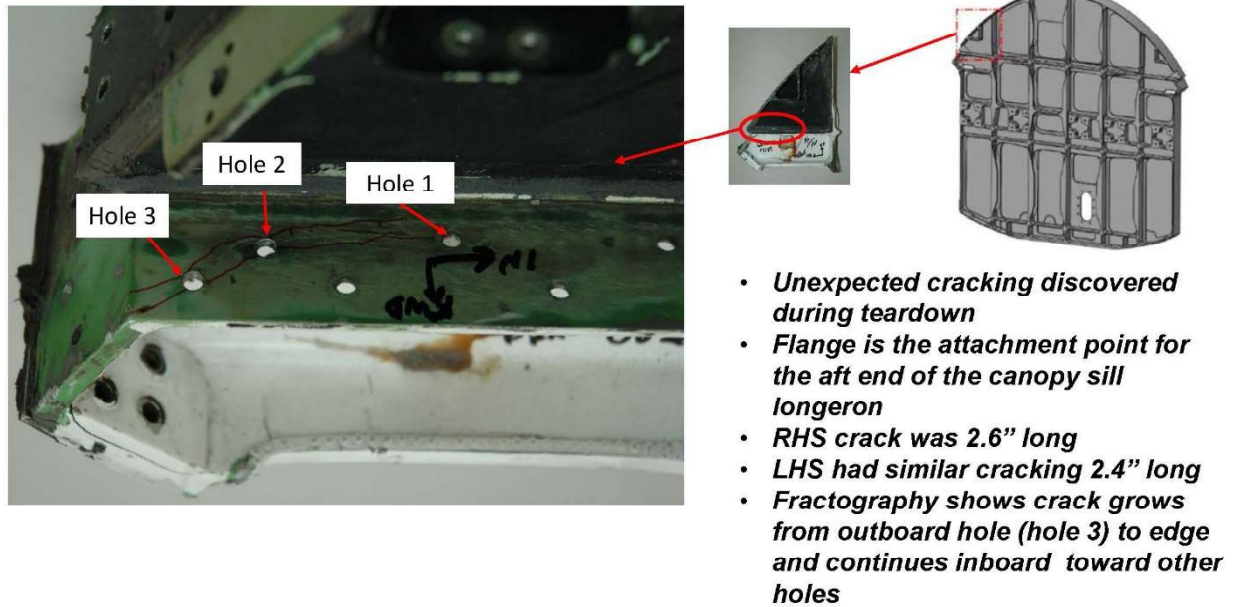


Figure 9.4-12. Bulkhead Cracking at FS 189

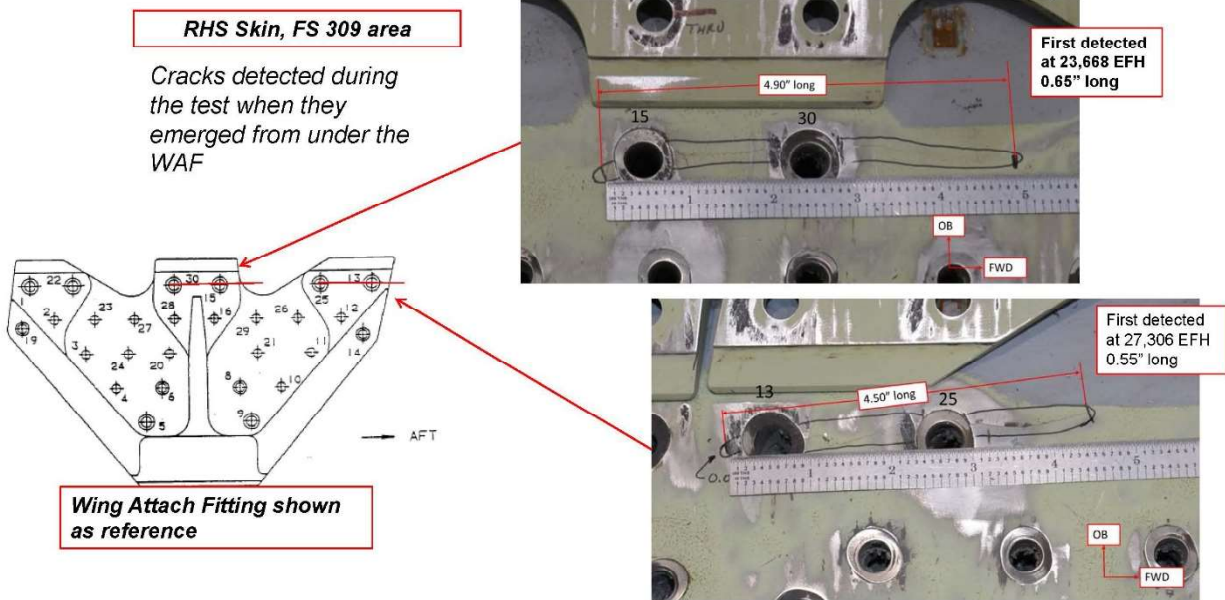


Figure 9.4-13. Lower Wing Skin Cracking



Figure 9.4-14. Horizontal Tail Outboard Support Beam Cracking

9.4.4. Structural Teardown Analysis

Gregory Shoales and James M. Greer, Jr., USAFA – CASTLE

CASTLE continues to assist fleet management decisions and the U.S. Air Force Aircraft Structural Integrity Program (ASIP) through multiple programs whose focus is assessing the condition of aging structures. Teardown analysis programs are required by MIL-STD-1530C at various points in the life

cycle of all USAF aircraft. CASTLE has been part of teardown analysis programs since 2002 and wrote the USAF best practices guide for teardown in 2008 [1] as well as detailed protocols for performing each phase of such a program. This publication and the results of various teardown analyses have been previously reported in ICAF and other forums.

Since ICAF 2015 CASTLE updated and republished the eight (8) CASTLE protocols to document lessons learned and to capture new process elements based on our experiences over the five years that have passed since their original publication. As before, the updated eight protocols include; five protocols to document the typical processes executed during any structural teardown (referred to by CASTLE as execution protocols), two protocols to capture critical administrative processes (referred to by CASTLE as administrative protocols), and one protocol to document specialized analysis of typical fuselage structural joints. The overall subject of each protocol remains as documented in the 2015 ICAF review and as presented to ICAF in 2009. The CASTLE Teardown Analysis Program protocols are recommended by the USAF for all such programs and are referenced in an ASIP structures bulletin [2].

The progression of the execution protocols from Protocol 3 through Protocol 4 is depicted in Figure 9.4-15, which has been repeated from the previous publication [3]. The continued progression of the same part from Protocol 4 through the analysis phase processes captured in Protocols 7 and 8 is depicted in Figure 9.4-16, which has been adapted from the previous publication [3]. Since ICAF 2015 CASTLE has continued to conduct teardown analysis of multiple aircraft of different aircraft types. This includes completion of the largest program in history—that of a four aircraft nose-to-tail, wingtip-to-wingtip, tanker/transport program.

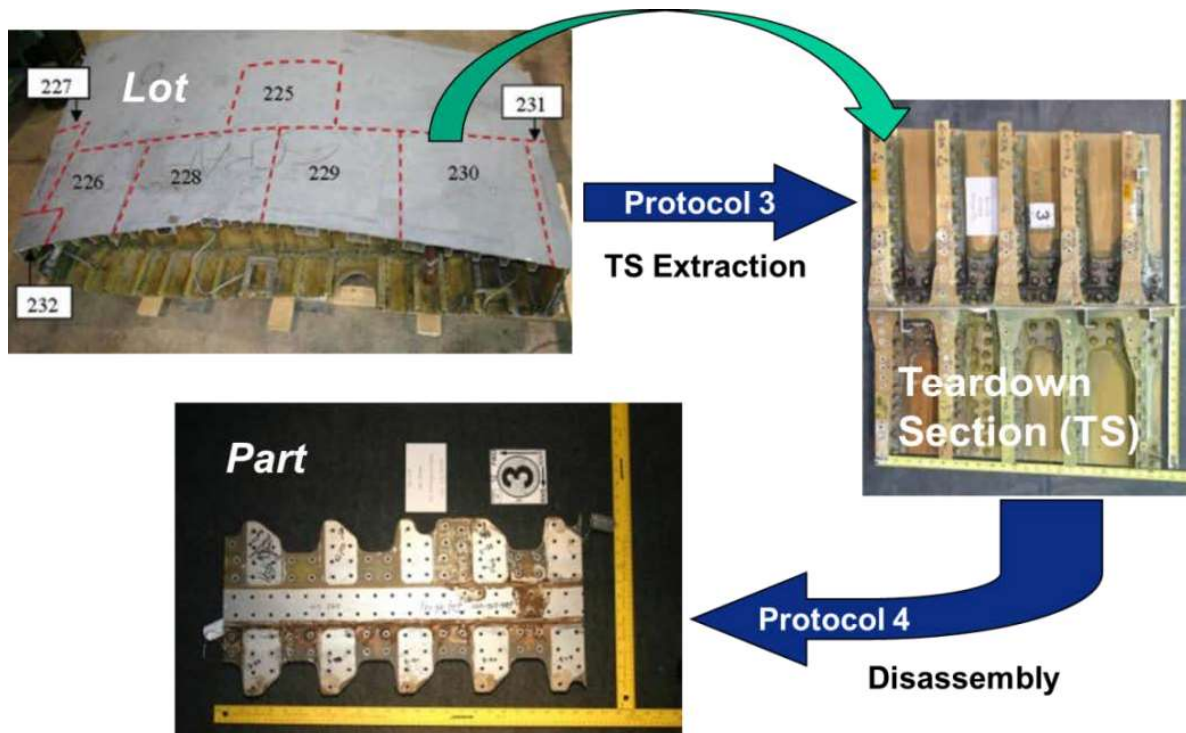


Figure 9.4-15. The Progression of Execution Protocols to Include Extraction of Structure of Interest, Called a “Teardown Section,” From Larger Aircraft Structural Element via Protocol 3 and Subsequent Disassembly of the Teardown Section into Individual Parts via Protocol 4

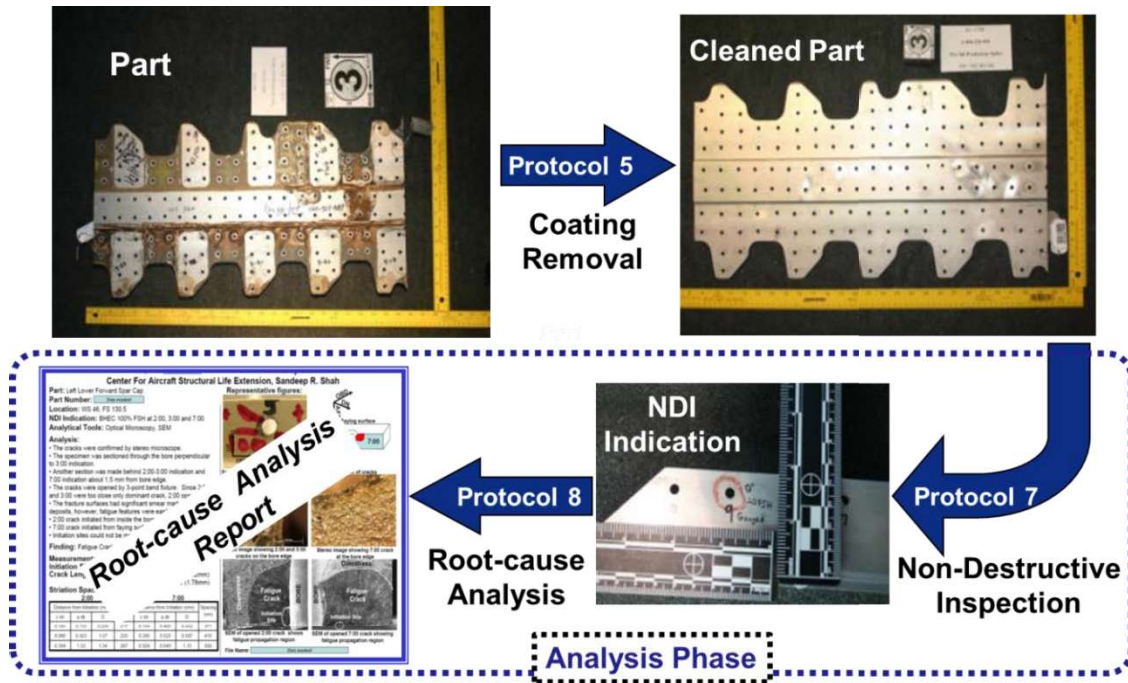


Figure 9.4-16. Continued Progression of Part Through Coating Removal via Protocol 5 and the Analysis Phase Which Includes Nondestructive Inspection via Protocol 7 and Root-Cause Analysis via Protocol 8

To date CASTLE has conducted or participated in analyses for more than fifty (50) different aircraft of a dozen different types from small trainer class aircraft to large transport/bomber class aircraft. In that time more than 100,000 indications have been documented during the Protocol 7 nondestructive inspection portion of the analysis phase with several thousand of those warranting extended root-cause analysis via Protocol 8.

References

- [1] Shoales, G.A., Brausch, J.C., Shah, S.R., Arunachalam, S.R., and Fawaz, S.A., "Procedures for Aircraft Structural Teardown Analysis," USAF Academy TR-2008-02, USAF Academy, CO, May 2008.
- [2] EZ-SB-15-001, "Aircraft Structure Teardown Inspection and Evaluation Program Protocols," USAF ASIP Structures, Wright-Patterson AFB, OH, 30 January 2015.
- [3] Shoales, G.A., G. Gann, and J. Wilterdink, "C/KC-135 Teardown Analysis Program: Program Update and Aircraft 1 Report," 2012 Aircraft Airworthiness and Sustainment Conference, Baltimore, MD, 2-5 April, 2012.

9.4.5. T-38 Wing Teardowns

Michael Blinn, USAF T-38 ASIP; Isaac Grothe and David Wieland, Southwest Research Institute

The T-38 ASIP office has been performing destructive teardown analysis of retired T-38 -29 model wings. The teardown articles were retired for cause (i.e., fatigue damage that had grown past repair limits). The primary focus of the teardown analyses were to evaluate the lower wing skin (LWS); however, on select wings the substructure and the upper wing skins (UWS) were also inspected.

This effort has been completed by the Sabreliner Aviation, LLC, team under contract with the CASTLE at the USAFA. The Sabreliner team consists of Sabreliner Aviation as the prime contractor and the Southwest Research Institute (SwRI) as the subcontractor. The foundation for all teardown activities

as required by the contract was established by the *CASTLE Procedures for Aircraft Structural Teardown Analysis* (PASTA) handbook [1] and the *CASTLE Teardown Analysis Program Protocols*, all of which are formally recommended by the USAF for use in all teardown analyses by the USAF Structures Bulletin EZ-SB-15-001 [2].

The detailed and disciplined teardown protocol procedures as well as the robust analyses performed within the efforts of this program provide valuable data that are highly relevant for assuring structural integrity of the T-38 -29 wing. The information has and will assist the USAF in the management of the dated -29 wings and their eventual retirement and replacement with -33 wings. In addition, the teardowns help the assessment and management of the T-38's Structural Critical Safety Item (SCSI) list, and contribute additional data towards evaluating new and existing fatigue critical locations (FCLs).

The data collected from these teardown activities also provide for improved equivalent initial flaw size (EIFS) distributions, understanding wing cracking trends, and better defining FCL locations (see Figure 9.4-17 for a sample of NDI results on a wing). Of great importance, the teardown outcomes assist with higher fidelity risk assessments. All of these activities help to characterize and capture the status of the structure, in order to effectively and efficiently manage the service life of the fleet of T-38 fleet. Finally, these data are invaluable for correlating damage tolerance analysis with actual field cracking experience (see Figure 9.4-18, a sample durability correlation of an FCL to field findings).

References

- [1] Shoales, G.A., Brausch, J.C., Shah, S.R., Arunachalam, S.R., and Fawaz, S.A., "Procedures for Aircraft Structural Teardown Analysis," USAF Academy TR-2008-02, USAF Academy, CO, May 2008.
- [2] EZ-SB-15-001, "Aircraft Structure Teardown Inspection and Evaluation Program Protocols," USAF ASIP Structures, Wright-Patterson AFB, OH, 30 January 2015.

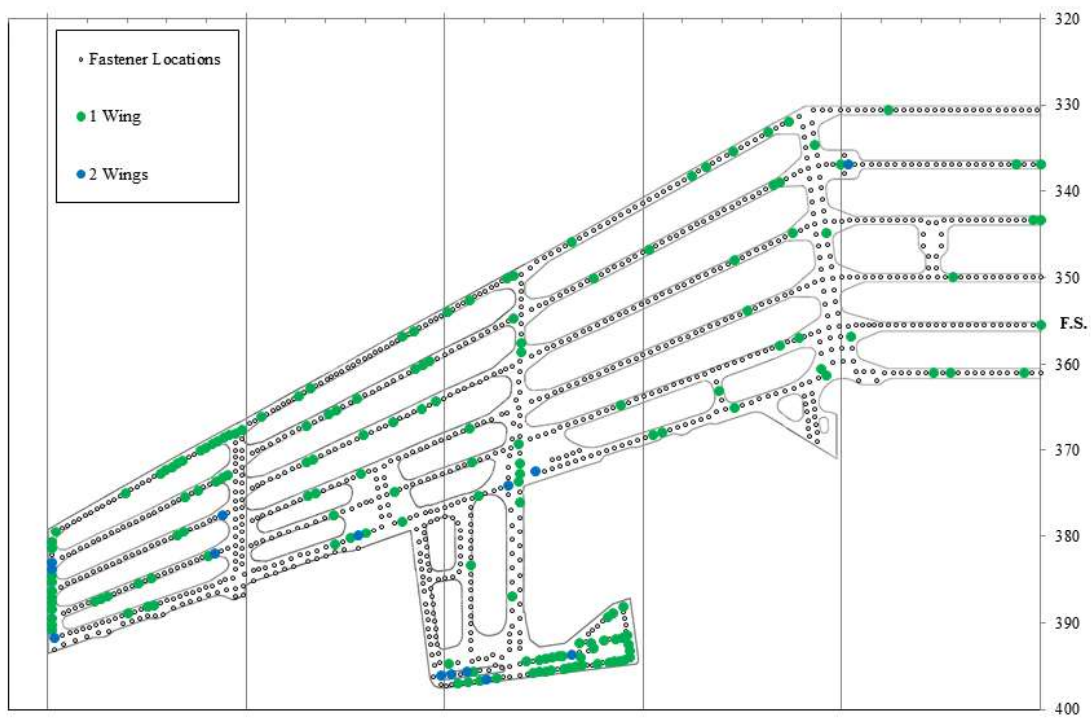


Figure 9.4-17. Summary of the Two Wings with Crack Indications at Each Hole on the Left Side of the Wing

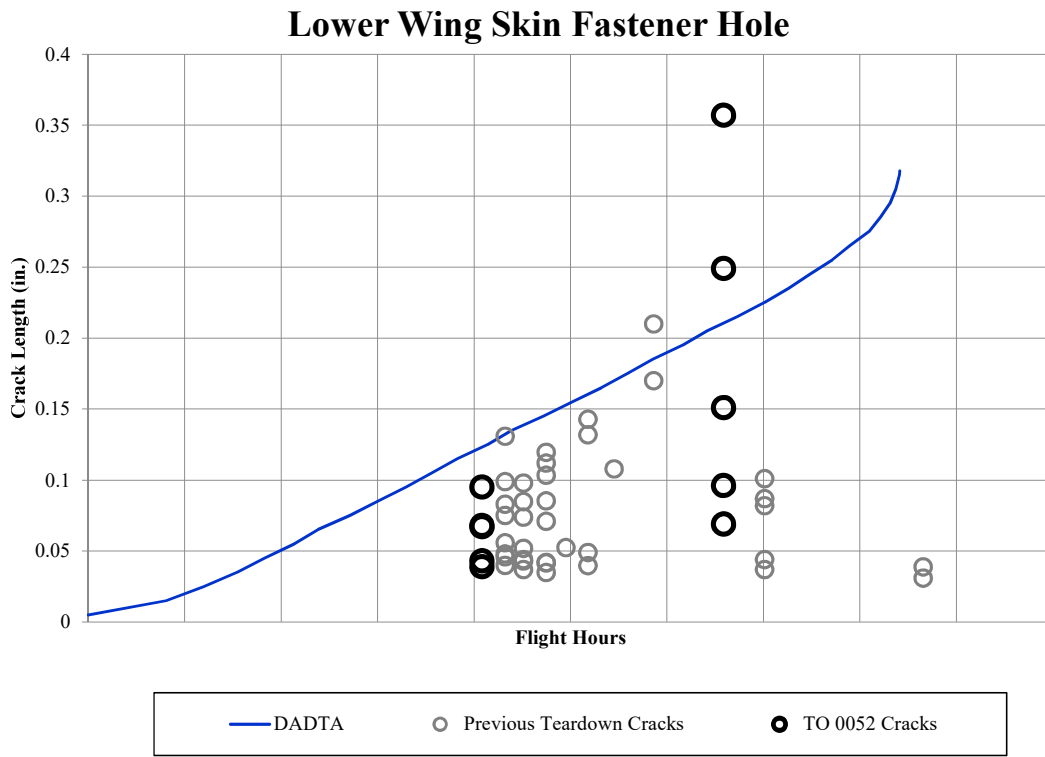


Figure 9.4-18. Durability Analysis Compared to Teardown Findings (TO 0052 Cracks are Recent)

9.5. LOADS AND ENVIRONMENT CHARACTERIZATION

9.5.1. Determination of Vibratory Loads for the HH-60G Pave Hawk Helicopter

Robert McGinty, Gregory Wood, and Jeffrey Brenna, Mercer Engineering Research Center (MERC); Kevin Reid, USAF HH-60G ASIP

The United States Air Force (USAF) tasked Mercer Engineering Research Center (MERC) to implement several Aircraft Structural Integrity Program (ASIP) initiatives to quantify and extend the service life of the HH-60G Pave Hawk helicopter fleet. This effort is complicated by the extensive, mission-specific modifications that have been performed on the weapons system over its 25+ years of service. For example, current mission usage deviates significantly from the original Black Hawk design specifications, and modifications to the aircraft structure and mission usage are expected to result in changes to the platform's operational flight loads. MERC was able to leverage several ASIP initiatives to develop a new set of comprehensive loads specific to the current HH-60G airframe (Figure 9.5-1). The initial testing and analysis methods used to do so were presented at the 2014 ASIP Conference; however, that addressed only the quasi-steady portions of the aircraft flight loads. This effort extends the work to include the vibratory components of flight loads that ride on top of the quasi-steady, or DC portions presented earlier. Together, the DC and vibratory parts provide a complete picture of the structural vibrations of the aircraft and can be used to produce stress spectra needed for fatigue and damage tolerance analyses. While the quasi-steady analyses used basic linear static finite element (FE) analysis methods, the vibratory analyses discussed here require modal analyses and Fourier transforms, followed by multivariable statistical regressions applied to complex valued quantities because of the necessity of accounting for phase lags (Figure 9.5-2). Furthermore, the analyses are performed on a second-by-second basis in order to capture transients in the load levels during flight. In all, the analyses are systematic, but involved and draw on a broad range of disciplines to complete. The analysis procedures permit the determination of magnitude and phase (at each vibration frequency) of the driving forces throughout the aircraft on a second-by-second basis. The derived force data is then recombined with FE modal analyses to predict load and stress oscillations for any point in the structure (Figure 9.5-3). Combined with the DC levels presented last year, it becomes possible to derive load spectra for any portion of the aircraft, thus supporting damage tolerance analyses. The new computed forces will make it possible to better support service life extension efforts for the helicopters in their new configurations and flight usage regimes as opposed to the original design specs from the 1970s. The new load sets also permit the HH-60G program office to more accurately assess structural damage and repairs and perform risk analyses on the fleet.

- Use data from instrumented flight tests to compute flight loads for HH-60G aircraft to support structural analyses

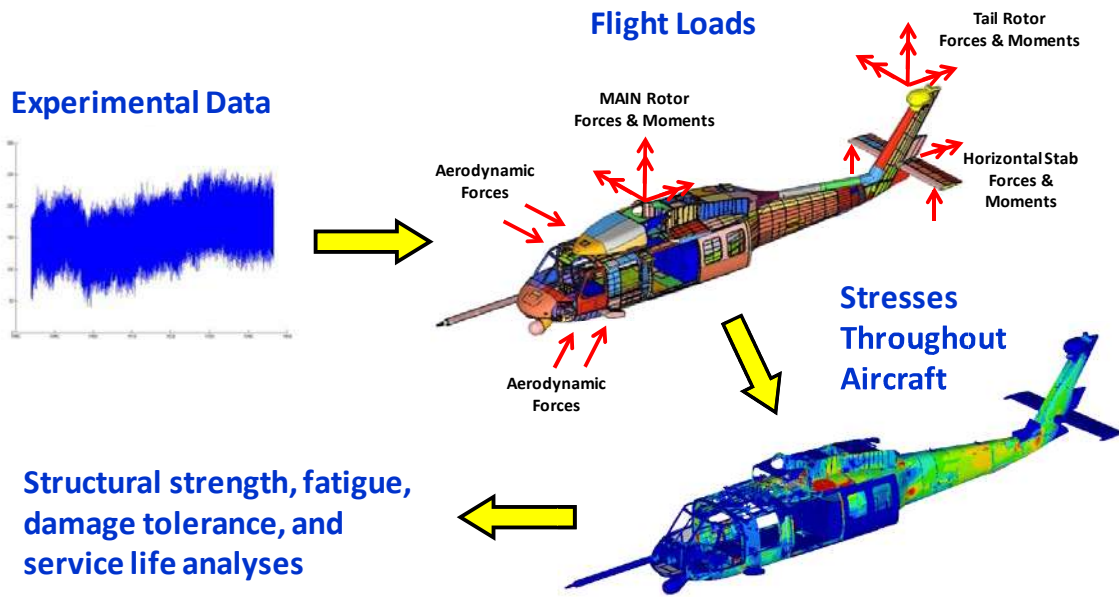


Figure 9.5-1. Loads Calculation Overview

Validated according to USAF guideline EN-SB-11-001

Validation performed in two phases:

Phase 1 – Static sling load from rotor head

Phase 2 – Design flight loads

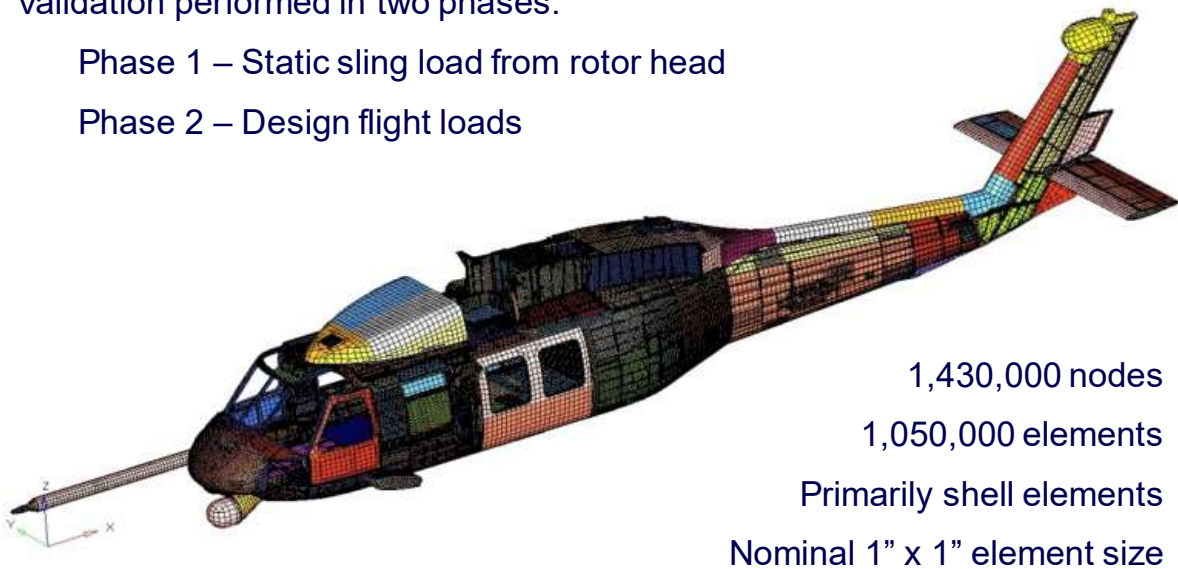


Figure 9.5-2. Finite Element Model

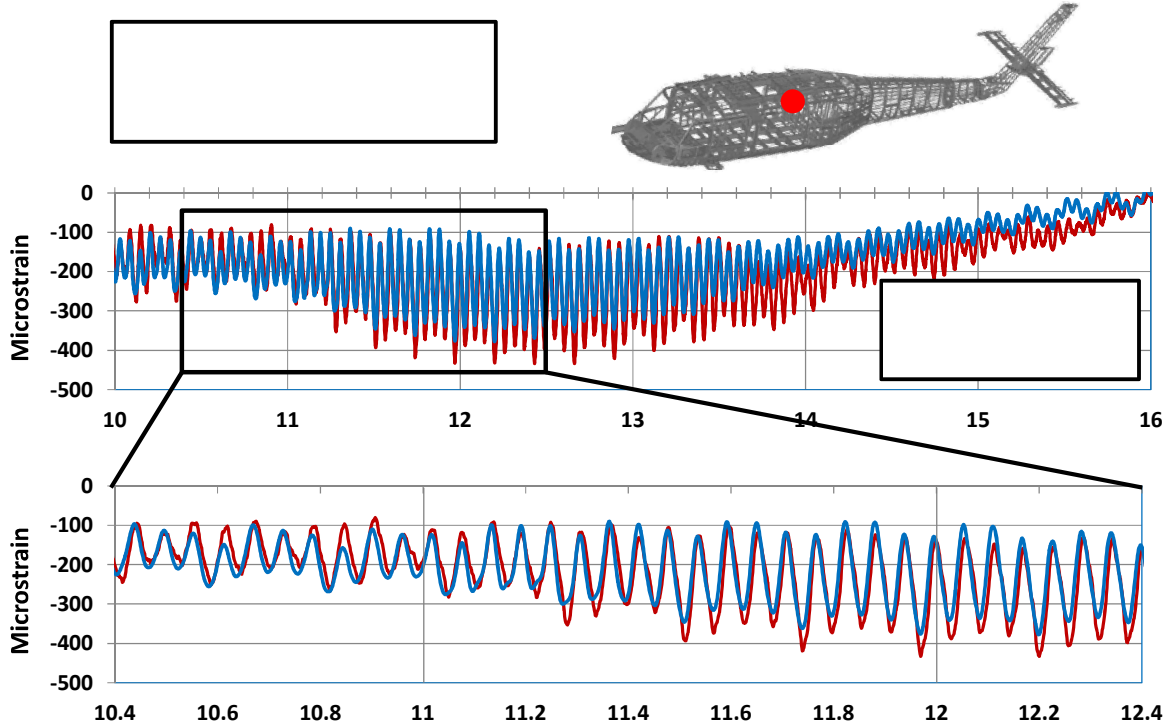


Figure 9.5-3. Comparison to Measured Strains

9.5.2. Flight Maneuver Recognition for the UH-1N Helicopter

Nathan Branch, Joshua Finn, James Bozarth, and Nick Hatcher, Mercer Engineering Research Center (MERC); Allen Craven and Scott Stringer, USAF UH-1N ASIP

The United States Air Force (USAF) is working to update the usage spectrum of the UH-1N helicopter (Figure 9.5-4). The current usage spectrum was generated by a pilot survey in 2004. The UH-1N SPO determined that the best method for updating the spectrum was to use flight data recorded by the Loads/Environment Spectra Survey (L/ESS) system. MERC was tasked with developing an algorithm to recognize maneuvers in this flight data and output a usage spectrum. This technical effort discusses the challenges with regime definition, recognition, and data processing in the development of a robust L/ESS processing script that can be used to continually update the UH-1N usage spectrum for the remainder of its life. To aid the process of translating the flight parameters into recognizable regimes, MERC coordinated with the USAF to perform a flight test on a UH-1N outfitted with the L/ESS system (Figure 9.5-5). Flight test cards were composed of regime descriptions, pilot instructions, and ordered in a way to facilitate execution and post processing. MERC engineers were aboard each of the four flight tests to coordinate and document the effort. The reduction in man-hours required to develop the regime recognition algorithm and improve accuracy of regime detection was a direct benefit of the documented and observed flight test. Several challenges presented themselves during the regime recognition development, including: - Lack of a "weight on wheels" switch to discern flight and ground regimes - Lack of some necessary parameters, including rotor tach - Reliability / data quality of analog signals on the circa 1970 aircraft. These challenges were addressed and a robust algorithm was developed as MERC coordinated with SPO and OEM engineers. The new maneuver recognition algorithm can be used to

quickly determine the usage spectrum of the UH-1N fleet at any time during the rest of its service (Table 9.5-1). It can also be used to develop a usage spectrum for a specific command, base, or tail number for instrumented aircraft. Finally, the algorithm can be leveraged for future individual aircraft tracking (IAT) or rotorcraft dynamic component tracking (RDCT) / health and usage monitoring (HUMS) efforts to help ensure aircraft safety.



Figure 9.5-4. UH-1N Twin Huey

- Four test flights were performed at Andrews AFB in November 2014
- Several scripted flight maneuvers were performed and compared to algorithm-predicted maneuvers
- Helped clarify how regimes should be defined
- Allowed fine-tuning and validation of the algorithm



Figure 9.5-5. Flight Tests

Table 9.5-1. UH-1N L/ESS Usage Spectrum

L/ESS Usage Spectrum Represents:

- 2376 hrs event time (power on to off)
- 10 hours overlapping regimes (0.4%)
- 1810 hrs flight time (1st TO - last landing)
- 6360 GAGs
- 1125 flights
- 11 UH-1N Aircraft

Regime	Time (hours)	Time (%)
Normal Start	93.5	3.94%
Shutdown (w/Coll)	21.3	0.90%
Flight Idle	156.8	6.60%
FPG (Nr ~100%)	294.6	12.39%
Takeoff	15.4	0.65%
Hover	173.8	7.31%
Hover Control Reversal	26.8	1.13%
Landing/Approach	52.1	2.19%
Level Flight	863.7	36.34%
Climb	138.4	5.83%
Pull-ups	0.9	0.04%
Level Flight Left Turn	130.7	5.50%
Level Flight Right Turn	196.0	8.25%
Flight Control Reversal	7.8	0.33%
Descent	112.6	4.74%
Twin to Single	0.1	0.00%
Single to Twin Descent, 1 sec	0.0	0.00%
Fire Sup. Push-Over, Dive, Pull-Up	2.6	0.11%
Fire Sup. Left Turn	9.4	0.39%
Fire Sup. Right Turn	73.9	3.11%
Autorotation	13.2	0.55%
Other	3.5	0.15%
Total	2386.9	100.4%

9.5.3. Comparison of Flight Loads of Single-Engine Air Tankers with Agricultural Operations

Kamran Rokhsaz and Linda Kliment, Wichita State University

Wichita State University investigated flight loads from a fleet of Single-Engine Air Tankers (SEATs) for comparison with their agricultural use. Federal Aviation Administration funded this investigation as an element of its Operational Loads Monitoring program.

Under this program, digital flight data recorders were installed on four aircraft consisting of two Air Tractor AT-802As and two PZL-M18s. One of the latter airframes was used exclusively for agricultural spraying. These aircraft were also equipped with a single strain gauge mounted on the upper side of the lower main spar cap. Data were also acquired from a fifth aircraft, an Ayers Thrush S2R-T45, by the United States Forest Service and made available to Wichita State University. All five aircraft were powered by turboprops and their takeoff gross weights ranged from 10,000 to 16,000 pounds. A total of 454.5 hours of SEAT operation were compared with 104 hours of agricultural spraying.

Flights were divided into various phases (Figure 9.5-6) and results developed for all, in addition to the results from the entire mission (Figure 9.5-7). Basic flight parameters, such as airspeed, altitude, duration, and bank and pitch angles were extracted and shown in statistical formats consistent with previous reports in this area. Load factors were separated for each phase into gust and maneuver loads using the two-second rule. Exceedance charts were constructed for each phase, as well as for the entire flights. Additionally, load factors were normalized based on estimated instantaneous aircraft weight and used to develop a second set of exceedance charts.

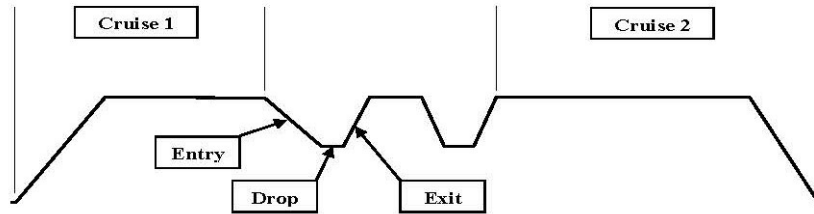


Figure 9.5-6. Various Flight Phases

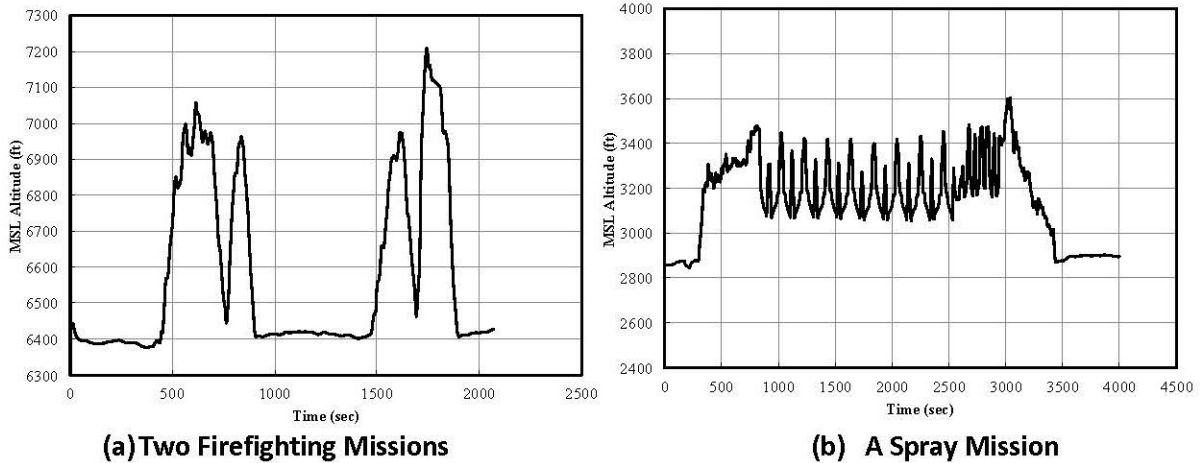


Figure 9.5-7. Typical Altitude Time History

The results were presented in formats that allowed easy comparison of the design criteria with actual usage, thereby creating a better understanding of those factors that influence the structural integrity of these aircraft. The major conclusions of this program were as outlined below.

1. SEAT aircraft are used for shorter missions than those flown for agricultural applications. Therefore, the former airframes are subjected to a larger number of takeoffs and landings per 100 hours. This necessitates shorter inspection intervals of the landing gear components for these aircraft.
2. Traditionally, severity of structural loads is inferred from measured normal load factors. However, in the case of agricultural and firefighting operations, where up to half of the weight can be in the form of retardant or chemicals, this practice may result in erroneous conclusions concerning airframe fatigue life. Generally, the largest vertical load factors are associated with the drop phase on SEAT aircraft, but the largest wing bending moments occur when the aircraft is flown near maximum takeoff weight (Figure 9.5-8).
3. SEAT aircraft experience relatively large load factors during the drop phase. These load factors, mostly driven by the release of nearly half of the aircraft weight, occur once per flight. On the other hand, aircraft used for agricultural applications are subjected to more moderate loads, but with a significantly higher frequency per flight (Figure 9.5-9).

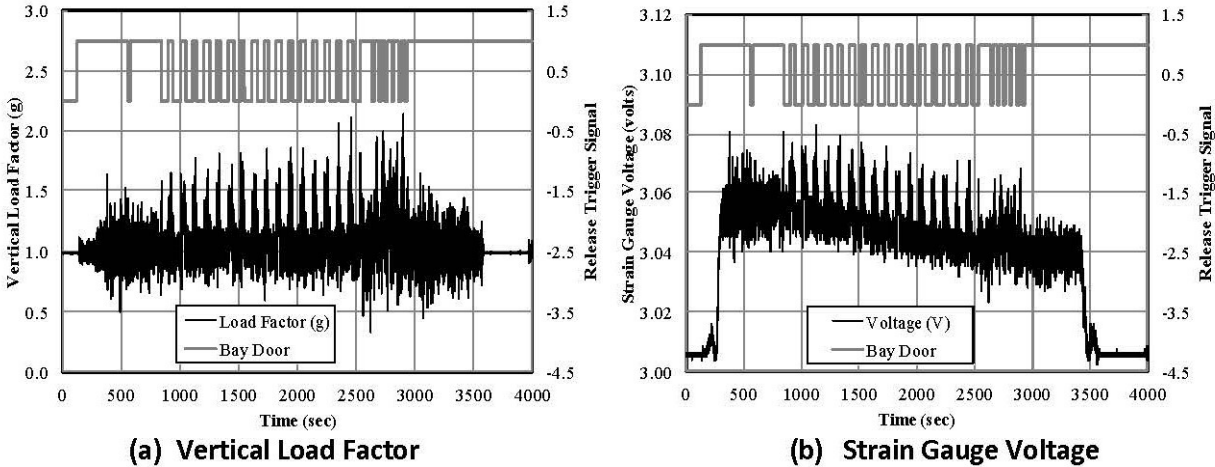


Figure 9.5-8. Time History of Load Factor During a Spray Operation

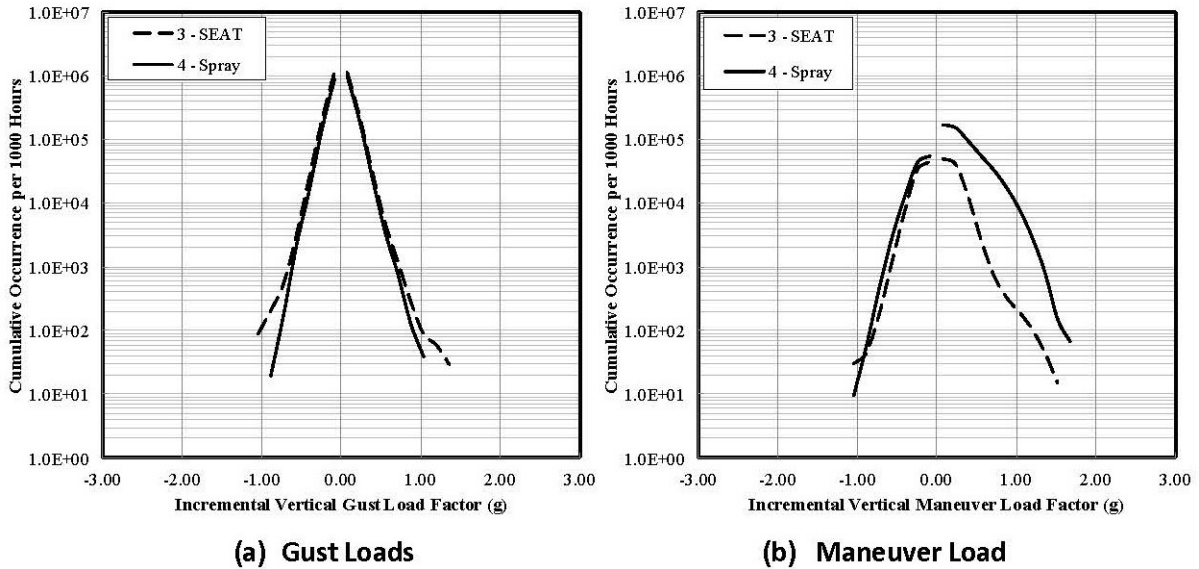


Figure 9.5-9. Cumulative Occurrence of Vertical Load Factor

9.5.4. Mission Utilization Impact on Individual Aircraft Tracking Data

Jeff Newcamp, USAF AFIT

Individual aircraft tracking (IAT) programs have operated for decades, resulting in a vast repository of aircraft utilization data. These data show trends in historical utilization that can be mined to aid decision makers who can move towards optimizing usage of end-of-life aircraft. This project, sponsored by the Air Force Institute of Technology’s Civilian Institution Program, sought to correlate IAT data to mission utilization as a way to infer the fatigue condition of aircraft structural components. The methodology was validated using 11 years of A-10 aircraft data from the Aircraft Data Acquisition and Distribution System. Specifically, the study proved that there exists a significant loading difference among mission types. Figure 9.5-10 shows Surface Attack (SA), Functional Check Flight (FCF) and

Navigation (NAV) counting accelerometer data from the A-10 dataset. These three mission types were chosen to illustrate the range of loading conditions. These data were translated into expected loading models for various mission types. A subset of these models is shown in Figure 9.5-11. More information on this aspect of the work can be found in Reference [1].

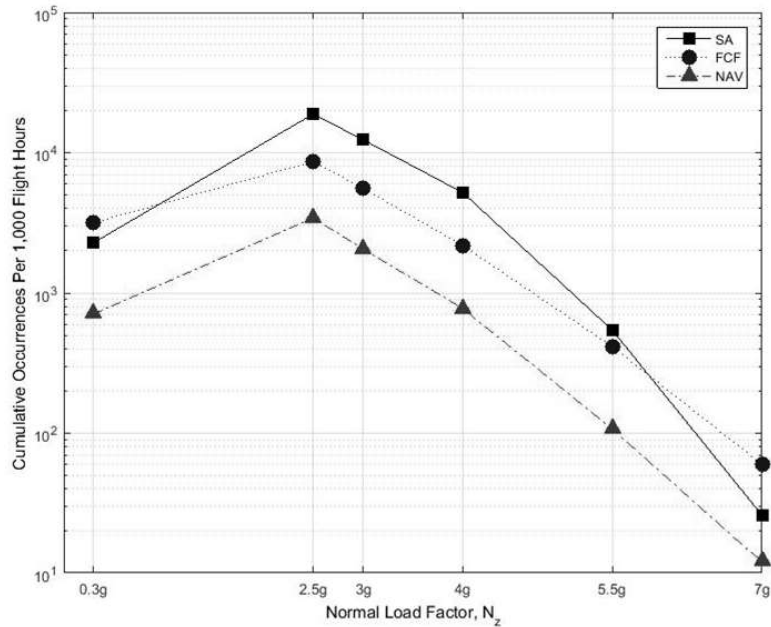


Figure 9.5-10. A-10 Counting Accelerometer Data for Three Mission Types

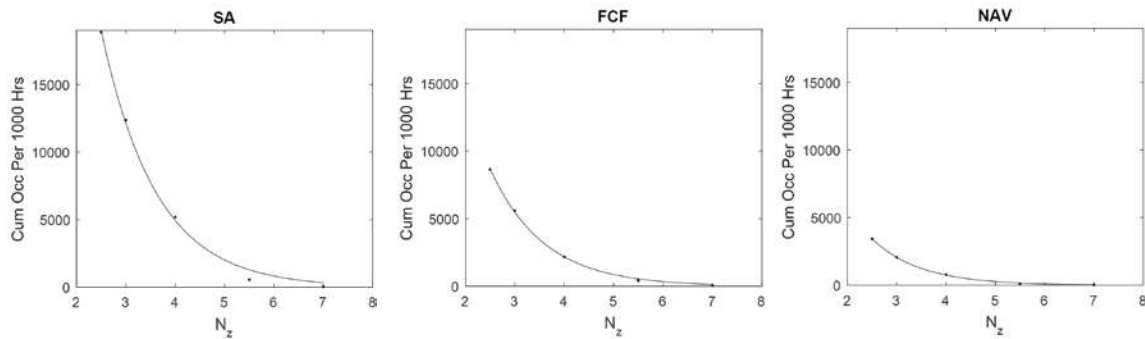


Figure 9.5-11. Model Development for Counting Accelerometer Data

IAT data also capture the effects of aircraft basing. Aircraft have been moved between bases for a variety of reasons but an emerging suggestion is for SmartBasing, the concept of capitalizing on base utilization differences to achieve an objective function. This project has shown that regular rotations can equalize equivalent flight hours within a fleet – or increase deviation – depending on a fleet manager’s preference. IAT historical data were used to show that yearly aircraft rotations could transform a fleet’s useful life prediction.

Reference:

[1] Newcamp, J., Verhagen, W., Curran, R., “Correlation of Mission Type to Cyclic Loading as a Basis for Agile Military Aircraft Asset Management,” *Journal of Aerospace Science and Technology*. (55) (2016) 111-119.

9.6. CHARACTERIZATION, MODELING & TESTING

9.6.1. Comparing Starting Crack Size Estimates (EPS and EIFS) Based on the Same Experimental Crack Growth Life Data

J.P. Gallagher, Independent Consultant; Lorrie Molent, DSTG

The technical activity discusses starting crack data (i.e., initial material discontinuity size) and reports on methods for establishing starting crack sizes for damage tolerance and durability analyses. These starting crack data are generated using corner crack growth life data from a total of 68 low stress concentration (k_t) test coupons made from 7050-T7451 aluminum alloy (Figure 9.6-1). The test coupons were subjected to five fighter aircraft wing variable amplitude (VA) stress histories (the applied test stress histories were scaled by either two or four stress scaling factors). The starting condition was associated with internal and near surface material inclusions that rapidly turned into cracks and subsequently propagated. Crack growth was measured using quantitative fractography subsequent to the test. Two methods for generating the estimates for starting crack data are presented: (1) one estimate utilized the Australian crack growth life fitting method (Figure 9.6-2) and (2) the other estimate relied on a fracture mechanics (FM) analysis method (Figure 9.6-3). The Australian life fitting method is based on the use of the exponential equation: $a = a_0 \exp(Bt)$, where a is the crack size, a_0 is the initial crack size and t is the time in flight hours; this equation has been demonstrated to accurately describe small crack behavior for a number of variable amplitude fatigue cracking situations. The equivalent pre-crack size (EPS) values ($= \alpha_0$) are based on a back extrapolation of the $\ln(a)$ vs. flight hour fit to 0.0 flight hours. The FM method is based on developing experimental da/dt data from the VA crack growth histories and describing these data using a simple power law relationship where $da/dt = C K_{ref}^m$. The power law constants C and m were developed for each set of crack growth data available for each fighter aircraft wing stress history. The fitted power law exponent (m) values for the individual spectrum da/dt behaviors are found to be slightly greater than 2.0. The equivalent initial flaw size (EIFS) results are based on the integration of the fits of derived da/dt data. The technical activity summarizes and compares the EPS values with EIFS values (Figures 9.6-4, 9.6-5, and Table 9.6-1). The EIFS and EPS values compare extremely well; EIFS values are also compared to historical results.

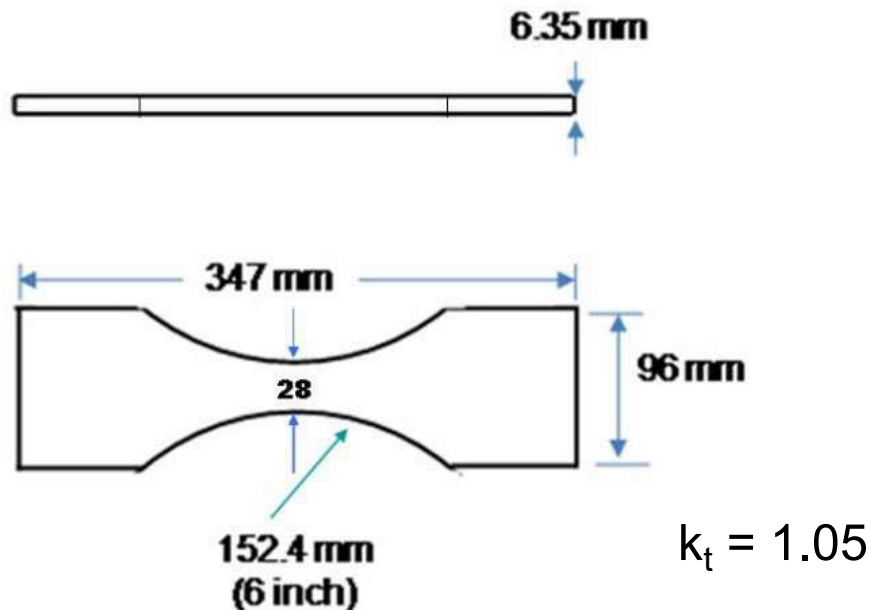
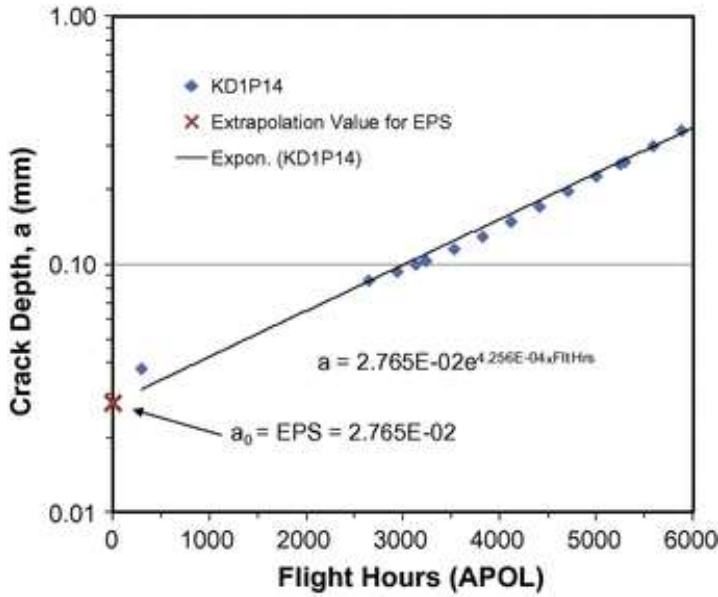


Figure 9.6-1. Test Specimen Geometry



$$a = a_0 \exp(B t)$$

$$a_0 = 0.0276 \text{ mm}$$

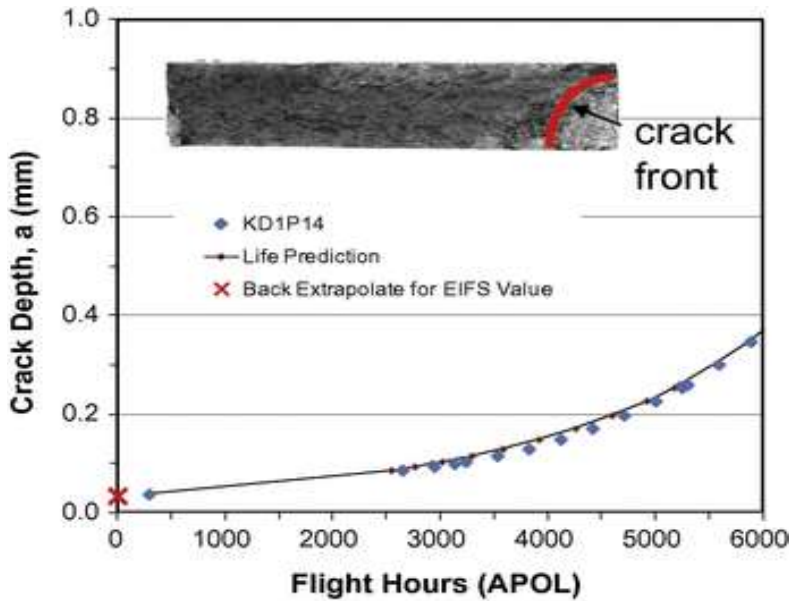
$$a_0 = 0.0011 \text{ inch}$$

a_0 referred to as the Equivalent Pre-Crack Size (EPS)

1 inch = 25.4 mm

Spectrum = APOL, Stress Scaling = 396.5 MPa (57.5 ksi)

Figure 9.6-2. Australian DSTG Approach to Determining a_0



$$t = \int_{a_0}^a \frac{da}{CK_{\max}^m}$$

K based on Newman Raju published results

Figure 9.6-3. Estimate of a_0 by Fracture Mechanics Method

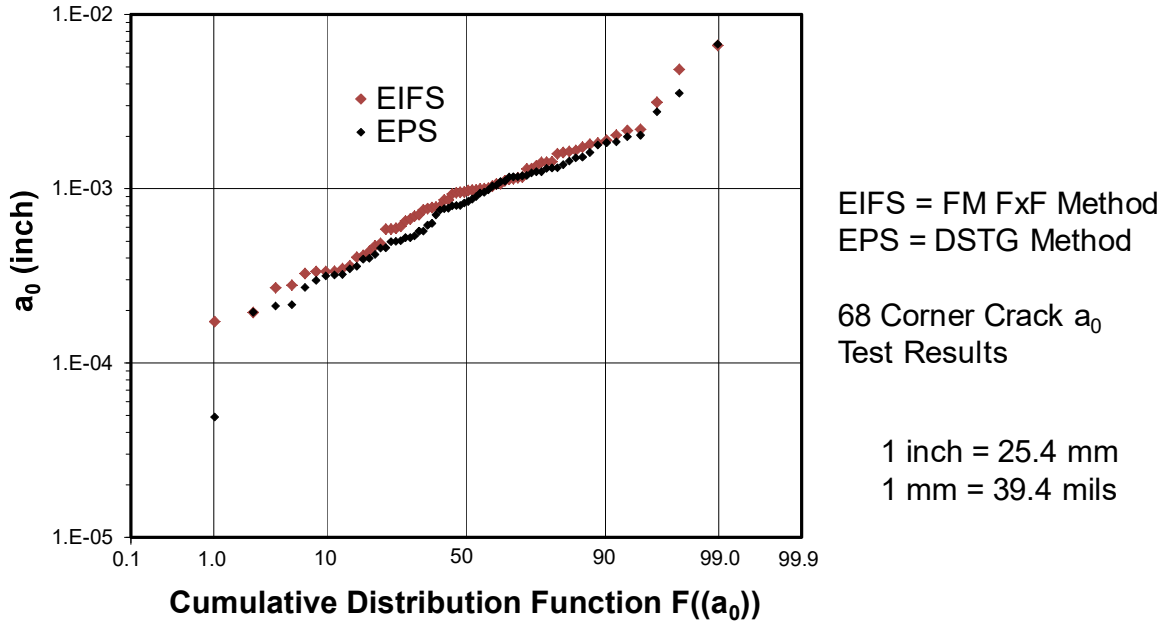


Figure 9.6-4. Comparison of Experimental FM FxF and DSTG Methods for Establishing a_0

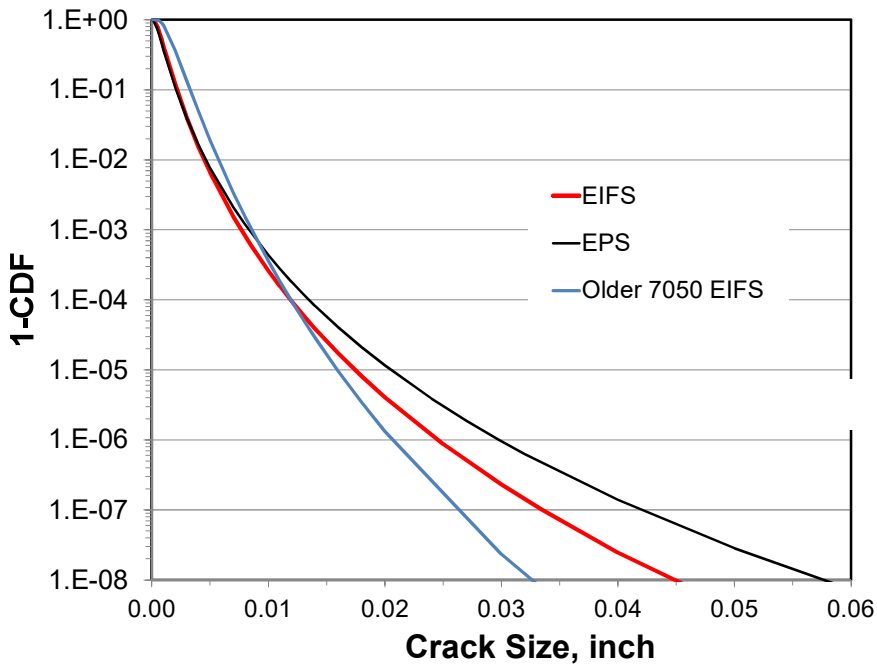


Figure 9.6-5. Comparison of Exceedance Probability

Table 9.6-1. Summary of Lognormal Distribution Results

Data Set	No. of a_0 Tests	Lognormal Parameters (inch)		a_0 value at CDF = 0.5 (inch)	a_0 value at 1-CDF = 10^{-7} (inch)	% of 0.050-inch DT Safety Value
		μ	σ			
EIFS	68	-7.028	0.698	0.00089	0.033	67.0
EPS	68	-7.154	0.766	0.00078	0.042	83.9
Older EIFS	35	-6.3907	0.5279	0.00168	0.0261	52.2

9.6.2. Effective Corrosion Prevention Control Plans

Terry Gabbert, USAF Research Laboratory - Materials and Manufacturing Directorate; Charles Babish IV, USAF Life Cycle Management Center

In December 2002, Congress, concerned with the high cost of corrosion (Figure 9.6-6), enacted legislation 10. U.S.C. 2228 which placed added emphasis in the Department of Defense management and technical focus on corrosion prevention and control measures. In response to a GAO recommendation, a standardized methodology for collecting and analyzing corrosion cost, readiness, and safety data was developed. This analysis included measures for both the cost of corrosion and availability related effects of corrosion on DoD's military equipment and infrastructure. LMI's Estimated Effect of Corrosion on the Cost and Availability of Air Force Aircraft and Missiles: 2013-14 update stated that the Department of Defense spends an estimated \$23.5 billion which represents 20.3 percent of total maintenance expenditures. The annual corrosion cost for Air Force aviation and missiles was estimated to be \$6.0 billion, or 24.9 percent of the total maintenance costs. Additionally, it was estimated that corrosion contributed to 2.3 million non-available hours or 14.0 percent of total non-availability for all Air Force aviation assets. Program managers and procuring agencies should consider corrosion prevention and control (CPC) as a key issue in designing, procuring and maintaining any DoD system or facility. CPC planning features two aspects: (1) management of the planning, and (2) technical and design considerations (requirements, tradeoffs, etc.) that lead to viable CPC planning. The Corrosion Prevention and Control Plan (CPCP) should be prepared as early in a program/project as possible, but in the case of weapons systems, no later than Milestone B - Program Initiation, at which time the Program Manager should generate the document. This technical activity will cover what a comprehensive and effective CPCP should contain (Figure 9.6-7); this will include references and venues for the program offices to use for tactical and strategic corrosion management planning. Additionally, emphasis will be put on program transition into the sustainment phase to address issues such as time in severe environments, wash cycles based on TO guidance, process to evaluate wash cycle waiver requests, and when a plan should be updated. Potential use of corrosion sensors will be discussed along with corrosion assessments and corrosion consideration for replacement materials. Accurate and up to date information provided within a current Corrosion Prevention and Control Plan can assist the ASIP engineer in making operational and maintenance decisions.

- **Basic Design**
 - Dissimilar metals
 - Crevices
 - High stress levels
 - Lack of lubrication provisions
 - Poor drainage
 - Poor access
 - Improper material selection
- **Finish Deterioration**
 - Chipping
 - Scratches
 - Breaks around fasteners
 - Abrasions
 - Deposits
 - Erosion
 - Age
- **Maintenance Problem Areas**
 - Neglect
 - Improper repair
 - Poor cleaning practices
 - Improper material selection
 - Inadequate corrosion control program
- **Conditions with the Aircraft**
 - Condensation
 - Microbial growth
 - Human transport
 - Animal transport
- **Accidental Contamination**
 - Chemical spills
 - Galley spills
 - Lavatory spills
- **Operational Environment**
 - Hot humid climate
 - Industrial pollutants
 - Landing areas
 - Snow removal chemicals

Figure 9.6-6. Some Causes of Corrosion

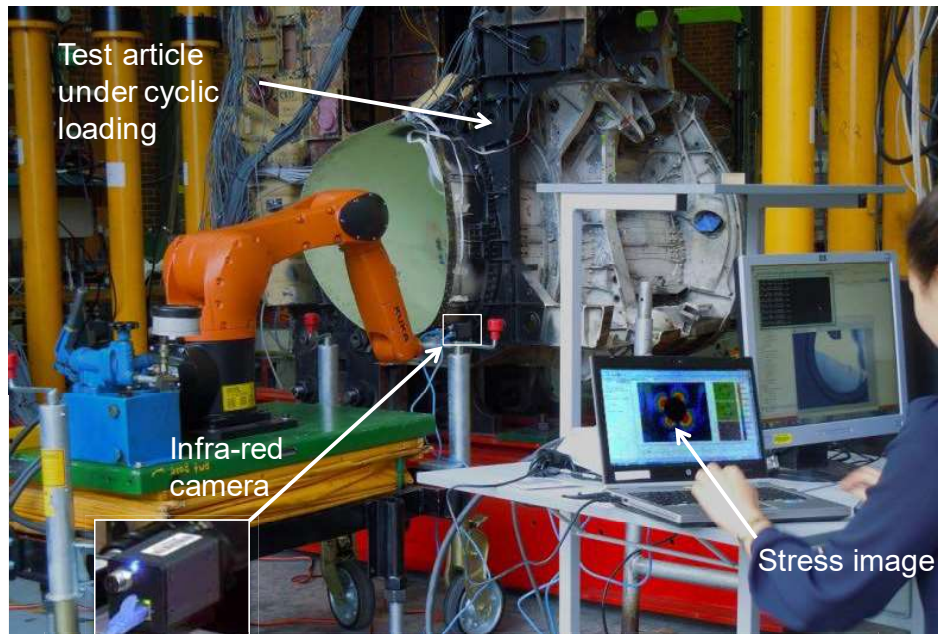
1. Introduction
2. Organization and Responsibilities
3. Corrosion Prevention and Control Requirements
4. Operational Environment
5. Design Considerations
6. Corrosion Assessments
7. Corrosion Prevention and Control Processes
8. Corrosion Surveys
9. Metrics
10. Lessons Learned
11. TO Cross Reference
12. References

Figure 9.6-7. CPCP Content: Table of Contents

9.6.3. In Situ Thermoelastic Stress Analysis of the F-35 – An Improved Approach to Airframe Structural Model Validation

D. McSwiggen and D. Whiteley, Lockheed Martin Aeronautics; N. Rajik and M. McDonald, DSTG

A recent innovation in thermoelastic stress analysis (Figure 9.6-8) offers an opportunity to improve the validation basis for structural finite element modelling of complex airframe components. In the aerospace context, model uncertainties can lead to inaccurate airframe lifing predictions and premature test failures that delay and add cost to full-scale durability test programs. A compact low cost thermoelastic stress analysis capability developed by the Australian Defence Science and Technology Group enables models to be validated against full-field stress imagery obtained from an airframe under full-scale structural durability testing. Traditional validation practice relies on a sparse set of observations drawn primarily from discrete electrical resistance strain gauge, structural deflection and load cell measurements. Full-field stress imagery, used in conjunction with traditional validation practice, represents a significant improvement over the use of traditional validation practice alone. This technical activity provides an overview of the full-field stress imagery capability and outlines the results of recent trials on the F-35 full-scale durability test program (Figures 9.6-9 and 9.6-10). These trials represent the most comprehensive full-field stress survey of an airframe done to date and the findings prove the efficacy of this new approach. The results show that structurally attached microbolometers (Figures 9.6-11 and 9.6-12) can furnish full-field stress imagery in airframe components of arbitrary geometric complexity which enables a direct assessment of model fidelity in areas of potentially life-limiting stress concentration where predictive accuracy is difficult to ascertain and needs to be most assured (Figure 9.6-13). Factors affecting the practical application of thermoelastic stress analysis to full-scale durability testing are also discussed, including constraints around loading rate and the effects of rate limitations, the selection of an appropriate load reference, the influence of surface imperfections and the emissivity properties of airframe primer on thermoelastic response measurements.



Enables detail stresses to be measured.

Figure 9.6-8. Thermoelastic Stress Analysis (TSA)



**165 Load Rams, 1849 Strain Gage Channels
525 K Maneuver, 4560 K Buffet Endpoints/Life**

Figure 9.6-9. F-35A Full Airframe Durability Test

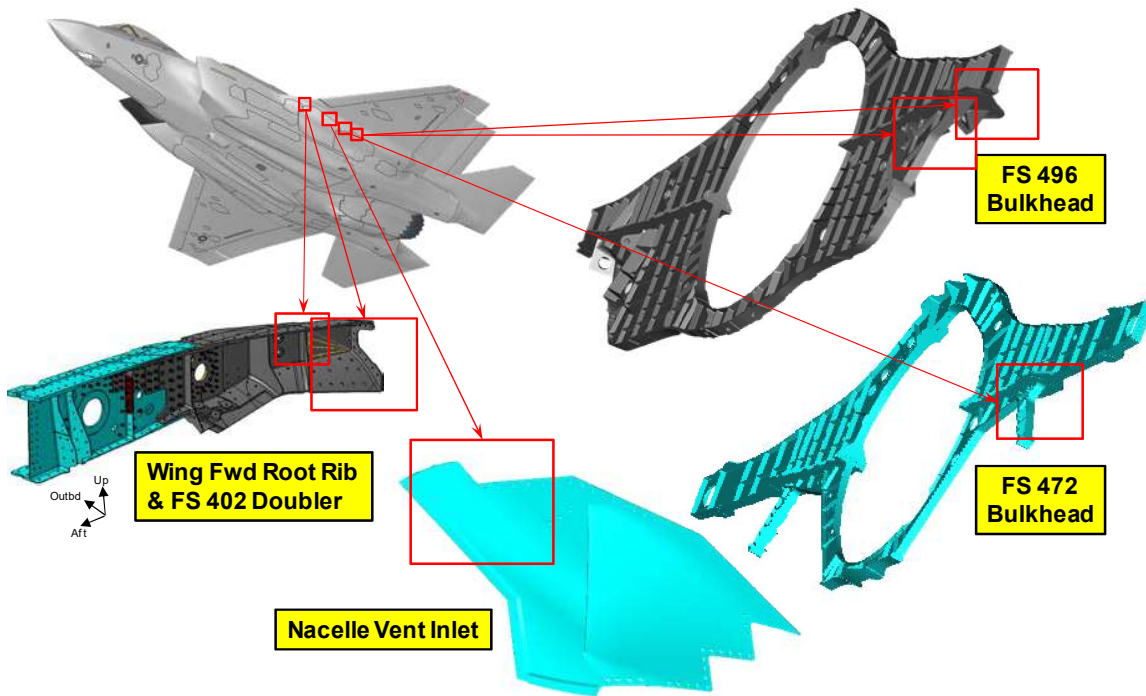
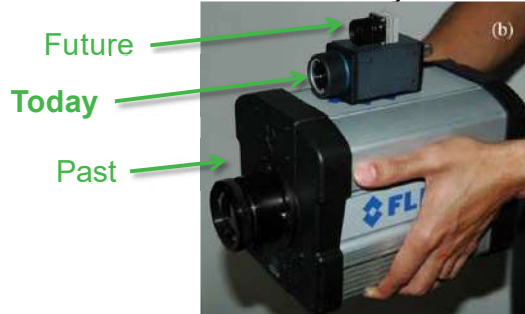


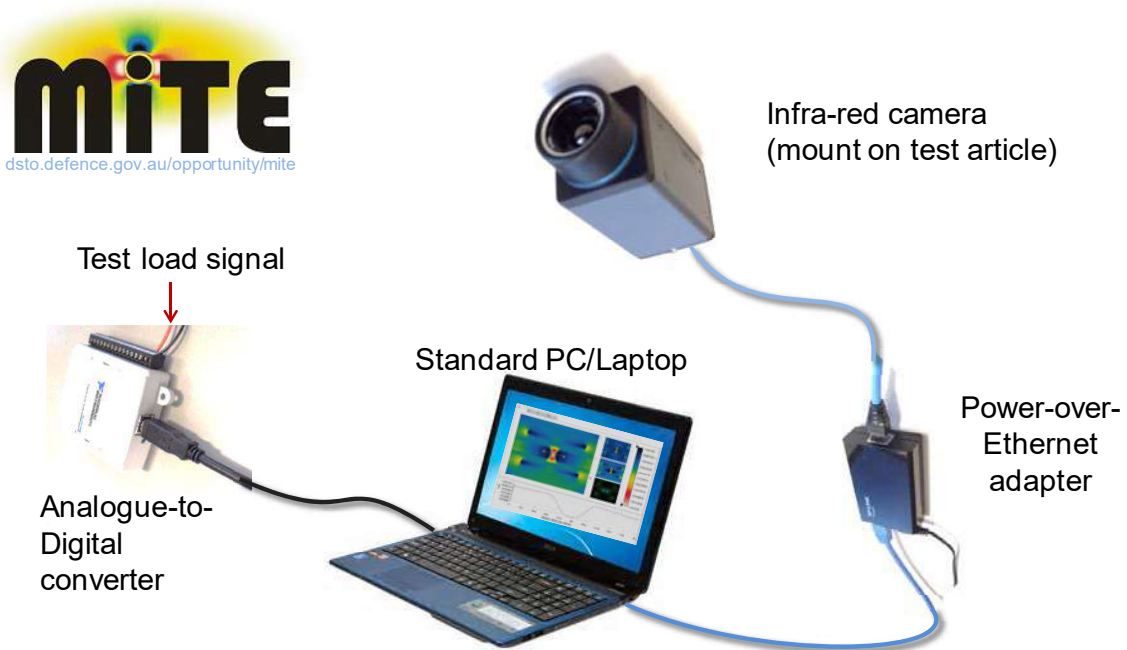
Figure 9.6-10. F-35A Locations

- **Commercial development of microbolometers have created:**
 - **Small, light-weight infra-red (IR) cameras**
 - **Room temperature cameras with very high sensitivity and high signal-to-noise ratios (don't need to cool a microbolometer like you do with a photon sensor)**
 - **Low cost cameras <\$10k**



Enables cameras to be mounted to test articles.

Figure 9.6-11. Microbolometers



Hardware all COTS. Software public released.

Figure 9.6-12. Equipment

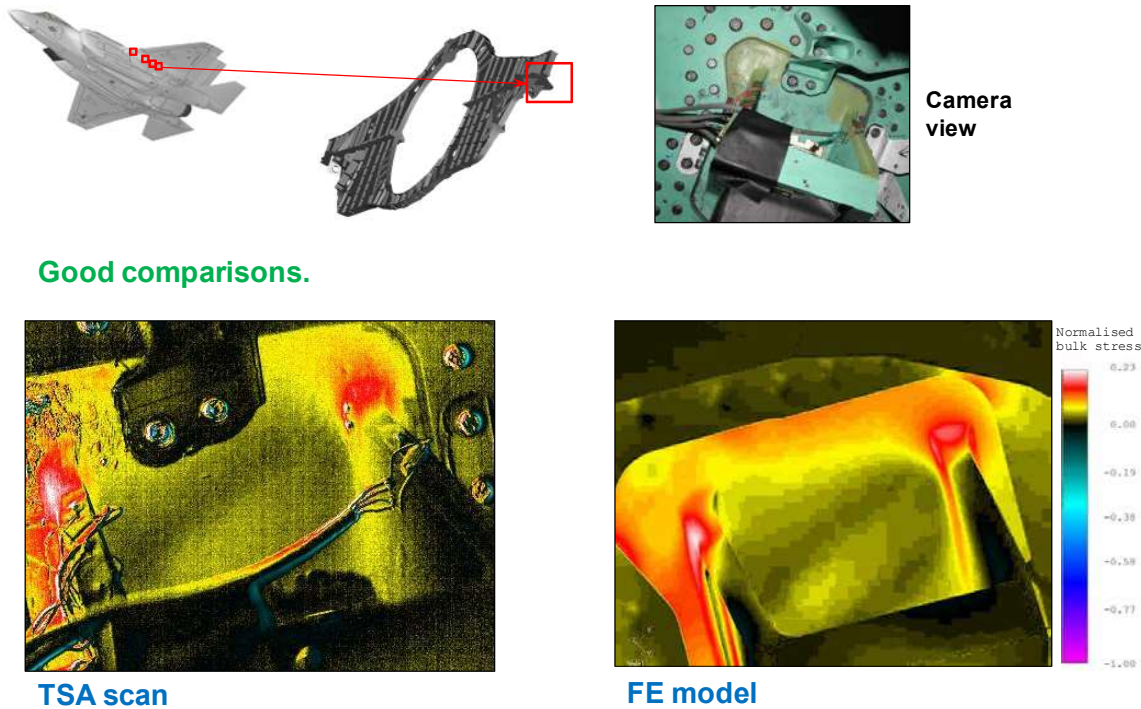


Figure 9.6-13. FS496 LHS Trunion Runout

9.6.4. Impacts on Crack Growth Analysis of Titanium 6Al-4V Small Crack Test Data

Ji Eun Park, Lockheed Martin Aeronautics; Wirt Garcia and Jake Warner, F-22 ASIP

The updated da/dN data of titanium 6Al-4V β A is developed from the combination of F-22 (Figure 9.6-14) current design curve, ASTM Load Reduction (LR) test and compression pre-cracking constant amplitude (CPCA) test completed in December 2014 (Figure 9.6-15). The CPCA test predicted lower threshold data than the ASTM LR or constant K_{max} tests. The results of the ASTM LR and constant K_{max} tests were almost identical. It was concluded that both test data experienced load history effects of compressive residual stress created by tension pre-cracking, and the CPCA test produced the most conservative and reasonable threshold values. The development process of the updated design material property curve using the Adjusted Compliance Ratio (ACR) method is presented (Figure 9.6-16). The ACR method is a technique to combine fatigue crack growth rate (FCGR) data into a single curve by removing residual stresses and closure effects. The final normalized master curve consists of CPCA test data for below $7.7 \text{ ksi}\sqrt{in}$ of K_{norm} , ASTM LR test data for K_{norm} of $7.7 \sim 27.61 \text{ ksi}\sqrt{in}$ and the current design curve for the rest of K_{norm} range. The cutoff stress ratio, R_c , is adjusted to get a better correlation for highly compressive spectra. It allows additional negative R cycles in crack growth calculations. To verify the master curve, the K_{norm} curve is regenerated for different K_{max} and adjusted to include crack closure effects using Newman's crack opening stress equation, and then the readjusted curves are compared with the CPCA test data. The expanded K table is derived using the Walker relationship with the set of K_{norm} data. The comparisons of the previous design material property and updated FCGR data are presented next (Figure 9.6-17). The Ti 6Al-4V small crack Phase 3 test, which was the damage tolerance crack growth verification test, concluded that the faster crack growth in the threshold region did not affect damage tolerance dramatically for most spectra tested. However, it must be noted that the test success criterion of the Phase 3 test was $L_{test} / L_{prediction} > .80$ and the test results showed the shorter

damage tolerance life with wing bending spectrum. Some of F-22 components including the center frames are made of Ti 6Al-4V β A and subjected to wing bending. Also, the ASTM LR and constant K_{max} test data used for the update of the part of transition range (Region II) showed faster crack growth than the current design FCGR and that update affects damage tolerance crack growth analysis. The damage tolerance crack growth analyses at various locations subjected to wing bending are performed with the updated FCGR data and the changes due to the material properties are discussed. Comparison of the durability and damage tolerance crack growth lives using the legacy and updated crack growth rate data are presented (Figures 9.6-18 through 9.6-20).



Figure 9.6-14. F-22 Aircraft

Development of Fatigue Crack Growth Rate Data



Figure 9.6-15. FCGR Test Specimen

- Adjusted Compliance Ratio (ACR) was used to Generate a Single Mean FCGR Data with CPCA Test Results for 6 Different Stress Ratios: R=0.9, 0.7, 0.4, 0.05, -0.5 and -0.95.
- ACR Method Eliminates Effects from Residual Stress, Crack Roughness, Crack Front Plasticity, etc.
- With the ACR data, Normalized K Curve is Obtained using

$$K_{norm} = \Delta K_{ACR}^{1-n} \cdot K_{max}^n$$

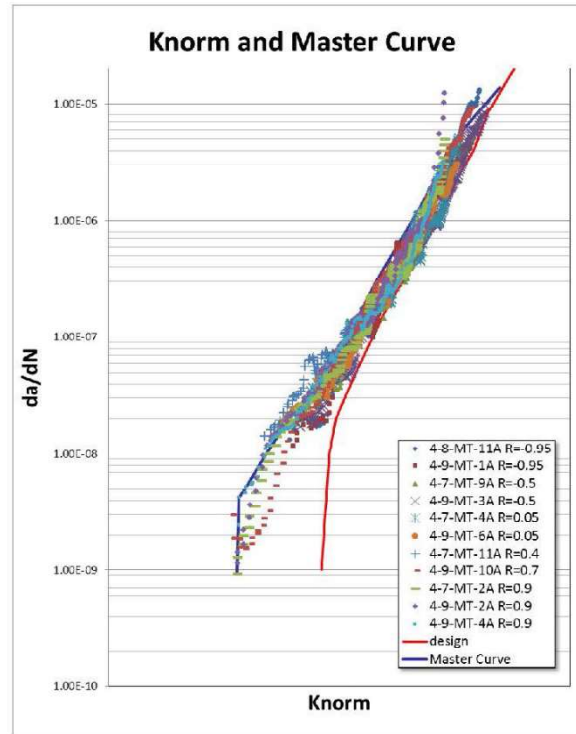


Figure 9.6-16. Adjusted Compliance Ratio (ACR) Method

- The Proposed da/dN Consists of Three (3) Parts:
 - Region I: CPCA
 - Region II: ASTM LR
 - Region III: Current F-22 Design
- The Cut-off Ratio is Decreased to -0.3 from -0.06 to Get a Better Correlation for Highly Compressive Spectra.
 - Allows Additional Negative R Cycles in CG Calculations.
 - Effects Only Highly Compressive Spectrum.

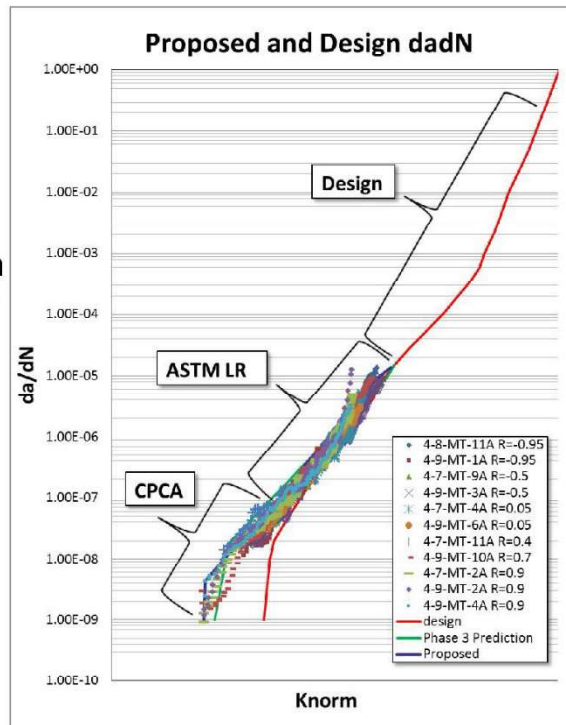


Figure 9.6-17. Proposed and Design da/dN

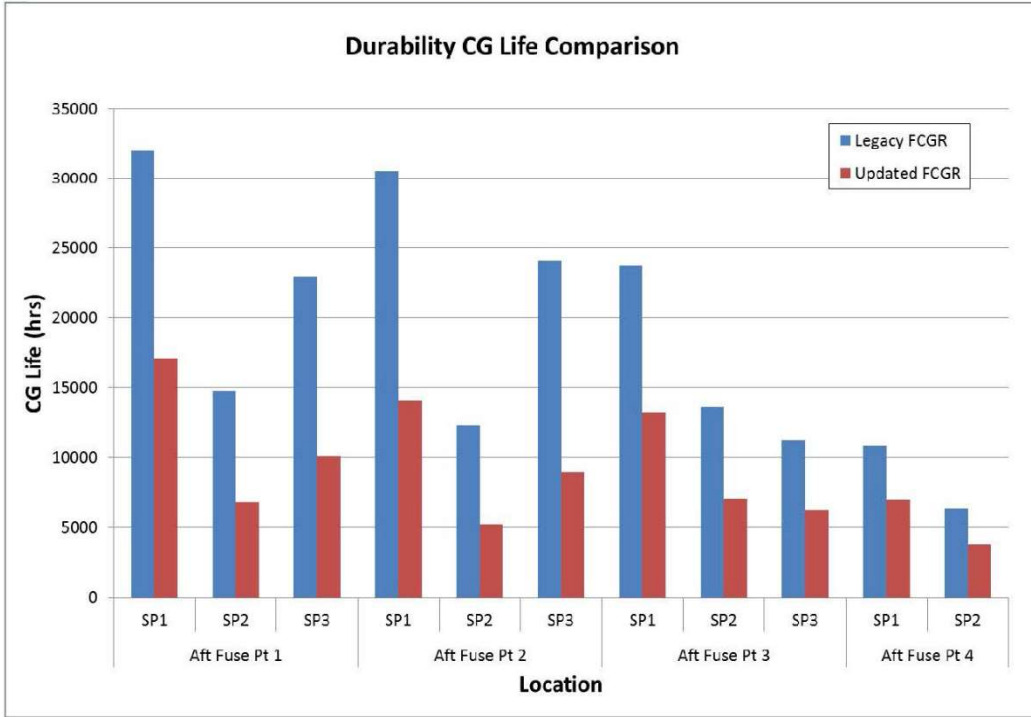


Figure 9.6-18. Durability Crack Growth Life Comparison

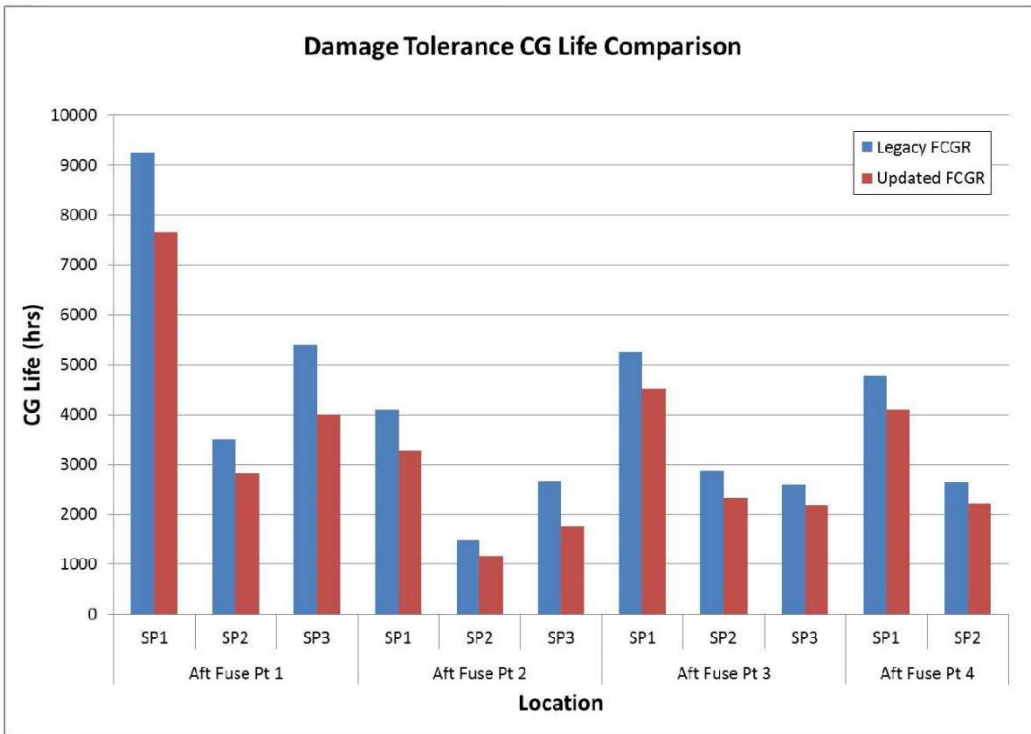


Figure 9.6-19. Damage Tolerance Crack Growth Life Comparison

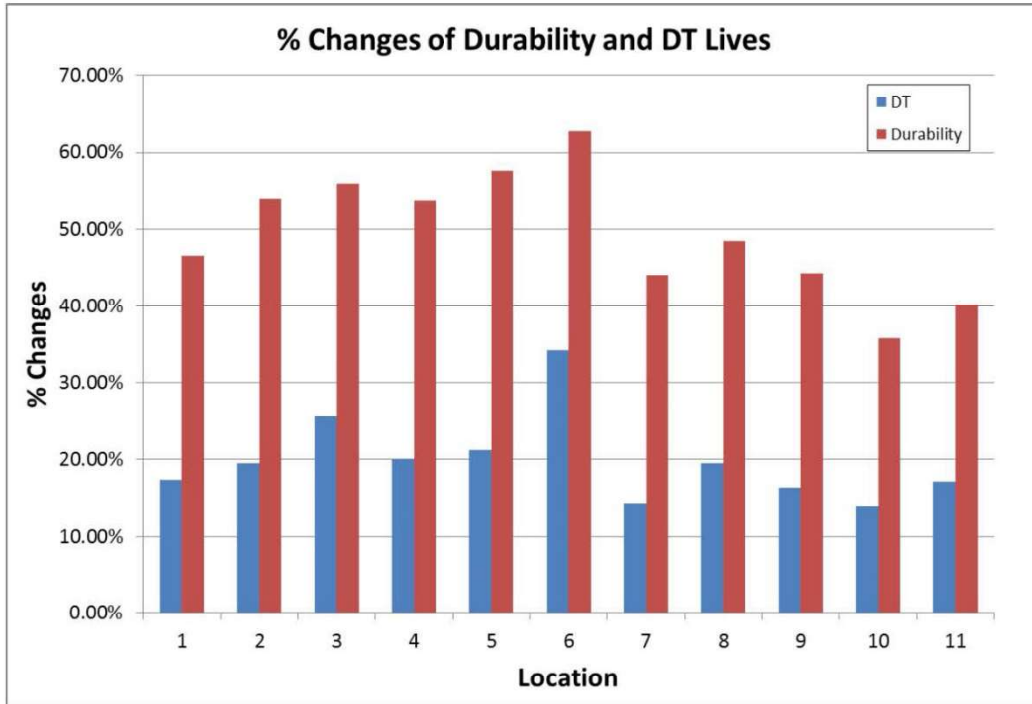


Figure 9.6-20. Percent Changes of Durability and Damage Tolerance Lives

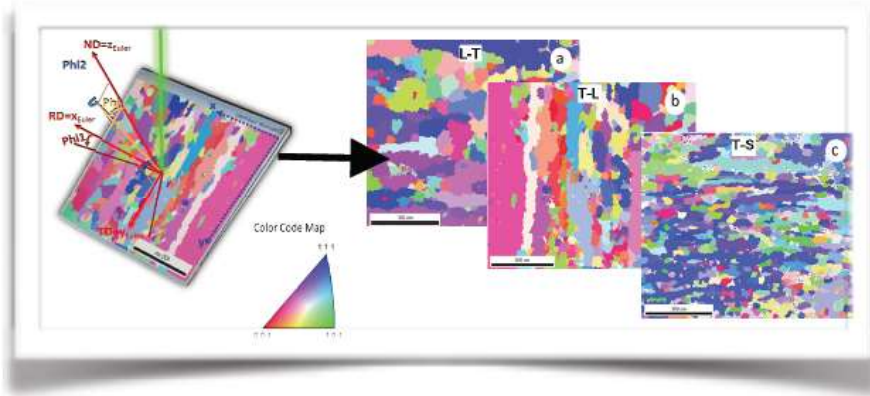
9.6.5. Relationship Between Galvanic Corrosion and Local Plastic Deformation – A7050-T7451

Alberto Mello, Andrea Nicolas, and Michael Sangid, Purdue University; Ricardo Lebensohn, Los Alamos National Laboratory

Aluminum alloys still are the preferred material for aircraft's primary structures in worldwide aviation. It means that the majority of the load carrying components and fatigue critical locations are made of this material, which are frequently stressed in multiple directions and under complex loading conditions. Component failure is a result of deformation accumulating in small regions within a part. In fact, strain localization is a precursor to material failure. Understanding the strain localization and the role of microstructure, e.g. grain's orientation and boundaries, on the strain energy accumulation is a key factor for improving the application of such materials under aggressive loading and environments. We investigate the strain accumulation for three textures orientation (L-T, T-L and T-S) of standard ASM AA7050-T-7451 (Figure 9.6-21). We also work with columnar aluminum with the ASM 7050 composition, treated to condition T7451 (Figure 9.6-22). For the columnar material, fatigue experiments are conducted with pristine, corroded and under corrosion specimens in the presence of a AISI 316 Stainless Steel cathode and 3.5% saline solution. The results establish the corrosion rates for resting and under fatigue specimens, as well as display the evolution of sub grain level deformation as the material is cycled until failure. These results provide an important basis in forecasting structure degradation, typically found in aging aircraft. To accomplish the experiments, each specimen is patterned using a novel micro stamping procedure to allow for strain mapping by digital image correlation (DIC). Electron backscatter diffraction (EBSD) is used to identify spatial maps of local grain orientations. The measured microstructures are used as input in a crystal plasticity model allowing comparisons between the strain maps obtained experimentally and the simulations for all tested textures. The comparisons show that the predicted levels of strain concentration are reasonable for all specimens from a statistical perspective. The results also show that the strain varies according to grain orientation and it is clearly affected by the

neighbor grains, and the maximum residual strain at grain level is much higher than the average strain on the specimen. In addition, the present work establishes the interconnection between galvanic damage and plastic deformation. This is quite an important ramification for design and structural analysis: even macroscopic loadings that are firmly within the elastic region of the material's behavior may create local plastic strains, thus resulting in hot spots that are prone to failure, especially for fatigue.

- The method used for mapping the strain field of the L-T, T-L, and T-S specimens was ex situ digital image



correlation. After mapping the grain orientations through EBSD, each specimen was stamped with a 10 μm pattern.

- The specimens were loaded axially to 3% strain and unloaded. Vic-2D was used for the DIC measurements. The strain mapping is the residual strain field after plastic deformation.

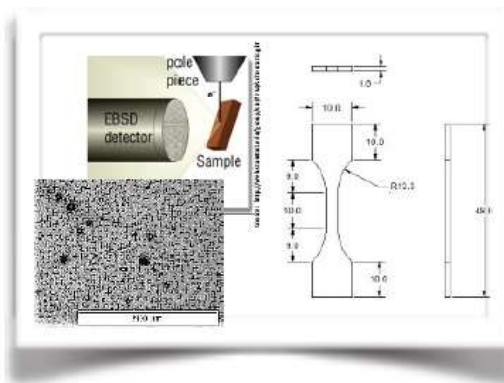


Figure 9.6-21. Microstructural Performance

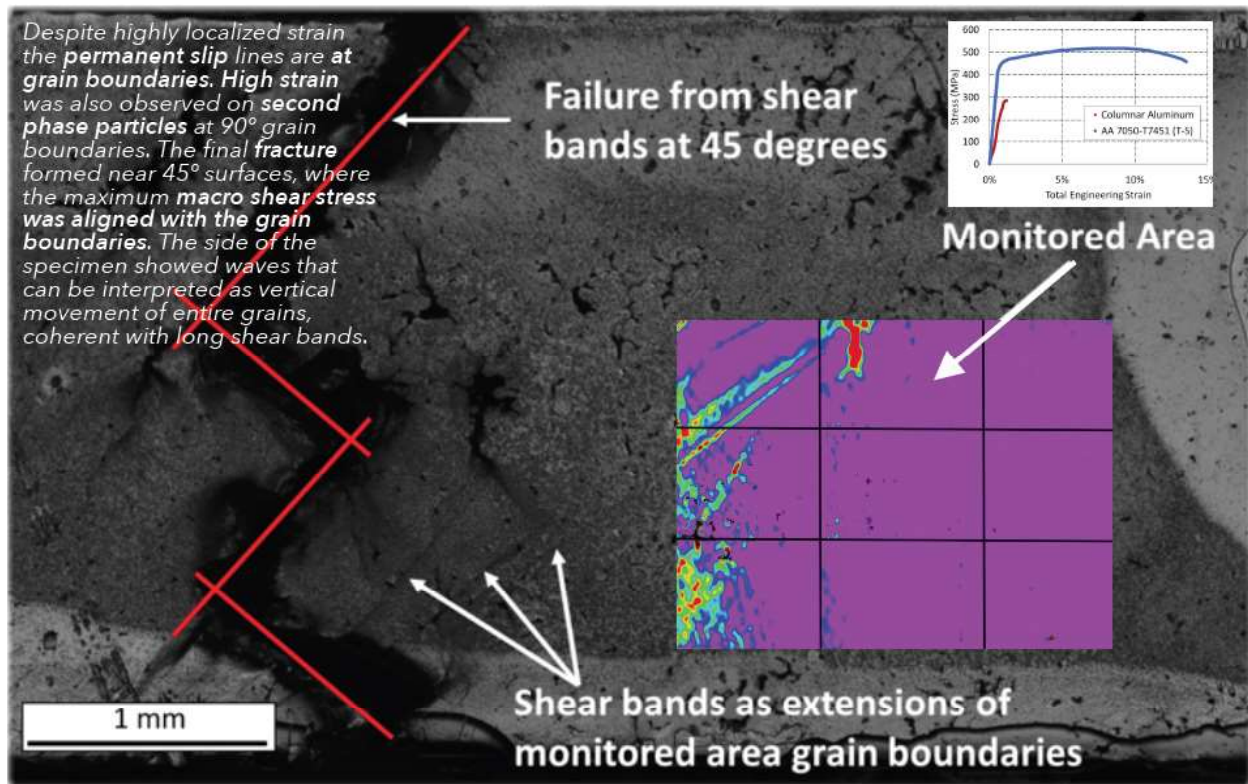


Figure 9.6-22. Columnar Aluminum

9.6.6. Progress Toward Accelerated Corrosion Testing and Asset Management Tools

Douglas Dudis, USAF Research Laboratory – Materials and Manufacturing Directorate

Corrosion of aircraft and missiles costs the Air Force an estimated \$6B per year and accounts for about 16% of system non-availability. In 2012 the Air Force Research Laboratory established the Corrosion Integrated Product Team with the vision to transform the Air Force from a “Find and Fix” to a “Prevent, Predict, Detect, Manage” approach toward corrosion. This technical activity will highlight selected AFRL activities with an emphasis on recent developments of accelerated corrosion testing methodologies (Figures 9.6-23 and 9.6-24) and approaches toward proactive means to manage corrosion in aircraft, missiles and ground support equipment. The development the Advanced Combined-Effects Simulation (ACES) chamber is progressing well, and efforts to define and evaluate protocols are being initiated. The ACES chamber is intended to provide a much more realistic and credible laboratory-based simulation of real-world environmental conditions (Figures 9.6-25 and 9.6-26). The environmental conditions can include not only weather, but pollutants as well as static and dynamic loading, depending upon the problem at hand. In a parallel effort, the advent of the Cumulative Corrosion Damage Model (CCDM) has opened up new possibilities with respect to proactive corrosion management. The CCDM provides a reasonable scientific framework for considering environmental factors impacting corrosion, can be extended and tailored to specific problems, and can (in principle) be implemented in operational environments. The ACES and CCDM are mutually supportive and part of an integrated program which will be discussed.

Accelerated aging should not change the target aging mechanism!

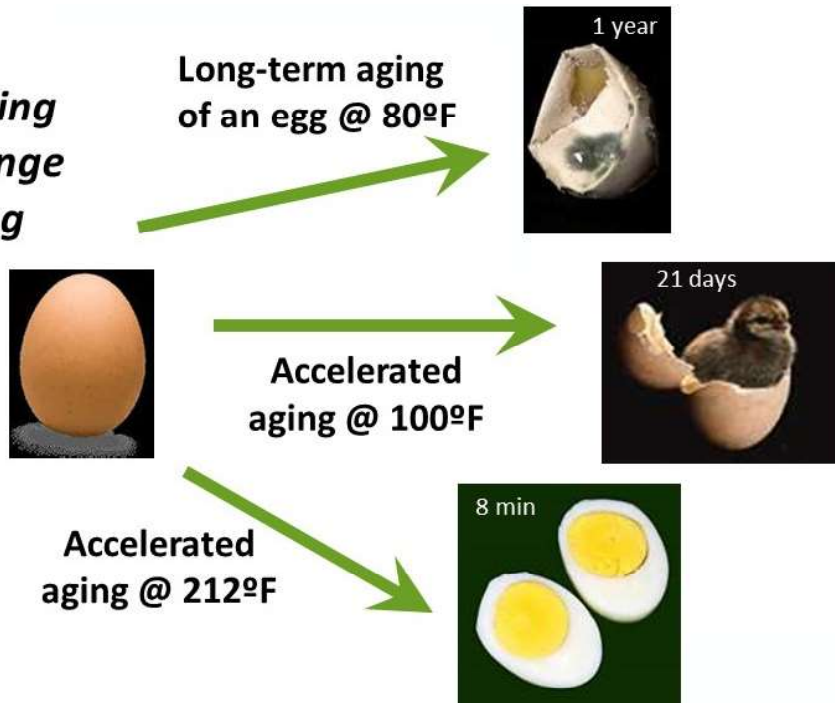


Figure 9.6-23. Accelerated Aging

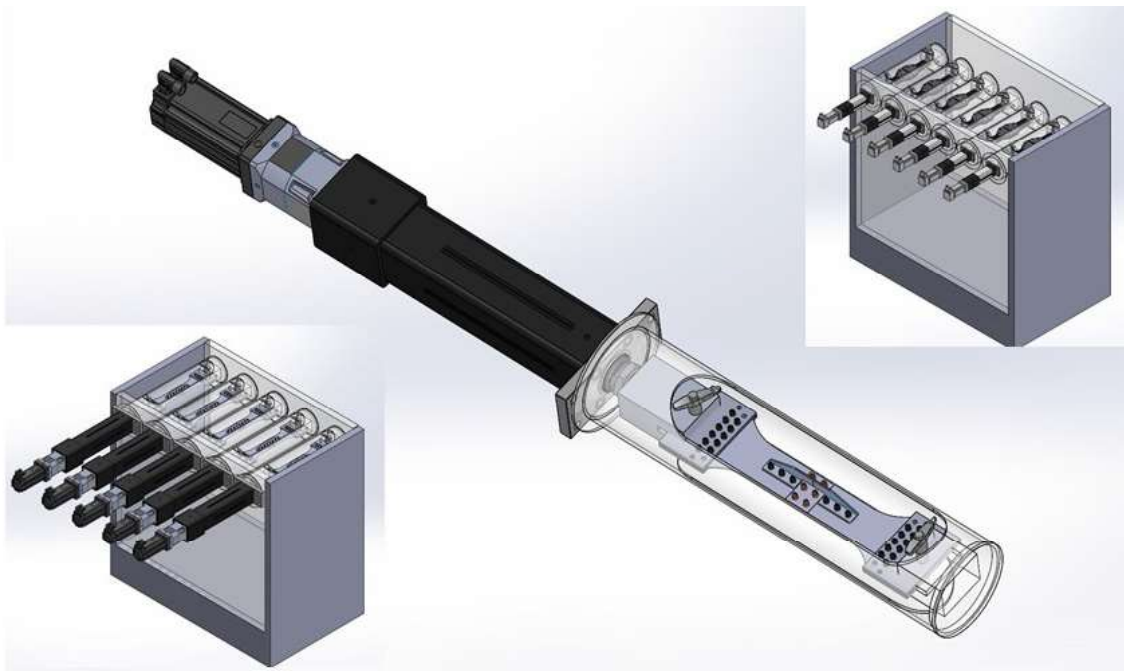


Figure 9.6-24. Fatigue Testing

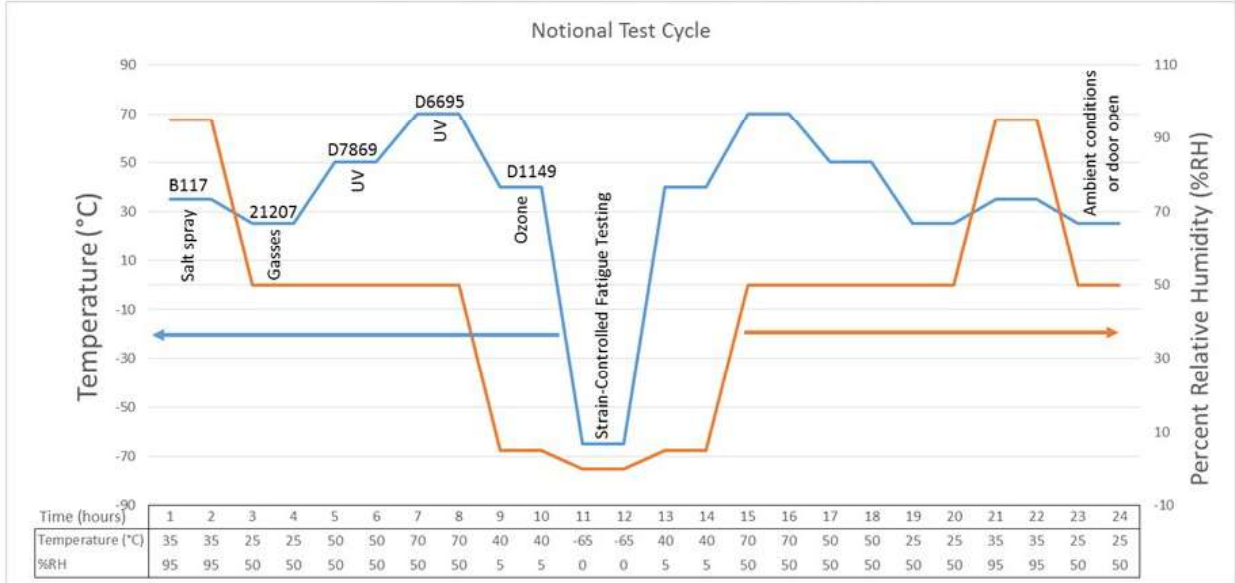


Figure 9.6-25. Notional Test Sequence

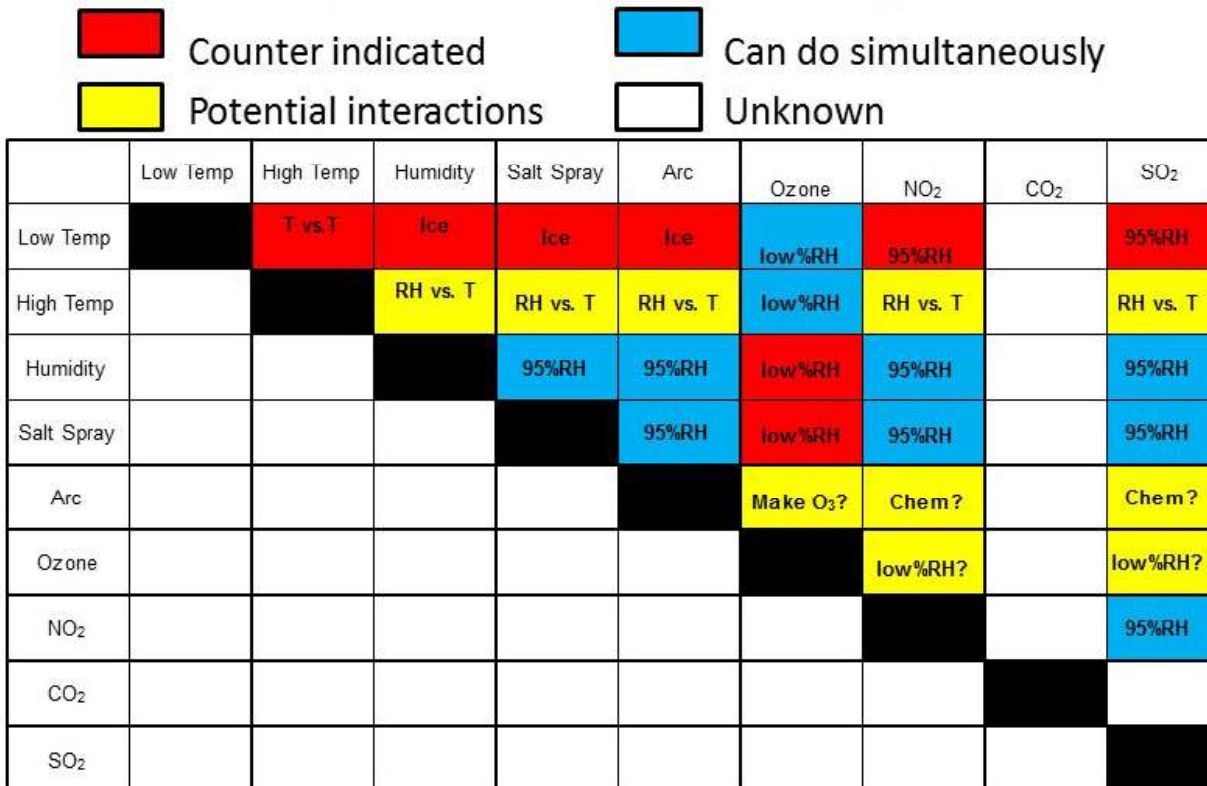


Figure 9.6-26. Environmental Conditions Matrix

9.6.7. Cumulative Corrosion Damage Modeling: A Novel Approach to Evaluating Environmental Attack on Aerospace Alloys

David Rose, Adirondack Analytics; Scott McCombie, Booz Allen Hamilton

Past attempts at predicting atmospheric corrosion rates have primarily employed statistical regression or power-law models. These approaches enable predictions based upon consideration of long-term (e.g., annual) average chloride and/or SO₂ deposition rates. In addition, they often employ a simplistic approach to considering relative humidity, which is a factor referred to as “Time of Wetness”. Most past models ignore temperature effects and those that do consider the factor are limited to using average values. Legacy models like those described here make linear or simple nonlinear predictions. They can be highly accurate but only when they are calibrated and used to make predictions for locations that have similar environmental conditions. When they are calibrated and employed using diverse data measured at locations with significantly different environmental conditions, they make predictions that are far less accurate. Generally speaking, the inability of these types of models to accurately work under diverse conditions results from their failure to explicitly account for interactions (both synergistic and competing) between the numerous, highly variable acceleration factors that come together to initiate and sustain corrosive reactions. Accurate models that can be employed under diverse conditions can only be developed through use of an entirely different modeling approach and formulation. A novel, simulation-based approach has been developed and is currently being improved and expanded upon that considers atmospheric corrosion as a cumulative damage process. Constructing a cumulative corrosion damage model (CCDM) as described here follows a similar path as was used to develop random amplitude fatigue models for composites. Specifically, equal levels of exposure to damage-causing acceleration factors leads to equal levels of damage. Rather than consider the effect of random oscillatory stresses as is the case with fatigue models, the CCDM approach enables the prediction of short-time corrosion damage increments based upon short-term (e.g., hourly) measurements of temperature, relative humidity, sulfur dioxide, and ozone combined with longer-term chloride deposition rates. Longer-term corrosion rates are developed through summation of the short-term increments. This approach enables predictions based upon the explicit consideration of diurnal and seasonal weather factors combined with stochastic atmospheric contaminant levels (Figures 9.6-27 through 9.6-29). The proof-of-concept CCDM appears to possess unprecedented accuracy when compared to past modeling efforts (Figures 9.6-30 and 9.6-31). Computerized simulations are underway in order to further optimize the mathematical formulation of models and to apply them to different materials such as aerospace aluminum alloys. There are several advantages to CCDM that could enable the implementation of new approaches to aircraft sustainment. Currently, predictions are made using historical weather, air pollution, and chloride deposition data. Such predictions can be useful for design purposes and they can easily be updated later using actual environmental parameter measurements made during the specific times and locations that a system is exposed to atmospheric conditions. As a result of how it considers the impact of short-term exposures, the CCDM approach can enable predictions based upon individual aircraft flight and deployment histories. The ability to update predictions in such a fashion while directly considering flight cycles and deployments enables the development of new CBM+ approaches to aircraft sustainment.

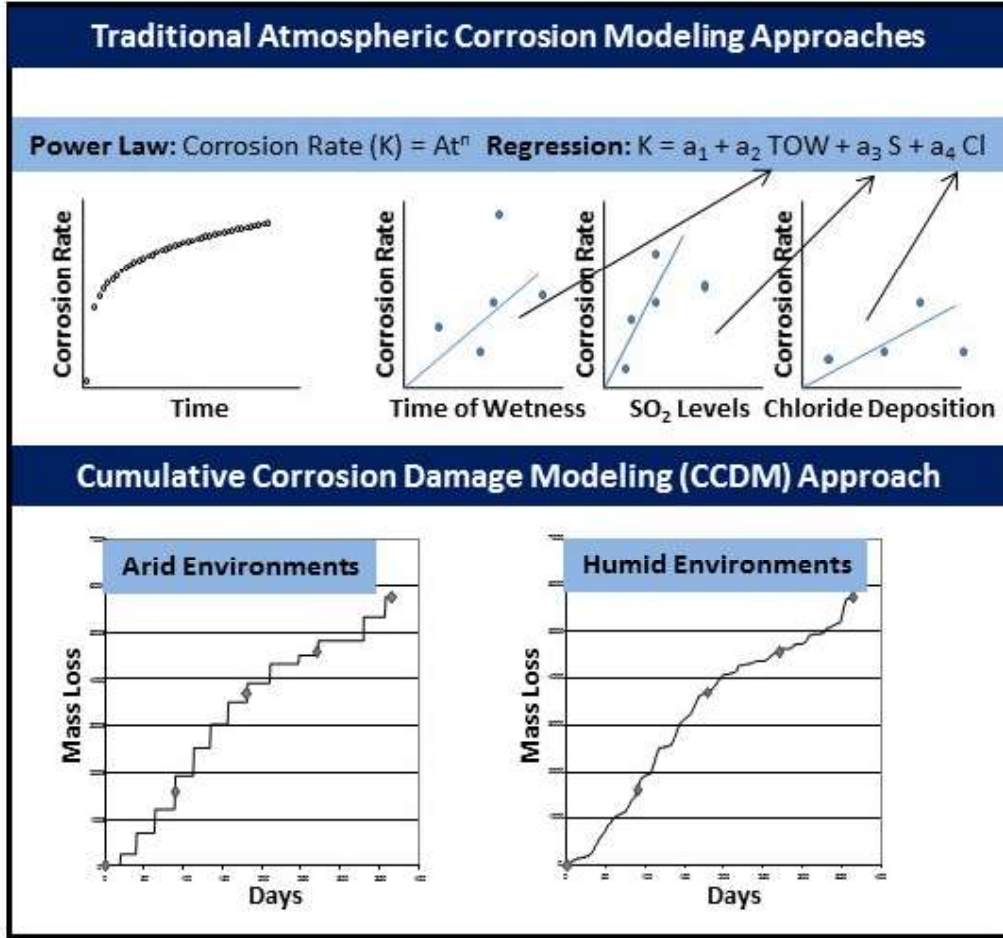


Figure 9.6-27. Comparison of CCDM to Traditional Corrosion Models

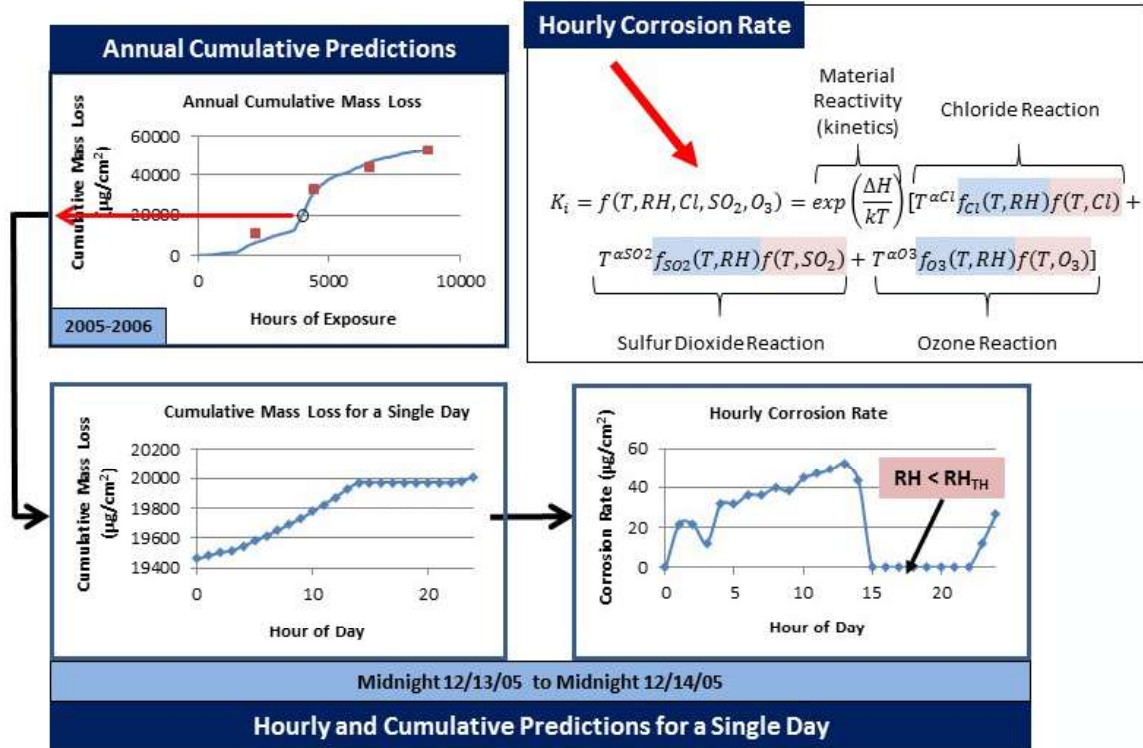


Figure 9.6-28. Illustration of Cumulative Predictions

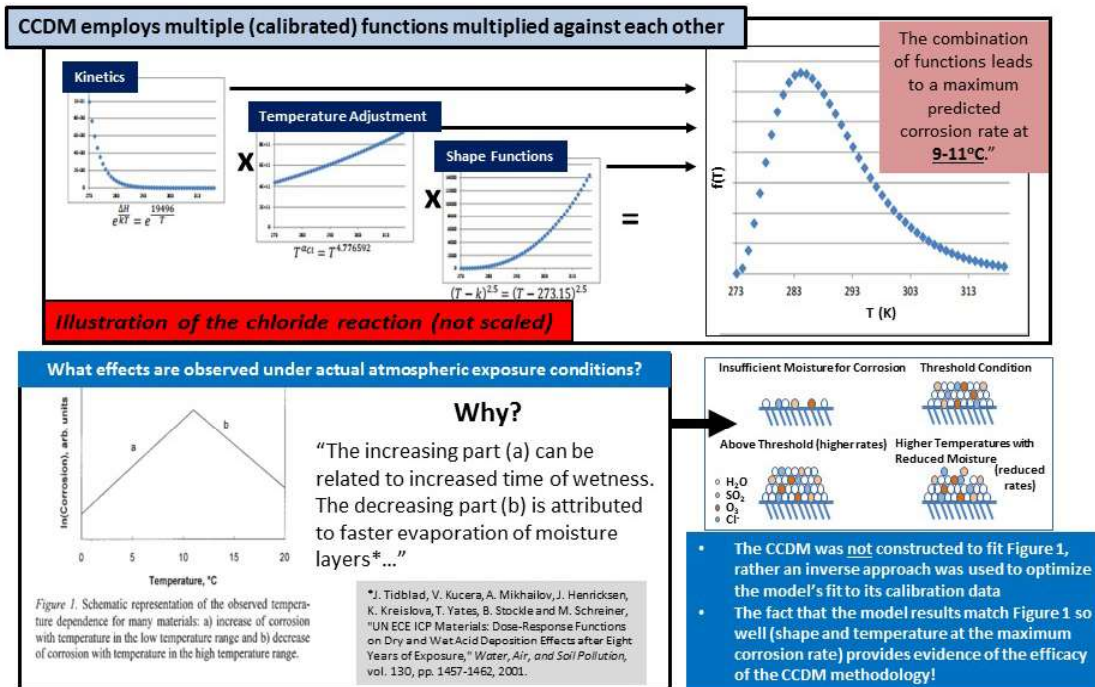


Figure 9.6-29. Comparison of CCDM to Observations

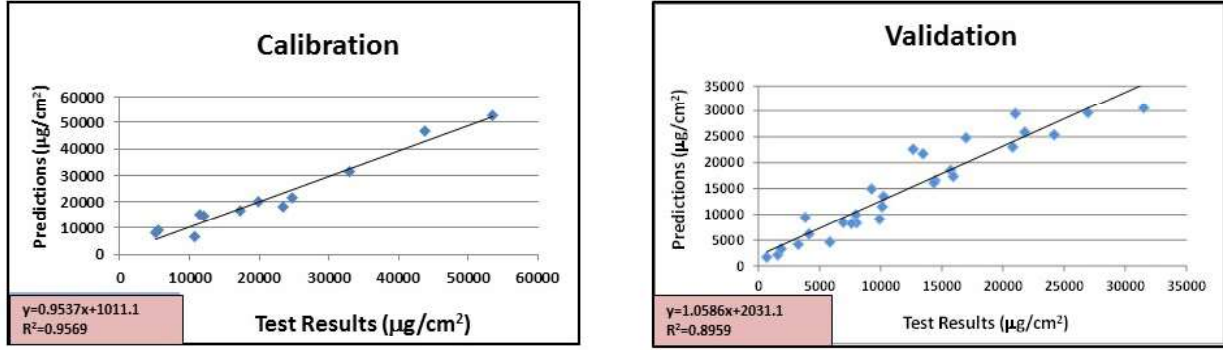
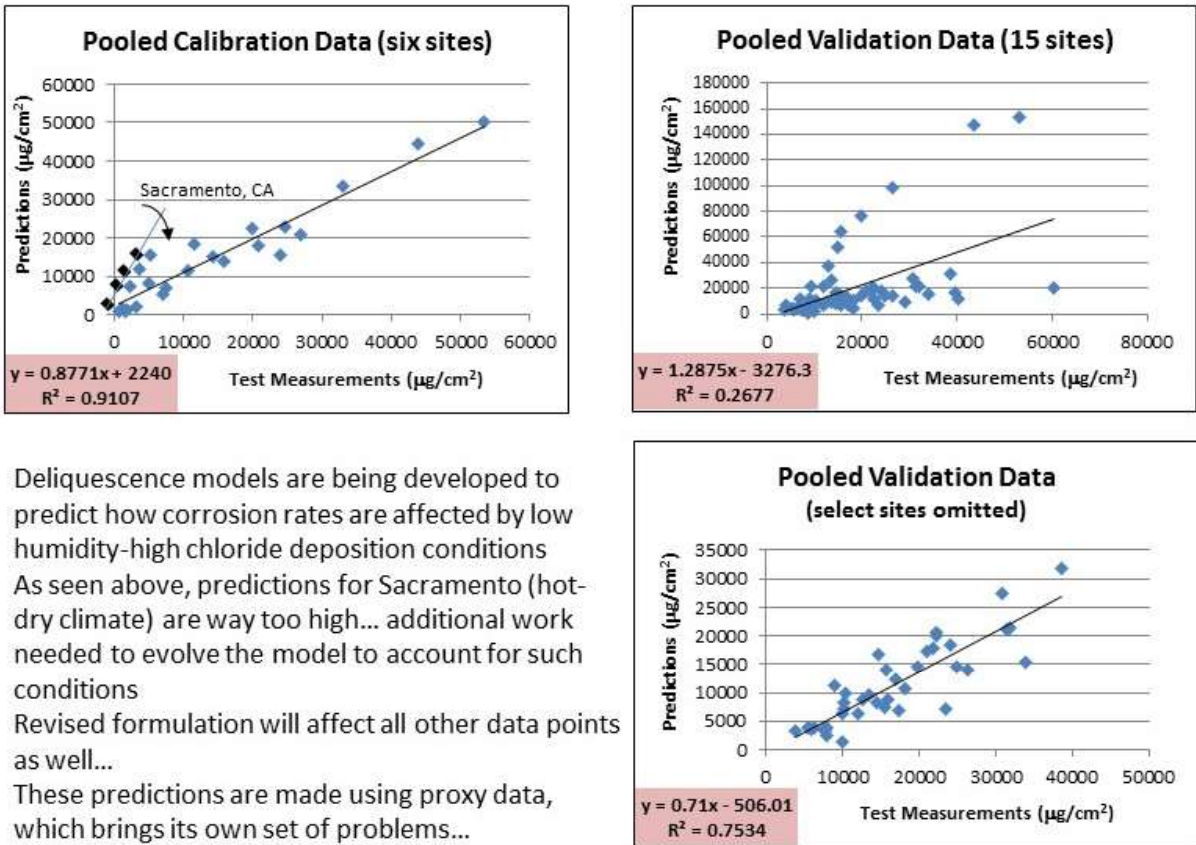


Figure 9.6-30. Final Proof-of-Concept CCDM



- Deliquescence models are being developed to predict how corrosion rates are affected by low humidity-high chloride deposition conditions
- As seen above, predictions for Sacramento (hot-dry climate) are way too high... additional work needed to evolve the model to account for such conditions
- Revised formulation will affect all other data points as well...
- These predictions are made using proxy data, which brings its own set of problems...

Figure 9.6-31. Model Evaluation

9.6.8. Improved Life Cycle Management Tools for Prediction of Corrosion Damage of Airborne Systems

Michael Oja, Robert Tyron, Animesh Dey, Robert McDaniels, Ketan Kulkarni, and Nick French, VEXTEC; James Burns, University of Virginia

Corrosion damage is important to the management of the structural integrity of an airframe, and current corrosion damage modeling methods are expensive and provide only rough estimates of damage. Cracking due to corrosion is a multi-disciplinary, multi-scale problem that needs to integrate multiple physics for accurate simulation of the damage state and better prediction of failure risk. These disciplines include electrochemistry, mechanical metallurgy and structural analysis. VEXTEC is developing a multi-disciplinary and multi-scale computational model and software that integrates computational models for multiple damage mechanisms (Figures 9.6-32 and 9.6-33). The model will address prediction of remaining useful life of structures suffering from corrosion fatigue and stress corrosion cracking (Figure 9.6-34). VEXTEC's approach has had preliminary success in developing an integrated computational materials engineering (ICME) approach that simulated the effect of corrosion induced surface damage on fatigue crack initiation in airframe aluminum alloys. In order to account for the variability that exists in the material and loading conditions, the approach is probabilistic (Figure 9.6-35). The software will be used to optimize inspection and maintenance of aging aircraft (Figure 9.6-36).

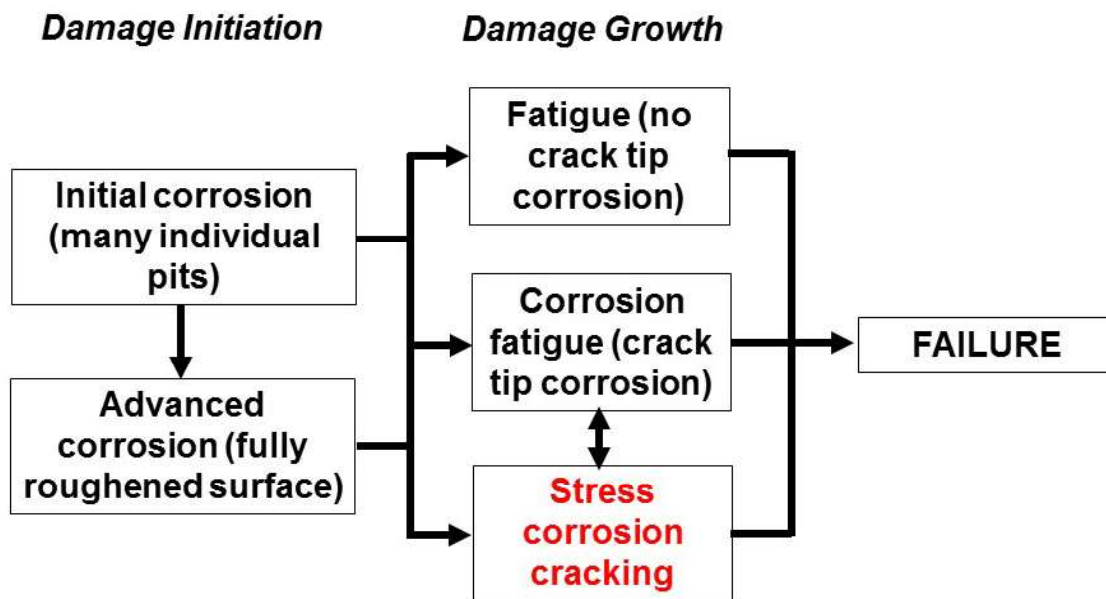


Figure 9.6-32. Overview of Corrosion Damage Software

- Material da/dt
- Applied Potential
- Initial Defect Size
- Applied Stress
- Residual Stress
- Crack Geometry

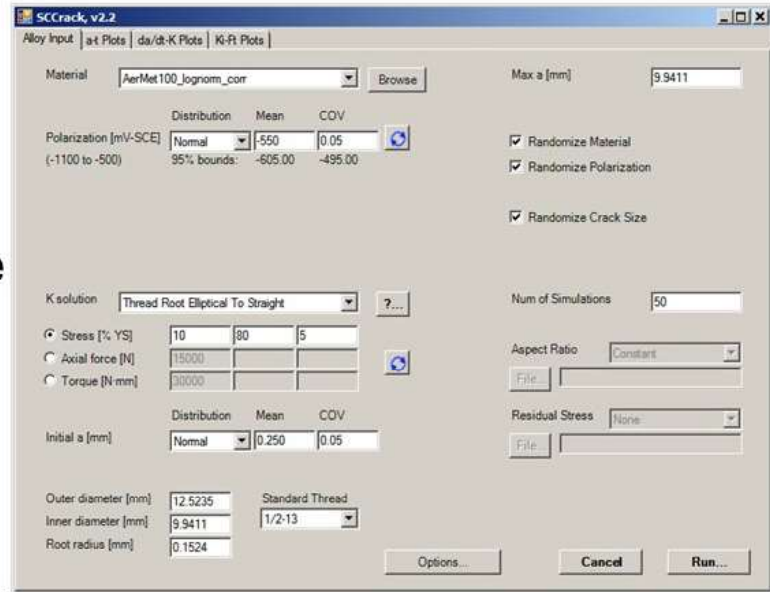
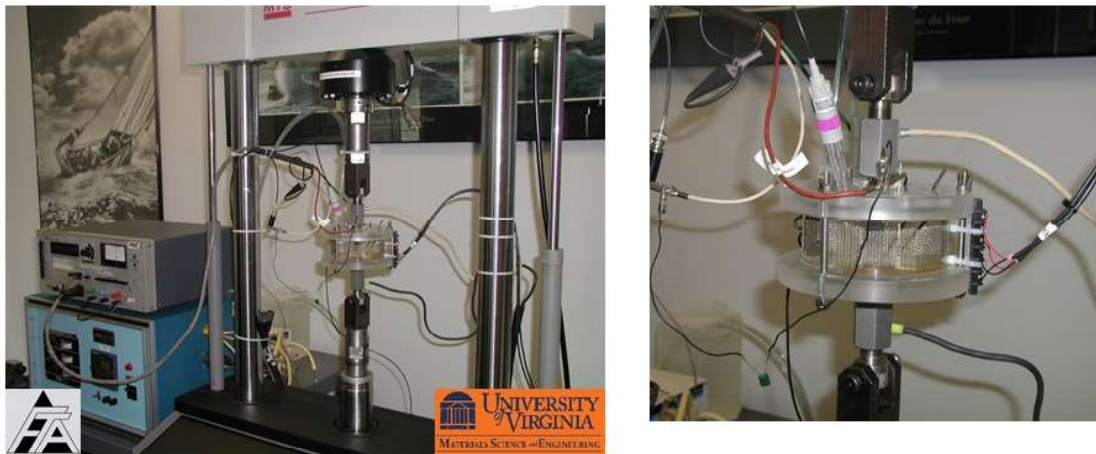


Figure 9.6-33. Software Inputs

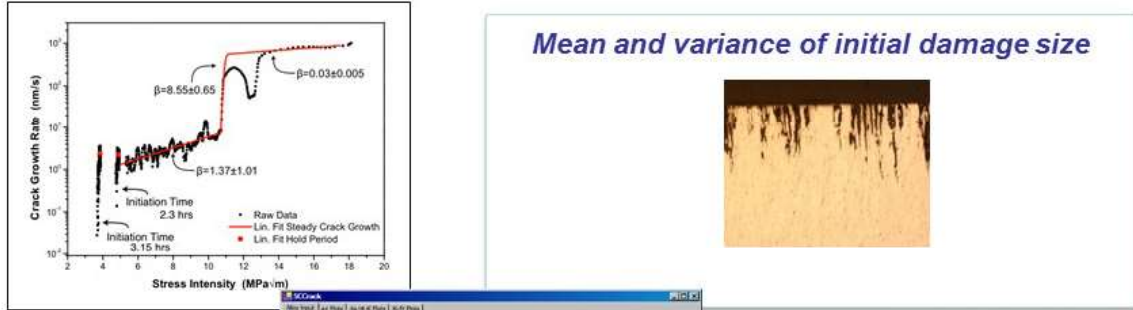


*FTA is Fracture Technology Associates (Bethlehem, PA)



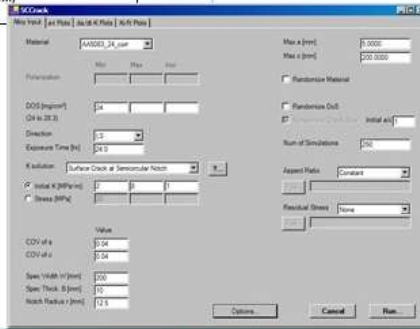
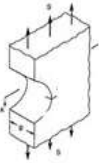
- DC Potential Drop (DCPD) measurement of crack growth (*months* hours of test time)
- Programmed slow dK/dt loading

Figure 9.6-34. Accelerated SCC Test Method



(Lim, Scully, and Kelly)

$$\left(\frac{da}{dt}\right)_i = C_i 10^{n_i} K$$



1. Monte Carlo selection of initial damage size and da/dt vs. K
2. Stress intensity solution for application (assumed crack shape)
3. Integration of crack growth rate

Figure 9.6-35. Probabilistic SCC Simulation

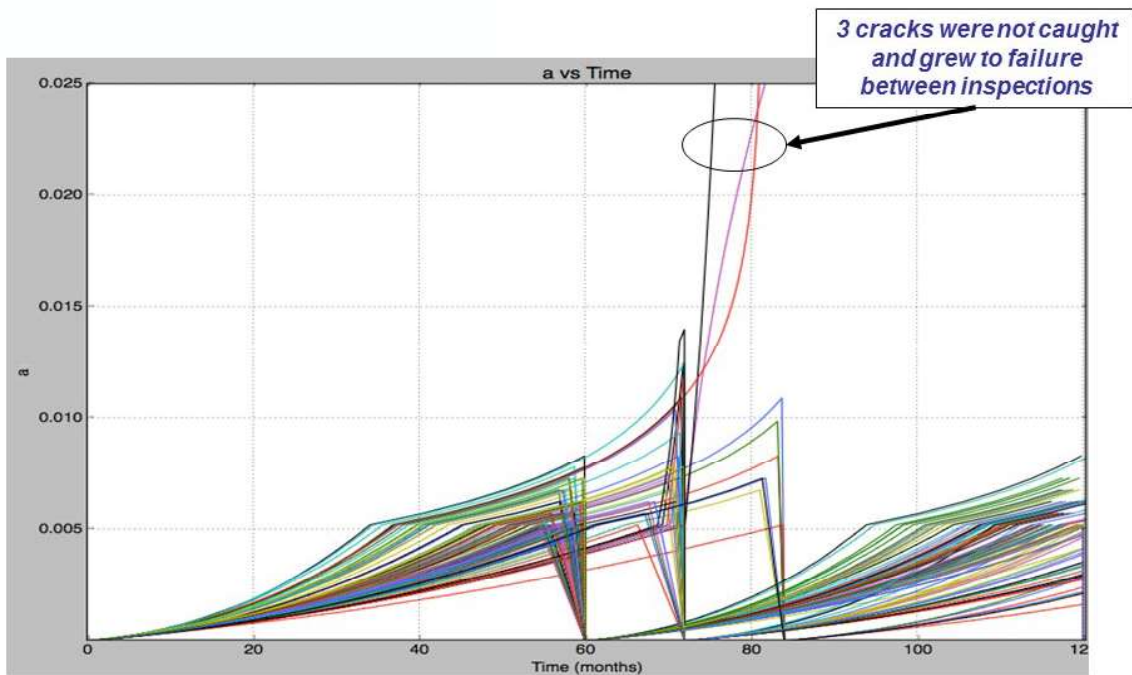


Figure 9.6-36. Output: Crack Length vs. Time with Inspections

9.6.9. Damage-Tolerant Analyses Using Load-Shedding ΔK -Rate Data is Inappropriate for Aircraft Spectrum Loading Life Predictions

James Newman, Jr., Mississippi State University; Kevin Walker and R. Boykett, DSTG Australia

Standard ASTM test method to generate fatigue-crack-growth-rate data in the low-rate regime has been the load-shedding method, which has been shown to produce elevated thresholds, slower crack-growth rates, and different Paris slopes in mid-rate regime than steady-state behavior (Figures 9.6-37 and 9.6-38). Compression pre-cracking methods have been shown to produce lower thresholds and faster rates than the ASTM method (Figures 9.6-39 and 9.6-40). However, both methods show elevated levels of crack closure for low- and high-stress ratio tests in the low-rate regime due to plasticity, roughness and debris. This technical activity presents results of crack-growth-rate tests conducted on middle-crack-tension, M(T), specimens under constant-amplitude loading. These results are compared with previous tests on compact, C(T), specimens made of 7075-T6/T651 and 7249-T76511 alloys. A crack-closure analysis was used to collapse the data into a fairly narrow band over many orders of magnitude in rates (Figure 9.6-41 and 9.6-42). Measured and calculated crack-opening loads were used to generate the effective-stress-intensity factor (ΔK_{eff}) against rate relation, which was significantly lower than the ΔK -rate data in the low-rate regime. Tests and crack-growth life predictions have been made on the two alloys using two wing spectra. One spectra was a short sequence ($\sim 300,000$ cycles), while the other was a very long spectra (~ 1.5 million cycles). In addition, some analyses were also made on tests using the very long spectra conducted by IMP Aerospace in Canada on the CP140 life-extension program. The latter spectrum includes a very large number of small stress amplitude that would cause stress-intensity factors to be below the traditional threshold using the ASTM load-shedding method. However, these small stress amplitudes have a significant influence on crack-growth predictions using the lower threshold and faster rates generated from the compression pre-cracking method. Fatigue-crack-growth predictions were made with FASTRAN Version 5.53. Results from the spectrum tests and analyses generally agreed to within about $\pm 25\%$. This work was sponsored by Australian DSTO.

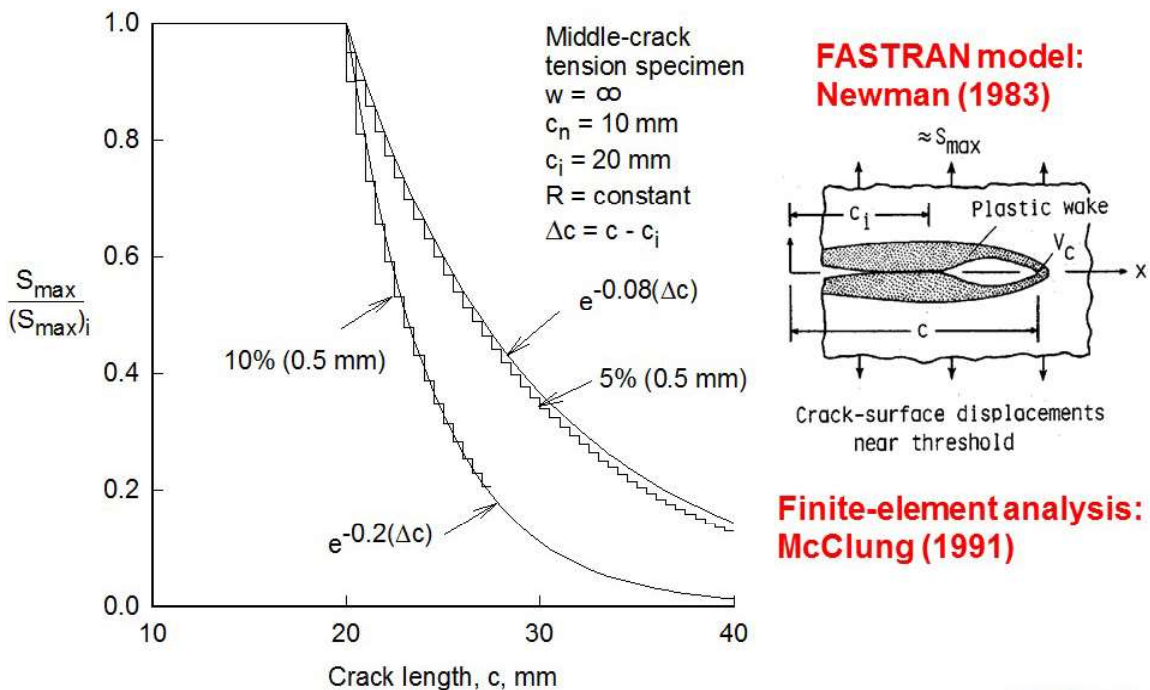


Figure 9.6-37. Traditional Load-Reduction Test Procedure

AFML TR 78-40; Hudak, Saxena, Bucci and Malcolm (1978)

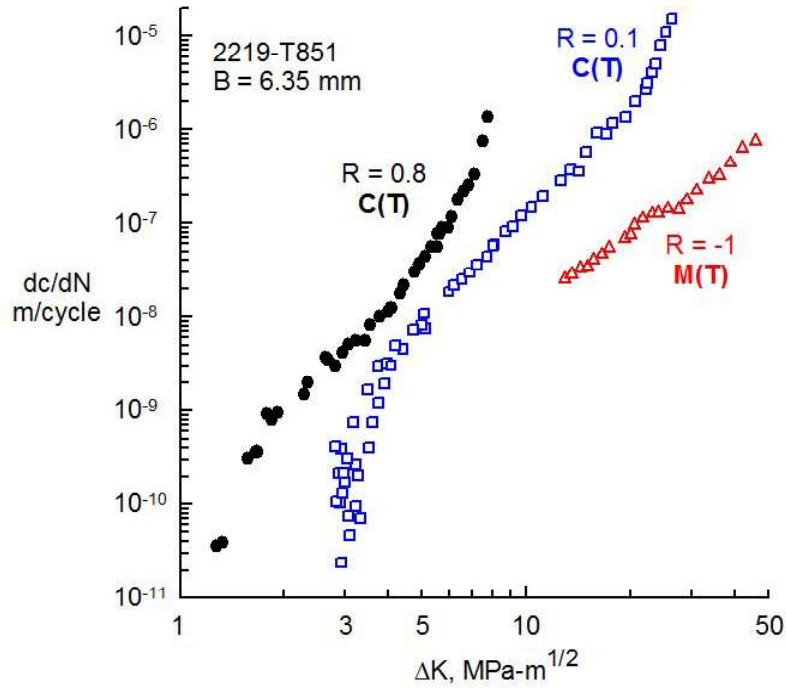


Figure 9.6-38. Data Used in Original Development of Standard Load-Reduction Test Procedures

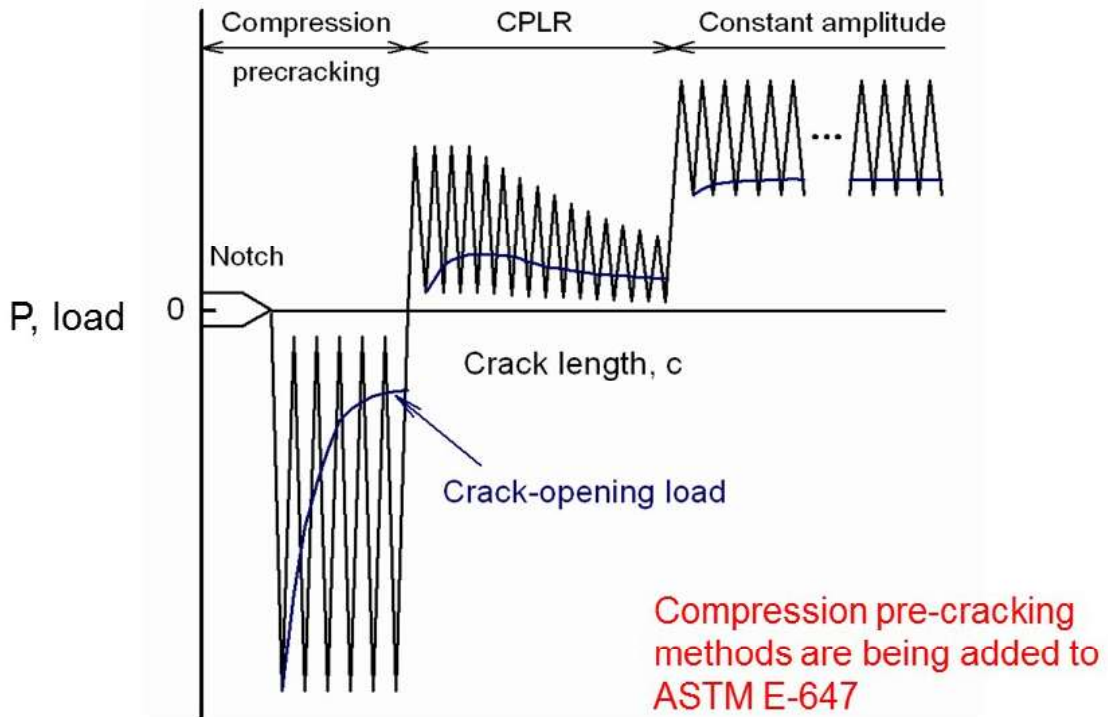


Figure 9.6-39. Compression Pre-Cracking Load-Reduction (CPLR) Procedures to Minimize History Effects

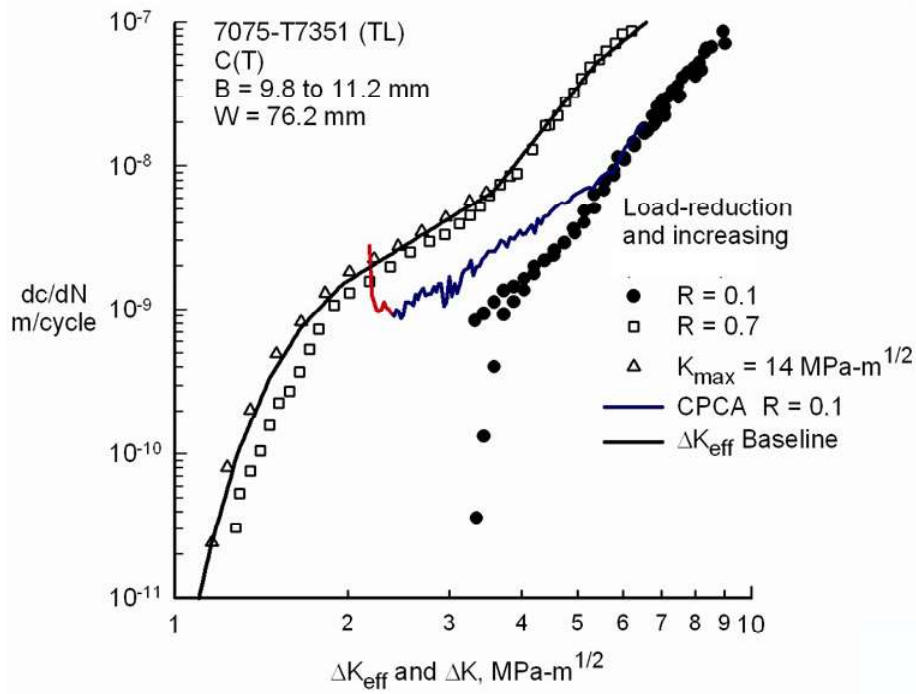


Figure 9.6-40. Fatigue-Crack-Growth-Rate Data on 7075-T7351 Aluminum Alloy (3)

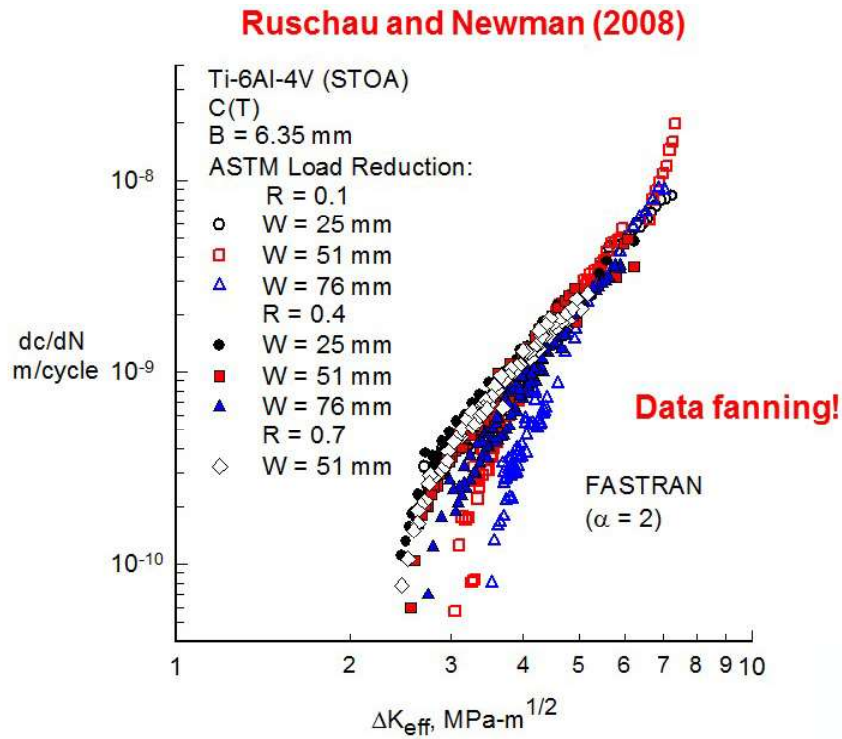


Figure 9.6-41. Crack-Closure Analyses for LR Test Data

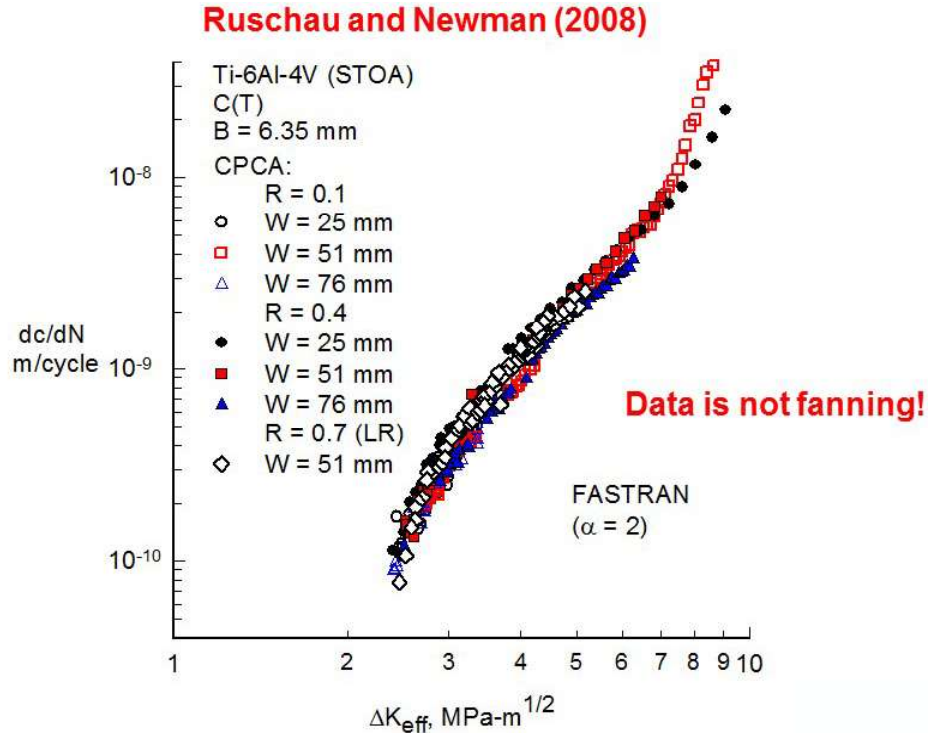


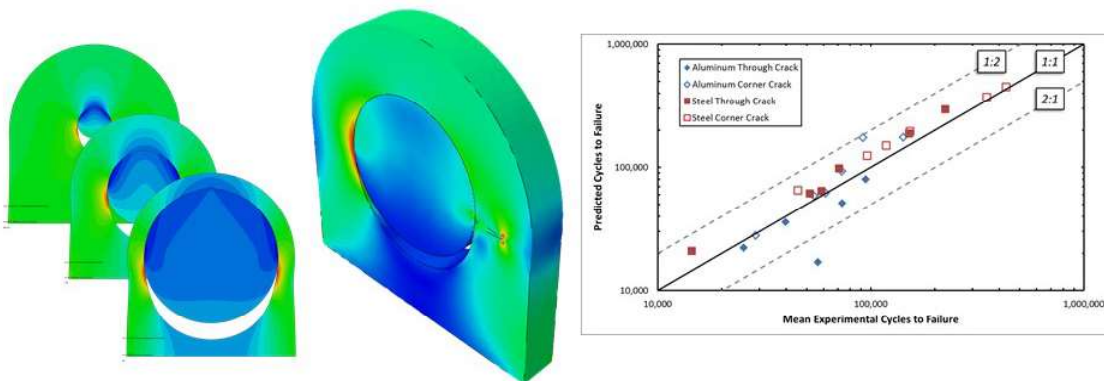
Figure 9.6-42. Crack-Closure Analyses for CPCA Test Data

9.6.10. Modeling Cracks in Obliquely Loaded and Tapered Lugs

James Sobotka, Yi-Der Lee, Craig McClung, and Joseph Cardinal, Southwest Research Institute

Airframe structures usually incorporate fracture critical pin-lug connections that are susceptible to crack growth under cyclic loading. Sustainment activities require analysis of these lugs using stress-intensity factor (SIF) solutions to relate the loading, geometry, and crack size to the driving force for fatigue and fracture. Legacy SIF solutions for lugs almost always set very simple short and straight geometries (Figure 9.6-43) under a vertical loading, propose bearing stresses to transfer load from pins to lugs instead of modeling contact, and assume fixed crack planes normal to the loading angle. In this effort, new and unique SIF solutions were developed for through cracks and corner cracks in obliquely loaded and tapered lugs using weight function (WF) solutions. In contrast to legacy solutions, these new WF SIF solutions expand the range of applicable geometries for cracks at lugs to include variable oblique loading angles (Figure 9.6-44), lug taper angles (Figure 9.6-45), and variable lug height (Figure 9.6-46); transfer loads directly through pin-to-lug contact; and determine crack planes (Figure 9.6-47) based on peak opening stresses at the uncracked lug's socket. Furthermore, WF solutions easily accommodate residual stresses, thermal stresses, and other loading features than may prove intractable using dense tables of numerically calculated SIFs. WF methods instead compute SIFs using integral kernel functions (the weight function) for the appropriate geometry and uncracked stress gradients. The new WF SIF solutions rely on uncracked stress gradients from advanced finite element analyses. Analyses explicitly model the neat-fit pin/socket connection with state-of-the-art contact algorithms that support contact between deforming objects – i.e., the pin and lug. Several thousand analyses of cracked and uncracked geometries inform lessons learned on the complex interactions among non-dimensional geometric parameters, crack shape, contact, friction, pin-lug material mismatch, lug height, taper angle, oblique loading angle, crack-location, and crack angle. These analyses suggest inconsistencies between

traditional approaches with assumed contact pressure distributions (e.g., the cosine squared distribution) and fixed crack angles that may lead to overly conservative designs. Results from the analysis database also lead to the development of stress prediction routines for tapered and obliquely loaded lugs. Extensive verification of these WF solutions supports the credibility of the new SIFs. The verification process generates independently calculated SIFs determined by domain integral methods that are applied to finite element results of cracked lugs. This verification process creates the SIF database using the python scripting interface available in Abaqus CAE to automate model development, execution, and extraction of key results. Due to the large solution space, the verification process employs a modified Latin-Hypercube Sampling to ensure a space filling design of experiment. Verification reveals that WF solutions usually deviate by no more than 10% from numerical SIFs and are often much closer (Figures 9.6-48 and 9.6-49). Relative to the independent SIF database, new WF SIF solutions are more accurate than earlier legacy SIF solutions. In validation studies, the new lug solutions predict lives within 50% of mean experimental values and have less experimental scatter than legacy solutions.



- Investigated methods to apply pin loading
- Confirmed applicability of weight function methods
- Verified new solutions for through, corner, and surface cracks
- Validated new solutions against crack growth measurements
- Sobotka et al, "Modeling Cracks at Pin-Loaded Holes in Plates and Lugs: Assumptions, Verification, and Validation," AA&S, Grapevine, TX, 2016.

Figure 9.6-43. Earlier Work with Straight Lugs

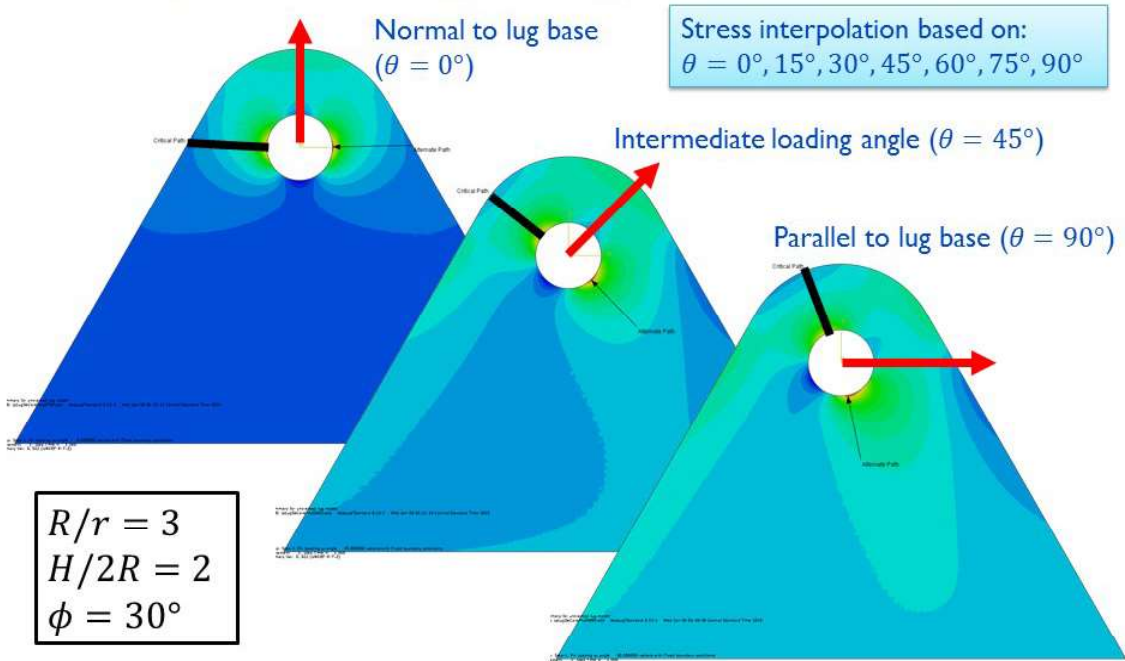


Figure 9.6-44. Oblique Loading Range

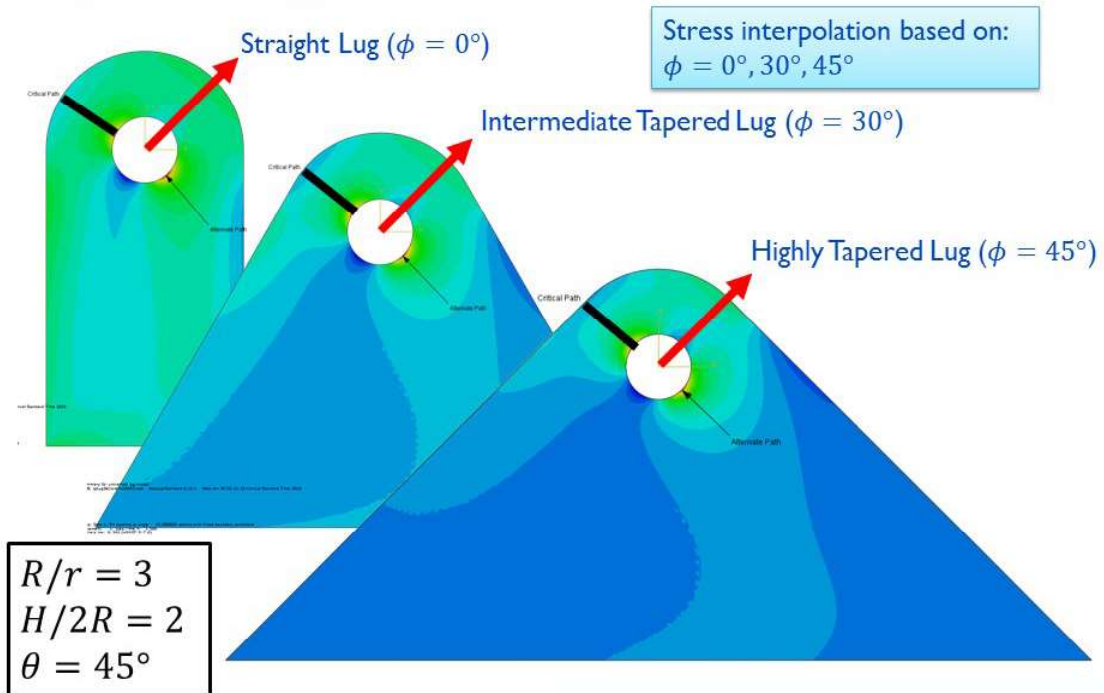


Figure 9.6-45. Taper Range

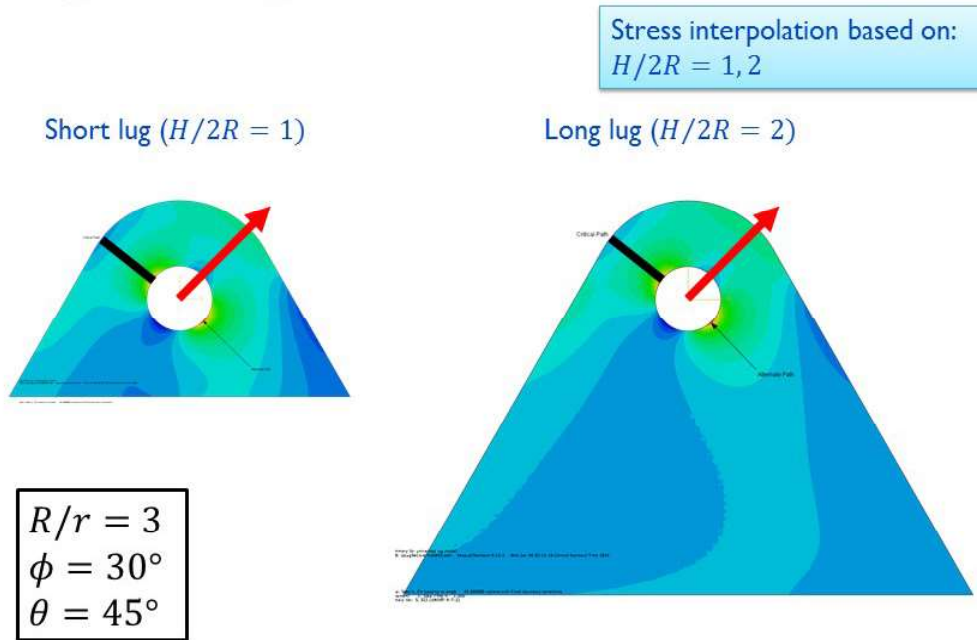
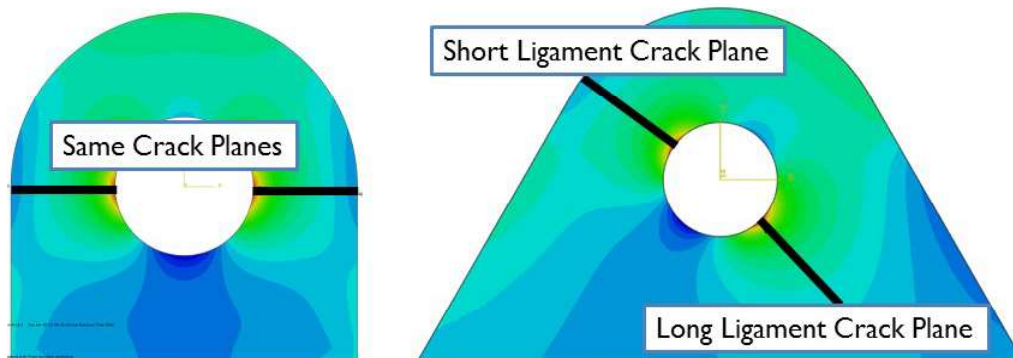


Figure 9.6-46. Height Range



- Previous solutions restrict crack plane to be normal to loading
- Reasonable assumption for straight lugs loaded perpendicular to crack plane
- For tapered and obliquely loaded lugs need a variable crack path location and need to distinguish between two possible paths
- New solutions base crack angle on the maximum opening stress angle and shorter ligament length

Figure 9.6-47. Crack Plane

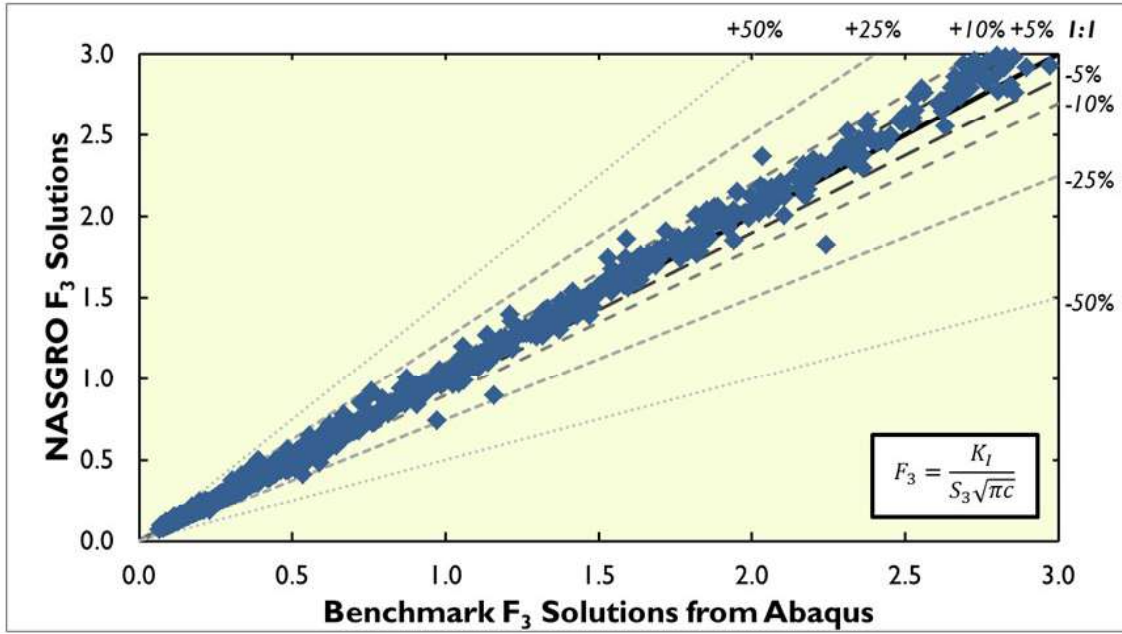


Figure 9.6-48. Through Crack Solutions: TC30 (3/3)

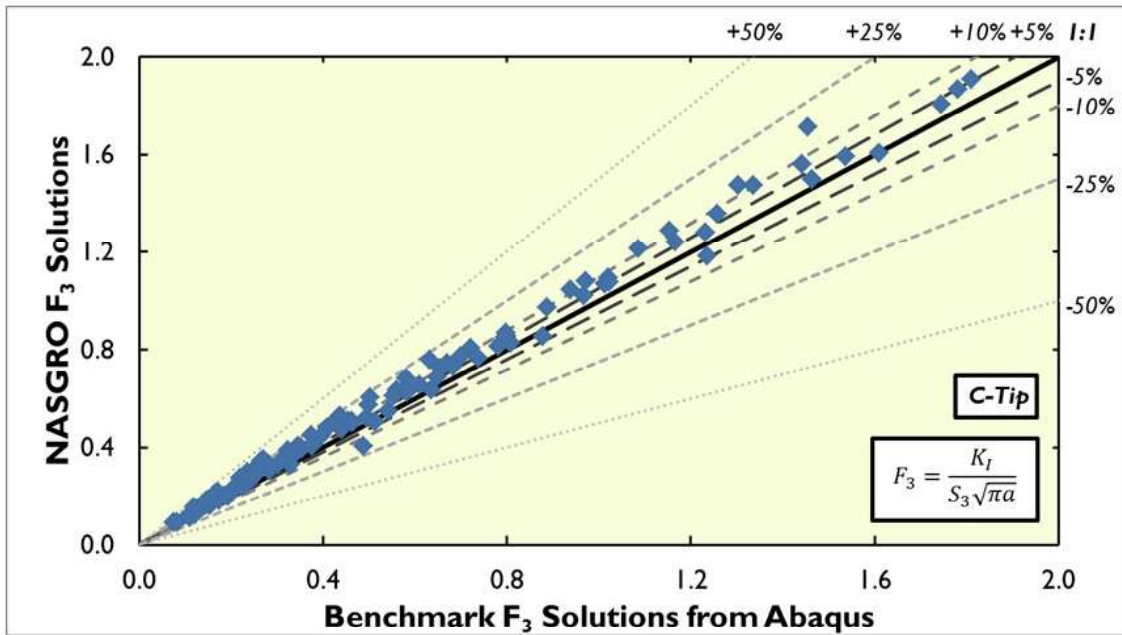


Figure 9.6-49. Corner Crack Solution: CC23 (5/5)

9.6.11. StressCheck + Fracture: Best Practices and Live Demo

Eric Buettmann, ESRD, Inc.

StressCheck v10.2 by ESRD, Inc. is renowned in the aerospace finite element analysis community for extracting high quality stress intensity factors (SIFs) for complex parts and assemblies. This technical activity focuses on the features and capabilities that make StressCheck v10.2 ideally suited for ASIP applications and other challenging damage tolerance projects. Practical FEA examples are demonstrated and crack meshing best practices are discussed to enhance StressCheck productivity. The technical effort emphasizes key post-processing capabilities that enhance the quality and reliability of fracture mechanics analysis results. The following is a break-down of the topics to be explored: 1. Brief overview of StressCheck's fracture mechanics module (Figure 9.6-50) and key features for ASIP analysis tasks; 2. Best practice meshing tips for extracting high quality SIFs (Figure 9.6-51) – benchmark studies; and 3. Example: SIF Analysis of a complex 3D aerospace structural component with non-elliptical cracks in critical regions + contact (Figure 9.6-52).

- SIFs in 2D or 3D
 - Superconvergent contour integral method
 - Through-cracks or corner cracks
- Automatic crack path analysis in 2D
- Energy release rate in 2D or 3D
 - Elastic-plastic or linear materials in 2D
 - Separated J-integral J_I , J_{II} , J_{III} in 3D
 - Cracks at multi-material interfaces
- Arbitrarily-shaped cracks
- Influence of residual stresses
 - K_I via loaded crack face if one residual stress tensor component is known
 - K_I , K_{II} , K_{III} if all residual stress components are known
 - Simulate cold working to produce residual stress input for fracture analysis

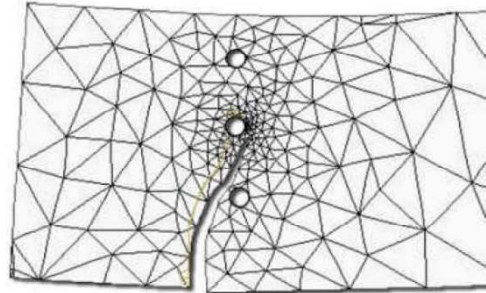


Figure 9.6-50. Fracture Capabilities

- Meshing Tips - 3 considerations when computing SIFs in a 3D cracked body:

- 1. Approximability of the exact solution**

- How can we best converge on the exact solution?

- 2. Element mapping**

- How can we avoid highly distorted elements while still minimizing the number of elements required?

- 3. Path-independence**

- Computation of SIFs by CIM and size of the integration path.

Figure 9.6-51. Best Practices for Fracture Analysis

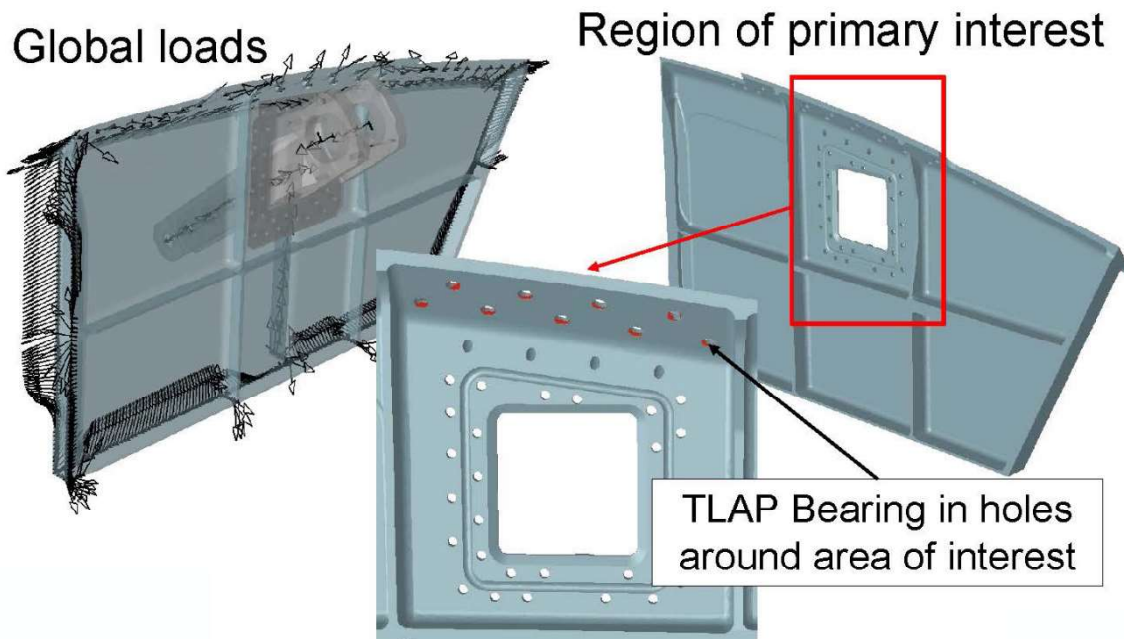


Figure 9.6-52. Problem Description

9.6.12. A-10 Failure Analysis Case Study of High Strength Nuts

Dallen Andrew, John Macha, and Scott Carlson, Southwest Research Institute; Robert Pilarczyk, USAF A-10 ASIP

The United States Air Force experienced failures of three separate zero-time, 220 ksi Inconel 718 nuts, shown in Figure 9.6-53, that were installed on A-10 Thunderbolt II aircraft, also known as the “Warthog” (Figure 9.6-54). A thorough review of the procurement data revealed that all the failed nuts had passed lot tests successfully. This led to concerns that the current procurement test requirements

were insufficient to identify nuts that could unexpectedly fail in service. In order to determine the risk for potential future nut fractures, a novel experimental approach was developed and executed to evaluate the strength and integrity for all 220 ksi Inconel 718 nut manufacturers and sizes utilized on the A-10 aircraft. This technical activity discusses these experiments that were designed to have a combination of shanking and pre-load and push the nuts to extreme limits with the intent of uncovering sub-par capability. An example of a test setup as part of this technical activity is shown in Figure 9.6-55. In addition to these experiments, this technical activity presents the rigorous metallurgical evaluation that was performed to determine if there were any metallurgical anomalies within the fractured and tested nuts.

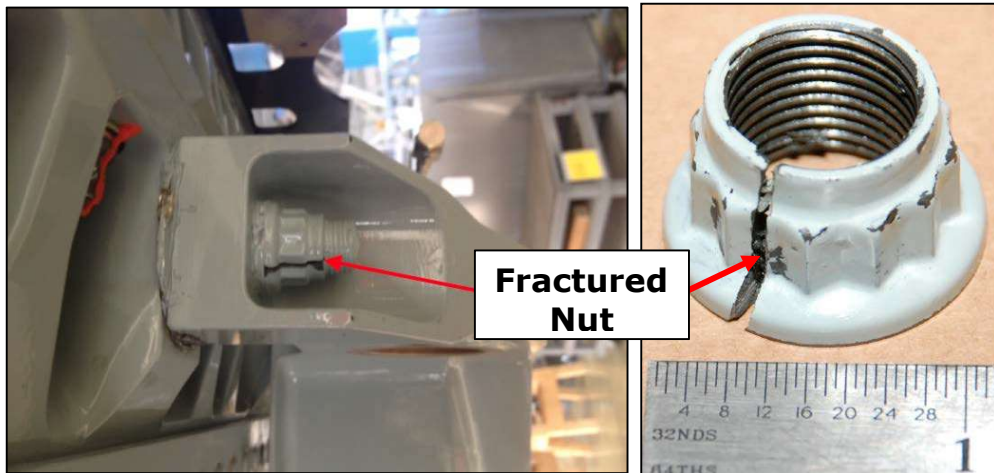


Figure 9.6-53. Examples of Fractured Nuts



Figure 9.6-54. A-10 Thunderbolt II "Warthog"



Figure 9.6-55. Torque Test Setup Example

The novel testing method in this technical activity provided quantitative data (Figure 9.6-56) to determine the impact of the manufacturing process on the performance of the bolt/nut combination and demonstrated that a characterization of the microstructure alone (Figure 9.6-57) may not provide evidence of corresponding nut performance.

Reference:

- [1] Andrew, D., Carlson, S., Macha, J., Pilarczyk, R., “Investigation and interpreting failure analysis of high strength nuts made from nickel-based superalloy”, *Engineering Failure Analysis*, Vol. 74, pg. 35-53, 2017.

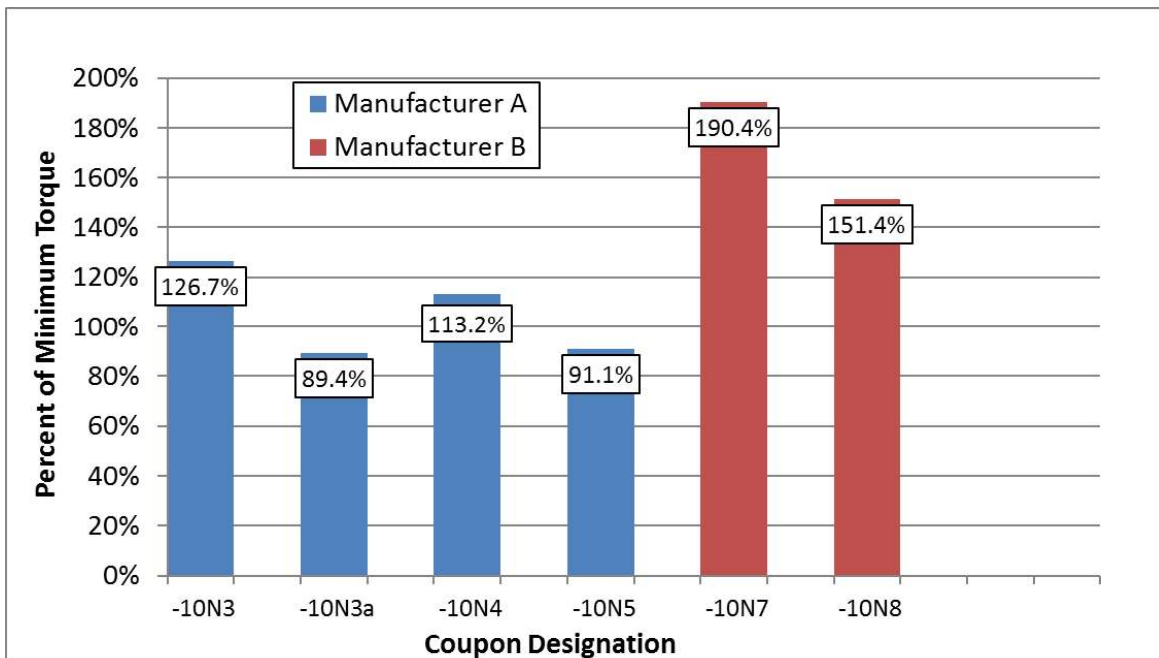


Figure 9.6-56. Percent of Minimum Torque Achieved for 10/16 Inch Size Nuts

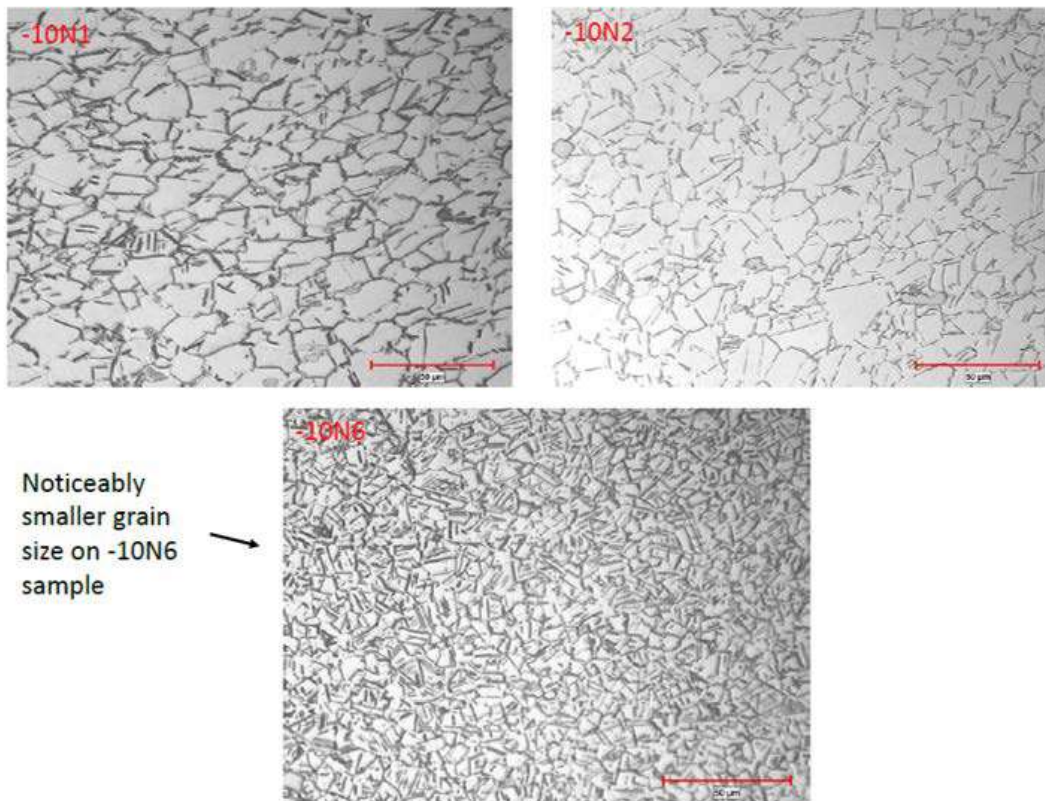


Figure 9.6-57. Nut Microstructure of Corner Region Showing Different Grain Sizes Based on Manufacturer for Three 10/16 Inch Size Nuts

9.6.13. Continued Development of the NASGRO Software for Fracture Mechanics and Fatigue Crack Growth Analysis

Craig McClung, Joseph Cardinal, Yi-Der Lee, James Sobotka, and Vikram Bhamidipati, Southwest Research Institute; Joachim Beek, NASA Johnson Space Center; Venkataraman Shivakumar, Randall Christian, Yajun Guo, and Michael Baldauf, Jacobs Technology, Inc.

The NASGRO® software for fracture mechanics (FM) and fatigue crack growth (FCG) analysis continued to be actively developed and widely used during 2015 and 2016. NASGRO is the standard fracture control software for all NASA Centers and is also used extensively by NASA contractors, the European Space Agency (ESA) and ESA contractors, and FAA Designated Engineering Representatives certified for damage tolerance analysis, as well as many aerospace companies worldwide. NASGRO has been jointly developed by NASA and Southwest Research Institute since 2001, with substantial financial support from NASA, the NASGRO Consortium, and the Federal Aviation Administration (FAA). The NASGRO Consortium concluded its fifth three-year cycle (2013-2016) and began its sixth cycle (2016-2019). The international participants currently include Airbus, Arconic, Blue Origin, Boeing, Bombardier Aerospace, Embraer, GKN Aerospace, Honda Aircraft Engines, Honeywell Aerospace, IHI Corporation, Israel Aerospace Industries, Korea Aerospace Industries, Leonardo, Mitsubishi Aircraft Corporation, Mitsubishi Heavy Industries, Siemens Energy, Sierra Nevada Corporation, Sikorsky, SpaceX, United Launch Alliance, and UTC Aerospace Systems. In addition to Consortium members and

NASA/ESA/FAA users, 115 single-seat and 5 site NASGRO licenses were issued in 2015-2016 to users in 20 countries.

Two new production versions of NASGRO were released in 2015 and 2016. Version 8.0 contained several new SIF solutions including a through crack at an edge (TC25) or internal (TC26) rectangular cutout with rounded corners (Figure 9.6-58). A new option was added to the edge through crack (TC02) model to restrain in-plane bending at the remote end. A new pin loading option was added to the weight function SIF solution for a through crack at a hole (TC13), and an improved finite-width correction factor was implemented for the corner-crack-at-hole solution CC16 under pin loading. Other v8.0 enhancements included an HCF threshold failure criterion, GUI plotting of the Failure Assessment Diagram (FAD) failure criterion, and the ability to input user-supplied SIF solutions as tables of K versus crack size.

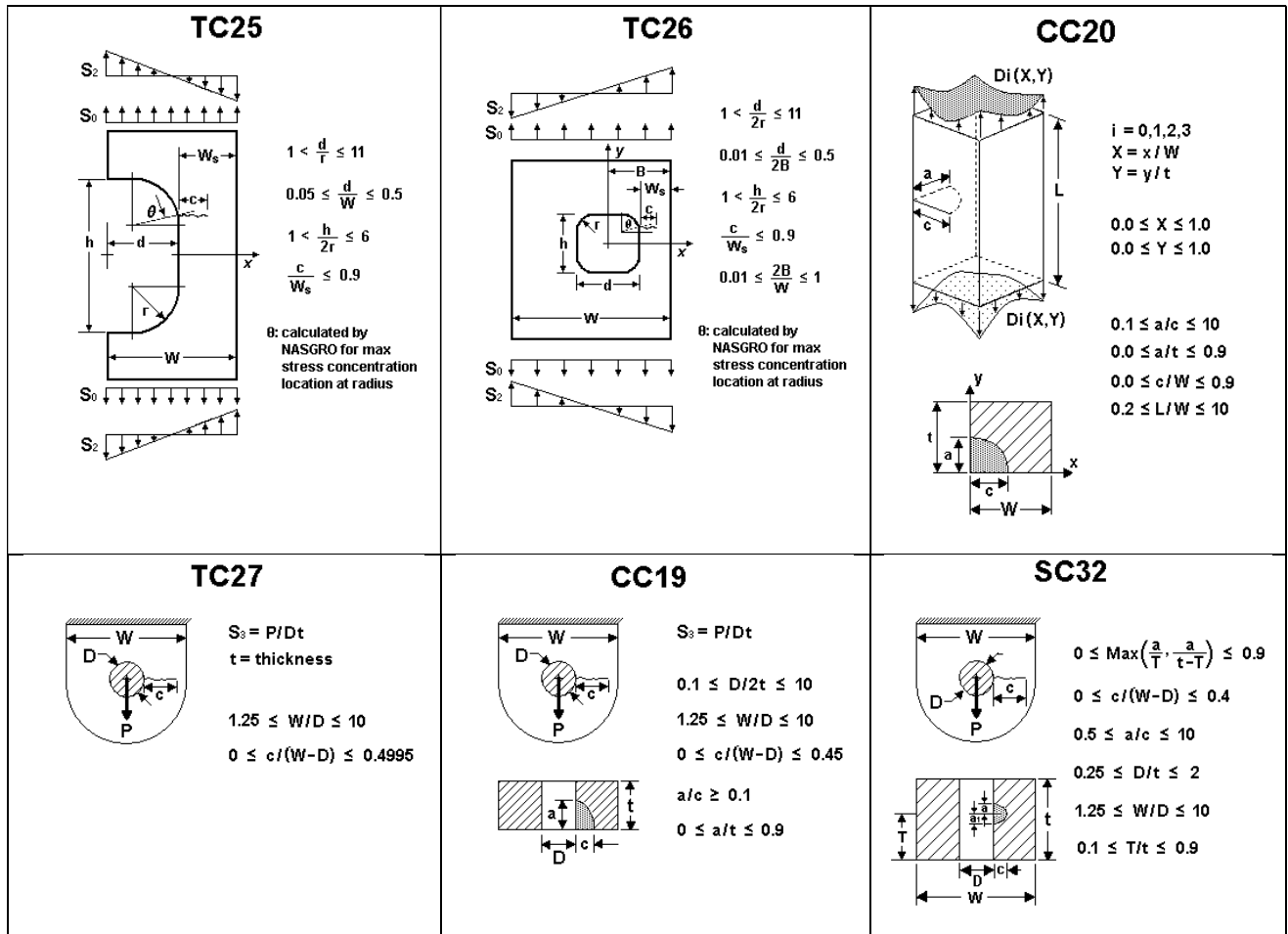


Figure 9.6-58. Selected New Stress Intensity Factor Solutions in NASGRO Versions 8.0 and 8.1

Version 8.1 included completely new SIF solutions for through, corner, or surface cracks in straight lugs (TC27, CC19, SC32) with significantly improved accuracy and expanded geometry ranges compared to legacy solutions. A new SIF solution for a corner crack in a plate under displacement control (CC20) was also added. See again Figure 9.6-58. Direct pin-loading capabilities were added to the weight function crack-at-hole solutions CC08 and SC18, and improved finite-width correction factors were introduced to the SIF solution for two unequal corner cracks at a hole (CC17) under pin loading.

Methods were significantly improved for inverse calculations of initial crack size or stress scale factor given a target life.

Significant progress was achieved on NASGRO 8.2, which was in Beta release at the end of 2016, with Production release anticipated for early 2017. Many new SIF solutions were implemented (see Figure 9.6-59), including a through or corner crack in a tapered lug under oblique loading angles ranging from zero to ninety degrees (TC30, CC23); a corner crack at an external or internal rectangular cutout with rounded corners (CC21, CC22); a curved edge through crack in a plate with a through-thickness stress gradient (TC28); and a through crack in a structural L-section (TC31, TC32). Additional SI units options were introduced for all calculation modes. The ASME FFS/API-579 FAD approach was implemented as a parallel option to the previous FITNET FAD capability.

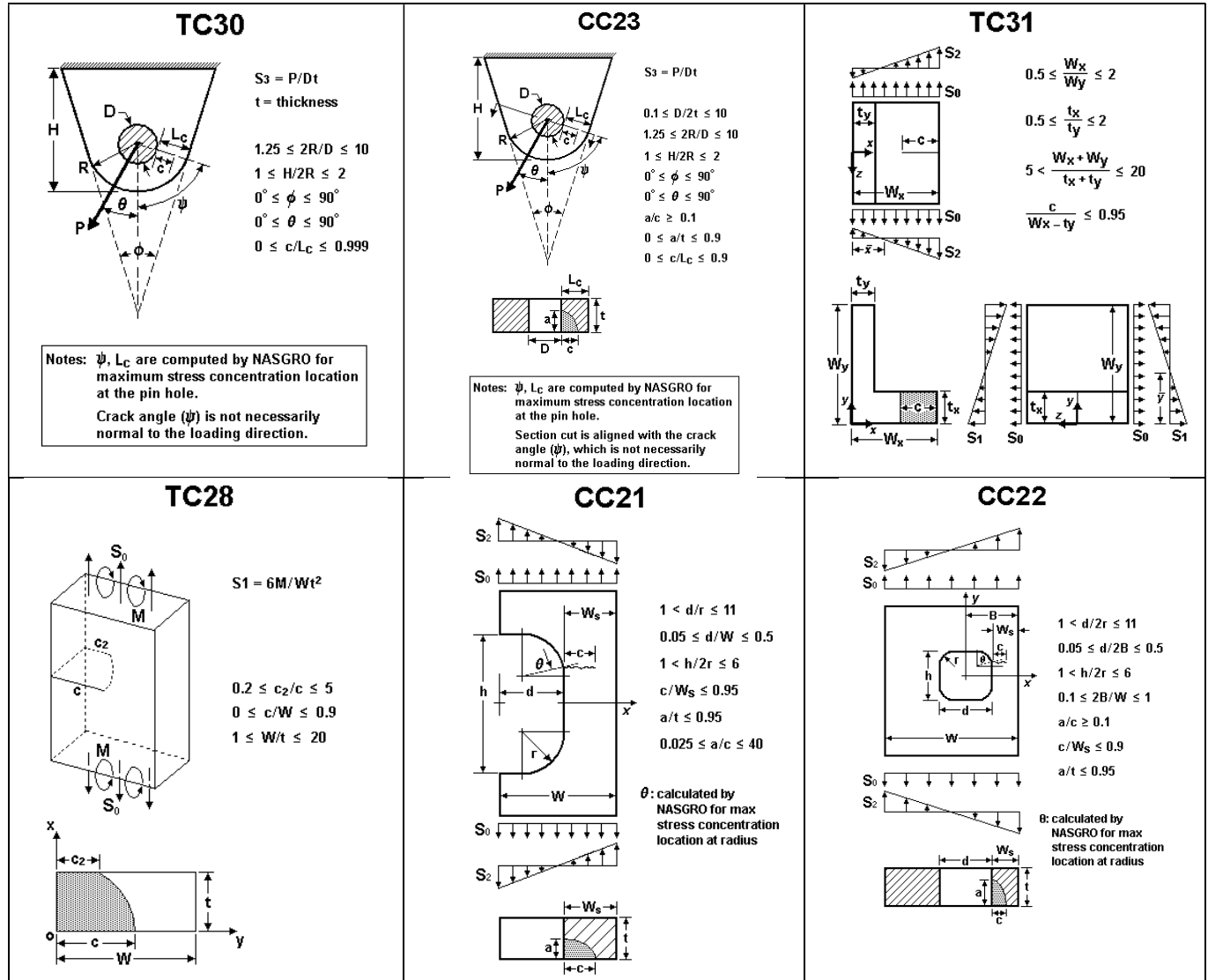


Figure 9.6-59. Selected New Stress Intensity Factor Solutions in NASGRO Version 8.2

Southwest Research Institute has been conducting NASGRO training courses since 2006. During 2015 and 2016, SwRI trained 145 students in 8 courses, including 4 courses in San Antonio, Texas, and 4

courses at remote sites including a major space access company, a Tier 1 aerostructures supplier, and the ESA Technical Center in the Netherlands.

Further information about NASGRO is available at www.nasgro.swri.org.

POC: Craig McClung, Southwest Research Institute, craig.mcclung@swri.org, 1-210-522-2422.

9.6.14. Advances in Boeing Composite Durability Analysis

Saeed Nojavan and Calvin Chen, The Boeing Company – Commercial Airplanes

Composite structures can develop progressive damage caused by cyclic loading, which can emanate from certain types of features in the structure, including joints, small manufacturing defects, or due to environmental effects or impact in service. The challenge with composites tends to be the ability in practice to inspect for and characterize the damage, which affects the manner for which durability is accounted. There are effective nondestructive inspection (NDI) methods capable of detecting most forms of composite damage; however, the cost to implement such inspections is often high. Additionally, composite fatigue and small damage progression analysis methods are not mature enough today to extend to composites for the same kinds of economic life and safety-by-inspection approaches that are traditionally applied to metallic structure.

Fatigue evaluation of composite structures used at Boeing Commercial Airplanes since the NASA 737 horizontal stabilizer demonstrator program in the 1980's, and now including the Boeing 787, has been typically based on the principle of No Detrimental Damage Growth (NDDG). This approach aims to assure no detrimental growth from undetectable defects and damage during the service life of the aircraft with a high reliability and confidence level, as substantiated by fatigue test evidence. Detrimental growth refers to any damage growth leading to the inability to meet load and stiffness requirements, or when the part is no longer capable of performing as intended. This approach considers potential initial defects and impact damage that can occur during manufacturing or while in service that may go undetected by production in-process inspections or in the course of scheduled or directed field inspections while the part is in service. Evaluation methods include:

1. A reliable design service life substantiated by element, subcomponent, or component fatigue testing (a building block approach) is developed for each primary structure component. In the substantiation fatigue tests, a Load Enhancement Factor (LEF) is often applied to reduce the test duration and cost while maintaining the required level of design reliability and confidence. Figure 9.6-60 illustrates the LEF approach along with a life factor approach using a conceptual S-N curve for the component under fatigue test. The test objective is to demonstrate 95 percent reliability with 95 percent confidence design life without any detrimental damage by testing the component under the enhanced load over the test duration, N_{test} .
2. A variation of the NDDG approach is to use a fatigue threshold, a stress or strain level below which negligible fatigue damage accumulates. In this method, the part is sized to the fatigue threshold. The fatigue threshold is adjusted to consider the effects of component size, undetectable damage, environment and other degradation sources. This method incorporates coupon/element tests with analysis. Because the test result is conservatively projected to the component level with the desired level of reliability and confidence, it achieves the design goal as would be demonstrated through component fatigue substantiation testing.

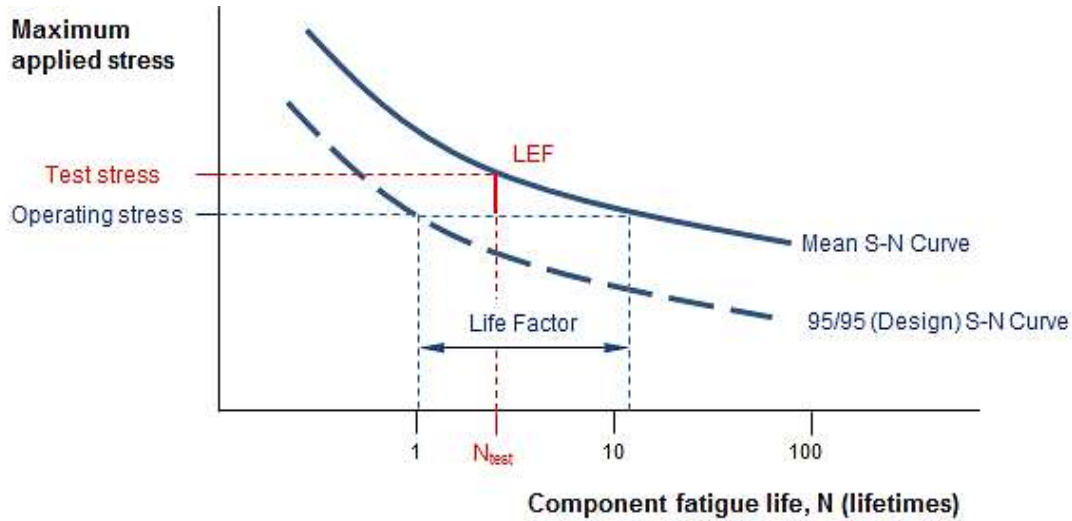


Figure 9.6-60. Component Fatigue Life (N) vs. Maximum Applied Stress (S)

The NDDG design approach in general results in a conservative airframe design with substantially reduced inspection and maintenance requirements. In order to reduce the large amount of fatigue tests in the NDDG approach, more emphasis is being placed on developing reliable numerical simulations of damage progression in composite structures under fatigue loading. While the prediction methods for interlaminar failure modes (delamination) are considered relatively mature, methods for in-plane damage prediction still need more work due to complex failure mechanisms, such as fiber breakage, matrix cracking, matrix crazing, fiber buckling, fiber-matrix interface failure, fiber pull-out, etc.

9.6.15. Revised Approach for Efficient Surface Crack Analysis

Zachary Whitman, The Boeing Company – Commercial Airplanes; Gregory Cass, The Boeing Company – Engineering Operations & Technology

A common approach to simplify crack growth analysis is to track and calculate crack extension in one direction only. For a part-through surface crack there are two critical directions to monitor; i.e., surface length, and depth (Figure 9.6-61). Typical simplified approaches are based on crack growth in either the surface (2c) or depth (a) direction using a fixed, constant aspect ratio crack chosen prior.

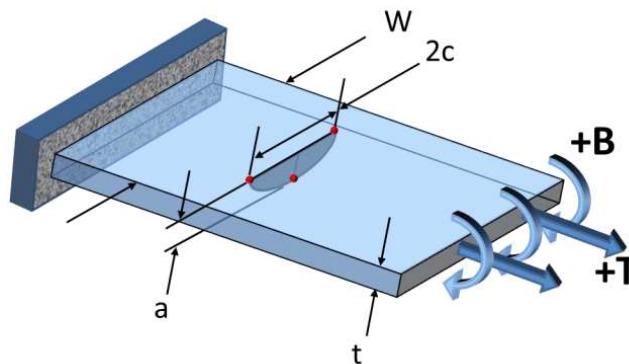


Figure 9.6-61. Depiction of a Surface Crack

A review of test and fleet data showed that a predefined, variable crack aspect ratio could be set as a function of two ratios: The ratio of the bending (B) and tension (T) stress, and the ratio of the crack depth and thickness. Even cracks starting at an unnatural aspect ratio will grow disproportionately until they conform to the basic trend as shown in Figure 9.6-62.

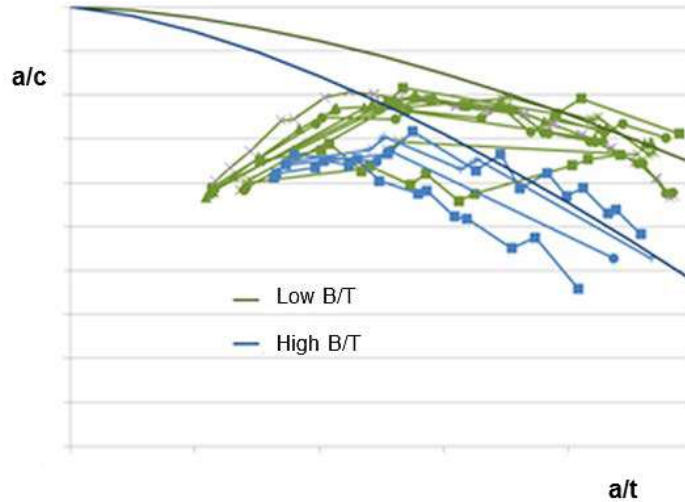


Figure 9.6-62. Aspect Ratio of Multiple Test Specimens and the Forced Aspect Ratio From the Revised Approach

The new approach was designed such that the crack aspect ratio is controlled using a mathematical function that emulates the collected data. This retains the simplicity of tracking a single crack direction while increasing the crack growth curve accuracy by closely matching the typical variation in the aspect ratio as shown in Figure 9.6-63. It also improves the accuracy of the calculated surface crack length when the crack breaks through to the opposite surface. This can have an impact on which type of inspection is performed. The new approach also eliminates variation in the assumed crack aspect ratio, which provides conformity and repeatability across many analysts.

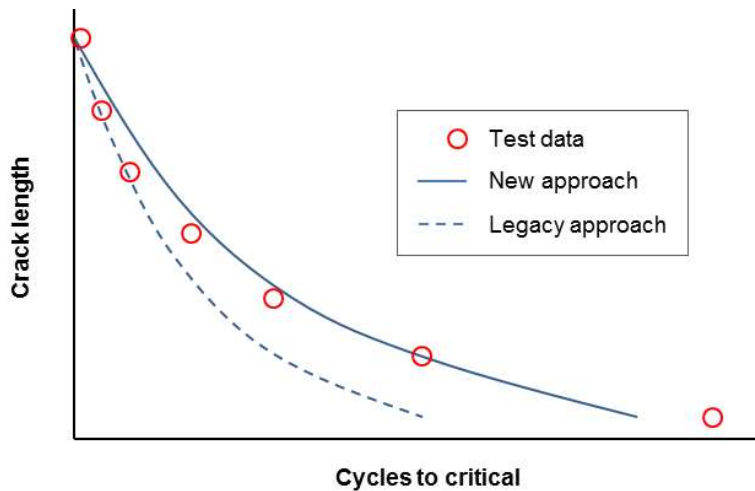


Figure 9.6-63. Cycles to Critical Crack Length for a Specimen Comparing the New Approach Against the Legacy Method

9.6.16. Fatigue and Damage Tolerance of Tension Fittings

Brandon Chapman and Gerald D. Gute, The Boeing Company – Commercial Airplanes

Tension fittings have numerous applications in aircraft primary structures (e.g., side-of-body terminal fittings, wing strut attachment fittings, flap support structure, nacelle attachments, and fin-to-body joint connections). A conventional structural analysis of tension fittings can be difficult to achieve with reasonable accuracy because the state of stress is generally very complex. Improved fatigue and damage tolerance analysis methods are needed to allow more structurally-efficient designs and to keep pace with recent trends toward lighter gage fittings that are typical of integral structures.

Boeing has been actively engaged in the testing and analysis of aluminum tension (“bathtub” channel and angle) fittings (Figure 9.6-64). The objective of this study was to obtain data to support the development and validation of new fatigue and damage tolerance analysis methods. Fifty aluminum fittings, consisting of both channel and angle geometries, spanning a typical design range were fabricated and tested in the laboratory. The specimens were loaded cyclically until fatigue cracking occurred. In a follow-up study, the fatigue crack flaws were characterized and the specimens were then monotonically loaded to determine the failure mode and the residual strength capability of each fitting configuration.

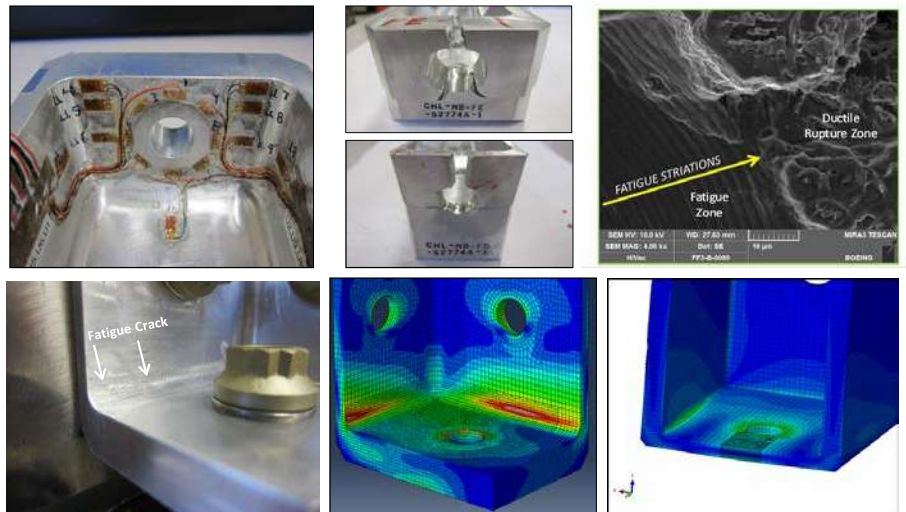


Figure 9.6-64. Fatigue and Residual Strength Testing and Analysis of Tension Fittings

To determine the distribution of stress around the end pad fastener hole, a subset of the specimens were instrumented for strain surveys. In addition, one channel fitting specimen was far-field imaged using the Digital Image Correlation (DIC) technique, which provided valuable quantitative information about the in-plane strains and out-of-plane deformations. These data have been used to validate the finite element (FE) modeling procedure being used to approximate the response of these types of fittings to various loading and boundary conditions. Excellent agreement between the results obtained from the FE models and the strain surveys has been demonstrated. An automatic FE model generator for the bathtub type fittings was recently completed. Current efforts are focused on expanding the capability of the automatic FE model generator to include the meshing of multiple distinct crack scenarios with varying crack front profiles, including linear, circular, and elliptical crack fronts.

9.6.17. Cost and Flow Reduction via “Smarter Testing” and Improved Analysis Methods

Amlan Duttchoudhury, Eric Sager, and Steven Chisholm, The Boeing Company – Commercial Airplanes

Structural testing is required as part of the Boeing Commercial Airplanes (BCA) certification approach – i.e., use of analysis methods validated by test evidence. Various types or levels of testing exist in the building block pyramid rubric (Figure 9.6-65), beginning with small coupon tests for foundational material property evaluation at or before the start of a program, moving to design detail evaluation and analysis method validation with mid-level element and sub-component parts, finally culminating with component and full-scale tests for high fidelity loads and analysis method verification. Many validated analysis methods are available for various types of metallic and composite aircraft structure within BCA, but most of these are not fully general and have only been validated within specific areas of a design space. New materials, architectures, or regions of the design space necessitate additional method validation and expansion via test. This need typically results in testing at the mid to lower levels of the building block pyramid, in which various sub-component and structural element tests are carried out for development of structural design values. Very large costs (more than 50%, typically) and long flow times are associated with this middle region of the pyramid; validating methods or design data in this domain is risky since the tests are relatively complex, and require a relatively mature production system – both of which lead to results coming later in the development cycle. Surprises late in an airplane development program are not welcome guests!

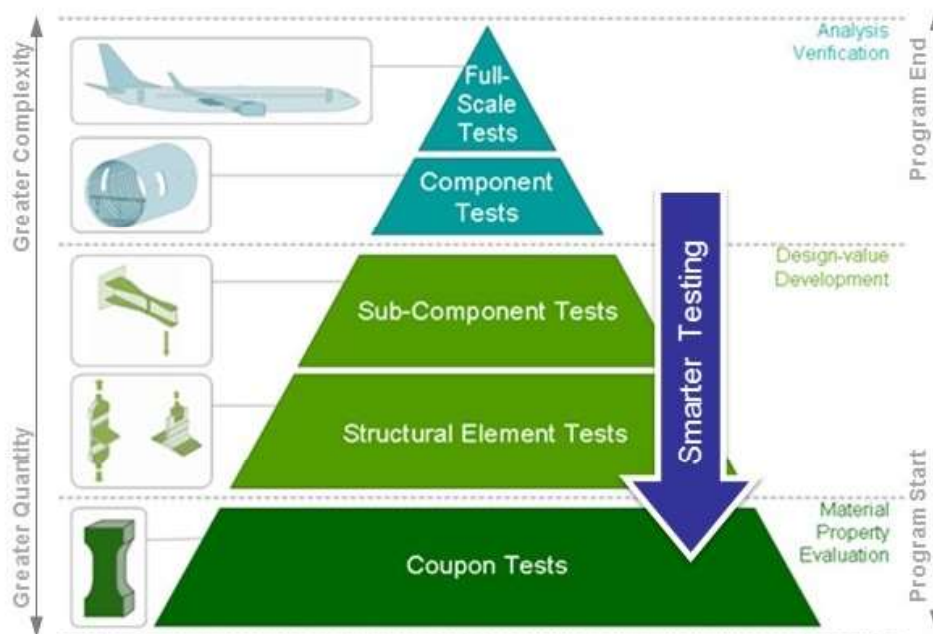


Figure 9.6-65. Structural Testing Pyramid

BCA Structures Engineering has developed a multi-year initiative that aims to standardize and simplify testing associated with methods and design values. Use of advanced analysis techniques using fundamental (coupon-derived) inputs and/or expanding existing standardized analysis methods using centralized “Core” engineering guidance can lead to reduced quantities of program-led mid-level structural tests, reducing Airplane Development costs and risks. The approach is referred to as “smarter testing.” Testing developed using the smarter testing approach is by definition less scattershot, more directed and timely, more cost effective, and therefore more valuable to BCA.

Smarter testing is built around some or all of the following key ideas and approaches:

- Better test goals definition
- Virtual testing precedes physical tests
- Analysis-enhanced test point allocation across the design space to target specific failure modes after appropriate analyses (less of a “shotgun” approach)
- Better test planning and execution; disciplined application of Design of Experiments (DOE) to reduce matrix sizes and focus on the important parameters
- Replacement of complex sub-component tests by element or coupon tests while keeping the failure mode the same; establishing the linkages between the various analysis scales
- Active test program control. The testing scope/sequence/goals are re-evaluated at every stage with analysis of the previous stage results.
- Data mining and standardization for future re-use

The fundamental set of ideas is to leverage advancing predictive abilities, reduce “brute force” testing and to go into remaining testing better informed, while using standard test approaches where possible. Smarter testing aims to decrease test expenses, increase test execution speed, and maintain the scope and accuracy of the experimental demonstration of method accuracy and efficacy. This approach also moves the high risk tests to earlier phases of development, de-risking the tests that remain. As mentioned, surprises in tests can lead to late design changes that are difficult to react to, and may require additional validation tests with associated schedule and budget challenges.

As part of this initiative, BCA Structures Engineering has brought together technology, tools and experience to form a “Blue Streak” Structural Test (BSST) protocol, which is a multi-disciplinary approach for quick and inexpensive tests conducted early in an airplane development cycle. BSST provides a streamlined path for execution, with much less overhead, saving time and money and decreasing the time required to traverse the spiral learning loop. Multiple successes have been realized to date and more projects are planned.

Composite structures present some unique analytical challenges and BCA has laid out a road map for continuing analysis method development (Figure 9.6-66) in the areas of stability, bolted joint, damage mechanics and residual strength evaluation. The strategy is to first mature traditional modeling approaches (e.g., Point Stress Failure criteria) for significant gains in cost reduction, followed by the use of failure-mechanism-based approaches (e.g., Peridynamics, Enhanced-Schapery-Theory) for further reductions.

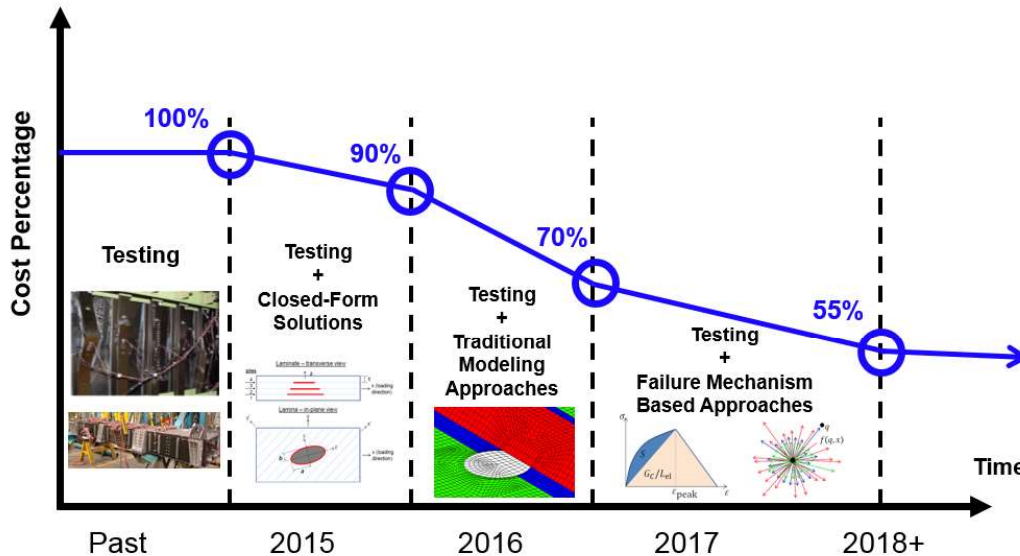


Figure 9.6-66. Analysis Methods Road Map for Composite Structures

9.6.18. Smarter Testing for Metallic Structures

Maheash Chengalva, The Boeing Company – Commercial Airplanes

Smarter testing is the reduction of physical testing to the absolute minimum possible, guided by intelligent decisions driven by proven analytical methods. At Boeing, smarter testing has moved from a concept to widespread application in a matter of a few years for metallic airframe components such as fittings and lugs. This has resulted in a highly significant reduction in the volume of testing. The key enabler for smarter testing is the capability of virtual testing, wherein a physical test is replicated via computer simulations (illustrated in Figures 9.6-67 and 9.6-68). This in turn requires an analysis methodology that is highly versatile, accurate, reliable and capable of rapidly analyzing configurations of interest.

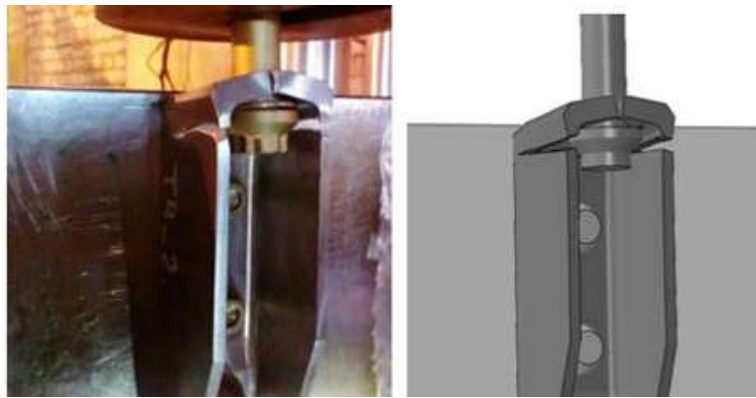


Figure 9.6-67. Virtual Testing of a Bathtub Fitting, Comparing Failure Mode Prediction with Test Results

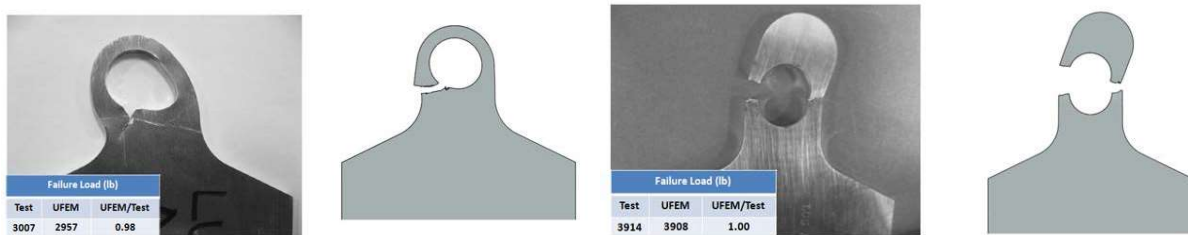


Figure 9.6-68. Virtual Testing of Airplane Lugs, Comparing Failure Mode Prediction with Test Results

To enable smarter testing for metallic structure, a FEM-based methodology has been developed at Boeing Commercial Airplanes, which involves internally developed material behavior and failure criteria. Static failure initiation and propagation are predicted directly from a Strength-of-Materials approach, without the need for fracture properties. It is implemented using Explicit FEM with Boeing-proprietary material subroutines that utilize only fundamental coupon level properties obtainable from basic uniaxial tests. Known as UFEM (User-material defined Finite Element Method), these methods are now in production usage at Boeing.

In addition to matching the failure mode, another Boeing requirement is that the predicted ultimate strength of the component be within 10% of the corresponding test. The UFEM approach meets this requirement, as shown in Figure 9.6-69 where the predicted strength is compared with the corresponding test value for a set of over 30 lugs across the design space, loaded both axially and transversely. In this plot, a value of 1.0 indicates perfect correlation.

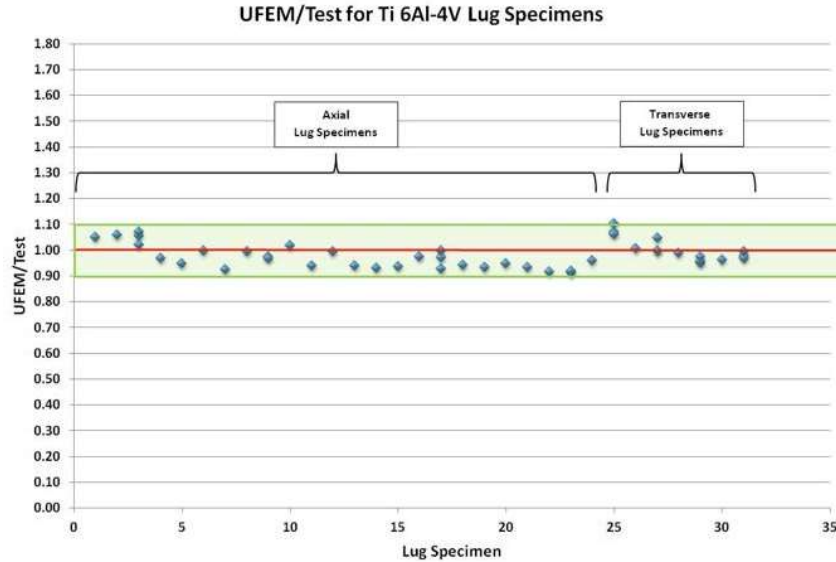


Figure 9.6-69. Comparison of Predicted versus Measured Strength of Various Lug Specimens

It should be noted that although UFEM predicts material behavior across the linear, nonlinear and plastic realms, along with failure propagation required for obtaining Figure 9.6-69, the only input required by UFEM are three sets of uniaxial tensile and compressive curves, one each along the L, LT and ST direction. Moreover, all results are verified for solution convergence due to mesh refinement. Only the converged solution results are reported with UFEM, as in Figure 9.6-69. The implications of this fact are that UFEM results are user-independent provided solution convergence due to mesh refinement is verified by the user.

Another key enabler of rapid virtual testing is the creation of parametric modeling tools for various component types such as lugs, bathtub fittings, angle clips and other structural parts commonly used in aircraft. With the implementation of these parametric modelers coupled with UFEM, it is possible for engineering customers to rapidly evaluate design changes in a matter of hours. This is currently being done at Boeing. The benefits go well beyond reduction of physical testing – the unprecedented value of knowledge generated by the parametric modeling approach has been instrumental in pushing the design space to a level that has been hitherto unattainable by evaluations based on physical testing.

Following the development and validation of these new structural analysis methods at the component level, significant progress has been made in the next logical step in the sequence, which is the application at the aircraft sub-assembly level. Figure 9.6-70 shows one such structure that has been analyzed consisting of an assembly of four bathtub fittings and the surrounding structure in a recent Boeing airplane design. Multiple virtual tests were conducted including a residual strength analysis wherein one of the two tension bolts in Figure 9.6-70 was removed. A similar evaluation is shown for a landing gear component in Figure 9.6-71. In both cases, in addition to residual strength, the propagation of failure through the structure is also a key component of the output of the virtual test.

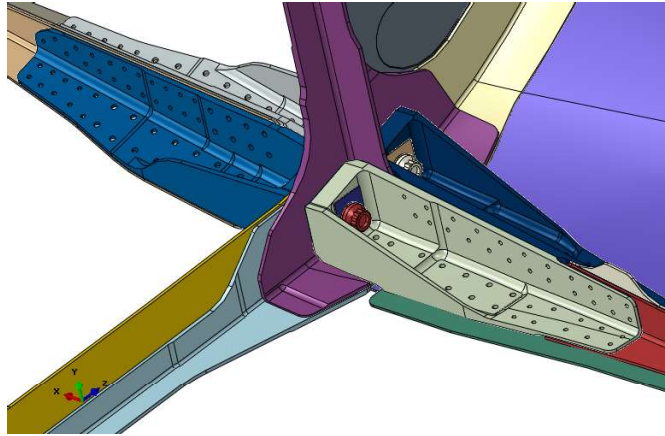


Figure 9.6-70. Aircraft Sub-Assembly Modeled with UFEM for Residual Strength Analysis

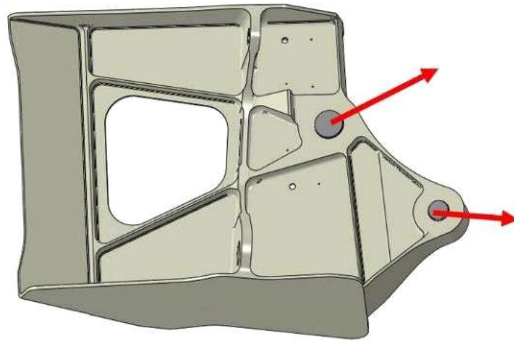


Figure 9.6-71. Landing Gear Component Evaluation with UFEM for Various Aircraft Load Cases

In conclusion, the realm of virtual testing at Boeing is gradually expanding into ever larger domains of structure. Because UFEM only requires basic material properties as input, it is scalable to a structure of any size. The only restriction is the available computing power, which has been exponentially increasing with time thanks to Moore’s law. The future of virtual testing is highly promising – having already delivered smarter testing at the component level, in the decade to come it would make a significant reduction in airplane development costs while at the same time improving performance.

9.6.19. Metallic Materials Properties Development and Standardization (MMPDS)

Jim Kabbara, FAA – Aircraft Certification Service; Mark Friesthler and Ian Won, FAA – Transport Airplane Directorate; John Bakuckas, Jr., FAA – William J. Hughes Technical Center; Jana Rubadue, Battelle Memorial Laboratories

The Metallic Materials Properties Development and Standardization (MMPDS) is an effort led by the FAA to continue the Handbook process “Metallic Materials and Elements for Aerospace Vehicle Structures” (MIL-HDBK-5). The Handbook is recognized worldwide as the most reliable source for verified design allowables needed for metallic materials, fasteners, and joints used in the design and

maintenance of aircraft and space vehicles. Consistent and reliable methods are used to collect, analyze, and present statistically-based aircraft and aerospace material and fastener properties.

The objective of the MMPDS is to maintain and improve the standardized process for establishing statistically-based allowables that comply with the regulations, which is consistent with the MIL-HDBK-5 heritage, by obtaining more equitable and sustainable funding sources. This includes support from government agencies in the Government Steering Group (GSG), from industry stakeholders in the Industry Steering Group (ISG), and from profits from Handbook and derivative products sales.

Towards this goal, the commercial version of the MMPDS-11 was released in April 2016 (Figure 9.6-72). Significant changes to the Handbook include the addition of five new metallic alloys, updated properties for six alloys, updated guidelines and requirements for fastener allowables, and new guidelines for material specification requirements. In addition, equitable and sustainable funding sources were secured in FY15, at which time 60%–70% was funded by the ISG and GSG, and 10% was funded from commercialization efforts.

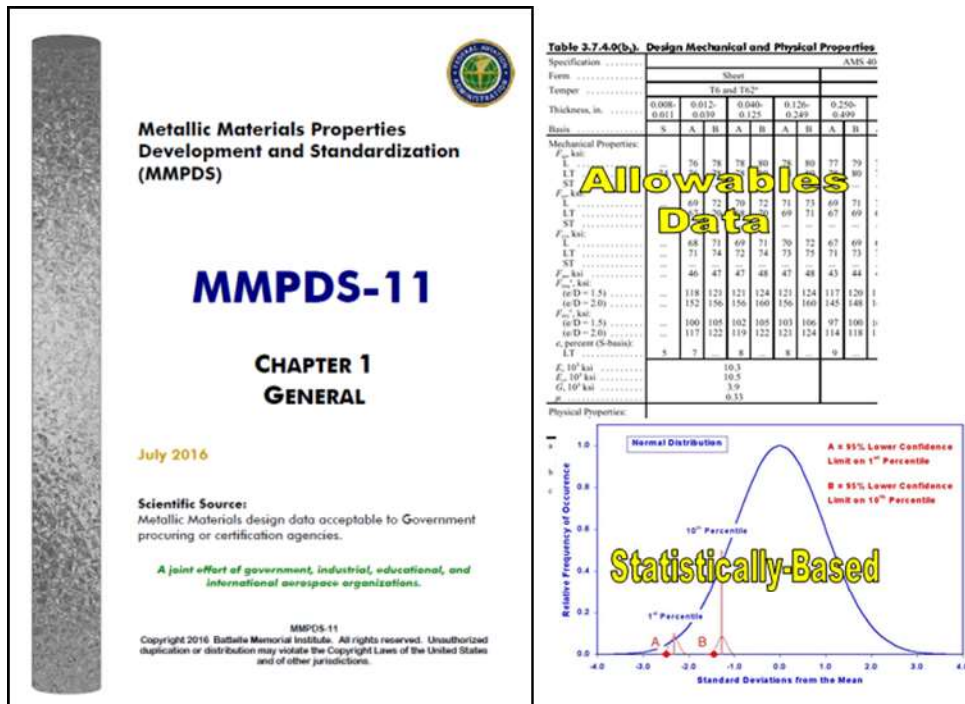


Figure 9.6-72. Cover of MMPDS-11

9.6.20. Methodology for Evaluating High-Temperature CMAS (Calcium-Magnesium-Aluminosilicate) Attack of Protective Coating Materials

Valerie Wiesner, Narottam Bansal, Bryan Harder, Gustavo Costa, and Dongming Zhu, NASA Glenn Research Center – Materials and Structures Division

Ceramic matrix composites (CMCs) are an attractive replacement for current metal-based parts used specifically in the hot section of air-breathing turbine engines in order to improve efficiency, due to the lower density and higher temperature capabilities of CMCs. Because silicon-based CMCs are susceptible to oxidation and corrosion in the harsh combustion environment encountered in turbine engines [1], environmental barrier coatings (EBCs) are being developed to protect CMCs. In addition to remaining stable in oxidizing environments, EBC material requirements include possessing low reactivity

with water vapor and a coefficient of thermal expansion (CTE) comparable to the underlying CMC [2, 3]. Ingested particulates, such as sand, volcanic ash and runway debris, pose a significant design hurdle in the development of robust protective coatings. When ingested by a turbine engine, the particulates melt at temperatures $\sim 2200^\circ\text{F}$ into glassy deposits with compositions loosely corresponding to calcium-magnesium-aluminosilicate (CMAS). Molten CMAS may chemically interact with and/or infiltrate pores of protective coatings and may deposit on the surfaces of various engine components adversely affecting the performance and life of the engine. NASA technical activities center on evaluating CMAS degradation mechanisms of EBCs in order to develop coatings resistant to CMAS attack for future air-breathing turbine engine applications.

Recent NASA CMAS-related efforts have focused on characterizing the properties, including mechanical and thermal [4, 5], as well as crystallization behavior [6], of CMAS glasses prepared from sand and synthetic mineral mixtures relevant to aviation to better understand CMAS interactions with protective coatings. For example, the CTE of a sand glass was found to be double that of leading EBC materials, suggesting that the CTE mismatch between CMAS and EBCs may hinder a CMAS-infiltrated coating's ability to accommodate residual stresses upon cyclical heating and cooling leading to coating spallation. The temperature-dependent viscosity of a synthetic sand glass was also experimentally measured to compare with three composition-based glass viscosity prediction methods [7]. Although none of the models precisely predicted the sand glass viscosity, two models were identified as more suitable viscosity models to aid in understanding CMAS infiltration of EBCs at temperatures relevant to aviation.

Other CMAS efforts have involved evaluating the high-temperature thermochemical interactions of CMAS with advanced EBC compositions. Building upon a previous investigation of a candidate EBC material of yttrium disilicate ($\text{Y}_2\text{Si}_2\text{O}_7$) [8], nominally dense $\text{Y}_2\text{Si}_2\text{O}_7$ substrates were exposed to CMAS, as well as pellet mixtures of $\text{Y}_2\text{Si}_2\text{O}_7$ and CMAS, $>2200^\circ\text{F}$ for various durations. The resulting thermochemical interactions were observed to follow a dissolution-reprecipitation mechanism such that yttrium was dissolved into the CMAS glass and mostly reprecipitated as an alternate $\text{Ca}_2\text{Y}_8(\text{SiO}_4)_6\text{O}_2$ oxyapatite silicate phase. To characterize CMAS effects on EBCs under conditions more representative of those in an engine, a laser high heat flux high cycle fatigue test rig (shown in Figure 9.6-73 and 9.6-74) and a laser high heat flux creep rupture test rig (refer to Figure 9.6-75) for longer durability testing have been utilized [9]. Ongoing work involves screening and identifying EBC materials resistant to CMAS attack to fully enable CMC technologies in next-generation air-breathing turbine engines.

References:

- [1] N.S. Jacobson, E.J. Opila, K.N. Lee, Oxidation and corrosion of ceramics and ceramic matrix composites, *Current Opinion in Solid State and Materials Science*, 5 (2001) 301-309.
- [2] K.N. Lee, Environmental Barrier Coatings for SiCf/SiC, in: N.P. Bansal, J. Lamon (Eds.) *Ceramic Matrix Composites: Materials, Modeling and Technology*, John Wiley and Sons, Hoboken, NJ, 2014, pp. 430-451.
- [3] C.G. Levi, Emerging materials and processes for thermal barrier systems, *Current Opinion in Solid State and Materials Science*, 8 (2004) 77-91.
- [4] V.L. Wiesner, N.P. Bansal, Mechanical and thermal properties of calcium-magnesium aluminosilicate (CMAS) glass, *Journal of the European Ceramic Society*, 35 (2015) 2907-2914.
- [5] N.P. Bansal, S.R. Choi, Properties of CMAS glass from desert sand, *Ceramics International*, 41 (2015) 3901-3909.
- [6] V.L. Wiesner, N.P. Bansal, Crystallization kinetics of calcium-magnesium aluminosilicate (CMAS) glass, *Surface and Coatings Technology*, 259, Part C (2014) 608-615.
- [7] V.L. Wiesner, U.K. Vempati, N.P. Bansal, High temperature viscosity of calcium-magnesium-aluminosilicate glass from synthetic sand, *Scripta Materialia*, 124 (2016) 189-192.
- [8] N.L. Ahlborg, D. Zhu, Calcium-magnesium aluminosilicate (CMAS) reactions and degradation mechanisms of advanced environmental barrier coatings, *Surface and Coatings Technology*, 237 (2013) 79-87.

- [9] D. Zhu, Advanced Environmental Barrier Coatings for SiC/SiC Ceramic Matrix Composite Turbine Components, in: T. Ohji, M. Singh (Eds.) Engineered Ceramics: Current Status and Future Prospects, Wiley2016.

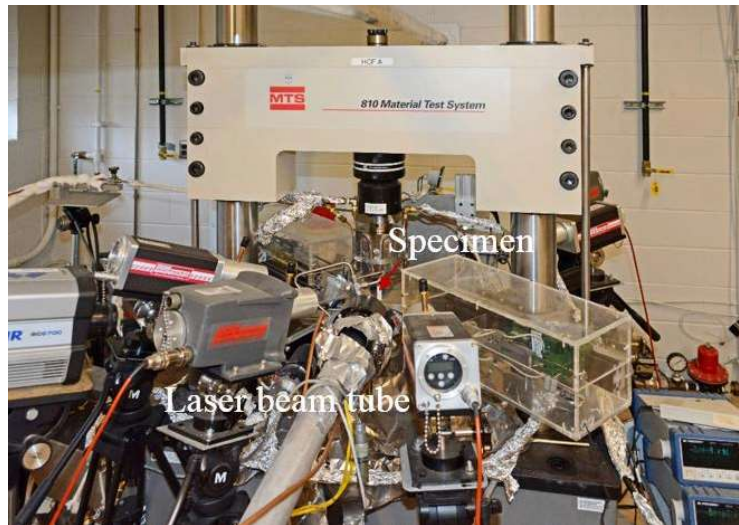


Figure 9.6-73. Laser High Cycle Fatigue (HCF) Test Rig Showing Extensometers and Various Temperature Measurement Instrumentation



Figure 9.6-74. An EBC-Coated SiC/SiC Specimen Under High Heat Flux Fatigue Testing in Steam and CMAS Exposure Conditions

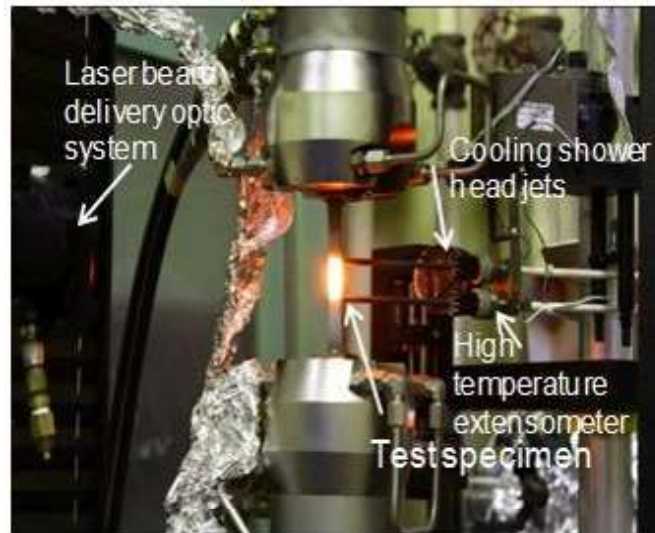


Figure 9.6-75. Laser Heat Flux Creep Rupture Test Rig Showing a Specimen Under Testing

9.6.21. Investigation of the Correlation Between Surface Topology Changes and Fatigue Crack Propagation

Randall Kelton, Jalal Fathi Sola, Efstathios Meletis, and Haiying Huang, University of Texas at Arlington

Changes in surface morphology have long been thought to be associated with crack propagation in materials. In this project, we are studying the changes in the surface profile of the crack-tip plastic zone with an attempt to understand the relationship between the plasticity-induced surface profile changes and the crack growth behavior. The experiment setup for performing fatigue tests and high-resolution surface profiling is shown in Figure 9.6-76. A mechanical tester that is capable of performing fatigue tests at up to 200 Hz is integrated with a scanning whitelight interferometer (WLI) microscope for measuring high resolution surface profile changes. A center crack specimen was designed based on ASTM standard E647 and machined from Nickel 200. The specimen was electropolished and etched to reveal the grain structure before fatigue testing. After growing the crack to a predetermined pre-crack length, an observation zone was selected to be outside of the plastic zone of the pre-crack, as indicated by the square in Figure 9.6-77(a). Fatigue testing was conducted at constant nominal K and ΔK with surface measurements performed every 200 cycles. The test was conducted over 400,000 cycles, growing the crack approximately 0.17 mm into the observation zone. The surface profile image of the specimen around the crack is shown in Figure 9.6-77(b). We observed that the crack growth rate is not uniform at the microscopic scale; the crack growth was retarded at crack arresting points and the crack grew at a fast rate when it propagates between the arresting points. Large changes in the surface profile of the crack-tip plastic zone were found when the crack was arrested and little surface roughness changes were created as the crack tip advanced. An imaging processing algorithm was developed to evaluate the changes of the surface profile at different fatigue cycles. We discovered that the crack path can be predicted based on the surface profile changes of the crack-tip plastic zone, as shown in Figure 9.6-78.

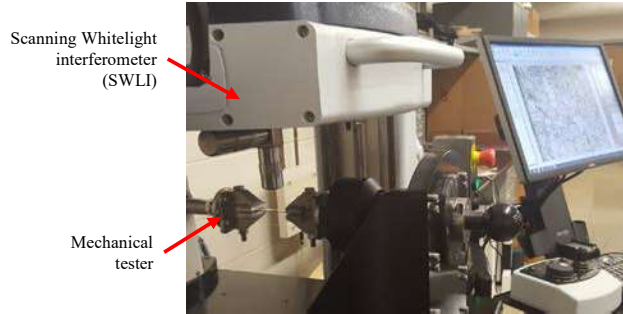


Figure 9.6-76. Fatigue Test with High Resolution Surface Profiling Capability

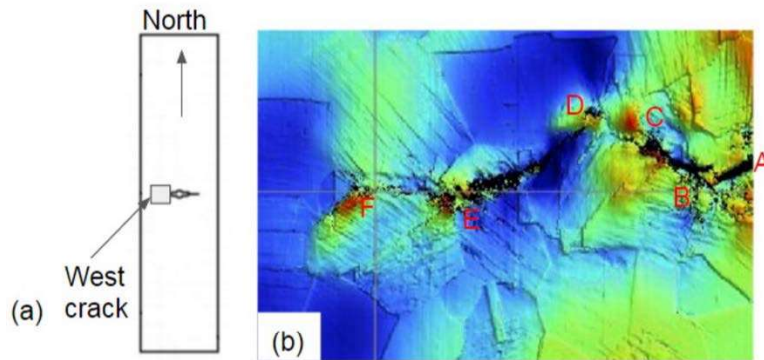


Figure 9.6-77. (a) Fatigue Specimen and the Location of the Imaged Area; (b) Surface Profile Image of the West Crack

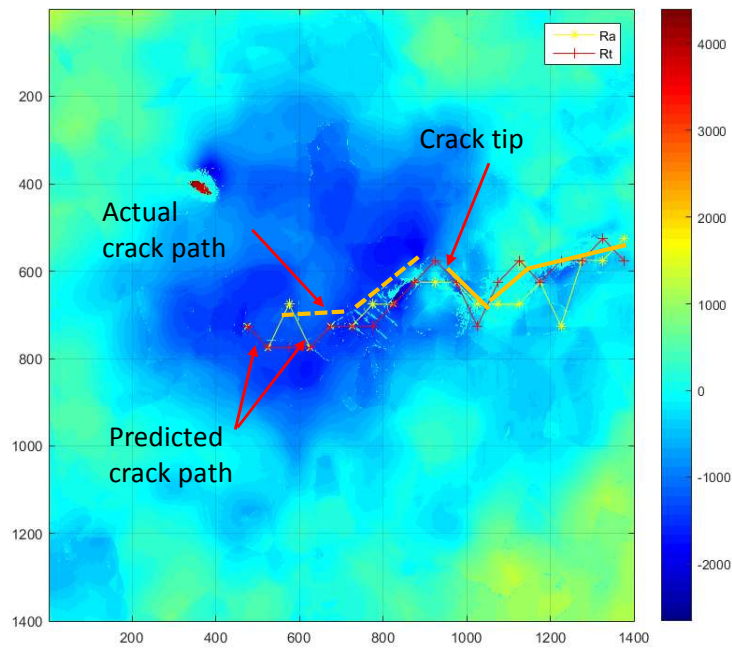


Figure 9.6-78. Comparison Between the Predicted Crack Path and the Actual Crack Path

Note: The crack path was predicted using two different surface roughness parameters, i.e. R_a and R_t .

9.6.22. A Combined Dislocation Fan – Finite Element (DF-FE) Method for Stress-Field Simulation of Dislocations Emerging at the Free Surfaces of 3D Elastically Anisotropic Crystals

Kranthi Balusu and Haiying Huang, University of Texas at Arlington

Understanding material plasticity is necessary for optimal design of structures undergoing fatigue loading. Plasticity, *i.e.*, the permanent deformation of materials, is generally attributed to internal dislocation activities. In recent years, discrete dislocation dynamics (DDD) simulation has made great advances in simulating plasticity at a microscopic scale, due to ever-increasing computation capabilities. The existing simulation methods, however, cannot efficiently simulate the stress field of a dislocation structure intersecting a free surface, due to the stress singularity at the intersecting point. In this work, we developed a combined dislocation fan-finite element (DF-FE) method for efficient and accurate simulation of dislocation nodal forces in 3D elastically anisotropic crystals with dislocations intersecting the free surfaces. As shown in Figure 9.6-79, the finite domain problem is decomposed into half-spaces with singular traction stresses, an infinite domain, and a finite domain with non-singular traction stresses. As such, the singular and non-singular parts of the traction stresses are addressed separately; the Dislocation Fan (DF) method is introduced to balance the singular traction stresses in the half-spaces while the Finite Element Method (FEM) is employed to enforce the non-singular boundary conditions. The accuracy and efficiency of the DF method is demonstrated using a simple isotropic test case shown in Figure 9.6-80(a) and the results are compared with the analytical solution as well as the FEM solution in Figure 9.6-80(b). The DF-FE method is subsequently used for calculating the dislocation nodal forces in a finite elastically anisotropic crystal shown in Figure 9.6-81, which produces dislocation nodal forces that converge rapidly with increasing mesh resolutions. In comparison, the FEM solution fails to converge, especially for nodes closer to the surfaces, as shown in Figure 9.6-82.

Reference:

- [1] Balusu, K. and Huang, H., (2017), A combined dislocation fan-finite element (DF-FE) method for stress field simulation of dislocations emerging at the free surfaces of 3D elastically anisotropic crystals, *Modelling and Simulation in Materials Science and Engineering*, v25, n3, 0355007 (14pp).

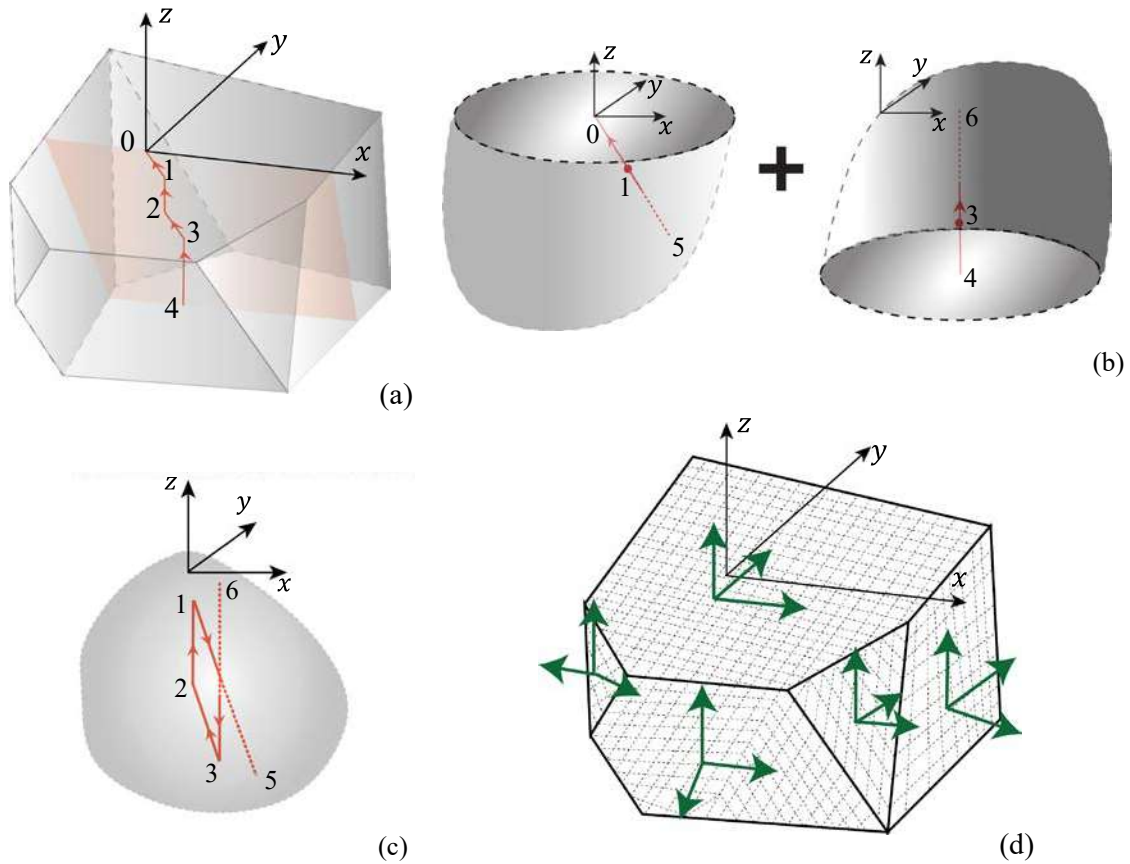


Figure 9.6-79. The Combined DF-FE Method Decomposes (a) as the Superposition of (b), (c), and (d); (a) a Dislocation Intersecting the Free Surfaces of a Representative Finite Domain; (b) Semi-Infinite Dislocations (0-1-5) and (4-3-6) Intersecting the Free Surfaces of the Half-Spaces; (c) the Original Dislocation Structure, with the Segments (0-1) and (4-3) Removed and Replaced by Corresponding Coincident Lines Extending to Infinity Away From the Free Surface; (d) the Body Meshed as Finite Elements to Enforce the Stress Boundary Conditions

Note: The image tractions are shown in green.

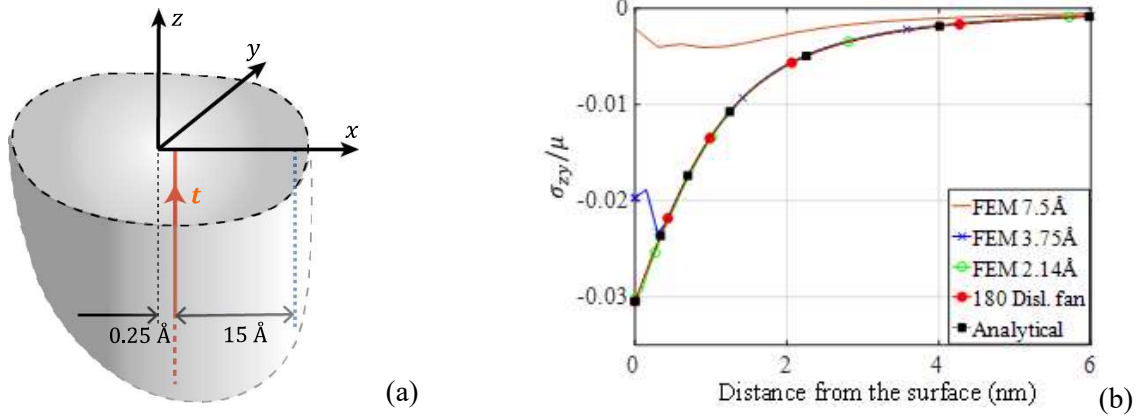


Figure 9.6-80. (a) An Isotropic Case for Validating the Discretized Dislocation Fan Method. (b) Comparison Between Results Obtained Using DF-FEM Method, FEM Method, and Analytical Solution

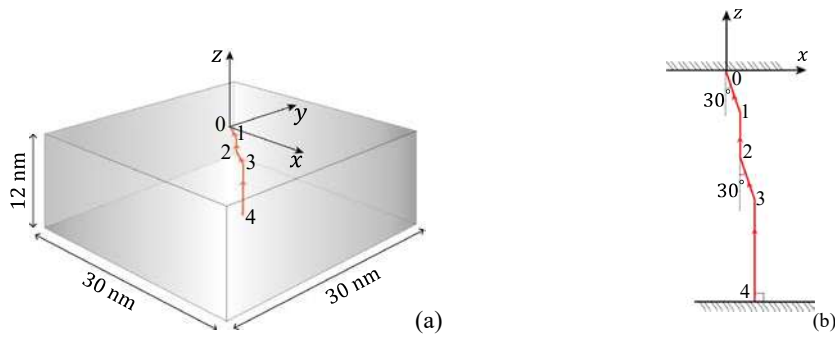


Figure 9.6-81. (a) A Finite Crystal with a Dislocation Structure Intersecting the Top and Bottom Free Surfaces; (b) Orientation of the Dislocation Structure in the zx-Plane

Note: It consists of three 2 nm long dislocation segments and segment (3-4) extends to intersect the bottom free surface normally.

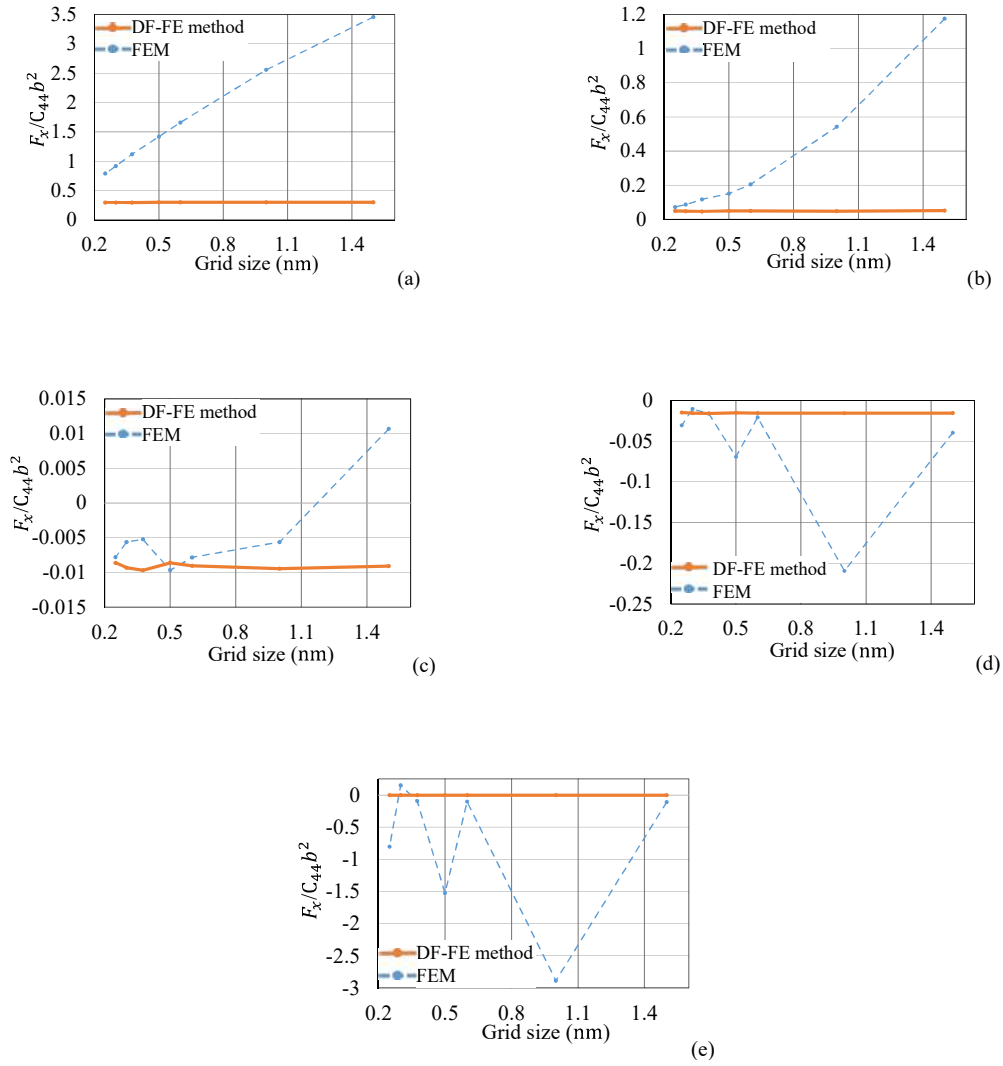


Figure 9.6-82. Simulated Dislocation Nodal Forces in x Direction. The Forces are Calculated Using Both the Hybrid DF-FE Method and FEM at Multiple Grid Sizes. The Forces are Non-Dimensionalized; (a) Force on Node 0, i.e. the Node on the Top Free Surface; (b), (c) and (d) Forces on Nodes 1, 2 and 3 Respectively; (e) Force on Node 4, i.e. the Node on the Free Surface at the Bottom

9.6.23. Open-Hole Tension-Tension Fatigue of Three-Dimensional Woven Composites

Kyle Warren, Harun Bayraktar, and Jonathan Goering, Albany Engineered Composites; William London and Roberto Lopez-Anido, University of Maine

Notched performance of composites is typically a design-limiting case for aerospace structures. Design allowable knock-down factors for various 2D composites used in the aerospace industry are in the 0.4 to 0.5 range [1-2]. This knock down represents a significant reduction from the un-notched load case. The incorporation of through-the-thickness fiber reinforcement found in 3D woven composites eliminates discrete lamina and associated resin-rich layers between layers of fiber reinforcement. This lack of lamina in 3D woven composites results in the design of a composite structure that isn't limited by delamination like traditional 2D composites.

The notched tension-tension fatigue behavior of a 3D woven composite has been evaluated. The composite was reinforced by a 3D woven preform made from 24K IM7 carbon and injected with Cytec PR520 toughened epoxy resin using a resin transfer molding (RTM) process. A graphical representation of the weave architecture is shown in Figure 9.6-83. Tension-tension fatigue evaluation was performed on these notched samples with an R-ratio of 0.1 and a test frequency of 5Hz at standard laboratory conditions of 50% relative humidity at 21°C. The SN curve illustrating results is shown in Figure 9.6-84. Samples shown in the curve that align with 1,000,000 cycles were considered runout specimens and the test was stopped. Figure 9.6-85 shows the notched sample loaded into the test machine on the left and a sample that has suffered a net-section tensile fatigue failure on the right.



Figure 9.6-83. Graphical Representation of Three-Dimensional Woven Fiber Architecture Used in the Fatigue Evaluation

Note: The warp tows are illustrated in red and the weft tows are shown in blue.

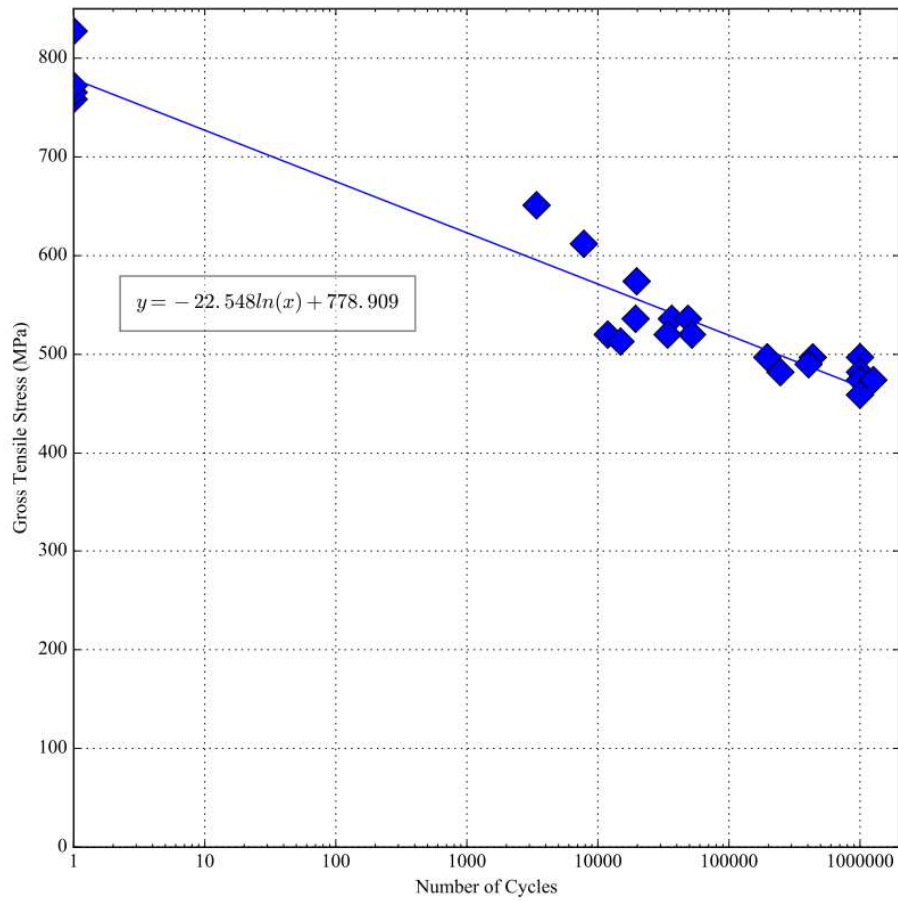


Figure 9.6-84. Open-Hole (Notched) Tensile Fatigue Curve for 3D Woven Composite

Note: Samples with a cycle count of 1,000,000 are runout samples and did not fail. Testing was done at 5Hz with an R-ratio of 0.1.

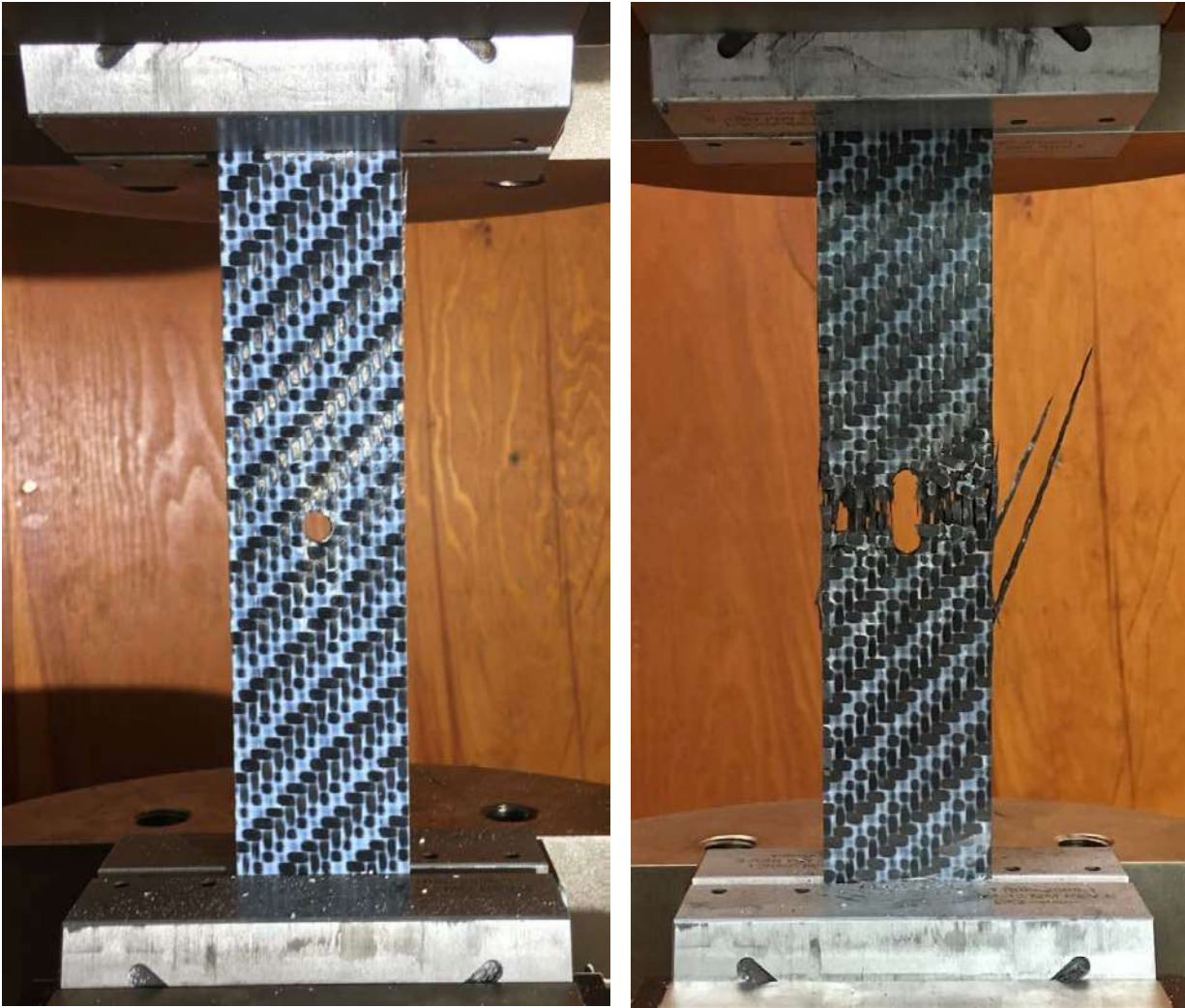


Figure 9.6-85. Notched Fatigue Sample During Testing (Left) and After Fatigue Failure (Right)

3D woven composites similar to that studied in this fatigue are currently flying on both Boeing 737 MAX and Airbus A320neo aircraft as both containment fan cases and fan blades for the CFM LEAP turbofan engine. Figure 9.6-86 shows the Airbus A320neo with CFM LEAP engines containing parts manufactured by Albany Engineered Composites. The un-notched quasi-static tensile strength of this 3D woven composite was evaluated and found to be 1,030 MPa, whereas the open-hole (notched) samples were found to have a strength of 768 MPa. This results in a quasi-static strength knock-down of 0.75 – notably higher than that currently used for 2D composites. Further understanding of the fatigue behavior and performance of 3D woven composites may enable designers to utilize smaller knock-down compensation factors when designing structures in the future.

References:

- [1] Ekvall, J. C., and C. F. Griffin. "Design allowables for T300/5208 graphite/epoxy composite materials." *Journal of Aircraft* 19.8 (1982): 661-667.
- [2] Mangalgi, Prakash D. "Design Allowable Considerations for use of Laminated Composites in Aircraft Structures." *Journal of the Indian Institute of Science* 93.4 (2013): 571-592.



Figure 9.6-86. Airbus A320neo Aircraft with CFM LEAP Engines

9.6.24. Tension-Tension Fatigue Investigation of Three-Dimensional Woven Composites: Effect of Various Epoxy Resin Matrices

Harun Bayraktar, Kyle Warren and Jonathan Goering, Albany Engineered Composites

This evaluation activity investigates the effect of changes in the epoxy resin matrix on the tension-tension fatigue performance of a three-dimensional (3D) woven composite. 3D woven composites have higher fracture toughness than 2D laminated composites while also eliminating delamination as a possible failure mode with the incorporation of through-the-thickness fiber reinforcement. These advantages have been exploited for use in both the blades and containment fan cases for the LEAP turbofan engine currently flying on both Boeing 737 MAX and Airbus A320neo aircraft, shown in Figure 9.6-87. New concept development for applications such as open-rotor blades and fuselage structural shielding will benefit from an enhanced understanding of the fatigue behavior of 3D woven composites.



Figure 9.6-87. CFM LEAP Turbofan Engine Used on Boeing 737MAX and Airbus A320neo Aircraft

Note: This cutaway highlights the fan blades and containment fan case, both manufactured from 3D woven composites.

All test samples were reinforced with the same 3D woven fiber preform. This ply-to-ply architecture, woven with 24K Hexcel IM7 carbon, was injected with a resin transfer molding (RTM) process to a nominal thickness of 4.2mm. A graphical representation of the 3D woven preform, including ply-to-ply interlocking, is shown in Figure 9.6-88. Warp tows are illustrated in gray, while weft tows are illustrated in blue. Tension-tension fatigue testing was performed at room temperature dry (RTD) conditions at 5Hz with an R-ratio of 0.1 to evaluate the effect of epoxy matrix resin system on the tensile fatigue life and performance of the 3D woven composite. Five different epoxies were evaluated: Cytec Cycom PR520 (toughened), Hexcel RTM230 ST (toughened), Hexcel RTM6, Cytec EP2400 (toughened), and Cytec Cycom 890. Collected fatigue data are shown in Figure 9.6-89 with a logarithmic regression line shown for each of the resin systems. These curves should be regarded as preliminary - three samples were evaluated at four different stress levels.

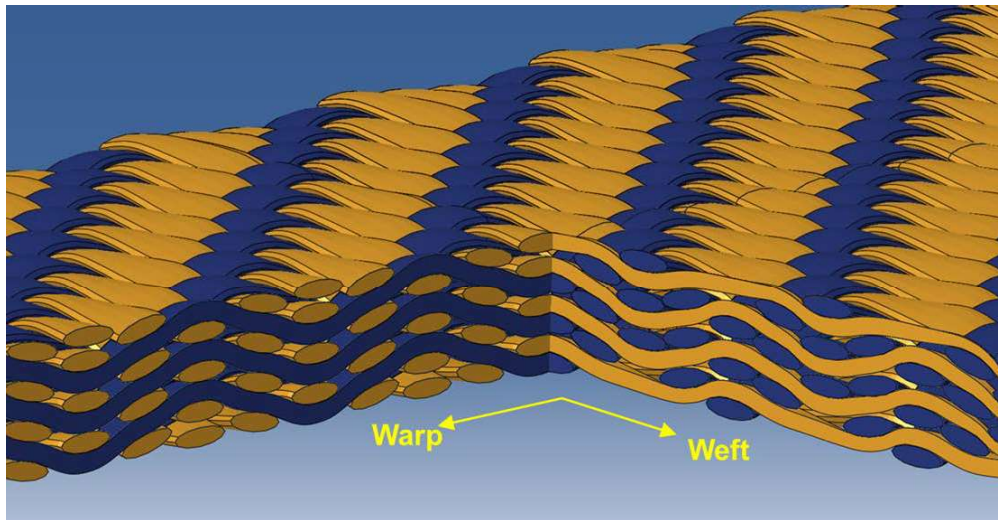


Figure 9.6-88. Graphical Representation of Three-Dimensional Woven Fiber Architecture Used in the Fatigue Evaluation

Note: The warp tows are illustrated in gray and the weft tows are shown in blue.

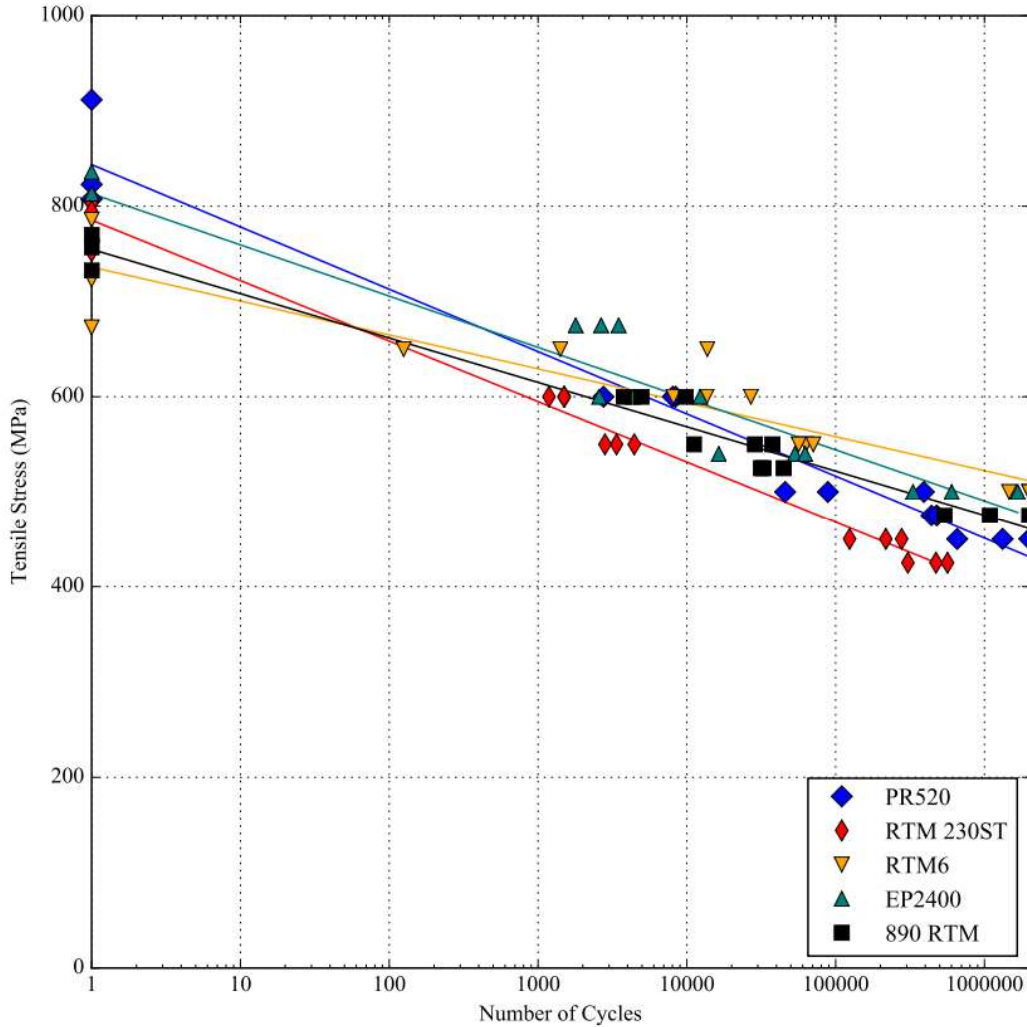


Figure 9.6-89. Tension-Tension Fatigue SN Curves for the Same Fiber Reinforcement Injected with Different Epoxy Resins

Note: Samples with a cycle count of 2,000,000 are 'runout' samples and did not fail.

Minor differences are seen in the performance of this 3D woven composite when evaluated with these various epoxy resin matrices, both toughened and un-toughened that can be brittle and are more susceptible to cracking. These results suggest that the connectivity of fibers (through-the-thickness reinforcement) found in this 3D woven composite may dominate in driving ultimate fatigue failure, rather than the matrix. The lack of delamination combined with the mitigation of crack propagation by the incorporation of through-the-thickness reinforcement found in 3D woven composites may improve the fatigue performance when compared with 2D composites that contain no through-the-thickness reinforcement.

9.6.25. Thermal Cycling Fatigue of Thermal Barrier Coatings

James L. Smialek, NASA Glenn Research Center – Materials and Structures Division

Thermal barrier coatings (TBC) are widely used on air-cooled superalloy airfoils in all jet turbine engines to protect the metal from hot combustion gases. The coatings are typically 7 wt.% Y₂O₃-ZrO₂ yttria partially stabilized zirconia (YSZ) over oxidation resistant NiCoCrAlY or Ni(Pt)Al bond coats. While the utility of such systems have been realized for the past few decades, the drive for higher temperatures or reduced cooling warrants continued development and improvement. Progress is often assessed by comparative lives in furnace cycling tests that exhibit thermal fatigue (cracking/spalling) of the external TBC layer. Here coated samples are inserted into a hot furnace, held for a standard interval (generally 1 h), and cycled to near room temperature, automatically. Periodically, e.g., every 24 h, the samples are inspected for coating damage, and the time to incur ~15-25% loss of the TBC is recorded as failure.

No individual study captures the effects of all variables so it is difficult to obtain a global view of TBC durability. Thus, appropriate furnace cycle test (FCT) data was assembled from the literature to define a fatigue life envelope for standard thermal barrier coatings (electron beam physical vapor (EB-PVD) deposited YSZ and a Pt-modified aluminide bond coat). [1] Figure 9.6-90 summarizes the results of 60 FCT life data from over 20 studies as a function of temperature. The primary pool of data refers to Pt-modified NiAl aluminide bond coats and Pt-only diffusion coatings (filled green circles). Various superalloy substrates were used (Rene'N5, Rene'142, CMSX4, CMSX10, PWA1484, AM1, and IN100), with perhaps a general benefit shown for the more oxidation resistant alloys. [1] Overall, there is about a 10x life reduction for every 100°C temperature increase. The solid blue line refers to a regression fit on an Arrhenius plot:

$$t_c \text{ (h)} = 2.0 \times 10^{-8} \exp(280 \text{ kJ/mol}/RT) \quad r^2=0.6$$

which can only be used as a general guideline because of the high degree of scatter between systems and investigations. Some systems, using oxidation resistant substrates (NiAl or Ti₂AlC), show superior lives or projections because they avoid the typical failure mechanisms associated with coating instabilities (rumpling, ratcheting) or have an excellent CTE match and did not fail. [2]

Al₂O₃ scale spallation triggered by those phenomena leads to TBC failure, often reported to occur at a thickness of ~7 μm when the thermal strain energy on cooling achieves a critical value. [3] Using published scale growth kinetic data, that failure locus is projected as the green dash-dot line in Figure 9.6-90. It is seen to roughly define an upper limit to the life data. A more direct comparison is offered in Figure 9.6-91, where the actual measured scale thickness is presented for various temperatures. Despite much scatter, there is still no clear trend with temperature. The average critical scale thickness was found to be ~6 ± 2 μm, statistically equivalent to the 7 μm criteria. (Larger values can be achieved for oxidation resistant bulk NiAl and Ti₂AlC substrates).

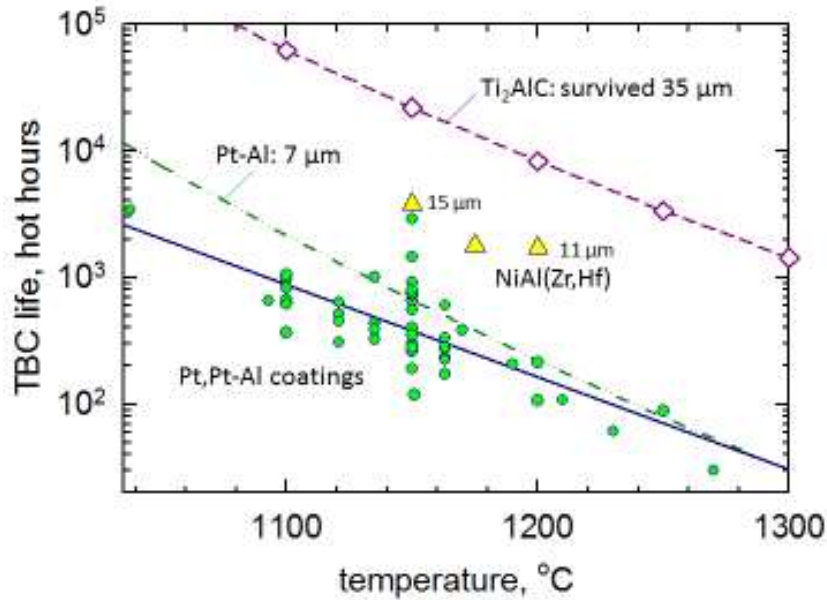


Figure 9.6-90. EB-PVD TBC FCT Life on Alumina-Forming Systems

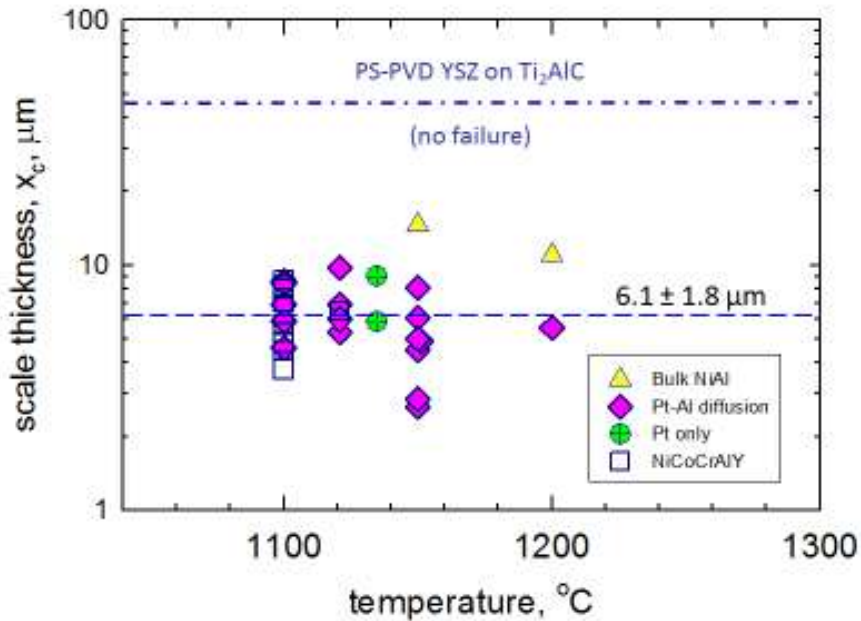


Figure 9.6-91. Alumina Scale Thickness at TBC Failure

These representations offer guidelines for thermal fatigue life for state of the art EB-PVD thermal barrier coatings on superalloys using typical Pt-only or Pt-aluminide bond coats. It can provide a comparative template against which to evaluate current or advanced formulations. While the cyclic life decreases dramatically with oxidative temperature, it appears that a constant strain energy in the scale, defined by its thickness, may offer a more invariant upper limit to life.

9.6.26. New Damage Tolerance Methodology to Model High Temperature Dwell Crack Growth in Nickel-Based Superalloys

J. Telesman, T. P. Gabb, and L. J. Ghosn, NASA Glenn Research Center

With the increase in the operating temperatures of the new generation of gas turbine engines, dwell crack growth of nickel-based powder metallurgy (P/M) superalloys has become a life limiting mechanical property for turbine disk components. While considerable research has been performed over the years to develop a new generation of alloys to improve dwell crack growth behavior, the understanding and modeling of this time dependent mechanism still needs considerable development. The existing damage tolerance life prediction methodologies utilize the linear elastic fracture mechanics (LEFM) crack driving force factor, ΔK , as the main parameter to estimate the remaining life of turbine components. This methodology was developed for lower temperature applications and is largely predicated on the assumption that crack growth is governed by cyclic plasticity. However, at higher operating temperatures crack growth is governed by complex interactions of cyclic, creep and environmental damage mechanisms which are not well understood.

The goal of the current work was to expand the understanding of the factors controlling dwell crack growth behavior and develop improved damage-tolerance-based life prediction methodology consistent with high temperature crack growth mechanisms. By decoupling the environmental damage from creep, it was demonstrated that at the higher operating turbine disk temperatures the use of the standard K-based parameter is no longer appropriate for correlating dwell crack growth rates due to significant stress relaxation effects at the crack tip. Thus the large differences in the observed dwell crack growth rates, for materials which have similar environmental resistance, are due to the inability of the K parameter to accurately describe the crack tip stress field (Figure 9.6-92).

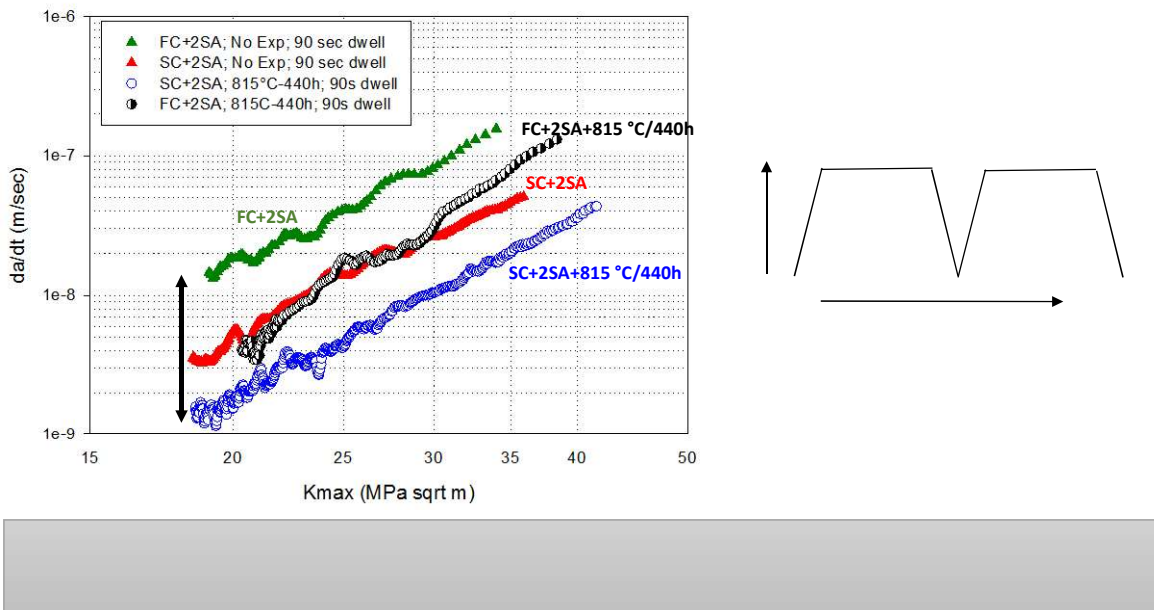


Figure 9.6-92. Turbine Disk Nickel-Based Superalloy Tested at 704 °C

It was shown that cracking of the continuously forming nano-scale oxide layer at the crack tip is the primary damage mechanism responsible for dwell crack growth. While the environment embrittles the crack tip region, the crack tip stress field driving crack extension is heavily influenced by visco-plastic behavior. The crack driving force was found to be proportional to the remaining stress level obtained

from simple uniaxial stress relaxation tests (Figure 9.6-93). Finally, a visco-plastic based correction to the LEFM, K parameter, was developed which accounts for and incorporates the differences in the stress relaxation behavior into its formulation. The new parameter called K_{srf} , was shown to do a good job in correlating the dwell crack growth behavior in this class of alloys (Figure 9.6-94).

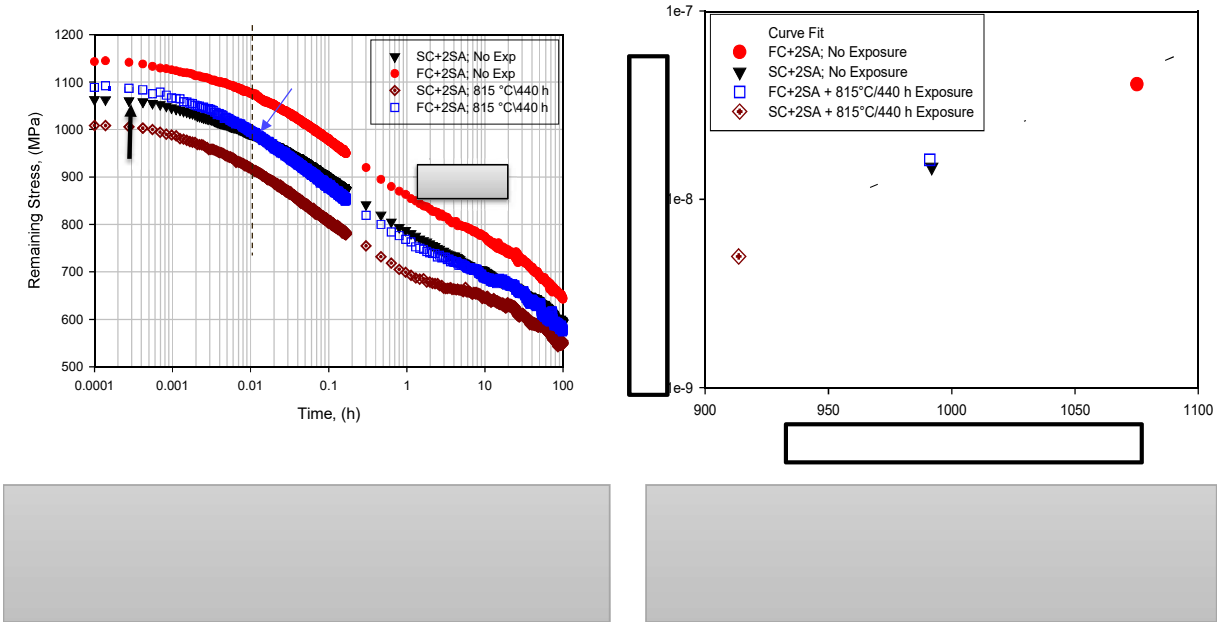
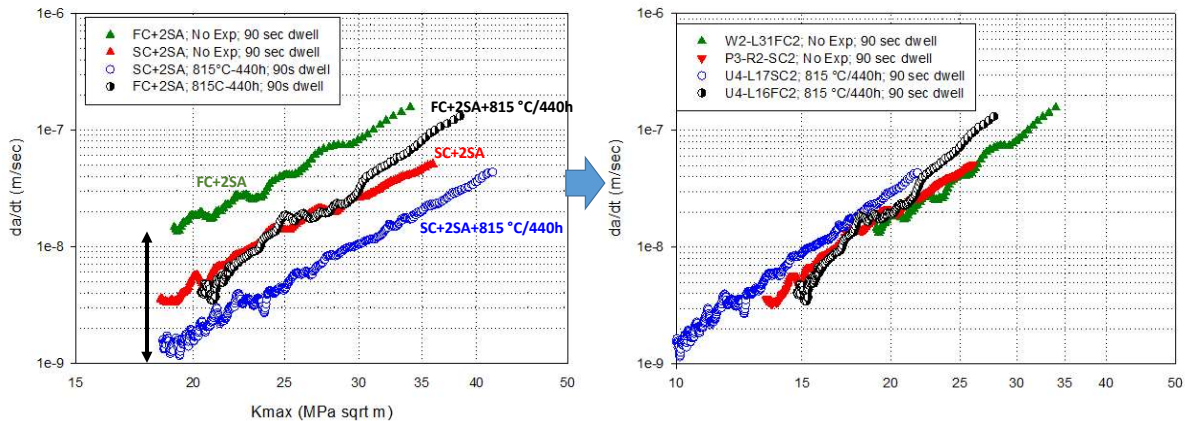


Figure 9.6-93. Relationship Between Stress Relaxation Behavior and Dwell Crack Growth at 704 °C



$$K_{srf} = K_{max} / SRF$$

SRF – stress relaxation factor dete
 srf – modified stress intensity fa
 K_{max} – Applied LEFM stress inten
 differences in crack tip stres:
 rates using standard linear ele

Figure 9.6-94. New Damage Tolerance Based K_{srf} Parameter does a Good Job in Correlating the Measured Dwell Fatigue Crack Growth Rates

9.6.27. Cyclic Fatigue and Dwell Fatigue Crack Growth Response of Ti-6Al-4V

Adam L. Pilchak, Air Force Research Laboratory – Materials and Manufacturing Directorate

The available specimen test data in the literature and the large volume of Ti-6Al-4V that has been successfully used in many commercial and military aircraft for many years suggests that Ti-6Al-4V is relatively insensitive to dwell fatigue failure under conventional engine operating conditions from the perspective of total lifetime. However, both crack initiation and crack growth lifetime contribute to the total lifetime debit and hence it is important to understand the role of dwell on fatigue crack growth rate in Ti-6Al-4V in the event that extrinsic factors (e.g., foreign object damage or machining defect) lead to early crack initiation. This is useful information when managing inspection intervals and setting safe operating limits. Hence, a study was undertaken to separate the contributions of crack initiation and crack growth to the total lifetime debit [1]. Smooth uniaxial fatigue samples were subjected to 20 Hz cyclic and 2-min dwell waveforms until failure in load-control. A 2.1X debit in lifetime was observed under dwell conditions confirming the relative insensitivity to early crack nucleation at least at the test conditions (peak stress 84% of the alloy yield strength) used in this work, Figure 9.6-95. Smooth, electropolished fatigue samples were preflawed using focused gallium ion beam to produce 30 micrometer wide micronotches. Dwell fatigue cracks were initiated from these micronotches and their growth rates measured with acetate replication. These measurements demonstrated the potential for anomalous crack growth rates during dwell fatigue loading of highly microtextured Ti-6Al-4V leading to debits in crack growth lifetime compared to conventional fatigue. This crack growth debit can potentially be severe as the anomalous rates are observed until the crack reaches the size of the microtextured region (MTR) in which it initiated. Only once the crack has reached the edge of this region, does it cease to behave as a microstructurally small crack, which coincides with a reduction in crack growth rate and more classical “long fatigue crack” behavior is observed.

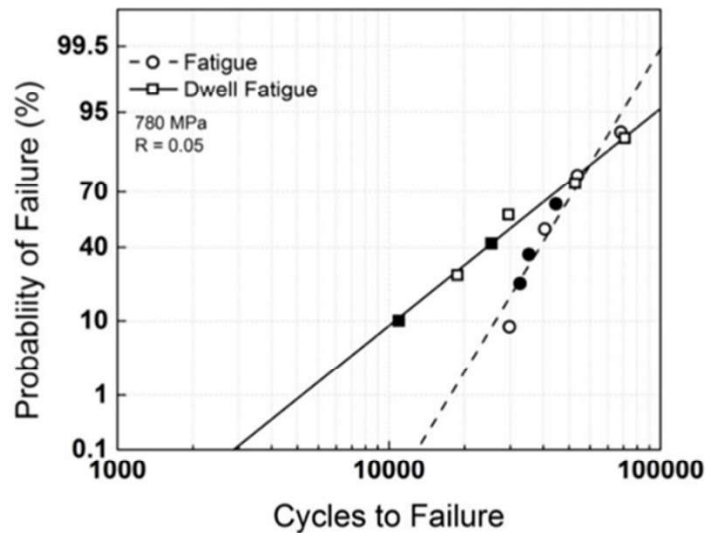


Figure 9.6-95. Fatigue Lifetime Data for Cyclic and Dwell Fatigue of Ti-6Al-4V. The Filled and Open Symbols Represent Samples with High and Low Degrees of Microtexture, Respectively

In addition to these general conclusions, the following specific results were obtained in this work: (1) Order-of-magnitude variations in the growth rates of small dwell fatigue cracks were measured within individual MTRs measured. These rates were often significantly faster than cyclic small cracks exposed to an equivalent driving force. (2) Local texture was a stronger contributor to crack growth rate

variability than local microstructure or the roughness developed in the crack wake. (3) There was a population of slow-growing dwell fatigue cracks where the growth rates were of the same order as the typical cyclic small crack effect in low-microtexture material. (4) There was no significant effect of dwell fatigue or microtexture on long crack growth rates other than to reduce slightly the long crack growth threshold stress intensity range for conventional cyclic fatigue. (5) A few dwell fatigue cracks growing in the low microtexture material grew at faster rates than the corresponding cyclic cracks, but still were not as fast as the fastest population of dwell cracks in the high microtexture condition (Figure 9.6-96).

Reference:

- [1] Pilchak, A. L., Hutson, A., Porter, W. J., Buchanan, D., and John, R., "On the Cyclic Fatigue and Dwell Fatigue Crack Growth Response of Ti-6Al-4V," *Proceedings of the 13th World Titanium Conference on Titanium*, Editor(s): Vashist Venkatesh, et al., John Wiley & Sons, Inc., Hoboken, NJ, published online, doi: 10.1002/9781119296126.ch169, pp. 993–998, 6 May 2016.

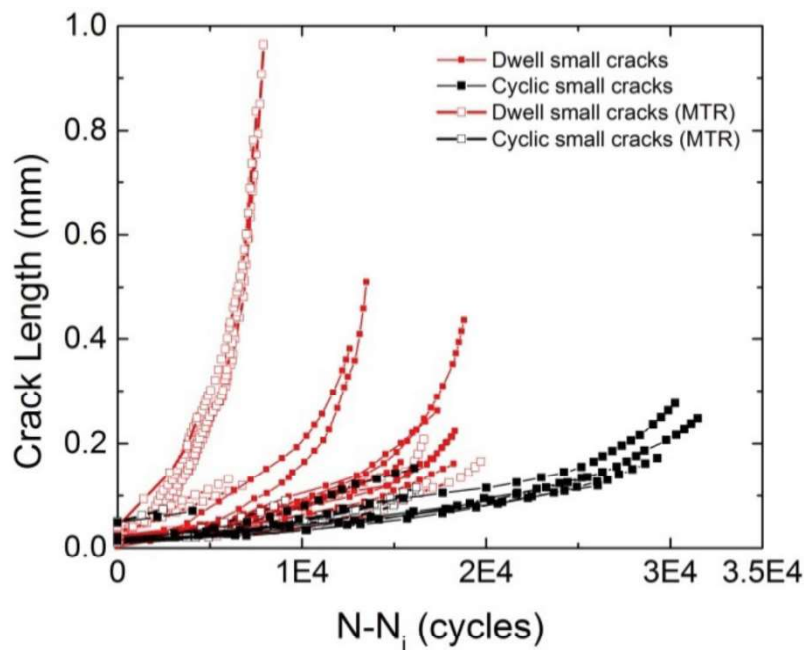


Figure 9.6-96. Small Crack Length versus Cycles as a Function of Microstructure and Waveform

9.6.28. Role of Deformation Heterogeneities in Life-Limiting Fatigue Failures in a Two-Phase Titanium Alloy

Reji John, Air Force Research Laboratory – Materials and Manufacturing Directorate

Fatigue crack-initiation sites in the alpha+beta Titanium alloy, Ti-6Al-2Sn-4Zr-6Mo were characterized with emphasis on distinguishing the microstructural neighborhoods and mechanisms that produce the life-limiting failures vs. those that promote the mean-lifetime behavior. The characterization methods included quantitative tilt fractography, focused ion beam milling across crack-initiation facets, and electron backscattered diffraction analysis. The motivation for discerning between the life-limiting and the mean-dominating crack-initiation microstructural neighborhoods stemmed from the previously developed understanding that the mean and the life-limiting behaviors respond differently to stress level (and other variables), leading to an increasing separation between the two subpopulations as the stress

level is decreased, thereby increasing the variability in lifetime, Figure 9.6-97. This study was ultimately aimed at developing an understanding of the occurrence rate of life-limiting failures. The following main conclusions can be drawn. (i) The fatigue lifetimes grouped into a life-limiting population that was dominated by the crack growth lifetime, and a mean-dominating population that was increasingly dominated by the crack-initiation lifetime with decreasing stress level. (ii) The mechanism of fatigue crack-initiation is not unique and can be produced by several random combinations of microstructural constituents even in the same nominal microstructure and under the same loading condition. (iii) The life-limiting failures initiated by a different mechanism than the mean-dominating failures where, for surface crack-initiation, the most notable difference was that the crack-initiation facet plane in the life-limiting case was inclined away from the maximum shear orientation with respect to the loading axis (on average 31 deg. based on characterization of 7 life-limiting specimens), whereas, in the mean-dominating case, the inclination with respect to the loading axis was close to the maximum shear orientation, i.e., about 45 degrees, Figure 9.6-98. (iv) Based on the characterization study, four classes of fatigue-critical microstructural configurations, with varying size and complexity, could be deduced in the given microstructure of Ti-6Al-2Sn-4Zr-6Mo, Figure 9.6-99. (v) A hypothesis in terms of hierarchy of fatigue deformation heterogeneities, accounting for various possibilities for microstructural arrangements and damage accumulation paths, is proposed, Figure 9.6-100. The hypothesis treats the microstructural arrangements probabilistically, and therefore allows for the occurrence of life-limiting failures with certain probability even at low applied stress levels.

Reference:

- [1] S.K. Jha, C.J. Szczepanski, R. John and J.M. Larsen, "Deformation heterogeneities and their role in life-limiting fatigue failures in a two-phase titanium alloy," *Acta Materialia*, Vol. 82, pp. 378–395, 2015.

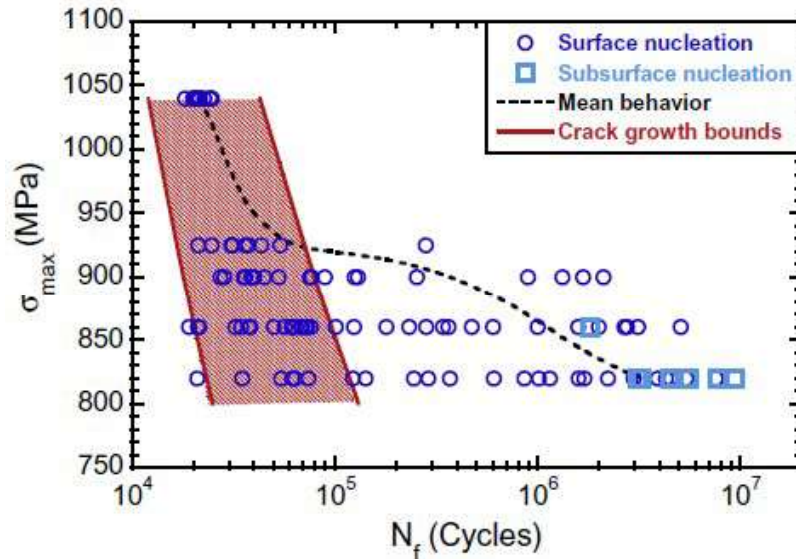


Figure 9.6-97. Mean versus Life-Limiting Fatigue Behavior of Alpha+Beta Alloy, Ti-6Al-2Sn-4Zr-6Mo: Distribution in Lifetimes with Respect to Stress Level in the S-N Space

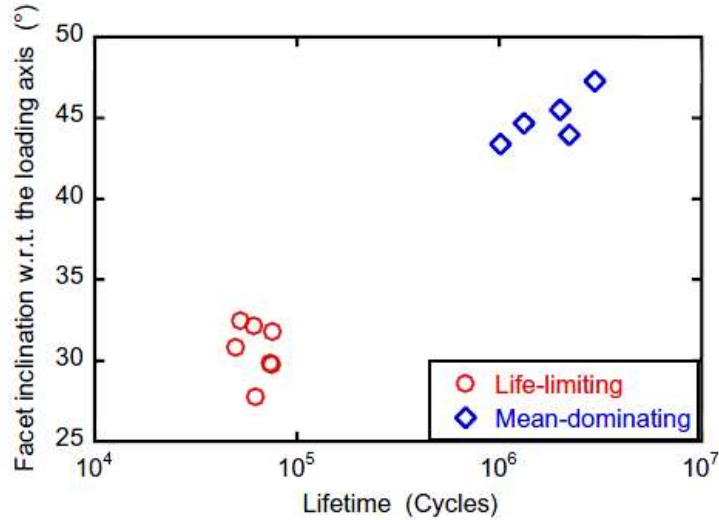


Figure 9.6-98. Compilation of Facet Inclination Data From Characterization of Multiple Life-Limiting and Mean-Dominating Specimens: Facet Inclination with Respect to the Loading Axis versus Lifetime

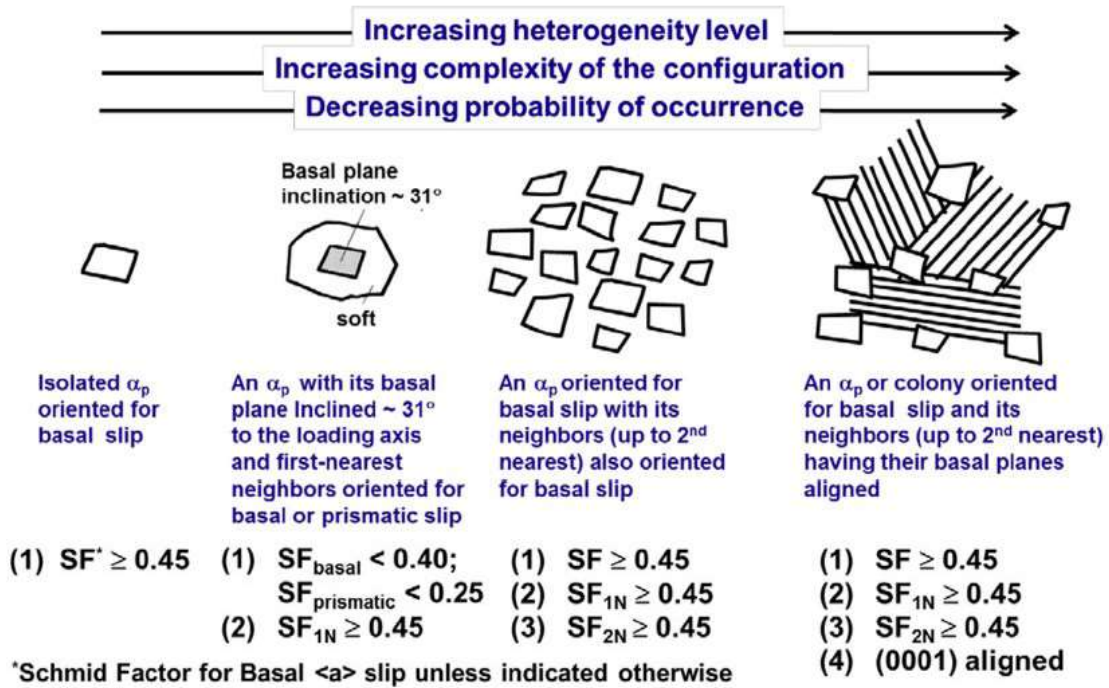


Figure 9.6-99. Deduced Crack-Initiating Microstructural Configurations in Ti-6Al-2Sn-4Zr-6Mo Based on the Characterization Study

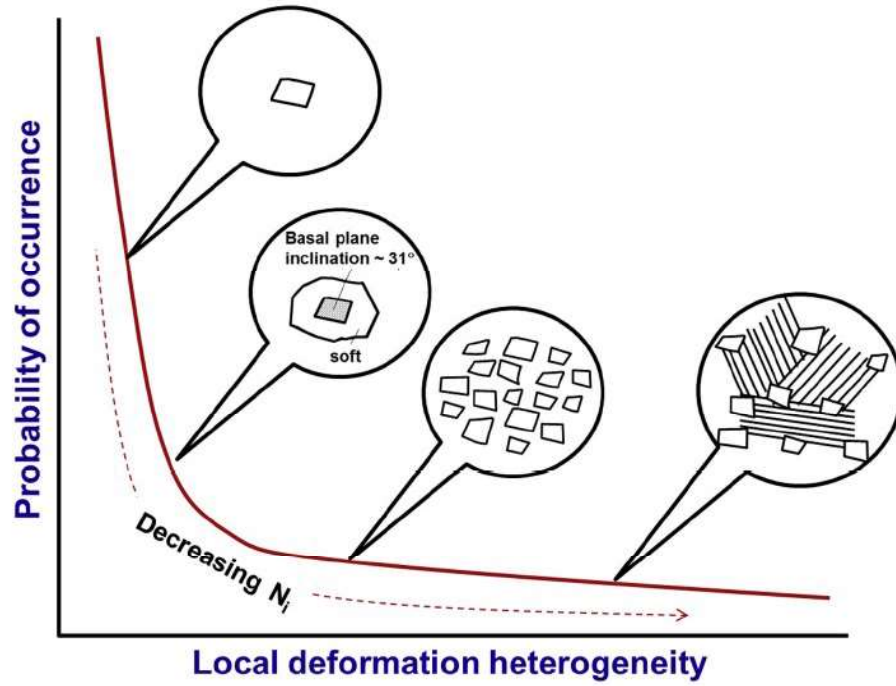


Figure 9.6-100. Schematic Depiction of the Hypothesis of Life-Limiting Failure Based on Hierarchy of Fatigue Heterogeneity Levels

9.7. PROGNOSTICS & RISK ANALYSIS

9.7.1. Risk Assessments per DoD System Safety, USAF Airworthiness and USAF ASIP

Charles Babish IV, USAF Life Cycle Management Center

Risk assessments are an integral part of decision making in regards to aircraft safety, airworthiness and structural integrity. Risk assessments require knowledge of the hazard, probability of occurrence for the hazard, and the consequence associated with the hazard occurrence. DoD MIL-STD-882 establishes the System Safety program and it includes a suggested or example risk assessment matrix table which contains five probability levels (frequent, probable, occasional, remote, and improbable) and four severity levels for consequence (catastrophic, critical, marginal, and negligible). The table includes probability of occurrence values for use when quantitative analysis is performed. Due to issues experienced where estimated failure rates were incorrectly compared to the suggested probability of occurrence values in the table, the USAF ASIP established risk thresholds in MIL-STD-1530C (2004) in terms of "probability of failure per flight" for structural integrity hazards. For similar reasons, the USAF Airworthiness Office established risk thresholds in terms of "frequency per flight hour" in Airworthiness Bulletin AWB-013A (2011) for all airworthiness hazards. This technical activity will provide background information on MIL-STD-882D (Table 9.7-1), MIL-STD-882E (Table 9.7-2), MIL-STD-1530C (Figure 9.7-1) and AWB-013A (Table 9.7-3) that relate to risk assessments for USAF aircraft (Table 9.7-4). A quantitative example problem using the Weibull model with "assumed to be known facts" will be used to illustrate the possible calculations and the different risk assessments that are possible based on various interpretations of failure rate, frequency, probability, and probability of occurrence in the life. The calculations will show five different risk assessment results, of which two are clearly not reasonable (Figure 9.7-2). A second example problem will be used to further illustrate potential reasonable and unreasonable risk assessment results for both the qualitative and quantitative methods established in MIL-STD-882 (Tables 9.7-5 through 9.7-7). The technical activity will conclude by stating that hazard rate and thresholds based on hazard rate provide the best basis for performing aircraft risk assessments

Table 9.7-1. DoD MIL-STD-882D (2000)

A.4.4.3.2.2 Mishap probability. Mishap probability is the probability that a mishap will occur during the planned life expectancy of the system. It can be described in terms of potential occurrences per unit of time, events, population, items, or activity. Assigning a

TABLE A-II. Suggested mishap probability levels.

Description*	Level	Specific Individual Item	Fleet or Inventory**
Frequent	A	Likely to occur often in the life of an item, with a <u>probability of occurrence greater than 10⁻¹ in that life.</u>	Continuously experienced.
Probable	B	Will occur several times in the life of an item, with a <u>probability of occurrence less than 10⁻¹ but greater than 10⁻² in that life.</u>	Will occur frequently.
Occasional	C	Likely to occur some time in the life of an item, with a <u>probability of occurrence less than 10⁻² but greater than 10⁻³ in that life.</u>	Will occur several times.
Remote	D	Unlikely but possible to occur in the life of an item, with a <u>probability of occurrence less than 10⁻³ but greater than 10⁻⁶ in that life.</u>	Unlikely, but can reasonably be expected to occur.
Improbable	E	So unlikely, it can be assumed occurrence may not be experienced, with a <u>probability of occurrence less than 10⁻⁶ in that life.</u>	Unlikely to occur, but possible.

“probability of occurrence ... in that life”

Observation 2:
Text states “it can be described in terms of potential occurrences per unit of time...” (per flight hour instead of per life = 1,000 hours or more ?)

Table 9.7-2. DoD MIL-STD-882E (2012)

A.3. Quantitative Probability Example. For quantitative descriptions, the frequency is the actual or expected number of mishaps (numerator) during a specified exposure (denominator). The denominator can be based on such things as the life of one item; number of missile firings, flight hours, systems fielded, or miles driven; years of service, etc.

TABLE A-II. Example probability levels

Probability Levels				
Description	Level	Individual Item	Fleet/Inventory*	Quantitative
Frequent	A	Likely to occur often in the life of an item	Continuously experienced.	Probability of occurrence greater than or equal to 10^{-1} .
Probable	B	Will occur several times in the life of an item	Will occur frequently.	Probability of occurrence less than 10^{-1} but greater than or equal to 10^{-2} .
Occasional	C	Likely to occur sometime in the life of an item	Will occur several times.	Probability of occurrence less than 10^{-2} but greater than or equal to 10^{-3} .
Remote	D	Unlikely, but possible to occur in the life of an item	Unlikely but can reasonably be expected to occur.	Probability of occurrence less than 10^{-3} but greater than or equal to 10^{-4} .
Improbable	E	So unlikely, it can be assumed occurrence may not be experienced in the life of an item	Unlikely to occur, but possible.	Probability of occurrence less than 10^{-4} .
Eliminated	F	Incapable of occurrence within the life of an item. This category is used when potential hazards are identified and later eliminated.		

* The size of the fleet or inventory should be defined.

Observation 1:
Added “Quantitative” column & moved PoO values to it & deleted “in that life”

Observation 2:
“probability”, “frequency” and mishaps/exposure (a rate!) used in text

Observation 3:
“in the life” of an “Individual Item”

Table 9.7-3. USAF Airworthiness (2011)

Translation	HAZARD CATEGORIZATION	SEVERITY*			
		CATASTROPHIC (1)	CRITICAL (2)	MARGINAL (3)	NEGLIGIBLE (4)
>E-03	F FREQUENT (A) = or > 100/100K flt hrs	1	3	7	13
E-03 to E-04	R PROBABLE (B) 10-99/100K flt hrs	2	5	9	16
E-04 to E-05	Q OCCASIONAL (C) 1.0-9.9/100K flt hrs	4	6	11	18
E-05 to E-07	U REMOTE (D) 0.01-0.99/100K flt hrs	8	10	14	19
<E-07	N IMPROBABLE (E) = or < 0.01/100K flt hrs	12	15	17	20

HIGH CAE Risk Acceptance
HRI = 1 through 5

MEDIUM PM Risk Acceptance
HRI = 10 through 17

SERIOUS PEO Level Risk Acceptance
HRI = 6 through 9

LOW Risk Acceptance As Directed
HRI = 18 through 20

Observation:
Frequency per flight hour

Table 9.7-4. Summary of Quantitative Values

Probability	Individual Item	Fleet / Inventory	Catastrophic Severity	MIL-STD-882 (Prob or Freq or Rate)?	AWB-013A (Rate per Flight Hour)	MIL-STD-1530C (Rate per Flight)
Frequent	Often	Continuous	High	$\geq 10^{-1}$	$\geq 10^{-3}$	$\geq 10^{-5}$
Probable	Several	Frequent	High	$< 10^{-1}$ to $\geq 10^{-2}$	$< 10^{-3}$ to $\geq 10^{-4}$	
Occasional	Likely	Several	High	$< 10^{-2}$ to $\geq 10^{-3}$	$< 10^{-4}$ to $\geq 10^{-5}$	
Remote	Possible	Can Occur	Serious	$< 10^{-3}$ to $\geq 10^{-6}$	$< 10^{-5}$ to $\geq 10^{-7}$	$< 10^{-5}$ to $\geq 10^{-7}$
Improbable	Unlikely	Unlikely	Medium	$< 10^{-6}$	$< 10^{-7}$	$< 10^{-7}$

Observation of quantitative value differences:

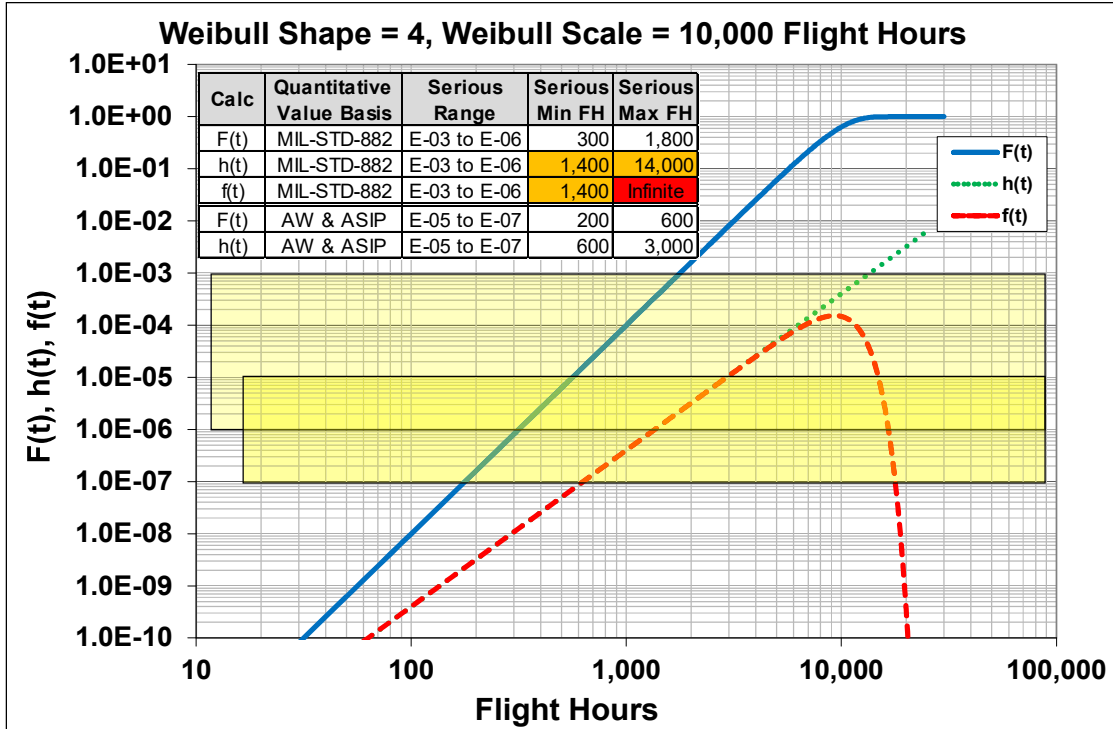
- 1. Serious maximum value varies from 10^{-3} to 10^{-5} (100X)**
- 2. Medium maximum value varies from 10^{-6} to 10^{-7} (10X)**

- “A probability of catastrophic failure at or below 10^{-7} per flight for the aircraft structure is considered adequate to ensure safety for long-term military operations”
- “Probabilities of catastrophic failure exceeding 10^{-5} per flight for the aircraft structure should be considered unacceptable”
- “When the probability of failure is between these two limits, consideration should be given to mitigation of risk through inspection, repair, operational restrictions, modification, or replacement”

Observation:

Probability of failure per flight (MIL-STD-1530C words taken from Dr. Lincoln paper “Risk Assessment of an Aging Military Aircraft” dated August 1985)

Figure 9.7-1. USAF ASIP MIL-STD-1530C (2004)



882 values is wrong, PDF shouldn't be used

Figure 9.7-2. Example Problem #1 Results

Table 9.7-5. Example Problem #2 Results: Method 2 and MIL-STD-882D

MIL-STD-882D RISK ASSESSMENT MATRIX						
Description	Probability of Occurrence in that Life for an Individual Item	Fleet / Inventory	Catastrophic (1)	Critical (2)	Marginal (3)	Negligible (4)
Frequent (A)	$>10^{-1}$	Continuous	High	High	Serious	Medium
Probable (B)	$<10^{-1}$ to $\geq 10^{-2}$	Frequent	High	High	Serious	Medium
Occasional (C)	$<10^{-2}$ to $\geq 10^{-3}$	Several	High	Serious	Medium	Low
Remote (D)	$<10^{-3}$ to $\geq 10^{-6}$	Can Occur	Serious	Medium	Medium	Low
Improbable (E)	$<10^{-6}$	Unlikely	Medium	Medium	Medium	Low

- Method 2: Use 10^{-4} in all “quantitative” locations with 10 expected fleet losses as before
- Result: either High or Serious risk

Not consistent & PoO risk basis is not reasonable

Table 9.7-6. Example Problem #2 Results: Method 1 & 2 and MIL-STD-882E

MIL-STD-882E RISK ASSESSMENT MATRIX							
Description	In the Life of an Individual Item	Fleet / Inventory	Probability of Occurrence	Catastrophic (1)	Critical (2)	Marginal (3)	Negligible (4)
Frequent (A)	Often	Continuous	$\geq 10^{-1}$	High	High	Serious	Medium
Probable (B)	Several	Frequent	$< 10^{-1}$ to $\geq 10^{-2}$	High	High	Serious	Medium
Occasional (C)	Likely	Several	$< 10^{-2}$ to $\geq 10^{-3}$	High	Serious	Medium	Low
Remote (D)	Possible	Can Occur	$< 10^{-3}$ to $\geq 10^{-6}$	Serious	Medium	Medium	Low
Improbable (E)	Unlikely	Unlikely	$< 10^{-6}$	Medium	Medium	Medium	Low

Use method 1 (failure rate times exposure) to obtain individual in the life & fleet/inventory probability levels

- Individual: 0.1 subjectively shown as "possible"
- Fleet: expected losses = 10 (frequent)

Use method 2 for probability of occurrence

Result: either High or Serious risk

Not consistent & PoO risk basis is not reasonable

Table 9.7-7. Example Problem #2 Results: AWB-013A & ASIP

HAZARD CATEGORIZATION		SEVERITY*			
		CATASTROPHIC (1)	CRITICAL (2)	MARGINAL (3)	NEGLIGIBLE (4)
FREQUENCY	FREQUENT (A) = or > 100/100K fit hrs	1	3	7	13
	PROBABLE (B) 10-99/100K fit hrs	2	5	9	16
	OCCASIONAL (C) 1.0-9.9/100K fit hrs	4	6	11	18
	REMOTE (D) 0.01-0.99/100K fit hrs	8	10	14	19
	IMPROBABLE (E) = or < 0.01/100K fit hrs	12	15	17	20

HIGH CAE Risk Acceptance
HRI = 1 through 5

MEDIUM PM Risk Acceptance
HRI = 10 through 17

SERIOUS PEO Level Risk Acceptance
HRI = 6 through 9

LOW Risk Acceptance As Directed
HRI = 18 through 20

9.7.2. Risk-Shaping the Building Block Development Process for Certification of Composite Structure

LeRoy Fitzwater, Herb Smith, and Mike Renieri, The Boeing Company – Research and Technology; Dick Holzwarth, USAF Research Laboratory – Aerospace Systems Directorate

As the use of composites has grown, so has the size and the associated cost and time of traditional test-intensive building block development programs. The cost of these test programs is becoming prohibitively large and has become an impediment to implementing new materials and structural concepts. To most effectively reduce the risk of high benefit, but unproven new technology, an ideal building block program should be designed and scheduled to address the high risks as soon as practical, thereby allowing more time for additional risk mitigation activity that may be required (Figure 9.7-3). Boeing is investigating the feasibility and benefits of applying the proven Failure Modes, Effects, and Criticality Analysis (FMECA) process (Figure 9.7-4) to the problem of identifying and characterizing design and manufacturing risks inherent in composite airframe structure during the design evolution. Boeing is also investigating the application of network theory to understand how specific development activities reduce the inherent risk. The envisioned product will be a management process in which the most critical risks can be readily identified and the most efficient risk reduction schedule can be found. The study focused on systematically assessing risk in a well-defined, portable, and repeatable manner and then using that data to build a diagnostic model of risk flow throughout a multilevel building block program. The model was then exercised to demonstrate the capability to define a sequence of activities that more quickly reduce the risk and uncover issues in a new composite material, design or manufacturing process. This approach will identify the most important tests to do first and will provide a basis for rationally leveraging analysis methods to supplant or augment selected testing.

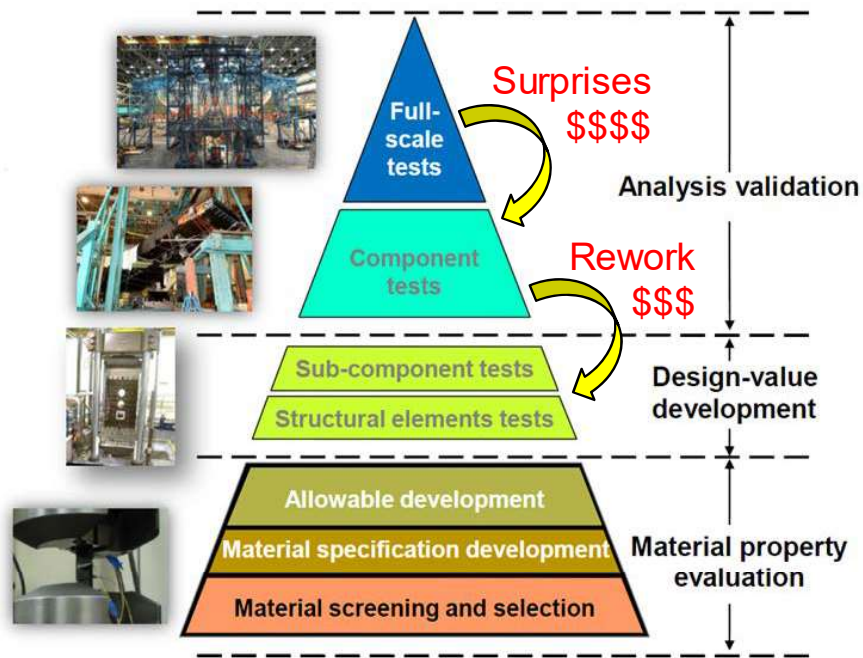


Figure 9.7-3. Building Block Risk Reduction Approach

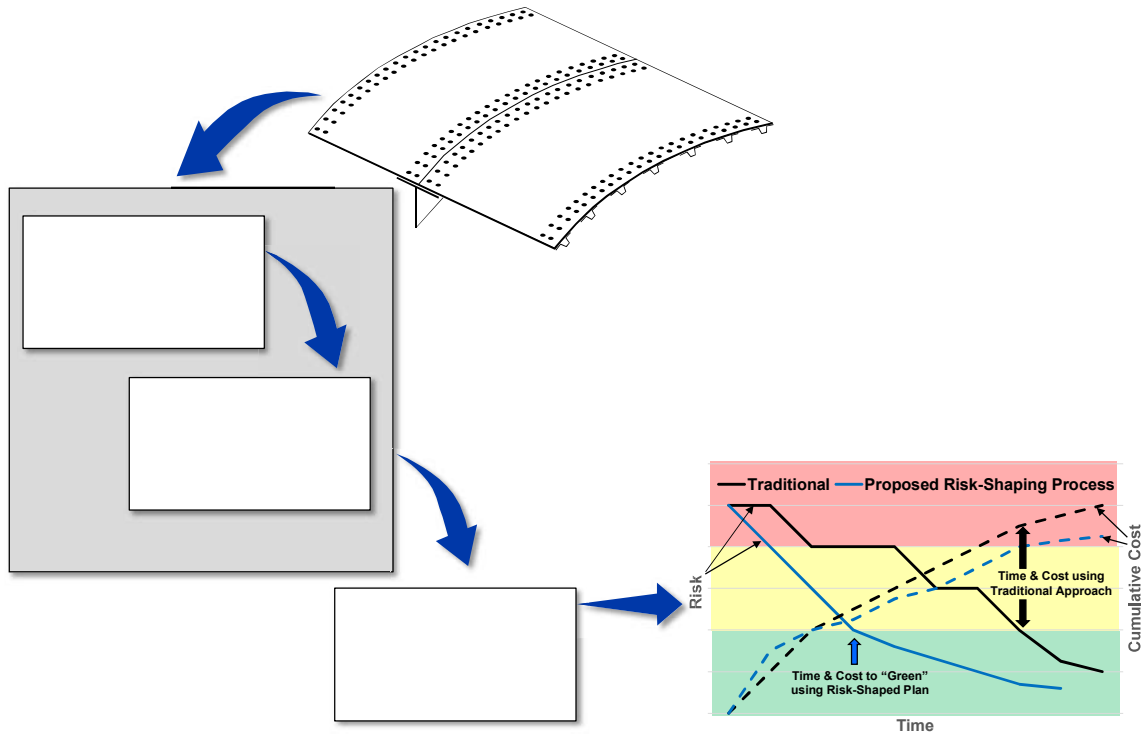


Figure 9.7-4. Failure Modes, Effects, and Criticality Analysis (FMECA) Process

9.7.3. Aircraft Structural Reliability Under the Cumulative Effect of Structural Repairs

Mohammad Khalessi, PredictionProbe, Inc.

Aircraft structural risk and reliability analysis is a vital and growing element of the USAF Aircraft Structural Integrity Program. As the age of the USAF inventory increases, the cumulative effect of structural repairs is a growing threat to aircraft structural integrity. The approach to be presented herein can account for the diversity and complexity of structural repairs and can accurately predict the structural reliability of various repair scenarios and their cumulative effect. This technical activity will describe a new 4-Step Process for performing condition-based aircraft post inspection reliability analysis. This process has been developed under the USAF SBIR Topic No.: AF141-067 based upon the concept originally developed and presented by Dr. Eric Tuegel on December 3, 2013 at the ASIP Conference. This new 4-Step Process shall provide: a) techniques for correctly modeling the physics of the variety of possible post-inspection structural repair options, b) methodologies for accurately performing probabilistic structural reliability analysis calculations for metallic aircraft structures subject to fatigue, and c) a framework for developing a new structural reliability analysis tool. This technical activity describes each step of the 4-Step Process, namely: Input Data, Analysis, Output Data, and Updating. One of the key elements of this process is the use of a condition tree. The condition tree defines the number of conditions found at each inspection (e.g., possible repair types, no crack found, etc.) (Figure 9.7-5). These conditions may be used to define the potential paths during a selected time period. For example, for two (2) repair types there will be three (3) conditions between the first and second inspections, and nine (9) conditions between the second and third inspections. These conditions define a total of nine (9) paths for the period between $t=0$ to just before the third inspection (Figure 9.7-6). This condition tree can be expanded to define all paths for any number of repairs and inspections. In our approach, we track the performance of the structure along each path separately, and then integrate the performances across all

paths to predict the behavior of the structure. Typical analyses performed along each path include calculation of the crack size distribution, cumulative probability of failure, single flight probability of failure, etc. Conclusions and Significance of this technical activity: The proposed approach enhances the capability of the current methods by providing a systematic approach for considering various repair types in reliability analysis of the aircraft after inspection. Although the focus of the approach has been for USAF applications, the technology will have technical leverage which can be applied to other branches of the armed forces, Federal Aviation Administration, National Aeronautics and Space Administration, aerospace, airline industries, maritime, etc. The tools to be developed using this approach will decrease the threat of cumulative effects of structural repairs to structural integrity of aircraft, spacecraft, and ship fleets while ensuring the safety and reliability of such valuable fleets with considerable benefits to both industry and the U.S. Government.

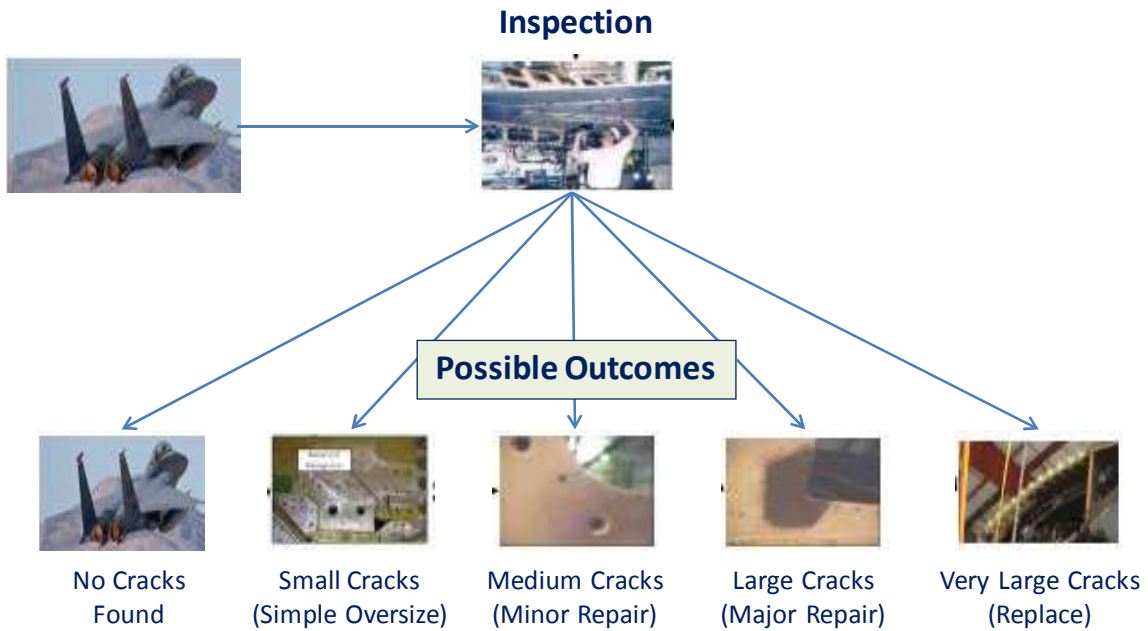


Figure 9.7-5. Notional Repair Options

- The construction of a Condition Tree is a key step in the modeling of the condition-based processes.
- The Condition Tree is made up of many branches with multiple conditions with associated probabilities of P_{ij} , where “i” is the inspection number and “j” is the condition number (e.g., Branches 1 and 27 each have 3 conditions).

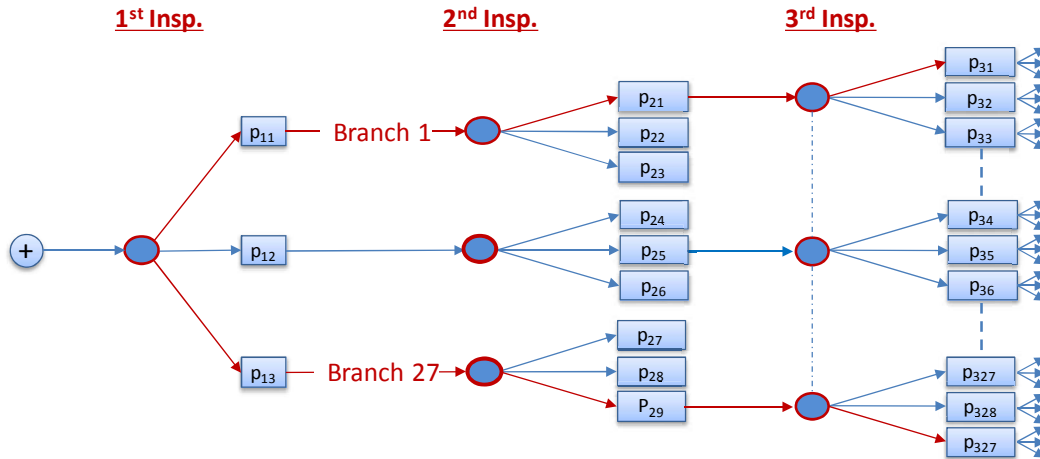


Figure 9.7-6. Modeling Repair Options

9.7.4. Probabilistic Damage Tolerance Using the FAA-Sponsored SMART|DT Software

Harry Millwater, Juan Ocampo, and Nathan Crosby, University of Texas at San Antonio; Beth Gamble and Chris Hurst, Textron Aviation; Marv Nuss, Nuss Sustainment Solutions

Under FAA funding, the University of Texas at San Antonio (UTSA), in consort with Cessna Aircraft and Nuss Solutions, has developed probabilistic damage tolerance software (SMART|DT) in support of risk assessment of aging aircraft (Figure 9.7-7). The emphasis of the program has been to provide the analyst a comprehensive risk assessment tool through the incorporation of: a) state-of-the-art lifing methods, e.g., NASGRO, AFGROW, and FASTRAN, for through, surface and corner cracks, b) a wide range of random variable options, and c) a complete repair and replace option (Figure 9.7-8). These features allow the analyst to consider a wide range of scenarios and to perform a realistic safety and risk prediction. The computational support provided to the analyst consists of a number of innovative features. In particular, an adaptive error-based surrogate model is developed on-the-fly that interpolates the residual strength and crack size results from NASGRO, AFGROW, and FASTRAN, such that time-dependent Monte Carlo realizations can be computed in a significantly reduced computer time. In addition, the computations have been parallelized such that all available computer cores are utilized (Figure 9.7-9). The inspection and repair options are comprehensive in that the user can implement any number of inspections and execute multiple repair scenarios. For example, different structural configurations can be simulated dependent upon the crack size detected, e.g., employ a doubler for a large crack, apply a patch for a medium-sized crack, and simulate the reaming of hole for a small crack. In each case, the entire fracture mechanics model can be redefined. The statistical tools available allow the analyst to consider a comprehensive list of random variables such as: initial crack size, crack aspect ratio, da/dN variability, hole diameter, edge distance, yield stress, ultimate stress and others. Finally, probabilistic sensitivities are computed in order to assess the relative importance of the random variables. In summary, a comprehensive risk assessment tool is now available that can integrate with existing lifing modules and codes and provide rich inspection, repair, and random variable options.

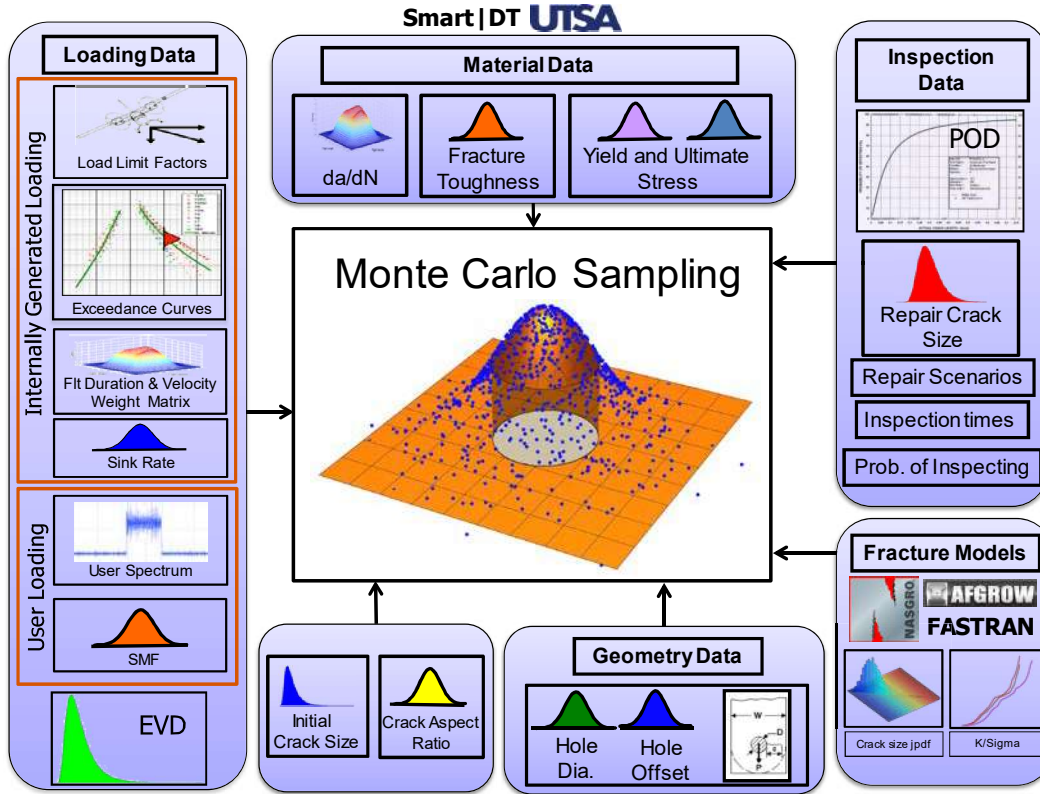


Figure 9.7-7. SMART | DT Software

➤ Run any crack growth model



➤ Consider any repair scenario



Oversized Hole

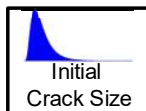


Doubler



Replacement

➤ Consider any random variable



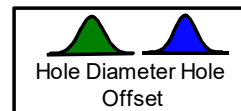
Initial Crack Size



da/dN



Fracture Toughness



Hole Diameter Hole Offset

Etc.

Figure 9.7-8. Development Philosophy

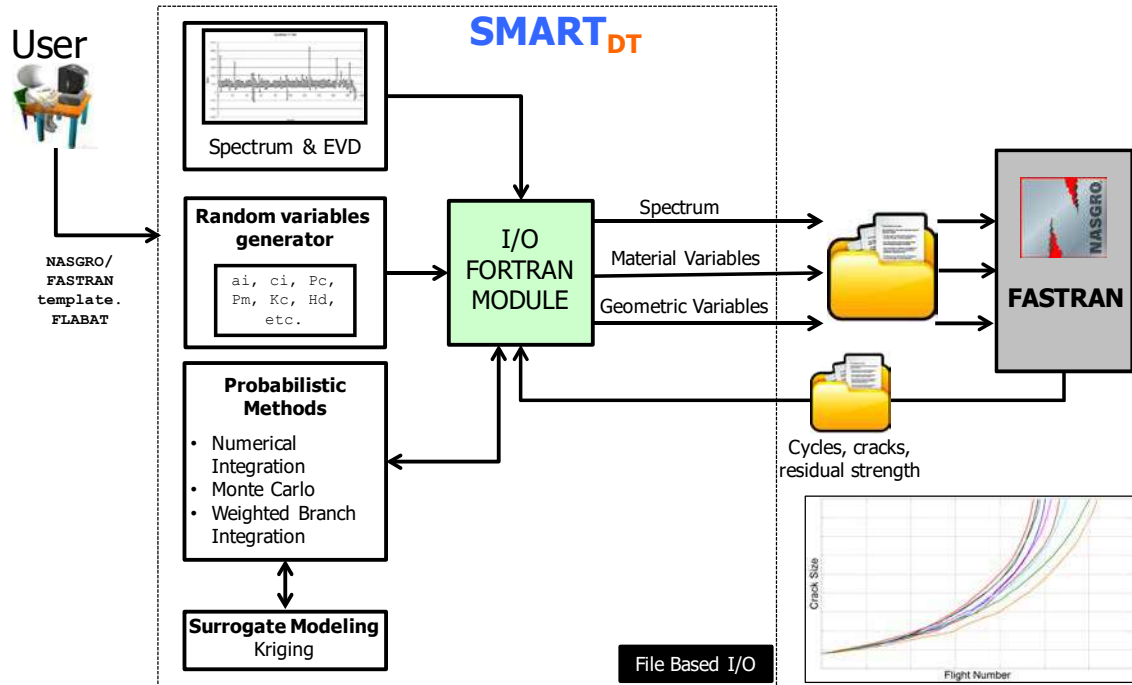


Figure 9.7-9. FASTRAN/NASGRO Interface Runs in Parallel

9.7.5. HH-60G Risk-Based Service Life Assessment

Nathan Branch and Gregory Wood, Mercer Engineering Research Center (MERC); Kevin Reid, HH-60G ASIP; Thomas Brussat, Tom Brussat Engineering, LLC

This technical activity discusses the development and substantiation of a certified service life for the USAF's HH-60G fleet (Figure 9.7-10). Development of a certified service life can be particularly challenging for legacy helicopters for several reasons. Full-scale fatigue tests are not practical due to the loading profile, which contains a large amount of small amplitude cycles in addition to GAG and maneuver loads typical of fixed-wing aircraft. The construction of the HH-60G lends itself to economic replacement of all structure, with no life-limiting components that cannot be replaced (e.g., C-130 center wing). Finally, the monocoque structure of the HH-60G is inherently redundant and capable of sustaining limit load under complete failure of primary structure. Given these facts, previous characterizations of the HH-60G service life as "unlimited" were proposed. However, as the fleet ages, the risk of widespread fatigue damage (WFD) must be evaluated. MERC conducted this study in order to quantify the risk level associated with WFD. Several previous HH-60G ASIP initiatives lent themselves to the risk-based assessment. Crack history and component replacement records were used to catalog crack-prone locations and determine equivalent initial flaw size (EIFS) distributions. MERC utilized a previously developed and validated global HH-60G finite element model (FEM) to determine the combinations of component failures that, if undetected, would cause loss of aircraft. Durability and damage tolerance analyses (DADTA) at these locations were performed using MERC in-house code to determine the crack growth at critical locations subjected to the usage spectrum for both intact and failed neighboring structure (Figure 9.7-11). The maximum stress per flight distribution for these components was obtained from flight strain survey data, Loads / Environment Spectra Survey (L/ESS) data, and the HH-60G finite element model (Figure 9.7-12). The SFPOF for catastrophic component failures on the HH-60G were determined by MERC using a new Fast Monte Carlo risk analysis program designed for multi-element damage (MED) evaluation (Figure 9.7-13). The MED Monte Carlo accounts for fail-safety of multiple

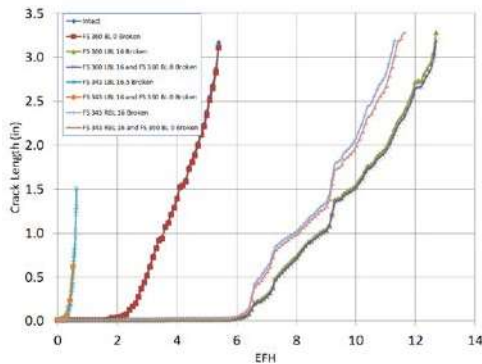
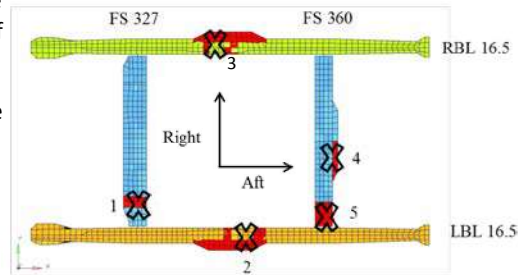
components, faster crack growth rates when neighboring parts are broken, and the capability of different NDI methods. The risk of structural failure as the fleet ages can be determined for different NDI and maintenance strategies. Program runtimes can be just a few minutes by only considering the critical inspections before and after the first component failure when cracks are most likely to be found. The result of the probabilistic SFPOF provided data to the HH-60G SPO and MAJCOMs to allow determination of a maintenance and inspection approach for the aircraft in order to ensure acceptable risk levels (Figure 9.7-14). It is believed that this approach can be generalized to other rotary-wing platforms where full-scale fatigue testing is impractical and that do not have other life-limiting characteristics.



Figure 9.7-10. HH-60G Pave Hawk

- Analysis with global finite element model identified five critical locations along four main transmission beams of HH-60G upper cabin
- Choice of locations supported by crack history database
- All five are failsafe: Any combination of three failed locations is catastrophic, three scenarios of two failures are not catastrophic

Top View of main transmission beams



- DTAs were performed to determine a(t)'s for these locations under various fail-safe scenarios
- Total of 34 a(t) curves
- FS 327 a(t) goes critical in 5 to 12 hours from 0.01 inch a_0

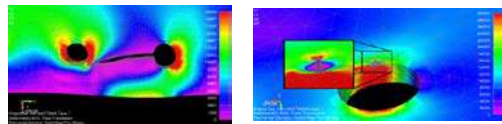
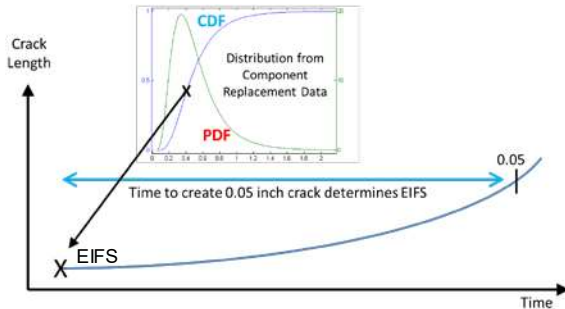
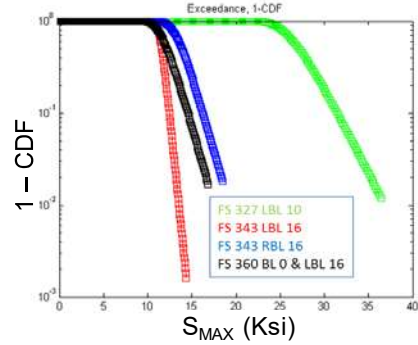


Figure 9.7-11. Finite Element Model and Damage Tolerance Analyses

- Max stress per flight (S_{MAX}) distributions for all locations:
 - Flight data taken from 1100 L/ESS flights
 - Correlated to IVHMS strain survey and global FEM
 - Used to create S_{MAX} exceedance curves for each location



- Component replacement history from depot records determine component life distribution
- Used to determine EIFS distribution for each beam
- Component life represents time for the EIFS to grow to a 0.05 inch size crack on a(t) curve
- Rogue flaw adjustment imposed, so a 0.05 inch flaw occurs with $1e-7$ probability

Figure 9.7-12. Max Stress Per Flight Distributions

- MERC also developed a Simple-Sampling (SS) MED Monte Carlo program
- Inspired by work published by Halbert et. al. AIAA 2013-1604 (Monte Carlo, 1 part)
- Similar to Fast Monte Carlo MED with exceptions:
 - Simulates every flight and every inspection
 - Each trial is equally-weighted
 - Runtimes range from hours to days depending on SFPOF magnitude
 - Can improve runtime by performing selective sampling

Example MED SFPOF Results →

Red = Simple Sampling MC
Blue = Fast MC

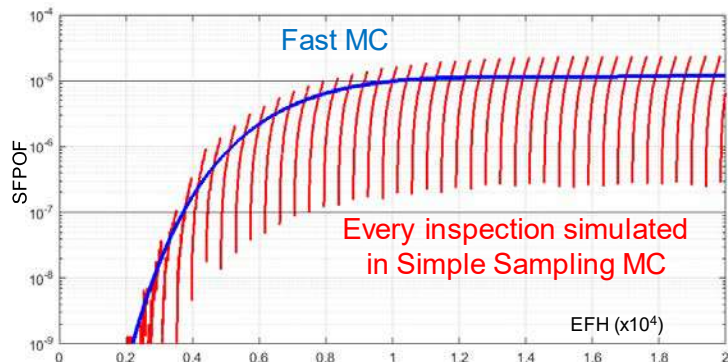


Figure 9.7-13. MED Monte Carlo Program

- Chart below shows that there is little benefit from performing inspections unless the structure is failsafe
- Infrequent poor visual POD has little effect if one part failure is catastrophic and suffers from fast crack growth
- Combination of fail safety and inspections needed to manage risk

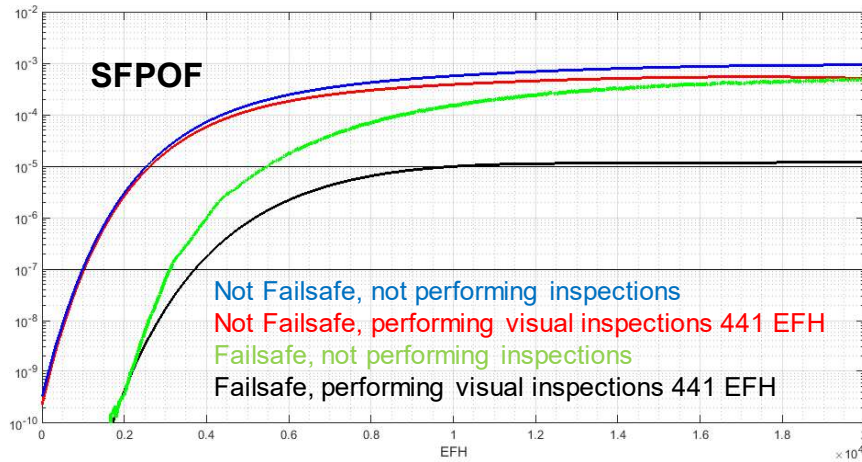


Figure 9.7-14. SFPOF Results

9.7.6. Probabilistic Risk Assessment – The SMART Approach to Continued Operational Safety Beth Gamble, Textron Aviation

Cessna and Beechcraft (a.k.a. Textron Aviation) have delivered 250,000+ airplanes over the past eighty-five years with the combined fleet exceeding 100 million flight hours (Figure 9.7-15). These airplanes are used to fulfill a variety of roles including military training and combat, government special missions, commercial airline service, in addition to corporate and personal use. Textron Aviation's fleet is aging with many aircraft in the fleet being legacy designs that predate damage tolerance regulations. Over a typical airplane's life, it may have several owners and fly a wide range of missions. In many cases, the current owner may not know how the previous owner(s) used the airplane. Some of those missions may be far more severe than what the manufacturer intended. This makes determining the appropriate inspection requirements difficult due to the inherent variability in construction and operations. Therefore, a risk assessment evaluation of the continued operational safety of the fleet can provide important insight to the criticality/severity when potentially serious structural issues arise. To address the inherent variability in aircraft usage, flight loadings, material properties, fabrication quality and initial flaw sizes, a probabilistic methodology for fatigue and damage tolerance of general aviation aircraft has been developed and implemented. The methodology and computer code, SMART|DT (Small Airplane Risk Assessment Technology - Damage Tolerance), was created by the University of Texas-San Antonio under FAA sponsorship, to address risk assessment and risk management of general aviation structural issues (Figure 9.7-16). The architecture of the software, however, allows the software to be applied to transport category and military aircraft in addition to general aviation. To evaluate the SMART|DT methodology and software, a twin-engine airplane with a history of fatigue cracking was chosen (Figure 9.7-17). This airplane has been used in a wide variety of missions including low level "sightseeing" and short "island hopping" missions (Figure 9.7-18). The results from SMART|DT are compared to the results of an extensive fatigue and damage tolerance assessment developed by the manufacturer for

continued operational safety inspections. This technical activity gives an overview of SMART|DT and how it was used to resolve a current airworthiness concern. The overview will include: 1) a comparison of SMART|DT results to those developed by the manufacturer, 2) a technical evaluation of the SMART methodology, 3) a comparison of the spectrum capabilities within SMART|DT to OEM generated spectra, 4) a technical evaluation of the effect of initial flaw size and comparison to observed damage in the field, 5) geometric and/or material variability, 6) a derivation of an inspection program using SMART|DT, 7) a technical evaluation of geometric and material variability and 8) opportunities for software enhancements.



Figure 9.7-15. Cessna and Beechcraft Airplanes

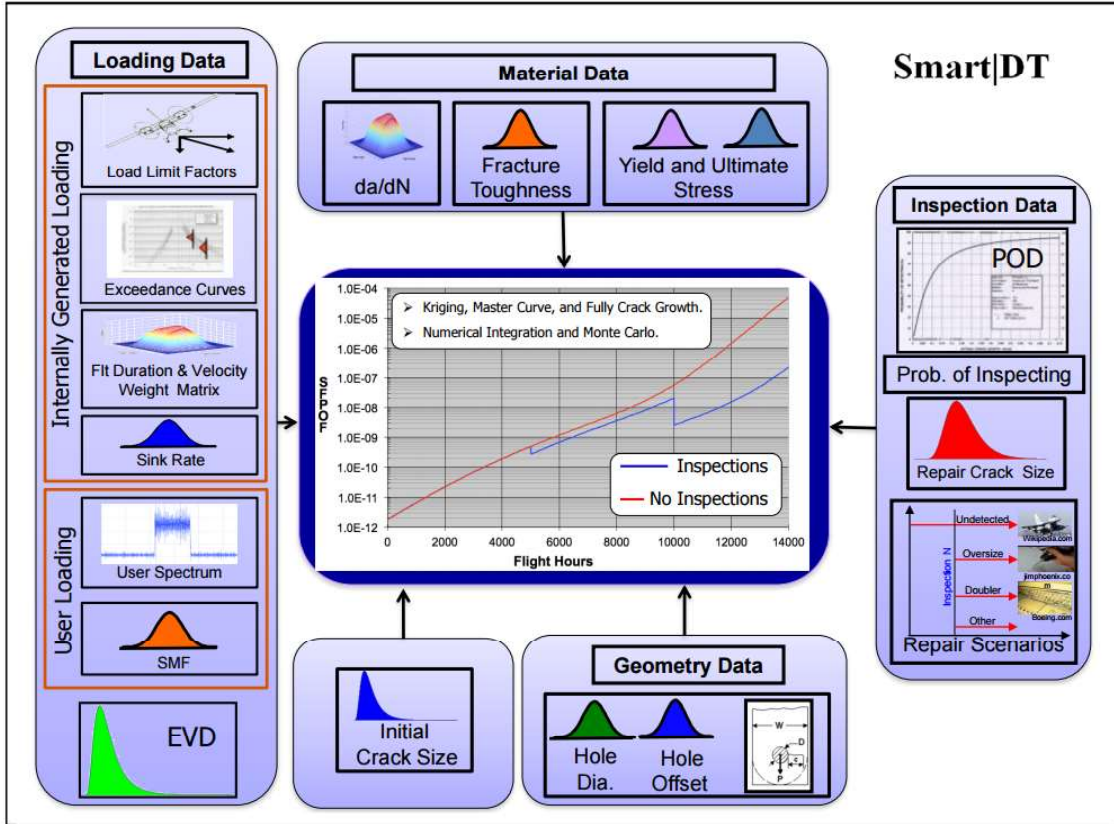


Figure 9.7-16. SMART | DT Methodology



Figure 9.7-17. Cessna Model 402C

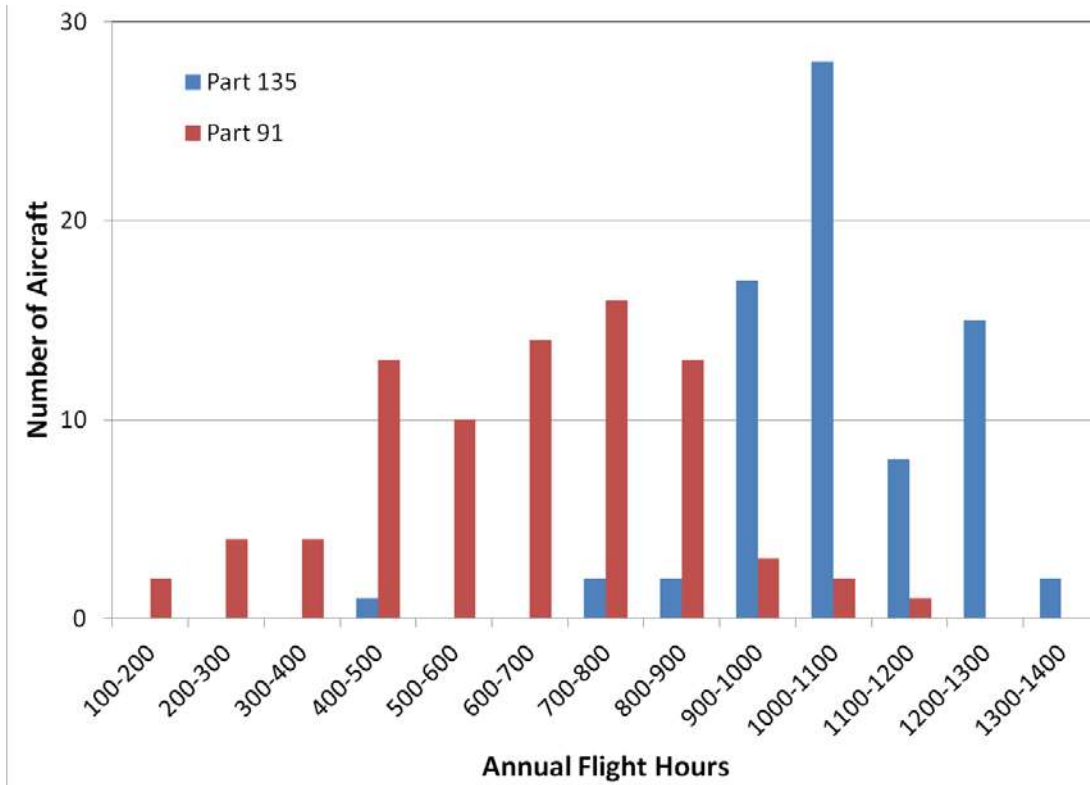


Figure 9.7-18. Model 402C Fleet Annual Flight Hours

9.7.7. Building Robust Initial Flaw Size Distributions for T-38 Risk Analysis

Laura Domyancic, Southwest Research Institute

Probabilistic risk analysis is essential to maintain the continued operational safety of aging fleets, such as the USAF T-38 (Figure 9.7-19). The technical substance of a probabilistic risk analysis is contained within the single flight probability of failure (SFPOF) calculation, and previous risk analyses of T-38 fracture critical locations (FCLs) have shown that the SFPOF is often most sensitive to the initial flaw size (IFS) variable. Since this variable is the most difficult for which to obtain data, Southwest Research Institute (SwRI) has performed significant work in recent years to accurately characterize IFS distributions. The traditional way to characterize this variable is to use findings from aircraft teardown results to build an equivalent initial flaw size (EIFS) distribution (Figure 9.7-20). However, it is also important to incorporate non-findings, known as suspension data, to prevent an over-conservative prediction. The question then arises as to what flaw size should be used to represent the suspended data points. Using suspension flaw sizes based on the capability of the non-destructive inspection (NDI) method (as suggested in the PROF software manual) can lead to poor distributions, especially if the NDI method cannot detect small flaws or if there is large scatter in the usage of fleet airframes (Figure 9.7-21). This effort seeks to address this issue by representing suspensions with a separate initial flaw size distribution based on the material microstructure. Then, both the teardown EIFS distribution and suspension distribution are combined into a single bimodal IFS distribution for input into the risk analysis. By accounting for separate crack nucleation mechanisms (e.g., natural fatigue vs. gouges) in this way, this method can reduce variability and over-conservatism in risk analysis results. The material-based distribution can also be used as a standalone input for risk analysis of locations which do not yet have crack findings. An example risk analysis using the new method showed the significant effect that

using a bimodal, material-based IFS distribution can have on the SFPOF results. An example (Figure 9.7-22) set of IFS data was represented by the traditional method and was known to be over-conservative due to the lack of inspection findings. A bimodal distribution was created using the new method, and a risk analysis was then run using each distribution as an input (Figure 9.7-23). The SFPOF results revealed that the new method delays the need for risk mitigation measures by approximately 2,000 flight hours, and thus reduced the over-conservatism (Figure 9.7-24). This technical activity will cover the improved method, updates made to T-38 IFS distributions using this method, and the various “best practices” learned along the way.



Figure 9.7-19. T-38 Aircraft

- Concept was introduced in the late 1970s
- The EIFS is a hypothetical crack size that results in the equivalent life to a crack that was in the structure at time zero
 - Entire life of crack is estimated by Stage II crack growth

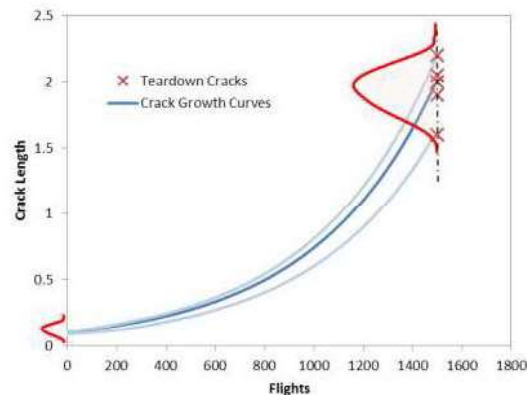
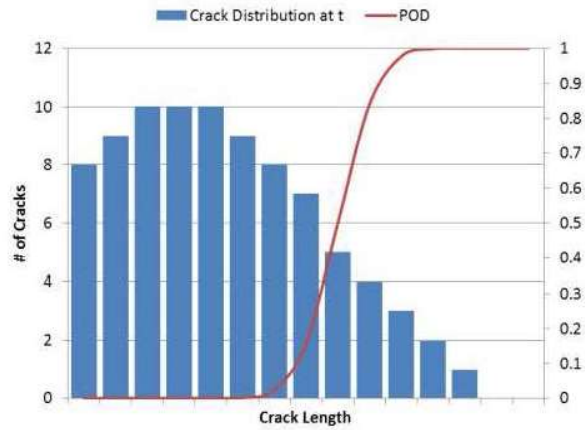


Figure 9.7-20. Equivalent Initial Flaw Size Method

- **POD Curve (PROF Manual)**
- The probability of detection (POD) curve and the distribution of detected cracks are used to infer the suspension crack size distribution
- The suspended locations are then assigned a crack size from the distribution $M(a)$

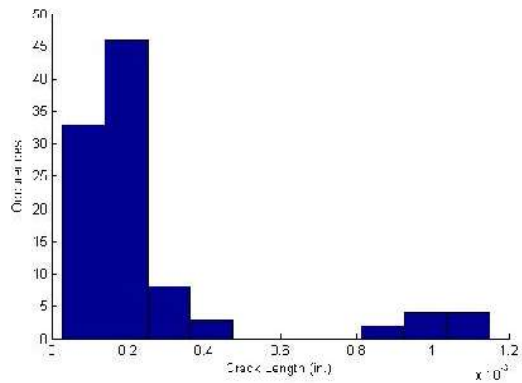
$$f(a) = \frac{P_D(\infty)}{POD(a)} \frac{d}{dx} (D(a))$$



$P_D(a)$ is the proportion of cracks less than a that are detected

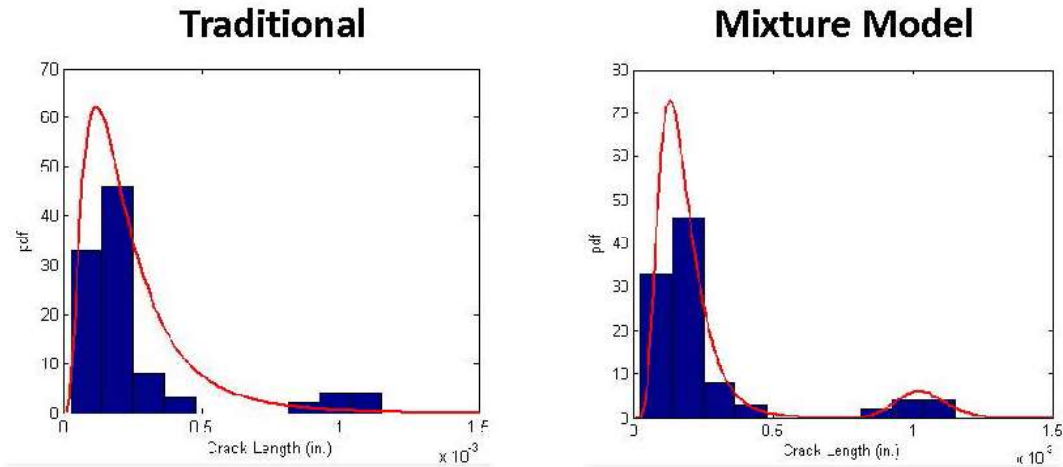
Figure 9.7-21. Traditional Method for Suspension Distributions

- **Structural detail in 2024-T351 plate**
- 100 similar details are inspected
 - 10% have mechanical damage and recorded flaw sizes
- Suspensions assumed to follow distribution for 2024-T351 crack nucleating particles (Laz)
 - LN(1.76e-4, 8.08e-5) in.



Sampled IFS Data

Figure 9.7-22. Notional Example



- Mixture model is a much better representation of the data

Figure 9.7-23. Representation of Data

- Traditional unimodal distribution – Maintenance (Mx) action required before 18,700 hours
- Finite mixture distribution - Mx action required before 20,900 hours
- **2,200 flight hour difference**

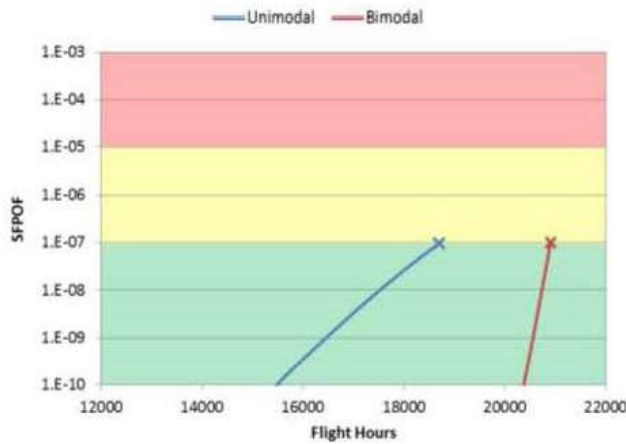


Figure 9.7-24. Time Required for Risk Mitigation

9.7.8. Fatigue Path Probability Integration (FPPI) for Fatigue Management with Multiple Maintenance Options Using Nondestructive Inspections (NDI) or In-situ NDI

Michael Shiao and Tzikang Chen, USA – Vehicle Technology Directorate

To improve aircraft availability and readiness at reduced operating cost throughout the system/component life cycle, the industry and Government are developing capabilities to move beyond conventional flight-hour based maintenance towards a reliability-based maintenance framework. In fatigue-critical structural maintenance, the probabilistic structural risk assessment (PSRA) methodology using conventional nondestructive inspection (NDI) for single maintenance scenario has been well developed based on the assumption of independent inspection outcomes. However, when using the emerging NDI with in situ sensors, the independent assumption no longer holds, and the existing PSRA methodology must be modified. Army Research Laboratory has derived a new NDI and in situ NDI-based framework with a proper probabilistic modeling of correlations among multiple inspection outcomes from the same structural component considering multiple maintenance options. The framework and the associated probabilistic algorithm FPPI (Fatigue Path Probability Integration) are based on the principles of fatigue damage progression, NDI reliability assessment, and structural reliability methods (Figure 9.7-25 and 9.7-26). Multiple maintenance options include multiple repair types (Figure 9.7-27) and inspectional schedules, multiple loadings and multiple inspection techniques to allow for a more realistic probabilistic modeling. FPPI can incorporate a wide range of uncertainties including material properties, repair quality, crack growth related parameters, loads, and probability of detection for risk prediction. In addition, FPPI probabilistic algorithm is capable of modeling the correlation among inspection outcomes from in situ NDI. If the correlation is set to zero, it simulates the independent inspections for risk assessment using NDI for health monitoring. In this technical effort, we will demonstrate the computational efficiency and accuracy of PFFI for multiple maintenance options using various repair scenarios and inspection schedules, and present a preliminary verification study. We will also present the effect of inspection correlations on risk prediction. As shown in the study, the assumption of independent inspection events using in situ NDI for health monitoring gives non-conservative risk prediction while the prediction with the assumption of fully correlated inspection events is too conservative.



Figure 9.7-25. FPPI for Fatigue Risk Management

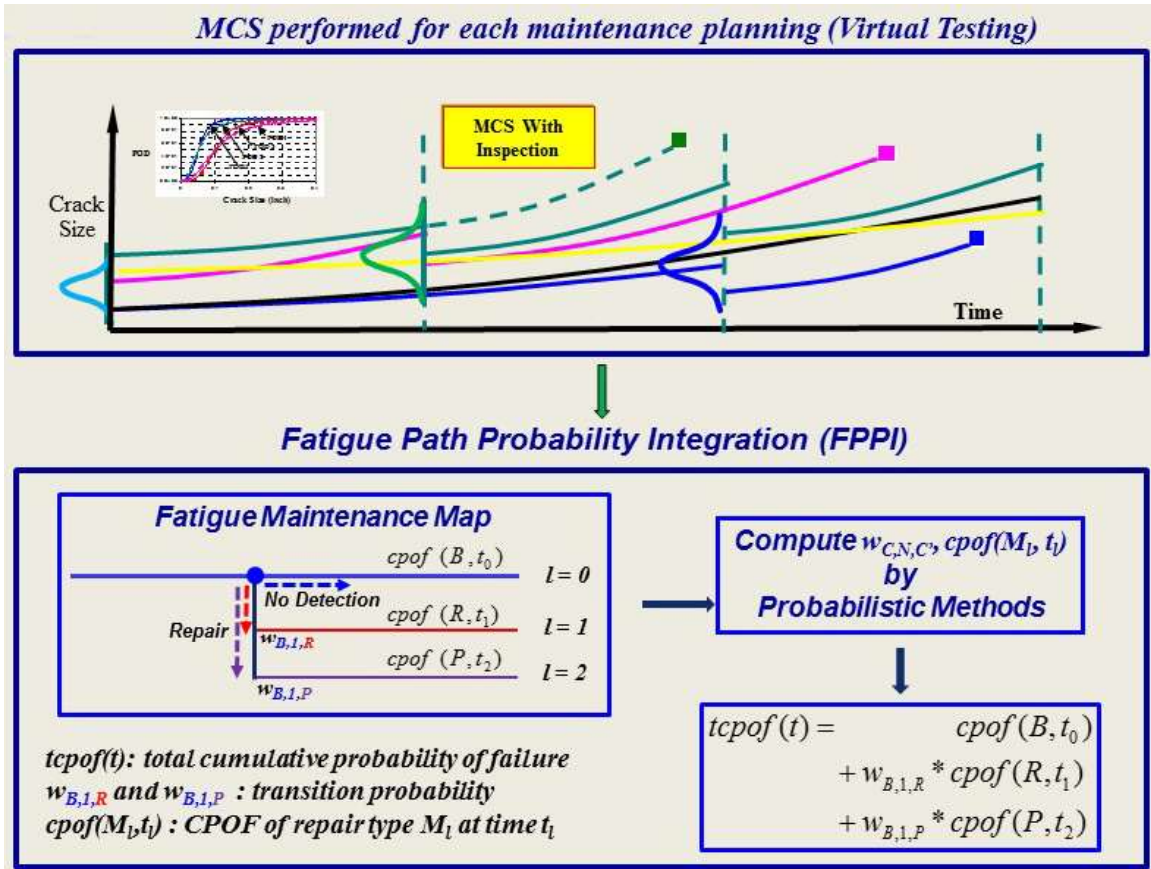


Figure 9.7-26. Visual Testing Supporting FPPI

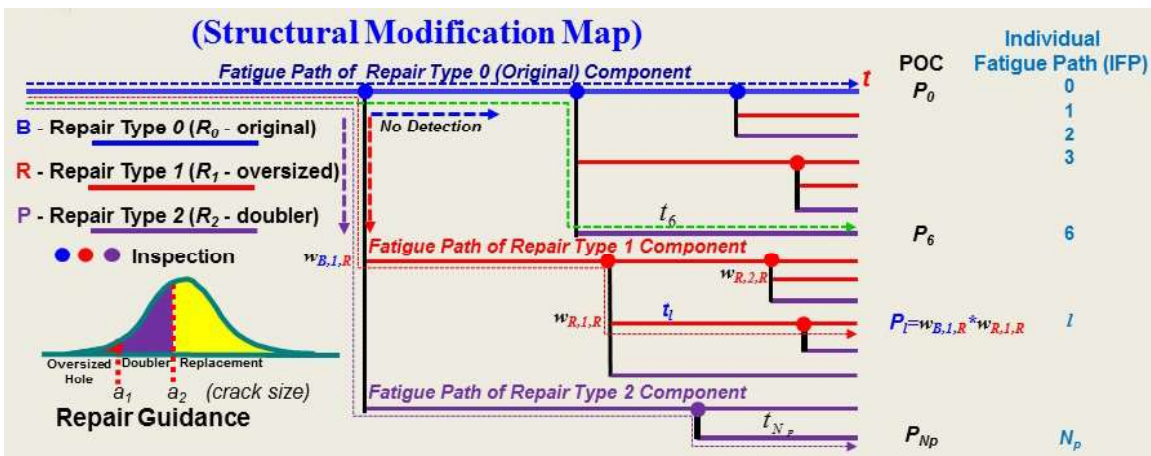


Figure 9.7-27. Fatigue Maintenance Map for Multiple Repair Types

9.7.9. A Comparison of Risk Methods in Problems of Varying Complexity

Mark Ryan and Jeff Mock, Lockheed Martin Aeronautics

The differences between various methods to calculate risk will be investigated. First, the hazard equation will be derived from probability theory and a method for the treatment of multiple failure modes will be presented. Second, the hazard equation will be compared to two methods used to estimate risk; the probability density function (PDF) and the cumulative distribution function divided by the aging parameter (CDF/t) (Figure 9.7-28). A quantitative example comparing the methods will be given for a single-point failure with no inspections (Figure 9.7-29). Another example will be given for a single-point failure with inspections (Figure 9.7-30). A third example will be given for the case of a redundant design (Figure 9.7-31). Although the PDF is often satisfactory for simple cases (single-point failure) where it diverges from the hazard equation above 10^{-5} , it is unsatisfactory for the more complex cases (redundancy) where it may diverge earlier than 10^{-9} . It is concluded that the hazard equation is the best method for risk calculation.

Cumulative Distribution Function (CDF)/time

- Results in negative risk and infinite life

$$R(t) = \frac{CDF(t)}{t}$$

Probability Distribution Function (PDF)

- Initially accurate, but diverges
- Instantaneous PDF is CDF/time

$$R(t) = PDF(t) \quad \text{(instantaneous)}$$

$$\mathbb{R}(t, \Delta t) = CDF(t + \Delta t) - CDF(t) \quad \text{(risk over period of time)}$$

Hazard Equation

$$R(t) = \frac{PDF(t)}{1 - CDF(t)} \quad \text{(instantaneous)}$$

$$\mathbb{R}(t, \Delta t) = \frac{CDF(t + \Delta t) - CDF(t)}{1 - CDF(t)} \quad \text{(risk over period of time)}$$

Figure 9.7-28. Overview of SFPOF Risk Methods

- For simple cases, PDF is good enough.
 - PDF typically diverges from the risk equation above 10^{-5} .

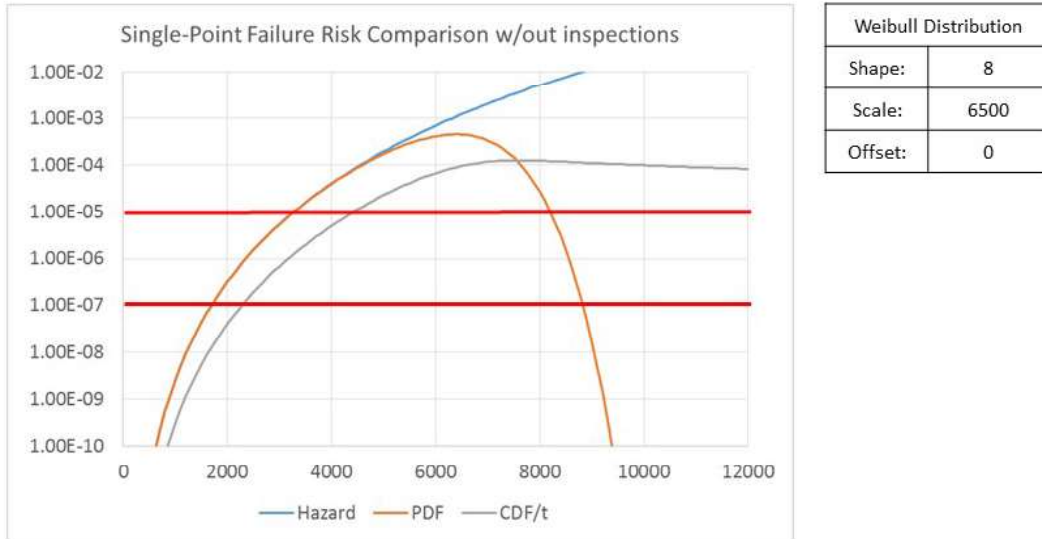


Figure 9.7-29. Single-Point Failure with No Inspection

- For simple cases with inspections, PDF creates non-intuitive results
 - Risk starts decreasing after a point
 - Risk goes negative

Weibull Distribution	
Shape:	8
Scale:	6500
Offset:	0

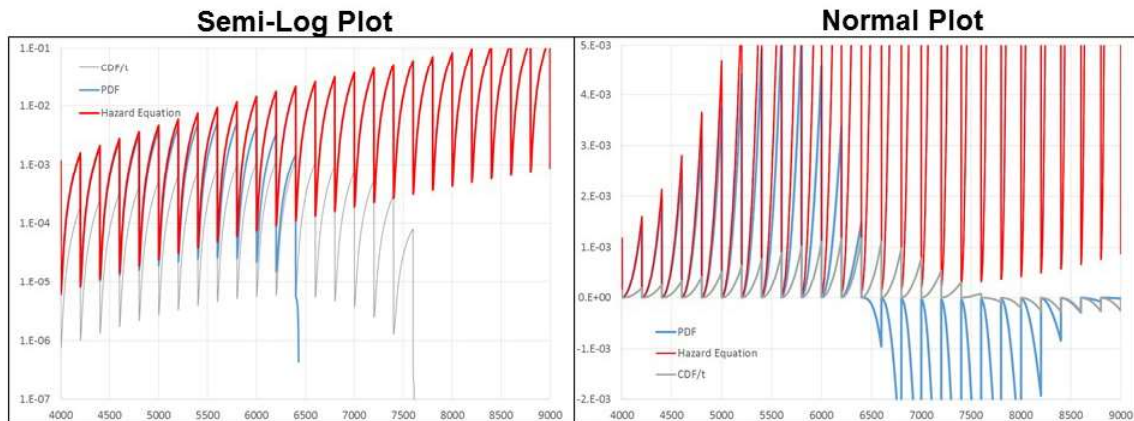


Figure 9.7-30. Single-Point Failure with Inspections

- **Binomial Distribution can be used to calculate risk on redundant systems with no load transfer**
- **With redundant systems PDF can diverge from Hazard Equation below 10^{-7}**

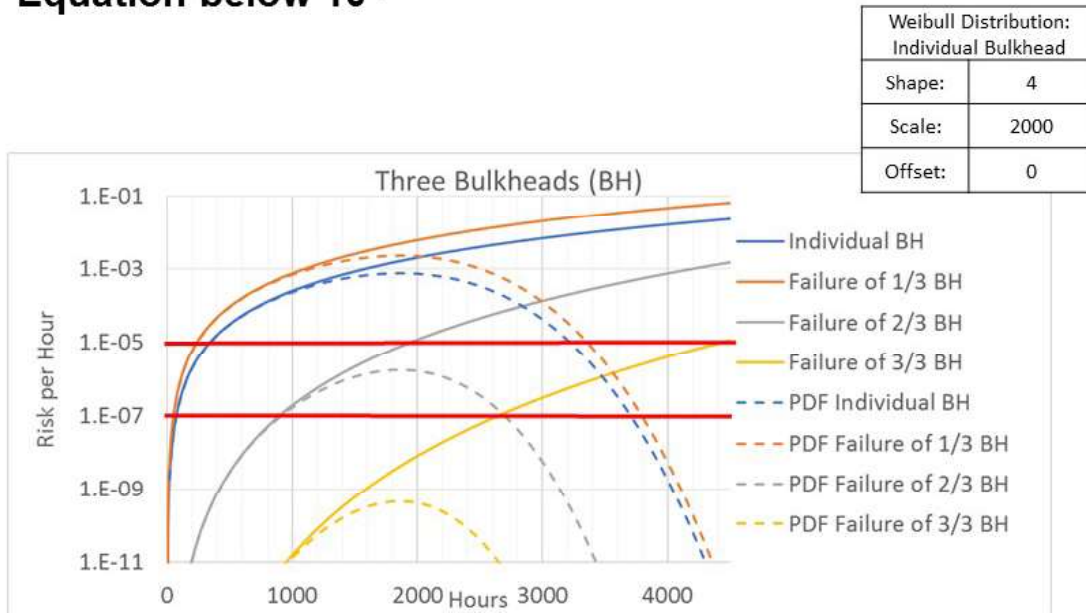


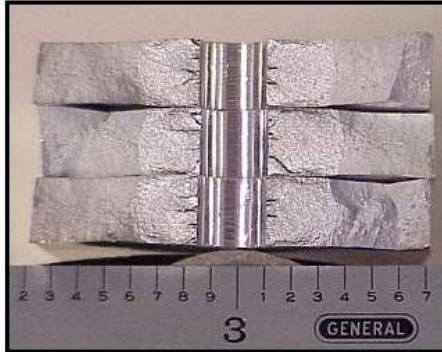
Figure 9.7-31. Redundant Structure with Similar Lives

9.7.10. Durability Risk Analysis for Random Double Cracks at a Hole

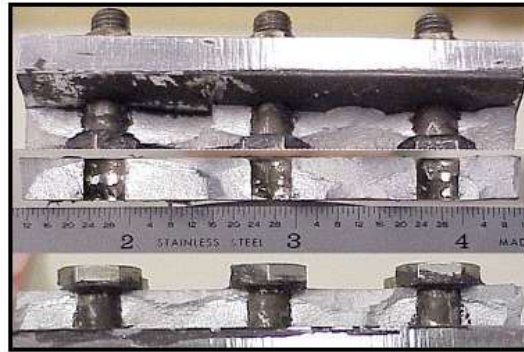
Thomas Brussat, Tom Brussat Engineering, LLC

By tradition in the durability and damage tolerance analysis for fatigue cracking at a hole, a single crack is assumed on one side of the hole. Typically, the same assumption is made in risk analyses, despite the fact that cracks on both sides of a hole are a common cracking scenario and that double cracks can grow to critical size more than twice as fast as a single crack (Figure 9.7-32). Efforts at a rigorous durability analysis of double cracks at a hole are a challenge because there are an infinite number of possible double crack scenarios. A worst-case durability analysis that assumes equal double cracks would be straightforward but would likely be overly conservative. The methodology proposed in this technical effort is a risk-based durability analysis that develops and uses a probability distribution for all possible relative sizes of double cracks. The demonstration example, with the hole near an edge, adds the complexity of non-symmetry that typifies most practical cases (Figure 9.7-33). Current approaches to this problem appear inadequate. Even a Monte Carlo risk analysis seems daunting because each of the thousands of random trials would require a unique AFGROW analysis to calculate the crack growth life. Furthermore, each trial would also require the crack lengths at the specific times when an inspection is scheduled, requiring a separate regression equation for each AFGROW result. This technical effort demonstrates a very manageable risk analysis approach for random double cracking at a hole located off-center, including the effects of periodic in-service inspections. Only a handful of AFGROW analyses are required. Total life is defined as the sum of the time to nucleate a .02 inch crack (driven by peak stress at the hole) plus the crack growth time to failure (driven by stress intensity factor). The crack growth life and the effects of periodic inspections on failure probability are calculated for eight representative double

crack cases. An interpolation scheme extends these results to the entire range of double crack scenarios. In a manner analogous to an EIFS distribution, the probability distribution for the nucleation time of the first crack is estimable from service cracking data. A rationale is devised to also estimate the probability distribution for relative time to nucleate the second crack. The accelerating effect of the growing main crack on that secondary crack nucleation time is estimated using beta-factor output from the AFGROW crack growth analyses. From these results, Single Flight Probability of Failure can be calculated for the random double crack case. The methodology is developed in detail and applied to the example of a hole near a free edge. Single-flight-probability-of-failure results for the random double crack are compared to those of both the traditional single crack and the equal double crack (worst) case (Figure 9.7-34).



Fracture surface for
open hole coupons
7050-T7451 Aluminum

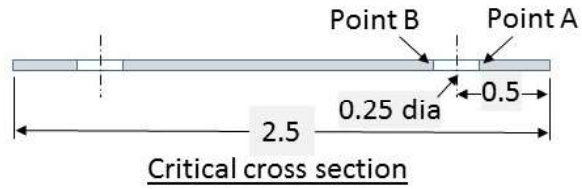


Fracture surface for
single lap joints
7050-T7451 Aluminum

What are the probability and consequences of double cracking?

Figure 9.7-32. Double Cracks Often Occur in Laboratory Fatigue Tests

- 7075-T6 Aluminum
- Uniform remote tension
- Spectrum loading; $S_{REF} = 34.8$ ksi
- Stress concentration factors:
 - At point A: $K_{TA} = 3.19$
 - At Point B: $K_{TB} = 3.11$



N_B and N_A

- Definition: relative nucleation times at Points B and A
- $(N_B - N_A)$ determines relative crack sizes
- Goal here is to randomize $(N_B - N_A)$

POD/INSPECTION:

- $a_{NDE} = 0.10$ in. is based on 90/95
- Use mean curve for risk analysis.
- Lognormal CDF;
 - $\mu = -3.219$;
 - $\sigma = 0.5409$
- POI = 0.97

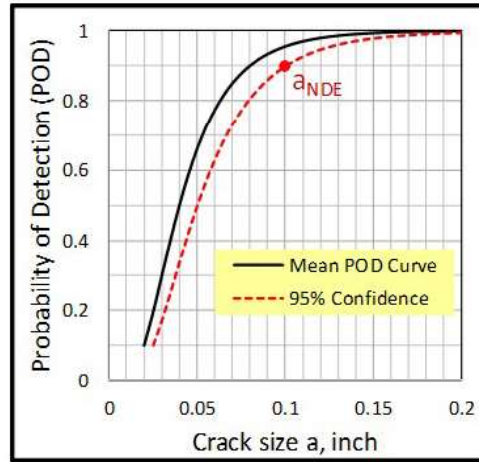


Figure 9.7-33. Example Problem of Tension Strip

$$SFPOF(N+\Delta N) = [\text{Conditional PoF}(i)] \{f(N)/[1-F(N)]\}$$

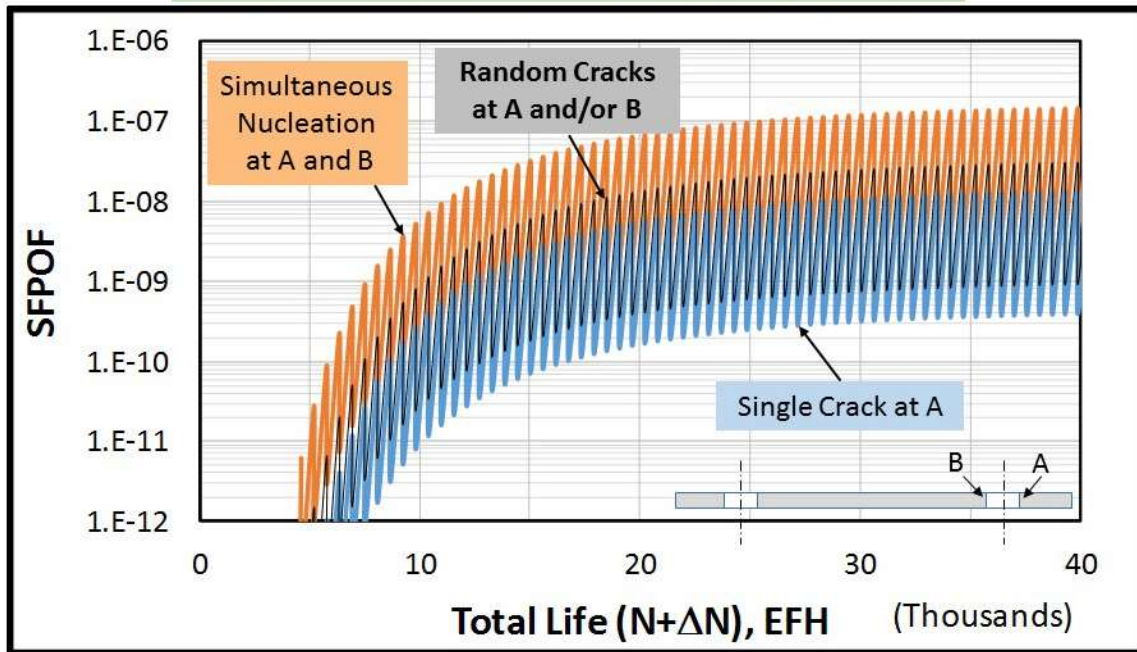


Figure 9.7-34. Comparison of SFPOF Results

9.7.11. Continued Development of the DARWIN Software for Probabilistic Damage Tolerance Analysis and Risk Assessment

Craig McClung, Michael Enright, Yi-Der Lee, Jonathan Moody, James Sobotka, Vikram Bhamidipati, and John McClure, Southwest Research Institute; Ben Guseman, Elder Research

High-energy rotating components in aircraft gas turbine engines may contain inherent or induced anomalies that can lead to rare but potentially catastrophic failures. Federal Aviation Administration (FAA) Advisory Circulars address specific types of inherent and induced anomalies (AC 33.14-1 and AC 33.70-2, respectively) and establish a general framework for all life-limited engine parts (AC 33.70-1). The associated risk of fracture can be predicted using DARWIN[®], an award-winning probabilistic fracture mechanics software code developed by Southwest Research Institute[®] under FAA R&D funding.

DARWIN (Design Assessment of Reliability With INspection) integrates 2D and 3D finite element (FE) models and stress/temperature results, advanced fracture mechanics models, material anomaly data, NDE probability of detection curves, and inspection schedules with advanced probabilistic methods and a powerful graphical user interface (GUI) to determine the probability of fracture of a component as a function of operating cycles, with and without inspections. Originally developed to address specific threats to the integrity of high energy rotating components in aircraft engines, DARWIN now includes general deterministic and probabilistic damage tolerance capabilities relevant to many applications, including airframes. DARWIN has been under continuous development since 1995, and recent advances have significantly enhanced its ease of use, efficiency, and accuracy.

DARWIN development activities during 2015-2016 focused on Versions 9.0 and 9.1.

Previous versions of DARWIN provided autozoning capabilities for risk assessment involving inherent anomalies in components modeled using 2D and 3D finite element (FE) geometries. These techniques automatically build DARWIN zones based on user-defined property regions that consider anomaly size and occurrence rate, material properties, and other parameters. Autozoning leads to consistent results among users and reduces the human time required for zone definition. However, the computation time associated with autozoning may be significant for component models with large numbers of finite elements. **DARWIN 9.0 provides a new optimal Gaussian Process (GP) pre-zoning capability for the efficient automatic creation of zones in large complex 2D and 3D finite element geometries with inherent anomalies.** It defines pre-zones as groups of finite elements that are arranged based on similar stress ranges, temperatures, and distance-to-surface values. It then identifies the risk limiting location within each pre-zone via an approximate risk surface that is based on risk values at training points within the pre-zone. The previously developed optimal autozoning methodology is then used to determine the optimal zone break-up of the model. For large models where the number of pre-zones is significantly smaller than the number of finite elements, the optimal pre-zoning capability can significantly reduce the computation time associated with risk assessment. Initial studies indicate that the new pre-zoning algorithm is up to two to three orders of magnitude faster than the previous optimal autozoning algorithm, and up to four to five orders of magnitude faster than the previous exhaustive algorithm. Furthermore, the pre-zoning method requires less memory than either the exhaustive or optimal methods. This feature enables the pre-zoning method to solve much larger models than either previous method.

Rotating engine components often have 3D geometric features that repeat cyclically around an axis. Previously, DARWIN only supported full 3D models, or 2D axisymmetric models where the cross section was constant about the axis of rotation. **DARWIN 9.0 provides a new capability for risk assessment of components that are defined via 3D sector finite element model geometries.** When the sector model option is selected, DARWIN displays the original sector model and the exterior component boundaries based on cyclically repeating sectors. For life and risk assessments, fracture models are based on the full FE model geometry. This new capability is available for both manually and automatically zoned models.

DARWIN 9.0 includes a new stress intensity factor (SIF) solution (CC18) for part-elliptical cracks that originate at corners with a 135-degree angle, such as one corner of a chamfered edge. Cracks modeled using the CC18 SIF solution are capable of transitioning to the CC12 SIF solution, which is the bivariate SIF model for a crack that spans the entire length of a chamfered corner (Figure 9.7-35).

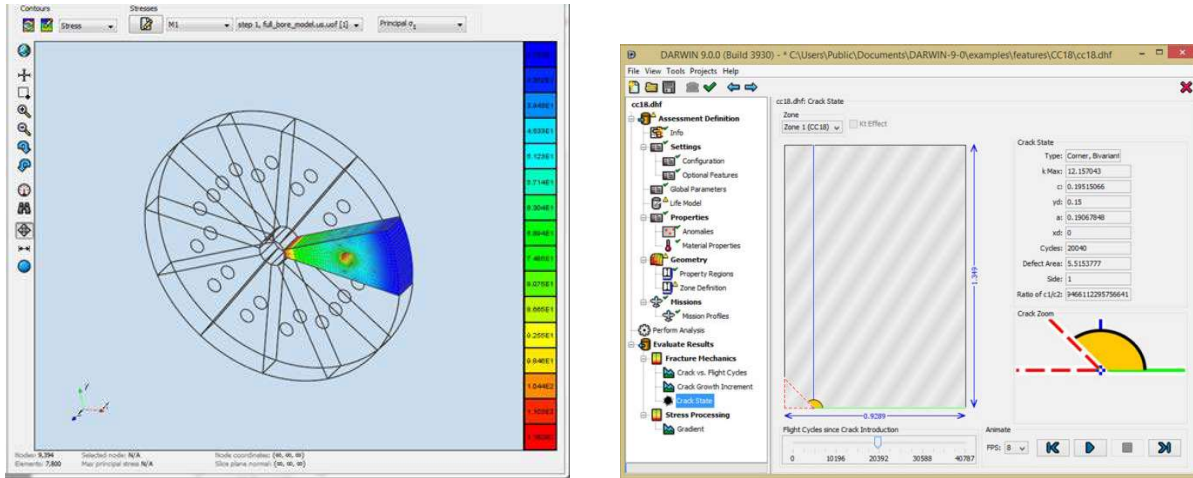


Figure 9.7-35. DARWIN 9.0 Provides a New Capability for Risk Assessment of Components that are Defined via 3D Sector Finite Element Model Geometries (Left) and a New Bivariant Stress Intensity Factor Solution (CC18) for Cracks that Originate at Corners with a 135 Degree Angle, Such as One Corner of a Chamfered Edge

DARWIN 9.0 also includes several new features that were supported by supplementary funding from the U.S. Air Force Research Laboratory, the U.S. Naval Air Systems Command, and DARWIN commercial licensing revenue. Several of these features facilitate the integration of DARWIN with manufacturing process simulation software so that DARWIN can be used to support Integrated Computational Materials Engineering (ICME). This ICME framework addresses the impact of manufacturing parameters (and manufacturing variability) on the integrity and reliability of components. The manufacturing process has a direct impact on bulk residual stresses, material microstructure, and anomaly orientation, each of which can affect life and fracture risk in the finished product. Specific new ICME capabilities included in DARWIN 9.0 include inputs of random unrecrystallized grain sizes, prediction of crack formation lives based on these unrecrystallized grain sizes, prediction of location-specific fatigue initiation lives related to persistent slip bands in recrystallized or unrecrystallized grains as well as supergrains, and support for anomaly distributions that are assigned at the billet stage and tracked to the final component shape. Related ICME features have been implemented in other recent versions of DARWIN.

Previous versions of DARWIN did not provide adequate support for large finite element (FE) models with large numbers of load steps. The time required to import and display large FE models in the GUI could be measured in double digit minutes or even hours. The time required to process FE models in the risk assessment code (RAC) was also extensive. This was primarily due to the use of text-based FE model files. **DARWIN 9.1 introduced a new hierarchical binary file format HSIESTA to store FE results data. This substantially reduces computation time and memory requirements for large FE models.** HSIESTA replaces an earlier FE model file format that stored data as ASCII text. These enhancements have significantly reduced the time required to read and display the stresses and temperatures associated with large FE models. For example, an FE model with approximately 100,000 nodes and 1,000 load cases required nearly ten minutes to import and display in the previous DARWIN version for a single load case. Using the HSIESTA capability implemented in DARWIN 9.1, the same FE model was imported and displayed in approximately ten seconds, or roughly sixty times faster than

DARWIN 9.0. The DARWIN computational engine was also enhanced to read and process data from HSIESTA. The RAC was enhanced with new random access functions that enable it to read data from specific regions of the HSIESTA file rather than importing the entire file into memory. Preliminary results indicate reduced memory usage for large FE models when the number of zones is much smaller than the number of elements/nodes.

The DARWIN “Autoplate” algorithm rapidly identifies the size and orientation of fracture mechanics models (i.e., rectangular plates) based on the geometry, temperature, and stresses at a specified location in an FE model. In previous versions of DARWIN, users could invoke the Autoplate algorithm when manually creating zones, but this capability was limited to 2D FE models. For 3D FE models, users were required to use their own engineering judgement to determine the size and orientation of fracture mechanics models when building zones manually. Initial crack locations for 3D FE models were also limited to surface nodes. **DARWIN 9.1 enables use of Autoplate for automatic creation of fracture mechanics models when creating zones manually in 3D FE models.** When the user selects an initial crack location on the 3D FE model, the slice plane and fracture model are created simultaneously using a single mouse click. DARWIN 9.1 also enables users to specify an initial crack location anywhere on the surface of a 3D FE model. These enhancements provide a common interface for creating zones manually in both 2D and 3D FE model geometries.

DARWIN provides several probabilistic methods for computing the fracture risk of components, including a method entitled “Monte Carlo with GP Response Surface.” This method creates a Gaussian Process (GP) response surface model to estimate the relationship among input variables and fatigue crack growth (FCG) lifetimes. Monte Carlo Simulation is then applied to the response surface for fracture risk computations. In previous versions of DARWIN, this method was limited to five random variables. **DARWIN 9.1 extends the Monte Carlo with GP Response Surface method to provide treatment for all DARWIN random input variables except those related to manufacturing process models.** New random variables include anomalies introduced at shop visits and anomalies with six degrees of freedom (three orthogonal dimension variables and three orthogonal orientation variables). A new response surface capability was implemented to model the relationship among formation life and its associated input random variables. The FCG life response surface was also enhanced to support additional random variables. This enhancement provides significant reductions in computation time for assessments employing additional random variables that were not previously supported by this method.

DARWIN was originally designed to assess the risk of fracture of components containing rare anomalies, and the original DARWIN GUI workflow was intended to support the zone-based risk assessment methodology described in AC 33.14-1 and 33.70-2. However, many analysts also use DARWIN to assess deterministic FCG life as described in AC 33.70-1. Previous versions of DARWIN enabled users to perform deterministic FCG analysis, but the risk assessment-based GUI workflow required additional input that was not required for deterministic analysis. For example, users had to define a zone for each initial crack location in a deterministic FCG life analysis, but much of the zone information was not used in the analysis. **DARWIN 9.1 enables users to perform deterministic life assessments without zones (Figure 9.7-36).** A new GUI workflow was developed specifically for deterministic assessments in which a new “life assessment” mode is defined in the first (configuration) GUI menu. This enables the GUI to display the analysis configuration settings that apply only to deterministic life assessment.

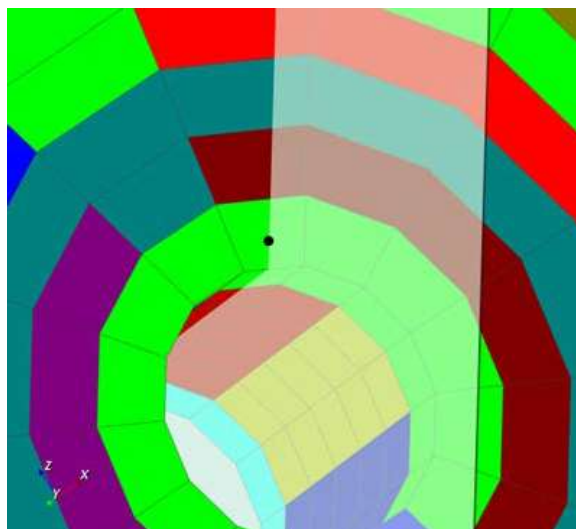


Figure 9.7-36. DARWIN 9.1 Enables Users to Place an Initial Crack Anywhere on the Surfaces of 3D FE Models and Automatically Create a Fracture Mechanics Model Using the DARWIN Autoplate Algorithm

More information about DARWIN is available at www.darwin.swri.org.

POC: Craig McClung, Southwest Research Institute, Craig.McClung@swri.org, 1-210-522-2422.

9.7.12. Risk Assessment and Risk Management Methods for Small Airplane Continued Operational Safety (COS), SMART Software

Sohrob Mottaghi, FAA – William J. Hughes Technical Center; Michael Reyer, FAA – Small Airplane Directorate; Harry Millwater, University of Texas at San Antonio; Juan Ocampo, St. Mary's University

The objective of this activity is to develop the Small Aircraft Risk Technology and software (SMART). The SMART software is based on a standardized Continued Operational Safety (COS) risk assessment method for small and transport airplanes that is consistent with the FAA safety management principles. It is focused on developing state-of-the-art software that uses advanced statistical and probabilistic methods in risk assessment and risk management of structural issues in general aviation. The outcome of this project will assist the FAA and industry to proactively manage the risk associated with fatigue failure.

The general aviation (GA) aircraft can be traced to more than 100 manufacturers, some of which no longer exist. The GA fleet includes approximately 150,000 airplanes that were certified with no fatigue evaluation requirements. The average age of the GA fleet was approximately 40 years in 2010, and the projected average fleet age reaches close to 50 years in 2020. During the past decade, the effects of aging on GA airplanes have caused primary component failures, some of which led to fatal accidents. As a result, the Small Airplane Directorate has recognized both the need to address the aging issues and that the GA community needs methods and tools to develop adequate Fatigue Management Programs. The principle goal of this requirement is to mitigate the risk associated with fatigue failure.

In 2006, the FAA's roadmap for GA aging airplane specified that the FAA shall initiate the development of risk-assessment and risk-management methods in fiscal year 2007 (FY07) and continue developing them beyond FY09 [1]. In 2009, the FAA issued a report on recommendations for general aviation for the next 20 years [2]. Finding 3.1 of this report states that the Instruction for Continued Airworthiness (at the time the report was written) assumes static airplane condition (i.e., factory new).

Therefore, the recommendation was made that airframe and system degradation associated with aging must be considered. Given the large and diverse GA fleet with little information regarding fatigue, the FAA has understood the need to develop tools that can proactively assess and mitigate the risk. To do so, statistical risk analyses are required to be performed on various measurable events that are related to undesirable events. Therefore, various probabilities must be estimated with regard to individual risk and fleet risk to establish a maintenance schedule. This is one of the goals of this multi-year project.

The Small Airplane Directorate has been committed to developing the tools required to overcome the above issues. Therefore, the FAA has partnered with the University of Texas at San Antonio and completed three phases of this project between 2007 and 2016, as follows:

- FY 07-11:** Developed SMART|LD software, based on Linear Damage (LD) methodology, for probabilistic fatigue analysis for small airplanes.
- FY 09-13:** Developed SMART|DT software, based on probabilistic Damage Tolerance (DT) concept, for risk assessments and including the tool that enables the assessment of the effect of inspection and repair on the risk and other required random variables.
- FY12-16:** Verification with in-service findings and developing numerical tools for decreasing the computational time.

In FY16, Phase 3 was completed. SMART|LD and SMART|DT software were both verified. In addition, modifications and advancements were made to increase the accuracy of the software predictions and reduce the required computational time. This was done by adding High Performance Computing Capability (OpenMP and Vectorization) and new Kriging capabilities (to avoid overtraining), and by developing an approximate and an exact method to compute the probability of failure. Figure 9.7-37 represents an example of SMART outputs. An interested reader may refer to [3-8] for more information.

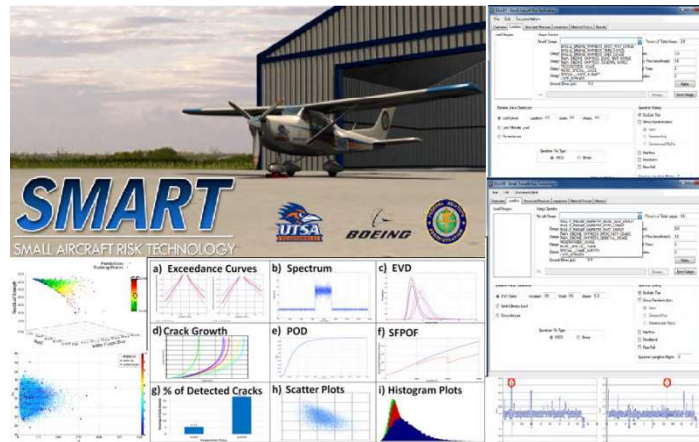


Figure 9.7-37. Some Representative Outputs of SMART Software

References:

- [1] The Federal Aviation Administration, “Roadmap for General Aviation Aging Airplane Programs”, September 2006. Link (as of 2/8/2017): https://www.faa.gov/aircraft/air_cert/design_approvals/small_airplanes/cos/aging_aircraft/media/roadmapGAagingAirplane.pdf.
- [2] The Federal Aviation Administration, “Part 23 – Small Airplane Certification Process Study. Recommendations for General Aviation for the Next 20 Years”, July 2009. Link (as of 2/8/2017): https://www.faa.gov/about/office_org/headquarters_offices/avs/offices/air/directorates_field/small_airplanes/media/CPS_Part_23.pdf.
- [3] B. Gamble and C. Hurst, “Using SMART|DT to Ensure the Continued Structural Safety of Textron Aviation’s Fleet,” Aircraft Airworthiness & Sustainment Conf., Grapevine, TX, April 2016.

- [4] B. Gamble, C. Hurst, P. Saville, “Probabilistic Continued Operational Safety Risk Assessment for General Aviation Airplanes,” Aircraft Airworthiness & Sustainment Conf., Grapevine, TX, April 2016.
- [5] J. Ocampo and H.R. Millwater, “Efficient Methods for Probabilistic Damage Tolerance Analysis of Aircraft Structures,” Aircraft Airworthiness & Sustainment Conf., Grapevine, TX, April 2016.
- [6] H.R. Millwater, J. Ocampo, N. Crosby, B. Gamble, C. Hurst, and M. Nuss, “Probabilistic Damage Tolerance using the FAA-Sponsored SMART|DT Software,” Aircraft Structural Integrity Program Conference, San Antonio, TX, November 2015.
- [7] B. Gamble, “Probabilistic Risk Assessment—The SMART Approach to Continued Operational Safety,” Aircraft Structural Integrity Program Conference, San Antonio, TX, November 2015.
- [8] J.D. Ocampo*, H.R. Millwater, G. Singh, H. Smith, F. Abali, M. Nuss, M. Reyer, M. Shiao, “Development of a Probabilistic Linear Damage Methodology for Small Aircraft,” AIAA J. Aircraft. 48, 6 (2011), 2090-2106 doi: 10.2514/1.56674.

9.8. LIFE ENHANCEMENT CONCEPTS

9.8.1. Fatigue Enhancement of a Critical A-10 Structural Detail Using Engineered Residual Stress

Michael Hill, Hill Engineering LLC

It is well established that compressive residual stresses provide improved fatigue performance and damage tolerance enhancement. To take advantage of this concept, many surface treatment processes have been developed over the past 60+ years that are capable of imparting compressive residual stress into the surface layer of a component (e.g., shot peening, cold working of fastener holes, and laser shock processing). The compressive stress near the material surface acts to slow the growth of fatigue cracks and can provide substantial benefits (e.g., reduced sustainment costs and increased aircraft availability). Recent work has developed computational tools and engineering processes that enable faster, more cost effective evaluation of the benefits from compressive residual stress treatments. With funding and support from AFRL, Hill Engineering and A-10 ASIP are in the process of developing and implementing a structural modification on the A-10 that uses laser shock peening to enhance fatigue performance. The technical effort provides an overview of the proposed modification, and describes the design and optimization of the surface treatment process. Surface treatment design uses computational tools that predict: 1) residual stress from surface treatments (Figures 9.8-1 and 9.8-2), and 2) the effects of residual stress on fatigue performance (Figure 9.8-3). Predicted behavior is validated against test data from experiments in element (Figures 9.8-4 through 9.8-7) and full-scale articles. The predictive capabilities, and the validating test data, provide for estimates of benefit, including potential cost savings, life extension, or increases in time between structural inspections.

Process region

- Select area near fillet

Simplified model

- Small
- Reduced features

Example results for LSP

- Predicted residual stress

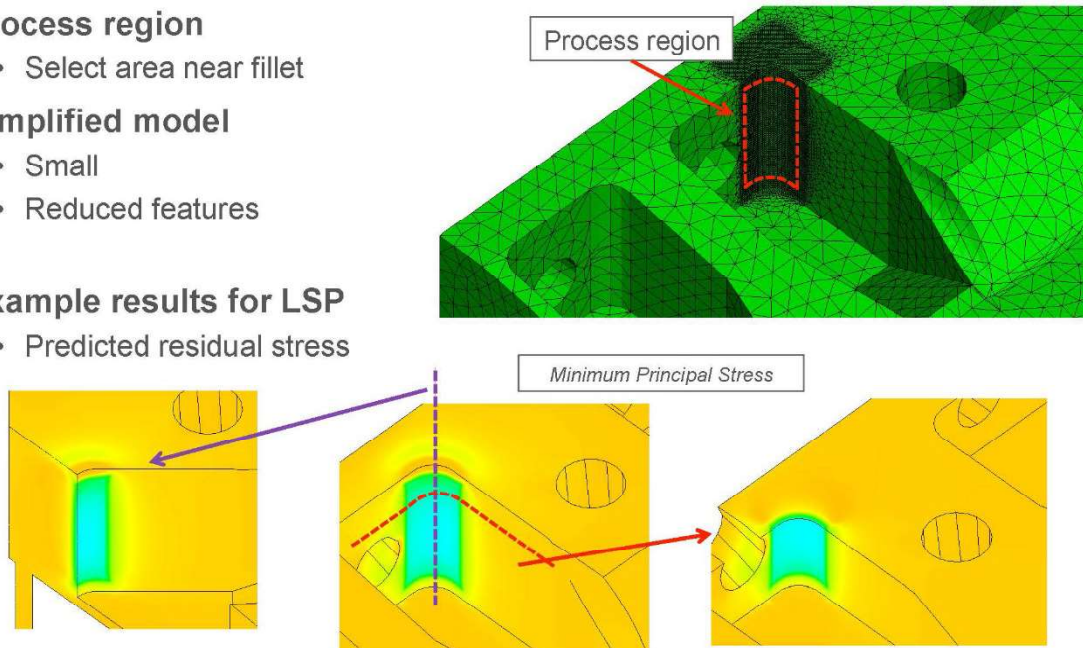


Figure 9.8-1. Residual Stress Prediction

Simple coupons

- Material 7050-T7451 (vs. 7175-T736)
- Two geometries
 - Rectangular blocks
 - Representative geometry

Measured stress in reasonable agreement with model

- Stress differences consistent with geometry difference
- Measurement in small part
- Model reflects larger splice fitting

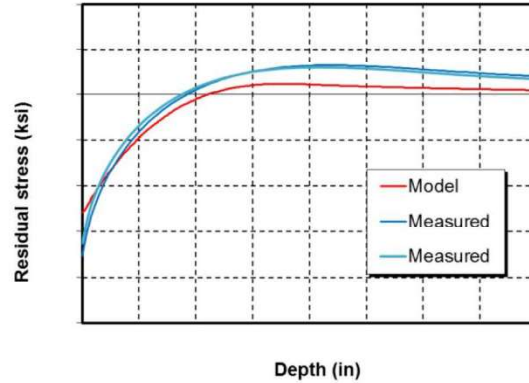
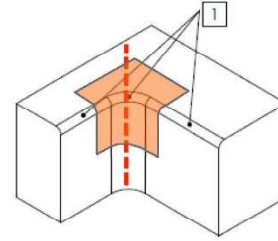
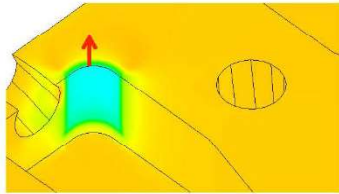
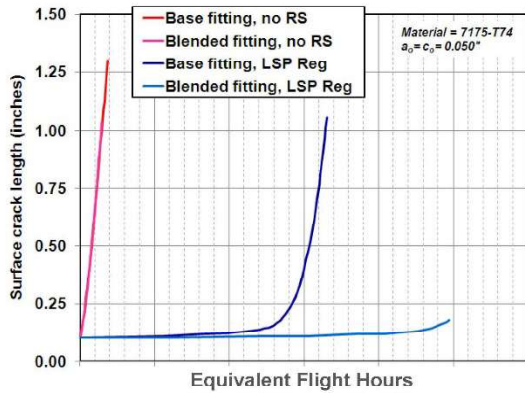
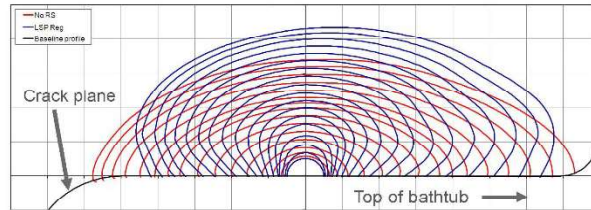
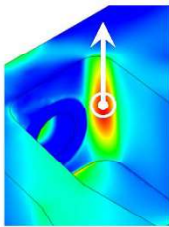


Figure 9.8-2. Residual Stress Measurements

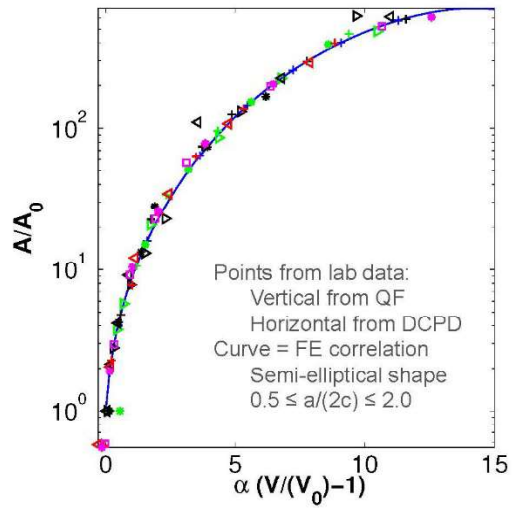
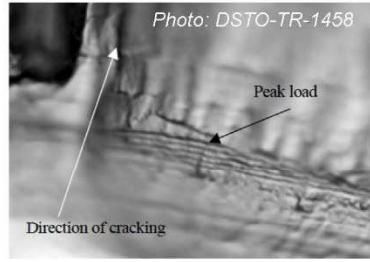


Estimated FCG Benefits:	
Unrepaired baseline:	1X
Blend repaired:	1X
LSP:	14X
Blend+LSP:	20X

Figure 9.8-3. Predicted Crack Growth Benefits

QF provides crack shape periodically during the test

- Somewhat expensive, but very valuable; 6 crack front profiles per test



DCPD provides cracked area

- Inexpensive, continuous

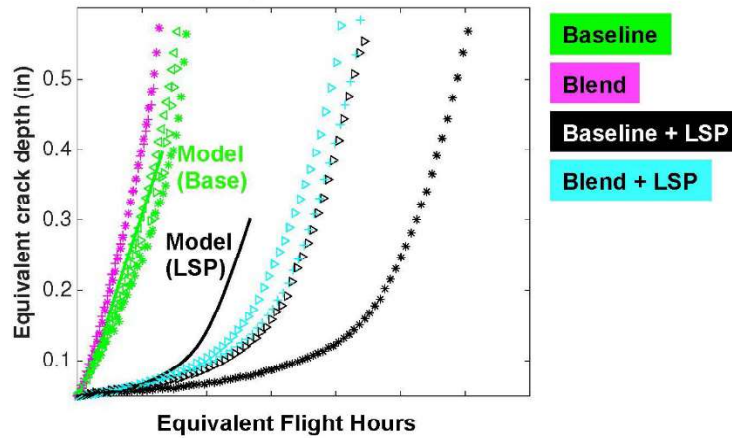
Reporting based on QF-correlated DCPD area

- Correlation expected, and follows electrostatic FE

Figure 9.8-4. Crack Measurement Correlation

Equivalent crack size vs Flight hours

- DCPD gives cracked area, Equivalent crack size $a_e = (2A/\pi)^{0.5}$
 (Using QF-correlated DCPD area)



*Blend repair results in small life reduction
 LSP provides significant life improvement*

Figure 9.8-5. Element Fatigue Life Validation

Area growth rate (per block) vs crack size

LSP offers benefit

- For small cracks
- Also for fairly large cracks (to $a_e \approx 0.2$ inch)

Crack growth correlation:

- Excellent for baseline model
- Conservative and within 2X of data for LSP model

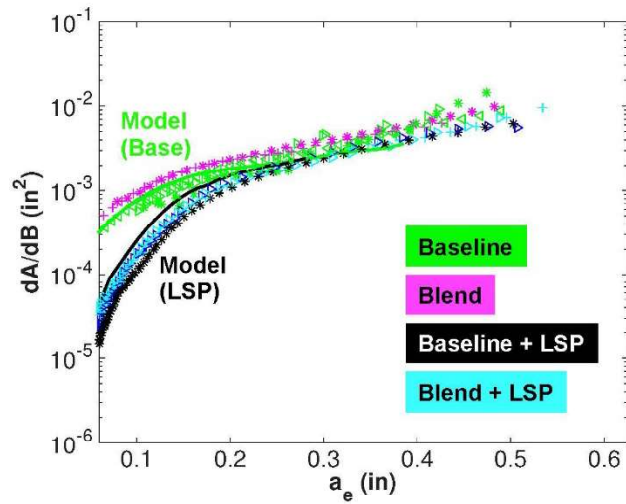


Figure 9.8-6. Element Crack Growth Rate Validation

Consistent crack shape evolution in model and QF measurements

- Baseline has typical semi-elliptical shape (examples shown are typical)
- LSP has slower growth near surface, faster growth in depth
 - Typical for LSP
- Accounting for crack shape necessary for accurate crack growth estimate

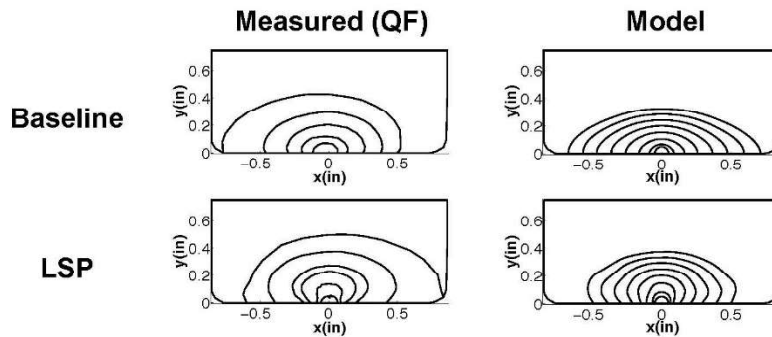


Figure 9.8-7. Element Crack Shape Validation

9.8.2. Residual Stress Management Using X-Ray Diffraction and Slitting Methods to Assess Significant Stress Corrosion Cracking in Extruded 7075-T651 Wing Skin Integral Risers on Australian Air Force P-3C Aircraft

Michael Hill and Adrian DeWald, Hill Engineering LLC; Kevin Walker, DST Group Australia; Justin Hill, RAAF DGTA

The wing structure on Australian Air Force P-3C maritime surveillance aircraft is manufactured from 7075-T651 aluminium alloy (Figure 9.8-8). The wing skins are primary structure and feature integral blade risers or stiffeners. The skins are chemically and mechanically machined from thick-section extruded billet which includes the basic form of the risers. The 7075-T651 material manufactured in this way is susceptible to stress-corrosion cracking (SCC). Any instances of SCC have been successfully managed for many years of service through a maintenance program which includes routine inspections and the application of corrosion prevention compounds where needed. But recent eddy-current surface scan inspections, which extended further than usual on one particular aircraft initially, revealed widespread crack indications at locations significantly remote from the fastener holes where any SCC would normally have been anticipated (Figure 9.8-9). This new form of SCC indication occurred at various locations on the risers, including at the radius where the riser meets the skin or at mid-height. The crack indications ran parallel to the primary load path direction and in most cases were shallow (about 0.01 inches deep in a 0.1 inch thick riser), but in some cases ran for several inches in the span-wise direction. These findings were unexpected, particularly since the surface finish (epoxy based paint) was in very good condition with no obvious entry point for the environment needed to facilitate SCC. Investigation of this matter included a program to measure the residual stress profile through the thickness of the risers in representative samples from the affected aircraft and sections of wing skin from similar but retired aircraft (Figure 9.8-10). The measurements were performed using three independent methods in two laboratories (USA and Australia); X-Ray diffraction (Figure 9.8-11) with electro-polishing through the depth, and compliance based slitting (Figure 9.8-12) and slotting. The results from the slitting/slotting and the X-Ray diffraction (Figures 9.8-13 and 9.8-14) were similar and consistent, and showed a region of significant compression of about 10-15 ksi on the outer layer which transitioned to low-level tension of less than 1.5 ksi at a depth of about 0.01 inches. The crack indications were also subjected to detailed metallographic assessment using sectioning and optical and Scanning-Electron Microscopy (Figure 9.8-15). The investigation revealed that the eddy current indications were indeed cracks, or at least very much crack like. Many more (small) cracks were also evident below the detectability limit for the eddy current technique. Rather than definite SCC, the cracks are now thought to be more accurately described as intergranular corrosion (IGC) cracks, and they have likely been present since manufacture. It seems that the most likely scenario for their development is that there was an anomaly in the manufacturing process for some wing planks in that they were left in the machined/etched but bare state for an extended period. The IGC cracks then developed in the presence of the ambient environment, despite the presence of a significant compressive stress layer. A summary of this work is presented, including how the results assisted with the development of a strategy to address and manage this issue. The work enabled the Australian Air Force to continue P-3C fleet operations with minimal impact on aircraft availability and operational effectiveness.

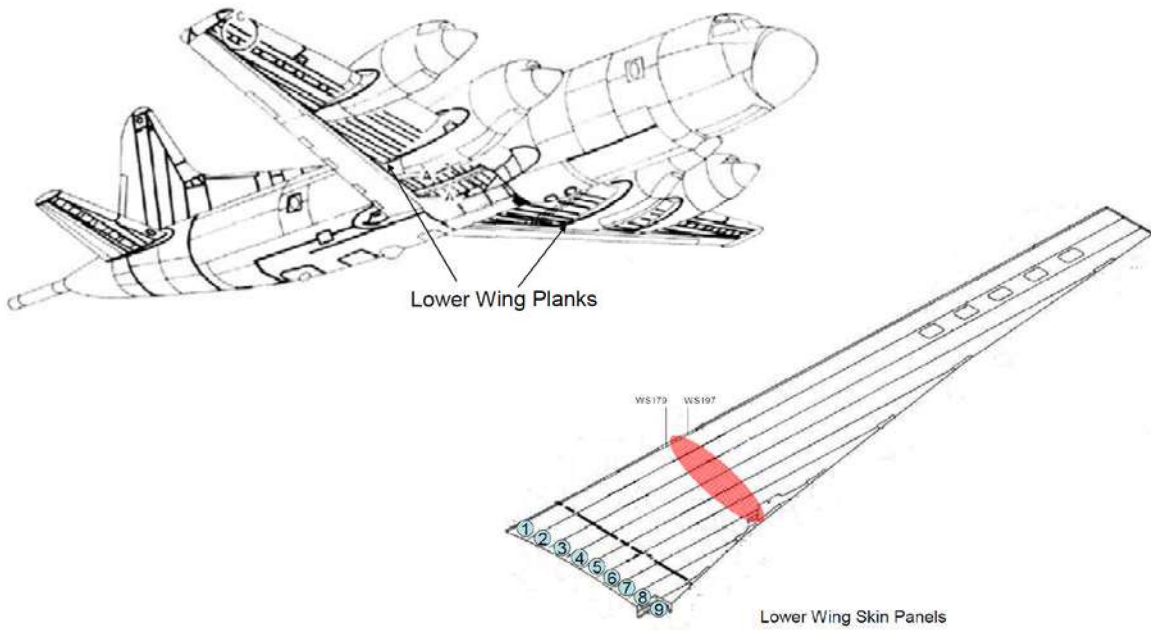


Figure 9.8-8. Wing Plank Structure

- During BHEC inspection for H-Clip cracking between WS179-197 on A09-759, unexpected indications observed in adjacent areas on risers
- Further investigation over a wider inspection region using ECSS resulted in over 1,100 crack like indications (one aircraft) in the lower wing panels.

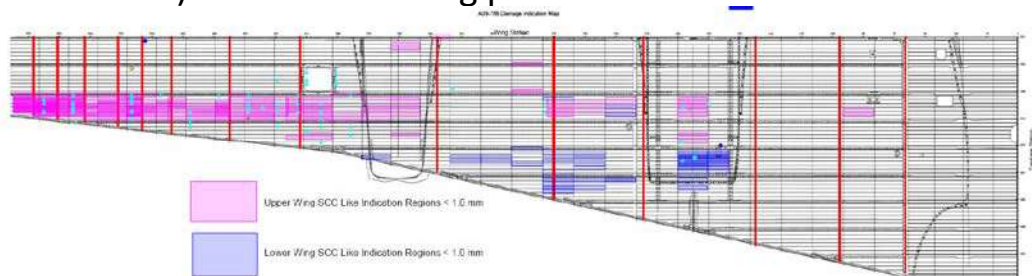


Figure 9.8-9. Widespread Crack Indications in Wing Plank Risers

- RS measurements on selected segments from a range of risers from A09-755
- Three methods:
 - Slitting (Hill Engineering)
 - Slotting (Hill Engineering)
 - X-Ray Diffraction (DST Group)
- Findings consistent for all riser locations and all methods.

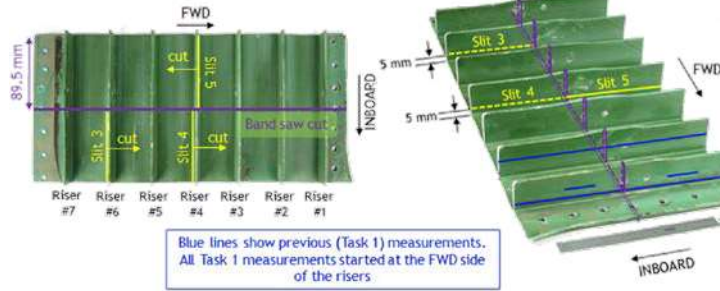
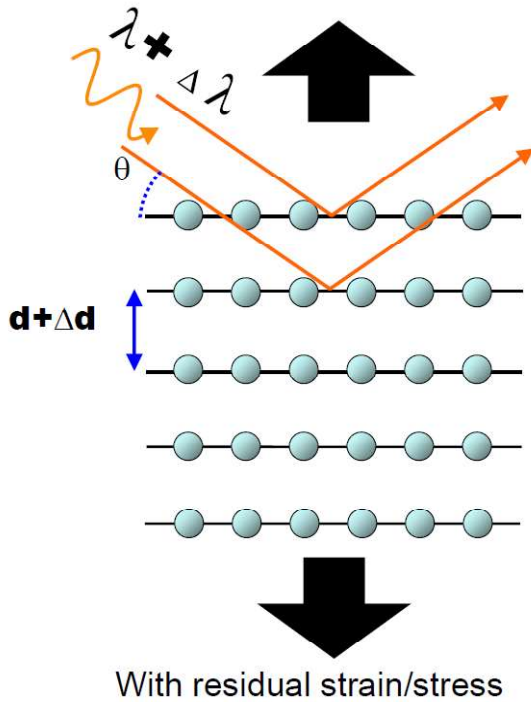
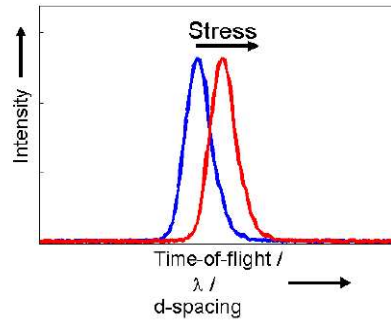


Figure 9.8-10. Residual Stress Measurements



Bragg's Law:
 $d = \lambda / (2 \sin\theta)$

Fixed angle θ : $\epsilon = \frac{\Delta d}{d} = \frac{\Delta \lambda}{\lambda}$



Diffraction peak shift is used to determine residual strain and stress

Figure 9.8-11. X-Ray Defraction Method

- Slitting method principle
 - Incrementally cut slit into test coupon
 - Measure strain release at specific locations
 - Compute residual stress from strain release
- Description of results
 - Residual stress profile (stress versus depth)
 - Single stress component (per measurement)
 - Multiple cuts for multiple stress components
- Useful for
 - 1D stress distributions
 - Bulk residual stress distributions
 - Large useful depth range (thin to thick)
 - Parts with large or complex geometry
 - Wide range of material types (e.g., metals and non-metals)
 - Not dependent on microstructure

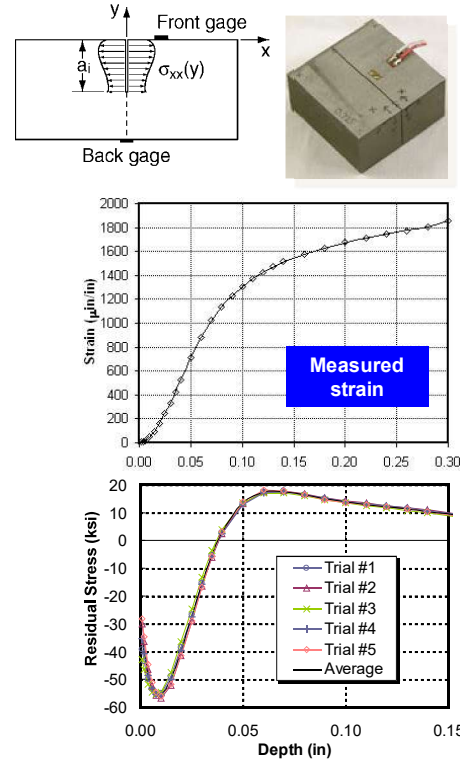


Figure 9.8-12. Slitting Method

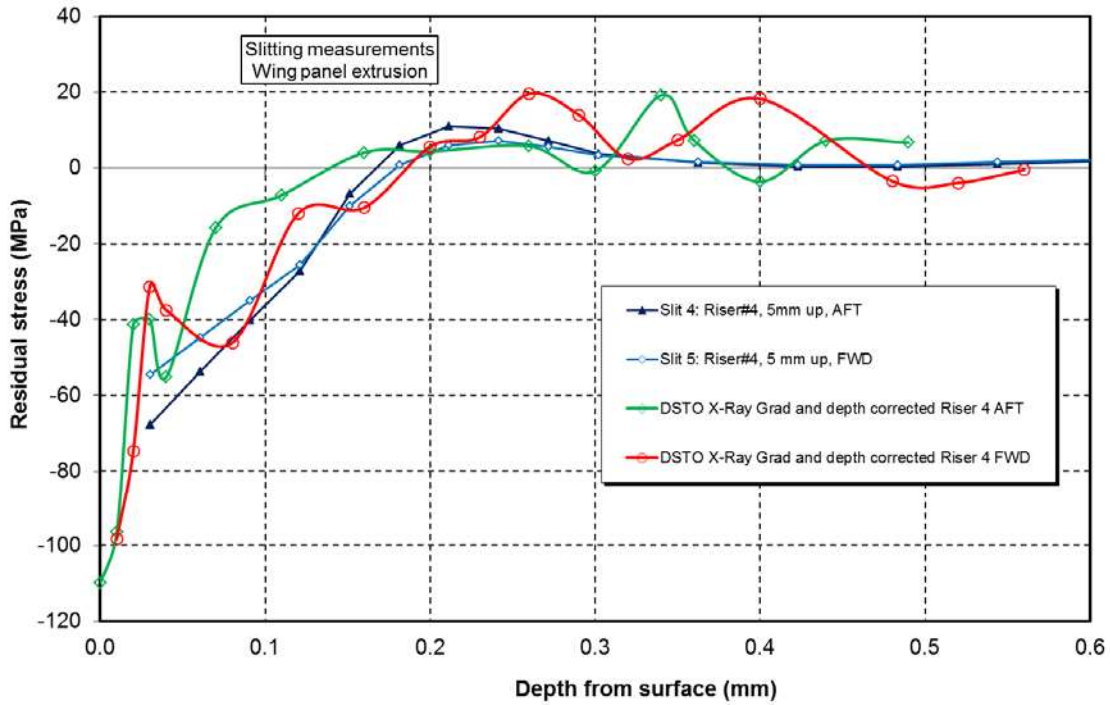


Figure 9.8-13. Slitting and X-Ray Diffraction Results

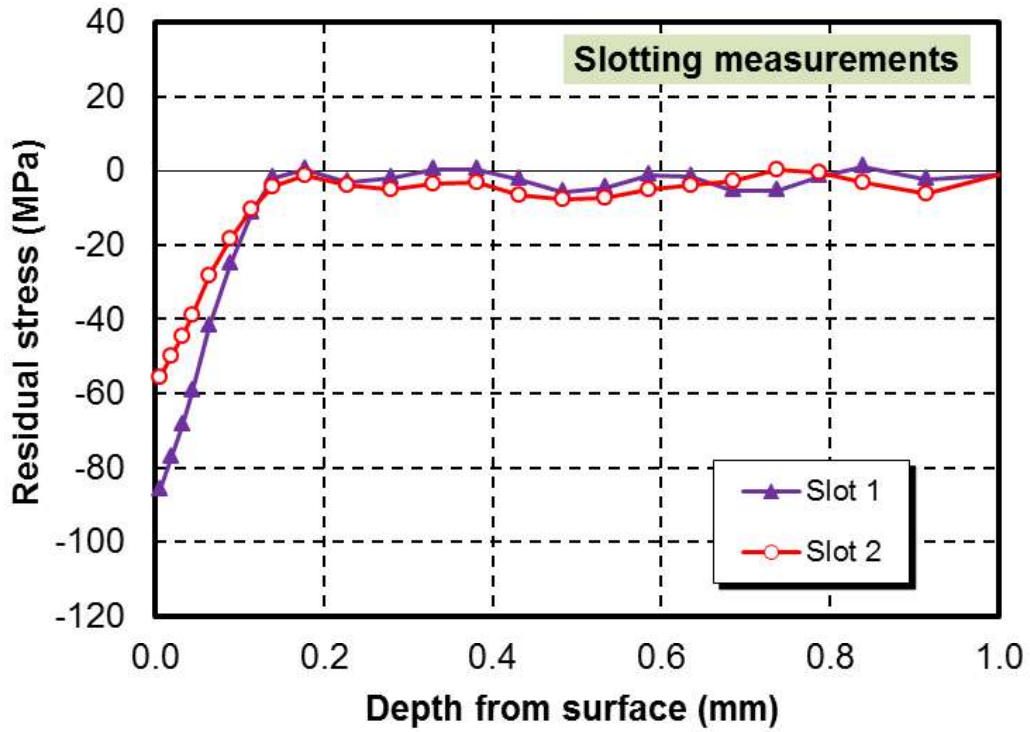


Figure 9.8-14. Slotting Results

A09-759 RH LWR Panel 7 Riser 3 WS175-184

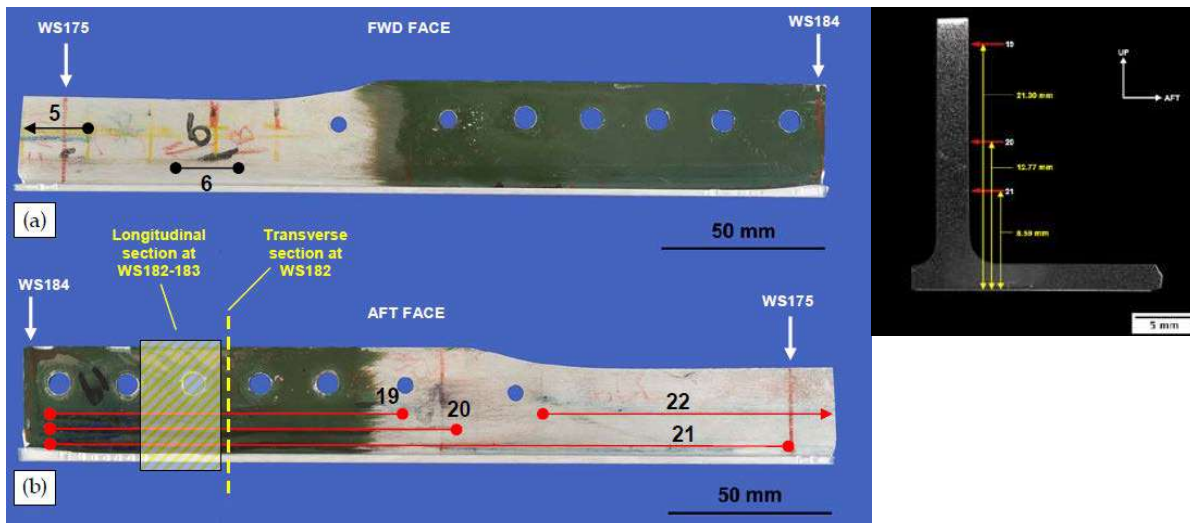


Figure 9.8-15. Metallographic Investigation

9.8.3. B-1 Wing Repair – Unique Hole Geometry Cold Expansion Solutions

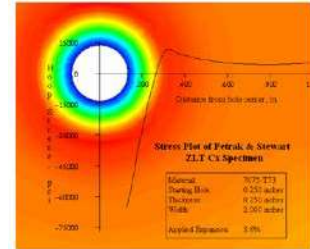
Dean Madden, Fatigue Technology, Inc.

Boeing Cold expansion is an industry known process for extending the fatigue life and crack growth life of holes in metallic structures by inducing a beneficial compressive stress in the material around the hole (Figures 9.8-16 and 9.8-17). Dealing with unique hole geometric and access conditions can be a challenge for the standard system of cold expansion (Figure 9.8-18). Unique hole conditions can include non-round holes, elliptical countersunk holes, blind holes, or limited backside access holes (Figure 9.8-19) and have been successfully cold expanded in prior applications. However, designing tooling to translate compressive stresses in the correct location around the hole and not creating undesirable tensile stresses in adjacent areas is required to achieve the optimum enhancement. The recent B-1 (Figure 9.8-20) Wing Repair program, lower skin fatigue cracking problem, presented a new unique hole configuration - countersunk and counterbore hole (CSK/Cbore) (Figure 9.8-21), as well as back side clearance challenges. FTI was requested by Boeing and USAF to develop a cold expansion solution. Several unique and new tooling design concepts were developed to successfully cold expand the CSK/Cbore geometry, with extensive use of FEA to characterize and optimize both the residual stresses around the hole as well as tool strength. Coupon fatigue testing was then accomplished to validate fatigue life improvements. Successful completion of the fatigue testing then allowed for application of the tooling to test aircraft, and ultimately the fleet. FTI is capable of producing a variety of custom tooling solutions for cold expanding a variety of unique hole configurations, including limited backside access, zero backside access, "D-shaped" holes, and out-of-round holes. These custom tooling solutions produced the desired life improvement target and provided significant material, labor and downtime cost savings versus alternative options, such as wing skin replacement in this program. By being able to apply cold expansion to a variety of hole configurations, the end user is able to cold expand their structure with minimal alterations as well as apply cold expansion to hole shapes that otherwise would require alternative costly repairs. This is especially advantageous in rework or repair scenarios where the task of cold expanding is made more difficult by limited accessibility. By being able to cold expand unique hole geometries, engineers are allowed more flexibility in their component designs and MRO facilities could use cold expansion technologies to both extend structural life and restore damaged holes to original size.

Split Sleeve Cold Expansion (cold working) induces a zone of residual compressive stress around and through a hole.

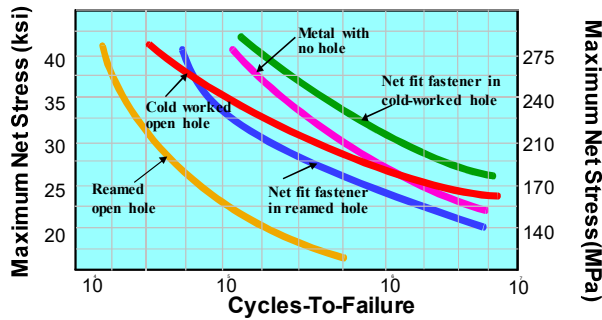


Hole is effectively "shielded," reducing effective stress intensity factor and therefore the growth of fatigue cracks.



Improves fatigue life, durability and damage tolerance of structure.

Figure 9.8-16. Fatigue Life Improvements of Holes with Cold Expansion



USAF DTA Approach

– Assume 0.050-inch initial flaw

With hole cold expansion:

- Allow smaller initial flaw
- Typically 0.005 inch

- Improve fatigue life
- Retard crack growth
 - No weight penalty
 - No change in stiffness & dynamics

Figure 9.8-17. Durability and Damage Tolerance Improvements

- **Short Edge Margin ($e/D < 1.5$)**
- **Parent Structure Features**
 - Designed non-round holes
 - Pad ups
 - Webs
 - Radii
 - Countersinks
 - Counterbores
 - Multiple lug locations

Proximate features often pose challenges in the form of access restrictions, in addition to stress/strain/displacement challenges.

- **Thin Materials ($t/D < 0.4$) and/or Damaged Holes**

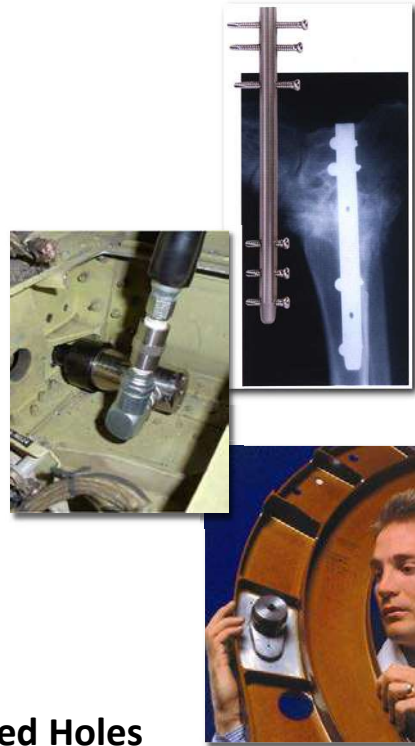


Figure 9.8-18. Geometric Challenges

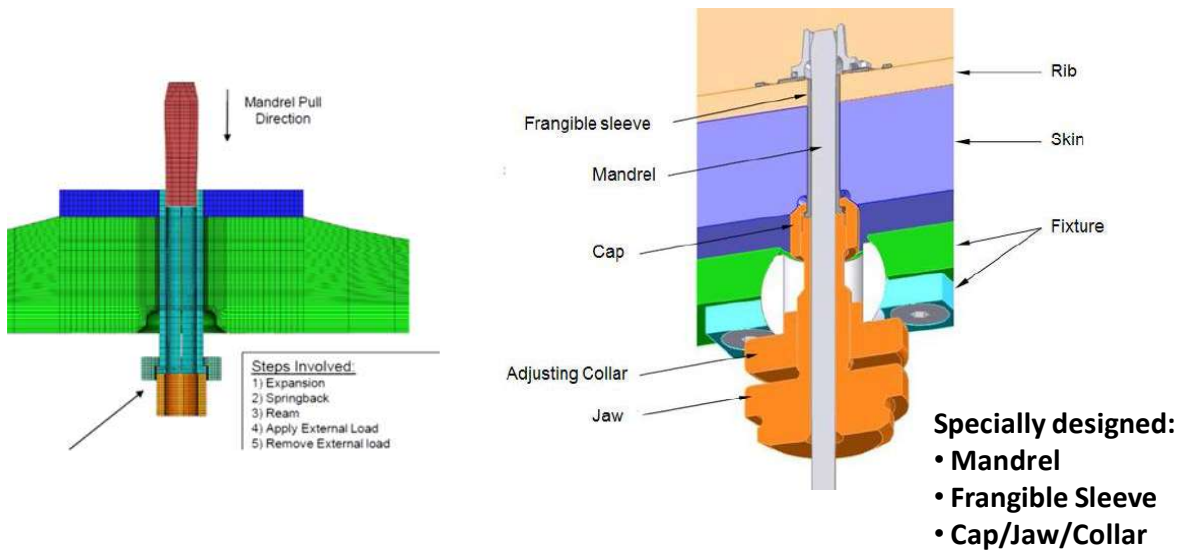


Figure 9.8-19. Cold Expansion of Straight Hole Bore with Backside Nutplate



Figure 9.8-20. B-1 Aircraft

Specially designed:

- Pintle
- Expanding Jaw
- Puller

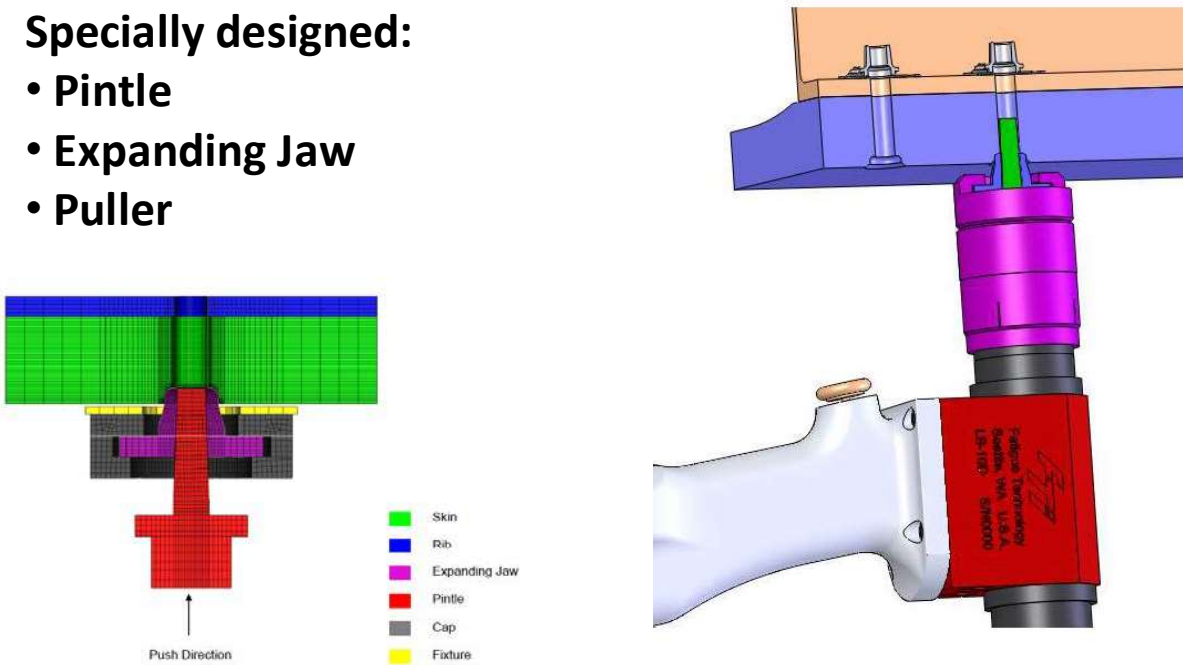


Figure 9.8-21. Cold Expansion of the C-Bore/CSK Detail

9.8.4. Implementation of Deep Engineered Residual Stresses into the Damage Tolerance Paradigm – Reducing Sustainment Costs and Improving Aircraft Availability

Scott Carlson, Southwest Research Institute

As weapon systems within the United States Air Force (USAF) and other Department of Defense (DoD) agencies continue to have retirement dates extended (Figure 9.8-22) and budgetary constraints tighten, the benefits of residual stress processes have become an area of special interest among airframe structural integrity communities. The proper application of engineered residual stress processes has been demonstrated through test and fleet history to extend service lives (Figure 9.8-23). The current DoD guidance for damage tolerance analysis of critical airframe structure imposes a non-physics-based reduction in Initial Flaw Size (IFS) to a minimum 0.005 inch corner crack to account for processes such as cold expansion of fastener holes. A new methodology for implementing deep residual stresses for the calculation of recurring inspection intervals has been in the process of being developed for over a decade and has been demonstrated to be effective for one-off analysis for fatigue and fracture critical locations on the A-10. Advances in modeling, fatigue crack growth software, and residual stress measurement techniques provide opportunities to move damage tolerance assessments forward, away from the limited reduced IFS approach, to a physics-based methodology. This technical effort will provide an overview of over a decade worth of research, focused on the ability to accurately model, measure, inspect and analyze the fatigue crack growth characteristics of cracks forming and propagating through deep residual stress fields. The technical effort will not focus on specific tools used to calculate recurring inspection intervals in the presence of a deep residual stress fields, but instead will provide the systems engineering approach to how this paradigm shift may be implemented within any given weapon system. It will also provide the major outcomes of the first, USAF sponsored, Engineered Residual Stress Implementation workshop, which has the charter to develop a Structures Bulletin for the USAF outlining the methodology for implementing deep residual stresses into Damage Tolerance Analyses for critical structure. As our budgets become smaller and the demand to extend the service lives of our airframes becomes greater, engineered deep residual stresses provide a viable means to accomplish each. In order to safely use engineered residual stresses there must be a robust implementation plan and sound engineering guidance, outlining how data are to be developed, analyzed and used. The goal of this technical effort is to provide methods for this to the ASIP community, along with lessons learned from the past 15 years as we have worked towards the goal of a more physics-based approach to engineered residual stress implementation.

	Major USAF Weapon Systems							
	A-10	F-16	F-15	KC-135	B-52	B-1	F-22	F-35
Number of Aircraft Procured	713	2230	1619	803	744	104	186	1763
Current Number in Fleet	283	964	472	417	76	66	123	167
Projected Age at Retirement	60	36	42	84	80	52	?	?

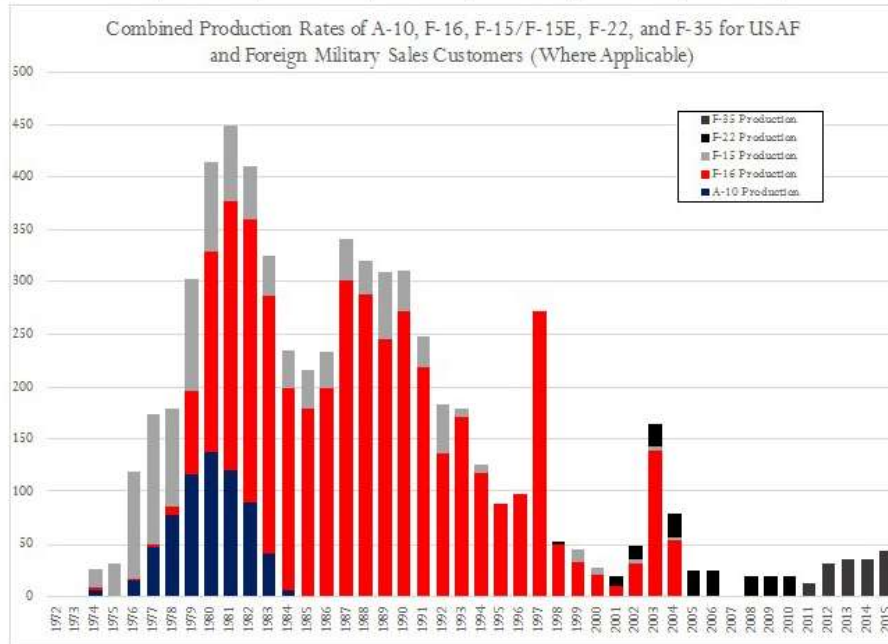


Figure 9.8-22. Aging USAF Weapon Systems

- Demonstrated Damage Tolerant Life Improvements Through the Cold Expansion Process
- Limited Analytical Advantage for Recurring Inspection Intervals

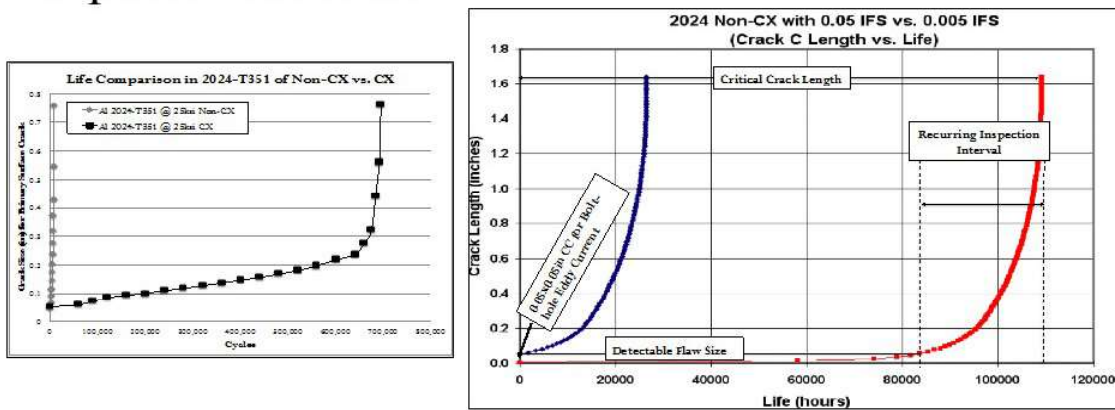


Figure 9.8-23. Benefits of Engineered Residual Stresses

9.8.5. Structural Certification of Laser Peening for F-35 Safety Critical Aluminum Forgings

Pete Caruso, Stephanie McMillan, Matthew Edghill, and Phil Gross, Lockheed Martin F-35 Program

The effect of laser shock peening (LSP) in the crack initiation and damage tolerance behavior of 7085-T7452 forgings was investigated. The F-35B (STOVL variant) (Figure 9.8-24) utilizes very large 7085-T7452 forgings for wing carry-thru bulkheads that have experienced fatigue cracking prior to one lifetime of full-scale durability testing (Figure 9.8-25). Additional fatigue cracking has occurred between one and two lifetimes of cycling, which requires repair (Figure 9.8-26). A comprehensive structural certification plan has been developed to qualify laser shock peening (LSP) to restore F-35B aircraft service life for fielded aircraft and apply in new production (Figures 9.8-27 through 9.8-29). LSP lessons learned during qualification of safety critical titanium bulkheads on legacy aircraft have been applied to reduce the certification risk. Three test phases shall be performed to qualify the LSP process for safety critical aluminum forgings. Phase 1 is the LSP process characterization testing conducted at the coupon level (Figure 9.8-30). Representative cross-section details shall be laser peened and residual stress measurements shall verify finite element predictions. Test spectra truncation and marker band methods shall be verified in coupon level tests. Phase 2 is the element level durability and damage tolerance testing to characterize the variability of the LSP process on mechanical properties (Figure 9.8-31). Element durability tests shall develop the crack initiation life improvement benefit. Element damage tolerance tests shall develop crack growth rate data in the presence of artificial flaws introduced preceding and subsequent to the LSP process (Figure 9.8-32). Phase 3 is the subcomponent level durability test to verify the LSP process. A critical step is to develop acceptable baseline (unpeened) fatigue test results to verify the durability test set-up. The LSP subcomponent durability test results shall be used to certify the safety critical aluminum forgings. LSP expected benefits are to restore the durability and damage tolerance life of delivered and new F-35B aircraft. Lessons learned from the LSP certification testing shall be applied to improve the life of F-35A and F-35C variants, if warranted from interpretation of full-scale airframe test results.



Figure 9.8-24. F-35B (STOVL Variant)

- **Bulkhead A, 7085-T7452 Forging**
Crack Location

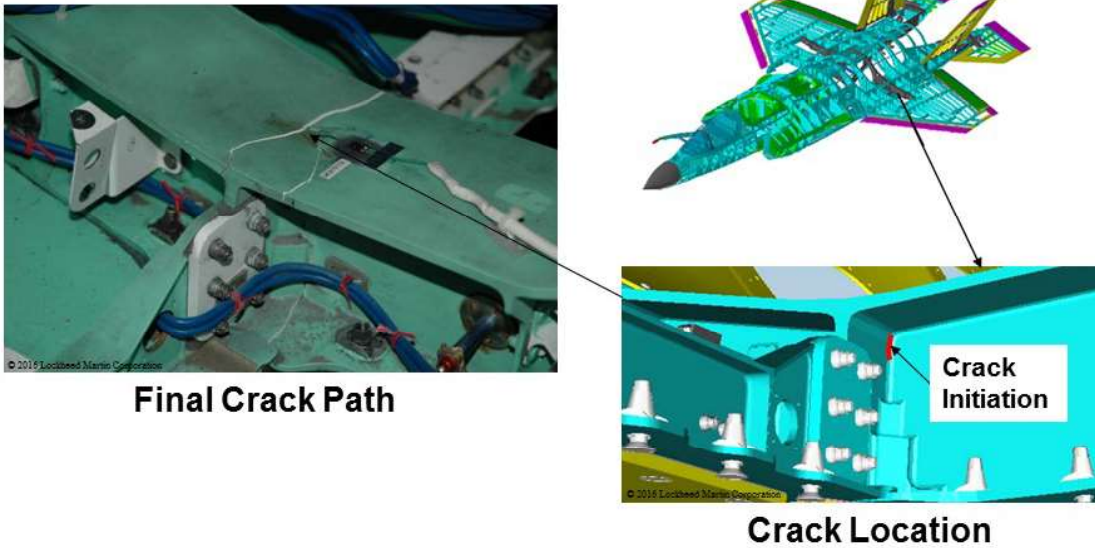


Figure 9.8-25. Durability Test Finding #1

- **Bulkhead B, 7085-T7452 Forging**
Crack Initiation

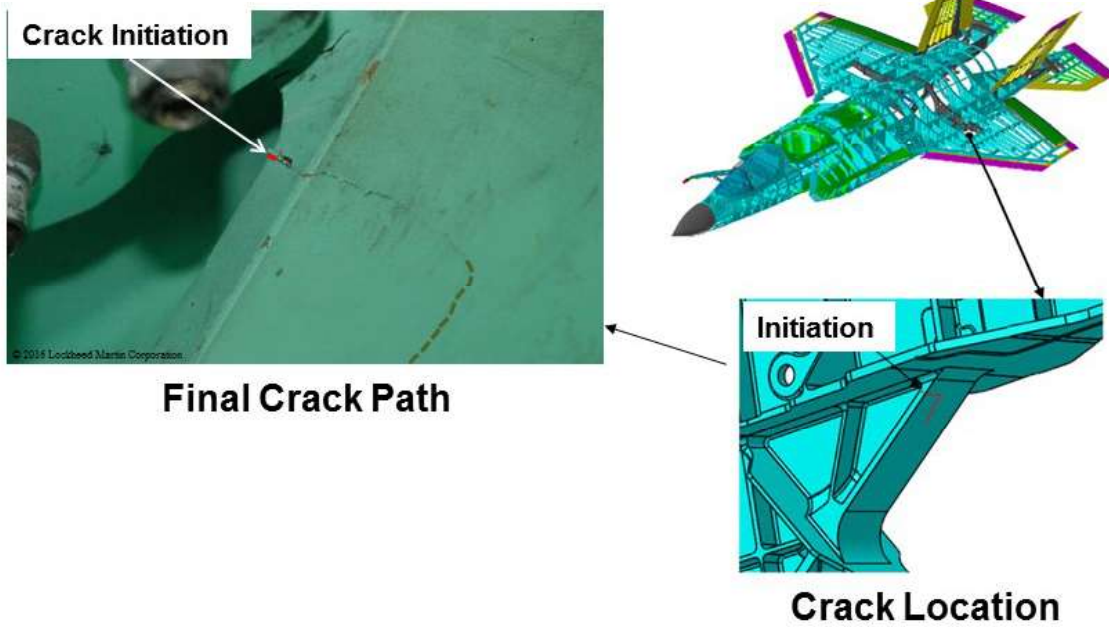


Figure 9.8-26. Durability Test Finding #2

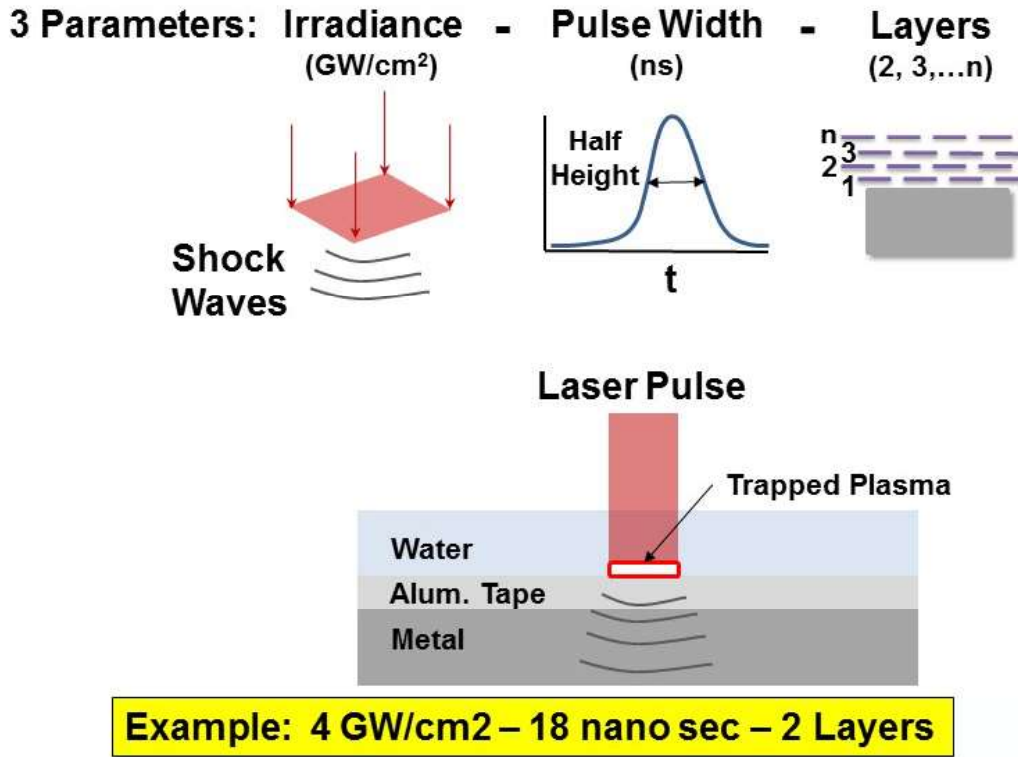
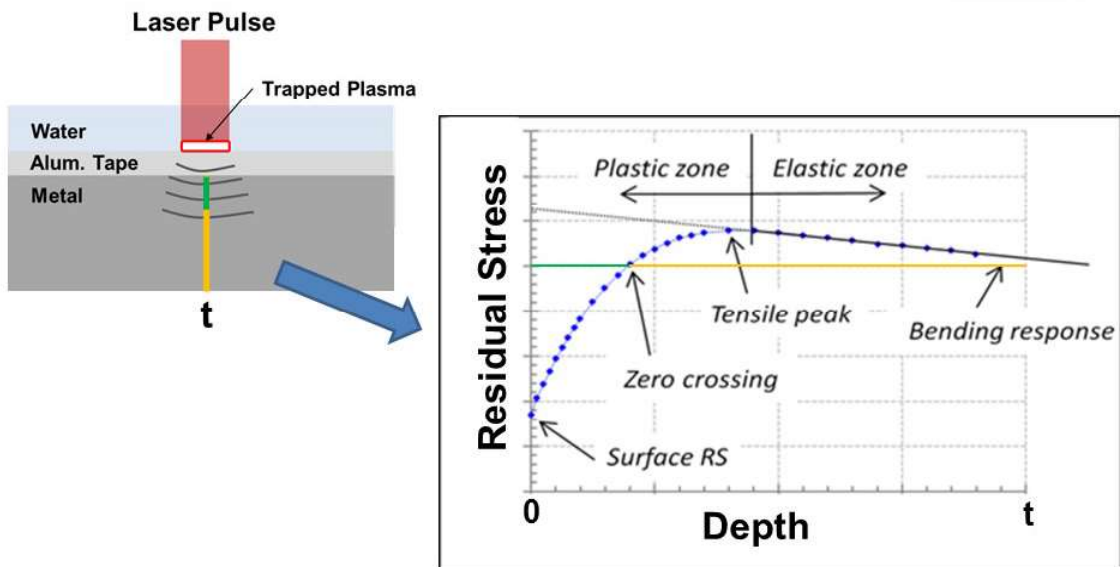


Figure 9.8-27. Laser Shock Peen Process



LSP Develops Deep Residual Stress

Figure 9.8-28. LSP Residual Stresses

• **Building Block Approach Reduces Risk of Qualification**

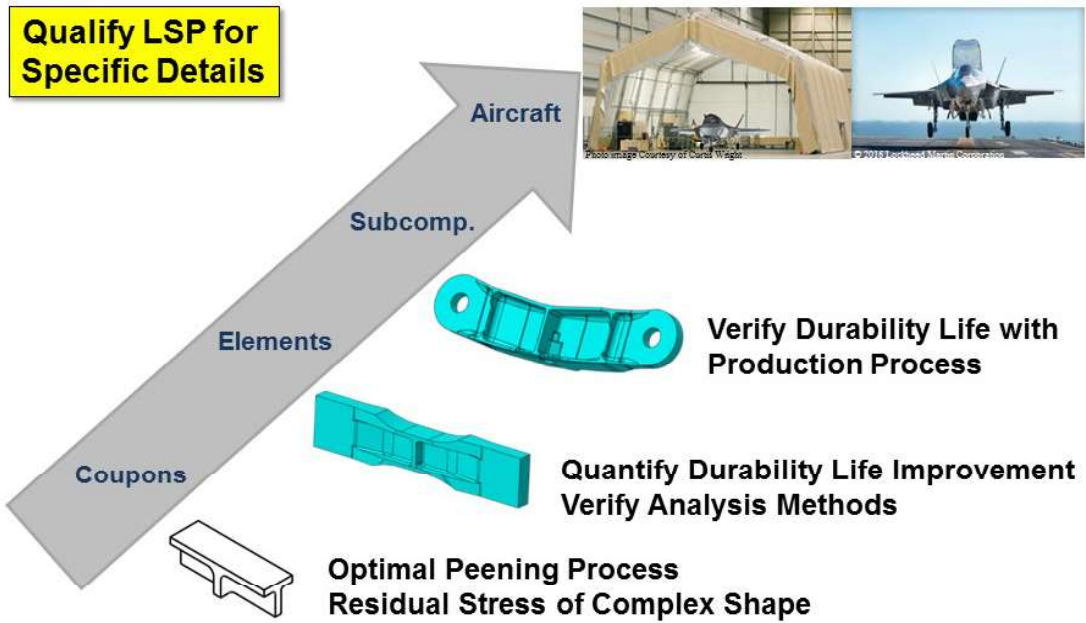
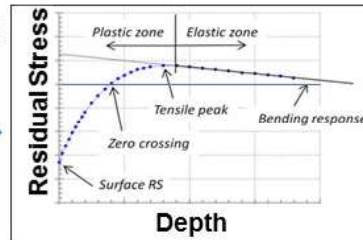
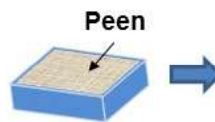


Figure 9.8-29. LSP Qualification Process

• **3 Types of Coupon Building Blocks:**

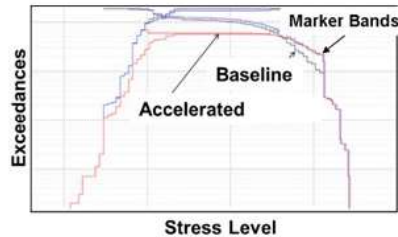
– **Process Characterization**

- Vary LSP Parameters
 - Irradiance, Layers



– **Spectrum Truncation**

- Verify Analysis Methodology



– **Geometric Coupons**

- Contour Method to Measure LSP Residual Stress

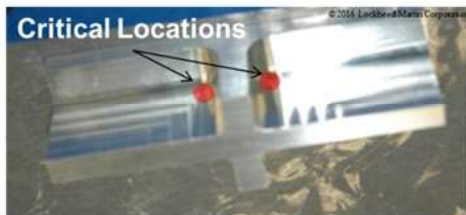


Figure 9.8-30. Phase 1: Coupon Tests

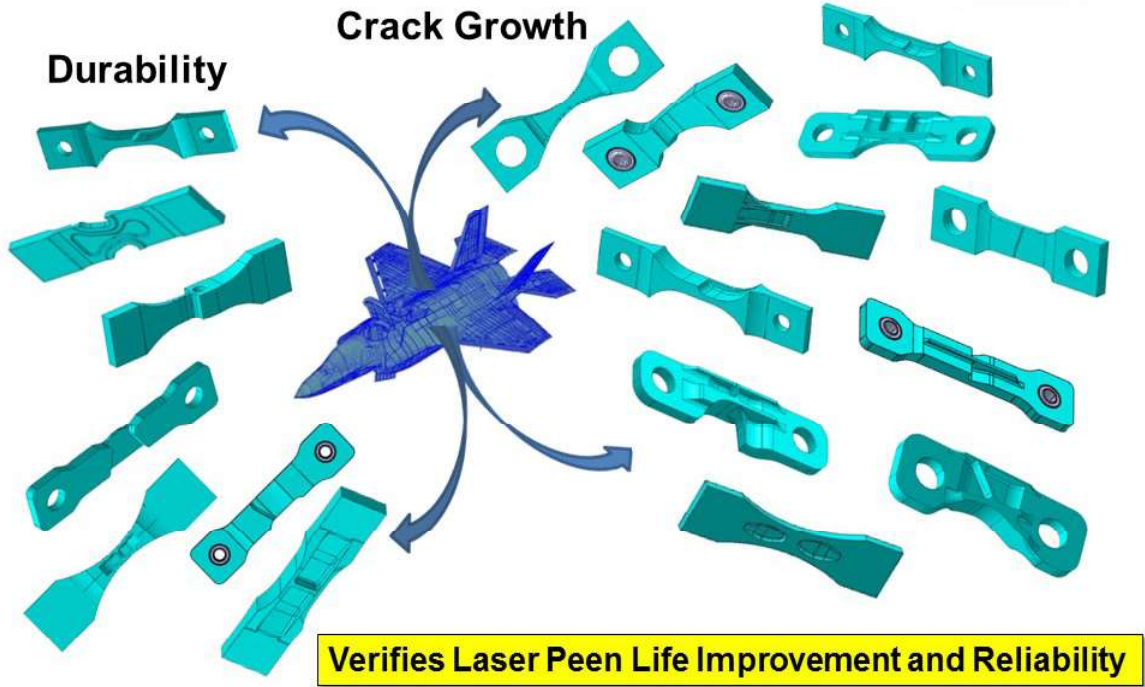


Figure 9.8-31. Element Test Specimens

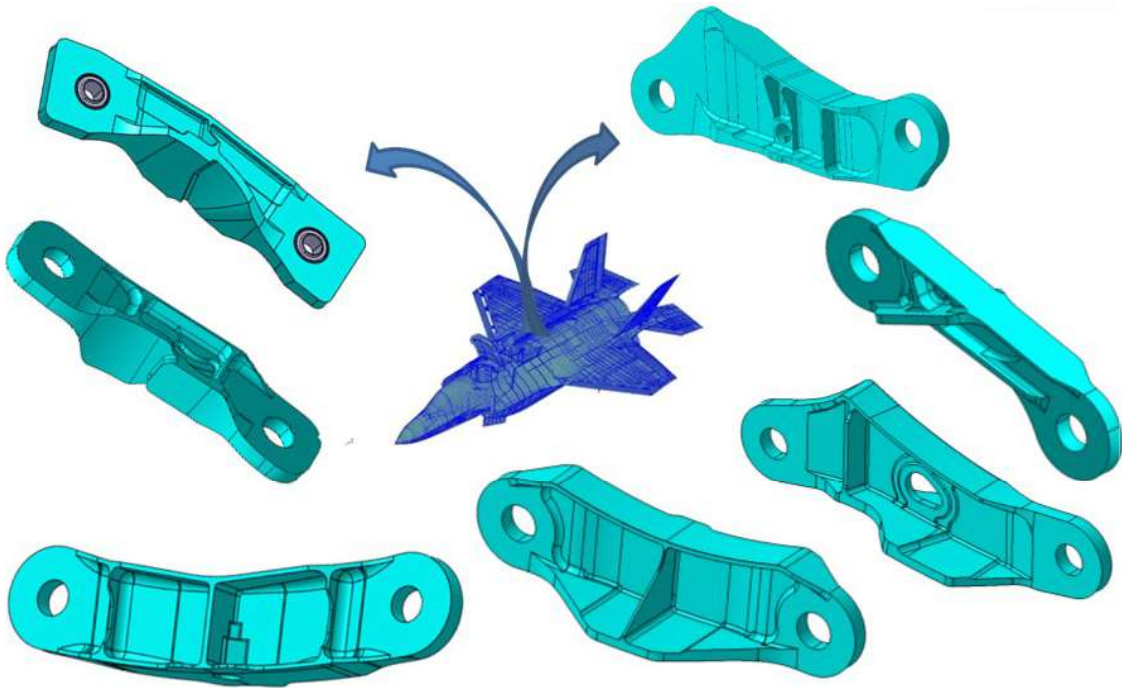


Figure 9.8-32. Phase 3: Subcomponent Specimens

9.8.6. Analytical Tools for CX Holes: Where We Are and Where We're Headed

Robert Pilarczyk and Michael Hill, Hill Engineering, LLC; Scott Carlson, Southwest Research Institute

The fatigue life benefits of engineered residual stress processes such as cold expansion of fastener holes and laser shock peening are well known and have been demonstrated by test in countless applications over the past few decades (Figure 9.8-33). Typical United States Air Force (USAF) methodologies do not directly account for the effects of residual stress and consequently often do not accurately replicate the fatigue life improvement from these processes (Figure 9.8-34). This has contributed to the USAF hesitation to take advantage of these benefits in damage tolerance analyses. Recent collaboration between the USAF, NRC-Canada, and multiple contractor partners have resulted in significant strides to establish and refine the analytical tools for cold expanded fastener holes and other engineered residual stress processes. This technical effort will give an overarching review of engineered residual stress tools and the contributions from the various team members in the sustainment community. The key developments to date, focus areas in work, gaps remaining, and the transportability of the analytical approaches and tools to other “deep” residual stress inducing processes will also be reviewed. Actions items resulting from the first Engineered Residual Stress Implementation (ERSI) workshop will be reviewed. As weapon systems continue to age, sharpened analytical tools are paramount to sustain and efficiently manage these fleets. Engineered residual stresses, and the ability to accurately predict their benefits (and limitations), must be part of the structural integrity engineer’s toolkit.

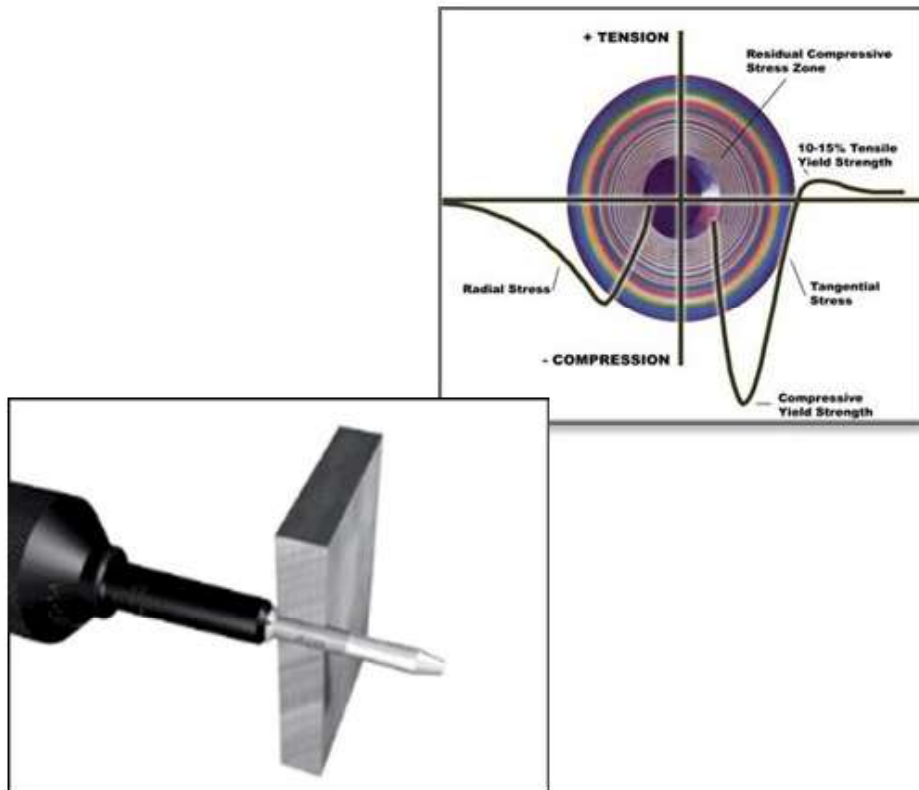


Figure 9.8-33. Cold Expansion of Fastener Holes

❑ Reduce Initial Flaw Size in Damage Tolerance Analysis

- Based upon guidance from JSSG-2006



❑ Limitations of this approach

- NOT PHYSICS BASED
- One size fits all...
- Doesn't account for:
 - Residual Stress (RS) field
 - Changes/Interaction between RS field and geometric notches
 - Crack shape evolution
- Limited benefit in sustainment scenarios
 - Recurring inspection intervals based on NDI Detectable Flaw Size

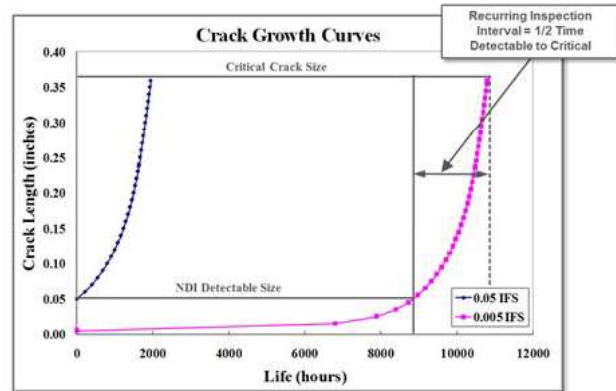


Figure 9.8-34. Classical USAF Approach

9.8.7. SMA Sleeve Method to Coldwork Holes

Albert S. Kuo, A.S.K. INTERNATIONAL, Inc.

A new method, named SMA sleeve method, to coldwork holes is developed, which utilizes seamless sleeve made of shape memory alloys (SMA) having a property of superelasticity. The method is introduced to the industry in the USAF ASIP 2016 conference for the first time. The property of superelasticity enables the sleeve to be seamless, re-useful, and an one-sided operation of coldworking. The operation of the SMA sleeve and split sleeve methods are quite similar.

The seamless feature of the SMA sleeve does not create a ridge and/or shear discontinuity/crack in the coldworked holes. Thus, the final reaming required by the split sleeve and split mandrel methods to clean-up and size the coldworked hole is not necessary for the SMA sleeve method.

Coupon test results of 7075-T651 shown in Figure 9.8-35 for the maximum stress around a hole (KtS) of 93 ksi (641 MPa) indicate that i) the fatigue life improvement factor (LIF) of the SMA sleeve method is superior to, in terms of the magnitude of the LIF and the data-scattering band, the split sleeve and split mandrel methods; ii) the SMA sleeve method can consistently provide a LIF of 4 within the conventional tolerance of start-hole sizes of 0.003 inch (0.08 mm) and even greater than 4 at a tighter tolerance of 0.002 inch (0.05 mm). The test results shown in Figure 9.8-36 for a KtS of 124 ksi (855 MPa) demonstrate the effectiveness of the SMA sleeve method to improve fatigue lives of holes at high stresses.

7075-T651, Constant Amp., R=0.10, Gross Stress = 30 ksi (207 MPa), KtS=93 ksi (641 MPa),
 D=0.25" (6.35 mm), T=0.25" (6.35 mm), W=1.5" (6.35 mm)

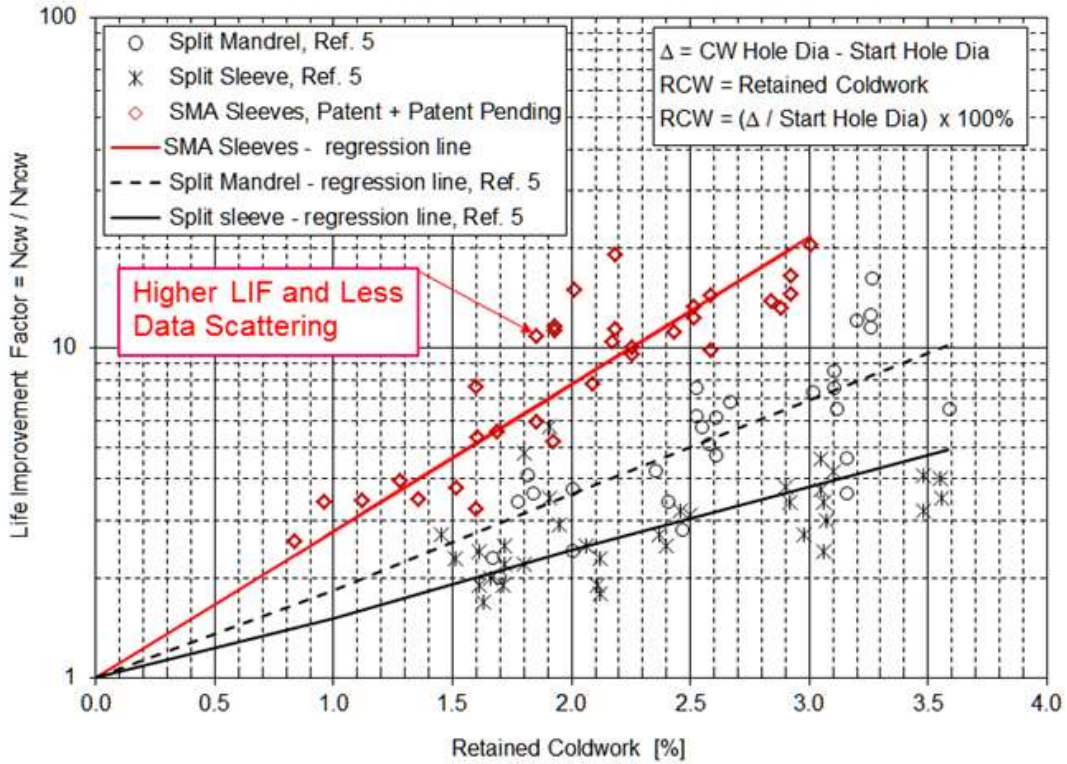


Figure 9.8-35. LIF of Three Hole-Coldworking Methods

7075-T651, Constant Amp., R=0.10, Gross Stress = 40 ksi (276 MPa), KtS = 124 ksi (855 MPa), D=0.25" (6.35 mm), T=0.25" (6.35 mm), W=1.5" (38.1 mm)

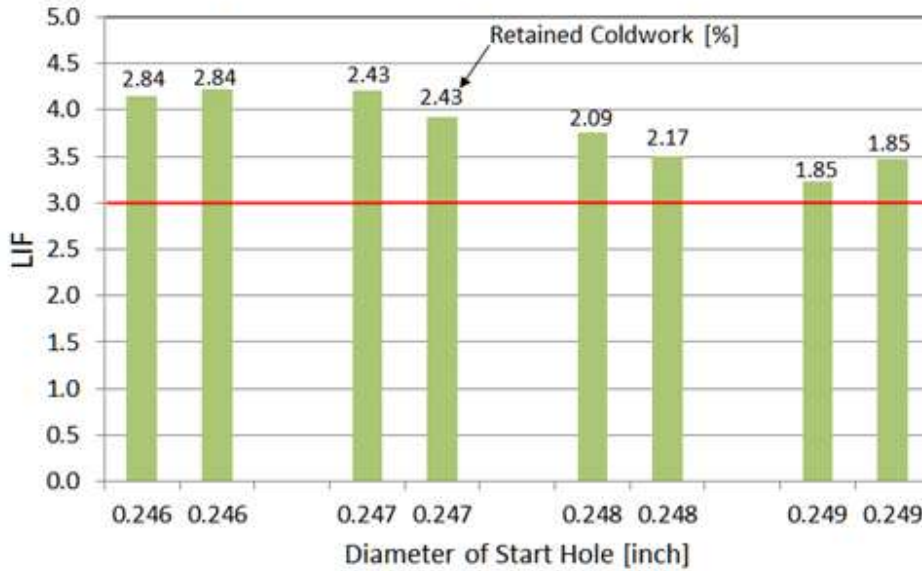


Figure 9.8-36. LIF of SMA Sleeve Method at KtS of 124 ksi

The sleeve durability test results indicate that a SMA sleeve is able to cold work more than 100 holes at the low end of coldworking interference level (3.64%) and 77 holes at the high end of coldworking interference level (5.72%) as shown in Figure 9.8-37. Without final reaming, all of the diameters of the coldworked holes are within an industry process specification. As shown in Figure 9.8-38, sleeve durability test results indicate that the LIF exhibits a variation as the re-use of a sleeve progresses, yet such variation is still within the data-scattering band shown in Figure 9.8-35 for the SMA sleeve method.

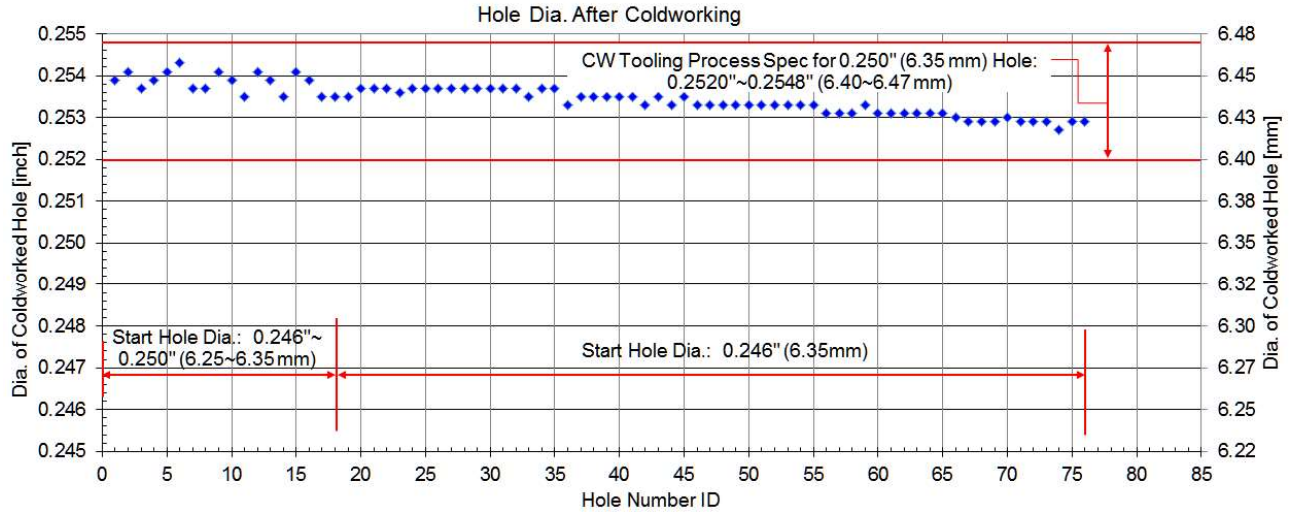


Figure 9.8-37. Final Diameter of Holes Coldworked by Sleeve NNP-15 at Coldworking Interference of 5.72%

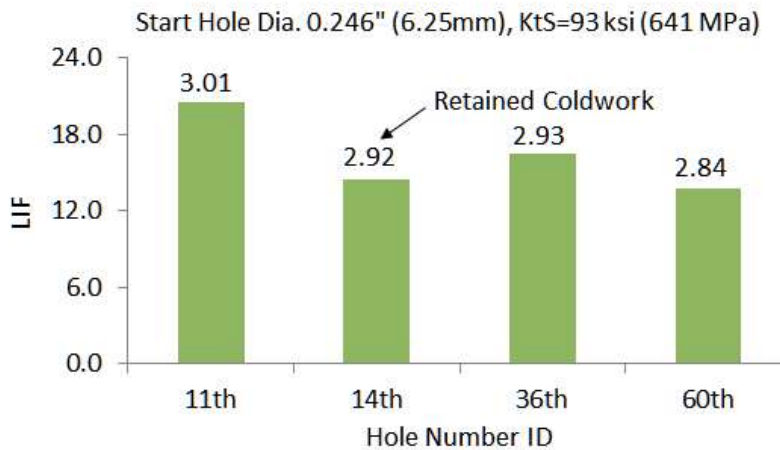


Figure 9.8-38. LIF for Holes Coldworked by Sleeve NNP-15 at Coldworking Interference of 5.72%

Coupon specimens in the short-transverse direction were machined from a 7 inch thick 7050-T7451 aluminum plate and were tested for three hole edge distance ratios of 1.0, 1.25 and 1.5. After coldworking, all of the holes in all specimens were inspected with liquid fluorescent dye penetrant inspection per ASTM E1417, level 3 sensitivity. No crack was detected for a hole edge distance ratio of 1.5 or greater and coldwork up to 3% was retained for the high end of coldworking interference levels.

The capability of the SMA sleeve method to provide consistently high LIFs would enable additional structural weight reduction beyond the current practice due to the split sleeve and split mandrel

methods, and would avoid the costly repair doubler or fitting, or even a re-design part for those tasks such as life extension of existing aircraft, salvaging the out-of-spec parts during manufacturing, and repair of fleet aircraft.

9.8.8. B-1 Wing Lower Skin Repair and Structural Life Enhancement

Lenny Phillip and Mark Moss, The Boeing Company – Defense, Space & Security; Bob Lee, The Boeing Company – B-1 ASIP; Brian Koehl and Rodney Harberson, USAF B-1 ASIP

Fatigue cracking has been discovered in B-1 wing skin holes common to the wing ribs during scheduled ASIP inspections (Figure 9.8-39). The wing lower skin holes contain a counterbore located between the hole and the countersink (Figure 9.8-40). Fuel is stored internally in the wing structure and the counterbore feature was designed to accommodate seating of an o-ring under the fastener head to provide the sole means of sealing the hole from fuel leakage. This feature also creates a geometric stress concentration that is more severe than would occur in a conventional straight bore-type hole. The cracks initiate near the corner formed by the counterbore and straight bore of the hole. In order to meet the service life objective for the B-1 airframe in an economical manner until 2040 and beyond, application of a cold work fatigue life improvement repair process is required. A two phase test program was developed to determine the most appropriate rework method available to extend the life of the wing skin. Phase I test program includes basic dog-bone fatigue testing to generate relative life improvement data for the various candidate repair processes through coupon level fatigue testing. The coupons are idealized representations of wing skin hole geometry. The processes to be evaluated are counterbore cold expansion (thru segmented jaws), adapted thick sleeve cold expansion (or cold work) and expanded bushing processes such as ForceMate™. Also to be evaluated are cold expansion of large holes with limited backside access. Life improvement data from the coupon test program will be used to determine the fatigue life benefit for a given repair process on the B-1 fleet (Figures 9.8-41 through 9.8-43 and Table 9.8-1). Follow-on Phase II testing will be covered in using more representative subcomponent level specimens to generate data for refinement of analytical models and life predictions to support fleet management (Figures 9.8-44 and 9.8-45). Objectives are to obtain durability and damage tolerance life predictions and inspection intervals, multi-site damage (MSD) behavior, K solutions for analytical crack growth curves, and correlation to historical testing and test spectra. Phase I testing completed with very favorable results and will be presented in this technical effort. As a result of this structural repair, the entire B-1 fleet aircraft were repaired within three (3) and one half years. The enhanced fatigue life will carry the B-1 wing beyond the expected service life.

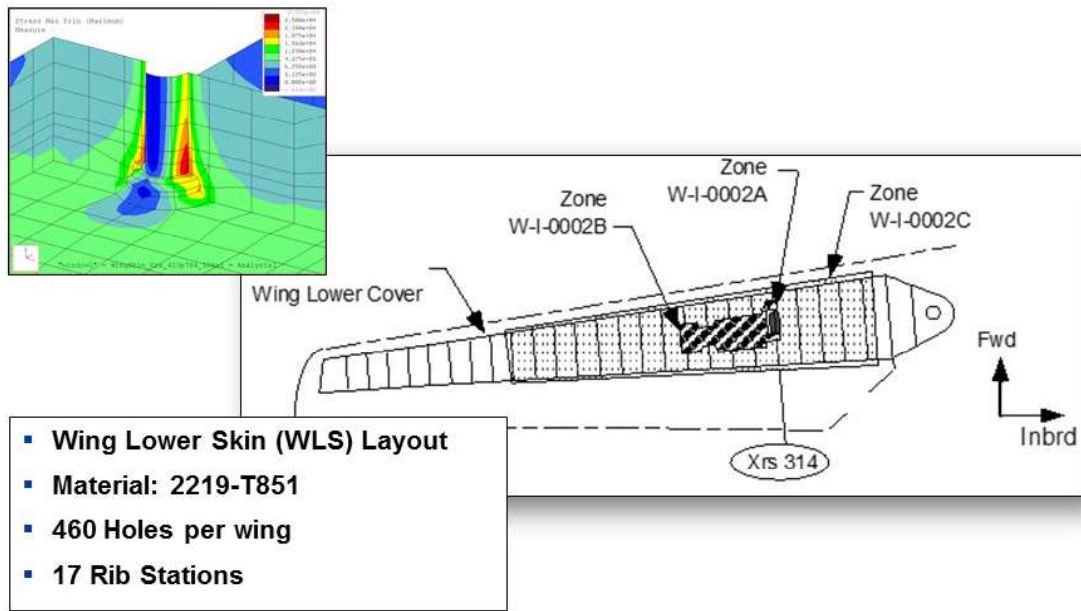


Figure 9.8-39. Inspection Zone

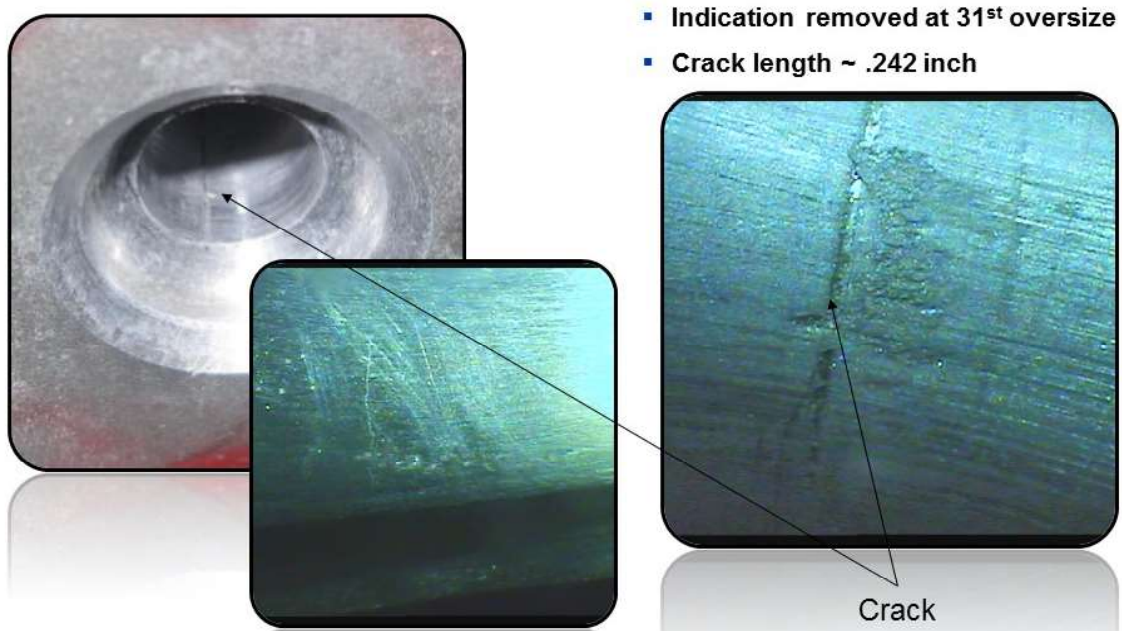


Figure 9.8-40. Crack Findings



Figure 9.8-41. Phase I Coupon Design

Table 9.8-1. Phase I Coupon Test Matrix

Coupon type	Hole Size	Quantity	Spectrum	Rate (Hz)	Location	Test Duration
Baseline	5/16"	9	2003 DADTA	5	HB	May - Jul 2011
Cx0	5/16"	5	2003 DADTA	5	HB	Sep - Oct 2011
FmCx0	5/16"	5	2003 DADTA	5	HB	Oct - Nov 2011
Cx0^	5/16"	5	2003 DADTA	5	HB	Dec - Feb 2012
FmCx0^	5/16"	5	2003 DADTA	5	HB	Jan - Feb 2012
Baseline	1/2"	6	2003 DADTA	5	Sea	Oct - Nov 2011
Baseline - Wide	5/16"	6	2003 DADTA	5	HB	Apr-12
FmCx3^	5/16"	5	2003 DADTA	5	HB	Jun-12
BaCx	5/16"	5	2003 DADTA	5	HB	Aug-12
Cx0^	1/2"	5	2003 DADTA	5	Sea	Apr-12
FmCx0^	1/2"	5	2003 DADTA	5	Sea	May-12

Cold Work Abbreviation	
Cx	Thick Frangible Sleeve Cold Expansion
FmCx	ForceMate Bushing Cold Expansion
BaCx	Large Crack Cold Expansion
Cx^	Counterbore Cold Expansion
^	Denotes Counterbore was cold expanded

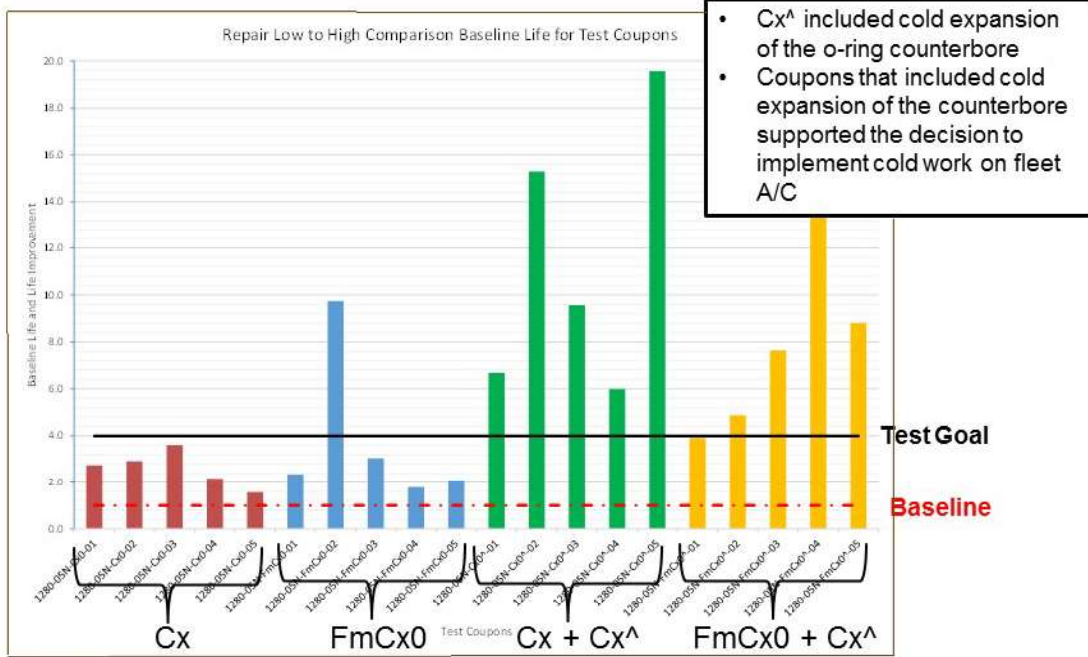


Figure 9.8-42. Phase I Life Improvement Results

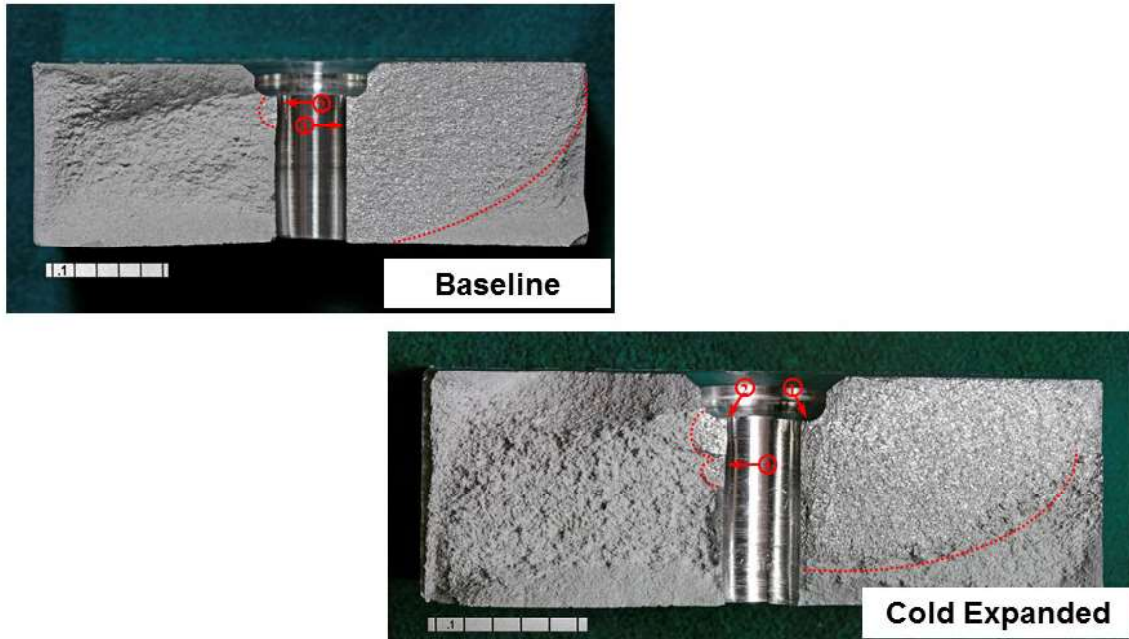


Figure 9.8-43. Phase I Failure Photos

- Phase II testing currently in progress



Figure 9.8-44. Phase II Specimen Design

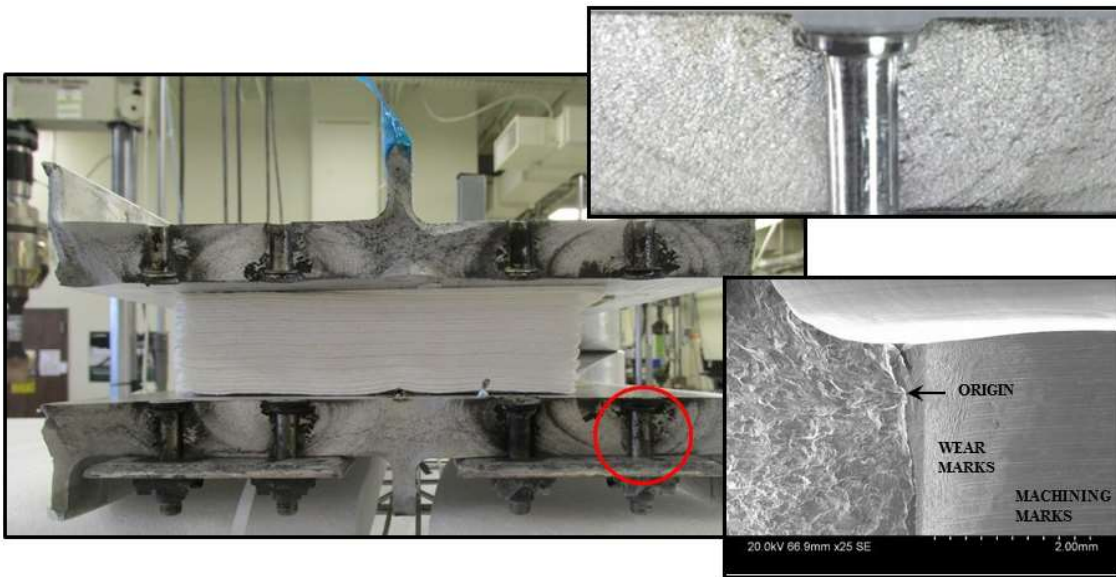


Figure 9.8-45. Phase II Specimen Fracture Face

9.8.9. Aleatory Uncertainties in Crack Propagation Life Predictions From Cold-Expanded Holes

Ricardo Actis and Matt Watkins, Engineering Software Research & Development, Inc.

In life prediction of structural components containing an initial flaw, it is particularly important to determine stress intensity factors (SIFs) to a high degree of accuracy. In the case of cracks emanating from cold-expanded holes, a very important factor affecting the prediction of fatigue crack propagation (FCP) life is the aleatory uncertainty associated with the use of experimentally obtained residual stress (RS) distributions.

The results of simulations of FCP when considering uncertainties in the input RS distribution were compared with experimental fatigue life data of aluminum alloy test coupons. The model of crack propagation was based on the following assumptions: (1) the driver of crack propagation is the SIF amplitude (ΔK) and the RS only affects the load cycle ratio R ; (2) da/dN - ΔK curves obtained from calibration experiments at fixed R using thru cracks are applicable for corner cracks; (3) the direction of crack propagation is normal to the crack front and the crack grows in the plane of the initial flaw. The effects of the aleatory uncertainties associated with the measured residual stress were investigated by scaling the RS profile while keeping all other variables constant.

The 1/4" thick 2024-T3 dogbone specimen with a 1/4" diameter hole and a 2.0" test section width shown in Figure 9.8-46 was one of the specimens used for life prediction. The coupon was pre-cracked with a surface length of 0.0281" and a bore length of 0.0349" after the cold-working operation. The RS profile determined by the Contour Method [1] along the symmetry plane where the crack is located is also shown in the figure. Figure 9.8-47 shows the life prediction for constant amplitude loading accounting for aleatory uncertainty in RS by introducing a $\pm 10\%$ variation in the profile: (1) as-measured RS (100%), (2) 90% of the measured RS and (3) 110% of the measure RS. The results show a spread in the predicted life of $N_{110\%}/N_{90\%} = 3.4$, with the closest to the experimental fatigue life (121,312 cycles) for the 100% RS (137,305 cycles). The figure also shows a typical crack propagation map and the predicted crack front shape.

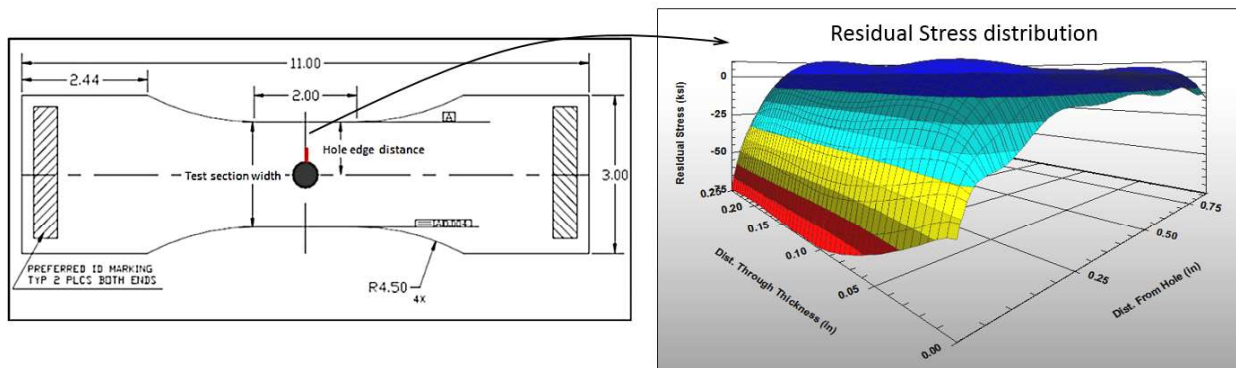


Figure 9.8-46. Typical Test Specimen and Residual Stress Distribution at a Cold Worked Hole

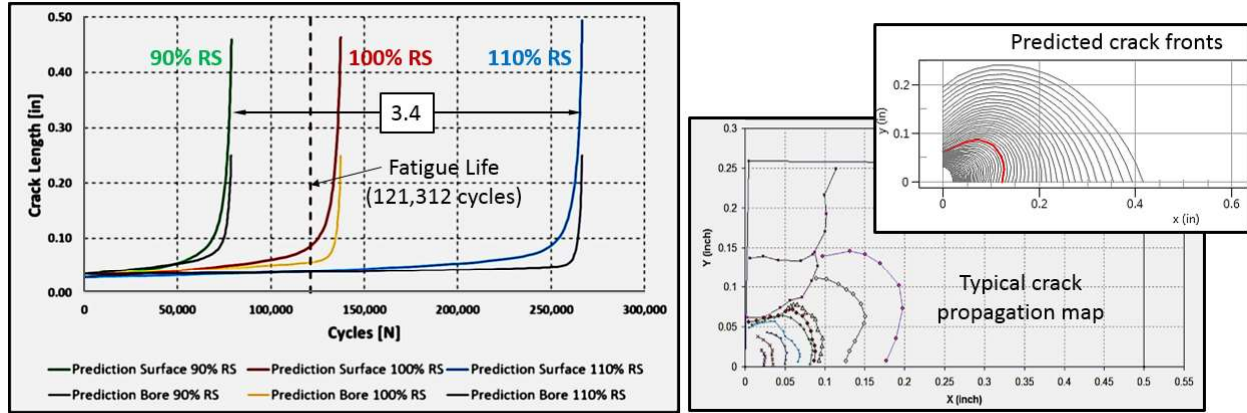


Figure 9.8-47. Crack Propagation Life Predictions Due to Variation in Residual Stresses. Typical Crack Propagation Map and Predicted Crack Shape During the Simulation

A prototype software tool was developed to perform the predictions for cracks emanating from cold worked holes. The software was designed for straight and countersunk (CSK) holes, it has a database of RS profiles for typical aerospace alloys; it accounts for constant-amplitude or variable-spectrum loading it; includes a cold-work simulation module to consider the effect of overload and underloads in the distribution of RS; and it communicates with StressCheck to determine accurate SIFs at points along the crack front. Residual stresses may also be imported from other software or experimental measurements, and it communicates with AFGROW for interpolation of crack growth curves. The prototype software is available for evaluation by contacting support@esrd.com.

It is well known that the prediction of fatigue life is affected by the statistical dispersion of the input data. In this work we addressed the effect of variation in measured RS for cracks in cold-worked holes and found that $\pm 10\%$ variation in RS resulted in a factor larger than 3 in fatigue life estimates. Additional examples are presented in Ref. [2], including specimens of 7075 and the effect of spectrum loading in life predictions.

This work was performed as part of a United States Air Force (USAF) program to incorporate residual stresses into structural life assessments to reduce inspection burden, increase asset availability, and reduce inspection cost for the A-10, F-16, and T-38 Aircraft Structural Integrity Programs (contract No. FA9453-12-C-0218). Analytical Processes/Engineered Solutions (AP/ES), Inc. (www.apesolutions.com) was the prime contractor for the program. Engineering Software Research & Development (ESRD), Inc. (www.esrd.com) was a subcontractor.

References

- [1] M. Prime, Cross-Sectional Mapping of Residual Stresses by Measuring the Surface Contour After a Cut. *Journal of Engineering Materials and Technology* 123(2):162-168.
<http://www.lanl.gov/contour/>
- [2] R. Actis, Factors Affecting Fatigue Crack Propagation from Cold-Expanded Holes. AFGROW User's Workshop, September 2015, Layton UT.
<http://www.afgrow.net/workshop/workshop2015.aspx>

9.8.10. Low Plasticity Burnishing Mitigates Fretting Fatigue Failures in AV-8B Harrier Engines Restoring Fleet Readiness

Julie Prev y, Lambda Technologies

The blade-disk contact faces of LPC1 disk post slots in F402-RR-404 (Pegasus) engines, which power U.S. Marine Corp’s AV-8B Harrier jets (Figure 9.8-48), are prone to fretting induced microcracks. Fretting damage occurs at the edge-of-contact (EOC) zones between the disk post and blade dovetail faces. If untreated, these shallow, shear stress (mode II) induced microcracks can grow through normal (mode I) fatigue crack growth’, potentially ending in catastrophic disk failure. Figure 9.8-49 shows the crack progression to failure in a F402-RR-404 LPC1 disk. Risk of disk failure posed an ongoing safety concern for the fleet, limiting fleet readiness and increasing both inspection and maintenance costs.



Figure 9.8-48. U.S. Marine Corp’s AV-8B Harrier

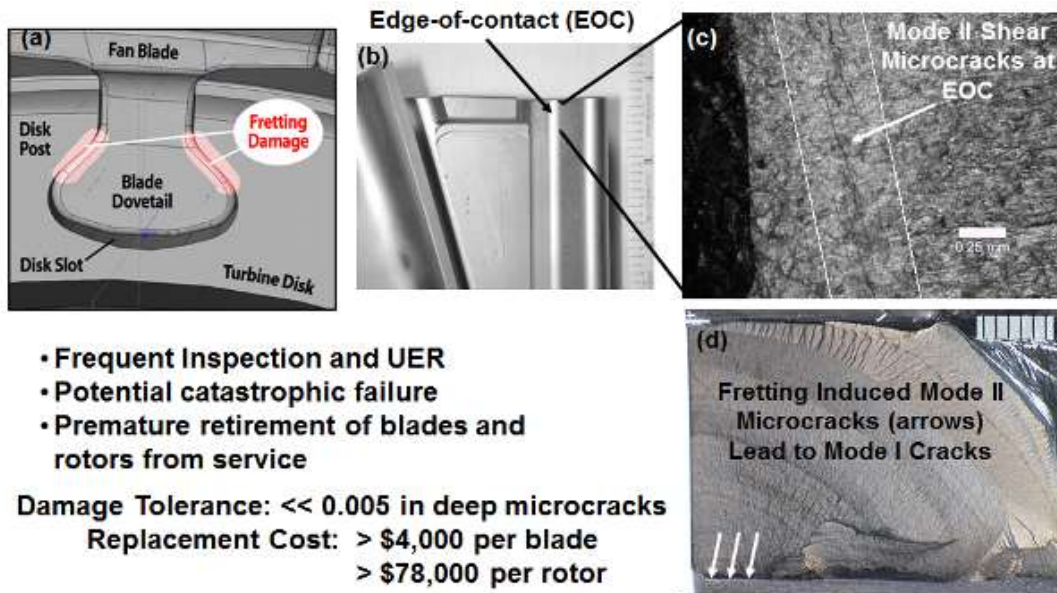


Figure 9.8-49. F402-RR-404 LPC1 Disk Microcracking

The F402-RR-404 LPC1 blade dovetail and disk slots were excellent candidates for the application of low plasticity burnishing (LPB[®]) treatment to improve damage tolerance and safety of operations. Having established that LPB induced compression completely mitigated fretting induced fatigue cracking, LPB production processing was developed for treating the disk posts and blade dovetail contact faces. Figure 9.8-50 shows the LPB treatment of the disk slots. Fatigue tests of full components with simulated fretting damage of up to a depth of 0.03 inches on the EOC zones showed a >15X improvement in life for the LPB treated parts over the baseline condition (Figure 9.8-51).



Figure 9.8-50. LPB Treatment of F402-RR-404 LPC1 Disk

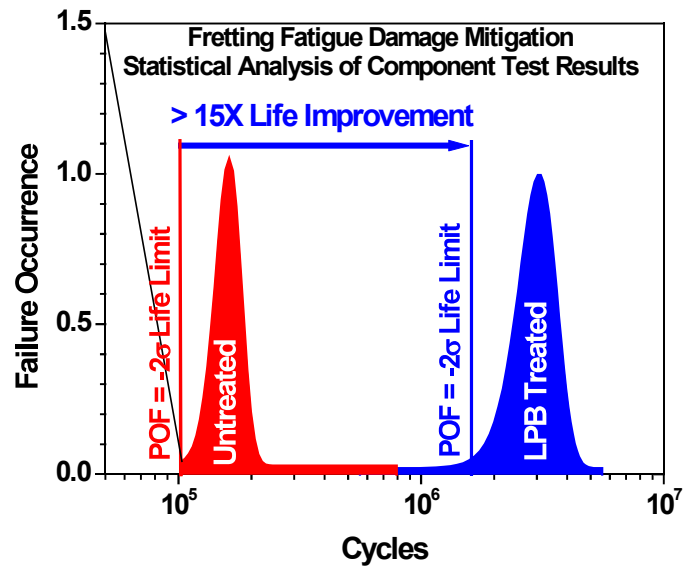


Figure 9.8-51. Component Life Extension From LPB Treatment

NAVAIR approved Lambda's LPB process for improving the damage tolerance of both new and in-service F402-RR-404 LPC1 disks. Over 60 in-service disks have been LPB treated and placed in service over the last decade. The improved damage tolerance has eliminated a major flight safety issue threatening continued operation of the AV-8B Harrier fleet. The ease of implementation of LPB into the

existing manufacturing process in CNC mills has made it very cost-effective and provided substantial cost savings for the USMC. LPB treatment of the blade dovetail EOC regions is pending final approval.

9.8.11. LPB Treatment of P-3 and C-130 Propellers Reduces Maintenance and Ownership Costs

Julie Prev y, Lambda Technologies

U.S. Navy's P-3 Orion (Figure 9.8-52) and USAF's C-130 Hercules (Figure 9.8-53) are powered by T-56 turboprop engines using similar Hamilton-Sundstrand propellers. The propeller blades are manufactured from high strength aluminum alloy forgings with hollow shanks. An aluminum bronze bushing is fitted into the propeller bore in the shank as part of the blade feathering mechanism. Contact between the dissimilar aluminum and bronze bushing alloys renders the bore surface prone to stress corrosion cracking (SCC), as seen in Figure 9.8-54. To mitigate SCC, the bore was heavily shot peened to introduce a deep layer of beneficial compressive residual stress. Peening left an extremely rough surface requiring reaming to correctly fit the bronze bushing. Because the reamed surface is conical, the circular face of the shank had to then be machined. After three machining cycles propellers reach dimensional limits and must be retired. The peening-machining overhaul and replacement blades cost nominally \$1,000 and \$35,000, respectively. But more imperative than cost, limited availability of replacement blades threatens fleet readiness.



Figure 9.8-52. U.S. Navy's P-3 Orion



Figure 9.8-53. USAF's C-130 Hercules

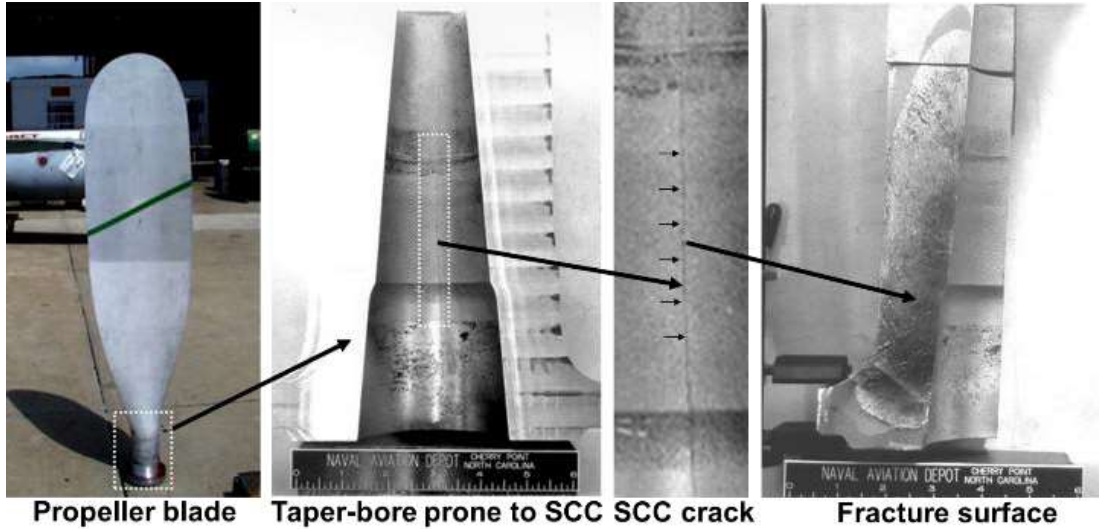


Figure 9.8-54. Taper Bore of the Propeller Blades Prone to Stress Corrosion Cracking

Low plasticity burnishing (LPB) treatment of the taper bore surface was chosen to replace the heavy shot peening process. The depth and magnitude of LPB produced compression exceed that from the heavy shot peening. LPB generates very low cold work so the beneficial compression is stable during service. LPB leaves a very smooth surface, eliminating the need for reaming and machining. Therefore, LPB eliminates blade retirement. Blades can be overhauled and returned to service indefinitely, ensuring fleet readiness. Implementation of the LPB process in an MRO (Maintenance, Repair and Overhaul) shop on a robot controlled system is logistically convenient.

Figure 9.8-55 shows the robotic LPB treatment of a propeller blade. Residual stress vs depth profile plots in Figure 9.8-56 compares the results for LPB treated and shot peened and reamed blades. Both deeper and higher magnitude compression are achieved by LPB. Also, as seen in Figure 9.8-57, LPB treatment leaves to a nearly polished ($18 \mu\text{m rms}$) surface, eliminating the need for any other finishing operations.

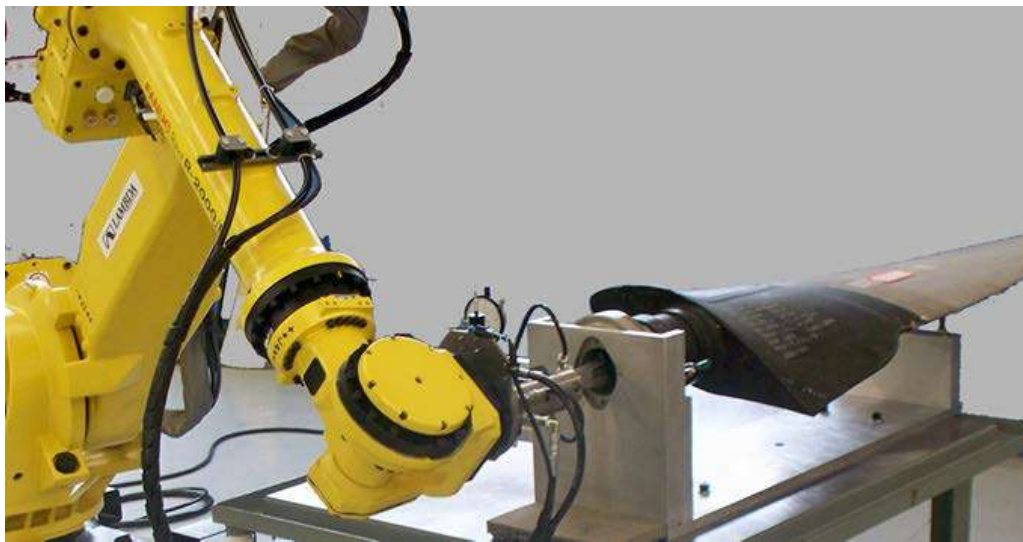


Figure 9.8-55. Robotic LPB Treatment of Propeller Taper Bore

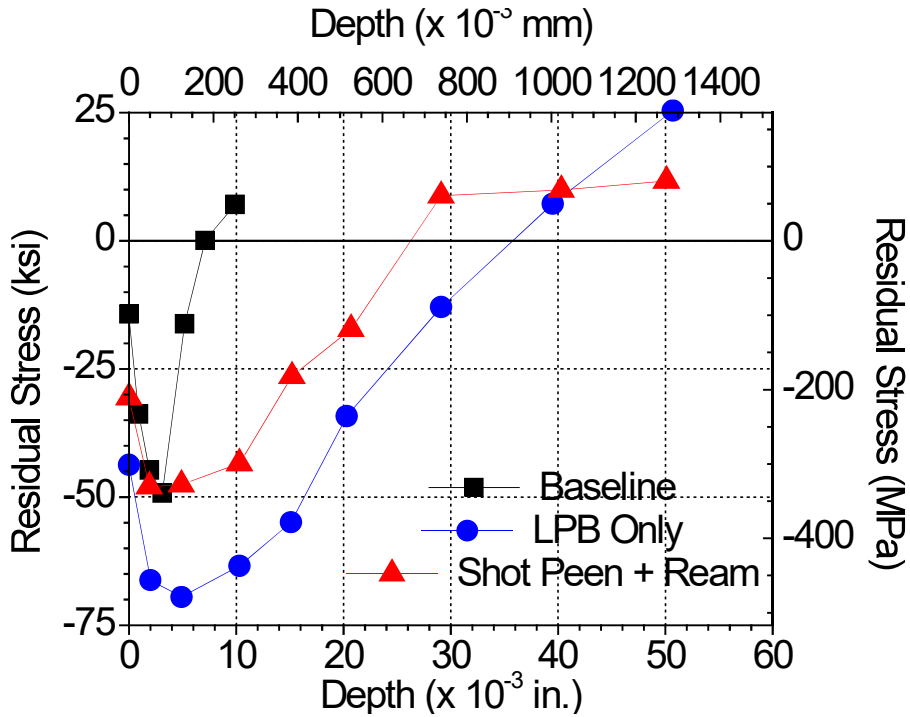


Figure 9.8-56. Residual Stress vs. Depth Plots for Propeller Bores

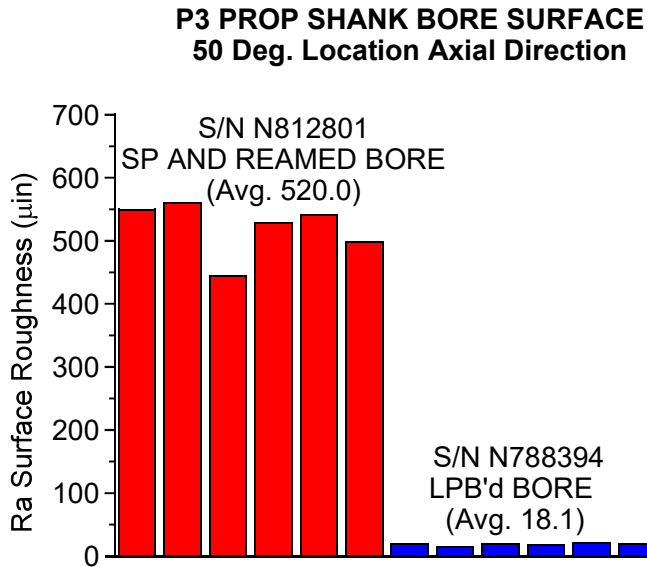


Figure 9.8-57. Surface Roughness Comparison of Treated Propeller Bores

Robotic LPB systems have been operational treating both P-3 and C-130 propellers for nearly six years at U.S. Navy's Cherry Point depot, Warner Robbins Air Force Base, and Pacific Propeller International. Nearly 3,000 P-3 and C-130 propeller blades have been LPB treated to date. Substantial

cost savings for both the U.S. Navy and USAF have been achieved, and the estimates are shown in Figure 9.8-58. Fleet readiness has been ensured by LPB processing existing blades to allow continued service.

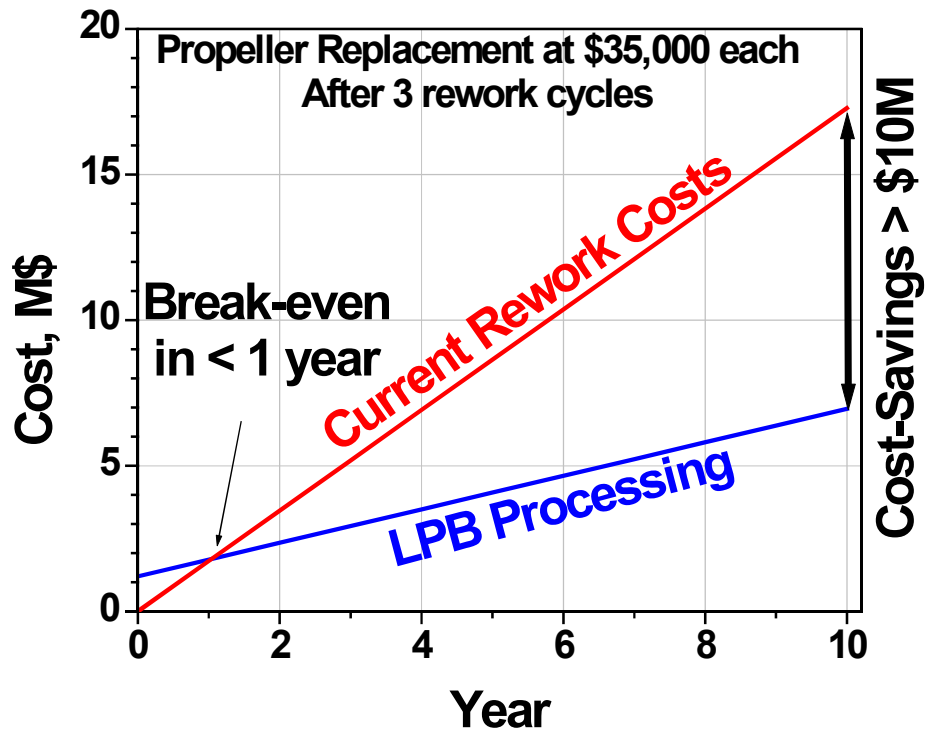


Figure 9.8-58. Cost Benefit Analysis

9.8.12. Low Plasticity Burnishing of LPC1 Vanes Mitigates Fatigue Failures of AV-8B Harrier Engines

Julie Prev y, Lambda Technologies

The LPC1 (1st stage low compressor) vanes of the F402-RR-404 (Pegasus) engine powering the USMC AV-8B Harrier (Figure 9.8-59) have failed in fatigue causing several Class A mishaps, initially grounding the fleet, and creating an ongoing safety concern. Cracks occurred in the inboard trailing edge (TE) of the airfoil near the platform (Figure 9.8-60). The LPC1 vane foreign object damage (FOD) tolerance was less than 0.005 inch, requiring frequent inspection and vane replacement, reducing fleet readiness. Limited replacement vane availability threatened fleet readiness and potential grounding.



Figure 9.8-59. U.S. Marine Corps AV-8B Harrier

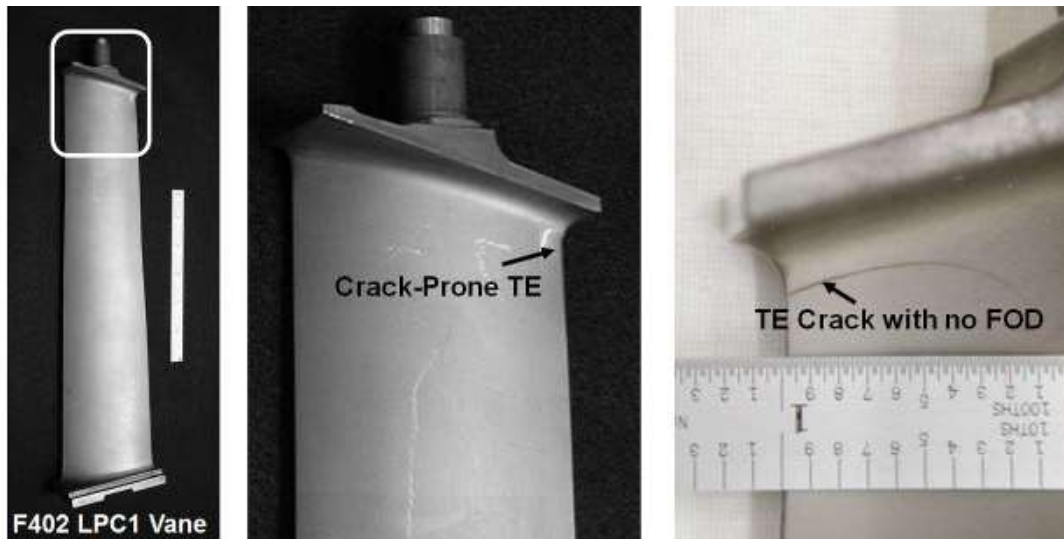


Figure 9.8-60. F402-RR-404 LPC1 Vane, Close-Ups of Crack-Prone Trailing Edge

Low plasticity burnishing (LPB[®]) was used to put the critical leading edge in high residual compression to improve the damage tolerance F402-RR-404 LPC1 vanes. The level of LPB compression needed to mitigate FOD and restore fatigue properties was determined through coupon studies. Production LPB processing was then developed to treat the TE regions of the airfoil, putting the entire thickness of the LE in high compression, completely arresting fatigue crack growth. Figure 9.8-61 shows the LPB processing in a CNC mill, LPB treatment in progress, and a close-up view of the resulting LPB induced residual compressive zone. Fatigue tests of LPB processed LPC1 vanes with 0.020 inch deep FOD on the trailing edge verified an improvement in life over the baseline exceeding 1000X (Figure 9.8-62). OEM conducted ASMET engine testing for over 600 hours proved that LPB treatment resulted in complete mitigation of even 0.025 inch ballistic FOD (Figure 9.8-63).

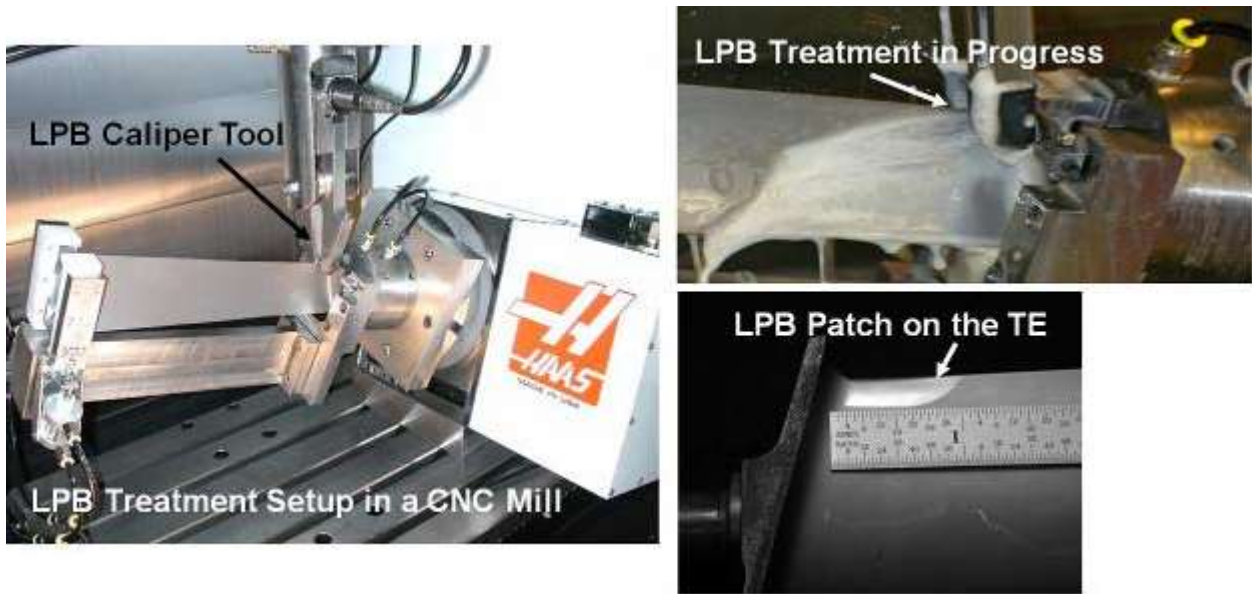


Figure 9.8-61. LPB Treatment in a CNC Mill, Resulting LPB Patch

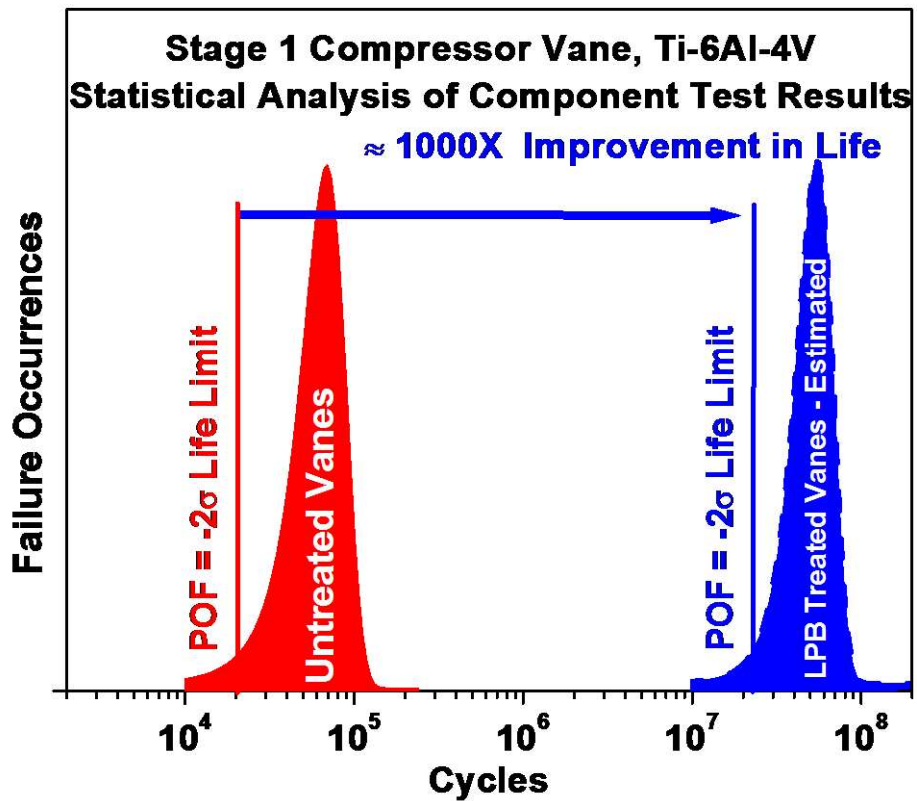


Figure 9.8-62. Fatigue Life Improvement From LPB Treatment



Figure 9.8-63. LPB Passed >600 Hr ASMET Engine Test

NAVAIR approved Lambda's LPB process for improving the damage tolerance of both new and in-service LPC1 vanes. Over 16,000 in-service vanes have been LPB treated and installed in F402-RR-404 engines over the last decade. The improved damage tolerance has eliminated a major flight safety issue, ensuring continued operation of the AV-8B Harrier fleet, improved time on wing, and provided substantial cost savings for the USMC.

9.8.13. Shot Peen Residual Stress Redistribution During Bending Loading

Reji John, Air Force Research Laboratory – Materials and Manufacturing Directorate

The effect of bending loading on the redistribution of shot peen residual stresses in a Ni-base superalloy, IN100 was investigated [1]. The bend specimen configuration used in this study is shown in Figure 9.8-64. The complete load-unload computed bending stress versus measured strain deformation response of the four-point bend samples for three maximum applied stresses of interest in shot peened IN100 at room temperature are shown in Figure 9.8-65. The elastic modulus, measured in the elastic region of the curve was determined to be 207 GPa. This was within 1.5 % of the measured value from the uniaxial tensile tests. The plastic strain levels for maximum applied surface stresses of 1,268, 1,364, and 1,512 MPa were approximately 0.0022, 0.0035, and 0.006, respectively. All the compressive strains shown in Figure 9.8-65 were measured on the top surface of the specimens with the sign changed to plot as positive values. Interestingly, strain measurements recorded simultaneously on the bottom surface were practically identical in magnitude to the top surface showing no difference in yield behavior under tension and compression. Measurements of retained residual stress depth profiles on the tensile and compressive surfaces of shot peened IN100 four-point bend samples tested at 23 °C are shown in Figures 9.8-66 and 9.8-67. The residual stress profiles in Figure 9.8-66 were measured on the bottom surface in the long-axis orientation, which is the applied loading direction for applied maximum tensile stresses of +1,268, +1,364, and +1,512 MPa based on elastic beam theory. On the bottom surface the applied tensile stress from bending is superimposed with the compressive residual stress from shot peening, which after unloading results in some level of relaxation. The maximum applied stress of +1,268 MPa appears to exhibit little or no relaxation in residual stress whereas the other two profiles exhibit increased relaxation with increased applied tensile stress. In contrast, residual stress profiles shown in Figure 9.8-67 were measured on the top surface in the long-axis orientation, which is the applied loading direction for applied

minimum compressive stresses of -1,268, -1,364, and -1,512 MPa. On the top surface the applied compressive stress from bending is superimposed with the compressive residual stress from shot peening, which after unloading results in some measure of relaxation. However, on the top surface of the specimen, the final residual stress profiles are similar with only a limited difference in relaxation with increased applied compressive stress. The residual stress relaxation behavior on the two surfaces of the bend geometry are clearly different from each other. This difference in relaxation behavior between the two surfaces is intuitive, given the interaction of an asymmetric applied stress gradient with a symmetric residual stress profile.

References

- [1] Buchanan, D.J. and John, R., "Effect of Large Plastic Strains and Strain Gradients on Residual Stress Relaxation in Shot Peened IN100," *Superalloys 2016: Proceedings of the 13th International Symposium on Superalloys*, Edited by: Mark Hardy, Eric Huron, Uwe Glatzel, Brian Griffin, Beth Lewis, Cathie Rae, Venkat Seetharaman, and Sammy Tin, TMS (The Minerals, Metals & Materials Society), pp. 841-848, 2016.

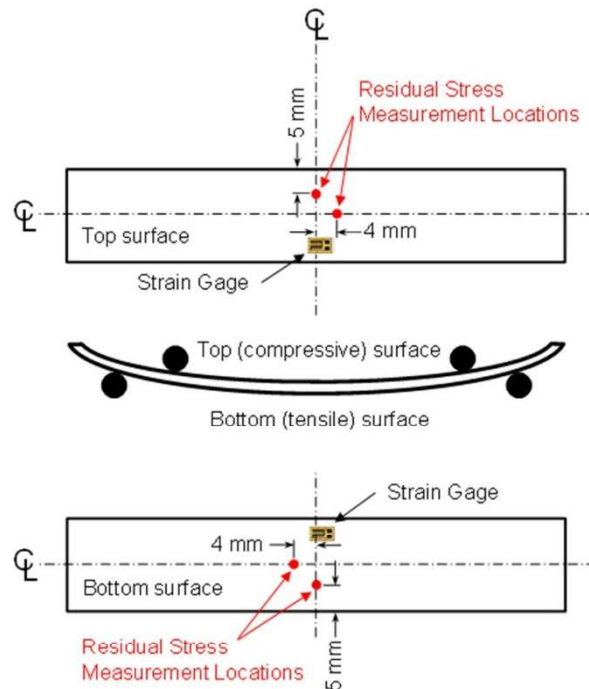


Figure 9.8-64. Bend Specimen Schematic Showing Locations of Strain Gages and Residual Stress Measurement Locations on Both the Top (Compressive) and Bottom (Tensile) Surfaces

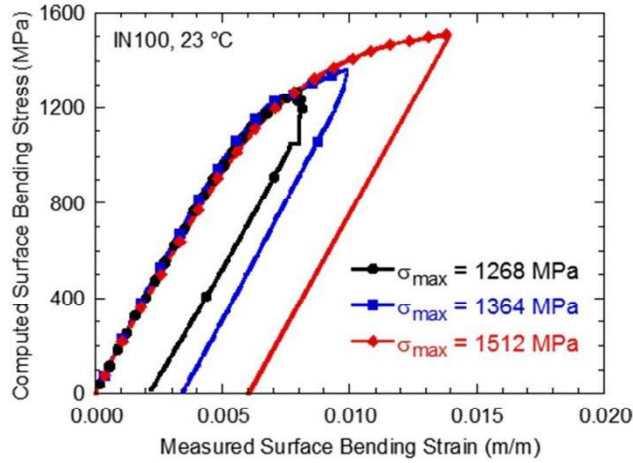


Figure 9.8-65. Stress-Strain Response and Resulting Plastic Deformation for Shot Peened IN100 at 23 °C for Different Levels of Maximum Bending Stress

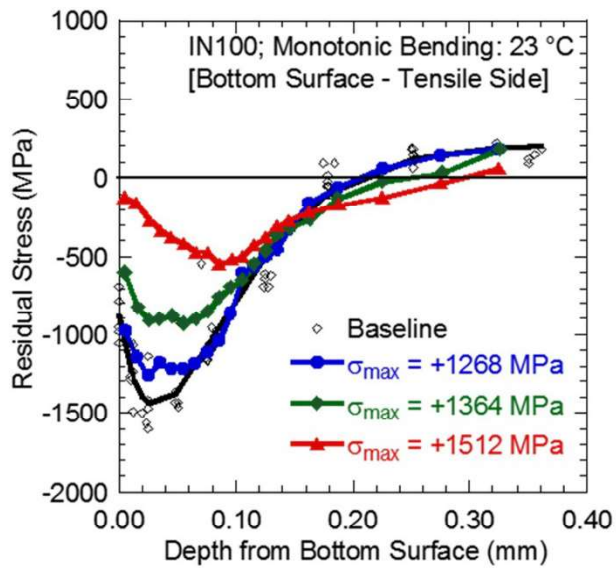


Figure 9.8-66. Effect of Applied Stress Gradient on Retained Residual Stress on the Bottom Surface of the Bend Specimen for Different Levels of Applied Tensile Stress

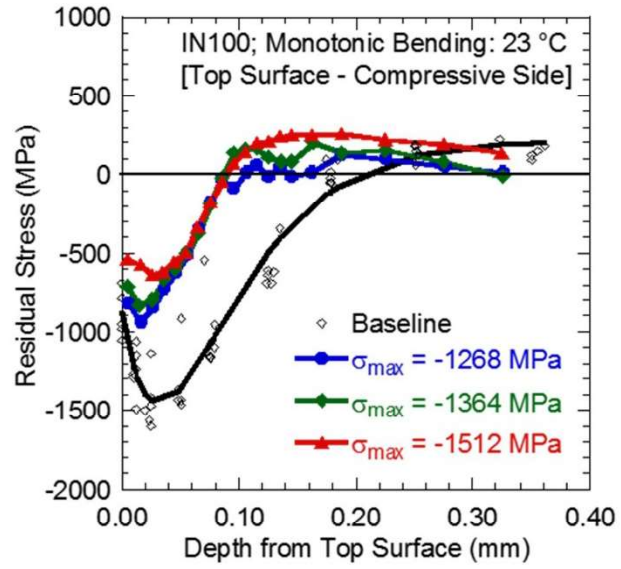


Figure 9.8-67. Effect of Applied Stress Gradient on Retained Residual Stress on the Top Surface of the Bend Specimen for Different Levels of Applied Compressive Stress

9.9. REPAIR CONCEPTS

9.9.1. TRAINING: Design of the Full Strength, Damage Tolerant Repairs for Metallic Aircraft Structure: The Art Behind the Science

Scott Carlson and Rachel Heller, Southwest Research Institute

As the modern United States Air Force's fleet continues to age, the effects of usage, corrosion and maintenance intrusion have caused repair costs to increase while at the same time increasing the length of time needed to design, validate and install repairs. One reason for this is the lack of specialized training, focusing on the design of full-strength, damage tolerant repairs, provided by the USAF. The A-10 ASIP Analysis Group has invested in the development of a 17-week, graduate level training course that covers all of the topics necessary to enable the new structures engineer to become familiar with aerostructure terminology, e.g., spar cap, web, doubler, Hi-Lok, and to understand basic aircraft structure, loads, materials, how materials behave under monotonic and cyclical loading and how to integrate with the USAFs Non-Destructive Inspection (NDI) offices at their individual depot. This course has been provided across multiple sites to Air Force Life Cycle Management Center and Air Force Sustainment Center engineers whose areas of responsibility range from structures and mechanical systems to tooling and processing, enabling them to more effectively, efficiently and most importantly safely design, analyze and produce full-strength damage tolerant repairs for critical aircraft structures. This training course provides an overview of the material covered in the semester long course. Topics include: epistemology of aircraft structural design and safety management paradigms (ultimate strength, safe life/fail-safe, and damage tolerance), external to internal loads, materials and mechanisms for strengthening metals, introduction to advanced strength of materials, fastener selection and use, design of stepped splice repairs, doublers for skins, damaged hole repair, and finally lessons learned from repairs that failed. In addition to these static strength repair concepts an introduction into damage tolerant design is provided. This introduction includes an overview of the application of Linear Elastic Fracture Mechanics (LEFM), and residual strength calculations to determine the recurring inspection interval for fatigue and fracture critical parts, in the presence of a repair. Through this instruction we hope to enhance the learning environment by providing valuable training, focused on practical depot-level repair design for metallic aircraft structure (Figures 9.9-1 through 9.9-4).

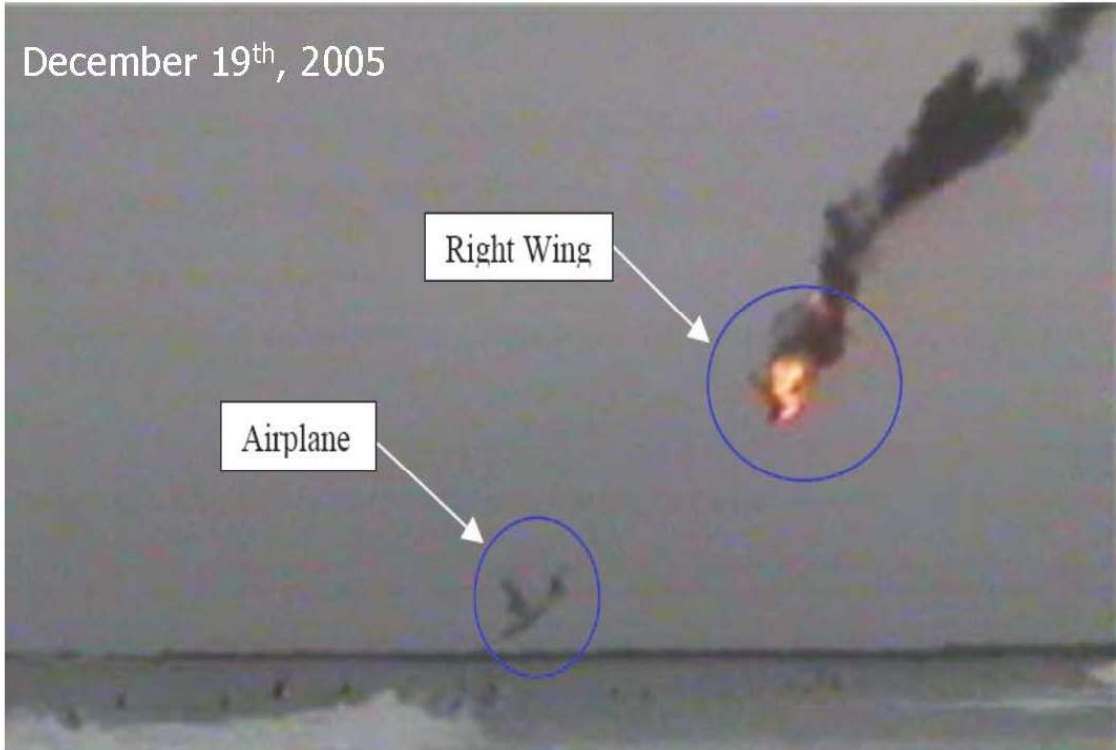


Figure 9.9-1. Case Study 1: Chalk's Ocean Airways Flight 101 (2005)



Figure 9.9-2. Case Study 2: C-130A N130HP and N135FF

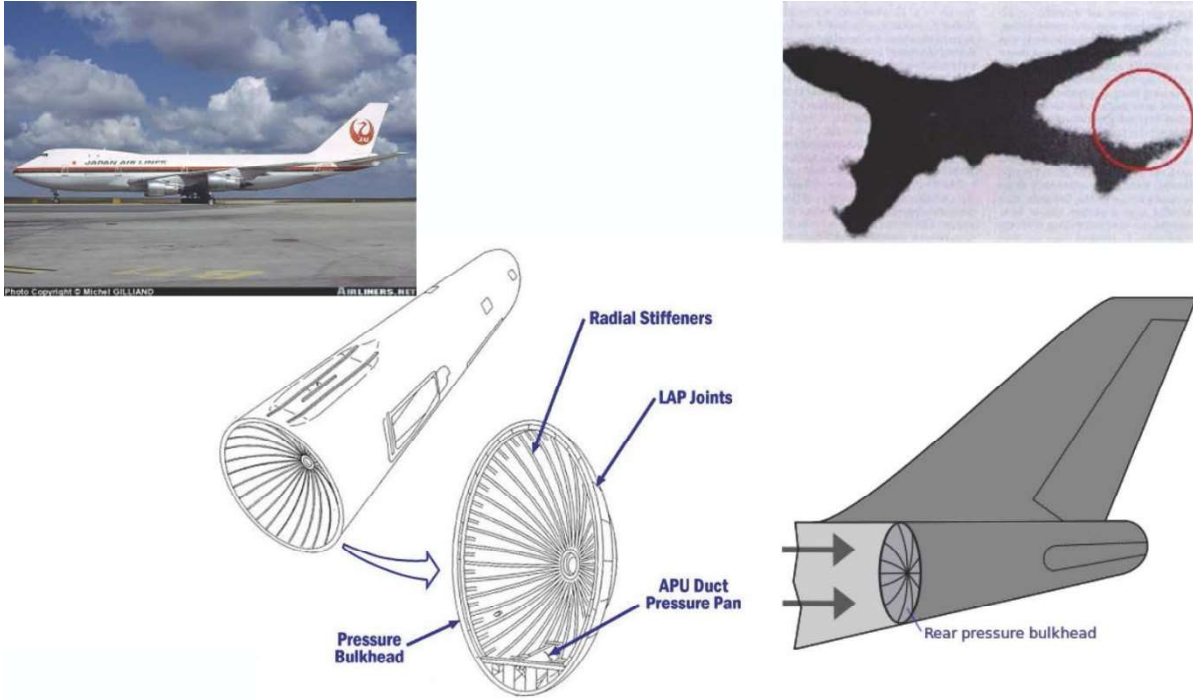


Figure 9.9-3. Case Study 3: Japan Airlines Flight 123 (1985)

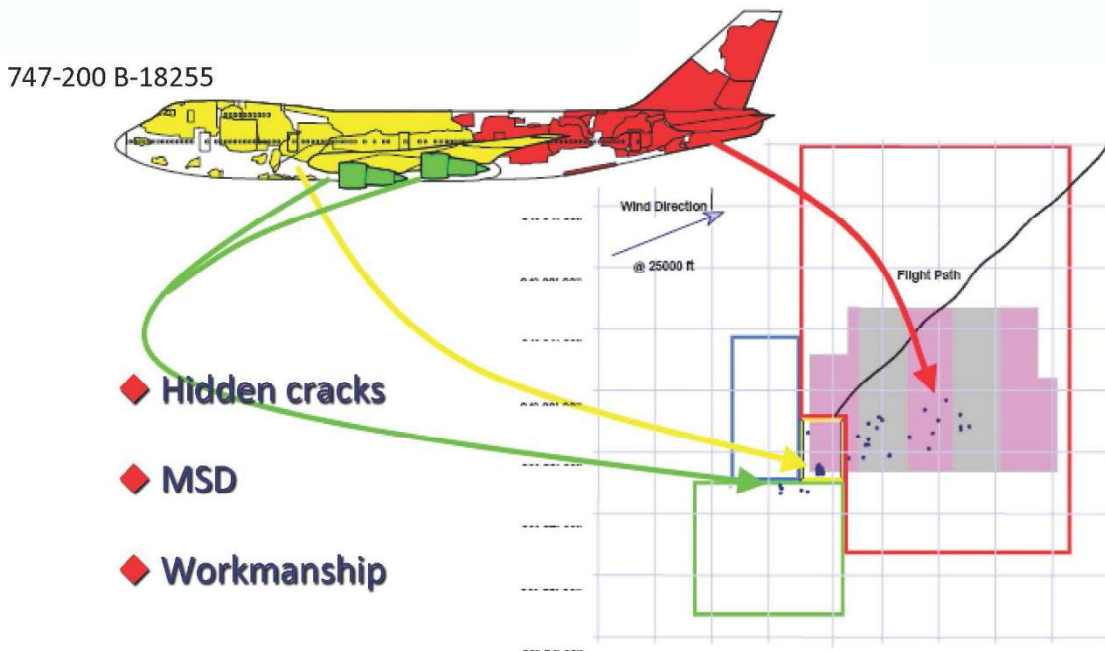


Figure 9.9-4. Case Study 4: China Airlines Flight CI611 (2002)

9.9.2. Finite Element Analysis of Bonded Repairs and Analysis Methods for the ASIP Engineer Lawrence Stoker, USAF Life Cycle Management Center

Bonded repairs on aircraft can provide a repair alternative with the unique benefit of creating a non-invasive repair on existing structure. Historically, bonded repairs were modeled in Finite Element Analyses and Models (FEAs and FEMs) via correlation to test data to determine bond stiffness. Some have attempted to model the bond-line with elements and an appropriate thickness. This introduces at least two problems associated with element size and shape. For a reasonable sized element, the aspect ratio due to a thin bond layer (0.005" to 0.05") can create high errors within the solution. One can decrease the element size such that aspect ratio is not an issue; however, the number of elements required drastically increase run- and post-processing times. To address these problems Siemens NX has implemented a "glue" feature specifically designed to represent an adhesively bonded layer. There are several options available within NX allowing the engineer to account for bond stiffness without physically modeling the bond layer. Following an NX NASTRAN simulation, the resultant loads were applied within the p-element FEA software package, StressCheck™, to allow for the development and extraction of Stress Intensity Factors (SIFs) for various crack sizes using tools contained within StressCheck™. This technical activity will provide an outline of this process allowing the ASIP engineer to assess and predict the damage tolerance behavior of aircraft structure in the presence of a bonded repair. This methodology was developed in order to predict the behavior of the lower aft wing skin of the B-1 during its full-scale wing fatigue test (Figures 9.9-5 and 9.9-6). A series of milled, tapered, 0.35" thick steel repairs were bonded to the B-1's aluminum wing plank (Figures 9.9-7 and 9.9-8). These bonded repairs covered cracks originating at the trailing edge of the wing plank growing forward. Almost 200 individual SIFs were developed for a series of cracked locations along the lower aft skin. These SIFs allow the ASIP engineer to develop a specific beta (β) solution table, which can be utilized in standard crack growth software to predict the crack growth behavior in the presence of a bonded repair. The technical activity will provide some of the simulation results as well as their correlating SIFs.

- B-1 Fatigue Test Currently Taking Place
- Experienced a High Number of Cracks in Lower Wing Skin
- Contacted A-10 ASIP for Support

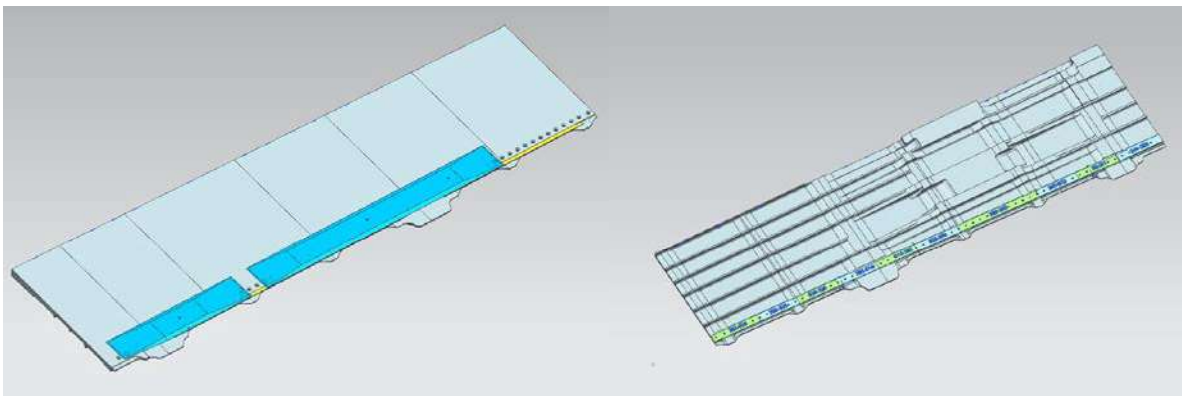


Figure 9.9-5. B-1 Lower Aft Wing Skin

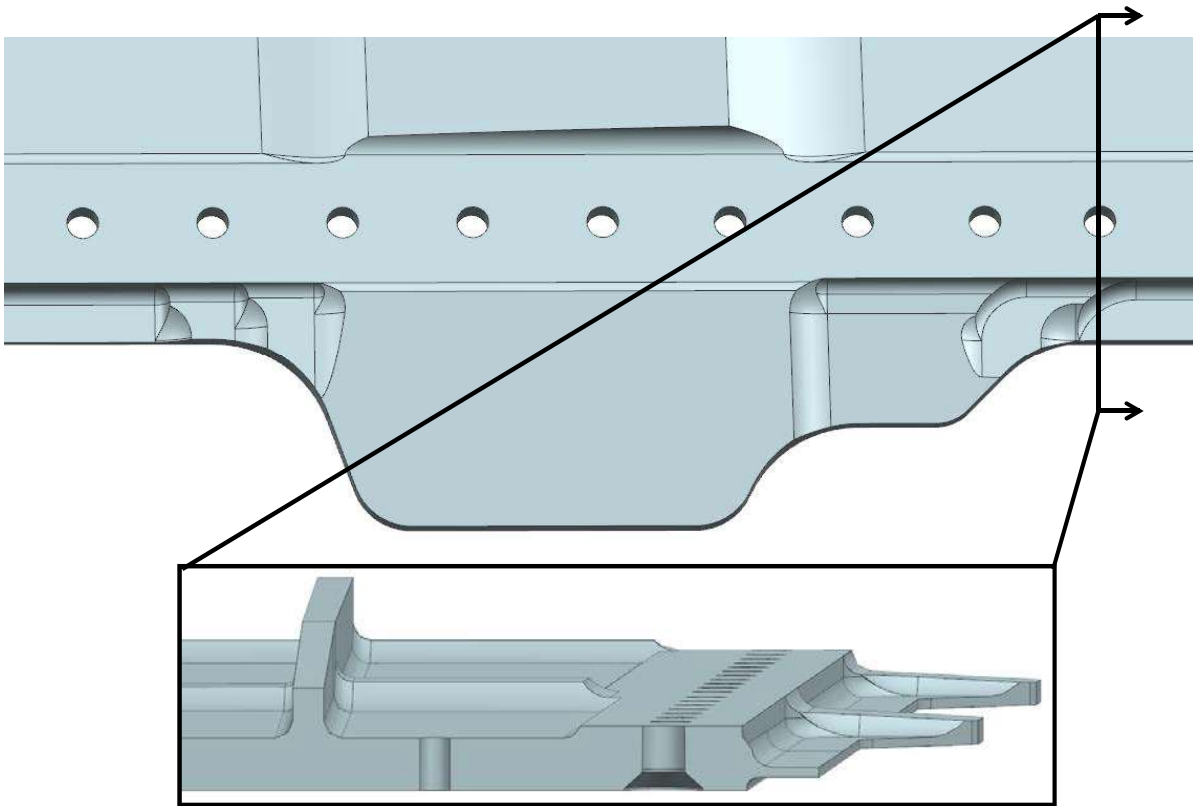


Figure 9.9-6. Detail of Cracking Location

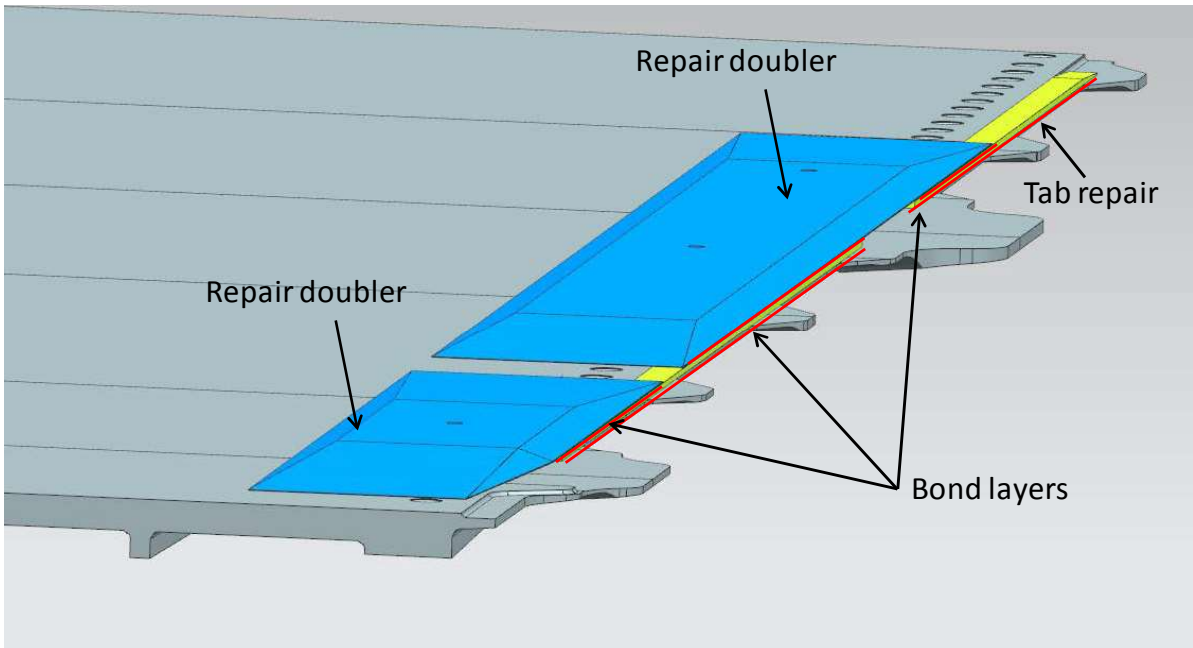


Figure 9.9-7. Method of Repair

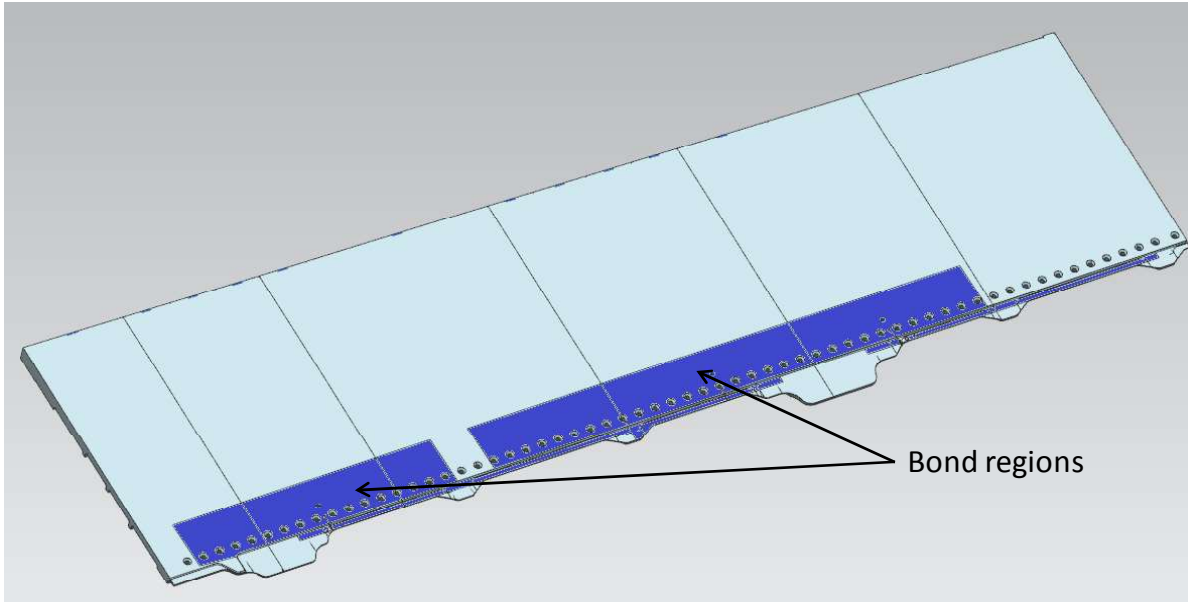


Figure 9.9-8. Bond Regions

9.9.3. Lower Forward Corner Fitting Life Extension

Timothy Philbrick, Robert McGinty, Jeffery Brenna, and Alyson Engle, Mercer Engineering Research Center (MERC); Kristina Langer, Thomas Spradlin, Captain Lanser and Stephanie Flanagan, USAF Research Laboratory – Aerospace Systems Directorate; Randy Cliett and Darren Fritz, USAF C-130 ASIP

In the early 2000 decade, the C-130 System Program Office (SPO) noted multiple failures of wing production joint fittings at the lower front corner of the center wing box (Figure 9.9-9). These failures were due to fatigue cracking and occurred well before the parts reached their predicted service lives. In fact, in several cases the corner fittings were completely severed upon discovery during inspection. MERC was tasked by the U.S. Air Force Special Operations Forces C-130 Engineering Office and the Air Force Research Laboratory (AFRL) to develop a new corner fitting having comparable strength and stiffness as the current design, but with improved fatigue life and crack growth resistance. MERC evaluated new materials, part geometry, and various fastener sizes and types during development of the new fitting. MERC began the corner fitting investigation by conducting a thorough maintenance records investigation to establish a baseline of failure occurrences. MERC also performed a Damage Tolerance Analysis (DTA) of the current (Figures 9.9-10 through 9.9-12) and redesigned candidate corner fittings and developed coupon tests to evaluate materials and fastener modifications in the new design. MERC developed multiple coupon configurations with varying materials, surface treatments, and fastener types to determine which would best improve the life of the corner fitting. The configurations tested included combinations of 7075-T73 Al forging (baseline), 7249-T76511 Al extrusion, 7085-T4751 Al plate materials, shot peening and laser peening surface treatments, and TL200-4 Taper-lok and HL328-10 Hi-Tigue fasteners with cold-worked holes. Results of this testing show that the shot peened Al 7085-T7451 Al plate specimens with cold-worked holes and Hi-Tigue fasteners have the highest fatigue life of all configurations (Figure 9.9-13 and 9.9-14). This configuration will undergo coupon-level testing to observe behavior in a loading scheme more closely representative of the loads experienced by corner fittings during flight. Part geometry was evaluated through development of a detailed Finite Element Model (FEM) and DTA. MERC performed DTA's on both the original corner fitting and a redesigned

fitting that slightly increased the thickness on the lower flange. The lower flange thickness was increased by 0.122", the maximum amount allowable while retaining the current forging, and this improved the time to critical crack length by approximately 30 service years.

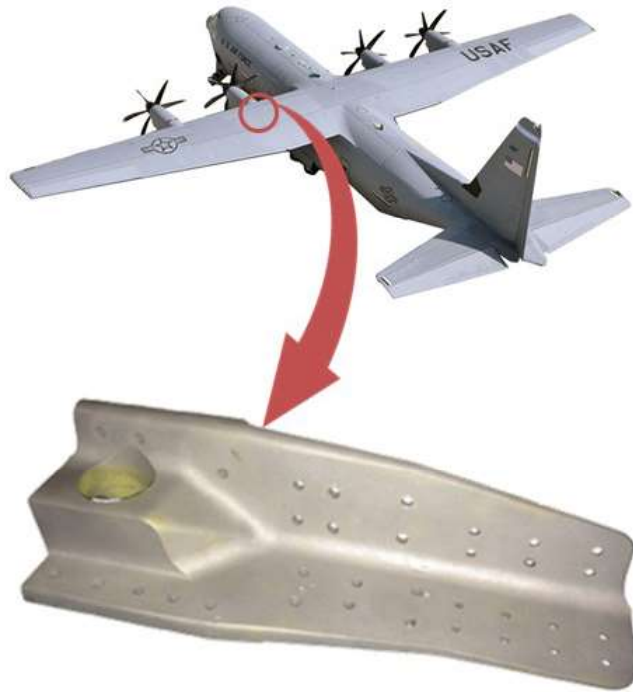


Figure 9.9- 9. Wing Production Joint Fitting

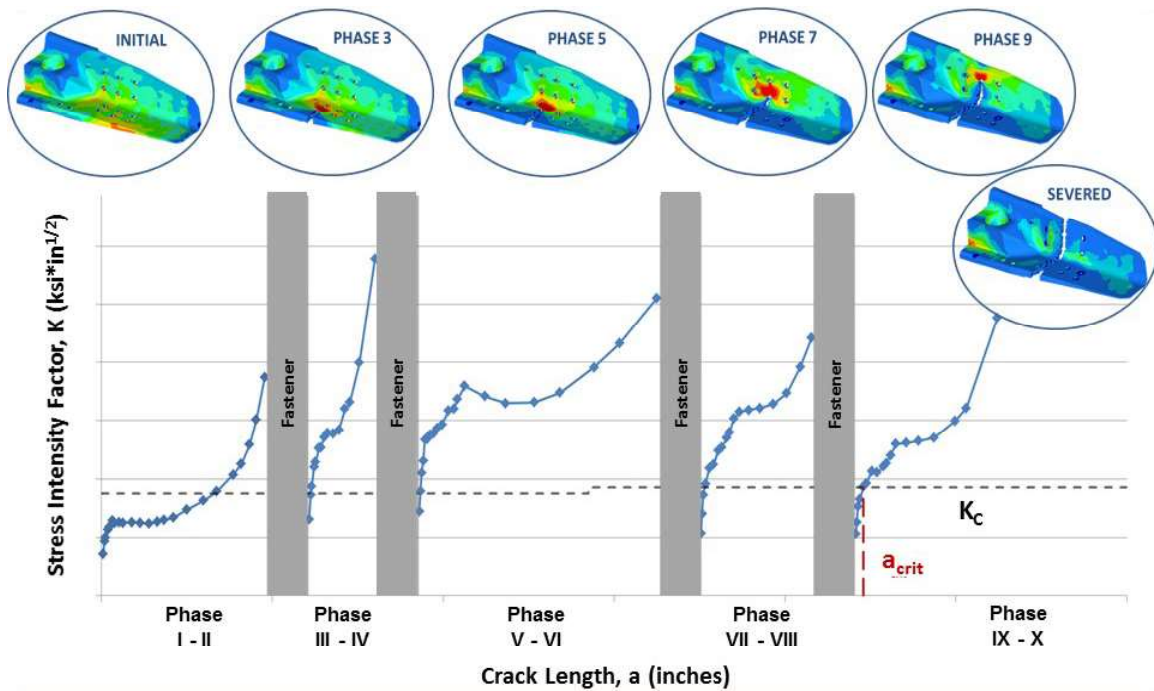


Figure 9.9-10. Stress Intensity Factors for Current Geometry

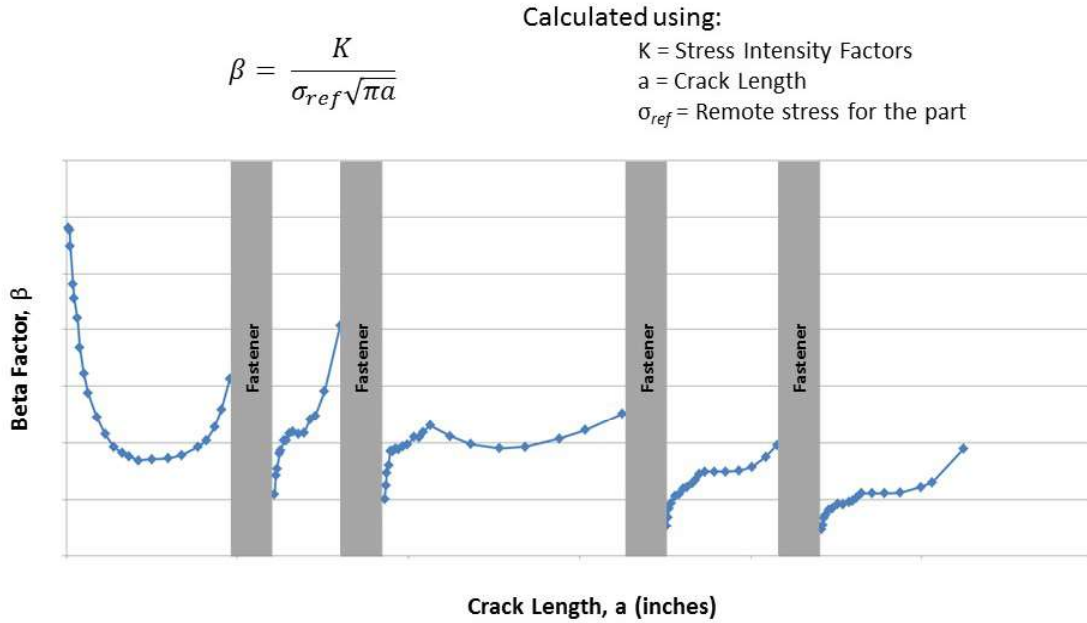


Figure 9.9-11. Beta Factors for Current Geometry

- Crack Growth

- AFGROW used to simulate the propagation of the crack
- Al 7075-T73 material using the defined stress spectrum and calculated β factors

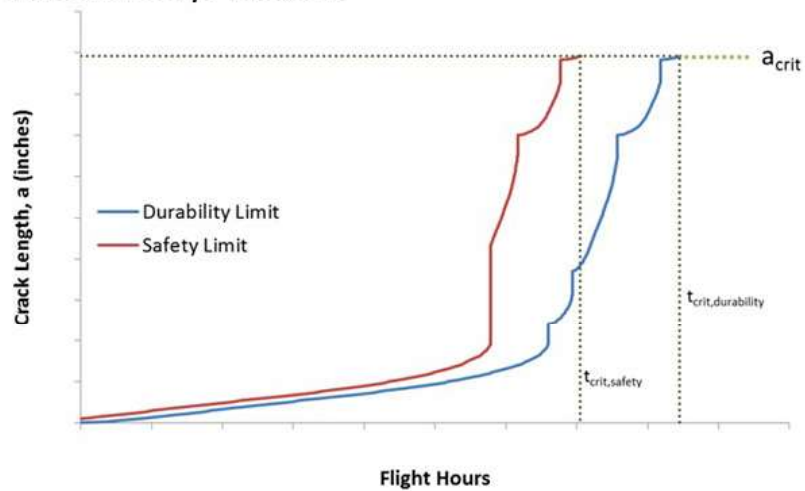


Figure 9.9-12. Crack Growth Results for Current Geometry

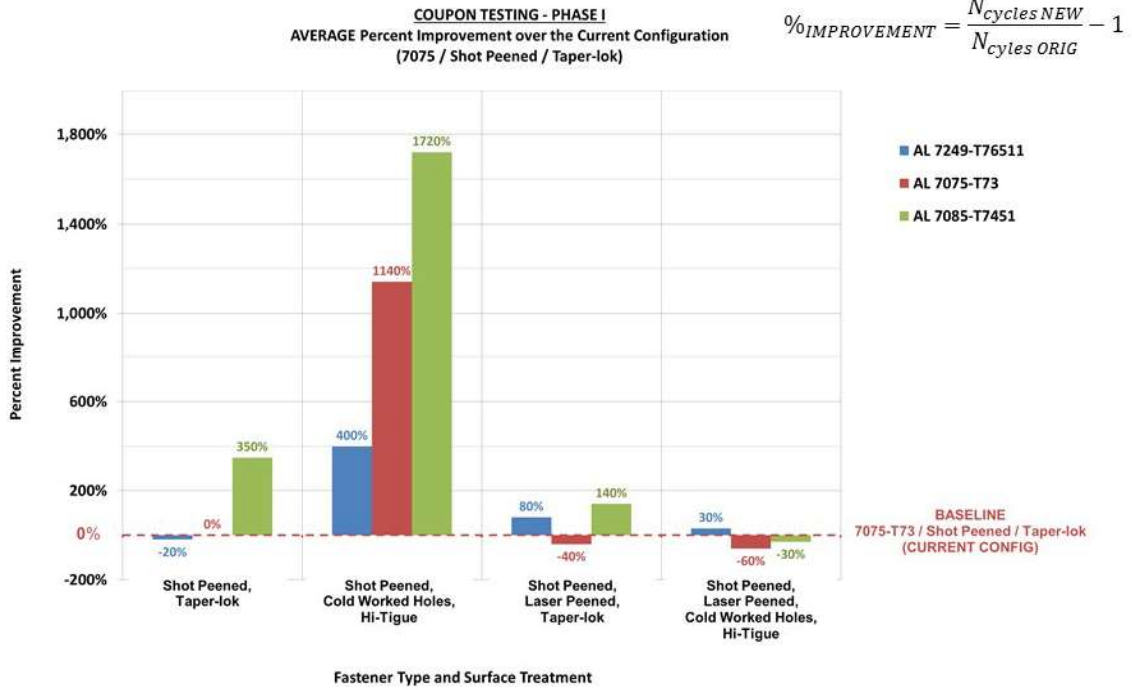


Figure 9.9-13. Life Improvement Results (Phase 1)

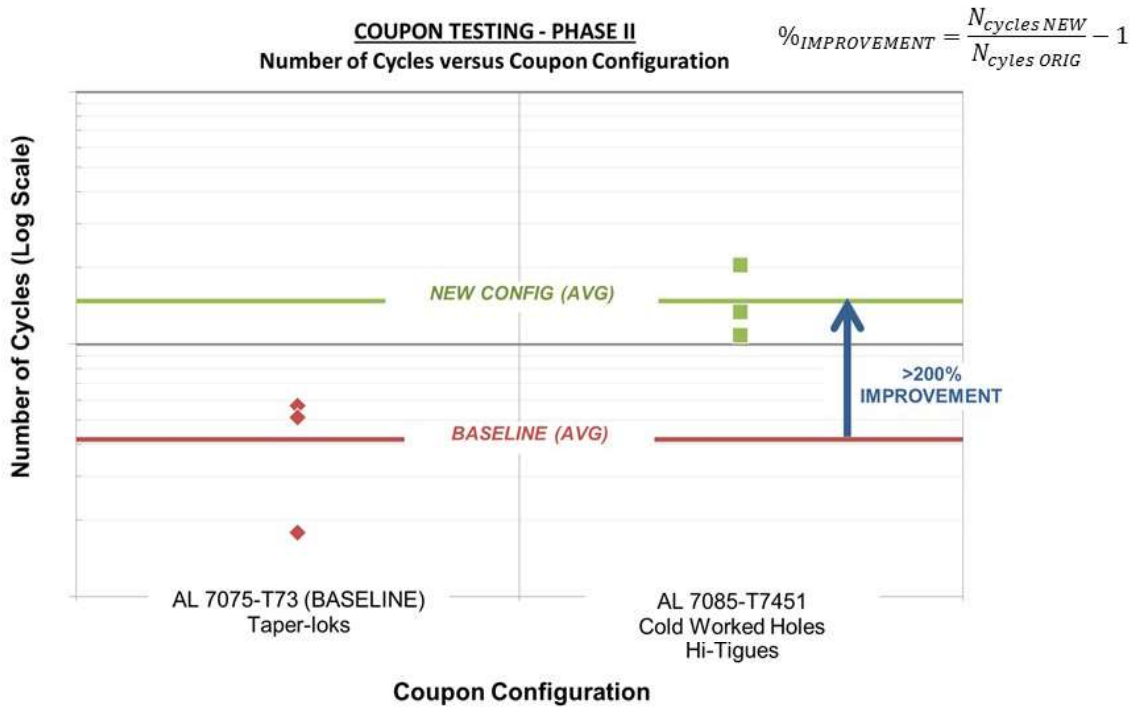


Figure 9.9-14. Life Improvement Results (Phase 2)

9.9.4. Bonded Repairs in Metallic Structure

Jeffrey Tom, The Boeing Company – Commercial Airplanes

Repairs to metallic airplane skins typically take the form of one or more doublers, attached externally with fasteners. A promising new approach is to attach the metallic repair using adhesives rather than fasteners. Advantages include lower cost and reduced dependency on spare parts, especially when the inside of the skin is difficult to access and/or includes integrally-machined stiffeners. For this reason, bonded metallic repairs have been used by the USAF in the C-141, A-10, and F-16. But how durable are such repairs? Can disbonding be prevented, accurately predicted, and/or reliably detected by NDI during regularly scheduled maintenance?

When fatigue cracking was observed in the horizontal stabilizer upper skins of the MD-80/90 fleet (which include integrally-machined stringers similar to those in military airplanes), the Boeing Commercial Airplanes (BCA) Southern California Design Center tackled the challenge of developing and certifying bonded repairs to this structure, including solutions to all concerns regarding disbonding, damage tolerance, and maintenance inspections (Figure 9.9-15). The work involved design, analysis, full-scale tests, a unique combination between the philosophies behind metallic and composite structures, and close collaboration with maintenance facilities. Now that bonded repairs are certified and flying, they could significantly reduce the cost of various repairs – and, potentially, of joints in baseline structure – on all airplane models.

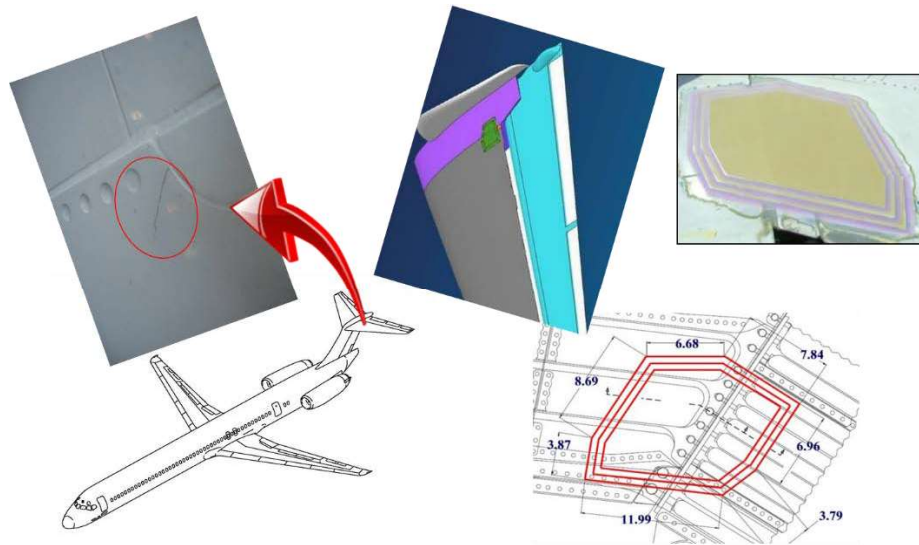


Figure 9.9-15. MD-80/90 Horizontal Stabilizer Skin Panel Bonded Repair Solution Concept

9.9.5. Effect of Environment on the Mechanical and Fatigue Behavior of Adhesive Bonded Repairs

John Bakuckas, Jr., Ryan Neel, and Yongzhe Tian, FAA – William J. Hughes Technical Center; Ian Won and Mark Freisthler, FAA – Transport Airplane Directorate; Kelly Greene, Jeong-Beom Ihn, and Cong Duong, The Boeing Company – Research & Technology; Jonathan Awerbuch and Tein Min Tan, Drexel University

In a joint effort, the Federal Aviation Administration (FAA) and The Boeing Company are investigating the structural robustness and damage-resistance capabilities of adhesively bonded repair technology through the testing and analysis of metallic B727 fuselage panels at the FAA Full-Scale Aircraft Structural Test Evaluation and Research (FASTER) facility. The program objectives are to

characterize the fatigue performance of bonded repairs under simulated service load conditions and to investigate tools for evaluating and monitoring the repair integrity.

A phased approach has been taken involving the testing and analysis of several panels containing boron-epoxy (B/Ep) and aluminum (Al) bonded patches. A variety of loading and environmental conditions, damage scenarios, and repair conditions have been considered. To date, the testing of three panels has been completed, and the results were reported in references 1–5. In general, baseline results from Panel 1 demonstrated that properly designed and installed bonded repairs can be durable under fatigue and capable of effectively containing significant damage under severe loading conditions [1, 2]. Repair patches were intentionally made deficient to permit damage growth in Panel 2 to demonstrate the effectiveness of several nondestructive inspection methods and a prototype piezoelectric-based structural health monitoring system [3, 4]. Initial studies were conducted on Panel 3 to assess environmental effects under hot-wet conditions on repair performance [5]. Those studies revealed slower crack growth under hot-wet conditions in the B/Ep composite repairs as compared to the ambient conditions. Mismatches in the thermal coefficient of expansion in the repair and panel resulted in the development of residual stresses ahead of the notch during the initial patch-installation curing process. At elevated temperatures, these residual stresses are relaxed, which may contribute to slower crack growth.

In this latest panel test, Panel 4, investigations continued in the assessment of environmental effects under both hot-wet (74°C and 85% humidity) and cold (-32°C) conditions on repair performance. Efforts were focused on assessing residual strains during the curing cycle of patch installation and during conditioning under hot-wet environment for a 4-week period. Fatigue testing was then conducted under cold conditions for 60,000 cycles. Results and other major findings include:

- Thermal residual strains in and around the repair that developed during the installation and curing process were measured for model development purposes. For the B/Ep repairs, high thermal residual strains developed within the patch footprint and surrounding areas because of thermal property mismatches in the B/Ep patch and aluminum fuselage panel. For the Al repairs, thermal residual strains were much lower and often insignificant.
- Mechanical strains along the notch-centerline were measured under ambient, hot-wet, and cold conditions. For the B/Ep repairs, the mechanical strains increased as temperature decreased (Figure 9.9-16(a)). The effect of environment was limited for the Al repairs.
- After repair installation, selected repairs were conditioned for 4 weeks under hot-wet conditions during which strains were continuously monitored. For the B/Ep repairs, thermal-viscoelastic-plastic behavior was observed where thermal strains relaxed (Figure 9.9-16(b)). The Al repairs were not affected by the conditioning.
- The panel was then fatigue tested under cold conditions, during which crack growth and strains were continuously monitored. Results from the Panel 4 test for a B/Ep repair as-installed and another B/Ep repair subjected to hot-wet conditioning (post-conditioned) are shown in Figure 9.9-16(c). Also shown are results from Panel 2 (tested under ambient conditions) and Panel 3 (tested under hot-wet conditions). As indicated, the fatigue crack growth (FCG) under the cold conditions for the as-installed B/Ep was the highest (Panel 4) followed by ambient (Panel 2) and then hot-wet (Panel 3). These followed similar trends shown in Figure 9.9-16(a) where the notch-tip strains were highest under cold conditions, followed by ambient and then hot-wet. The post-conditioned B/Ep repairs in Panel 4 exhibited slower crack growth compared to the as-installed B/Ep repairs, which correlated with lower notch-tip strains (Figure 9.9-16(d)).

Data from this program will be used to assess tools and methods for evaluating and monitoring the repair integrity over the life of the part.

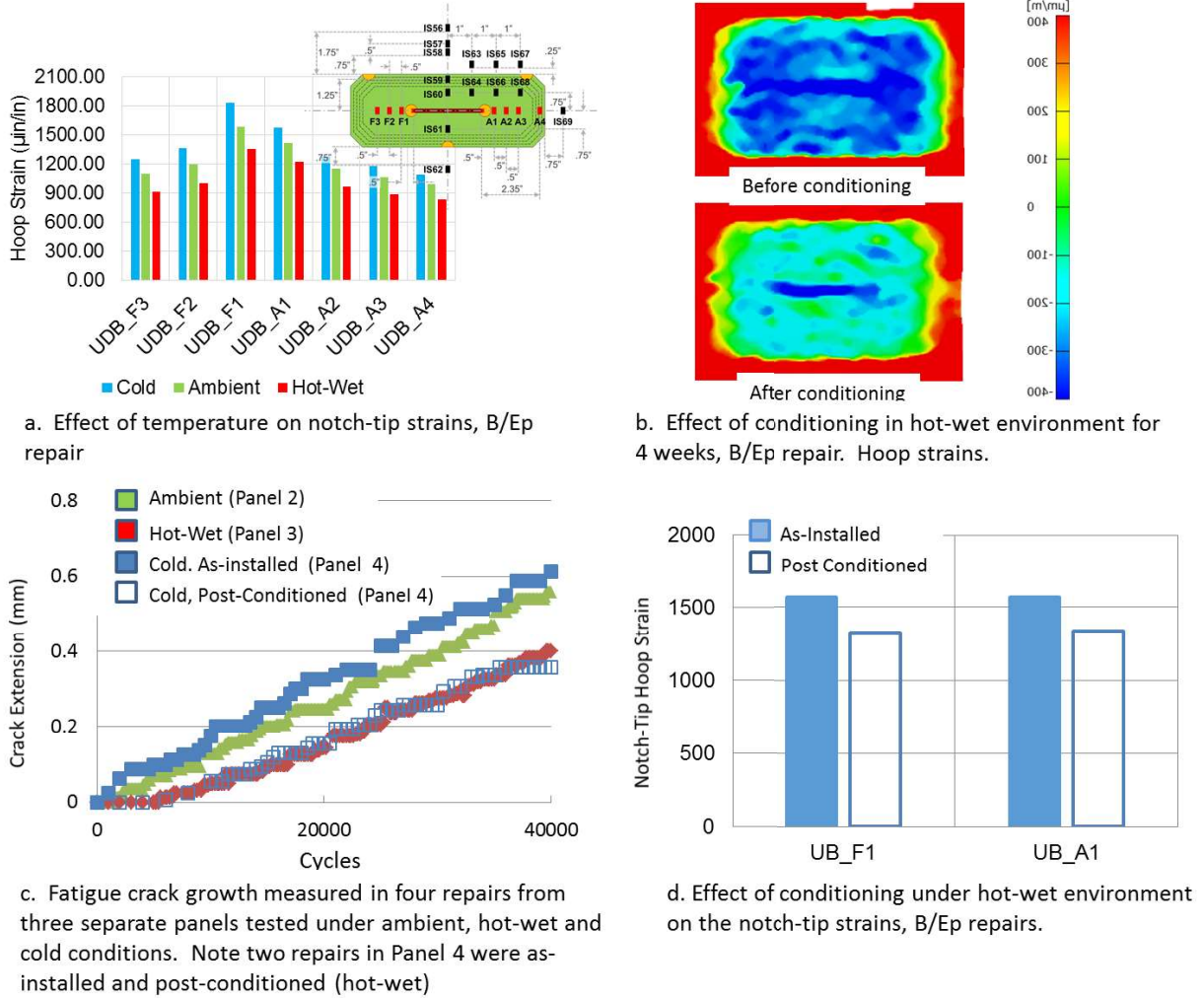


Figure 9.9-16. Effect of Environment and Conditioning on Mechanical and Fatigue Response of B/Ep Repairs

References:

- [1] Bakuckas, J. G., McIver, K., and Hsu, C., “Durability and Damage Tolerance of Bonded Repairs to Metallic Fuselage Structure,” *Proceedings of the 25th ICAF Symposium*, Rotterdam, May 27–29, 2009.
- [2] Chadha, R. and Bakuckas, J., “Adhesively Bonded Repairs to Metallic Fuselage Structure: Test 1, Fatigue and Residual Strength Performance,” DOT/FAA/AR-11/4, April 2013.
- [3] Bakuckas, J. G. and Westerman, B., “Fatigue and Residual Strength Performance Bonded Repairs to Metallic Fuselage,” *Proceedings of the 26th ICAF Symposium*, Montreal, Canada, June 1–3, 2011
- [4] Chadha, R., Bakuckas, J., Duong C., and Hunziker, K. “Adhesively Bonded Repairs to Metallic Fuselage Structure: Test 2, Monitoring Damage Growth,” DOT/FAA/TC-15/3, September 2015
- [5] Bakuckas, J., Lei, B., Tian, T., Won, I., Freisthler, M., Greene, K., Brewer, C., Korkosz, G., Awerbuch, J. and Tan, T., “Evaluation of Adhesively Bonded Repairs to Fuselage Structure Subjected to Environmental Conditions,” *Proceedings of the 28th ICAF Symposium*, June 3–5, 2015, Helsinki, Finland.

9.9.6. Bonded Repairs of Composite Airframe Beam Structure

John Bakuckas, Jr. and Reewanshu Chadha, FAA – William J. Hughes Technical Center; Michael Fleming and Megan Watson, The Boeing Company – Research & Development; Mark Freisthler and Ian Won, FAA – Transport Airplane Directorate

Under a Cooperative Research and Development Agreement (CRDA), the Federal Aviation Administration (FAA) and The Boeing Company are investigating the safety and structural integrity issues of bonded repair technology through test and analysis. To date the focus has been on fuselage structure applications. These are relatively thin and are subjected primarily to in-plane loads. Additional efforts have been identified for bonded repairs of thicker structures such as a primary beam structure representative of typical wing or stabilizer components which are subjected to much more complex loads. In efforts to further leverage resources and to take advantage of the experience and expertise of both Boeing and the FAA, the partnership has been extended to include bonded patch and scarf repairs to generic primary beam structure (composite).

For this new effort, the structural robustness and damage-resistance capabilities of adhesively bonded repairs will be investigated through the testing of simple flat and stiffened composite panels at the FAA's William J. Hughes Technical Center in Atlantic City, NJ. The program objectives are to characterize through test the durability and fatigue performance of scarf repairs and doublers using simulated service load (SL) conditions over the typical design service goal of an airplane and to investigate methods and tools used for analysis and predictive performance of the repairs as well as those used for evaluating and monitoring the repair integrity over the life of the part.

As part of this effort, the design of an Airframe Beam Structure Test (ABST) fixture was completed, as shown in Figure 9.9-17. The ABST fixture will provide a new structural test capability within the FAA for a primary beam structure representative of typical wing, stabilizer, and floorboard components, Figure 9.9-18. The fixture is a self-reacting structure designed for fatigue and residual strength testing of flat panels, 24" in width by 40" in length. The fully integrated system will consist of the mechanical fixture, hydraulic components, and control and data acquisition systems. Four 50 Kip hydraulic actuators will be used to apply various modes of loading to maximum strain range of $\pm 6000 \mu\epsilon$, Figure 9.9-19.

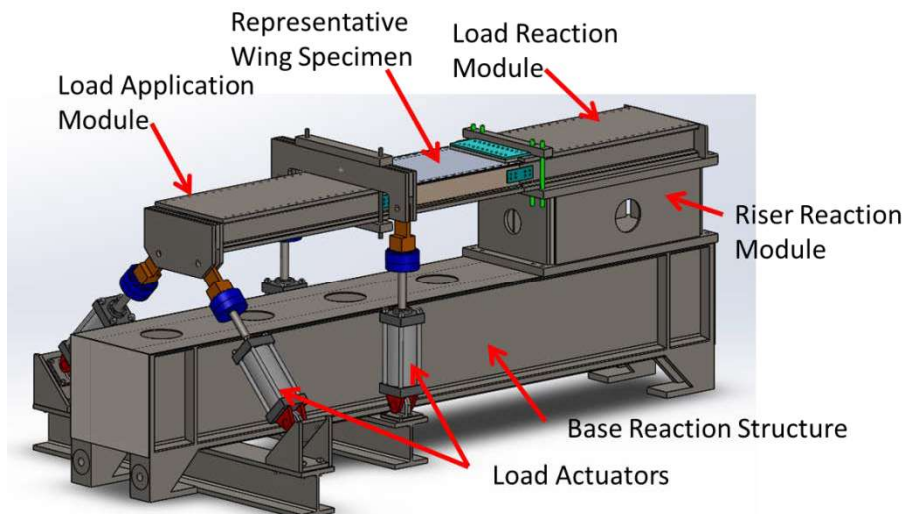


Figure 9.9-17. FAA Airframe Beam Structural Test (ABST) Fixture

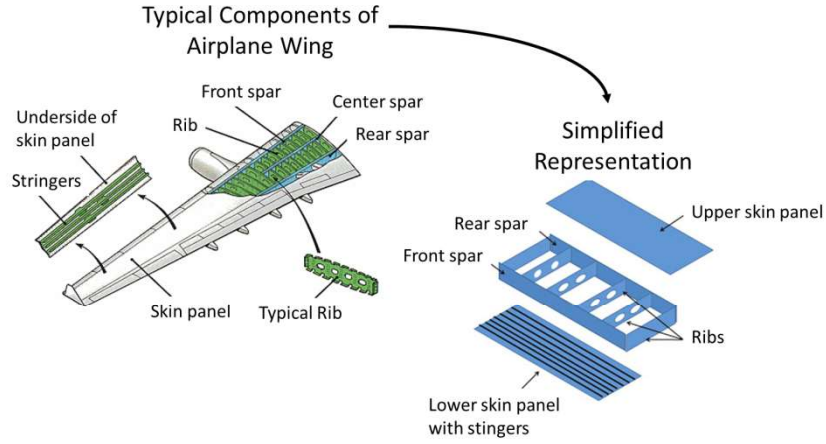


Figure 9.9-18. Designed to Test FAA Airframe Beam Structural Test (ABST) Fixture

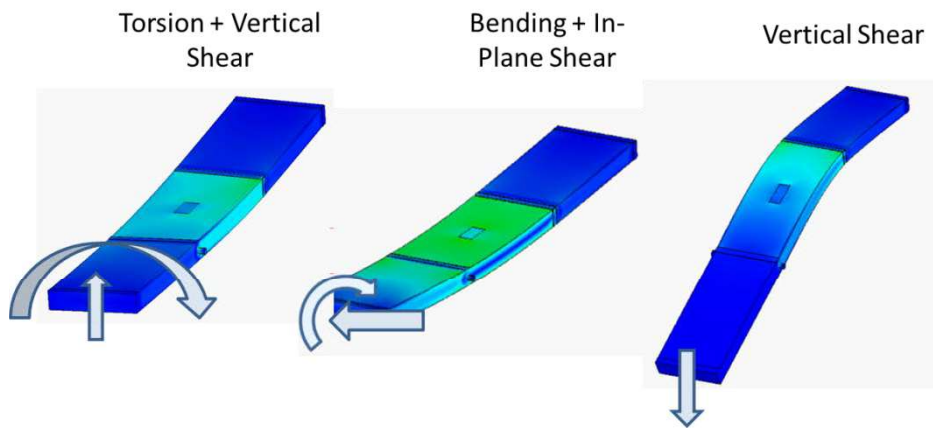


Figure 9.9-19. Modes of Loading

9.10. REPLACEMENT CONCEPTS

9.10.1. Process-Induced Bulk Residual Stress Finite-Element Model and Validation Measurements of an Aluminum Alloy Forged and Machined Bulkhead

John Watton, Alcoa Technical Center; Adrian DeWald, Hill Engineering LLC; Dale Ball, Lockheed Martin Aeronautics

The goal of manufacturing large monolithic forgings (Figure 9.10-1) with consistently low residual stress is aided by Alcoa developed finite-element tools to predict the heat treatment quench-induced residual stress (Figure 9.10-2) and the optimal process and efficacy of the compressive cold-work stress relief of aluminum die forgings. This predictive capability is integral to the design of Alcoa's Signature Stress Relief (Figure 9.10-3) forgings. Validation work completed as part of the AFRL Metals Affordability Initiative BA11 program is presented that quantitatively compares measured residual stress in the machined component bulkhead using the contour method and Alcoa's predicted residual stress. The contour method (Figure 9.10-4) is a destructive measurement technique that provides full-field data for a target cross section of the component. Alcoa's forging business is increasingly called upon to supply complete process-induced bulk RS field maps to OEMs for inclusion in design analysis, specifically to address fatigue life and weight optimization.

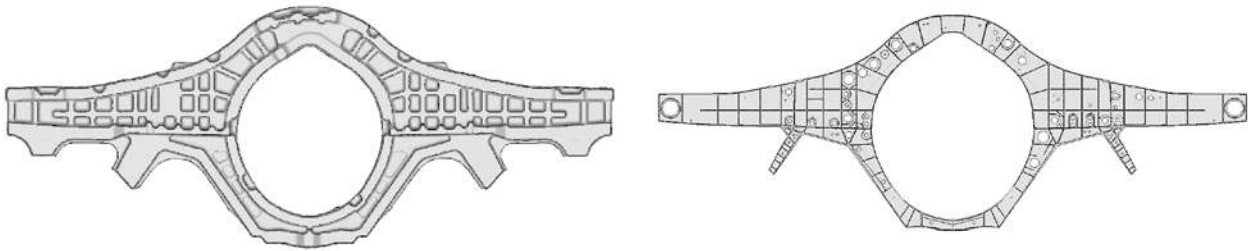


Figure 9.10-1. Forging and Machined Parts

1. Solution Heat Treatment (SHT) tempers T3 thru T9
 - Alloys 6061, 7085, 7050, 7020 @ $\geq 880^{\circ}\text{F}$
 - Allows alloy constituents to enter into solid solution.
 - Attenuates any fabrication stresses that may exist.
2. Quench - Water 70°F to 140°F
 - Rapid to hold the alloy constituents in solution.
 - But non-uniform cooling creates the quench-induced stress.
3. Stress Relief – a cold-working tensile stretch (T_51) or a cold-working compression (T_52)
 - Mitigates the quench-induced stress.
 - Achieve better properties (e.g. Al-Li materials improves fatigue strength and fracture toughness)
4. Artificial Aging at a series of elevated temperatures
 - Relaxes bulk RS by creep
5. Machining to final part shape
 - Can reduce bulk RS as part re-equilibrates.
 - But can introduce near surface machining-induced stress.
 - And part distortion!

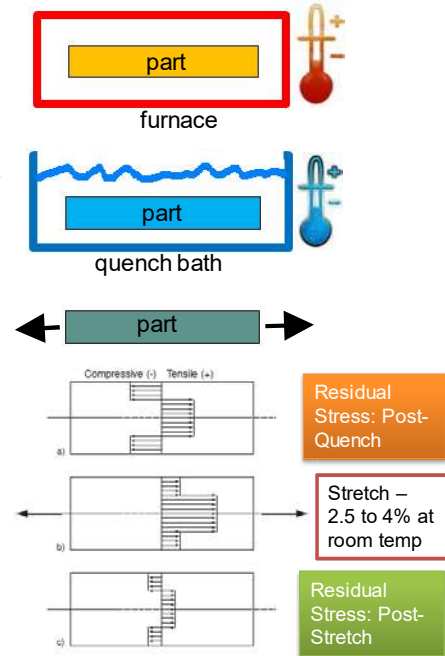
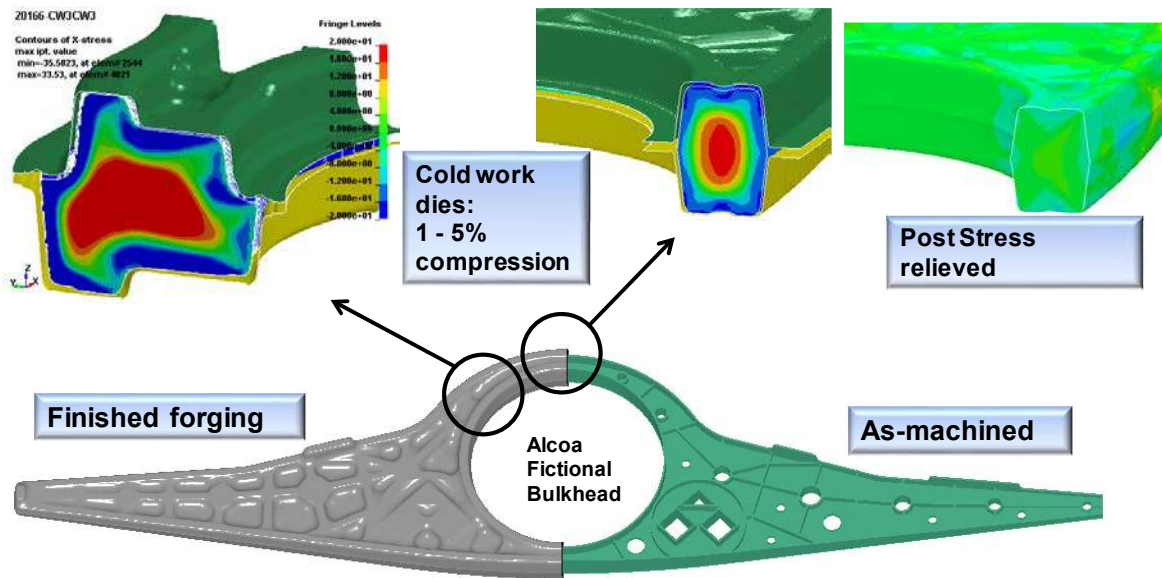


Figure 9.10-2. Quench-Induced Residual Stress



- SSR™ includes rules developed from practice and FEA simulation of solution heat treatment, quench, and cold-work to design cold work die sets:
 - Target 2.7% cold-work on rib and fillet features
 - Tapered segmented dies for large forgings
 - Inline application of segmented cold-work dies

Figure 9.10-3. Alcoa's Signature Stress Relief

- Cut the part
 - Wire EDM typical
 - Clamp part to rigid backing plate
- Measure surface deformation
 - CMM or laser scanner typical
 - Measure a grid of points on both cut surfaces
- Analyze experimental data
 - Filter out noise
 - Average data from both surfaces
- Compute residual stress
 - FEA model
 - Displacement boundary condition

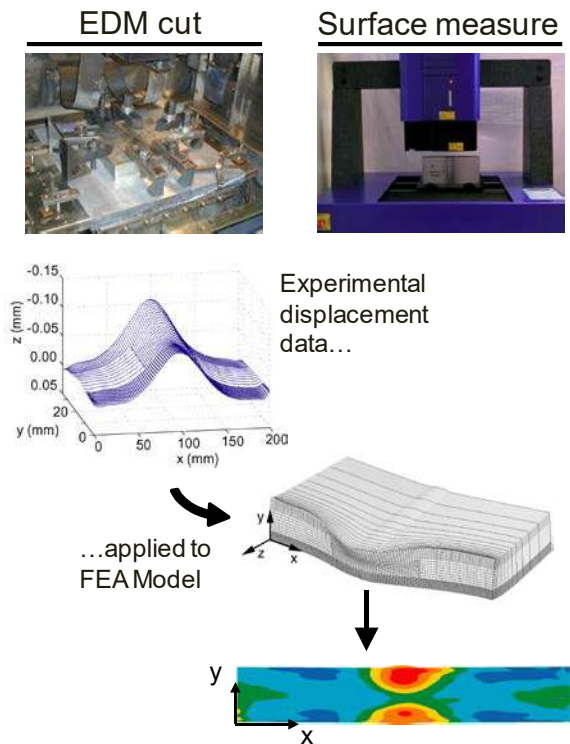


Figure 9.10-4. Contour Method of Residual Stress Measurement

9.10.2. Inclusion of Forging Residual Stresses in Large Component Structural Design

Dale Ball and Don Dubowski, Lockheed Martin Aeronautics; Thomas Spradlin, USAF Research Laboratory – Aerospace Systems Directorate

In a recently concluded Metals Affordability Initiative (MAI) program, the effects of forging process induced bulk residual stresses on both machining distortion and fatigue life were studied at both the coupon and large component level. During the coupon level methods development and validation program, it was demonstrated that the extraction of confounding residual stress effects from material property data (especially fatigue crack growth rate data), coupled with the explicit inclusion of forging residual stresses in the subsequent fatigue analyses of the coupons, resulted in a significant improvement in the fidelity of the analyses. By analyzing carefully designed and executed tests, it was shown that the newly developed methods resulted in analysis vs. test life correlation ratios that were either within the USAF required scatter factor of 2, or were conservative. This is in contrast to a much broader scatter band (5x) for calculations made using traditional (non-residual-stress-informed) methods. In the second phase of the subject MAI program, the residual stress design procedure was applied (to the extent possible) to the design and manufacture of a large, wing carry-through bulkhead (Figure 9.10-5). The objective of this phase of the program was to demonstrate, by way of two large component fatigue tests, that the technology would scale to the structural level, and that its use would result in components that are either lighter or more durable (or both) than their traditionally designed counterparts. In this technical effort, we compare and contrast the traditional vs. residual-stress-informed design procedures, and we describe in detail, the resulting baseline and ‘optimized’ test articles. A full description of the fatigue tests, along with comparisons between detailed fatigue calculations and test findings will be given.

Finally, an assessment of the extent to which the program objectives were achieved, along with recommendations for large component design, will be given.



Figure 9.10-5. Large Component Test Demonstration

9.10.3. Evaluation and Implementation of Additive Manufacturing Technologies for Structural Applications

Bernardo Malfitano, Vichai Rojanavanich, Andrew Stevens, Daniel Bazile, and Charles Park, The Boeing Company – Commercial Airplanes

Additive Manufacturing, also known as “3-D printing”, offers the potential to drastically change structural design. Complex curvatures and small details do not impact the fabrication cost of each component, as they would for traditional (“subtractive”) manufacturing processes. This means that highly optimized organic geometries may become practical for the first time. In addition, organizations that handle structural repairs and replacements could gain the capability to print components as needed, rather than stocking large inventories of spare parts, thus reducing costs and shortening the supply chain.

Boeing systems and interiors already use additive manufacturing technologies. Boeing Commercial Airplanes are currently flying 25,000 additively-manufactured parts, and the F-15 and F/A-18 fleets have about 40,000. Each 787 contains about 30 additively-manufactured parts (Figure 9.10-6). Most of them are components like air ducts and small parts in interiors such as buttons and covers. Until recently, metals produced by additive manufacturing technologies were inferior in strength and durability to wrought metals. However, various methods and technologies are currently being introduced that allow for additively manufactured metals to have structural properties comparable to wrought metals.

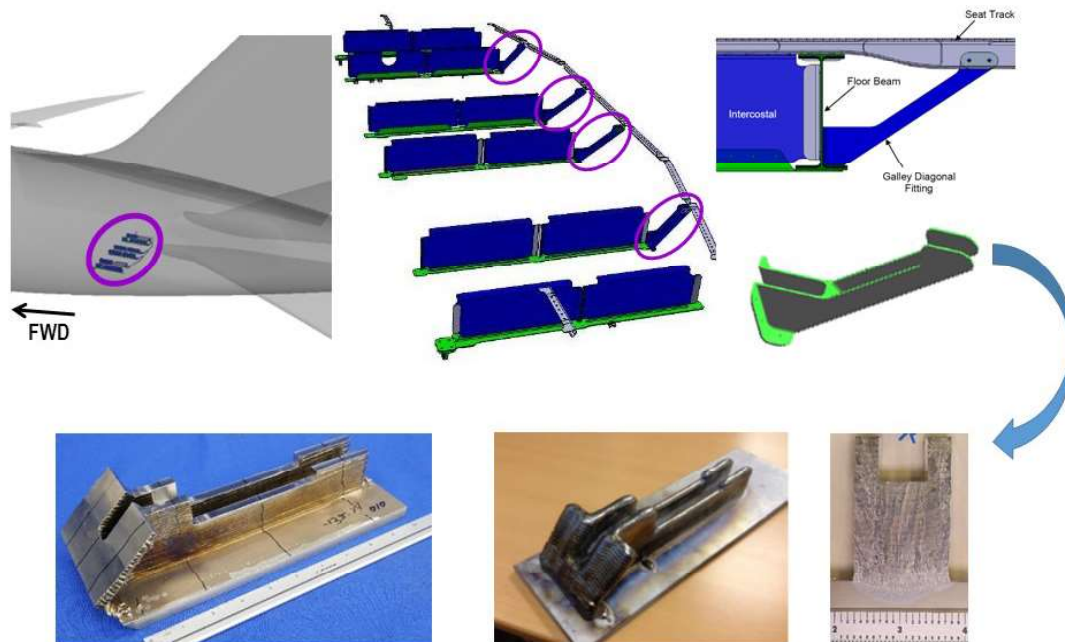


Figure 9.10-6. Example: 787 Aft Galley Diagonal Fitting

Two general categories of additive manufacturing for metallic structure are plasma/arc deposition and powder beds. In plasma/arc deposition, a nozzle travels over the component being built, depositing high-temperature material in a line as it travels. The nozzle is fed material via powder or wire, which is heated by various kinds of sources such as lasers. This allows for large components to be built up, as large as the range of motion of the mechanism that holds the nozzle. However, it is not possible to create smooth surfaces or small details, therefore substantial machining or surfacing is often necessary as one of the final fabrication steps. In powder-bed machines, the bottom of a container is covered by a layer of fine powder. An energy beam such as a laser or electron beam shines down from above this surface, “drawing” one layer of the part by melting or sintering the powder. This allows for the creation of small details and relatively smooth surfaces, but only for components small enough to fit inside the limited build volume.

Boeing has been partnering with various other companies and research laboratories to test the structural properties of these materials at the coupon level. Tests of 3-D printing processes are ongoing. These tests have explored the strength of the material in various orientations relative to the direction the material is deposited, in different thicknesses, and in different locations relative to the base plate onto which the material is deposited. These tests have served as the foundation for Boeing’s first implementation of metallic 3-D printing into 787 airplane structure. A second component substitution is currently in development, using a powder-bed approach to fabricate parts on the 777.

Fatigue and damage tolerance considerations currently pose challenges to the use of additively manufactured metals on airplane structures. One such challenge is surface roughness. When not machined or polished, the latest powder-bed metals tested at Boeing have fatigue properties similar to those of castings. This is unacceptably low for most applications in primary structure. Unlike castings, however, improving the surfaces of additively-manufactured metals can allow their mean fatigue behavior to approximate that of wrought materials. Variability, however, often remains high. The presence of inherent material defects randomly distributed throughout the volume of additively manufactured parts, which may be below the threshold of detectability, means that due consideration has to be given to size

effects and the possibility of cracks not always nucleating where they would ordinarily be expected based only on the magnitudes of local stresses associated with obvious macroscopic features such as geometric stress concentrations. This not only challenges the conventional understanding and characterization of crack nucleation (classical fatigue) properties but also, and more fundamentally, the principle of “safety by inspection” when it is tied to a presumption of certain crack morphologies and origins, which then define the means and frequency of inspections. It is further complicated by the difficulty of detecting internal bulk material defects that can act as potential fatigue crack nucleation sites. The solution may lie in the application of probabilistic fatigue analysis methods and perhaps a stronger reliance on fail-safety or safe life rather than directed inspections and prescribed inspection intervals. The impact of surface roughness, flaw size, structure thickness, and other factors on the effect and detectability of defects is still being quantified.

9.10.4. Advanced Aluminum-Lithium (AL-LI) for Primary Structure

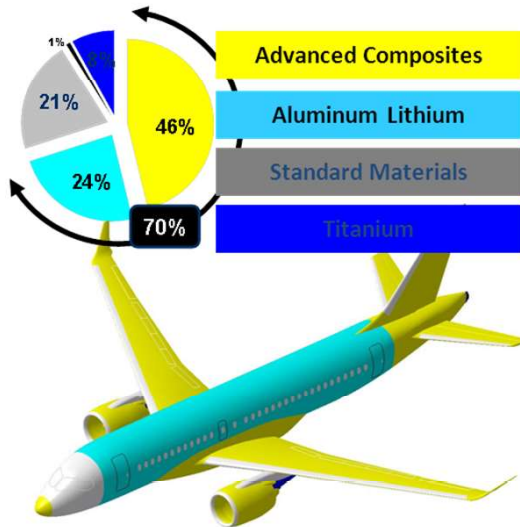
Kevin Stonaker and John Bakuckas, Jr., FAA – William J. Hughes Technical Center; Ian Won and Mark Freisthler, FAA – Transport Airplane Directorate; Bruce Thomas, Bombardier Inc.; Michael Niedzinski and Frank Eber, Constellium

The FAA, in partnership with Bombardier (airframe OEM) and Constellium (material producer), has undertaken an effort to gain a better understanding of the material properties, mechanical behavior, and unique characteristics of the typical next-generation aluminum-lithium (Al-Li) alloys being used in airframe structures through comparison to traditional aluminum alloys. The latest generation of Al-Li alloys offers significant weight savings over conventional aerospace aluminums, resulting in significant use in recent aircraft and aerospace applications as evidenced by the recently certified Bombardier C-Series with nearly a quarter of the aircraft utilizing Al-Li, Figure 9.10-7a. The alloys discussed herein are included in the Metallic Material Properties Development and Standardization (MMPDS) handbook and have been fully tested and qualified for the Bombardier C-Series program, but because previous generations of Al-Li alloys displayed material behaviors that limited their use for aerospace applications, the authors agreed to further explore the properties and behaviors of these new alloys.

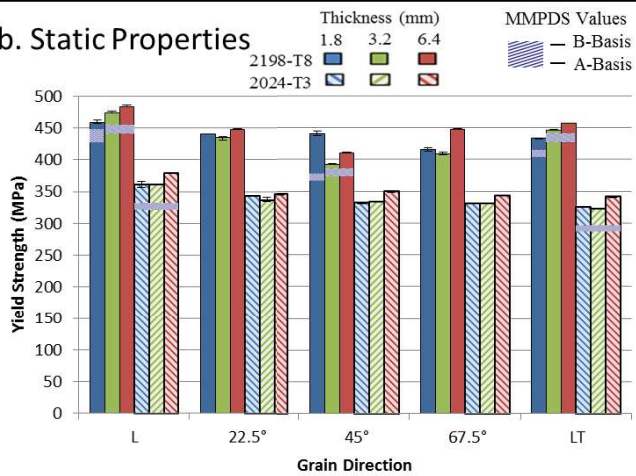
This study specifically looked at Al-Li alloys 2198-T8 produced in sheet form and 2196-T8511 produced in extruded form. Based on experience from earlier generations of Al-Li alloys, several properties were assessed and compared with baseline 2024-T3 and 7075-T6 alloys, including static properties, fatigue life and fatigue crack growth performance, corrosion resistance, machinability, as well as the damage and durability aspects. The initial phase of testing revealed that the static properties of 2198-T8, namely, tensile yield and ultimate strengths are above MMPDS published A and B values. In addition, anisotropic behavior is more pronounced in thicker gage material particularly in the 45° grain direction, Figure 9.10-7b. Measured fatigue crack growth rates for the 2024-T3 and 2198-T8 alloys were similar in the threshold and mid-range regions. When cycled under a simulated fuselage flight load spectrum, the 2198-T8 alloy displayed longer fatigue life in all orientations compared to the baseline 2024-T3, Figure 9.10-7c. In the standardized FAA Materials Fire Test AC 25.856-2A, 2198 T8 displayed longer burn-through time compared to 2024-T3.

When tested in a lap joint configuration designed to induce a large amount of secondary bending, 2198-T8 sheet material showed results between bare (higher) and clad (lower) compared to 2024-T3 baseline material. However 2198 T8 material displayed an interlaminar fatigue damage mode not observed in 2024-T3. The secondary bending was measured to be on the order of four times a typical narrow body aircraft fuselage lap joint. Though the lap joint design was not representative of a typical fuselage lap joint, the presence of interlaminar cracking (Figure 9.10-7d) has prompted a follow-on study to determine if the same behaviour is also characteristic of a realistic built-up structure.

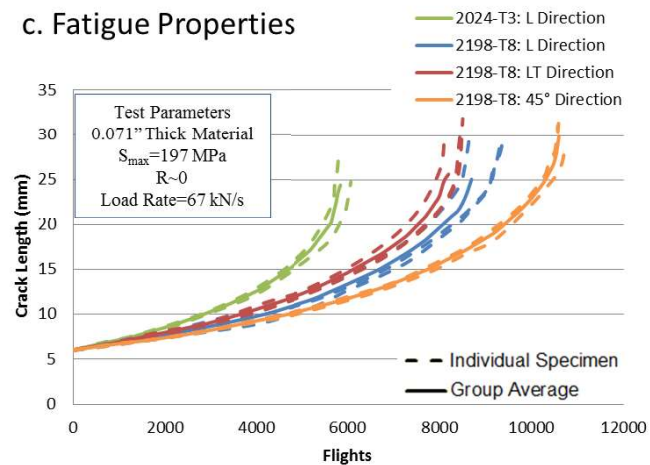
a. Application of Al-Li to Fuselage



b. Static Properties



c. Fatigue Properties



d. Interlaminar Cracking



Figure 9.10-7. Interim Test Results for Aluminum-Lithium

To further help the tests accurately reflect in-service conditions, Constellium will supply material finished to aerospace standards, and Bombardier will assist in building the test specimens to their own internal specifications.

9.10-5. Assessment of Emerging Metallic Structures Technologies Through Full-Scale Test and Analysis

John Bakuckas, Jr. and Kevin Stonaker, FAA – William J. Hughes Technology; Mike Kulak, Arconic Technical Center; Ian Won and Mark Freisthler, FAA – Transport Airplane Directorate

The aircraft industry is striving to improve performance and reduce costs in fabrication, operations, and maintenance by introducing advanced materials, construction methods, and production technologies. In response to the increased use of composite materials in aircraft such as the B787 and A350, the aluminum industry has made significant advancements in developing new aluminum alloy materials and product forms; improved structural concepts; and manufacturing processes that are lower cost compared to composites manufacturing. Collectively, these advances fall under the umbrella classification of Emerging Metallic Structures Technologies (EMST).

The introduction of a new material or concept in the aerospace industry can be quite challenging. A significant amount of test data at the coupon, substructure, and structural level is needed to fully vet and properly assess a new technology and understand any potential certification and continued airworthiness issues. This includes the assessment for continued relevance of existing regulations and potential development of additional safety standards and regulatory guidance, if needed, with the end goal of maintaining or enhancing the current level of safety afforded by the existing airworthiness standards. For these reasons, regulators and industry ideally should work together in preparation for the application and certification of EMST.

In recognizing these challenges, the Federal Aviation Administration (FAA) and Arconic (formerly Alcoa) have recently partnered in an effort to evaluate several EMST through full-scale test and analysis using the FAA's Full-Scale Aircraft Structural Test Evaluation and Research (FASTER) fixture. The goal is to demonstrate the potential for fuselage concepts using EMST to improve the durability and damage tolerance compared with the current baseline aluminum fuselage. Several technologies will be considered, including unitized welded structure, new metallic alloys (Al-Li), and hybrid construction (Figure 9.10-8). For this fiscal year, the majority of activities were focused on defining the test matrix and in the design and fabrication of EMST fuselage panels (Table 9.10-1). This involved conducting supplemental coupon tests and extensive finite element analyses to support panel design and for test preparations in the development of the applied loads used in panel testing using the FASTER fixture.

- **Advanced Alloys:**
 - 2524-T3 (Baseline)
 - 2060-T8E30 Al-Li
 - 2029-T8 Clad
 - 7075-T62 (Baseline)
 - 7150-T77511(Baseline)
 - 2055-T84 Al-Li
 - 2099-T83 Al-Li
- **Bonding and Fiber Metal Laminates**
 - GLARE Reinforcement Straps
 - Bonded stringers
- **Friction Stir Weld**
 - Solid state process can be applied to major aluminum alloys
 - Multiple materials can be joined
 - Excellent mechanical properties

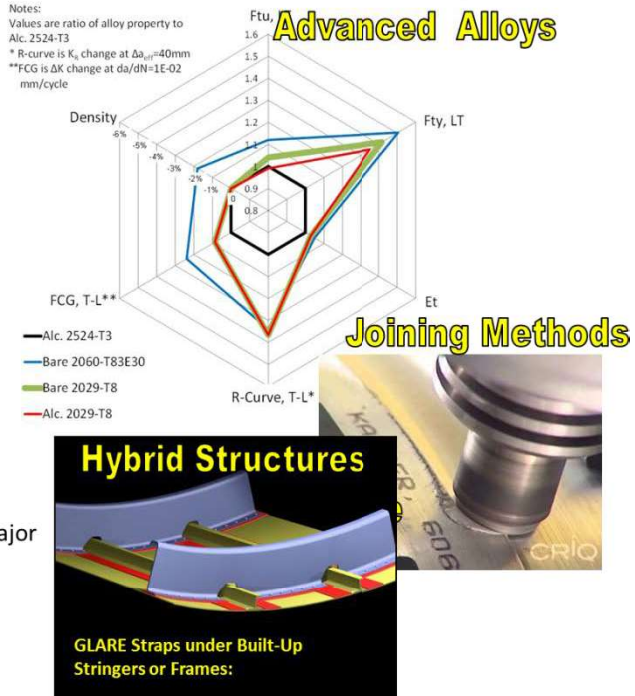


Figure 9.10-8. EMST Considered

Table 9.10-1. Text Matrix

		1	2	3	4	5	6	7
		Baseline	Advanced Density Reduction	Advanced Materials	Advanced Materials, FSW	FSW and Bonded Stringers	Baseline MSD	Advanced Density Reduction MSD
Component	Skin	2524-T3 sheet	2060 - T8 Al-Li sheet	2029-T8 sheet	2029-T8 sheet, FSW	2060 Al-Li sheet, FSW joint and bonded FML straps	2524-T3 sheet	2060 - T8 Al-Li sheet
	Stringer	7150 extrusions, riveted	2055 or 2099 Al-Li extrusions, riveted	2055 or 2099 Al-Li extrusions, riveted	2055 or 2099 Al-Li extrusions, FSW	2055 or 2099 Al-Li extrusions, bonded	7150 extrusions, riveted	2055 or 2099 Al-Li extrusions, riveted
	Frame	7075-T62 - shear tied, extruded, riveted	2055 or 2099 Al-Li integral extrusions, riveted	2055 or 2099 Al-Li integral extrusions, riveted	2055 or 2099 Al-Li integral extrusions, FSW	2055 or 2099 Al-Li integral extrusions, riveted	7075-T62 - shear tied, extruded, riveted	2055 or 2099 Al-Li integral extrusions, riveted

9.11. OVERVIEWS

9.11.1. Damage Tolerance for Life Management of Composite Structures – Part 1: Modeling

David Mollenhauer and Eric Lindgren, USAF Research Laboratory - Materials and Manufacturing Directorate; Endel Larve, University of Texas at Arlington; Kevin Hoos and Eric Zhou, University of Dayton Research Institute; Mark Flores, University of Texas at El Paso; Greg Schoeppner, USAF Life Cycle Management Center

It has long been desired to understand through modeling the damage tolerance of composite laminates (Figures 9.11-1 and 9.11-2) subjected to impact events. Impacted laminated composites typically display varying degrees of matrix and fiber damage. Matrix damage takes the form of ply cracking and delamination between plies. Long-term Air Force Research Laboratory (AFRL) investments in progressive damage analysis simulation methods are on the cusp of yielding viable damage tolerance assessment tools for composite laminates with pre-existing damage. AFRL's efforts have produced software codes that allow for modeling of individual ply cracking and delamination between plies in a framework referred to as Discrete Damage Modeling (DDM) (Figure 9.11-3). Briefly, the background and details of the DDM methodology will be described in this technical effort. Application of the DDM approach to a combined experimental and modeling study of impacted laminated composites will also be covered (Figure 9.11-4). In this effort, laminates are impacted at sufficient energies to induce damage. They are then examined with standard and advanced NDE techniques (Figure 9.11-5) (the subject of Part 2 of this technical effort). Subsequently, the impacted laminates are modeled using representations of the impact-induced damage as a starting point (Figure 9.11-6). Both compression-strength-after-impact (CSAI) and compression-compression fatigue loadings will be considered. Finally, extensive post-impact testing in both CSAI and compression-compression fatigue will examine damage evolution for correlation with modeling results. The full-field displacement measurement method, digital image correlation (DIC), will be used to track surface strains and global/local buckling events. Results-to-date from the modeling efforts will be presented in comparison with experimental results (Figure 9.11-7). Concluding remarks will include comments on the future direction of this potentially significant advance in life management of composite materials.

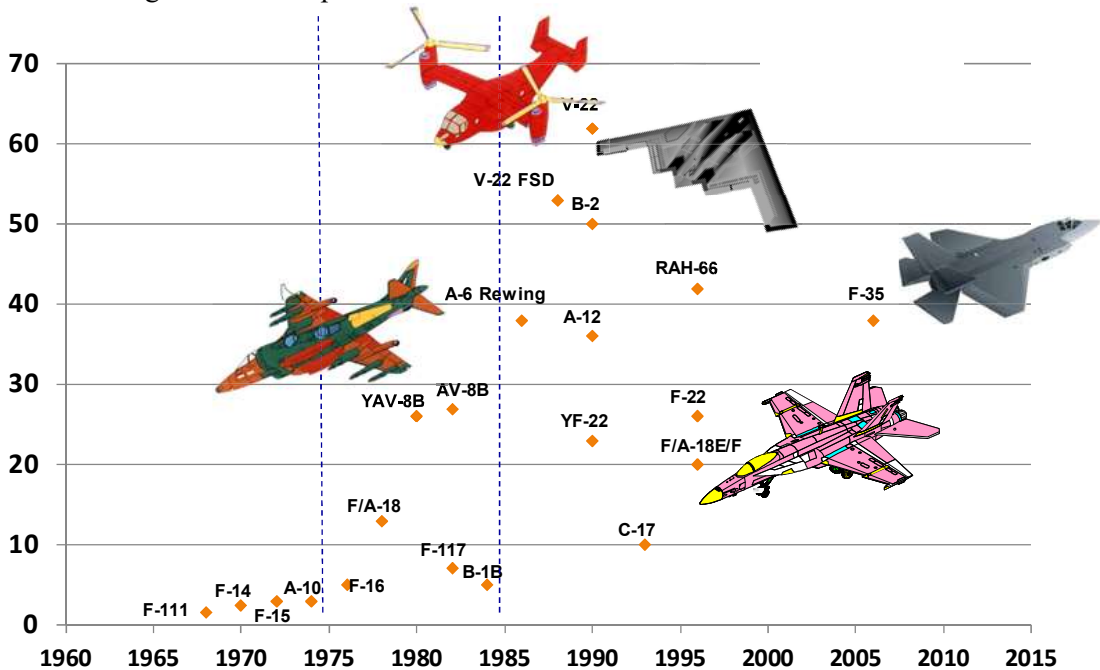


Figure 9.11-1. Composites in Military Airframes

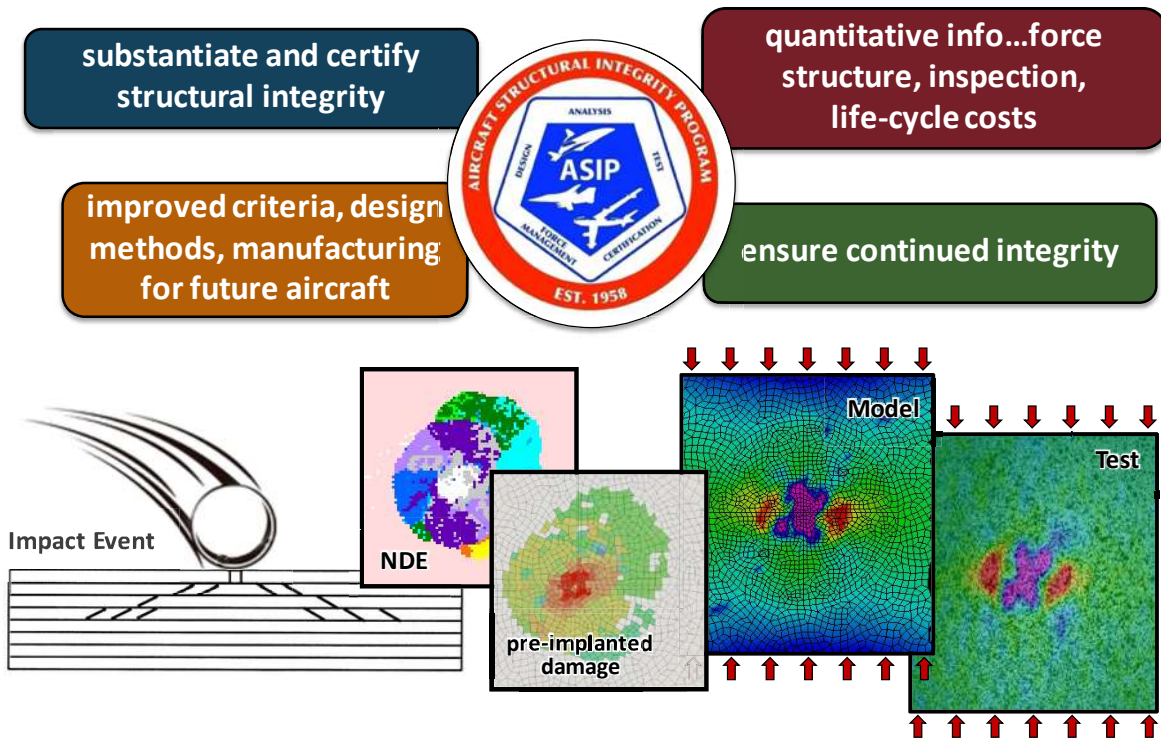
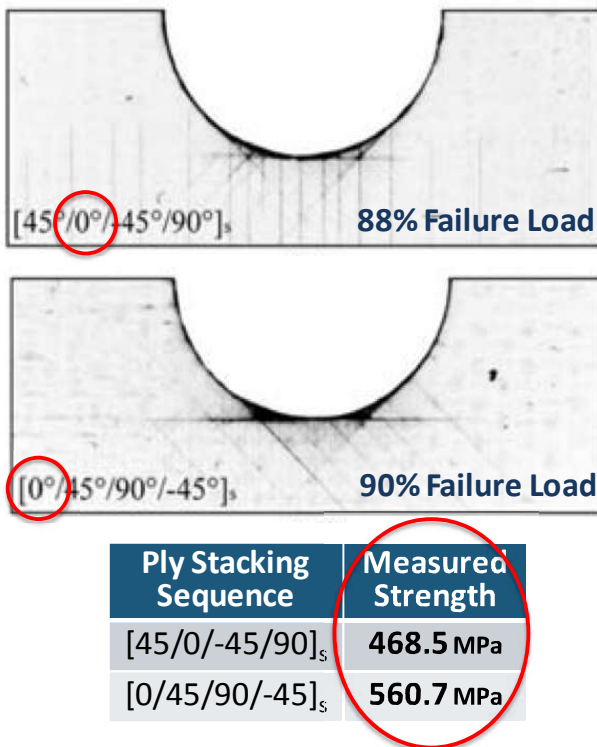


Figure 9.11-2. Damage Tolerance Modeling (Impact Damage)



- Matrix damage accumulates in laminate
- Cracks are not “diffuse”
- Damage patterns are clearly stacking sequence dependent
- 0° ply generally, but not always, governs final strength of laminate

Figure 9.11-3. Discrete Damage Modeling

Impact

- 1" impactor
- 55 ft-Lbs impact energy

CAI

- Multiple strain gages
- 0.05" loading rate
- Digital Image Correlation

All Specimens
[45/90/-45/0] _{4s}

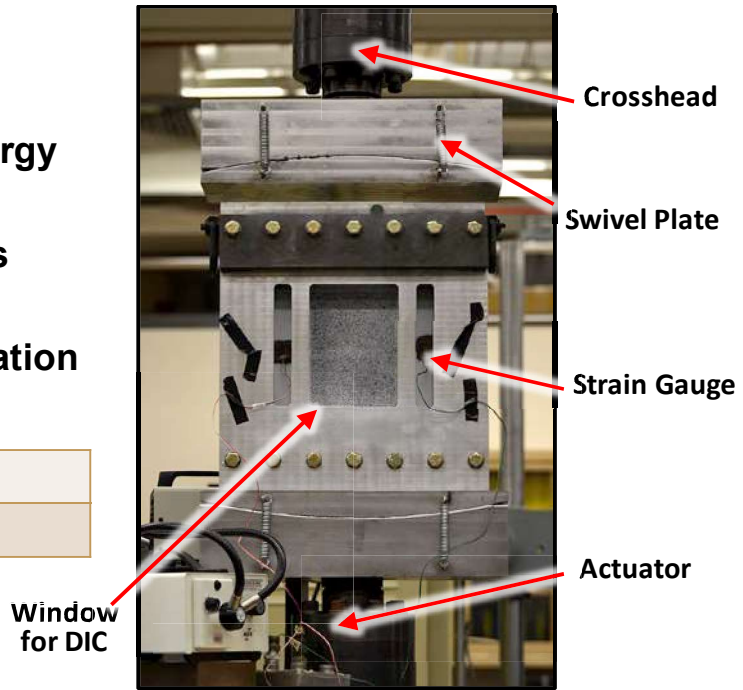
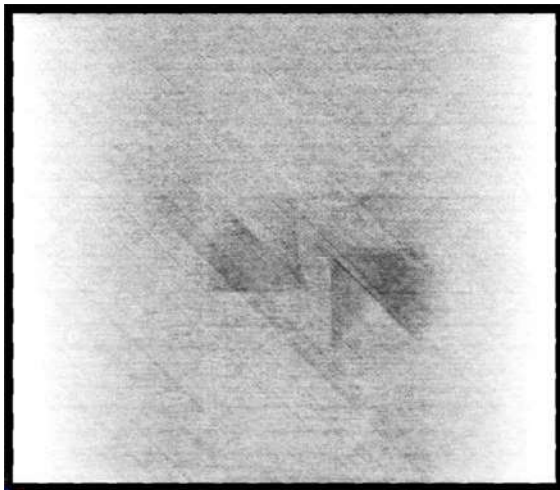
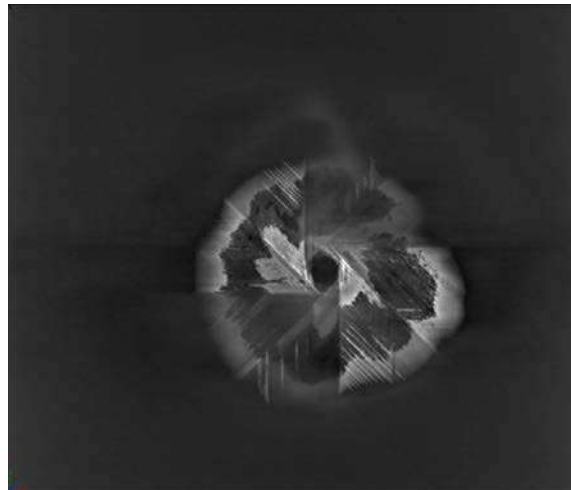


Figure 9.11-4. Impact Modeling and Experiments (Large Panels 10" x 12")

- Six large specimens impacted
 - 3 sectioned for X-ray CT
 - 3 CAI tested
 - X-ray CT untreated & ZnI treated



Untreated



Zinc Iodide Treated

Figure 9.11-5. X-Ray CT Inspection (Large Panels)

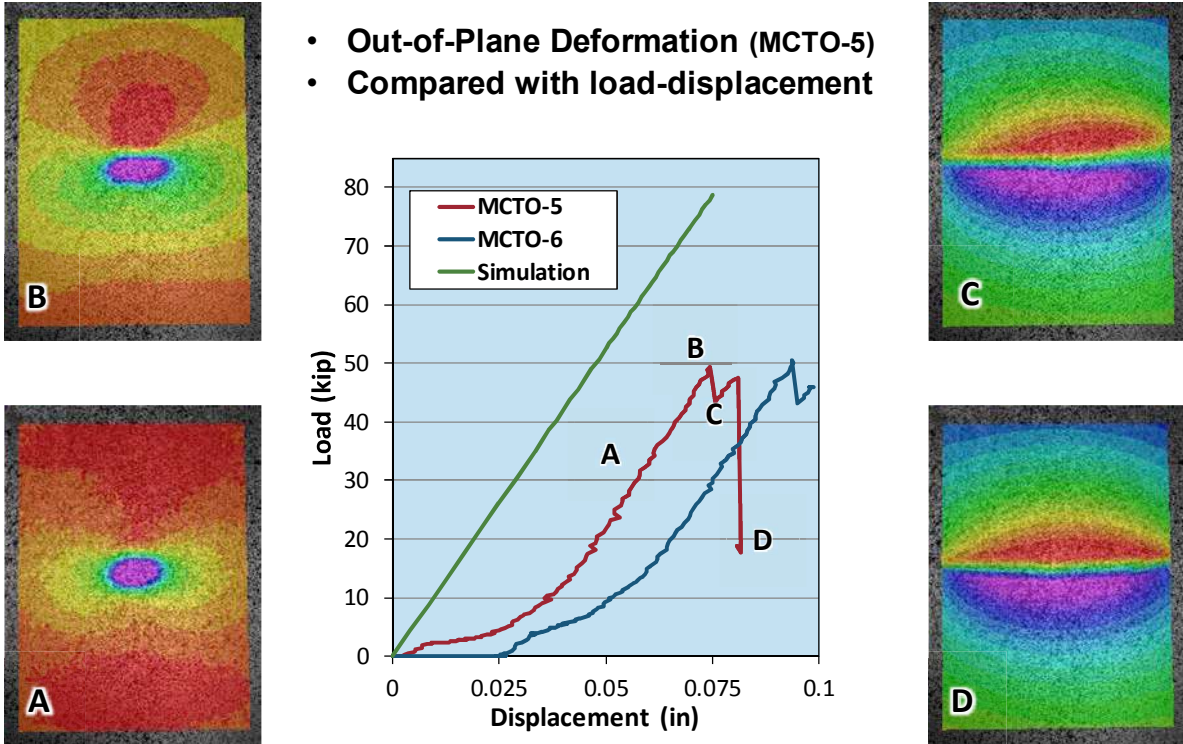


Figure 9.11-6. Damage Tolerance Modeling (Large Panel Results)

- Residual strength after fatigue
- Tension-tension fatigue, 200,000 cycles
- Laminate stacking sequence $[60/0/-60]_{3s}$

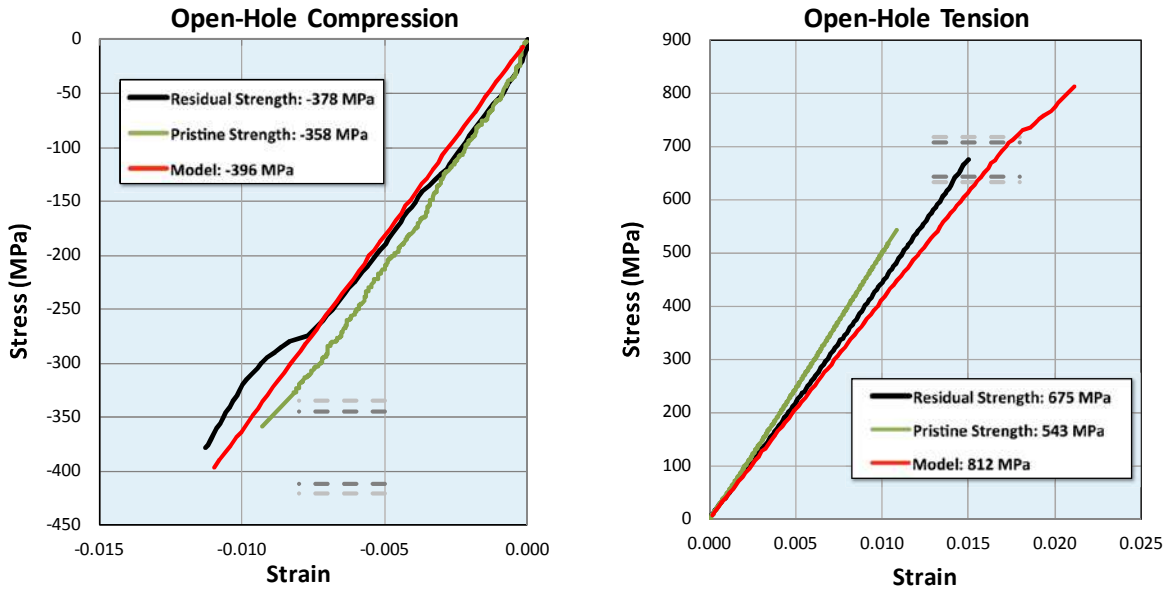


Figure 9.11-7. Fatigue Damage in Laminates

9.11.2. Damage Tolerance for Life Management of Composite Structure – Part 2: Nondestructive Evaluation

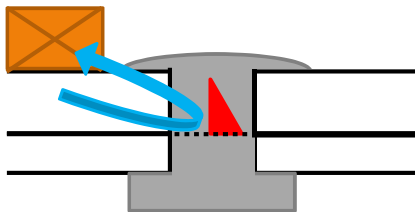
Eric Lindgren, David Mollenhauer, Sarah Wallentine and John Welter, USAF Research Laboratory - Materials and Manufacturing Directorate; Mark Flores, University of Texas at El Paso

The recent advances in the development of model-based methods to predict damage evolution for organic matrix composites (subject of Part 1 of this technical effort) has set the stage for using the same predictive capability to manage composites as is currently used within the damage tolerance framework for metals via fracture mechanics. As with current metal-based damage tolerance approaches, the use of Nondestructive Evaluation (NDE) to determine the presence of damage is a critical step in this process. The validated capability to detect and quantify the damage as a result of impact is an important input to the composite damage prediction framework referred to as Discrete Damage Modeling (DDM). This technical effort presents a brief overview of current NDE methods used to detect damage in composites with a focus on impact damage. It highlights the shortfalls of current methods for their use for the DDM framework which is optimized to use the full three-dimensional characteristics of damage from impact. Therefore, new approaches to generate volumetric representation of damage that do not require the use of computed tomography are needed. This technical effort provides a description of specific research and development efforts that focus on two techniques, one based on ultrasound and the other on thermal imaging. The ultrasonic method is based on the well-known angle-beam shear interrogation to detect fatigue cracks, but includes augmented analytics to enable additional characterization of the extent of impact damage (Figure 9.11-8). The thermal imaging method is assessing the sensitivity to sub-surface morphology using controlled thermal diffusion excitation as an alternative to the planar thermal gradient introduced by commercial flash-based systems (Figure 9.11-9). Current research and development activities are focused on making this capability realistic for depot maintenance environments. This includes developing methods to assess and validate the capability to provide statistical metrics of accuracy. Successful realization of these methods will enable the implementation of the DDM framework as a mechanism to realize damage tolerance management of composite components.

Standard USAF flaw detection method

Angle beam pulse echo

- Cracks in metals
- Capability is geometry dependent



Straight beam pulse echo

- Delaminations in composites
- Detection only

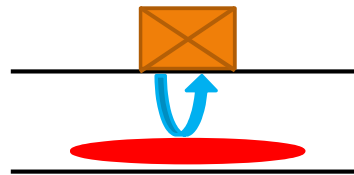


Figure 9.11-8. Overview of Ultrasound

Standard USAF flaw detection method

Pulsed Thermography

- Delaminations in polymer matrix composites
- Capability is geometry dependent

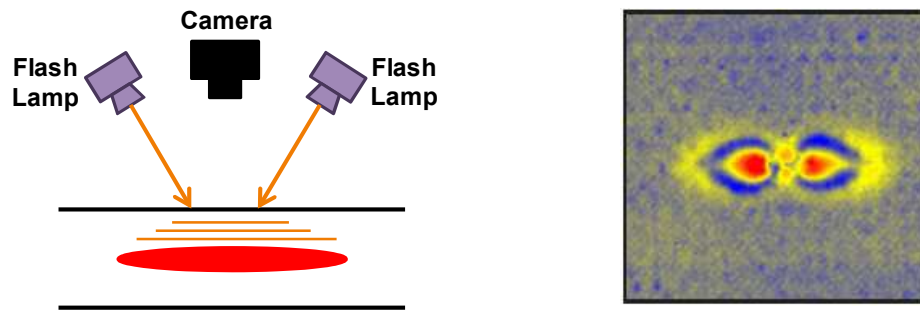


Figure 9.11-9. Overview of Thermography

9.11.3. ADS-89-SP: A Standard Practice for U.S. Army Rotorcraft Structural Integrity Programs

Robert E. Benton, Jr., USA - Aviation Engineering Directorate; Nate Bordick and Mark Robeson, USA - Aviation Development Directorate

The Army has identified challenges associated with its lack of a documented standard practice for ensuring rotorcraft structural integrity throughout the lifecycle. If unresolved, changes in loads due to new and modified configurations could drive increased airworthiness-related technical and programmatic risk for introducing necessary technologies into future rotorcraft. Traditional rotorcraft structural integrity methods vary by platform and include constraints imposed during historical structural flight testing. Evolutionary modifications, changes in usage and envelope, or integration of complex systems and similar technologies require expensive structural flight testing for new configurations or assessment of safety hazards for airworthiness impacts related to structural integrity. Rotorcraft loads analysis is not deemed valid for fatigue substantiation efforts, particularly for dynamic systems. Although additional insights and understandings are desired, it is the Army's current understanding that the MIL-STD-1530C (USAF) standard practice for an Aircraft Structural Integrity Program (ASIP) does not address key rotorcraft structural integrity concerns related to Army aircraft. Two key necessary distinctions would be the Army's desire for inclusion of an enhanced safe life methodology, and a reflection of differences between Army rotorcraft and USAF fixed-wing concepts of a flight loads survey and the associated rotorcraft fatigue methodology and substantiation. As such, MIL-STD-1530C has not been accepted for Army rotorcraft by the delegated airworthiness authority. However, it is viewed as an excellent pattern for a new standard practice for a Rotorcraft Structural Integrity Program (RSIP), and much of the draft 2x ADS-89-SP content has been adapted from MIL-STD-1530C (Figure 9.11-10). Similarly, JSSG 2006 may provide a similar pattern for related specification guidance for rotorcraft structural integrity. ADS-89-SP will be an Army Aeronautical Design Standard (ADS), which is a type of local Army military standard. The document will be a Standard Practice per MIL-STD-962D and may form the basis for a future MIL-STD-XXX if Air Force and Navy counterparts agree. The ADS will specify procedures on how to execute an RSIP, and should provide framework to allow programs to maximize the benefits of new loads, structures, and materials technologies. Regime recognition, structural health monitoring,

structural loads monitoring, and estimation tools discussed in the Army's ADS-79E-HDBK should be incorporated into the flight test configuration to enable validation. Initial efforts are underway with formation of Army co-authors from AMRDEC and a review team comprised of government and rotorcraft industry rotorcraft structural integrity experts, including representatives from the Army, Navy, and Air Force. This technical effort will provide a status of the effort to date. Co-authors are working through reviewer input from last year to produce the draft 2x ADS-89-SP for reviewers as soon as possible.

- **In accordance with MIL-STD-962D (and similar to MIL-STD-1530C)**

Section 1 Scope

Section 2 Applicable documents

Section 3 Definitions

Section 4 General requirements

Section 5 Detailed requirements

Section 6 Notes

Figure 9.11-10. Outline of Draft 2x ADS-89-SP

9.11.4. Digital Thread/Digital Twin Benefits Assessment

Joe Lougheed, Dale Ball, and Kevin Welch, Lockheed Martin Aeronautics

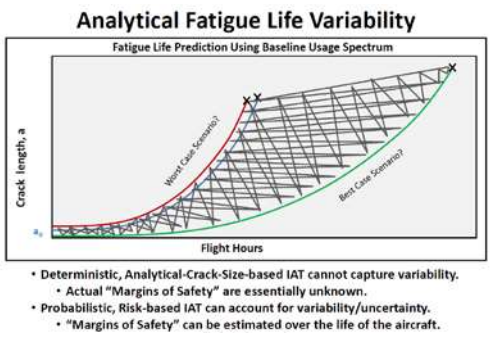
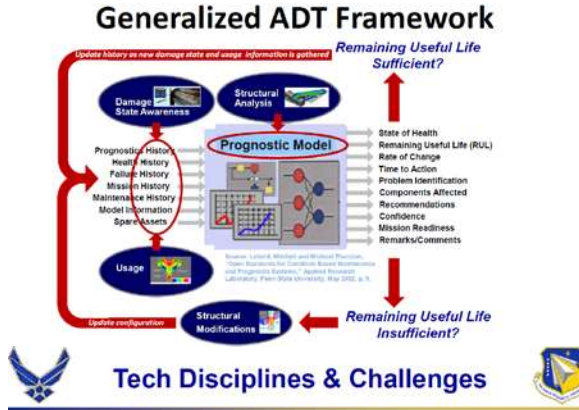
DoD and the services are currently exploring the application of current and emerging high performance computing and advanced modeling and simulation capabilities to enable development of a "Digital Thread" which can result in the digital integration of the entire product lifecycle. It is envisioned that a Digital Thread enabled acquisition process will provide for significant reductions in acquisition and support costs. According to the DAU Glossary of Defense Acquisition Acronyms and Terms the current definition of the Digital Thread is; "An extensible, configurable and component enterprise-level analytical framework that seamlessly expedites the controlled interplay of authoritative technical data, software, information, and knowledge in the enterprise data-information-knowledge systems, based on the Digital System Model template, to inform decision makers throughout a system's life cycle by providing the capability to access, integrate and transform disparate data into actionable information." A related activity is AFRL's Airframe Digital Twin (Figure 9.11-11) which is "An integrated multi-physics, multi-scale, probabilistic simulation of an as-built system, enabled by Digital Thread, that uses the best available models, sensor information, and input data to mirror and predict activities/performance over the life of its corresponding physical twin." Lockheed Martin Aeronautics recently completed a study effort for AFRL which explored the benefits that a Digital Thread/Digital Twin (DT/T) (Figure 9.11-12) capability could potentially provide. This technical effort will discuss the approach used, findings and recommendations that were identified during this study effort. In this technical effort we address benefits that could be

realized during Development (EMD) and Sustainment (SLAP/SLEP). The approach for Development involved looking at F-22 EMD and F-35 SDD and comparing and contrasting the structural design and analysis processes, tools and capabilities and outcomes as well as how the computing resources and analytical tools and capabilities have evolved. This evolution was used to identify the progress made toward achieving the objectives of the current Digital Thread initiatives and then we identified benefits that could be achieved if a complete Digital Thread capability were available. We identified benefits due to improved availability and quality of digital data, improved capability of the tools supporting the analysis, increased tool integration and improvements in the capability of computing infrastructure. The approach for Sustainment involved looking at several F-16 Service Life Assessment and Service Life Extension activities, comparing and contrasting the applied structural analysis processes, tools and capabilities and outcomes as well as how the computing resources and analytical tools and capabilities have evolved. Additionally, baselines for each major analysis task were established to be used a reference for estimating the benefits that could be realized if a complete "Digital Thread/Digital Twin" capability were available. As with Development we identified benefits due to improved availability and quality of digital data, improved capability of the tools supporting the analysis, increased tool integration and improvements in the capability of computing infrastructure (Figures 9.11-13 through 9.11-16).

CBM+SI Far-term Vision
per AFRL CBM+SI Workshop - Feb 2009

"Digital Twin": Real-Time, High-Fidelity Operational Decisions for Individual Aircraft Enabled by Tail Number Health Awareness

- When physical aircraft is delivered, a **Digital Model** of the aircraft – specific to that tail number, including deviations from the nominal design – will be delivered as well.
- The **Digital Model** will be **flown virtually** through the same flight profiles as recorded for the actual aircraft by its on-board SHM system.
- The modeling results will be compared to sensor readings recorded by the SHM system at critical locations to **update / calibrate / validate** the model.
- As **unanticipated damage** is found, it will be added to the Digital Model so that the model continually reflects the **current state of the actual aircraft**.
- Prognostics** for the airframe will be developed by "flying" the Digital Model through possible future missions.
- The Digital Model will be used to determine when & where structural damage is likely to occur, and when to perform maintenance.

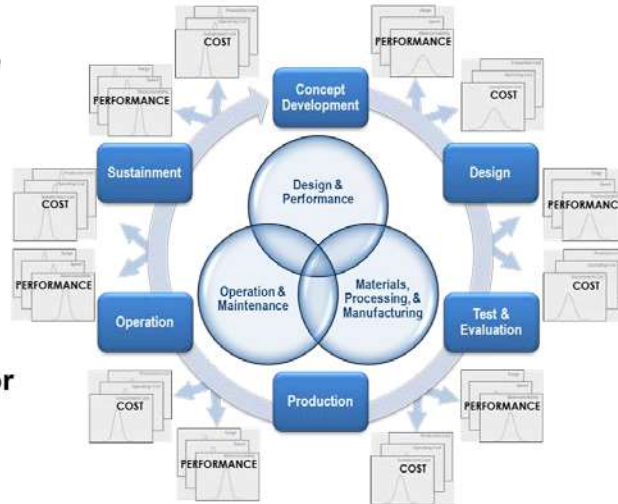



- Disciplines**
 - Aerodynamics
 - Structures
 - Materials and Manufacturing
 - Computer Science
 - Information Management
 - Challenges**
 - Developing parameterized, multi-disciplinary computational models of appropriate fidelity for the full-scale aircraft
 - Developing high-fidelity computational models of the relevant capability-controlling phenomena at physically appropriate length and time scales
 - Linking computational models across length/time scales at varying levels of fidelity
 - Understanding and incorporating all influential sources of uncertainty and variability into the models at each length/time scale
 - Developing analysis techniques for assessing and optimizing both capability and reliability of the aircraft
 - Integrating materials and manufacturing phenomena into the aircraft-level digital twin framework
 - Developing technologies and methods to track and update the state and behavior of both the actual aircraft and the digital twin based on real-world experience
- AFRL POC: Dr. Eric Tuegel, eric.tuegel@wpafb.af.mil
Upcoming Cross-organization Discussion Opportunities: AIAA SDM, AA&S2011, ICAF2011, ISHM Conference...

Figure 9.11-11. Airframe Digital Twin Concept

Key Attributes:

- Complete, fully accessible digital data
- Tools for accessing, integrating & transforming data
- Virtual representations of systems in a modeling & simulation environment
- Probabilistic framework for quantifying, forecasting, and updating system performance capability



*Create a **DIGITAL SURROGATE** of a materiel system*

Figure 9.11-12. Digital Thread/Twin Concept

- **SLAP Use Case:**
 - Identify airframe service life and inspection intervals for a change in baseline usage with no changes to the structural design requirements
- **SLEP1 Use Case:**
 - Identify structure not meeting service life and inspection interval objectives (which may be different than the design requirements)
 - Design modifications or improved replacement parts
 - Design requirements different from the baseline aircraft may be imposed on the new/redesigned structure as long as recertification is not required
- **SLEP2 Use Case:**
 - Extend the service life of the airframe beyond the design capability
 - New design requirements in addition to an extended service life requirement may be imposed
 - Structural/airworthiness recertification will be required

Figure 9.11-13. Definition of SLAP/SLEP Use Cases

• **Current State versus Final State**

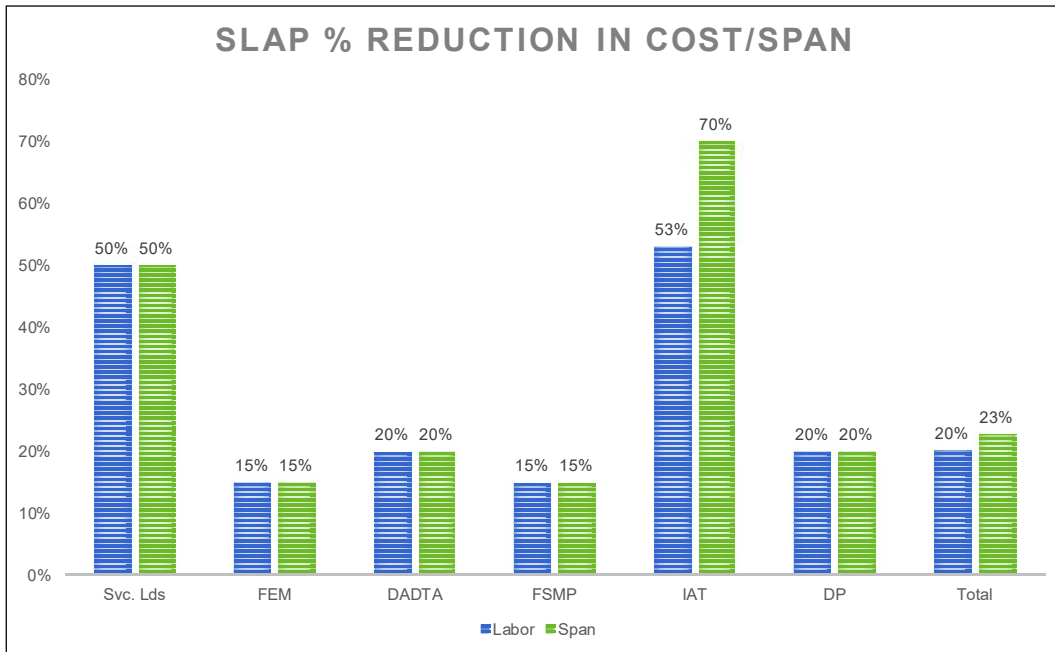


Figure 9.11-14. DT/T Benefits Comparison for SLAP

• **Current State versus Final State**

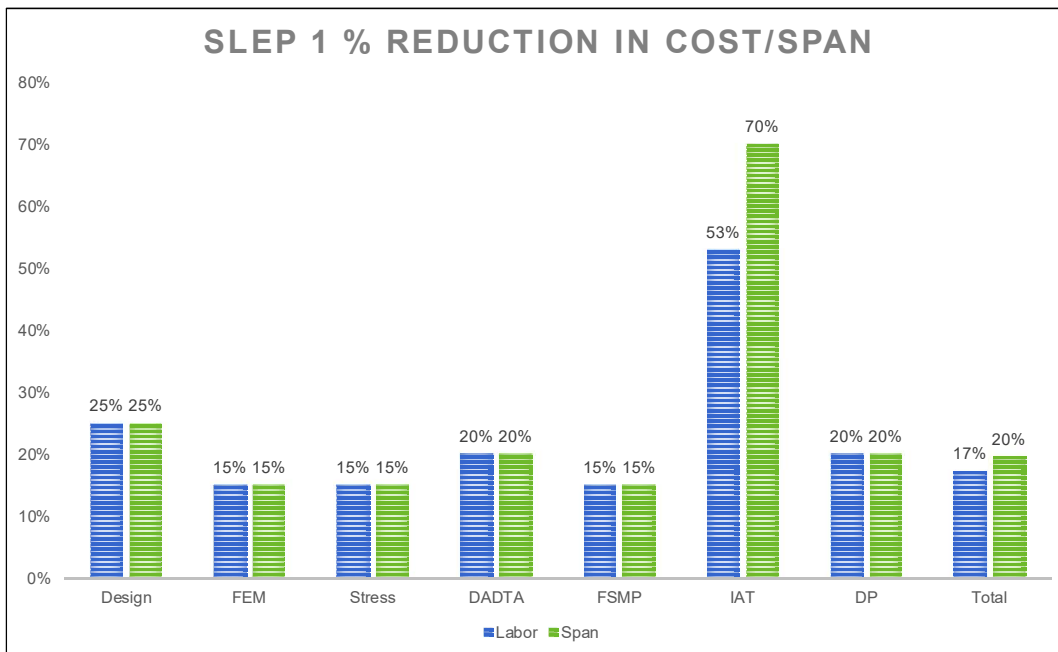


Figure 9.11-15. DT/T Benefits Comparison for SLEP1

- **Current State versus Final State**

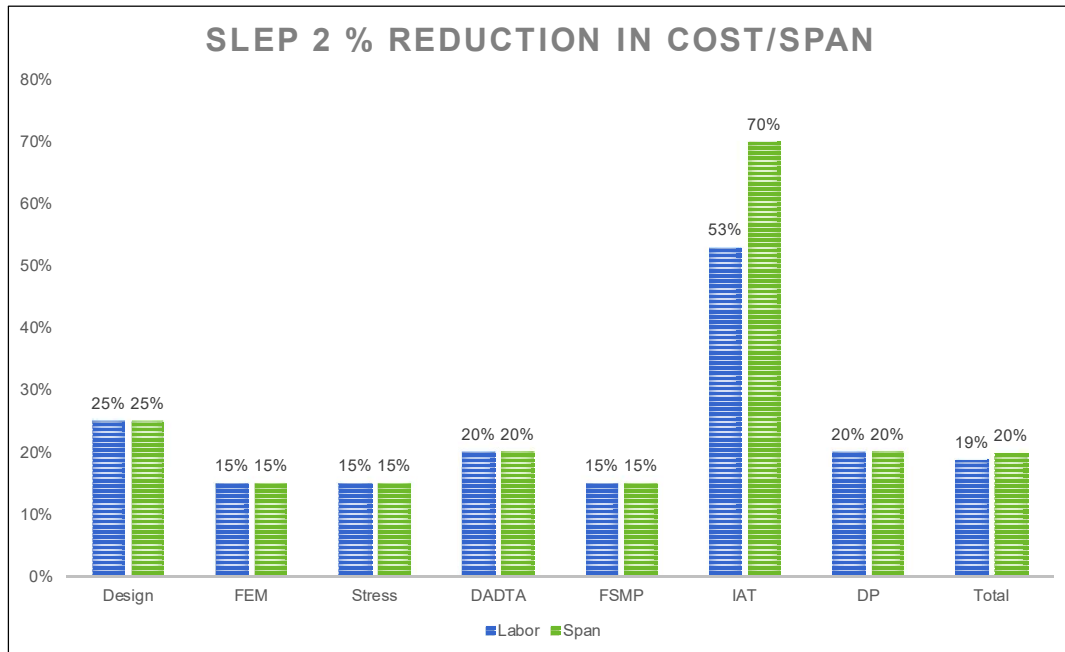


Figure 9.11-16. DT/T Benefits Comparison for SLEP2

9.11.5. B-1 Wing FSFT Progress and Lower Skin Trailing Edge DaDT Analysis

Bob Lee, Isaac Meier, and John Kowalczyk, The Boeing Company - B-1 ASIP; Ryan Rowten and Rodney Harberson, USAF - B-1 ASIP

The B-1 (Figure 9.11-17) Wing Full-Scale-Fatigue Test (FSFT) is ongoing and the goal is to achieve two times the flight hours estimated for lead-the-fleet aircraft in 2040 (Figure 9.11-18). At about 2.5 lifetimes of testing, cracks were discovered in the wing lower skin (WLS) trailing edge at multiple fastener hole locations. The WLS of the B-1 Wing is a primary load carrying structure and the Wing Outer Panel (WOP) lower plank is a fracture critical part. The lower wing skin consists of a single aluminum plank with a series of machined, milled and tapered steps from thickness of over 2 inches to 0.30 inch to accommodate several flap track, spoiler, and intercostal fittings. In the trailing edge location, a relatively thin skin tab is extended out from the thick rear spar attach section for the strap attach. In addition, fastener holes placed in series on the trailing edge tab act as an attach point for long straps along a major portion of the wing span. These attachments are located immediately adjacent to interference-fit taper-lok fasteners attaching the wing cover to the rear spar, trailing edge ribs and flap track. The first half of this technical effort presents the progress of the wing test, crack findings and the potential impact of these damages on the overall structural health of the wing. Due to the unique B-1 wing design in which upper and lower skins are not removable and have very limited access in the wing box, bonded doubler strap repair is developed for the test article. General finite element analysis of bonded repairs and stress intensity factor (SIF) methods will be addressed in a second technical effort from the A-10 team. In the design analysis, stress concentration was considered at the wing cover tab for attachment of the flap track. A high stress field was identified in the area of the straight-shank fastener holes. The current B-1B design calls out fastener hole cold work in the lock bolt holes to induce the presence of a beneficial residual stress condition in the subject fastener holes. However, the analysis did not account for complex

local geometry of compound stress gradients in the hole and tab-out area. Following NDI of the FSFT article along the WLS trailing edge, several locations along the skin tab showed crack-like indications in tab fastener holes in the forward and/or aft direction. Visual inspection detected a number of cracks emanating from the trailing edge through tab fastener holes and into rear spar taper-lok holes (Figure 9.11-19). It is suspected the cracks initiated at the tab fastener holes and grew to the aft ligament, followed by crack initiation at the forward edge of the fastener hole and growth forward through the thick skin and into rear spar taper-loks (Figure 9.11-20). With an understanding of the importance surrounding lock bolt hole cracks in the wing skin tab, an improved finite-element-based analysis of the WLS trailing edge was conducted (Figure 9.11-21). Local stress concentration through the thickness and stress-intensity-factor data were extracted from new finite element model results. The second half of this technical effort presents some basic crack growth analysis correlations with FSFT data and limited findings from fleet aircraft. Conclusions from this analysis and fatigue test results will be used to set fleet inspection (Figures 9.11-22 and 9.11-23).



Figure 9.11-17. B-1 Aircraft

- **ASIP 2013 presentation introduced the B-1 Full Scale Fatigue Test Program**
- **Objective: To validate the structure can survive two (2) times the predicted usage life of the B-1B fleet at year 2040**
- **Original design life: 30 years (or 9681 AFH)**

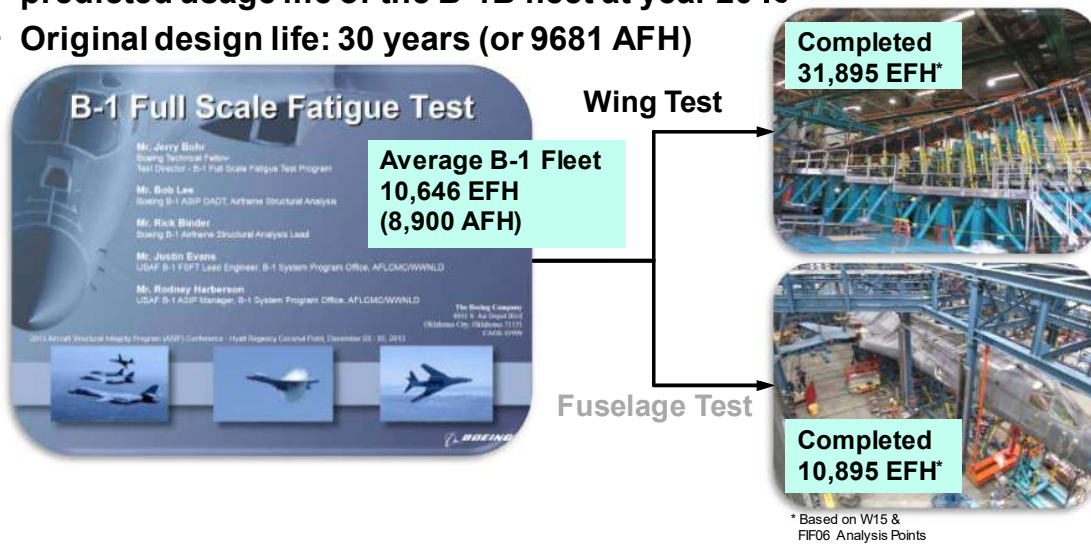


Figure 9.11-18. Background

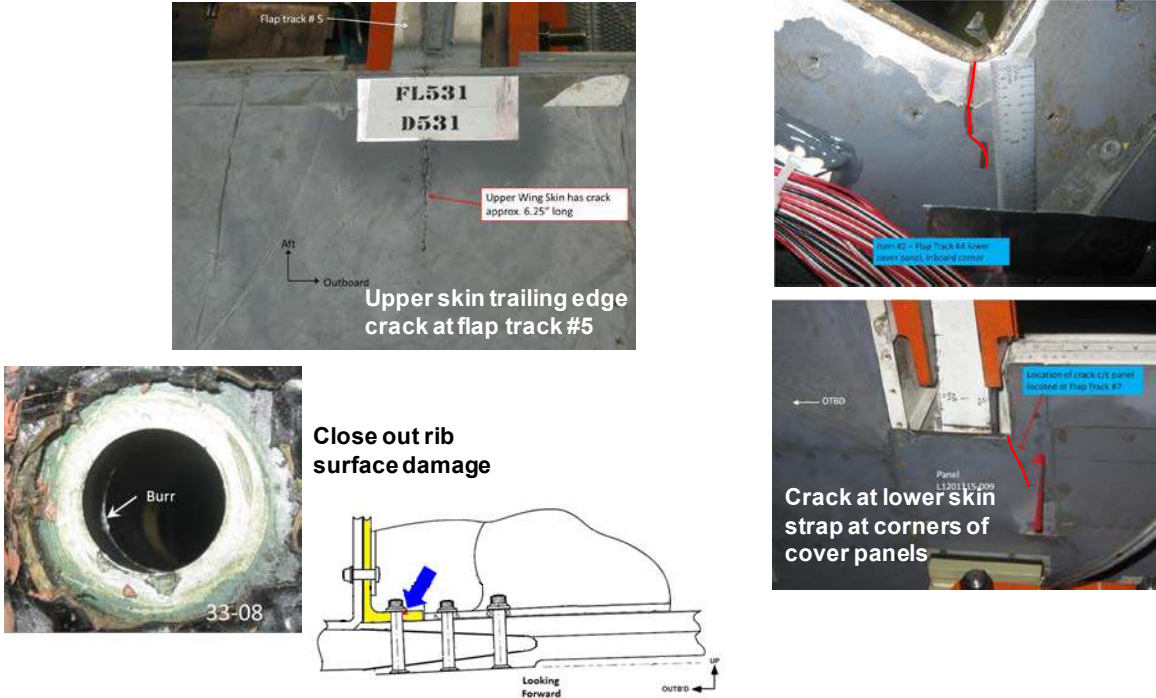
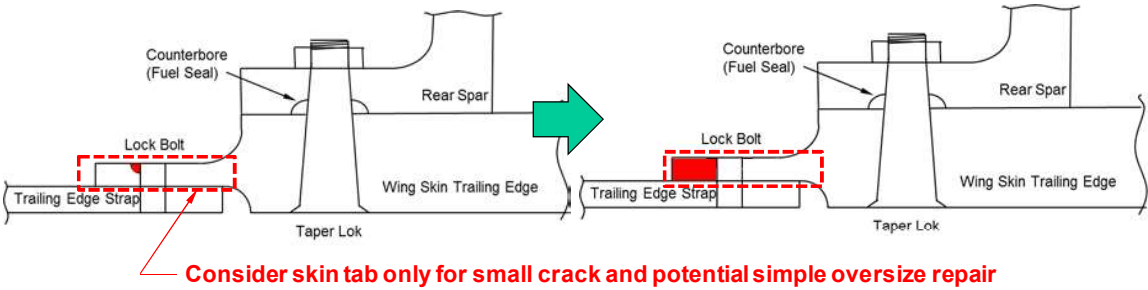


Figure 9.11-19. Selected Crack Findings

Stage 1: Corner Crack emanated at lock bolt hole aft edge and growth to trailing edge



Stage 2: Corner Crack emanated at lock bolt hole fwd edge and growth to skin transition

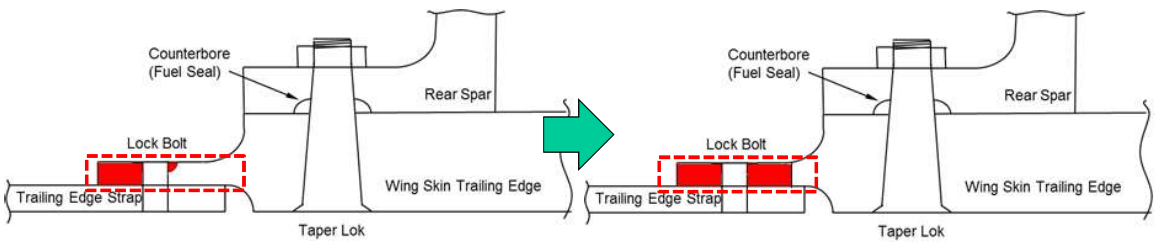
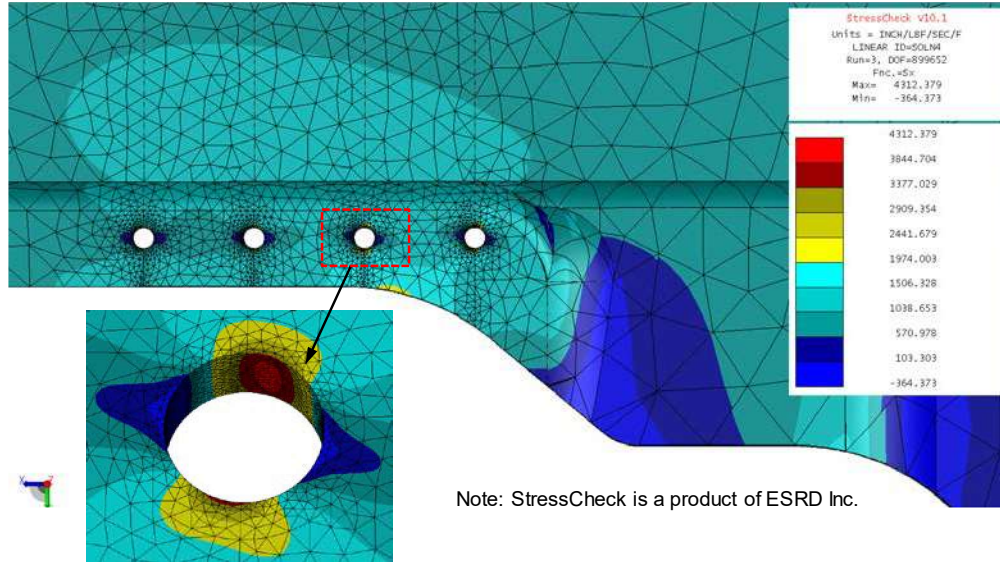


Figure 9.11-20. Trailing Edge Tab Crack Growth Sequence

- Modeled local WLS TE Tab using StressCheck™
- Loads/Constraints were from Global FEM
- Extracted stress gradient and SIF from results

Flap
Track #2
Example



Note: StressCheck is a product of ESRD Inc.

Figure 9.11-21. Local Finite Element Model

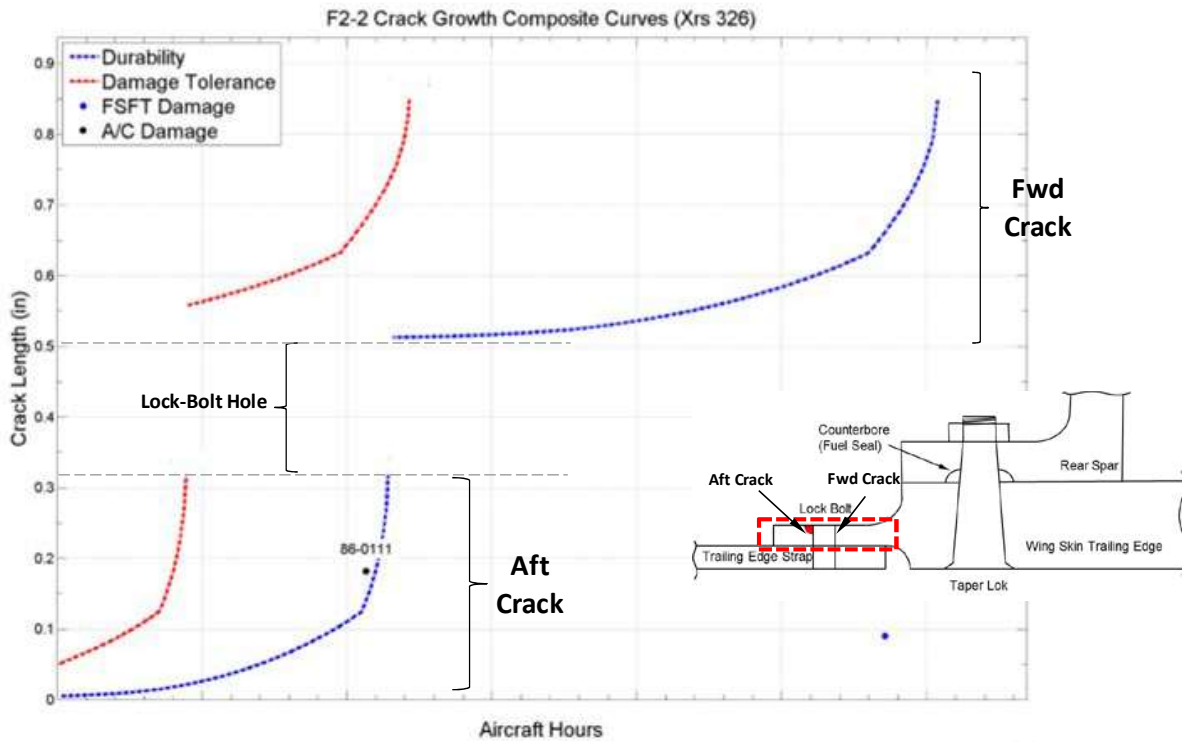


Figure 9.11-22. Crack Growth Curves

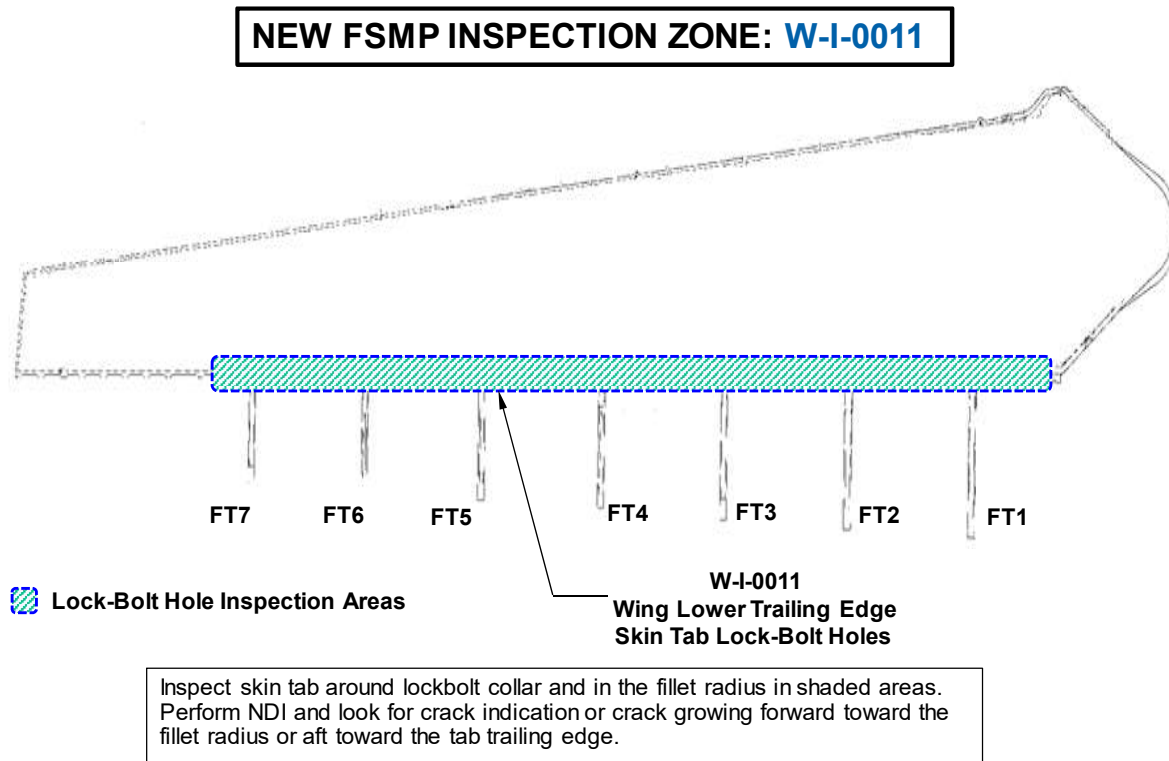


Figure 9.11-23. FSMP Inspection

9.11.6. C-130 Full-Scale Wing Durability Test with an ESL Wing: Coupon Test Program

Albert Arrieta, Lockheed Martin Aeronautics

The Lockheed Martin (LM) C-130 (Figure 9.11-24) Enhanced Service Life (ESL) center wing (Figure 9.11-25), which has been installed on all C-130J production aircraft beginning in 2006, has not received a full-scale durability test. The service life of the ESL center wing was not determined by testing, but estimated by analysis. The USAF Warner Robins Air Logistics Complex requested LM Aeronautics to develop a test spectrum for a C-130 full-scale wing durability test (WDT) to validate the durability of the ESL center wing. The untruncated C-130 Enhanced Service Life Wing Durability Test spectrum, referred to as the baseline spectrum, contained approximately 6 million load points or 3 million cycles. It is not possible to apply this test spectrum to the full-scale fatigue test article within the time and budget constraints. The spectrum size needed to be reduced or truncated. The primary purpose of the coupon test program was to ensure that the truncated fatigue test spectrum retained sufficient fatigue content to represent the untruncated spectrum. This technical effort provides the overall process whereby the baseline spectrum was reduced to a more manageable size, clipped to remove infrequent high loads, and modified with marker cycles to leave identifiable striations on fracture surfaces. It was also necessary to fine tune the da/dN crack growth rate models to improve correlation between test results and their predictions. The initial phase of the coupon test program (Figure 9.11-26) established that a truncation stress range of 1,900 psi was necessary to expedite the full-scale WDT to fit within reasonable time and budget constraints. The coupon test results in the initial phase of this project indicated that the crack growth rate predictions of the truncated spectra did not represent what was observed in testing (Figure 9.11-27). The C-130 7075-T73 crack growth (da/dN) properties were unsuitable to be used in predictions with these heavily truncated and factored spectra. This problem was solved by developing

new 7075-T73 da/dN properties tuned to the truncated and untruncated test results (Figures 9.11-28 and 9.11-29). In the subsequent phase, the Jack Loads Matrix (JLM) baseline spectrum was truncated from its original size of approximately 6 million load points down to approximately 1.2 million load points. Now, the truncated spectrum coupon test results were similar to the baseline coupon test results after factoring the stresses of the remaining cycles (Figure 9.11-30). The overall crack growth seen during coupon testing was a reasonable match to the analytical predictions once the new 7075-T73 da/dN properties were used.



Figure 9.11-24. C-130 Aircraft

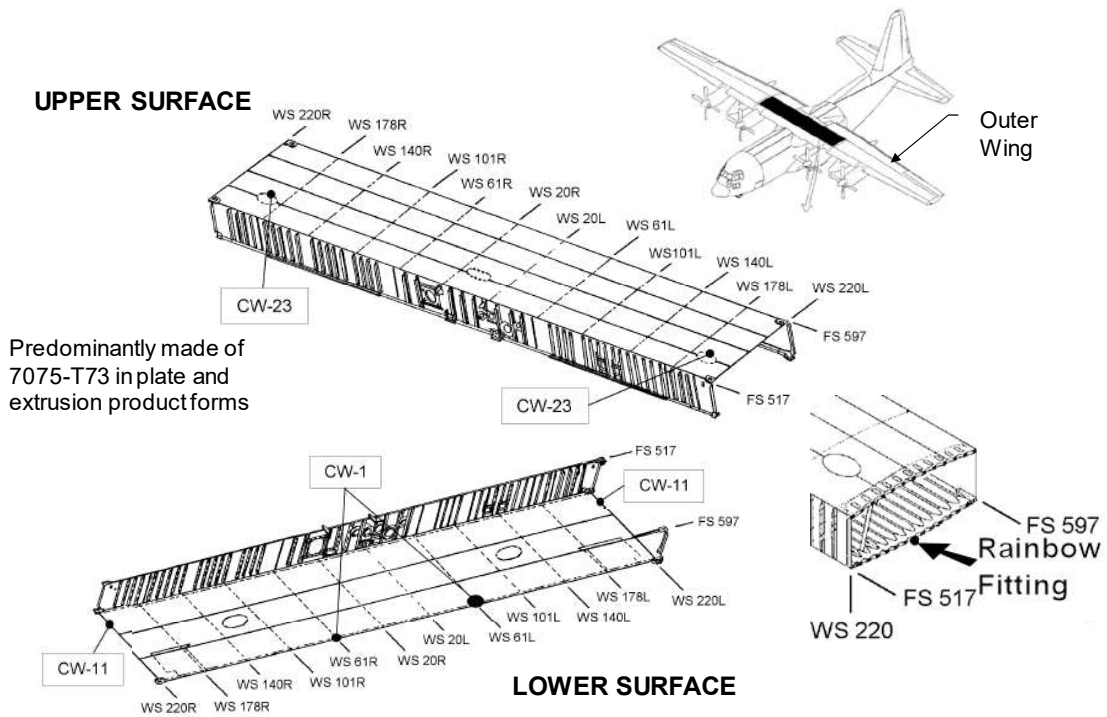


Figure 9.11-25. C-130 ESL Center Wing

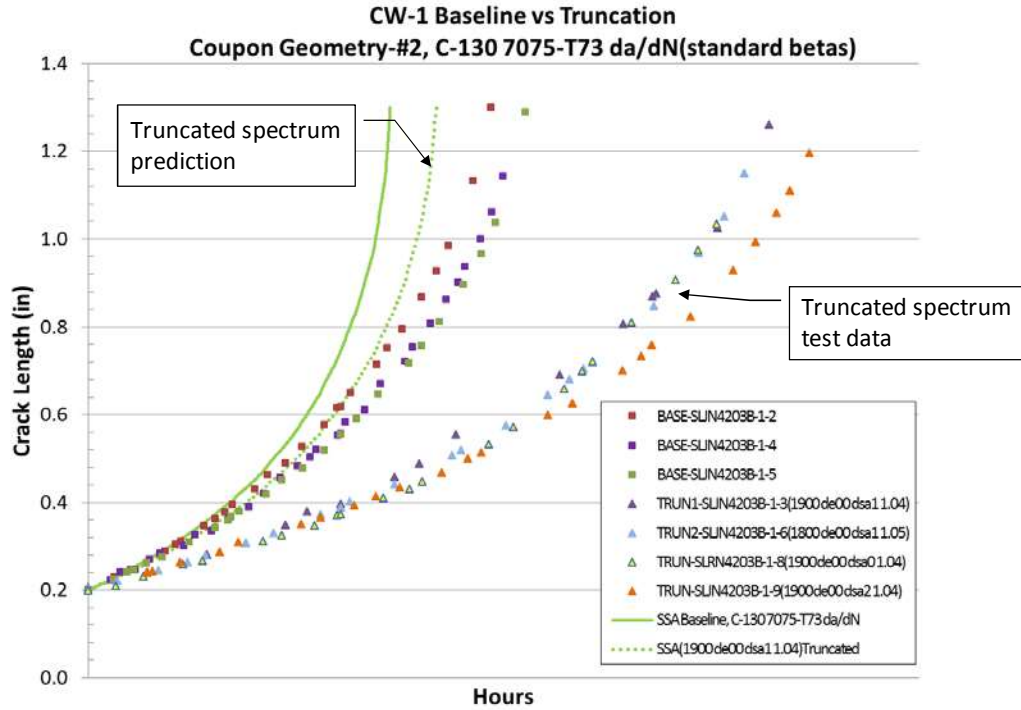


Coupon with hole & EDM notch



Typical Coupon Crack Growth Test

Figure 9.11-26. Coupon Testing



- Poor correlation between test and prediction

Figure 9.11-27. Initial Predictions and Test Results

- Tuned da/dN curve passes through data cloud

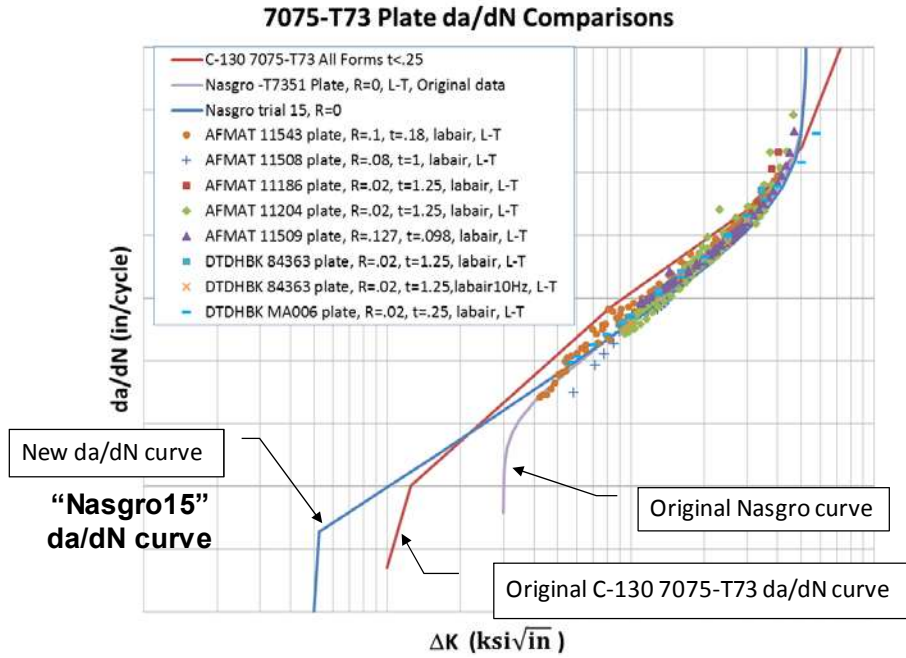
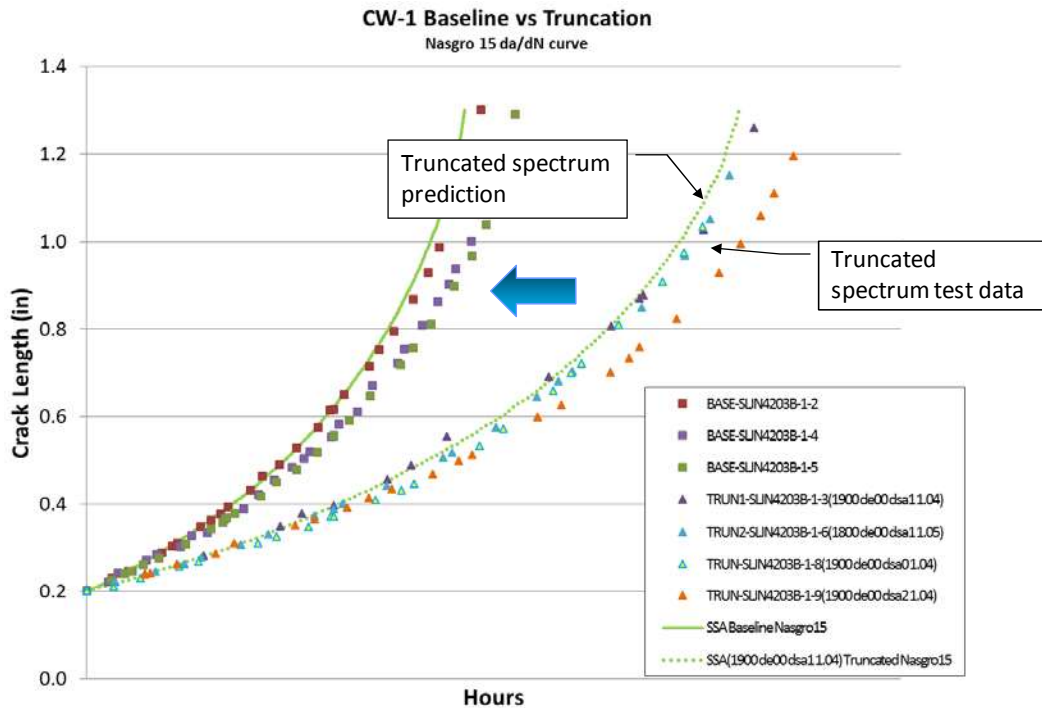


Figure 9.11-28. Material da/dN Evaluation



- Much better correlation but need more severity

Figure 9.11-29. New Prediction vs. Test Results

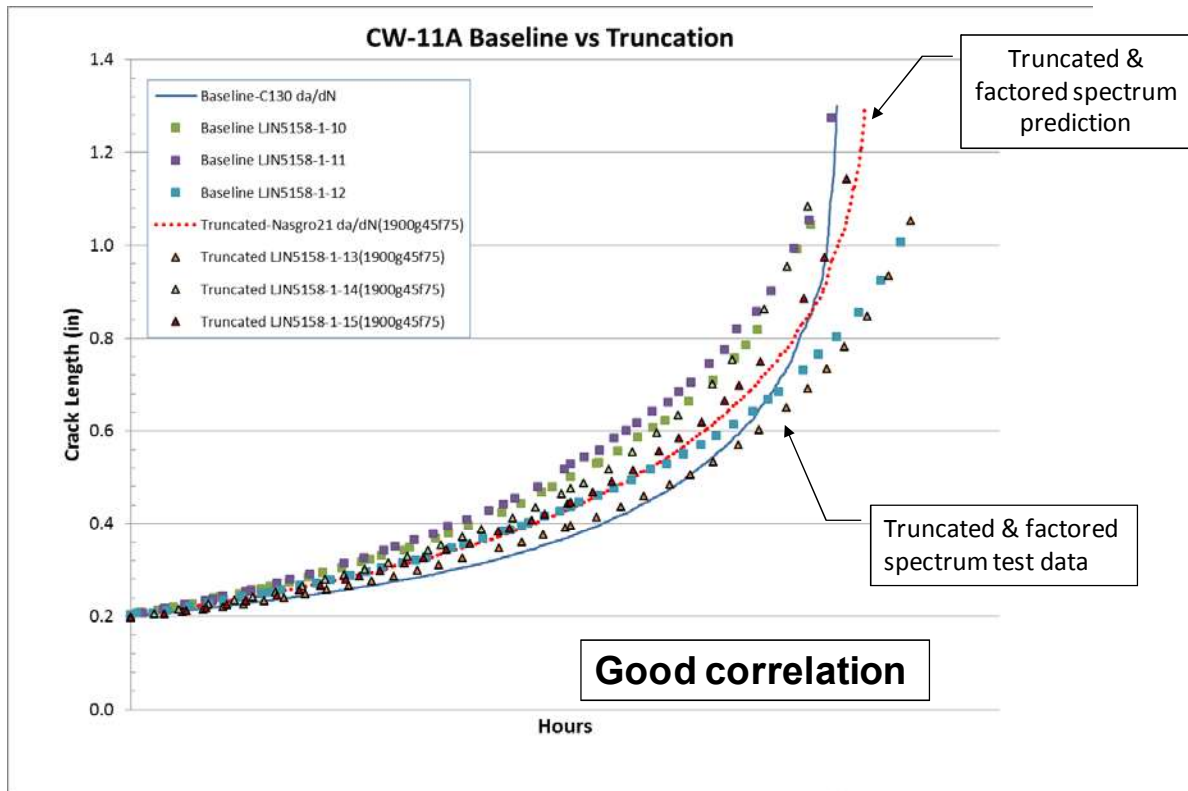


Figure 9.11-30. Baseline vs. Truncation Correlations

9.11.7. Long Term Viper: Flying the F-16 to 8,000 Hours and Beyond!

Kimberli Jones, Bryce Harris, Matt Regan, and Austin Rickards, USAF F-16 ASIP; Scott May and Kevin Welch, Lockheed Martin Aeronautics

The F-16 (Figure 9.11-31) is an important part of the aging United States Air Force (USAF) fighter inventory now and for the foreseeable future. However, with some aircraft nearing their service life limit, an Air Combat Command requirement was generated to create a program to extend the life of the Viper to a threshold of 10,000 hours, with a goal of 12,000 hours. To achieve this extended service life, a full-scale-durability test (FSDT) was conducted to identify structural modifications necessary to achieve the new service life (Figure 9.11-32). The FSDT reached the required test life of 24,000 Equivalent Flight Hours (EFH) in May 2015 to certify the 12,000 desired service life goal. Even though many areas of the FSDT aircraft were replaced and/or repaired during the test, there were no significant structural failures to signify the end of aircraft life. Therefore, an additional 3,200 EFH was applied to the test aircraft to further evaluate structural performance and extended life potential. Concurrent to the FSDT, the Service Life Extension Program (SLEP) was developed. This activity was critical for execution of a modification program (Figure 9.11-33) as soon as possible after test completion; once the FSDT teardown is completed and any additional findings identified for SLEP, the modification program can begin installation on the kit proof aircraft. This sequence of events minimizes the number of F-16 aircraft reaching the Certified Service Life (CSL) prior to SLEP full rate production capability, but may come at a price; concurrent activities may create a need to rework SLEP designed modifications due to findings in teardown. This technical effort provides the government perspective on F-16 life extension and fleet planning activities, with plans for implementing the FSDT results. Many of the test lessons learned with respect to future fleet management will be discussed.



Figure 9.11-31. F-16 Viper

- **FSDT reached 24000 EFH in May 2015**
 - 12k EFH life achievable, pending teardown results
 - No catastrophic structural failures, so test was continued for 2200 additional test hours (~3700 EFH)



Figure 9.11-32. Full-Scale Durability Test

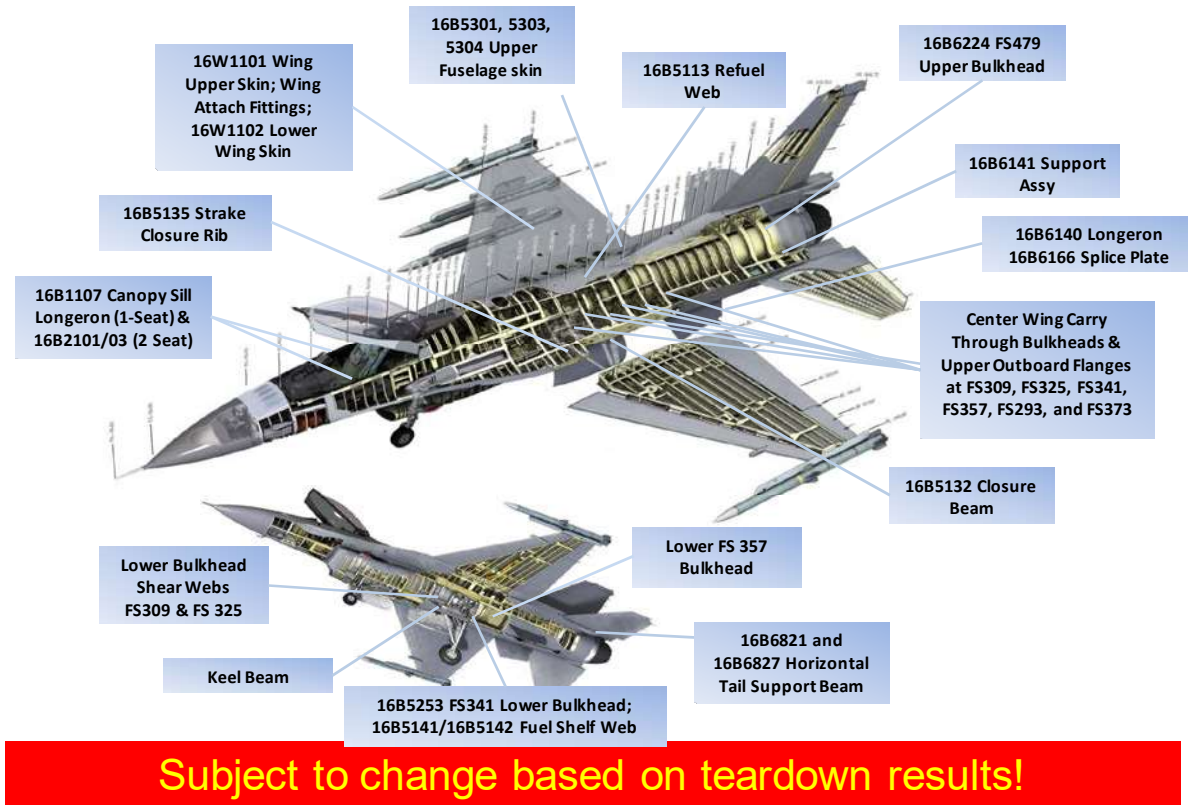


Figure 9.11-33. Current SLEP Modifications

9.11.8. F-16 Block 50 Full-Scale-Durability Test – Leveraging the Data

Keith Sundstrom, Lockheed Martin Aeronautics

The F-16 Program has recently completed its third Full-Scale-Durability Test. The current test was conducted in support of an extension of the Certified Service Life of the Block 40 and Block 50 configurations to 12,000+ hours. The test also provided data that will be used to support force management activities of the F-16 aircraft (Figures 9.11-34 and 9.11-35). These data include strain gage data (Table 9.11-1) recorded during the test, cracking data, fractography, and inspection methods and results. This information is valuable not only because it provides an insight of how the Block 50 aircraft structure ages but because it was generated under a known usage spectrum. This technical effort will focus on the different types of data collected during the Block 50 FSDT and how it will be used in the future to improve crack growth models, finite element models (Figure 9.11-36), risk analyses, and other fleet management tools.

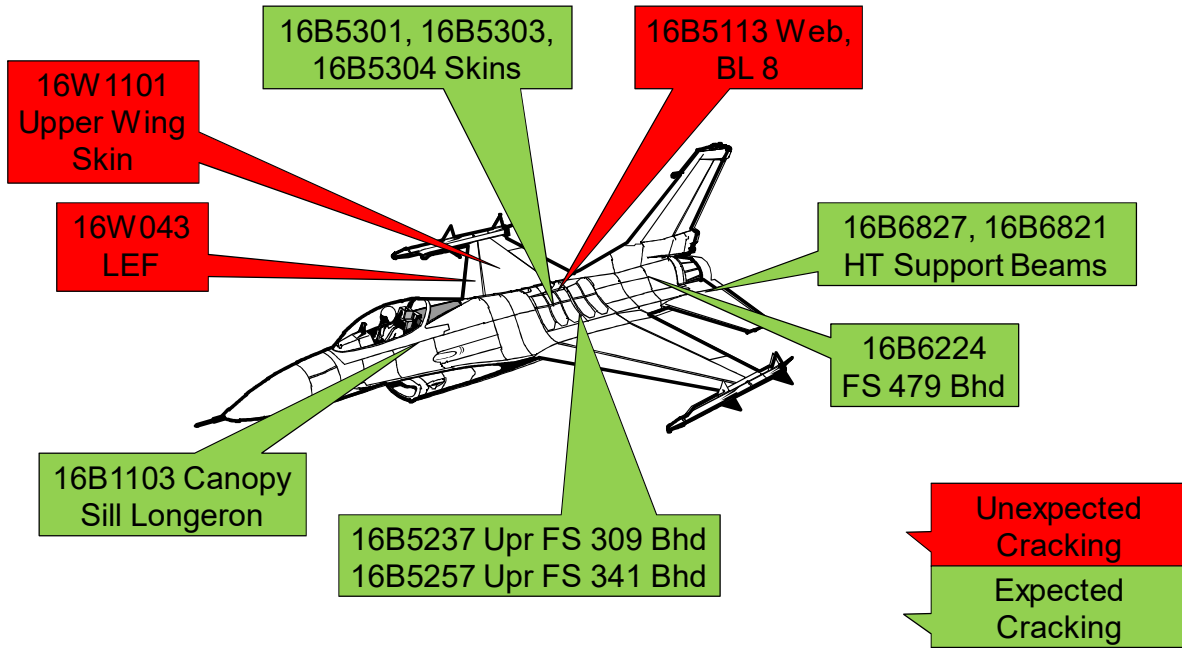


Figure 9.11-34. Significant Findings for Upper Fuselage

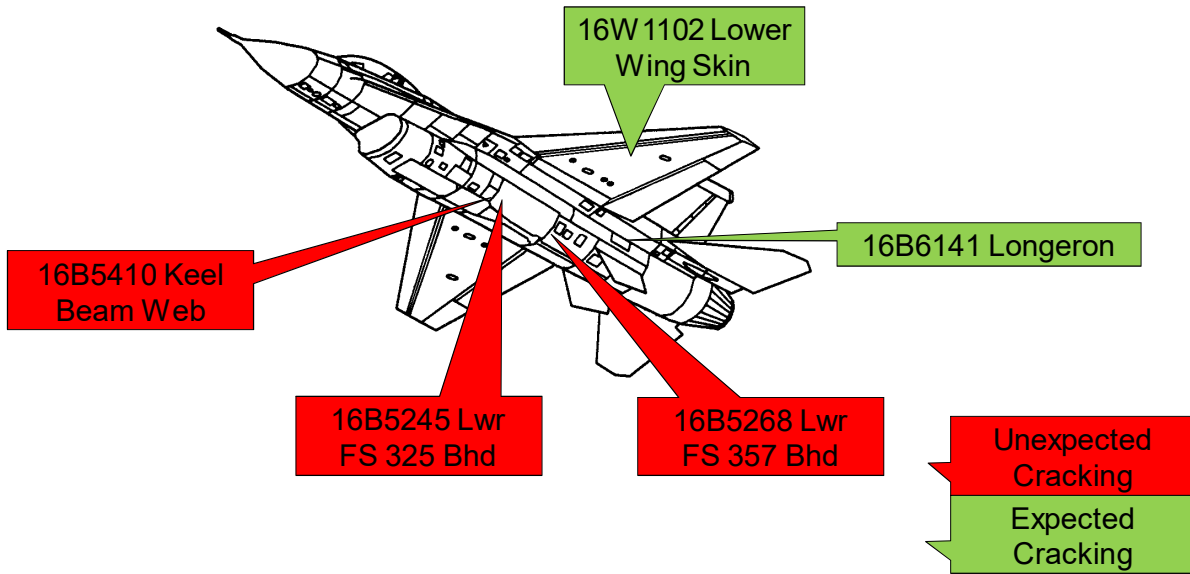


Figure 9.11-35. Significant Findings for Lower Fuselage

Table 9.11-1. Strain Gage Distribution

Summary	Axial Gages	Vesette Gages	Rosette Gages	Total Channels
Forward Fuselage	105	7	0	112
Center Fuselage	357	43	50	550
Aft Fuselage	176	120	10	326
Wing	192	0	80	432
Total	830	170	140	1420

- A unique airplane coarse grid finite element model has been developed to represent the FSDT article
 - Structural configuration
 - Loading configuration
- Finite element model to support initial evaluation and subsequent correlation effort

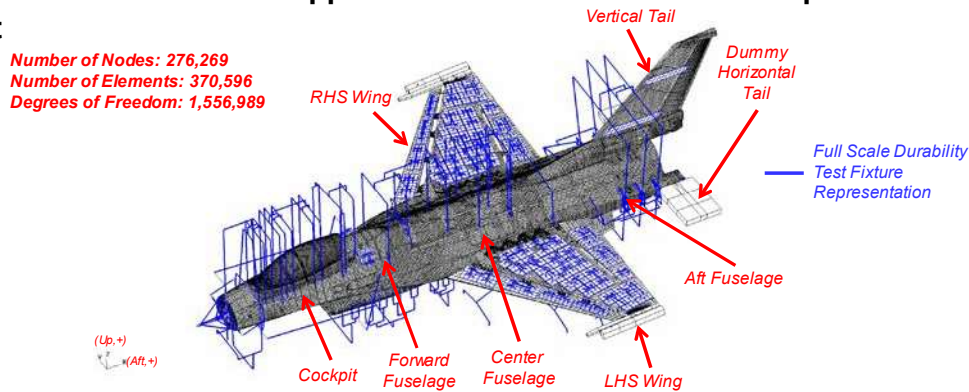


Figure 9.11-36. Course Grid Finite Element Model

9.11.9. The Evolution of the USAF Aircraft Structural Integrity Program

Dale Ball and Robert Burt, Lockheed Martin Aeronautics

The USAF Aircraft Structural Integrity Program came into being in 1958 after the loss of four B-47 aircraft due to structural fatigue. In its initial form, the ASIP called for all new aircraft to be designed using the safe-life approach, and for all existing operational aircraft to be subjected to a fatigue assessment, including a full-scale fatigue test. Eleven years after its inception, the loss of an F-111 led to the formulation of a new set of structural requirements based on fracture mechanics, and forced a major overhaul of the ASIP, both in terms of aircraft design and aircraft operation (Figure 9.11-37). In the 1970s and 1980s, damage tolerance requirements were imposed on new aircraft designs, and damage tolerance assessments were performed for existing USAF fleets. The F-16 was the first USAF aircraft produced in that time frame for which fracture-mechanics-based durability and damage tolerance requirements were a part of the initial design criteria (Figure 9.11-38). In the 1990s and early 2000s the ASIP was again re-evaluated, this time largely as a result of a commercial airliner incident (Aloha Airlines). This failure was found to be caused by the onset of widespread fatigue damage, which in turn was found to pose a significant threat to a large number of USAF aircraft, especially aging aircraft. As a result, the ASIP was again updated to ensure (among other things) that the onset of WFD was addressed

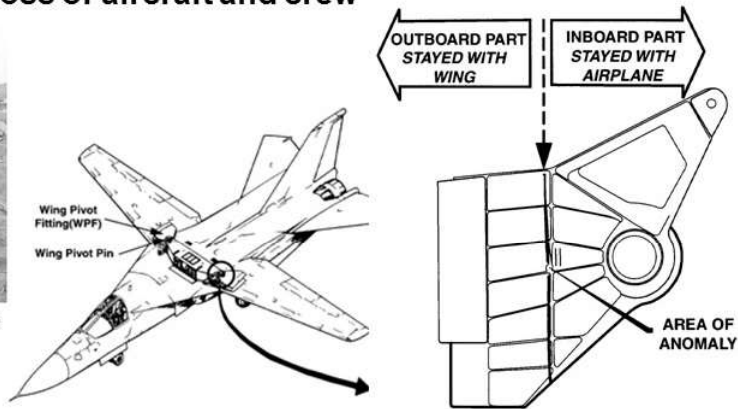
throughout the aircraft life-cycle. Now, in the latter half of the 2000s and during the 2010s, the efficacy of ASIP is again facing new challenges. In recent years both performance and affordability objectives have been forcing aircraft OEMs to consider the use of advanced materials and manufacturing processes for new designs. Many of these new materials, structural concepts and manufacturing techniques lead to damage behaviors that are not well treated using current (existing) analysis tools, and therefore may not be adequately managed by the ASIP in its current form. This has led to another detailed evaluation and update of the ASIP standard, as the USAF attempts to ensure durability and protect safety in the face of rapid structures technology advances. In this technical effort we will discuss the evolution of the ASIP with particular reference to four major fighter aircraft programs. The F-111 provides a prime example of the influence of the original, safe-life-based ASIP on structural design, and was the harbinger of the new, fracture mechanics based requirements to come. The F-16 is the quintessential example of the spectacular success that the USAF ASIP paradigm (which addresses all phases of the product life cycle) has had in protecting flight safety. And finally, the F-22 (Figure 9.11-39) and F-35 (Figure 9.11-40) programs provide examples of the challenges that rapid structures technology advances present to the ASIP and its ability to regulate air vehicle development and management.

F-111AAP#94 WPF FAILURE:

- **Lower plate of wing pivot fitting (WPF) failed during weapons delivery training mission, 22 Dec. 1969**
- **Aircraft had 105 accumulated flight hours**
- **Failure resulted in loss of aircraft and crew**



Left wing of AP#94 at crash site



Location of 'ROGUE' flaw that caused loss of aircraft

Figure 9.11-37. F-111 Limitations of Safe-Life Design



Figure 9.11-38. F-16A Full-Scale Fatigue Test



Figure 9.11-39. F-22 Full-Scale Fatigue Test



Figure 9.11-40. F-35A (CTOL) Full-Scale Fatigue Test

9.11.10. A-10 ASIP Adaption to Digital Data; Tactical Advantages, Lessons Learned and Future Plans

Hazen Sedgwick, USAF A-10 ASIP

There are many complexities when dealing with an aging fleet of aircraft like the A-10. To help reduce some of those challenges, the A-10 (Figure 9.11-41) program office has chosen to transition into a Product Lifecycle Management (PLM) environment to more effectively handle the intricacies of an aging fleet. A large part the PLM effort is to develop methods to capture digital maintenance data and use solid models in place of the traditional 2D part drawings. Presently the A-10 program is one of the leaders demonstrating the use of digital data to monitor and effectively communicate engineering decisions in support of the Aircraft Structural Integrity Program (ASIP). The A-10 program is developing digital tools that have already enabled the ASIP engineers to react quickly to individual aircraft issues and determine if fleet wide mitigation is necessary. This rapid response is due to several factors, some of which are: -The organic analytical capability of the A-10 ASIP team. -Owning the technical baseline and knowing how to apply it. -Moving to a Model Based Definition (MBD) environment and a fully digital data environment. -Controlling the data within a PLM scheme -Developing new tools to assist maintainers to produce valid data that is quickly assessable to the ASIP manager. Although the progression towards a digital solution for maintenance data collection, rapid engineering response and Risk Based Induction (RBI) has already shown significant benefit and cost savings to the A-10 program, there is still work to be done before fully deploying the new system to all aspects of maintenance. This technical effort will discuss: -A brief history and description of the organic capabilities of the A-10 ASIP team (Figures 9.11-42 through 9.11-46). -A brief overview of the USAF's vision for enabling a digital data environment and how the A-10 is leading this effort. -Implementation and current status of MBD within a PLM environment (Teamcenter). -Implementation and current status of a visual data communication tool (NLign) (Figure 9.11-47). -An example of using the current digital data environment to support fleet safety, cost and time savings for a 2016 mishap. -Lessons learned with the development and roll out of the PLM strategy and digital data collection. -Future efforts for progressing the digital environment.

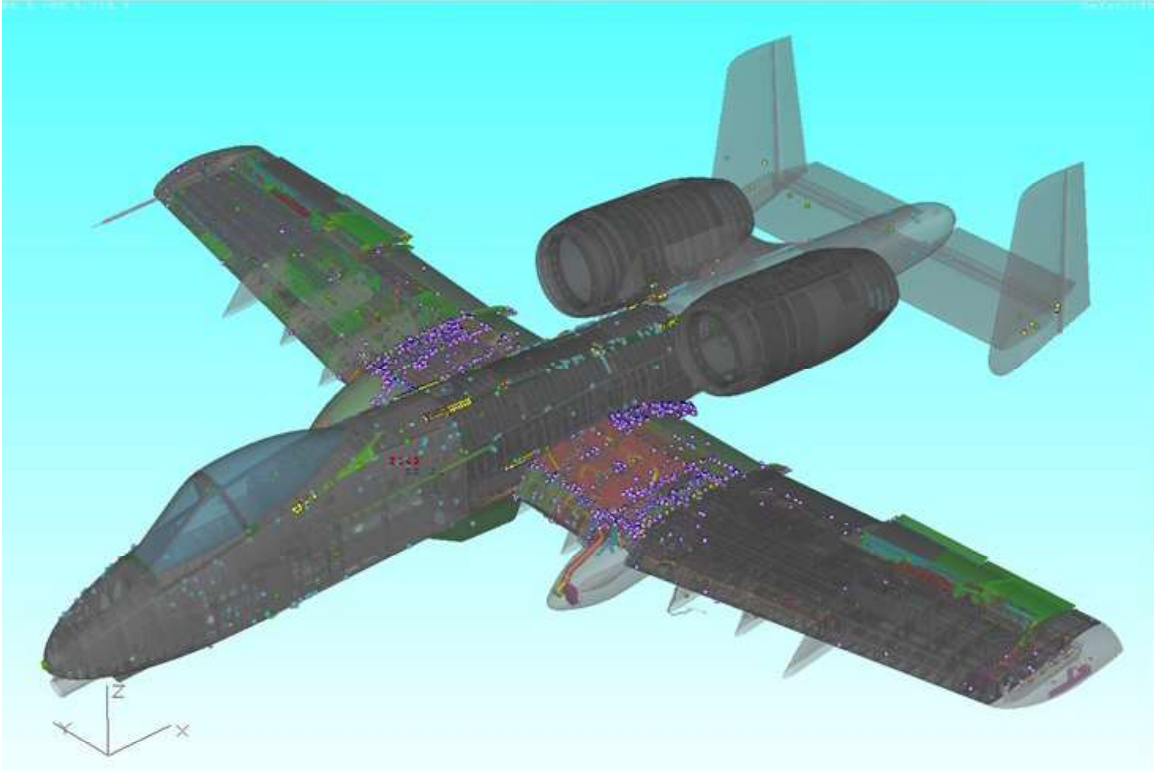


Figure 9.11-41. A-10 Aircraft

- 3D CAD NX & Teamcenter
- Finite Element Analysis (FEA)
 - Detailed Finite Element Model (FEM) inserted into a global loads FEM
 - Boundary conditions more accurately simulated
 - Strain gauge validated

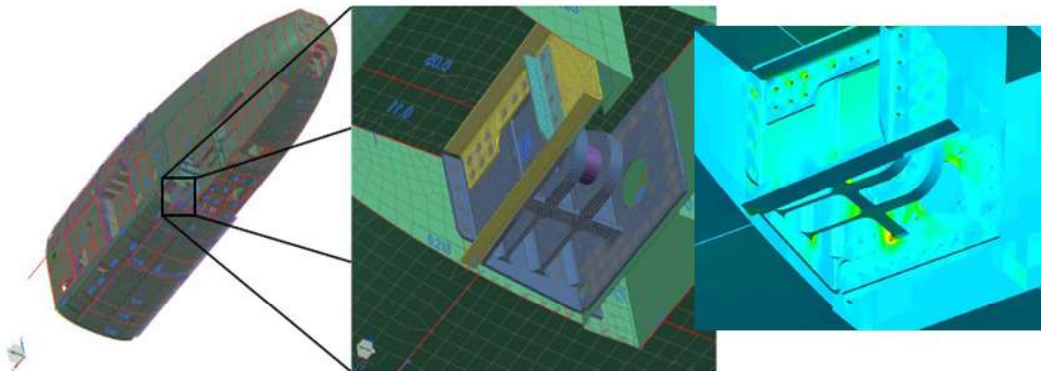


Figure 9.11-42. Finite Element Analysis (FEA)

- **FEA load distribution**

- **Baseline structure and repair configuration**
- **Fastener loads**
- **Contact surfaces**
- **Load re-distribution with crack propagation**

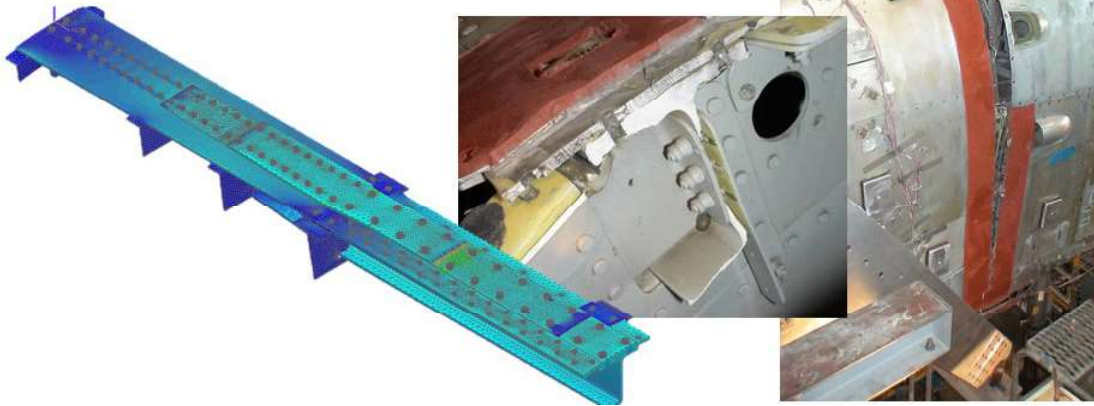


Figure 9.11-43. FEA Load Distribution

- **Stress intensity solution – StressCheck**

- **Unique Geometry/Loading not represented by standard solutions**

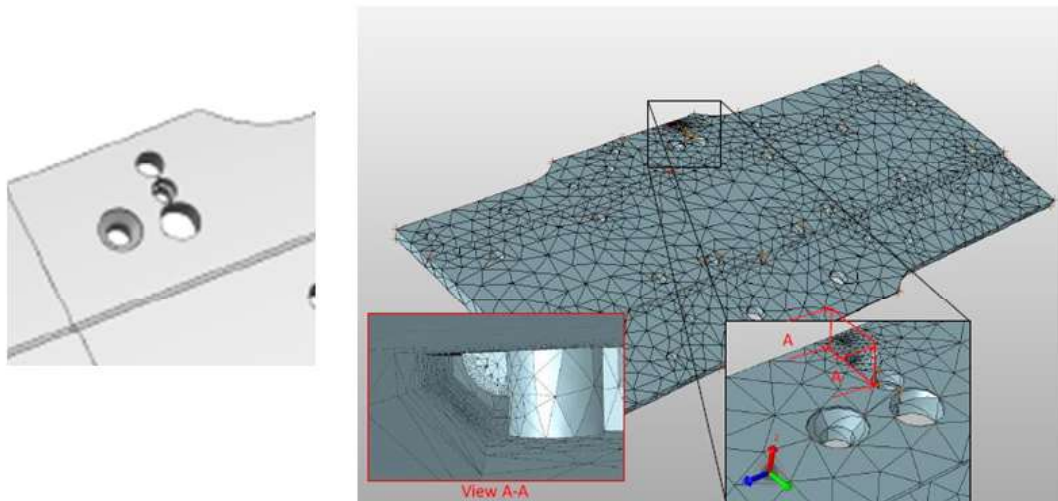


Figure 9.11-44. Stress Intensity Solutions

■ **Damage Tolerance Analysis (DTA)**

- AFGROW, StressCheck, BAMF

■ **Technical data required for organic DTA**

- Usage Data / Loads / Stress Analysis → Stress Spectra
- Material Data
 - Crack Growth Rate Data
 - Spectrum Testing

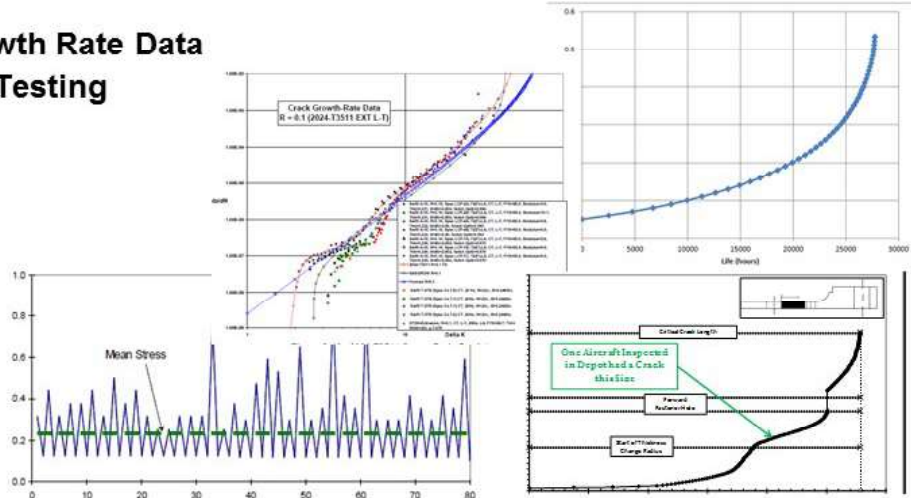
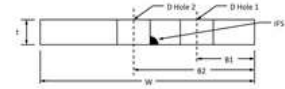


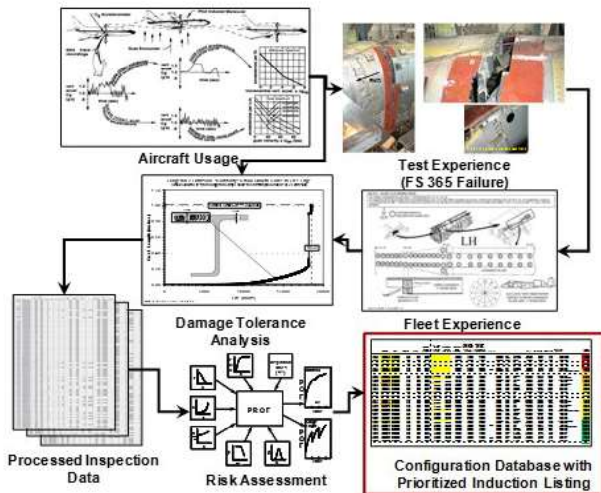
Figure 9.11-45. Damage Tolerance Analysis (DTA)

■ **Fleet health – PROF**

- Update 11/2015

■ **Risk based induction**

- Condition and need



■ **Fleet risk assessments**

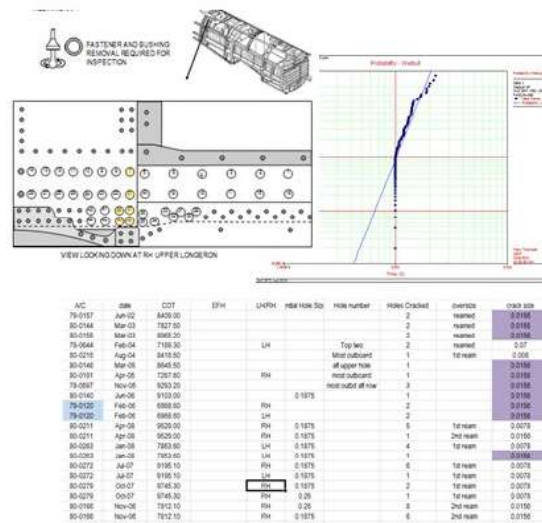


Figure 9.11-46. Risk Analysis

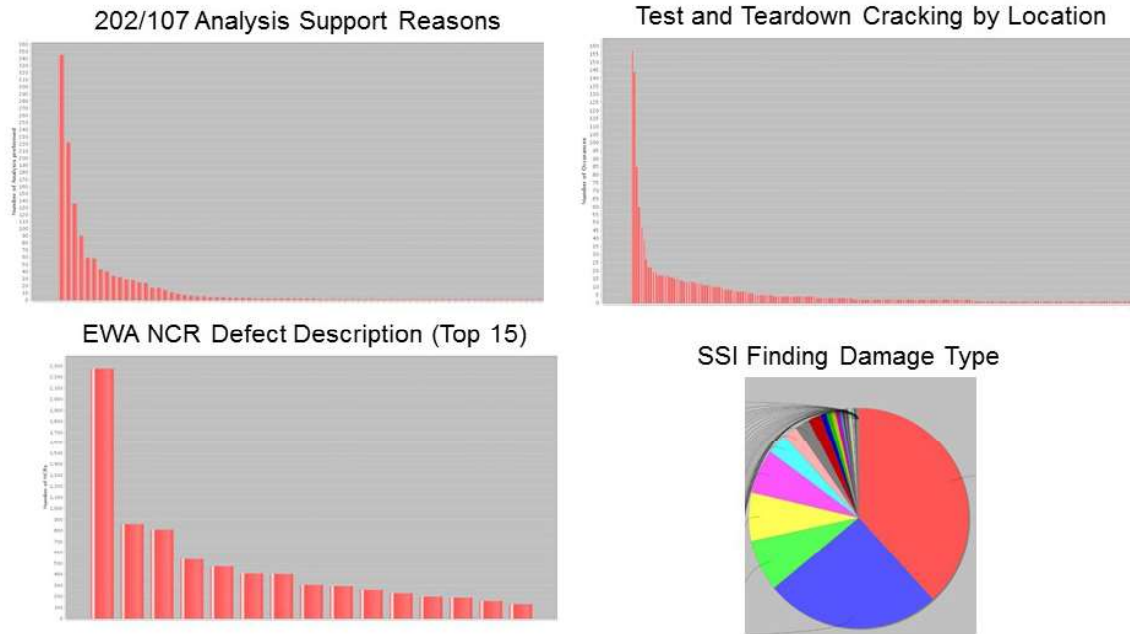


Figure 9.11-47. NLog Interaction Tool

9.11.11. F-35 Lightning II Joint Strike Fighter Full-Scale Durability Tests

Selen Minarecioglu, Lockheed Martin Aeronautics

Durability tests and correlation of structural analysis to test findings is a key component of the F-35 Lightning II Joint Strike Fighter Aircraft (Figure 9.11-48). Structural Integrity Program as well as Structural Certification. Full-scale airframe and horizontal and vertical tail component durability tests are being performed for each variant as part of the System Development and Demonstration phase (Figure 9.11-49). This technical effort will provide an overall status of the F-35 Lightning II Joint Strike Fighter full-scale airframe and component level durability testing. In addition, this technical effort will provide an overview of the real-time and daily-trend monitoring systems employed to protect the safety of the full-scale airframe durability test articles (Figures 9.11-50 and 9.11-51). The technical effort will also show the full scale airframe durability test article management through trend-based inspections. The trend-based inspections are being leveraged as a replacement to planned inspections to maximize the budget available for 3rd lifetime testing planned for the F-35 Lightning II Joint Strike Fighter variants.



Figure 9.11-48. F-35 Aircraft

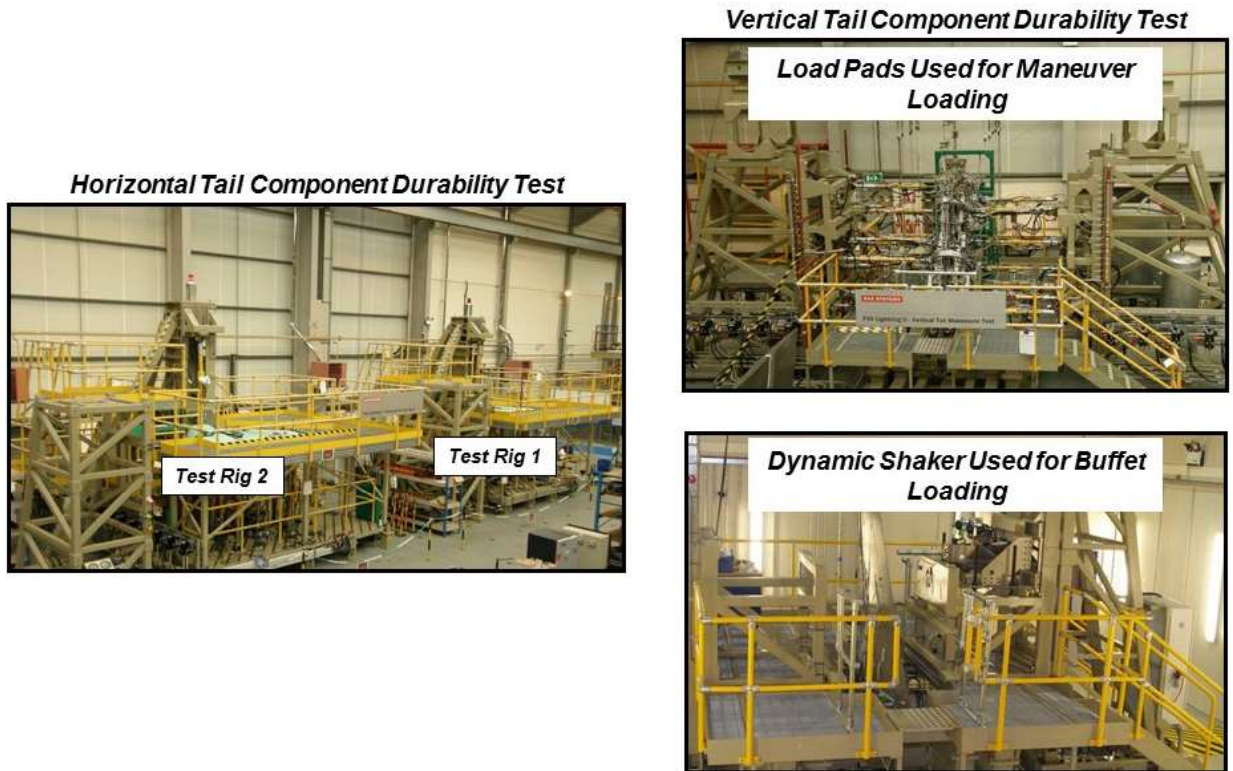


Figure 9.11-49. Horizontal Tail and Vertical Tail Component Durability Test Arrangement

FS 472 Bulkhead - View Looking Forward, LHS

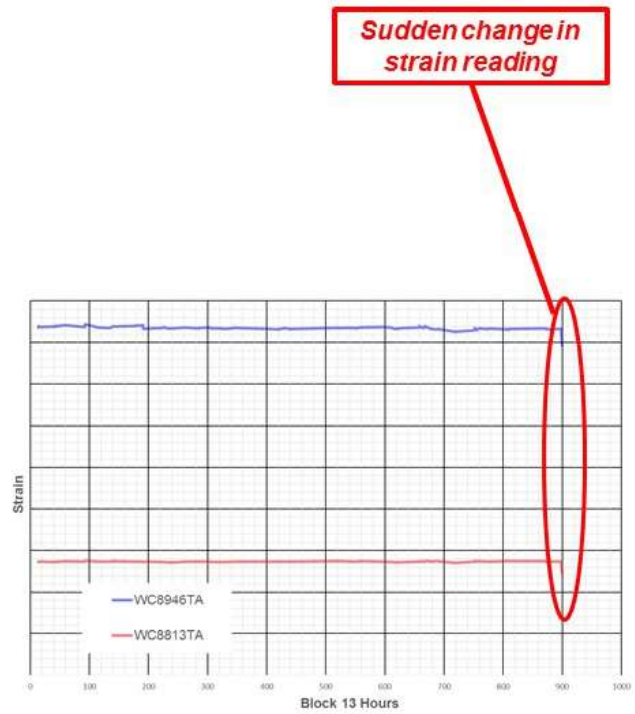
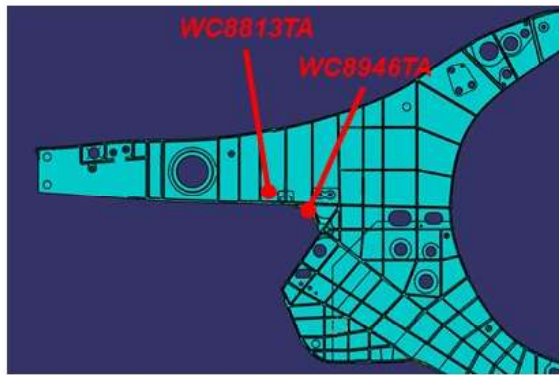


Figure 9.11-50. Real-Time Trend Monitoring Example

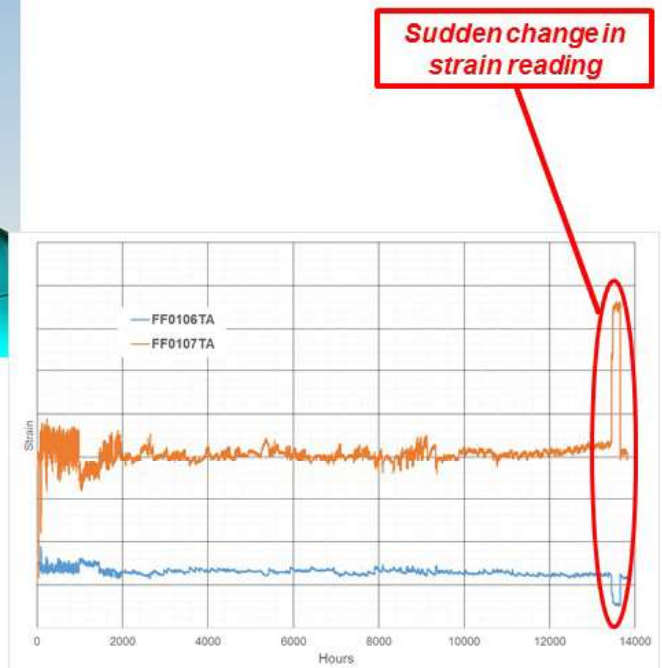


Figure 9.11-51. Daily Trend Monitoring Example

9.11.12. T-38 Full-Scale Fatigue Test of Two Legacy Wings (Milling Away at Durability Correlations)

David Wieland, Jon Cutshall and Clint Thwing, Southwest Research Institute; Mike Fallert, Sabreliner Aviation; Michael Blinn, USAF T-38 ASIP; James Greer, USAFA - CAStLE

The USAF/CAStLE/Sabreliner/SwRI team recently completed a project to perform two T-38 legacy (-29) wing full-scale fatigue tests (Figure 9.11-52). The overarching goals of the project were as follows: 1) determine the -29 wing's test demonstrated life for two unique usages (Figure 9.11-53) and 2) to determine the number of wings that will need to be purchased over the next 10 to 15 years. Further, results of the -29 wing fatigue testing, teardown, and analyses provide a valuable update to the baseline for continuing development of field-level repairs (Figure 9.11-54) and for the service replacement criteria. A big part of the project was to include both Introduction to Fighter Fundamentals (IFF) and Specialized Undergraduate Pilot Training (SUPT) usages. These two usages (one severe and one moderate) comprise the majority of the actively flying T-38 fleet. This technical effort will discuss the full-scale fatigue testing results of two T-38 -29 wings, lower wing skin milled pocket challenges, NDI improvements, durability correlation, and wing availability impact. As a capstone to this technical effort, one of the major findings of the -29 wing fatigue testing was a new fatigue critical location (FCL) at an inboard milled lower wing skin (LWS) pocket (Figure 9.11-55). While cracking at outboard milled LWS pockets are a known concern, cracking at the inboard pockets had not been manifest in the T-38 fleet. The technical effort will briefly discuss the problem, durability correlation to test results (Figures 9.11-56 and 9.11-57), NDI improvements, and fleet inspection results.



Figure 9.11-52. Whiffletree Design

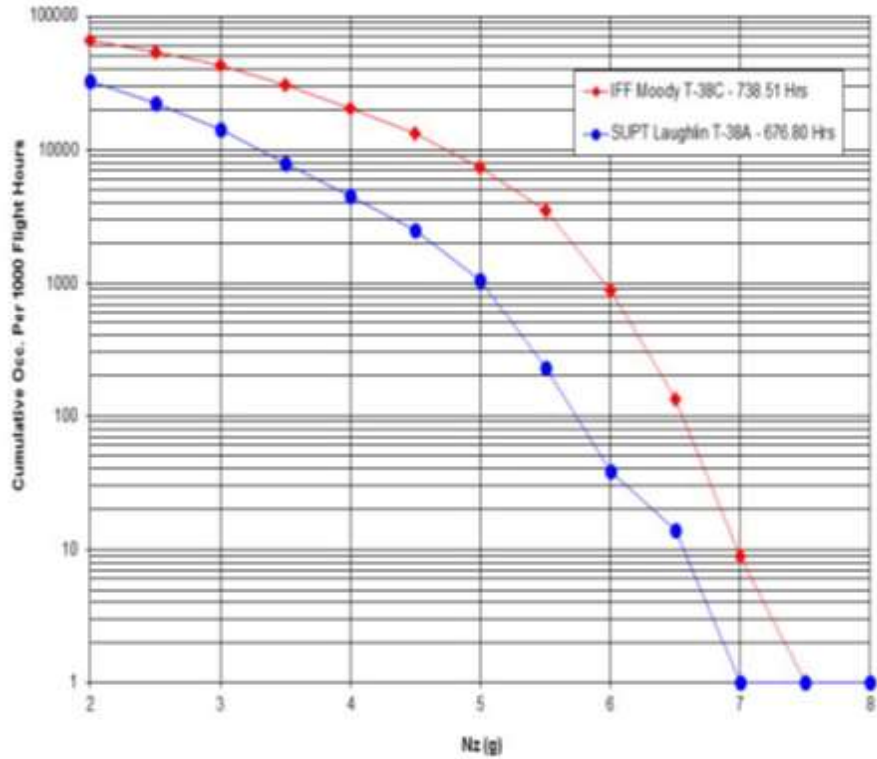


Figure 9.11-53. Two Unique Usages

- **Bonded repairs installed at 9,000 hours**
- **Picture on the left shows AFRL's curing of the bonded repair**
- **Picture on the right is the strain-gaged bonded repair**

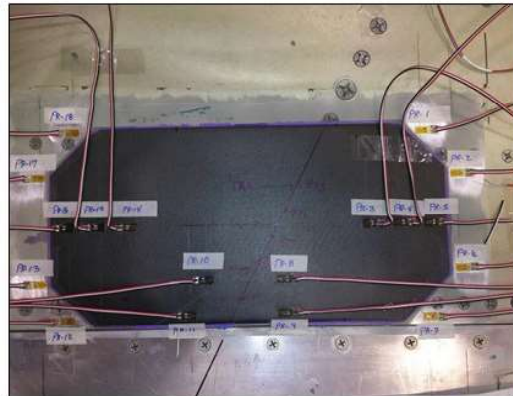
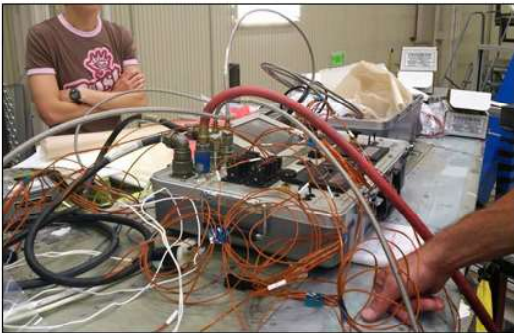


Figure 9.11-54. Repairs

IFF -29 Wing Fatigue Testing Major Results:

- A crack nucleating from the milled pocket at a new FCL location on the right side
- The constraint conditions for the wing test were then modified in order to continue testing on the left side only
- After an additional 370 hours, a crack beginning at the milled pocket near the new FCL on the left side; crack reached critical length and failed the wing box
- Picture of the crack nucleation area is shown below



Figure 9.11-55. New Fatigue Critical Location (FCL)

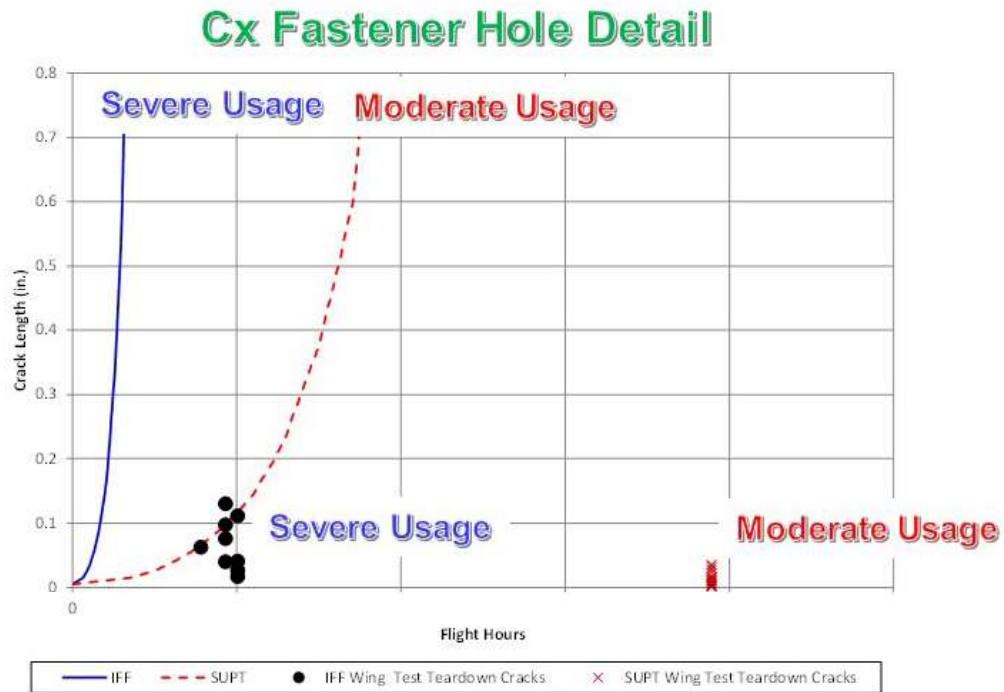


Figure 9.11-56. Durability Correlations for Cold-Worked Holes

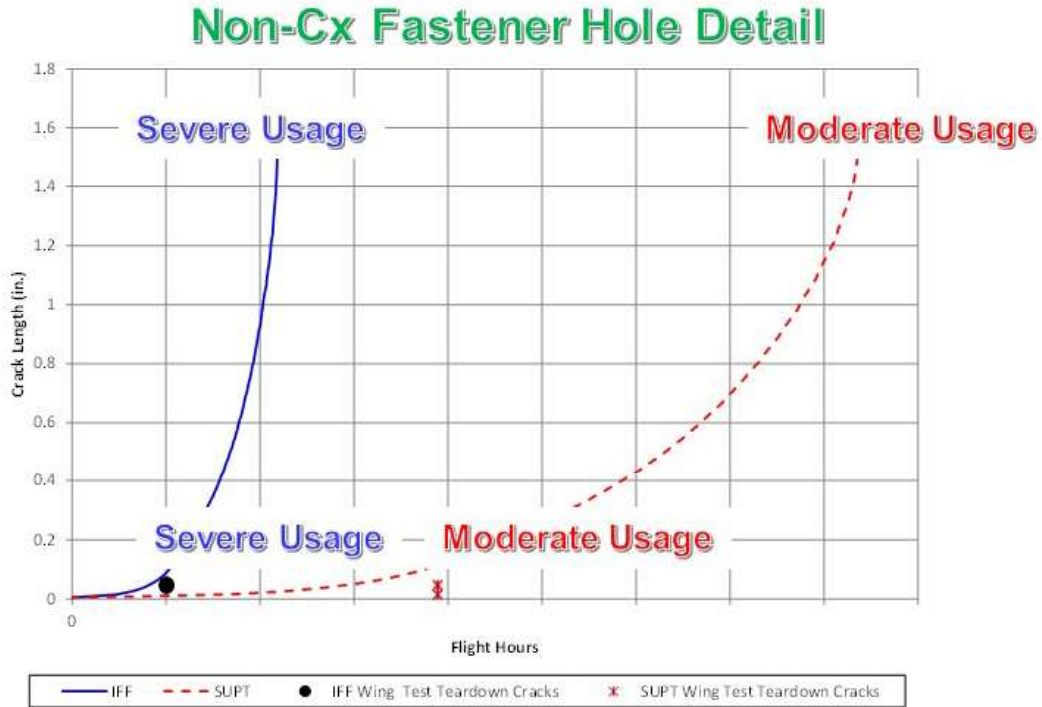


Figure 9.11-57. Durability Correlations for Non-Cold-Worked Holes

9.11.13. F-16s Fly with Cracks? Safely Dealing with the Reality of an Aging Airframe

Bryce Harris and Kimberli Jones, USAF F-16 ASIP; Kevin Welch, Lockheed Martin Aeronautics

The flight hours and maneuvers continue to accumulate on the proven and venerable F-16 airframe with a large worldwide fleet (Figure 9.11-58), decades of service life, and over 15 million worldwide flight hours. A crack database centralized at Lockheed Martin Aeronautics in Fort Worth, Texas has amassed over 9,000 structural cracks, covering nearly every significant piece of structure on the aircraft. The F-16 ASIP is robust and has been active since the early damage tolerant design phase of the F-16. This focused cognizance of the health of the airframe has resulted in an excellent understanding of the varying degrees of criticality for each different location on the airframe prone to fatigue, corrosion, and other damage (Figure 9.11-59). Notably, not all damage is found on critical structure or in critical locations. Sometimes damage can be categorized as “nuisance cracking,” or cracks that can be left in the structure unrepaired with continued operations and no flight restrictions. However, a sound understanding of the safety implications of that course of action is necessary prior to allowing continued flight operations. Examples of contributing factors that can reduce or control the safety risk are very large damage tolerant capability, fail-safe capability with a large Fail Safe Life Limit, low criticality or benign fracture consequences, etc. Detailed risk analysis also contributes by quantifying the probability of fracture, including the effects of Non-Destructive Inspections and associated intervals (Figure 9.11-60). Damage repair or component replacement requirements can have significant impacts to fleet operations and aircraft availability. Frequently it is very desirable, if possible, to delay the need for repairs in order to accomplish the planned missions, especially when damage is found on a high percentage of aircraft. This technical activity will detail some well-known areas of damage on the F-16 structure where cracks can be safely flown while minimizing fleet impacts. The benefits and significance of such an approach will be highlighted. A conclusion is that much of the F-16 fleet is likely flying with cracking/damage in

non-critical locations. It can be inferred that any given fighter aircraft fleet similar in metallic design and age to the F-16 likely has a sizeable population of cracks present in a significant percentage of the fleet.

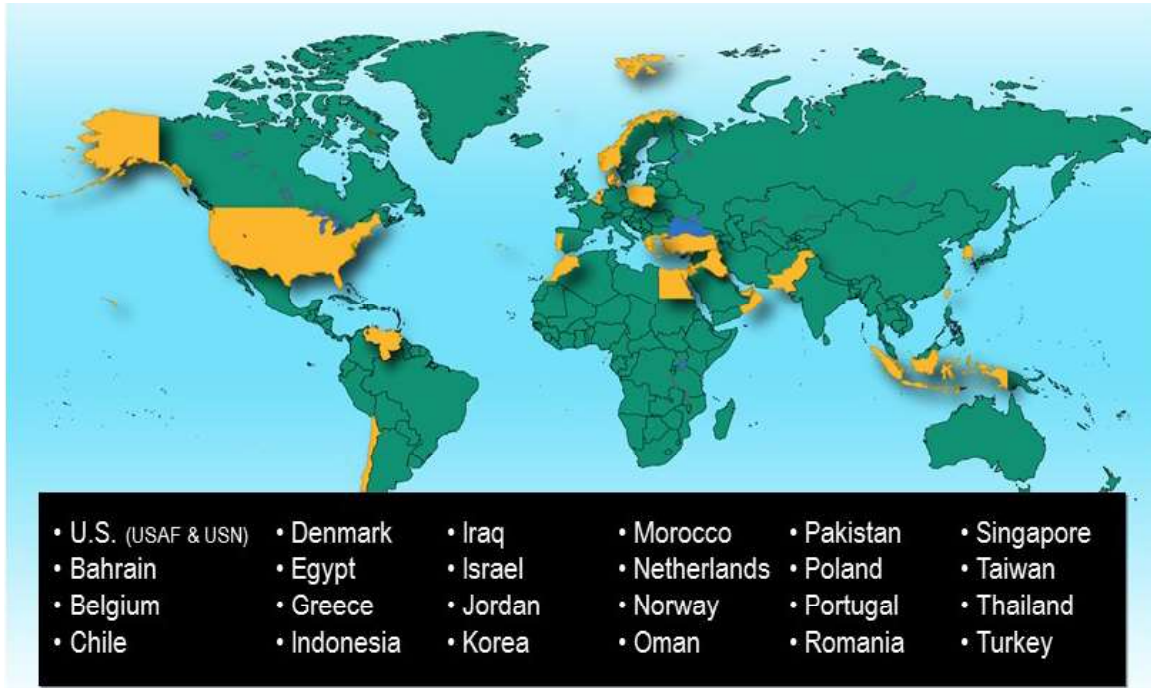


Figure 9.11-58. 24 Countries in Sustainment Program

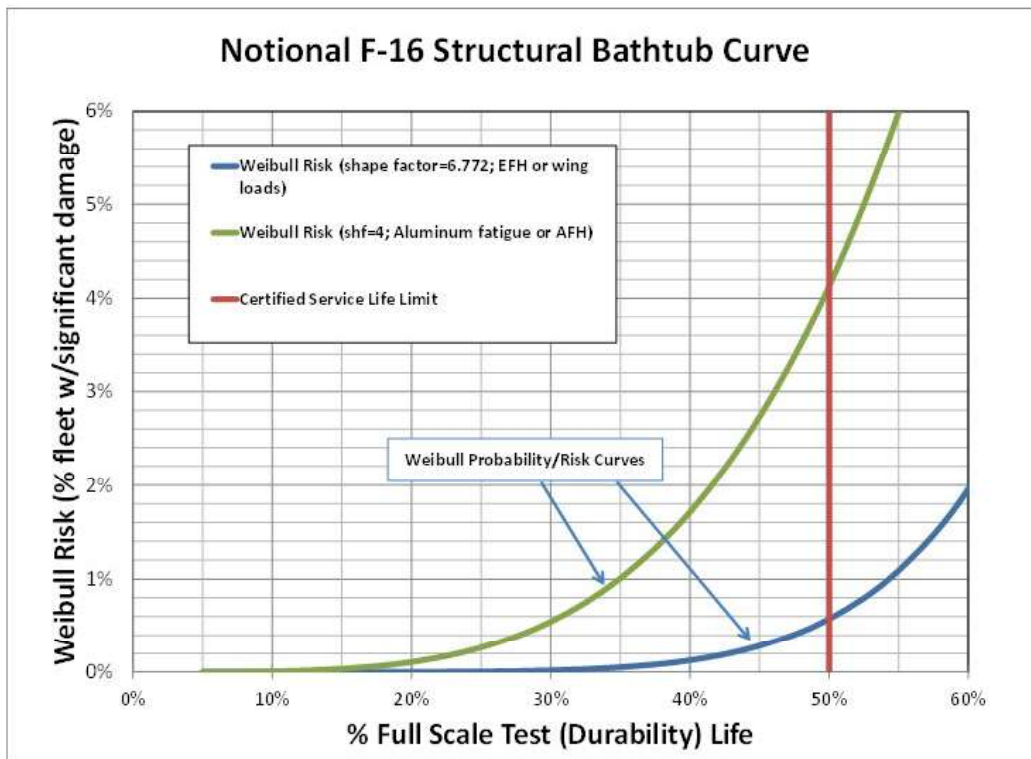
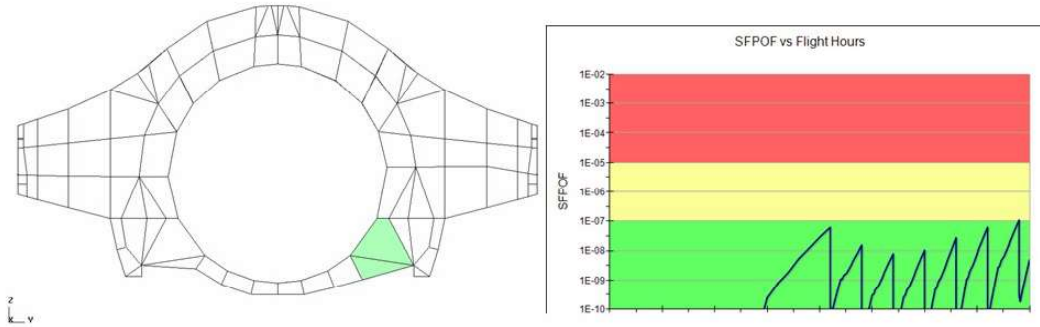


Figure 9.11-59. Challenges Come with Age



- **Fail-Safe capability if bulkhead and strap both severed**
 - Strap cracks have never been detected via NDI
 - Most a/c not yet at Fail Safe Life Limit (FSLL)
- **Safety is controlled with frequent NDI and recurring visuals**
 - Inspection method painstakingly tailored; bolts installed, nuts removed

Figure 9.11-60. FS337 Bulkhead – Risk Controlled

9.11.14. Structural Integrity in Aging USAF Landing Gear

Andrew Clark, USAF Sustainment Center

Landing gear (Figures 9.11-61 and 9.11-62) is generally under-represented as a topic in aircraft structural integrity discussions. The purpose of this technical activity is to highlight what the USAF supply chain is doing to ensure landing gear structural integrity is maintained as airframes age and landing gear is reworked during depot overhaul. Topics will include landing gear integrity approach, tools and methods used to address specific structural issues in landing gear, new technology that is being used or is being researched to aid in building surface coatings back, corrosion preventive coatings, and extension of landing gear service life.



Figure 9.11-61. Landing Gear



Figure 9.11-62. Supported USAF Systems

9.11.15. Expanded Dent Limits for C-5 Honeycomb Panels

Stefan Delin, Drew Bishop, and Matthew Harvey, Alion Science and Technology; David Wilkinson, C-5 ASIP

The aging USAF C-5 Galaxy (Figure 9.11-63) aluminum honeycomb panels require ever-increasing maintenance due to an extended service life and the demanding operational environment. Serving as primary and secondary structure on both the exterior and interior of the aircraft, these panels generally comprise aluminum facesheets and aluminum honeycomb cores. The Advanced Materials, Manufacturing and Testing Information Analysis Center (AMMTIAC) operated by Alion Science and Technology was tasked by the C-5 System Program Office to expand existing negligible damage limits for dents in these panels throughout the entire aircraft, with the objective of reducing maintenance efforts and expense. This technical activity reports the final deliverables of the completed C-5 Dent Limits Expansion program with emphasis on the new results achieved. The three-year program was organized as a three-phase approach, consisting of: Phase 1 - Alion created a database, which identified, categorized, and documented all C-5 aluminum honeycomb panels based on certain physical, structural characteristics, and specific locations of the aircraft. This deliverable encompassed 525 drawings, 2,749 panel dash numbers, and 3,864 panel configuration variations. Phase 2 - An innovative strategy to achieve significant data simplification was created in order to optimize the dent expansion engineering effort. All the panels were classified into 22 groups for analysis purposes, based upon geometry, materials, and loads. This allowed for generation of group-specific Finite Element Models (FEMs) (Figure 9.11-64), analysis methodology based on a single dent, and test criteria for model validation. Phase 3 - During the final phase, the analysis methodology was improved for two-dent simulation and implemented for the 22 dented panel groups. This methodology consisted of a structured multi-criteria finite element analysis algorithm for generation of expanded dent limits. It calculates single-dent parameters and dent separation constraints for multiple dents, as specified in Technical Order (TO) 1C-5A/M-3 for the panel index groups. Based on the assessment of the dented panel residual strength, the methodology quantifies the ability of a structural panel to withstand the aircraft loads with an adequate safety margin reserve. The methodology uses an enhanced version of the elastic criteria established in the C-5 legacy stress reports. Specifically, it defines a plasticity threshold marking the onset of plastic strain field growth, against which the panel stress response in a dented configuration can be compared. An essential and challenging part of the program was verification and validation of the analytical methodology (i.e., the FEMs) used to calculate the expanded C-5 dent limits (Figure 9.11-65). Model validation was achieved by correlating physical test (Figure 9.11-66) and analytical results for 10 representative panel groups, guided by the approach defined in ASIP Structures Bulletin EN-SB-11-001. A graphical method for documenting and seamlessly integrating new expanded dent limits into the C-5 structural repair TOs was also developed and delivered. On average, the dent limits expansion for C-5 aluminum honeycomb panels exceeds 500% (Figure 9.11-67). The successful implementation of the proposed expanded limits for allowable dents in TO's 1C-5A-3 and 1C-5M-3 will result in fewer panel repairs / replacements while maintaining the safety and mission readiness standards of the C-5 fleet.

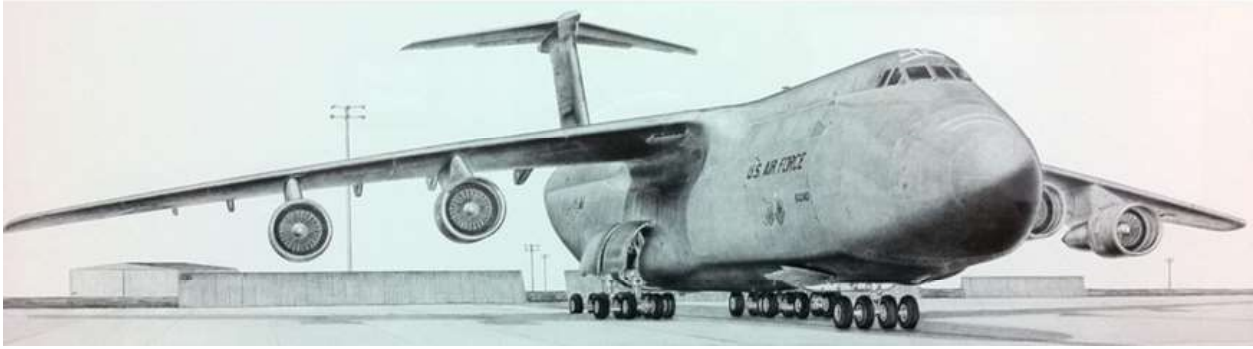
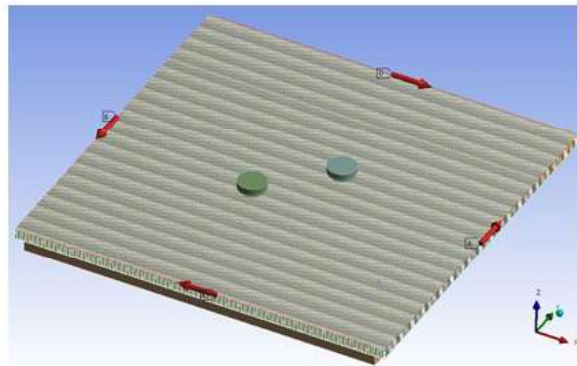
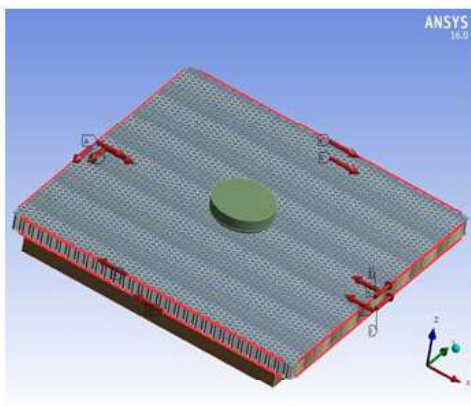


Figure 9.11-63. C-5A Galaxy



- Damaged honeycomb residual strength assessed using various FEM's
- 10"x10" models simulate single dent damage and typically comprise about 250,000 nodes and 300,000 elements
- 20"x20" models simulate 2-dent and 4-dent damage and incorporate about 850,000 nodes and over 1,200,000 elements

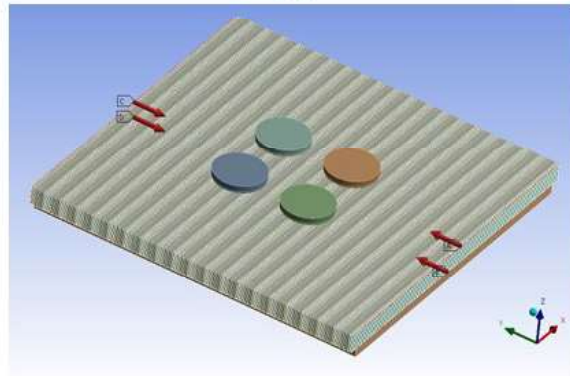
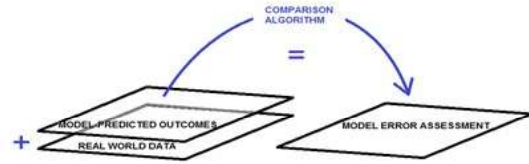


Figure 9.11-64. FEM Generation and Analysis

- How reliable and consistent is the predictive ability of the FEM?
 - Verification - Establish correctness of computational methodology
 - Validation – Define reliability of a specific model by comparing predictions to real-world observations



"Remember that all models are wrong; the practical question is how wrong do they have to be to not be useful."
 - Box, G. E. P., and Draper, N. R., (1987), Empirical Model Building and Response Surfaces, J Wiley & Sons, New York, NY.

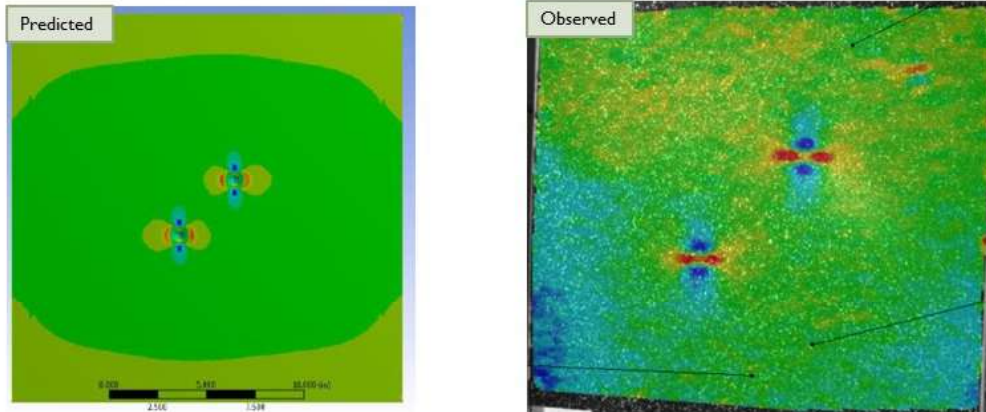


Figure 9.11-65. FEM Verification and Validation

Testing... in order to validate FE models and methodology

- Design and build test coupons
 - Biaxial (In-Plane) and Bending (Out-of-plane)
- Develop achievable "Lab Load" conditions
- Develop Test Plan
- Build 100 test coupons
- Perform Tests

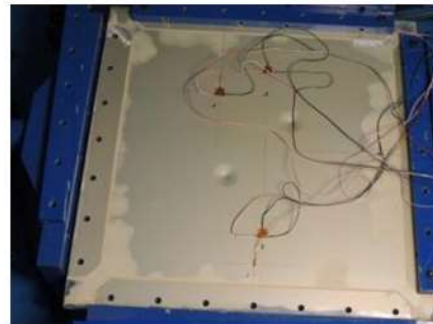
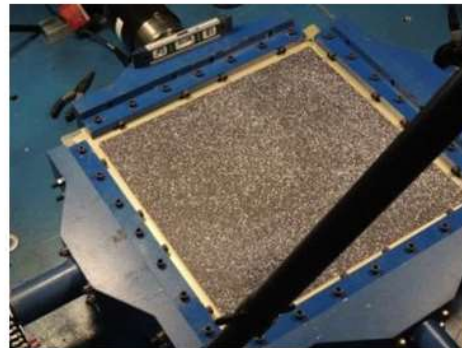
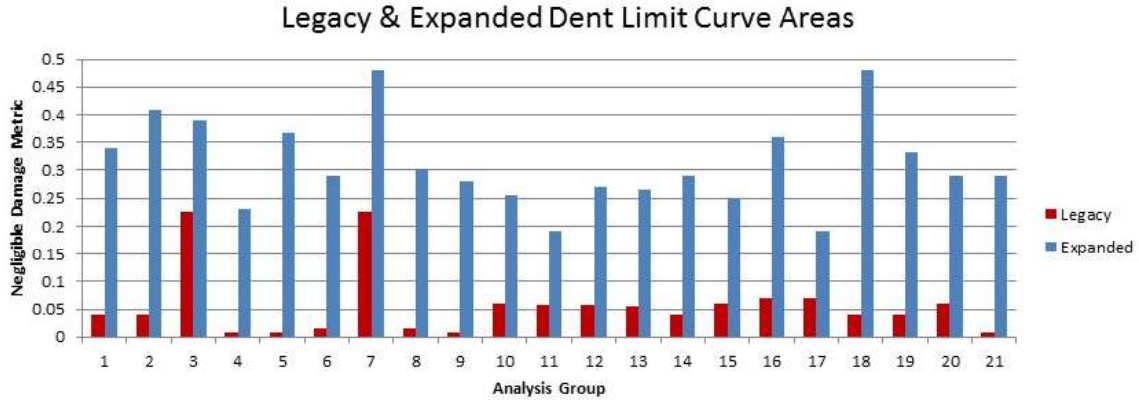


Figure 9.11-66. Physical Testing



- Most analysis groups exhibit sizable expansion of negligible dent limits
- Those analysis groups that are not sufficiently conservative undergo dent limit reduction methodology

Figure 9.11-67. Expanded Dent Limits

9.11.16. F-15 Full-Scale and Component Fatigue Tests

Roy Scheidter, The Boeing Company – F-15 Program

The F-15 (Figure 9.11-68) remains one of the most capable multirole strike fighters available today. During the past five decades, more than 1,600 F-15 aircraft have been manufactured, the latest variants being the F-15E Strike Eagle and a number of export versions. The U.S. Air Force plans to fly the F-15C/D and F-15E for many years to come; no sunset dates have as of yet been established.



Figure 9.11-68. USAF/Boeing F-15

Fatigue testing is being conducted to recertify the service life of the F-15C/D and F-15E airframes. The test articles have over one design lifetime of operational service. Three tests are being run:

- F-15C Full-Scale Fatigue Test (FTA7)

- F-15E Full-Scale Fatigue Test (FTE10)
- F-15C/E Stabilator Component Fatigue Test (FTA8)

The first two tests are being performed side-by-side at a Boeing major airframe test facility in St. Louis, MO (Figures 9.11-69 and 9.11-70). Figure 9.11-71 shows the stabilator in test. Cycling on the F-15C full-scale fatigue test began in September 2011 and is expected to continue through August 2015 under the current contract, then continue under a TBD follow-on contract until accomplishment of the cycling goal, evidence of widespread fatigue cracking or catastrophic failure of the test article. Wing replacement is anticipated/planned during the course of the test. Subsequent TBD contracts are planned for post-test teardown and analysis of the test article.



Figure 9.11-69. F-15 Full-Scale Fatigue Test Setup



Figure 9.11-70. F-15C and E Full-Scale Tests

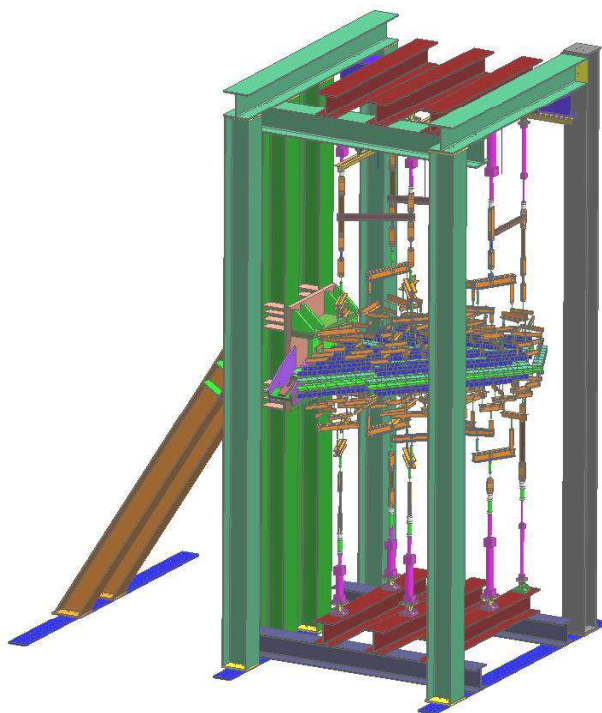


Figure 9.11-71. F-15C/E Stabilator Test

Cycling on the F-15E full-scale fatigue test started in November 2012 and is expected to continue through September 2015 under the current contract, and beyond with follow-on activities similar in scope to the F-15C test. Cycling on the F-15C/E Stabilator Component Fatigue Test was conducted in May - June 2012, successfully achieving the test goals. Teardown and analysis of the test article are underway. In addition to extending the rated life of the airframe, these tests will be used to evaluate the performance of repairs conducted prior to and during test, and their potential application to fleet aircraft will be identified.

9.11.17. F/A-18 Service Life Assessment Program (SLAP) and Service Life Extension Program (SLEP)

Matt Melliore, The Boeing Company – Military Aircraft

Military organizations have defined a need to fly aircraft beyond their original design service life. A Service Life Assessment Program (SLAP) and a Service Life Extension Program (SLEP) are in place to help achieve the new operational goals. SLAP and SLEP activities are ongoing across the F/A-18 U.S Navy fighter jet program (Figure 9.11-72). The F/A-18A-D SLAP started in 2001 with a focus on airframe components affected primarily by landings, catapult launches, arrestments, and landing gear retract cycles. A second more general SLAP phase covering structure affected by ground and flight loads began in 2005 and concluded in 2008. The F/A-18A-D SLEP is currently in work. The F/A-18E/F airframe SLAP started in 2008. Its first phases included the following technical tasks: (1) Fleet usage analysis and development of master event spectra representative of a 90th percentile aircraft in terms of fatigue damage; (2) Global finite element models to represent primary structure for the entire airframe. This finite element task included correlations with strain gage measurements made during the original full-scale tests; (3) Fatigue spectrum generation software; (4) Ground and flight loads analysis; (5) Selection of fatigue hot spots. The F/A-18E/F SLAP then transitioned to the fatigue life analysis of selected structural locations. SLEP activities for the F/A-18E/F are in their early stages.



Figure 9.11-72. F-18

9.11.18. Structural Life Management of International Space Station (ISS)

Kauser Imtiaz, The Boeing Company – Structures & Mechanical Systems

International Space Station (ISS) is the largest man-made, football field size, satellite (Figure 9.11-73). It was assembled 240 miles above earth in the zero-g Low Earth Orbit (LEO) environment from components built on Earth by 15 nations via spacewalk by a handful of astronauts over a 12-year span. Methodology for life management of earthbound structures is well established with design, analysis, testing, routine inspections, and maintenance guidelines. In contrast, ISS is a one-of-a-kind structure with no duplicates. Simulating on-orbit environments for a full-scale ground test was not feasible for many reasons including the phased assembly over 12 years. Astronaut mobility and field-of-vision constraints during spacewalk along with minimal tooling and techniques challenge detailed inspections that can be performed. Similarly, maintenance is not feasible due to the sheer size of ISS, limited spare parts, zero-g work environment, lack of space-rated tools, and manpower.

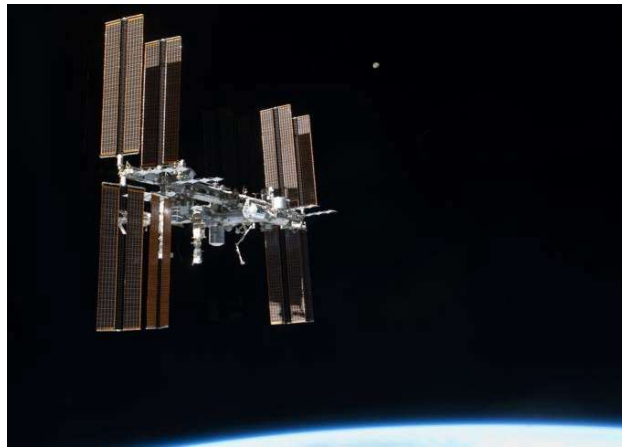


Figure 9.11-73. The ISS in Orbit

Life management of the ISS required a new set of rules. We have only design analysis and limited on-orbit instrumentation to predict and manage structural life of the ISS.

Each ISS component was designed to a 15-year life requirement. The clock for each component started at the launch. Upon completion of the assembly, the first ISS component had only a three-year analytical life remaining. Each new hardware addition changed the structural configuration of the ISS. Mass, center of gravity, damping, and natural frequencies changed continuously, making the prediction of loading spectra a moving target. During the 12 years of assembly, ISS was subjected to loads from orbital thermal cycles, station maneuvering, mechanical docking, large rotating mechanisms, and astronauts exercising. To make things more complicated, flight attitudes were continuously updated, resulting in an ever changing thermal spectrum.

In the early phase, pre-integrated structural health monitoring instrumentations for characterizing the on-orbit load environments were not feasible due to the lack of mature technologies. Limited instrumentation packages have since been flown to ISS and installed both internally and externally and are now providing invaluable data for math model correlation and structural health monitoring.

The challenges have been overcome and the analytical approaches taken adequately monitor the structural health and have resulted in life extension of the ISS through 2020 and beyond; almost doubling the life of each ISS component.

9.11.19. P-8A Poseidon Full-Scale-Fatigue Test

**Jude Restis, Thomas Turner, Hafizullah Wardak, The Boeing Company – Test & Evaluation;
James Cantela, Michael Edwards, Nam Phan, and Bradley Lloyd, USN - NAVAIR**

The P-8A Poseidon (Figure 9.11-74) is a military derivative of the commercial Boeing 737 aircraft. The P-8A is currently undergoing a full-scale fatigue test (Figure 9.11-75) to demonstrate the ability to fulfill its intended NAVY usage. The P-8A airframe is being fatigue tested to a two-lifetime test to validate the Design Service Objective (DSO) for the airframe per NAVY defined usage and requirements. The full-scale fatigue test requirements, test loads, test event tape with flight sequencing, and test fixtures were developed by the Boeing engineering team in a close collaboration with NAVAIR. Test loads were applied to a finite element model to compare design and verification internal loads. The fuselage, wings (including all wing surfaces), vertical fin and rudder are being tested on the aircraft. The landing gears, both nose and main, and horizontal stabilizer are being tested off aircraft. The wing-leading-edge and trailing-edge surfaces, weapon bay doors, and UARRSI will be block load tested. Cyclic load application started with initial block-load (local) test of the UARSSI, weapon bay door, and engine strut, all on the aircraft. Testing then progressed to fully distribute testing of the entire airframe. Block-load testing of the wing control surfaces on aircraft will follow distributed testing. This will complete one lifetime testing cycle. A second lifetime test will follow the same process. Lessons learned from this full-scale fatigue test, which is being tested with a severe loading environment, aggressive schedule, and budget constraints, will also provide data for future commercial airframe derivatives for military usage. The test program has taking extensive advantage of previous Boeing full-scale test program experience at Boeing (Figure 9.11-76).



Figure 9.11-74. P-8A Poseidon Aircraft

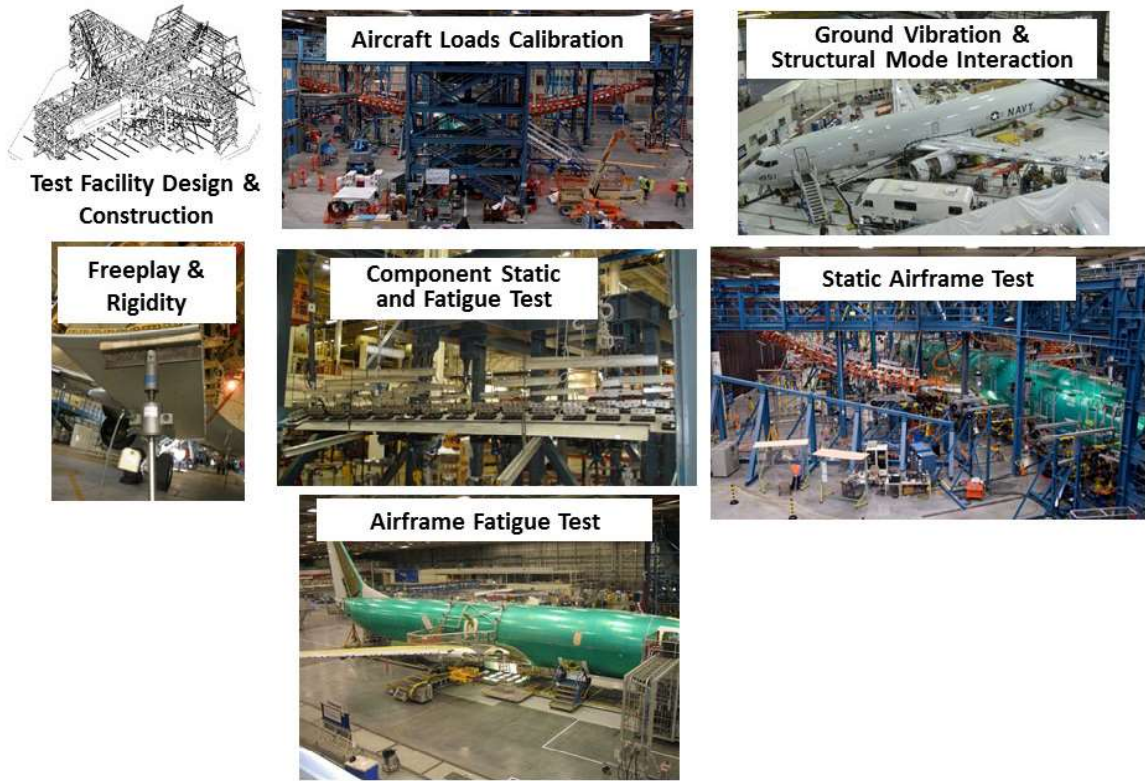


Figure 9.11-75. Elements of the P-8A Structural Test Program



Figure 9.11-76. P-8A Fatigue Test Set-Up

9.11.20. Boeing 767 Full-Scale Fatigue Test Program

Brandon Chapman, Shane Shaffner, Julie Smart, Timothy Adams, and Kevin Davis, The Boeing Company – Commercial Airplanes; P. Brownlow, The Boeing Company – Test & Evaluation

Full-scale fatigue testing of the 787 began August 15, 2010 at Boeing in Everett, WA and completed its 165,000th flight on September 28, 2015. The fatigue test airframe is a fully-structural representative production 787 airframe with the exception of non-critical and off-airplane tested items, and is tested in a test fixture specifically designed and built for the test. A photograph of the test article and test setup is shown in Figure 9.11-77.



Figure 9.11-77. 787 Full-Scale Fatigue Test Setup

Full-scale fatigue testing has long been a major part of Boeing structural performance data development, for both new models and airplanes retired from service. A full-scale fatigue test exposes a complete airframe to the typical operating loads experienced by an airplane model fleet. Though not the only evidence, such testing is primarily used to confirm the durability and damage tolerance characteristics of the primary airframe structure. Full-scale testing supports a verification of the Design Service Objective (DSO) of the airplane and the proposed inspection and maintenance program. Additionally, such testing offers significant economic benefits in terms of identifying unexpected durability issues or design deficiencies early in the life of the fleet. Finally, it provides test evidence demonstrating the effectiveness of the design to preclude the possibility of widespread fatigue damage (WFD) occurring within the DSO of the airplane, as required by the Federal Aviation Administration since 1998 and similar regulatory agencies worldwide. Companion to this is the substantiation of the limit of validity (LOV) that establishes the operational limit in the structural life of the airplane.

For the 787 airframe, Boeing set an objective to test to 165,000 flight cycles ($3.75 \times$ DSO, equivalent to 75 years of service) in an equivalent 5×5 fatigue spectrum. The test requirements, test loads, flight profile, flight sequencing, test designs and test fixturing were jointly designed by engineers from Boeing Commercial Airplanes (BCA) and Boeing Test & Evaluation (BT&E).

The 787 full-scale fatigue test spectrum load profile contained five unique flight types and load levels, and was applied in 5,000-flight repeating blocks. Each block contained 3,704 E-flights, 1,067 D-flights, 215 C-flights, 13 B-flights, and one A-flight, where the E-flight contains only the lowest load levels and the A-flight contained all load levels. In all, there were approximately 300 unique load cases. Prior to the start of testing, the test loads that had been developed were applied to a finite element model

to compare design and test loads, and validate that the applied fatigue loads met the targeted fatigue damage requirements at fatigue critical areas on the airplane.

A combination of 144 active and passive load systems were used to apply loads to the airframe and to achieve load balance – about 1.5 times the number of systems used for the 777 full-scale fatigue test. Counterbalance systems and/or tare loads were employed to offload test fixturing, horizontal load systems, and portions of the test article. Vertical loads are reacted through the main and nose landing gear, and horizontal loads were reacted through thrust/drag straps and lateral body whiffle tree systems. Test loads were applied to the airframe via bonded load pads, discrete fittings, dummy airframe structure, and load formers. The test control system continuously monitored load application and was programmed to provide an audible warning, put the test in a hold state, or shut down the test should established control limits be exceeded. Similarly a separate air control system monitored the pressurization of the fuselage main cabin. Test control limits, mechanical devices, and testing procedures provided the necessary protection of the test article. In addition, approximately 2,800 channels of strain and load measurement instrumentation were installed at specified locations of the airframe and data from these transducers were collected once during each flight block to monitor the health of the airframe structure.

Fatigue testing typically occurred 24 hours per day, seven days per week with regular inspections occurring every 6,000 flights. The inspection requirements were consistent with published 787 maintenance planning data and supplemental inspections for 787 aircraft. At the present time, teardown inspections are nearly complete. The test data have demonstrated quite clearly that the 787 outperformed the 767 and 777 in terms of fatigue performance. Figure 9.11-78 shows a comparison of the number of Fatigue Damage Reports generated by the 767, 777 and 787 major airframe fatigue tests throughout the first two DSOs.

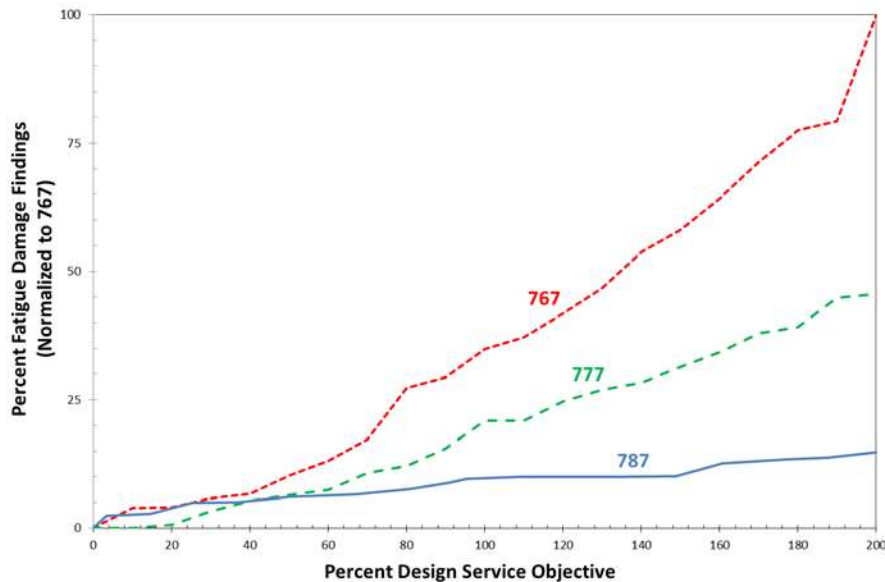


Figure 9.11-78. Comparison of Findings From Three Full-Scale Fatigue Tests: 767, 777, and 787

9.11.21. An Assessment of the Potential for Widespread Fatigue and Multi-Site Damage in the 727/737 Forward Pressure Bulkhead

G. D. Gute, Makoto Kosai, Girin Das, and Matthew Miller, The Boeing Company – Commercial Airplanes

A widespread fatigue damage (WFD) and multi-site damage (MSD) assessment was completed for the 727/737 forward pressure bulkhead (FPB) flat web. The 727 and 737 FPB share the same structural configuration and only differ in the thickness of the flat web. The assessment was accomplished by constructing finite element (FE) models of the 727 and 737 FPB structures and evaluating the distribution of stress in the flat web and, for the 737 FPB, the crack tip stress intensities and turning angles in terms of the crack tip location for a variety of crack scenarios (Figures 9.11-79 and 9.11-80). The stress survey for the 727 FPB only considered the normal operating load case. Results for both normal operating and residual strength load conditions were generated for the 737 FPB.

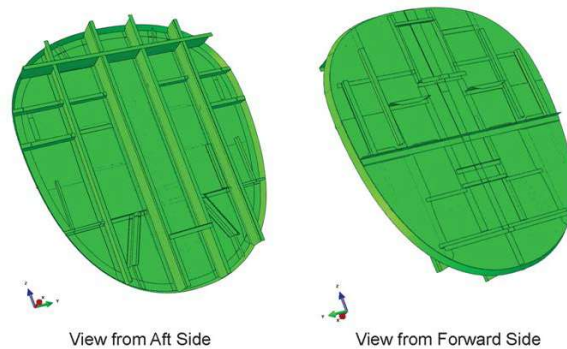


Figure 9.11-79. 727/737 Forward Pressure Bulkhead Geometry

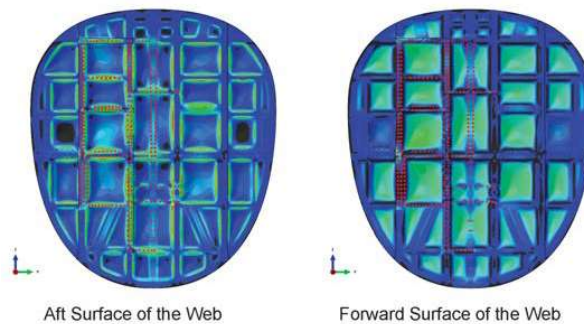


Figure 9.11-80. 737 FPB First Principal Stress Contour Plot, Normal Operating Pressure Load

The stress survey results obtained from the FE models indicate that there is sufficient variation in the resultant stresses to rule out the potential for WFD. However, the FE analysis results, in conjunction with available fleet data, indicate that MSD effects may be expected. As a result, five different crack scenarios were evaluated to determine the potential for cracks within the middle flat web section to traverse, or coalesce with other cracks, across bay boundaries. The results obtained from the stress survey and the various crack scenarios that were evaluated indicate vertically propagating cracks are not likely to traverse or coalesce across the FPB and floor junction. Similarly, the analysis results tend to support the conclusion that horizontally propagating cracks will not traverse.

9.11.22. Structural Damage Capability – Reintroducing Fail-Safety into FAA Part 25 Airworthiness Standards

Richard Kawaguchi, Mark Farthing, Wayne Lugg, David Polland, and Steven Chisholm, The Boeing Company – Commercial Airplanes

In 2015, the FAA formally tasked the Aviation Rulemaking Advisory Committee (ARAC); Transport Airplane Metallic and Composite Structures Working Group (TAMCSWG) to provide recommendations on § 25.571 and associated regulatory guidance material. As part of this effort, the TAMCSWG assigned the Airworthiness Assurance Working Group (AAWG) to re-introduce some fail-safe concepts (in the form of Structural Damage Capability (SDC)) into Part 25 of the Code of Federal Regulations (CFR). The AAWG consisted of representatives throughout the industry, including Original Equipment Manufacturers (OEM), airline operators and regulators. Although fail-safety has not been a structural requirement since the implementation of damage tolerance requirements, most OEMs have opted to continue fail-safe design practices for maintaining a level of safety against unexpected events. To encourage the continuation of these practices and to ensure new entrants to the field follow suit, the industry has considered the possibility of making SDC a regulatory requirement.

The AAWG attempted to draft guidance on addressing SDC which considered several factors and challenges, including, but not limited to the following:

1. SDC is strictly a design requirement and does not include any new maintenance program or inspection threshold requirements; it complements damage-tolerance-based inspection programs but is a separate requirement.
2. SDC needs to be applicable to composites, as well as metallic structure. There also needs to be a distinction between single load path, integral and built-up structure (see Figures 9.11-81 through 9.11-83).
3. Regarding residual strength requirements, it was difficult for the OEMs to agree upon a single damage size requirement.
4. The issue of detectability was challenging, partly because it forces one to address period of unrepaired use, which can blur the lines between SDC and damage tolerance.
5. Concerns from OEMs regarding the burden and cost associated with demonstrating compliance.



Figure 9.11-81. Single Load Path Structure

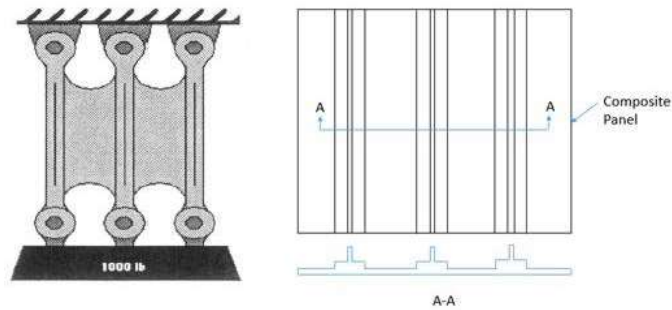


Figure 9.11-82. Integral Structure with Damage Containment Features

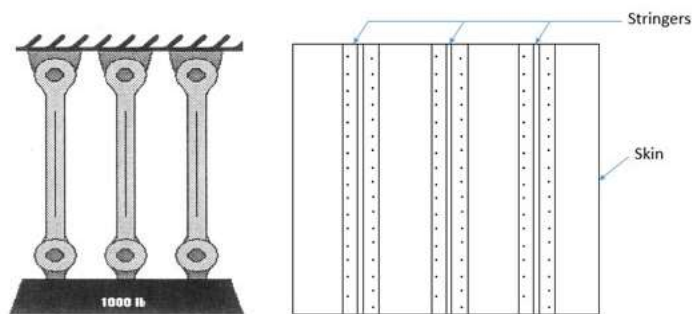


Figure 9.11-83. Multiple Element or Built-Up Structure

However, consensus could not be reached, due in part to some of the challenges listed above. Although all the AAWG-member OEMs include fail-safety in their structure, they do not necessarily design in the same level of robustness. The regulators recognize the difficulty in having the OEMs agree upon one specific set of SDC standards. To that end, current efforts are focused on making the guidance less prescriptive. Also, in addressing item #5 above, the regulators have proposed that as an alternative to making SDC a standalone requirement, it could be included as an “other consideration” as part of the OEM’s threat assessment. In other words, if an OEM can conduct a thorough threat assessment well supported by fleet history to support their findings, they could keep SDC as an internal design practice, rather than needing to show direct compliance. Conversely, a new OEM who may not yet have the capability to thoroughly address threat assessment may need to include SDC as part of their compliance findings. As of the writing of this summary, the approach to SDC is still a work in progress.

9.11.23. Active Flutter Suppression (AFS) – The Development of a Research Plan

Davis Westlund, FAA – William J. Hughes Technical Center; Wael Mour, FAA – Transport Aircraft Directorate; Eli Livne, University of Washington

Flutter is an aeroelastic instability that, once reached because of increasing flight speeds and Mach numbers, leads to airframe oscillations of magnitudes that may cause structural damage. Airplanes must be proven to be flutter-free throughout their flight envelopes, with safety margins. Manufacturers design flutter-free aircraft by building enough stiffness into the airframe and by a corresponding distribution of structural and systems weight. The use of active control technology for suppressing flutter has the potential for saving overall weight, but the technology, because of the safety issues involved, is not yet allowed in general.

The next generation of transports will use advanced “fly by wire” technology that will be capable of providing active flutter suppression (AFS) to reduce the impact of flutter requirements on the airplane design. Original equipment manufacturers (OEMs) are exploring AFS to optimize airplane design, improve operational safety, ensure continued airworthiness, and prevent and mitigate accidents. However, current regulations do not have provisions to address the safe application of these AFS systems and require the use of Special Conditions to certify airplanes with these unique features. The introduction of AFS systems requires the evaluation of: 1) relevant technical issues, 2) certification requirements and compliance issues, and 3) philosophical issues dealing with the application of this technology to commercial transports.

This multi-phase project will provide data to allow the FAA to develop new regulations, if needed, and to adjust regulatory guidance as needed to preserve current aviation safety standards. This research would be focused on the conventional type of Transport Category airplanes that are being designed today and in the near future. Recent accomplishments this fiscal year include the development of an AFS Research Plan to address the following fundamental questions:

- What are the risks/uncertainties of using AFS Systems?
- Are the current analysis methods capable of reliably predicting the behavior/effectiveness of AFS in flight?
- Are the current analysis methods capable of correctly predicting the sensitivities of AFS?
- What sensitivities should the FAA be aware of?
- What analysis validation methods are needed for an AFS design?

In developing this plan, the current state of AFS in the commercial airplane sector was assessed through surveys, interviews with airplane manufactures and operators, and discussions with technology developers. The plan explores leveraging resources with existing AFS projects, including the X-DIA wind tunnel model in collaboration with Milan Polytechnic (Figure 9.11.84). The major tasks of the AFS Research Plan over the FY17–20 timeframe include:

- Task 1: Collect all data from existing AFS programs (including models) and ground and flight test data
- Task 2: Develop or use existing control laws to determine appropriate margins of safety
- Task 3: Perform uncertainty and sensitivity analyses
- Task 4: Perform wind tunnel testing to validate analyses

The end goal of these tasks is to provide data to allow for the review of pertinent regulations and guidance material, and to prepare recommendations, if needed, for new, modified, or otherwise improved criteria.

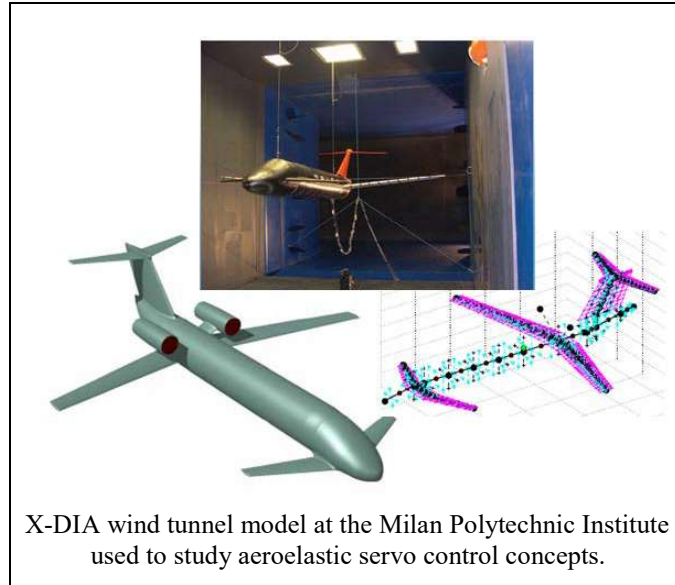


Figure 9.11-84. Active Flutter Suppression

9.11.24. U.S. Air Force Academy Center for Aircraft Structural Life Extension (CAStLE) Support to USAF Aircraft Structural Integrity Program (ASIP)

Gregory Shoales and James M. Greer, Jr., USAFA – CAStLE

Through multiple task orders and three contract vehicles, CAStLE has provided support to various aspects of the ASIP efforts of multiple USAF customers, including A-10, T-38, RQ-4B, RC-/KC-135 (Figure 9.11-85) and others.



**Figure 9.11-85. A Sampling of USAF Aircraft having CAStLE Support.
Clockwise From Upper Left: A-10, T-38, RC-135, RQ-4B**

CASTLE's involvement with various fleet manager customers ranges from minimal to "hand-in-hand". Aside from teardown analysis and the impact of environment on fatigue, ASIP support to these systems has included

- Reviews of and updates to ASIP-related documentation
 - ASIP Master Plan
 - Force Structural Maintenance Plan
 - Durability and Damage Tolerance Analysis (DaDTA)
 - Technical Orders (including Time-Compliance Technical Orders)
 - Corrosion Prevention and Corrosion Control plans
- On-site engineering support for the purposes of
 - Airworthiness certification/recertification support
 - Assessing engineering processes
 - Configuration management support
 - Engineering dispositions
- New Non-Destructive Inspection (NDI) tools
 - NDI fixtures for improved inspections (Figure 9.11-86a)
 - NDI probes and standards (Figure 9.11-86b)
 - Validation & verification of new procedures
 - Ergonomic tools for increasing probability of inspection
- Risk & EIFS analysis
- Coupon and subcomponent testing to support
 - DaDTA
 - Validation of modeling and simulation tools
 - Repairs & modifications
- Flight data collection and spectrum analysis
- Material processing (sealant removal and coating removal methods, CX effects)
- Software tools for crack growth modeling, maintenance and for tracking of damage & repairs
- Failure ("Root Cause") analysis of damaged/failed in-service parts

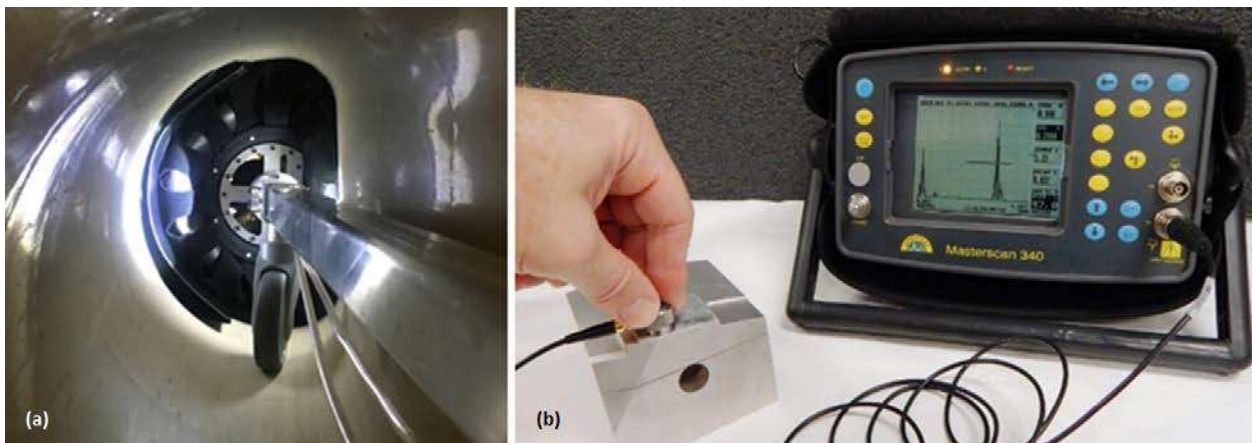


Figure 9.11-86. (a) NDI Tool for Nacelle X-Ray Inspection; (b) NDI Standard Development

9.11.25. U.S. Air Force Academy Center for Aircraft Structural Life Extension (CAStLE) Basic Research

James M. Greer, Jr., USAFA – CAStLE

A number of CAStLE researchers, including cadet researchers from the U.S. Air Force Academy (USAFA) took on a number of interesting basic research topics.

- Dr. Sandeep Shah and Mr. Kevin Gibbons (Sabreliner Aviation, LLC) examined the nucleation effects from oxide scales on aluminum.
- A cadet team instrumented and tested a fuel pump from a general aviation aircraft in an attempt to profile its electrical and thermal behavior during various modes of operation.
- Other cadets in a senior instrumentation course studied the effects of a crack at a critical fastener on the residual strength of structure removed from an in-service aircraft. Using the principles of Linear Elastic Fracture Mechanics, the cadets predicted the failure load and subsequently tested the structure (Figure 9.11-87).
- Dr. Ralph Bush, Dr. James Greer and a USAFA cadet, in conjunction with the supporting maintenance contractor, are studying the effects of a metal forming technique (hot joggling) on new 7000-series alloys.
- Dr. Börje Andersson, Dr. Ralph Bush, and Dr. James Greer are working on a project to generate stress intensity factors (and verify them) for a variety of crack geometries at a countersunk fastener hole (Figure 9.11-88).
- Dr. Sandeep Shah, Ms. Cindy Klahn and Mr. Todd St John examined the susceptibility of 7000-series aluminum alloys to in-place cracking (Figure 9.11-89) [1].
- Dr. Sandeep Shah, Cadet Jaspreet Singh, 2LT Timothy Welkener and Dr. James Greer studied the effects of corrosion pits and machining marks on fatigue crack growth in an aluminum alloy (Figure 9.11-90) [2].
- Cadets Despard and Chimento III, along with Dr. Saravanan Arunachalam, Mr. Collier McGehee (SAFE, Inc.), examined the topic of qualifying supersonic particle deposition (also known as Cold Spraying) for structural repair. This was presented at the Colorado Springs Undergraduate Research Forum in Colorado Springs. Cold Spraying for structural repairs is an attractive and cost effective option. However, the integrity of such repairs on critical components is difficult to guarantee and makes certifying structural repairs a lengthy process. This project attempted to understand the factors affecting the electrical conductivity of aluminum alloys, and to use the conductivity values to qualify the integrity of SPD repairs [3].
- Other basic research work to be presented at ICAF 2017 is cited below [4-7].

References:

- [1] Shah, S. and Klahn C. and St John, T., “In-Plane Cracking in Corrosion Susceptible AA7XXX Series Alloys and Its Effect on Mechanical Integrity of Structural Elements”, *Proceedings of the International Conference on Engineering Failure Analysis VI*, Lisbon, Portugal, 6-9 July 2014.
- [2] Shah, S. and Singh, J. and Welkener, T. and Greer, J., “The Effects of Corrosion Pits and Machining Marks on the Fatigue Crack Initiation and Propagation in AA7075-T73,” *Proceedings of the International Conference on Engineering Failure Analysis VII*, Leipzig, Germany, 3-6 July 2016.
- [3] Arunachalam, S. and McGehee, C. and Despard and Chimento III, “Qualifying the Use of Supersonic Particle Deposition for Structural Repair Using Electrical Conductivity”, Colorado Springs Undergraduate Research Forum (CSURF), Colorado Springs, Colorado, 2016.
- [4] Singh, J. and Shah, S. “Experimental Measurement of Small Crack Stress Intensity Factors, Poster, ICAF 2017.
- [5] Galyon Dorman, S. and Fawaz, S., “Effect of Chromate Inhibition on Corrosion Fatigue in Service Relevant Concentrations,” Paper, ICAF 2017.

- [6] Rausch, J. and Galyon Dorman, S. and Fawaz, S., "Corrosion Fatigue Pit-to-Crack Test Methodology," Poster, ICAF 2017.
- [7] Arunachalam, S.R. and Fawaz, S., "Structural Restoration Viability Using Cold Spray Technology," Poster, ICAF 2017.

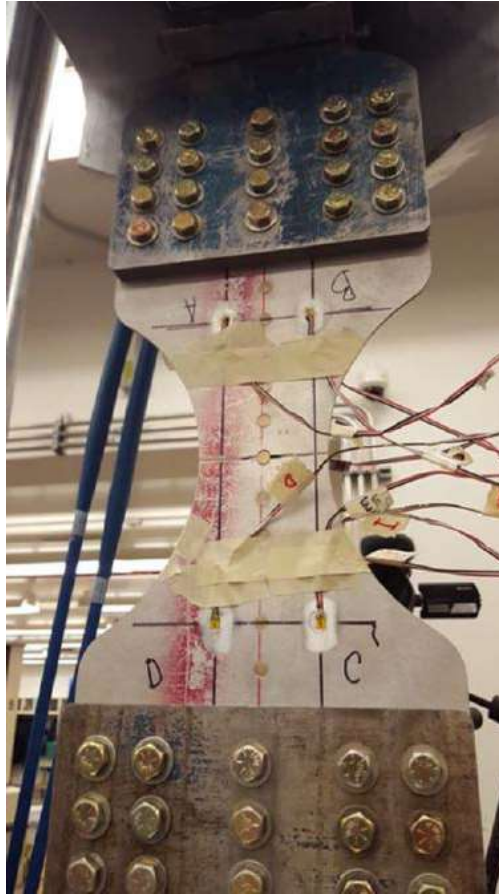


Figure 9.11-87. Specimen for Residual Strength Measurement

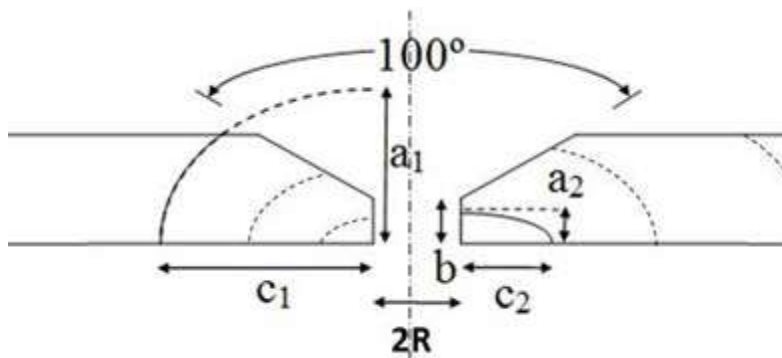


Figure 9.11-88. Countersunk Hole Geometry and Variables



Figure 9.11-89. Stiffening Element Exhibiting In-Plane Cracks

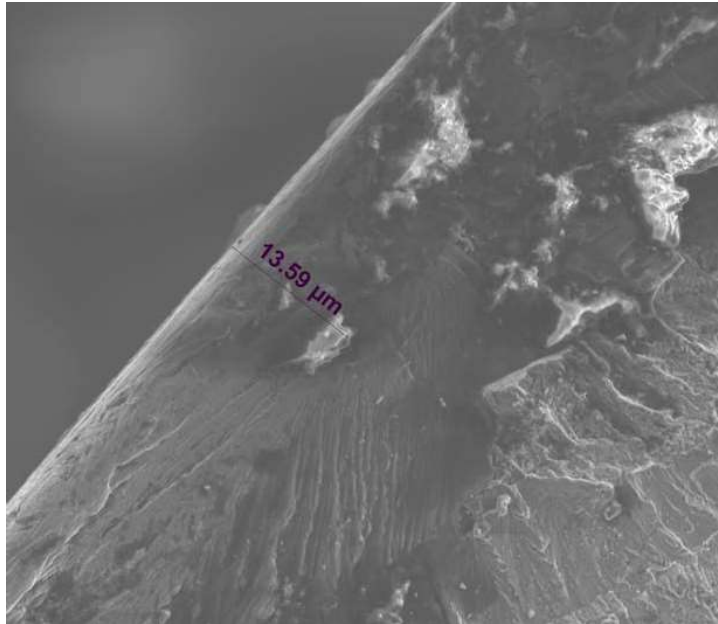


Figure 9.11-90. Crack Nucleation Site at a Machining Mark

9.11.26. Impact of Material Degradation on Fatigue

Gregory Shoales and James M. Greer, Jr., USAFA – CASTLE

CASTLE's experience continues to support the strong connectivity between fatigue crack damage mechanisms and corrosion damage mechanisms. The influence of chemical environment on fatigue damage is well established. Consequently, the advancement of material degradation (corrosion) science and technology (S&T) continues to be a national priority for the agencies of the U.S. Department of Defense, and therefore CASTLE, in order to facilitate the safe sustainment of aerospace structures. Just as important to the development of critical material degradation related S&T is the preparation of current professionals and future generations to address these challenges for years to come—such individuals have historically been in short supply. Accordingly CASTLE and the Office of the Secretary of Defense Corrosion Policy and Oversight (OSD-CPO) have the co-mission to execute a robust and diverse program to develop education, training and outreach programs which not only ensure a talented pool of individuals exist but also promote awareness of structural material degradation in the global society. The following is a brief overview of some of the activities in both the S&T research program and the education, training and outreach program since ICAF 2015.

Technical Corrosion Collaboration (TCC) Research and Technology Demonstration Projects

CASTLE has performed research in the area of structural material degradation for the past 20 years. Since the last ICAF report CASTLE has used CPO support to contract with a number of university and private entities to conduct a research program aimed at both educating students and furthering the body of critical knowledge in the corrosion sciences. The university and private companies along with relevant government research labs form the Technical Corrosion Collaboration or TCC. The TCC research programs are targeted at

- Developing appropriately experienced individuals to include students, faculty, and other researcher professionals
- Creating research products, which address the OSD-CPO research areas of interest. These areas include
 - Performance prediction through modeling, simulation and testing,
 - Surface finish and treatments research,
 - Coatings research, and
 - Product support research.
- Promoting collaboration between industry, government, university and commercial material degradation research entities.

For example, one such TCC participant, SAFE, Inc., has conducted a number of projects in the USAF Academy CASTLE facility. Abstracts of these projects are included in this year's ICAF report and include;

- Development of a Fatigue Testing Method for Analysis of the Corrosion Pit to Small Crack Transition
- Development of Equipment and Methods for Stress Spectra Structural Testing Combined with Environmental Spectrum
- Generating Stress Intensity Factors for Finite Width Plates

CASTLE assists the OSD-CPO to evaluate the technical merit of new projects, determine the best means to fund selected efforts, monitor technical performance, and conduct on-site reviews of all TCC participants. To further support the Areas of Interest (AoI) addressed by TCC research projects the OSD-CPO also sponsors numerous technical demonstration (Tech Dem) projects. Figure 9.11-91 shows a summary to date of the number of projects sponsored by OSD-CPO through both the TCC and the Tech Dem programs grouped by the AoI they support.



CPC Projects by Category

CORROSION POLICY AND OVERSIGHT

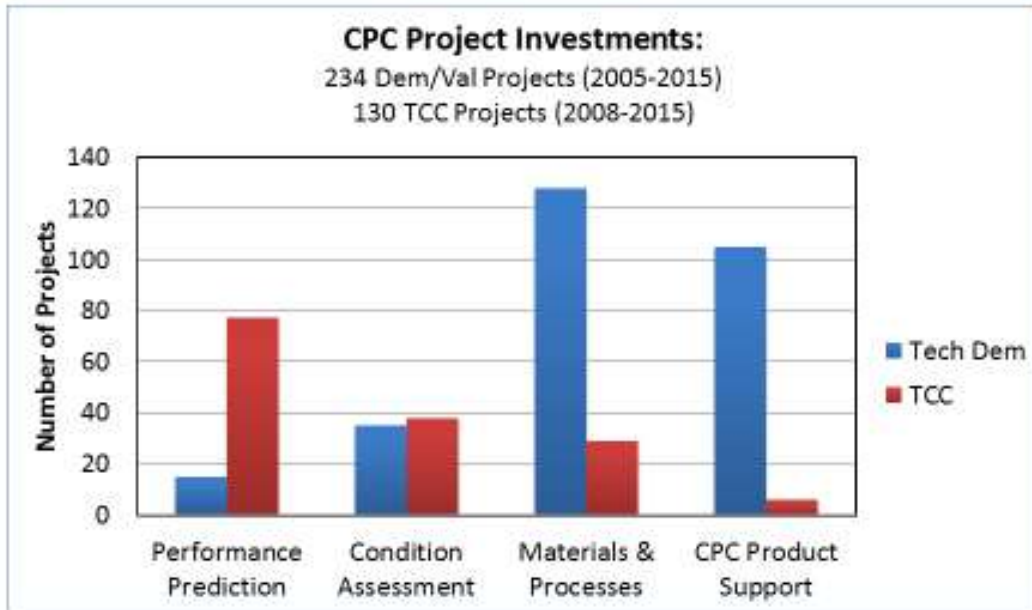


Figure 9.11-91. Summary of TCC and Tech Dem Projects by Area of Interest

As indicated previously, government labs are also TCC participants. As a USAF research lab, one of the ways CASTLE participates is by using TCC-inspired technology challenges to create projects for USAF Academy (USAFA) cadets that address the research goals of CASTLE, the TCC and the OSD-CPO. Since the last ICAF report USAFA cadets have participated in design challenges which

- Help catholically protect bridges and infrastructure, and
- Perform remote corrosion inspections of occluded, hard to reach areas in structures.

The latter of these challenges was fostered directly by CASTLE and OSD-CPO to create a new international “University Student Design and Applied Solutions Competition (USDASC).” The first ever USDASC competition was held 18-20 April 2016 in Houston, Texas. International participation in the event included both universities and U.S. service academies. Competitors were required to submit a written report, present their design via formal briefing, and finally demonstrate their design in an unknown structure. Cumulative scores in each element determined the final placing of the competitor teams. Figure 9.11-92 shows elements of two of the competitor designs during the demonstration element. The winning team, from the USAF Academy, is shown in Figure 9.11-93 with their winning design.

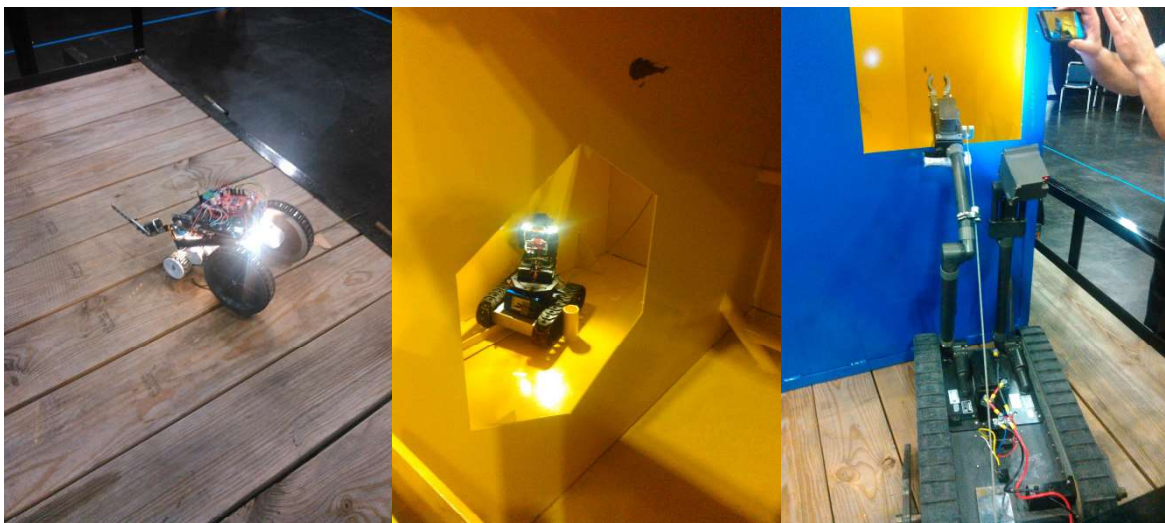


Figure 9.11-92. Examples of Various USDASC Design Solutions in Action During the Design Demonstration Competition Element

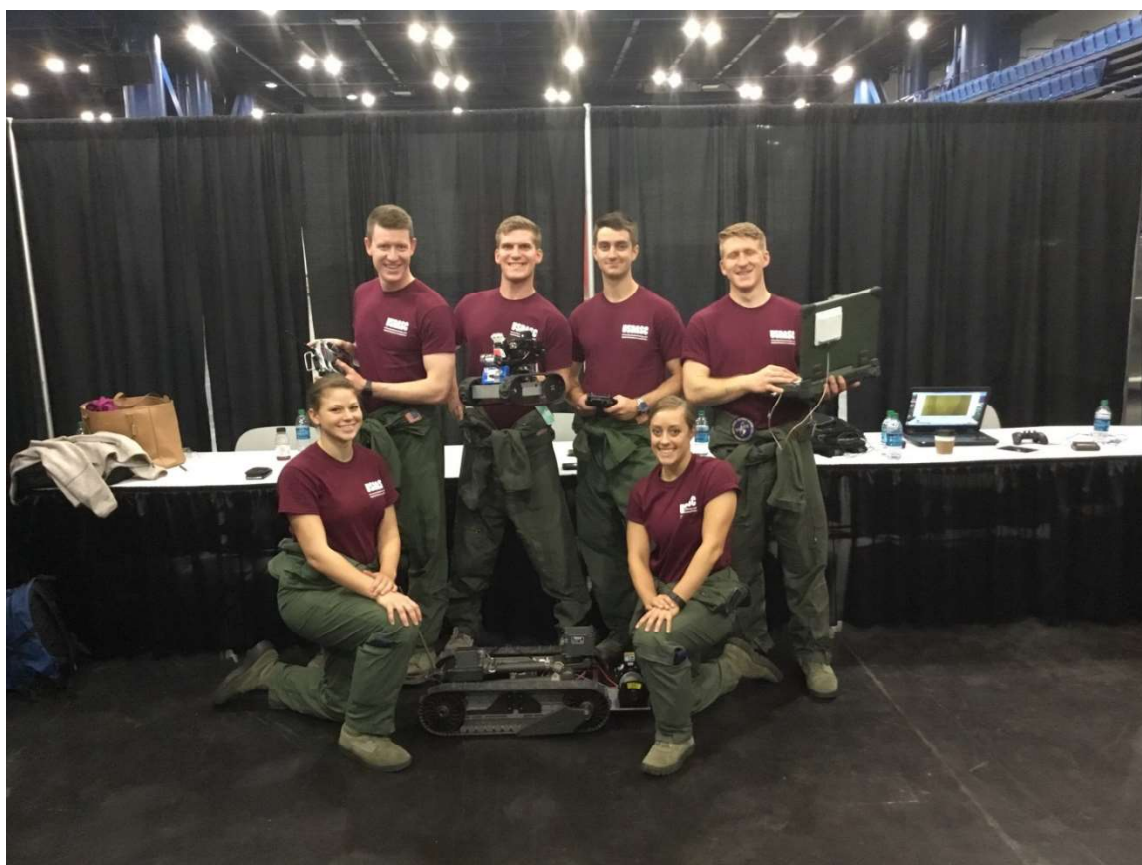


Figure 9.11-93. Winning Team From the First Ever University Student Design and Applied Solutions Competition (USDASC) in April 2016

Through the USAFA Cadet Summer Research Program (CSRP) and OSD-CPO support CASTLE has sent cadets to international research facilities to further their studies in material degradation related topics. In 2015, Cadets Gill and Weinberg were sent to work with Professor Tom Ladwein at Hochschule

Aalen in Germany. In 2015 USAFA Department of Engineering Mechanics faculty, Major Ben Steffens, began a USAF sponsored corrosion research program at BAM Federal Institute for Materials Research and Testing in Berlin. In 2016, Cadets Kyra Schmidt and Zane Wilburn participated in research of corrosion in high-strength landing gear steels at BAM under the guidance of Profession Thomas Böllinghaus and Major Steffens. The CSR work was presented at the TCC annual reviews of each year.

Corrosion Education and Outreach

OSD-CPO, through CASTLE, continues to foster an ever growing portfolio of education and outreach programs in corrosion topics. Since ICAF 2015, these projects have included:

- Development and prototyping of the aforementioned university student corrosion design-applied solution competition to address DoD's corrosion related problems
- Corrosion focused website
- Development of corrosion science education exhibits with hands-on interaction for application to U.S. public science centers
- Development of a material science long distance education course for advanced placement high school and college students
- Development of booths education exhibits for conference displays and public outreach media articles
- Updates to the annual corrosion impact studies